

AD-A076 093

WOODWARD-CLYDE CONSULTANTS CHICAGO IL

F/G 13/2

RESULTS AND INTERPRETATION OF PILE DRIVING EFFECTS TEST PROGRAM--ETCIL

DACW43-78-C-0005

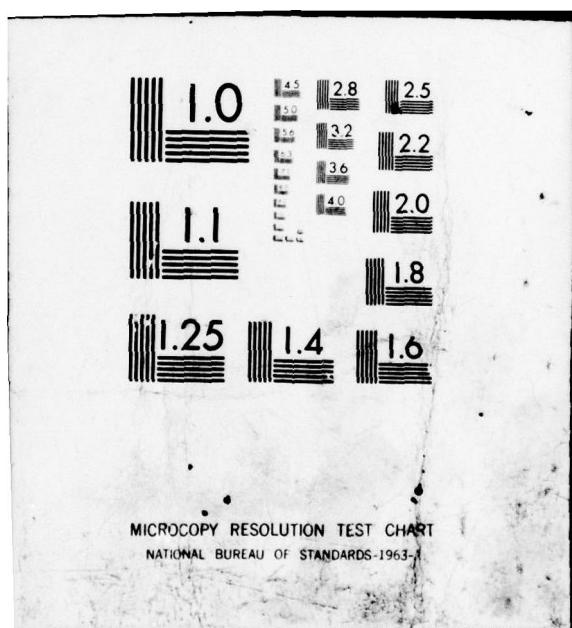
JUL 79 J PEREZ + D M HOLLOWAY

NL

UNCLASSIFIED

1 OF 5  
AD  
AD76093





PHASE IV REPORT  
VOLUME III

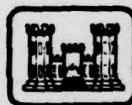
②  
**LEVEL**

RESULTS AND INTERPRETATION OF  
PILE DRIVING EFFECTS TEST PROGRAM

EXISTING LOCKS AND DAM NO. 26  
MISSISSIPPI RIVER, ALTON, ILLINOIS

A076093

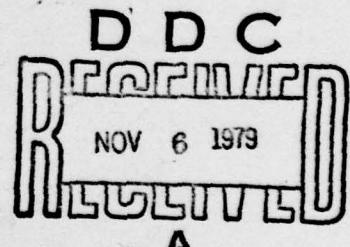
Prepared for



United States Army  
Corps of Engineers  
...Serving the Army  
...Serving the Nation

**St. Louis District**

By



Woodward-Clyde Consultants  
Chicago, Illinois

DDC FILE COPY

15 July 1979

Contract No. DACW43-78-C-0005

Y7C825

APPROVED FOR PUBLIC RELEASE - DISTRIBUTION UNLIMITED

79 11 05 155

# PHASE IV REPORT

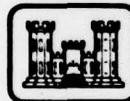
## VOLUME III

### RESULTS AND INTERPRETATION OF PILE DRIVING EFFECTS TEST PROGRAM.

EXISTING LOCKS AND DAM NO. 26,  
MISSISSIPPI RIVER, ALTON, ILLINOIS.

Volume III. Phase IV Report.

Prepared for



United States Army  
Corps of Engineers

... Serving the Army  
... Serving the Nation

St. Louis District

By

Final report,

D. Michael Holloway

(10)

Jean-Yves Perez

D. Michael Holloway

D. Michael Holloway

Woodward-Clyde Consultants

Chicago, Illinois

453

(11) 15 Jul 79

Contract No. DACW43-78-C-0005

(15) Y7C825

(12)

APPROVED FOR PUBLIC RELEASE - DISTRIBUTION UNLIMITED

411 445

mt

## Unclassified

SECURITY CLASSIFICATION OF THIS PAGE (When Data Entered)

REPORT DOCUMENTATION PAGE		READ INSTRUCTIONS BEFORE COMPLETING FORM																		
1. REPORT NUMBER	2. GOVT ACCESSION NO.	3. RECIPIENT'S CATALOG NUMBER																		
4. TITLE (and Subtitle) FOUNDATION INVESTIGATION AND TEST PROGRAM, LOCKS AND DAM 26, MISSISSIPPI RIVER, ALTON, ILLINOIS Volume III		5. TYPE OF REPORT & PERIOD COVERED Final report																		
7. AUTHOR(s) Jean-Yves Perez D. Michael Holloway		6. PERFORMING ORG. REPORT NUMBER																		
8. PERFORMING ORGANIZATION NAME AND ADDRESS Woodward-Clyde Consultants 11 East Adams Street Chicago, IL 60603		9. CONTRACT OR GRANT NUMBER(s) DACW43-78-C-0005																		
11. CONTROLLING OFFICE NAME AND ADDRESS U. S. Army Engineer District, St. Louis 210 North 12th Street St. Louis, MO 63101		12. REPORT DATE June 1979																		
14. MONITORING AGENCY NAME & ADDRESS (if different from Controlling Office)		13. NUMBER OF PAGES 365																		
		15. SECURITY CLASS. (of this report) Unclassified																		
		15a. DECLASSIFICATION/DOWNGRADING SCHEDULE																		
16. DISTRIBUTION STATEMENT (of this Report)  Approved for public release; distribution unlimited.																				
17. DISTRIBUTION STATEMENT (of the abstract entered in Block 20, if different from Report)  <table border="1" style="margin-left: auto; margin-right: auto;"> <tr><td>Vol I</td><td>Overview of Foundation Investigation and Test Program</td></tr> <tr><td>Vol II</td><td>Results and Interpretation of Chemical Grouting Test Program</td></tr> <tr><td>Vol IIIA</td><td>Appendices A through G, Results and Interpretation of Chemical Grouting Test Program</td></tr> <tr><td>Vol III</td><td>Results and Interpretation of Pile Driving Effects Test Program</td></tr> <tr><td>Vol IIIA</td><td>Appendices H through T, Results and Interpretation of Pile Driving Effects Test Program</td></tr> <tr><td>Vol IV</td><td>Results and Interpretation of Drilled-In Pile Test Program</td></tr> <tr><td>Vol IVA</td><td>Appendices A through E, Results and Interpretation of Drilled-In Pile Test Program</td></tr> <tr><td>Vol V</td><td>Results and Interpretation of Rock Anchor Test Program</td></tr> <tr><td>Vol VA</td><td>Appendices A through E, Results and Interpretation of Rock Anchor Test Program</td></tr> </table>			Vol I	Overview of Foundation Investigation and Test Program	Vol II	Results and Interpretation of Chemical Grouting Test Program	Vol IIIA	Appendices A through G, Results and Interpretation of Chemical Grouting Test Program	Vol III	Results and Interpretation of Pile Driving Effects Test Program	Vol IIIA	Appendices H through T, Results and Interpretation of Pile Driving Effects Test Program	Vol IV	Results and Interpretation of Drilled-In Pile Test Program	Vol IVA	Appendices A through E, Results and Interpretation of Drilled-In Pile Test Program	Vol V	Results and Interpretation of Rock Anchor Test Program	Vol VA	Appendices A through E, Results and Interpretation of Rock Anchor Test Program
Vol I	Overview of Foundation Investigation and Test Program																			
Vol II	Results and Interpretation of Chemical Grouting Test Program																			
Vol IIIA	Appendices A through G, Results and Interpretation of Chemical Grouting Test Program																			
Vol III	Results and Interpretation of Pile Driving Effects Test Program																			
Vol IIIA	Appendices H through T, Results and Interpretation of Pile Driving Effects Test Program																			
Vol IV	Results and Interpretation of Drilled-In Pile Test Program																			
Vol IVA	Appendices A through E, Results and Interpretation of Drilled-In Pile Test Program																			
Vol V	Results and Interpretation of Rock Anchor Test Program																			
Vol VA	Appendices A through E, Results and Interpretation of Rock Anchor Test Program																			
18. SUPPLEMENTARY NOTES																				
19. KEY WORDS (Continue on reverse side if necessary and identify by block number) Lock and Dam No. 26, Mississippi River      Timber piles Chemical grout test      Alluvial sands Rock anchor test      Benoto method Drilled-in pile test      Instrumentation of tests Pile driving effects test      Vibrational effects on structures																				
20. ABSTRACT (Continue on reverse side if necessary and identify by block number) A series of tests examining various foundation systems and construction techniques were conducted on Ellis Island near Locks and Dam No. 26 in alluvial sand deposits underlain by glacial deposits and limestone. The chemical grout test consisted of grouting the upper 20 feet of the alluvial sand by injecting a number of different silicate and cement-bentonite grout types, while varying the grouting method, hole spacing, and injecting rates. Heave, lateral displacement, and pore pressure were monitored during grout injection. The in situ properties of the sand were measured before and after grouting by standard																				

20. penetration tests, static cone penetration tests, pressuremeter tests, bore hole permeability tests, and shear wave velocity tests. Concurrently laboratory tests were conducted to investigate the strength and creep behavior of the grouted sand. After completion of grouting, the site was excavated to examine and evaluate the grouted sand. In the rock anchor test, inclined rock anchors were installed in limestone through 130 feet of alluvial and glacial deposits using a pneumatic down-the-hole hammer with an offset reamer. Load tests were conducted on three instrumented rock anchors and the feasibility of installation of the rock anchors was determined by evaluating loss of ground during installation, performance of the installation equipment, and rate of installation. The drilled-in pile test consisted of installation of large diameter high capacity pipe piles by the Benoto method. The feasibility of installing these piles was determined by evaluating loss of ground during installation, performance of the Benoto equipment, and rate of installation. In the pile driving effects test, pile founded monoliths were constructed, supported on either one, eight or twelve timber piles jetted and driven in alluvial sand to a depth of 35 feet. After applying lateral and vertical load to the monoliths, steel piles were driven at varying distances from the monoliths while monitoring movement of the monolith and supporting piles; shear, moment, and axial load in the timber piles; and pore pressure, movement, and particle velocity, in the soil. Parameters examined were pile type being driven (sheet, pipe, or H-pile), pile driving hammer (diesel, air-steam, or vibratory), distance of driven piles from monolith, driving of multiple piles at the same distance from the monolith, load level applied to the monolith, and soil properties (grouted and ungrouted). Vertical and lateral load tests were conducted on each pile founded monolith. Tests were also conducted to assess what effect grouted soil has on piles. Piles were driven in both grouted and ungrouted sand to examine driving characteristics and lateral load tests were conducted on H and pipe piles in both grouted and ungrouted sand.

**TABLE OF CONTENTS**

	<u>Page</u>
Title Page	i
Table of Contents	ii

**0 SUMMARY AND CONCLUSIONS**

Title Page	0-i
0.1 PILE DRIVING EFFECTS TEST PROGRAM	0-1
0.2 TEST AREA SUBSURFACE CONDITIONS	0-1
0.3 DESIGN AND CONSTRUCTION OF TEST FACILITIES	0-1
0.3.1 Test Program Design	0-1
0.3.2 Construction of Test Facilities	0-2
0.4 TESTING ACTIVITIES	0-3
0.4.1 Monolith Preloading	0-3
0.4.2 Pile Driving Effects Testing	0-3
0.4.3 Monolith Load Testing	0-4
0.4.4 Lateral Load Testing of Prototype Piles	0-4
0.5 SUMMARY OF TEST RESULTS	0-4
0.5.1 Monolith Preloading	0-4
0.5.2 Prototype Pile Driving Effects	0-4
0.5.3 Monolith Load Testing	0-6
0.5.4 Lateral Load Testing of Prototype Piles	0-6
0.6 INFERRRED MECHANISMS	0-6

Accession For	
NTIS GRA&I	
DDC TAB	
Unannounced	
Justification	
By _____	
Distribution/	
Availability Codes	
Distr.	Avail and/or special
A	

**TABLE OF CONTENTS**

(Continued)

	<u>Page</u>
<b>1 PURPOSE AND OBJECTIVES</b>	
<b>Title Page</b>	<b>1-i</b>
1.1 <b>PURPOSE</b>	1-1
1.2 <b>OBJECTIVES</b>	1-1
1.3 <b>ORGANIZATION OF VOLUME III</b>	1-2

**TABLE OF CONTENTS**

(Continued)

	<u>Page</u>
<b>2 TEST PROGRAM DESIGN</b>	
<b>Title Page</b>	<b>2-i</b>
<b>2.1 CONCEPT OF TEST PROGRAM</b>	<b>2-1</b>
<b>2.1.1 Test Area Selection</b>	<b>2-1</b>
<b>2.1.2 Approach</b>	<b>2-1</b>
<b>2.1.3 General Description</b>	<b>2-2</b>
<b>2.2 SELECTION OF VARIABLES</b>	<b>2-3</b>
<b>2.2.1 General</b>	<b>2-3</b>
<b>2.2.2 Number of Test Monoliths</b>	<b>2-4</b>
<b>2.2.3 Test Monolith Configuration and Geometry</b>	<b>2-4</b>
<b>2.2.4 Adjacent and Interior Piles</b>	<b>2-4</b>
<b>2.2.5 Timber Pile Installation</b>	<b>2-4</b>
<b>2.2.6 Applied Load Levels</b>	<b>2-5</b>
<b>2.2.7 Cyclic Preloading</b>	<b>2-5</b>
<b>2.2.8 Grouted/UngROUTED Soil</b>	<b>2-5</b>
<b>2.2.9 Prototype Piles</b>	<b>2-6</b>
<b>2.2.10 Pile Driving Hammers</b>	<b>2-6</b>
<b>2.3 SIGNIFICANT ASPECTS OF PERFORMANCE</b>	<b>2-7</b>
<b>2.3.1 General</b>	<b>2-7</b>
<b>2.3.2 Prediction Method</b>	<b>2-7</b>
<b>2.3.3 Predicted Performance</b>	<b>2-11</b>

**List of Tables**

<b>Table 2.1</b>	<b>SEQUENCE OF ACTIVITIES</b>
<b>Table 2.2</b>	<b>SUMMARY OF TEST MONOLITH VARIABLES</b>
<b>Table 2.3</b>	<b>SIGNIFICANT ASPECTS OF PERFORMANCE</b>

**List of Figures**

<b>Figure 2.1</b>	<b>CONCEPT OF TESTS</b>
<b>Figure 2.2</b>	<b>LOCATION OF TEST AREA</b>

**TABLE OF CONTENTS**

(Continued)

- Figure 2.3      GENERAL CONFIGURATION OF TEST AREA  
Figure 2.4      TYPICAL MONOLITH AND LOADING SETUP  
Figure 2.5      MONOLITH CONFIGURATIONS  
Figure 2.6      REFERENCE PEAK PARTICLE VELOCITY  $V_p$  AT  
                   $r_s = 1$  FT vs RATED HAMMER ENERGY AND BLOWCOUNTS  
                  FOR 14-IN. PILES  
Figure 2.7      PILE DRIVING EFFECTS DATA FROM DAM No. 11  
Figure 2.8      NORMALIZED RESPONSE OF FEAGIN'S TEST  
                  MONOLITH M2  
Figure 2.9      PREDICTED MONOLITH DISPLACEMENT CAUSED BY  
                  DRIVING WITH VULCAN 010  
Figure 2.10      PREDICTED MONOLITH DISPLACEMENT CAUSED BY  
                  DRIVING WITH DELMAG D22  
Figure 2.11      PREDICTED PERFORMANCE OF THE PRIMARY  
                  PILE DRIVING SYSTEM  
Figure 2.12      PREDICTED PEAK PARTICLE VELOCITY AT GROUND  
                  SURFACE CAUSED BY PROTOTYPE PILE DRIVING  
Figure 2.13      PREDICTED PROTOTYPE PILE DRIVING PERFORMANCE  
                  IN UNGROUTED AND GROUTED SOIL  
Figure 2.14      PREDICTED HORIZONTAL PILE-HEAD DISPLACEMENT  
                  UNDER LATERAL LOADING

**TABLE OF CONTENTS**

(Continued)

	<u>Page</u>
<b>3 INSTRUMENTATION</b>	
<b>Title Page</b>	<b>3-i</b>
<b>3.1 INSTRUMENTATION REQUIREMENTS</b>	<b>3-1</b>
<b>3.1.1 General Requirements</b>	<b>3-1</b>
<b>3.1.2 Response of Monoliths During Nearby Prototype Pile Driving</b>	<b>3-1</b>
<b>3.1.3 Performance of Prototype Piles During Driving</b>	<b>3-2</b>
<b>3.1.4 Wave Propagation in Soil</b>	<b>3-2</b>
<b>3.1.5 Response of Timber Piles During Nearby Prototype Pile Driving</b>	<b>3-3</b>
<b>3.1.6 Response of Soil Mass During Nearby Prototype Pile Driving</b>	<b>3-4</b>
<b>3.1.7 Static Load Testing of Monoliths</b>	<b>3-4</b>
<b>3.1.8 Driving Performance of Timber Piles</b>	<b>3-5</b>
<b>3.1.9 Lateral Load Tests on Prototype Piles</b>	<b>3-5</b>
<b>3.2 DESCRIPTION AND GENERAL EVALUATION OF INSTRUMENTATION</b>	<b>3-5</b>
<b>3.2.1 Optical Instrumentation and Controls</b>	<b>3-5</b>
<b>3.2.2 Monolith Instrumentation</b>	<b>3-6</b>
<b>3.2.3 Timber Pile Instrumentation</b>	<b>3-7</b>
<b>3.2.4 Ground Instrumentation</b>	<b>3-8</b>
<b>3.2.5 Steel Pile Instrumentation</b>	<b>3-10</b>
<b>3.2.6 Automatic Data Acquisition System (Cyber II)</b>	<b>3-11</b>
<b>3.2.7 Dynamic Data Acquisition System (Geophones)</b>	<b>3-11</b>
<b>3.2.8 Pile Driving Analyzer System</b>	<b>3-12</b>
<b>3.2.9 Details of Instrumentation for Monolith M2</b>	<b>3-12</b>
<b>3.3 CALIBRATION OF INSTRUMENTED TIMBER PILES</b>	<b>3-12</b>
<b>3.3.1 General</b>	<b>3-12</b>
<b>3.3.2 Pilot Test Program</b>	<b>3-12</b>
<b>3.3.3 Initial Calibration in Seattle</b>	<b>3-14</b>
<b>3.3.4 Recalibration of Timber Piles at Test Site</b>	<b>3-15</b>
<b>3.3.5 Summary of Calibration Results</b>	<b>3-16</b>
<b>3.3.6 Detailed Calibration Results for Piles Under Monolith M2</b>	<b>3-17</b>
<b>3.4 CALIBRATION OF INSTRUMENTED PROTOTYPE PILES</b>	<b>3-18</b>
<b>3.4.1 Calibration Procedures</b>	<b>3-18</b>

**TABLE OF CONTENTS**

(Continued)

	<u>Page</u>
3.4.2      Summary of Calibration Results	3-18
3.5          MEASUREMENT PRIORITIES	3-18

**List of Tables**

Table 3.1	<b>LIST OF INSTRUMENTATION</b>
-----------	--------------------------------

**List of Figures**

Figure 3.1	TYPICAL MONOLITH INSTRUMENTATION
Figure 3.2	LOCATION OF GROUND INSTRUMENTATION
Figure 3.3	TYPICAL TIMBER PILE INSTRUMENTATION
Figure 3.4	TYPICAL PROTOTYPE PILE INSTRUMENTATION
Figure 3.5	VERTICAL BENCHMARK
Figure 3.6	TYPICAL HORIZONTAL SURVEY INSTRUMENTATION
Figure 3.7	TYPICAL REFERENCE BEAM CONFIGURATION
Figure 3.8	DIAL GAGE AND LINEAR POTENTIOMETER ARRANGEMENT
Figure 3.9	TYPICAL SURFACE REFERENCE POINT
Figure 3.10	TYPICAL 3-D DEFORMATION GAGE
Figure 3.11	TYPICAL PNEUMATIC PIEZOMETER INSTALLATION
Figure 3.12	TYPICAL GEOPHONE INSTALLATION
Figure 3.13	DETAILS OF INSTRUMENTATION FOR MONOLITH M2
Figure 3.14	TIMBER PILE CALIBRATION SETUP
Figure 3.15	JACK POSITION FOR TIMBER PILE CALIBRATION

**TABLE OF CONTENTS**

(Continued)

Page

**4 TEST AREA SUBSURFACE CONDITIONS**

<b>Title</b>	<b>Page</b>
4.1 SUBSURFACE INVESTIGATIONS	4-i
4.1.1 Purpose and Scope	4-1
4.1.2 Soil Sampling	4-1
4.1.3 Dynamic Penetration Testing	4-2
4.1.4 Static Cone Penetration Testing	4-2
4.1.5 Pressuremeter Testing	4-3
4.1.6 Cross-Hole Shear Wave Velocity Measurements	4-3
4.1.7 Borehole Permeability Testing	4-4
4.1.8 Laboratory Testing	4-4
4.2 STRATIGRAPHY	4-5
4.2.1 General Geology	4-5
4.2.2 Flood Plain Deposits	4-5
4.2.3 Recent Alluvium	4-5
4.2.4 Alluvial Outwash	4-6
4.2.5 Wisconsinan Outwash	4-6
4.2.6 Illinoian Ice Contact Deposits	4-6
4.2.7 Limestone: St Genevieve Formation	4-7
4.2.8 Upper Stratigraphic Units	4-7
4.3 SOIL PROPERTIES	4-8
4.3.1 General	4-8
4.3.2 Grain-Size Distribution	4-8
4.3.3 Stresses	4-8
4.3.4 Relative Density	4-9
4.3.5 Stiffness	4-11
4.3.6 Shear Strength	4-13
4.3.7 Permeability	4-14

**List of Figures**

**Figure 4.1 LOCATION OF SUBSURFACE INVESTIGATIONS BEFORE  
TIMBER PILE INSTALLATION**

**TABLE OF CONTENTS**

(Continued)

- Figure 4.2      RESULTS OF IN SITU TESTS BEFORE TIMBER PILE INSTALLATION
- Figure 4.3      RESULTS OF CONE PENETRATION SOUNDINGS IN PROTOTYPE PILE DRIVING AREA
- Figure 4.4      IDEALIZED PRESSUREMETER TEST RESULTS
- Figure 4.5      SHEAR WAVE VELOCITIES BEFORE TIMBER PILE INSTALLATION
- Figure 4.6      PERMEABILITY TEST RESULTS BEFORE TIMBER PILE INSTALLATION
- Figure 4.7      GENERALIZED SUBSURFACE PROFILE IN VICINITY OF TEST AREA
- Figure 4.8      SUBSURFACE PROFILE A-A
- Figure 4.9      GRAIN-SIZE DISTRIBUTION OF UPPER STRATIGRAPHIC UNITS UNDERLYING TEST AREA
- Figure 4.10     INFERRRED OVERCONSOLIDATION PROFILE IN MONOLITH TRENCH
- Figure 4.11     IN SITU EFFECTIVE STRESS PROFILE BEFORE TIMBER PILE INSTALLATION
- Figure 4.12     RELATIVE DENSITY PROFILE BEFORE TIMBER PILE INSTALLATION
- Figure 4.13     LABORATORY MAXIMUM-MINIMUM DRY UNIT WEIGHTS
- Figure 4.14     ELASTIC DEFORMATION MODULUS DERIVED FROM STATIC CONE PENETRATION TESTS
- Figure 4.15     ELASTIC DEFORMATION MODULUS PROFILE BEFORE TIMBER PILE INSTALLATION
- Figure 4.16     ELASTIC DEFORMATION MODULUS FROM CROSS-HOLE SHEAR WAVE VELOCITY MEASUREMENTS BEFORE TIMBER PILE INSTALLATION
- Figure 4.17     ANGLE OF INTERNAL FRICTION PROFILE BEFORE TIMBER PILE INSTALLATION
- Figure 4.18     PRESSUREMETER LIMIT PRESSURE BEFORE TIMBER PILE INSTALLATION

**TABLE OF CONTENTS**

(Continued)

<u>Title</u>	<u>Page</u>
<b>5 CONSTRUCTION OF TEST FACILITIES</b>	
<b>Title Page</b>	<b>5-i</b>
5.1 GENERAL TEST REQUIREMENTS	5-1
5.1.1 Test Area	5-1
5.1.2 Reaction Structures	5-1
5.1.3 Test Monolith Construction	5-2
5.1.4 Chemical Grouting	5-2
5.2 TEST AREA PREPARATION AND DEWATERING	5-3
5.2.1 Location of Test Area Within Main Test Site	5-3
5.2.2 Excavations	5-3
5.2.3 Levees	5-4
5.2.4 Surfacing	5-4
5.2.5 Dewatering System	5-4
5.3 REACTION STRUCTURES	5-5
5.3.1 Horizontal Reaction Blocks	5-5
5.3.2 Reaction Rock Anchors	5-5
5.3.3 Reaction Frames	5-6
5.3.4 Jacking System	5-6
5.4 TEST MONOLITH CONSTRUCTION	5-7
5.4.1 Timber Pile Installation	5-7
5.4.2 Concrete Work	5-9
5.4.3 Effects of Timber Pile Installation on Soil Properties	5-10
5.5 CHEMICAL GROUTING	5-13
5.5.1 Sequence of Activities	5-13
5.5.2 Grouting Method and Equipment	5-13
5.5.3 Pattern and Sequence of Grouting	5-14
5.5.4 Grout	5-15
5.5.5 Evaluation of Grouting	5-16

Table 5.1

List of Tables  
**SUMMARY OF TIMBER PILE INSTALLATION INFORMATION  
FOR LOAD TESTED MONOLITHS**

**TABLE OF CONTENTS**

(Continued)

**List of Figures**

- Figure 5.1 DEWATERING SYSTEM
- Figure 5.2 AS BUILT TIMBER PILE LOCATIONS
- Figure 5.3 BORING LOCATION PLAN AFTER TIMBER PILE INSTALLATION
- Figure 5.4 STANDARD PENETRATION RESISTANCE PROFILES AFTER TIMBER PILE INSTALLATION
- Figure 5.5 STATIC CONE PENETRATION RESISTANCE PROFILES AFTER TIMBER PILE INSTALLATION
- Figure 5.6 IN SITU HORIZONTAL STRESS PROFILE AFTER TIMBER PILE INSTALLATION
- Figure 5.7 ELASTIC DEFORMATION MODULUS PROFILE AFTER TIMBER PILE INSTALLATION
- Figure 5.8 DRAINED ANGLE OF INTERNAL FRICTION PROFILE AFTER TIMBER PILE INSTALLATION
- Figure 5.9 PRESSUREMETER LIMIT PRESSURE PROFILE AFTER TIMBER PILE INSTALLATION
- Figure 5.10 CROSS-HOLE SHEAR WAVE VELOCITIES AFTER TIMBER PILE INSTALLATION
- Figure 5.11 PERMEABILITY TEST RESULTS AFTER TIMBER PILE INSTALLATION
- Figure 5.12 SCHEMATIC OF GROUTING PLANT
- Figure 5.13 LAYOUT OF GROUT HOLES
- Figure 5.14 BORING LOCATION PLAN AFTER GROUTING
- Figure 5.15 STANDARD PENETRATION RESISTANCE PROFILES AFTER GROUTING
- Figure 5.16 STATIC CONE PENETRATION RESISTANCE PROFILES AFTER GROUTING
- Figure 5.17 IN SITU HORIZONTAL EFFECTIVE STRESS PROFILES AFTER GROUTING
- Figure 5.18 ELASTIC DEFORMATION MODULUS PROFILES AFTER GROUTING
- Figure 5.19 PRESSUREMETER LIMIT PRESSURE PROFILES AFTER GROUTING

**TABLE OF CONTENTS**

(Continued)

<u>Title</u>	<u>Page</u>
<b>6 MONOLITH PRELOADING</b>	
<b>Title Page</b>	<b>6-i</b>
6.1 SCOPE OF TESTS	6-1
6.2 TEST PROCEDURES	6-1
6.2.1 General	6-1
6.2.2 Test Setup and Instrumentation	6-2
6.2.3 Sequence of Operations	6-2
6.3 TEST RESULTS	6-3
6.3.1 General	6-3
6.3.2 Monolith M1	6-3
6.3.3 Monolith M2	6-4
6.3.4 Monolith M3	6-5
6.3.5 Monolith M5	6-5
6.3.6 Monolith M6	6-5
6.3.7 Monolith M7	6-5
6.4 EVALUATION OF TEST RESULTS	6-5
6.4.1 Evaluation of Predictions	6-5
6.4.2 Monolith M1	6-6
6.4.3 Monoliths M2, M3, and M5	6-6
6.4.4 Monoliths M6 and M7	6-7

**List of Tables**

- Table 6.1      **SUMMARY OF MONOLITH DISPLACEMENT DURING PRELOADING**

**List of Figures**

- Figure 6.1      **HORIZONTAL DISPLACEMENT OF MONOLITH M1 DURING CYCLIC PRELOADING**
- Figure 6.2      **HORIZONTAL DISPLACEMENT OF MONOLITH M2 DURING CYCLIC PRELOADING**

**TABLE OF CONTENTS**

(Continued)

- Figure 6.3** HORIZONTAL DISPLACEMENT OF MONOLITH M3  
DURING CYCLIC PRELOADING
- Figure 6.4** HORIZONTAL DISPLACEMENT OF MONOLITH M5  
DURING CYCLIC PRELOADING
- Figure 6.5** HORIZONTAL DISPLACEMENT OF MONOLITH M6  
DURING CYCLIC PRELOADING
- Figure 6.6** HORIZONTAL DISPLACEMENT OF MONOLITH M7  
DURING CYCLIC PRELOADING

**TABLE OF CONTENTS**

(Continued)

<u>Title</u>	<u>Page</u>
	7-i
7.1 SCOPE OF TESTS	7-1
7.2 TEST PROCEDURES	7-1
7.2.1 General	7-1
7.2.2 Test Setup and Instrumentation	7-2
7.2.3 Sequence of Operations	7-3
7.3 TEST RESULTS	7-5
7.3.1 General	7-5
7.3.2 Prototype Pile Driving	7-5
7.3.3 Ground Vibration	7-7
7.3.4 Monolith Displacements	7-10
7.4 INFLUENCE OF TEST VARIABLES	7-14
7.4.1 General	7-14
7.4.2 Influence of Grouting	7-14
7.4.3 Influence of Load Level	7-15
7.4.4 Influence of Timber Pile Configuration	7-15
7.4.5 Influence of Pile Driving System	7-17

**List of Tables**

Table 7.1	CHARACTERISTICS OF PROTOTYPE PILES AND HAMMERS
Table 7.2	SUMMARY OF AVAILABLE DYNAMIC PILE DRIVING DATA
Table 7.3	DISPLACEMENTS OF MONOLITH M1 DUE TO PROTOTYPE PILE DRIVING
Table 7.4	DISPLACEMENTS OF MONOLITH M2 DUE TO PROTOTYPE PILE DRIVING
Table 7.5	DISPLACEMENTS OF MONOLITH M3 DUE TO PROTOTYPE PILE DRIVING
Table 7.6	DISPLACEMENTS OF MONOLITH M5 DUE TO PROTOTYPE PILE DRIVING

TABLE OF CONTENTS

(Continued)

Table 7.7	DISPLACEMENTS OF MONOLITH M6 DUE TO PROTOTYPE PILE DRIVING
Table 7.8	DISPLACEMENTS OF MONOLITH M7 DUE TO PROTOTYPE PILE DRIVING
Table 7.9	INFLUENCE OF PILE DRIVING SYSTEM ON MONOLITH DISPLACEMENTS

List of Figures

Figure 7.1	PLAN AND SECTION FOR MONOLITH M1
Figure 7.2	PLAN AND SECTION FOR MONOLITHS M2 AND M6
Figure 7.3	PLAN AND SECTION FOR MONOLITHS M3 AND M7
Figure 7.4	PLAN AND SECTION FOR MONOLITH M5
Figure 7.5	BLOWCOUNT DATA, PROTOTYPE PILE DRIVING, MONOLITH M1
Figure 7.6	BLOWCOUNT DATA, PROTOTYPE PILE DRIVING, MONOLITHS M2 AND M6
Figure 7.7	BLOWCOUNT DATA, PROTOTYPE PILE DRIVING, MONOLITHS M3 AND M7
Figure 7.8	BLOWCOUNT DATA, PROTOTYPE PILE DRIVING, MONOLITH M5
Figure 7.9	DYNAMIC MEASUREMENTS DURING PROTOTYPE PILE DRIVING, PRIMARY PILE DRIVING SYSTEM, MONOLITH M1
Figure 7.10	DYNAMIC MEASUREMENTS DURING PROTOTYPE PILE DRIVING, PRIMARY PILE DRIVING SYSTEM, MONOLITHS M2 AND M6
Figure 7.11	DYNAMIC MEASUREMENTS DURING PROTOTYPE PILE DRIVING, PRIMARY PILE DRIVING SYSTEM, MONOLITHS M3 AND M7
Figure 7.12	DYNAMIC MEASUREMENTS DURING PROTOTYPE PILE DRIVING, PRIMARY PILE DRIVING SYSTEM, MONOLITH M5

**TABLE OF CONTENTS**

(Continued)

- Figure 7.13** DYNAMIC MEASUREMENTS DURING PROTOTYPE PILE DRIVING,  
SECONDARY PILE DRIVING SYSTEM, MONOLITH M1
- Figure 7.14** DYNAMIC MEASUREMENTS DURING PROTOTYPE PILE DRIVING,  
SECONDARY PILE DRIVING SYSTEM, MONOLITHS M2 AND M6
- Figure 7.15** DRIVING PERFORMANCE OF PROTOTYPE PILES  
USING VIBRATORY HAMMER
- Figure 7.16** PRIMARY PILE DRIVING SYSTEM, NEAR-SURFACE  
PARTICLE VELOCITY AT MONOLITH M1
- Figure 7.17** PRIMARY PILE DRIVING SYSTEM, NEAR-SURFACE  
PARTICLE VELOCITY AT MONOLITH M2
- Figure 7.18** PRIMARY PILE DRIVING SYSTEM, NEAR-SURFACE  
PARTICLE VELOCITY AT MONOLITH M3
- Figure 7.19** PRIMARY PILE DRIVING SYSTEM, NEAR-SURFACE  
PARTICLE VELOCITY AT MONOLITH M5
- Figure 7.20** CUMULATIVE EFFECTS OF VIBRATION FOR  
MONOLITHS M1, M2, M3, AND M5
- Figure 7.21** SECONDARY PILE DRIVING SYSTEM,  
NEAR-SURFACE PARTICLE VELOCITY  
AT MONOLITH M1, AIR HAMMER
- Figure 7.22** SECONDARY PILE DRIVING SYSTEM,  
NEAR-SURFACE PARTICLE VELOCITY  
AT MONOLITH M2, VIBRATORY HAMMER
- Figure 7.23** SECONDARY PILE DRIVING SYSTEM,  
NEAR SURFACE PARTICLE VELOCITY  
AT MONOLITH M2, DIESEL HAMMER
- Figure 7.24** SECONDARY PILE DRIVING SYSTEM,  
NEAR-SURFACE PARTICLE VELOCITY  
AT MONOLITH M3, AIR HAMMER
- Figure 7.25** CUMULATIVE DISPLACEMENTS OF MONOLITH M1
- Figure 7.26** CUMULATIVE DISPLACEMENTS OF MONOLITH M2
- Figure 7.27** CUMULATIVE DISPLACEMENTS OF MONOLITH M3
- Figure 7.28** CUMULATIVE DISPLACEMENTS OF MONOLITH M5
- Figure 7.29** CUMULATIVE DISPLACEMENTS OF MONOLITH M6

**TABLE OF CONTENTS**

(Continued)

- Figure 7.30 CUMULATIVE DISPLACEMENTS OF MONOLITH M7  
Figure 7.31 INCREMENTAL DISPLACEMENTS OF MONOLITH M1  
Figure 7.32 INCREMENTAL DISPLACEMENTS OF MONOLITH M2  
Figure 7.33 INCREMENTAL DISPLACEMENTS OF MONOLITH M3  
Figure 7.34 INCREMENTAL DISPLACEMENTS OF MONOLITH M5  
Figure 7.35 INCREMENTAL DISPLACEMENTS OF MONOLITH M6  
Figure 7.36 INCREMENTAL DISPLACEMENTS OF MONOLITH M7  
Figure 7.37 INCREMENTAL DISPLACEMENTS OF MONOLITHS M1, M2, M3, M5  
Figure 7.38 DISPLACEMENTS OF MONOLITH M1 DURING SUCCESSIVE PILE DRIVING AT 20 FT  
Figure 7.39 DISPLACEMENTS OF MONOLITH M1 DURING SUCCESSIVE PILE DRIVING AT 30 FT  
Figure 7.40 DISPLACEMENTS OF MONOLITH M2 DURING SUCCESSIVE PILE DRIVING AT 20 FT  
Figure 7.41 DISPLACEMENTS OF MONOLITH M3 DURING SUCCESSIVE PILE DRIVING AT 20 FT  
Figure 7.42 DISPLACEMENTS OF MONOLITH M5 DURING SUCCESSIVE PILE DRIVING AT 20 FT  
Figure 7.43 DISPLACEMENTS OF MONOLITH M5 DURING SUCCESSIVE PILE DRIVING AT 15 FT  
Figure 7.44 DISPLACEMENTS OF MONOLITH M6 DURING SUCCESSIVE PILE DRIVING AT 20 FT  
Figure 7.45 DISPLACEMENTS OF MONOLITH M7 DURING SUCCESSIVE PILE DRIVING AT 20 FT  
Figure 7.46 INFLUENCE OF GROUTING ON NEAR-SURFACE PARTICLE VELOCITY FOR MONOLITHS M2 AND M3  
Figure 7.47 INFLUENCE OF GROUTING ON DISPLACEMENTS OF MONOLITHS M2 AND M3  
Figure 7.48 INFLUENCE OF LOAD LEVEL ON NEAR-SURFACE PARTICLE VELOCITY FOR MONOLITHS M2 AND M5

**TABLE OF CONTENTS**

(Continued)

- Figure 7.49** INFLUENCE OF LOAD LEVEL ON DISPLACEMENTS OF MONOLITHS M2 AND M5
- Figure 7.50** INFLUENCE OF TIMBER PILE CONFIGURATION ON NEAR-SURFACE PARTICLE VELOCITY FOR MONOLITHS M2 AND M1
- Figure 7.51** INFLUENCE OF TIMBER PILE CONFIGURATION ON DISPLACEMENTS OF MONOLITHS M2 AND M1
- Figure 7.52** INFLUENCE OF TIMBER PILE CONFIGURATION ON DISPLACEMENTS OF MONOLITHS M2 AND M6

**TABLE OF CONTENTS**

(Continued)

	<u>Page</u>
<b>8 MONOLITH LOAD TESTING</b>	
<b>Title Page</b>	<b>8-i</b>
8.1 <b>SCOPE OF TESTS</b>	8-1
8.2 <b>TEST PROCEDURES</b>	8-1
8.2.1    Instrumentation and Test Setup	8-1
8.2.2    Axial Load Tests	8-2
8.2.3    Lateral Load Tests	8-2
8.3 <b>TEST RESULTS</b>	8-3
8.3.1    Monolith M1 (Lateral Load Test)	8-3
8.3.2    Monolith M2 (Lateral Load Test)	8-4
8.3.3    Monolith M6 (Axial Load Test)	8-4
8.3.4    Monolith M6 (Lateral Load Test)	8-5
8.3.5    Monolith M3 (Lateral Load Test)	8-5
8.3.6    Monolith M7 (Lateral Load Test)	8-5
8.3.7    Monolith M5 (Axial Load Test)	8-5
8.4 <b>EVALUATION OF TEST RESULTS</b>	8-6
8.4.1    Evaluation of Predictions	8-6
8.4.2    Effects of Grouting	8-6
8.4.3    Effects of Pile Groups	8-6

**List of Tables**

Table 8.1      **SUMMARY OF MONOLITH LATERAL LOAD TEST RESULTS**

**List of Figures**

- |            |  |
|------------|--|
| Figure 8.1 | DISPLACEMENTS OF MONOLITH M1 DURING<br>LATERAL LOAD TEST |
| Figure 8.1 | DISPLACEMENTS OF MONOLITH M2 DURING<br>LATERAL LOAD TEST |
| Figure 8.3 | DISPLACEMENTS OF MONOLITH M6 DURING<br>AXIAL LOAD TEST   |

**TABLE OF CONTENTS**

(Continued)

- Figure 8.4** DISPLACEMENTS OF MONOLITH M6 DURING LATERAL LOAD TEST
- Figure 8.5** DISPLACEMENTS OF MONOLITH M3 DURING LATERAL LOAD TEST
- Figure 8.6** DISPLACEMENTS OF MONOLITH M7 DURING LATERAL LOAD TEST
- Figure 8.7** DISPLACEMENTS OF MONOLITH M5 DURING AXIAL LOAD TEST

**TABLE OF CONTENTS**

(Continued)

	<u>Page</u>
<b>9 DETAILED EVALUATION OF BEHAVIOR OF MONOLITH M2</b>	
<b>Title Page</b>	<b>9-i</b>
9.1 <b>SCOPE OF DETAILED EVALUATION</b>	9-1
9.2 <b>MONOLITH DISPLACEMENTS CAUSED BY PROTOTYPE PILE DRIVING</b>	9-1
9.2.1    General	9-1
9.2.2    Cumulative Peak Velocity vs Monolith Displacements	9-1
9.3 <b>DYNAMIC RESPONSE CHARACTERISTICS</b>	9-3
9.3.1    General	9-3
9.3.2    Component Peak Velocities	9-4
9.3.3    Velocity and Acceleration Time Histories	9-4
9.3.4    Response Spectra	9-5
9.3.5    Conclusions	9-6
9.4 <b>DEFORMATION OF THE TIMBER PILE-SOIL SYSTEM</b>	9-6
9.4.1    General	9-6
9.4.2    Deformation During Prototype Pile Driving	9-6
9.4.3    Deformation During Lateral Load Testing	9-8
9.5 <b>MONOLITH-PILE-SOIL LOAD TRANSFERS</b>	9-9
9.5.1    General	9-9
9.5.2    Load Transfer During Prototype Pile Driving	9-10
9.5.3    Load Transfer During Lateral Load Testing	9-11
9.6 <b>COMPARISON BETWEEN PREDICTED AND OBSERVED MONOLITH RESPONSE</b>	9-12
9.6.1    General	9-12
9.6.2    Predicted Performance	9-13
9.6.3    Comparisons	9-15
9.7 <b>APPARENT DEFORMATION MECHANISMS</b>	9-16
9.7.1    General	9-16
9.7.2    Pattern of Deformations During Static Load Testing	9-16
9.7.3    Pattern of Deformations During Prototype Pile Driving	9-16

**TABLE OF CONTENTS**

(Continued)

**List of Figures**

- Figure 9.1** INCREMENTAL DISPLACEMENTS OF MONOLITH M2 CAUSED BY DRIVING OF PROTOTYPE PILES 1 THROUGH 6
- Figure 9.2** CUMULATIVE PEAK VELOCITY FOR PROTOTYPE PILES 3 AND 4 AT MONOLITH M2
- Figure 9.3** INCREMENTAL DISPLACEMENTS VS CUMULATIVE PEAK VELOCITY FOR PROTOTYPE PILES 1 THROUGH 6 AT MONOLITH M2
- Figure 9.4** GROUND VIBRATION CHARACTERISTICS FOR PROTOTYPE PILE 1 AT MONOLITH M2
- Figure 9.5** GROUND VIBRATION CHARACTERISTICS FOR PROTOTYPE PILE 2 AT MONOLITH M2
- Figure 9.6** GROUND VIBRATION CHARACTERISTICS FOR PROTOTYPE PILE 6 AT MONOLITH M2
- Figure 9.7** PARTICLE VELOCITY RECORDED 50 FT BELOW GROUND SURFACE AT MONOLITH M2
- Figure 9.8** EXAMPLES OF GROUND VELOCITY TIME HISTORIES AT MONOLITH M2
- Figure 9.9** EXAMPLES OF GROUND AND MONOLITH MOTIONS TIME HISTORIES AT MONOLITH M2
- Figure 9.10** EXAMPLES OF RESPONSE SPECTRA FOR GROUND AND MONOLITH MOTIONS AT MONOLITH M2
- Figure 9.11** DEFLECTION OF TIMBER PILE INCLINOMETERS DURING PROTOTYPE PILE DRIVING FOR MONOLITH M2
- Figure 9.12** DEFLECTION OF GROUND INCLINOMETERS DURING PROTOTYPE PILE DRIVING FOR MONOLITH M2
- Figure 9.13** AVERAGE DEFLECTION OF INCLINOMETERS DURING PROTOTYPE PILE DRIVING FOR MONOLITH M2

**TABLE OF CONTENTS**

(Continued)

- Figure 9.14 SETTLEMENTS OF GROUND SURFACE AND MONOLITH DURING PROTOTYPE PILE DRIVING FOR MONOLITH M2
- Figure 9.15 DEFLECTION OF TIMBER PILE INCLINOMETERS DURING LATERAL LOAD TESTING OF MONOLITH M2
- Figure 9.16 DEFLECTION OF GROUND INCLINOMETERS DURING LATERAL LOAD TESTING OF MONOLITH M2
- Figure 9.17 CHANGES IN MOMENT AND SHEAR IN TIMBER PILES NEAR GROUND SURFACE DURING PROTOTYPE PILE DRIVING, MONOLITH M2
- Figure 9.18 CHANGES IN AXIAL LOAD AT BUTT AND STRAIN AT TIP OF TIMBER PILES DURING PROTOTYPE PILE DRIVING, MONOLITH M2
- Figure 9.19 SHEAR FORCE DISTRIBUTION ON TIMBER PILES DURING PROTOTYPE PILE DRIVING, MONOLITH M2
- Figure 9.20 BENDING MOMENT DISTRIBUTION ON TIMBER PILES DURING PROTOTYPE PILE DRIVING, MONOLITH M2
- Figure 9.21 AXIAL LOAD DISTRIBUTION ON TIMBER PILES DURING PROTOTYPE PILE DRIVING, MONOLITH M2
- Figure 9.22 SHEAR FORCE DISTRIBUTION ON TIMBER PILES DURING LOAD TESTING OF MONOLITH M2
- Figure 9.23 BENDING MOMENT DISTRIBUTION ON TIMBER PILES DURING LOAD TESTING OF MONOLITH M2
- Figure 9.24 AXIAL LOAD DISTRIBUTION ON TIMBER PILES DURING LOAD TESTING OF MONOLITH M2
- Figure 9.25 COMPARISON BETWEEN PREDICTED AND MEASURED PEAK PARTICLE VELOCITIES, MONOLITH M2
- Figure 9.26 PATTERN OF DEFORMATIONS DURING STATIC LOAD TESTING
- Figure 9.27 PATTERNS OF DEFORMATION DURING PROTOTYPE PILE DRIVING

**TABLE OF CONTENTS**

(Continued)

<u>Title</u>	<u>Page</u>
<b>10 LATERAL LOAD TESTING OF PROTOTYPE PILES</b>	
Title Page	10-i
10.1 SCOPE OF TESTS	10-1
10.2 PILE INSTALLATION AND TEST CONFIGURATION	10-1
10.2.1 Pile Driving	10-1
10.2.2 Grout Placement in Pipe Piles	10-2
10.2.3 Test Setup	10-3
10.3 TEST PROCEDURES	10-3
10.3.1 Initial Measurements	10-3
10.3.2 Short-Term Static Load Tests	10-3
10.3.3 Cyclic Load Tests	10-4
10.4 DATA ACQUISITION AND REDUCTION	10-4
10.4.1 General	10-4
10.4.2 Pile-Head Displacement	10-4
10.4.3 Bending Moment	10-4
10.4.4 Pile Deflection With Depth	10-5
10.5 TEST RESULTS	10-5
10.5.1 General	10-5
10.5.2 Piles Driven Into Ungrounded Soil	10-6
10.5.3 Piles In Postgrouted Soil	10-6
10.5.4 Piles Driven Into Pregrounded Soil	10-7
10.5.5 Cyclic Load Tests	10-7
10.6 EVALUATION OF TEST RESULTS	10-8
10.6.1 Piles Driven Into Ungrounded Soil	10-8
10.6.2 Piles In Postgrouted Soil	10-8
10.6.3 Piles Driven Into Pregrounded Soil	10-9

**List of Tables**

Table 10.1      **SUMMARY OF LATERAL LOAD TEST RESULTS  
ON PROTOTYPE PILES**

**TABLE OF CONTENTS**

(Continued)

**List of Figures**

- Figure 10.1 LOCATION PLAN FOR PROTOTYPE PILES T1 THROUGH T6
- Figure 10.2 LATERAL LOAD TEST SETUP
- Figure 10.3 STRAIN-BENDING MOMENT RELATIONSHIPS FOR PROTOTYPE PILES T2 AND T4
- Figure 10.4 SHORT-TERM LOAD BEHAVIOR PROTOTYPE PILES T3 AND T4, UNGROUTED SOIL
- Figure 10.5 BENDING MOMENT DISTRIBUTION, PROTOTYPE PILE T3, UNGROUTED SOIL
- Figure 10.6 BENDING MOMENT DISTRIBUTION, PROTOTYPE PILE T4, UNGROUTED SOIL
- Figure 10.7 SHORT-TERM LOAD BEHAVIOR PROTOTYPE PILES T1 AND T2, POSTGROUTED SOIL
- Figure 10.8 BENDING MOMENT DISTRIBUTION, PROTOTYPE PILE T1, POSTGROUTED SOIL
- Figure 10.9 BENDING MOMENT DISTRIBUTION, PROTOTYPE PILE T2, POSTGROUTED SOIL
- Figure 10.10 SHORT-TERM LOAD BEHAVIOR PROTOTYPE PILES T5 AND T6, PREGROUTED SOIL
- Figure 10.11 BENDING MOMENT DISTRIBUTION, PROTOTYPE PILE T5, PREGROUTED SOIL
- Figure 10.12 BENDING MOMENT DISTRIBUTION, PROTOTYPE PILE T6, PREGROUTED SOIL
- Figure 10.13 STATIC CONE PENETRATION RESISTANCE PROFILES POSTGROUTED VS PREGROUTED
- Figure 10.14 PROTOTYPE PILE DISPLACEMENTS AT GROUND SURFACE DURING CYCLIC LATERAL LOAD TESTS, PROTOTYPE PILES T1 THROUGH T4
- Figure 10.15 HORIZONTAL DISPLACEMENT OF PROTOTYPE PILES T1 THROUGH T6 UNDER SUSTAINED LATERAL LOAD
- Figure 10.16 TIME-DEPENDENT BEHAVIOR OF LATERALLY LOADED PROTOTYPE PILES T1 THROUGH T6

**TABLE OF CONTENTS**

(Continued)

	<u>Page</u>
<b>11 PILE INSPECTION AFTER EXTRACTION</b>	
Title Page	11-i
11.1      TIMBER PILES	11-1
11.2      PROTOTYPE PILES	11-1

**List of Figures**

Figure 11.1	PHOTOGRAPHS OF EXTRACTED TIMBER PILES MONOLITH M2
Figure 11.2	PHOTOGRAPHS OF EXTRACTED H AND SHEET PILES MONOLITHS M1 AND M2

**REFERENCES**

Title Page	R-i
REFERENCES	R-1

**PHASE IV REPORT**

**VOLUME III**

**RESULTS AND INTERPRETATION OF  
PILE DRIVING EFFECTS TEST PROGRAM**

**SECTION 0  
SUMMARY AND CONCLUSIONS**

## 0 SUMMARY AND CONCLUSIONS

### 0.1 PILE DRIVING EFFECTS TEST PROGRAM

The effects of nearby pile driving on axially and laterally loaded test structures supported on timber friction piles in sand were investigated near Locks and Dam No. 26 on the Mississippi River. The tests were designed to assess the magnitude of permanent displacements of test structures caused by nearby pile driving; assess the efficiency of chemical grout injection into the soil in reducing these displacements; and investigate the mechanisms governing pile driving effects. Adjunctly, the tests involved axial and lateral load tests on single timber piles and timber pile groups in ungrouted and grouted soil. The effects of chemical grouting on steel pile driving resistance and lateral load capacity of single steel piles were also assessed.

The tests were designed from November 1977 to May 1978. The test instrumentation was developed and installed from April to October 1978. The field tests were conducted from August 1978 to March 1979. Six test structures (monoliths) were constructed and tested. The test monoliths were founded on 46 instrumented timber piles having various configurations. Forty-two prototype steel piles were driven near the loaded test monoliths. Six prototype piles were laterally load tested. A total of 65,500 gal of low-strength silicate grout was injected into the soil surrounding two of the test structures. To a variable degree, these conditions also model other similar navigation structures on the Mississippi River. The tests involved a complex instrumentation system for manual and electronic data acquisition.

### 0.2 TEST AREA SUBSURFACE CONDITIONS

The test area was located on Ellis Island, about one mile downstream of Locks and Dam No. 26 on the Missouri side of the Mississippi River. The subsurface profile at the location of the test area consisted of approximately 100 ft of sand and gravel of alluvial and glacial origin, overlying the limestone bedrock. The subsurface conditions were investigated at the design stage, and reassessed at various times during the tests to detect changes caused by timber pile jetting and driving, prototype pile driving, and chemical grouting. The subsurface investigations relied primarily on the use of in situ testing methods (dynamic and static penetration, pressuremeter and permeability tests, and cross hole shear wave velocity measurements).

### 0.3 DESIGN AND CONSTRUCTION OF TEST FACILITIES

#### 0.3.1 Test Program Design

**Test Monoliths.** The pile driving effects test program was designed such that the test conditions generally modeled the conditions at nearby Locks and Dam

No. 26. The test structures represented the structural conditions of the dam to an acceptable degree of similitude; considerations were given to scale, timber pile configuration, construction details, and load levels and history on the existing structures. To a variable degree, these conditions also model other similar navigation structures on the Mississippi River. The test variables were selected consistent with the objectives of the program stated in Section 0.1.

Six monoliths were constructed; four were founded on 8- to 12-timber pile groups; two on single timber piles. The number, configuration, and other variables of the test monoliths permitted various comparisons and evaluations to be made:

- (1) effects of grouting on monolith performance;
- (2) effects of applied load level on monolith performance;
- (3) single timber pile vs timber pile groups;
- (4) effects of other adjacent timber piles on monolith performance; and
- (5) behavior of interior vs exterior timber piles.

The performance of the monoliths was predicted using empirical data. Only those aspects of performance which were necessary to meet the objectives of the program were considered. An instrumentation system was designed to be consistent with the ranking of the significant aspects of performance and predicted performance.

**Prototype Piles.** The prototype piles driven near the loaded monoliths were primarily H piles, a type of pile likely to be used in potential future construction on navigation structures. A few pipe and sheet piles were also driven for comparison purposes. The primary pile driving hammer used for the tests was a single-acting air hammer imparting a relatively constant impact energy to the piles. Other hammers (diesel and vibratory) were also used.

**Chemical Grouting.** The effects of grouting on monolith and pile performance were evaluated. A low-strength silicate grout, tested earlier in the chemical grouting test program (Volume II) was selected. The selection was based on the previous test program results. In situ test results and visual observations indicated that piles could be driven through soil injected with this grout; soil injected with all the other grouts tested in this program was considered to be too hard for pile driving by conventional methods.

### 0.3.2 Construction of Test Facilities

**Earthwork and Dewatering.** Construction of the test facilities involved extensive site preparation and construction of a dewatering and levee system to protect the site from Mississippi River floods. The dewatering system was used to maintain the groundwater level very close to the ground surface around the test monoliths. By maintaining the soil surrounding the monoliths submerged, the tests did not need to be conducted overwater.

**Reaction Structures.** The conduct of the tests required design and construction of appropriate reaction structures and systems capable of delivering large axial and lateral loads to the test monoliths. The size and capacity of these reaction structures were important factors in the selection of the scale and configuration of the test monoliths.

**Test Monolith Construction.** The timber piles under the test monoliths were installed by jetting and driving to a prescribed tip elevation; the installation method was similar to that used during construction of Locks and Dam No. 26. The timber piles were instrumented with inclinometer casings, and multiple levels of strain gages and telltales. Performance of the piles during driving was monitored with a pile driving analyzer. After timber pile installation, the soil properties were reassessed by in situ tests; the soil above the timber pile tips was generally made denser and stiffer by the timber pile installation.

**Chemical Grouting.** Chemical grout was injected in the upper 20 ft of soil surrounding two of the test monoliths. Grouting was done through sleeve pipes at 4-ft spacing. The grouting plant used was of the proportional type; the grout components were pumped separately and merged just before entering the grout pipes. Significant grout leakage and small grout takes were experienced under one monolith (M3); the grout appeared to leak from around the timber piles. Grouting was probably not very thorough under the monolith. Elsewhere, grouting was accomplished satisfactorily. After grouting, the soil properties were reassessed by in situ tests; the grouted soil properties were similar to those measured during the earlier chemical grouting test program for the type of grout used (Volume II); that is, an increase of about 20 percent in resistance to dynamic and static penetration, and to expansion of the pressuremeter was noted; somewhat greater increase in shear wave velocity was also observed.

## 0.4 TESTING ACTIVITIES

### 0.4.1 Monolith Preloading

Each monolith was first laterally loaded and unloaded for a number of cycles. This preconditioning was done to approximate the effects of load history on actual navigation structures.

### 0.4.2 Pile Driving Effects Testing

Prototype piles were driven at decreasing distances from a given monolith. Only the monolith being tested was axially and laterally loaded; the other monoliths were unloaded. The monolith displacement and surrounding soil deformation were monitored during prototype pile driving. Performance of the prototype piles during driving was monitored using a pile driving analyzer system. The dynamic responses of the soil mass and test monoliths were also measured. The prototype piles were generally driven 50 ft to 5 ft from the monoliths; for one monolith, at the beginning of the program, prototype piles were driven as far as 200 ft from the monolith.

#### 0.4.3 Monolith Load Testing

Upon completion of the pile driving effects stage of testing, each monolith was load tested to failure, either axially or laterally.

#### 0.4.4 Lateral Load Testing of Prototype Piles

Three instrumented H piles and three instrumented pipe piles were load tested to failure under lateral load. Four piles were driven into ungrouted soil. The soil surrounding two of these four piles was grouted (postgrouted); the soil around the other two piles was left ungrouted. The last two piles were driven through the previously grouted soil (pregouted).

### 0.5 SUMMARY OF TEST RESULTS

#### 0.5.1 Monolith Preloading

The predicted displacements of the monoliths were compared to the displacements measured during initial lateral loading. The comparisons show that the prediction overestimated the horizontal displacement of the monoliths, generally by a factor of approximately two. A large part of the overprediction is attributed to the presence of a berm in front of the monoliths; the effects of the berm were not considered in the predictions.

#### 0.5.2 Prototype Pile Driving Effects

**Performance of Prototype Piles During Driving.** The maximum energy and compression force transmitted from the hammer to the pile butt were predicted at 23 ft-k and 500 k, respectively. Measurements during driving indicated that these values were overestimated; maximum energy was generally between 10 and 17 ft-k, and maximum force was generally between 300 and 400 k. The differences are attributed to hammer assembly inefficiency. The pile driving resistance through grouted soil was approximately twice that in ungrouted soil.

**Vibrations Induced by Prototype Pile Driving.** The observed displacements of the monoliths during prototype pile driving correlated well with the measured ground vibration characteristics. The cumulative effects of ground vibrations were characterized by the summation with depth of the calculated product of peak vectorial particle velocity observed for each foot of prototype pile penetration times the blowcount for that foot (referred to as cumulative peak velocity). Horizontal displacement of the monoliths correlated well with cumulative peak velocity values derived near ground surface; settlement correlated well with cumulative peak velocity values derived at a depth of .50 ft below ground surface.

Detailed examination of the data for monolith M2 indicates that, after each hammer blow, the monolith continued to oscillate horizontally at a frequency close to its natural frequency; however, the amplitude of the horizontal vibratory motion of the monolith was much smaller than that of the ground at shallow depth.

The vertical motions of the ground at shallow depth and of the monolith were similar.

**Monolith Displacements.** The following table summarizes the displacements of the various monoliths during prototype pile driving. The total number, location, and type of piles, and the type of hammer used were different for each monolith; therefore, direct comparison of the values in the table cannot be readily made. The evaluation for each case is discussed in pertinent sections of the report.

Monolith No.	Timber Pile Configuration	Load* Level	Grouted	Total No. of Prototype Piles Driven	Measured Displacement in.	
					Average Horizontal	Average Vertical
M1	3 x 4	High	No	13	1.5	1.3
M2	2 x 4	High	No	14	1.9	1.1
M3	2 x 4	High	Yes	8	1.1	0.6
M5	2 x 4	Low	No	7	0.7	0.4
M6	Single	High	No	14	2.0	1.5
M7	Single	High	Yes	8	2.3	1.0

\* High-load level was 30 t/pile axially and 6 t/pile laterally; low-load level was 15 t/pile axially and 4 t/pile laterally

The following conclusions were drawn from the test results:

- (1) significant cumulative displacements of the monolith (that is, displacements larger than the accuracy of the measurements) were measured when prototype piles were driven at a distance of 50 ft or less from the loaded monoliths;
- (2) the cumulative displacements of a given monolith increased with the number of prototype piles driven;
- (3) when as many as four prototype piles were successively driven at the same distance from a given monolith, incremental displacement due to each pile generally did not show a stabilizing or decreasing trend;
- (4) grouting did not significantly reduce the displacement of the monoliths;
- (5) the horizontal displacement of the monoliths at low-load level was about 50 percent less than the displacement at high-load level; the settlement at low-load level was about 30 percent less than at high-load level;
- (6) the single timber piles and the pile groups were equally affected by prototype pile driving; and

- (7) the vibratory hammer induced much larger displacements of Monoliths J2 and M6 than the impact hammers (air or diesel); the impact hammers produced similar results.

#### 0.5.3 Monolith Load Testing

Static lateral load at failure in ungrouted soil ranged from 14.3 to 15 t/pile for the single timber pile and the two pile groups tested. It was 14.8 t/pile for the timber pile group and 20 t for the single pile in postgrouted soil. The timber pile group in grouted soil exhibited a stiffer response at low load levels than the groups in ungrouted soil. The reverse was found for the single timber piles; however, the load at failure for the single pile was 33 percent larger in grouted soil than in ungrouted soil. The response of the timber piles in grouted soil was affected by the creep characteristics of the grouted soil, and incomplete grouting near the ground surface under the pile groups (monolith M3, Section 0.3.2). The static axial load at failure for the single timber pile in ungrouted soil was 110 t; that for the pile group averaged 90 t/pile.

#### 0.5.4 Lateral Load Testing of Prototype Piles

The results of the lateral load tests on the six prototype piles are given below.

	H Piles		Pipe Piles	
	Load at 0.25 in. Horizontal Displacement t	Load at 0.5 in. Horizontal Displacement t	Load at 0.25 in. Horizontal Displacement t	Load at 0.5 in. Horizontal Displacement t
	Ungrounded Soil	8.5	15	5.5
Postgrouted Soil	12	16.5	4.5	8.5
Pregrounded Soil	7	10.5	8	12

The values for the ungrouted cases are in good agreement with the predicted values. The measured loads at the corresponding displacements were considerably smaller than the predicted values for the grouted cases. The differences are attributed to the time-dependent properties of the grouted soil and, to some extent, to the erratic penetration of the grout at shallow depth. The piles in postgrouted soil exhibited larger creep displacement than any other piles. The piles in pregrounded soil exhibited less creep than the piles in postgrouted soil; however, the creep rate in pregrounded soil was much larger than in ungrouted soil.

#### 0.6 **INFERRED MECHANISMS**

The behavior of monolith M2 was examined in detail in an attempt to explain the mechanisms governing the effects of pile driving on the loaded, pile-founded test structures. Mechanisms inferred from this analysis involve progres-

sive horizontal and vertical deformation of the soil in front of the monolith to a large depth as prototype piles are driven. The front piles closest to the driven piles deflect more than the rear piles. The deflection of the front piles is accompanied by a horizontal translation of the pile tips. The loads on the front piles are redistributed deeper along their shaft and to the other piles behind. This mechanism is basically different from the mechanism during static lateral load testing, which involves a uniform, shallow pile deflection, and small, shallow soil deformation.

**PHASE IV REPORT**

**VOLUME III**

**RESULTS AND INTERPRETATION OF  
PILE DRIVING EFFECTS TEST PROGRAM**

**SECTION 1**

**PURPOSE AND OBJECTIVES**

## 1 PURPOSE AND OBJECTIVES

### 1.1

#### PURPOSE

The pile driving effects tests described in this Volume III were part of an investigation and test program designed to provide comprehensive technical bases for the evaluation of various overwater construction schemes and techniques that could be used adjacent to existing loaded navigation structures such as Locks and Dam No. 26. Like many existing structures, where additional construction may be considered in the future, Locks and Dam No. 26 rest on short friction timber piles installed in granular soil. Potential additional construction schemes may involve driving high-capacity steel piles through the granular foundation soil to bedrock in areas close to or within the existing friction pile foundations. Of major concern are the effects such pile driving might have on the stability of the existing foundations. The purpose of the pile driving effects test program was to provide information regarding the magnitude of the effects of nearby pile driving on vertically and horizontally loaded pile-supported structures. Adjunctly, the test program was also designed to evaluate steel pile performance during driving and lateral loading in grouted and ungrouted soil.

The investigation and test program was conducted on Ellis Island approximately one mile downstream of Locks and Dam No. 26, on the Missouri side of the Mississippi River. In addition to the pile driving effects tests, it also included assessment of chemical grouting in alluvial sand (Volume II), and evaluation of construction feasibility of drilled-in piles (Volume IV) and rock anchors (Volume V). Summaries of conclusions for each of these tests are presented in Volume L

### 1.2

#### OBJECTIVES

The primary objectives of the test program were:

- (1) to assess whether or not test structures founded on vertical timber piles and subjected to vertical (axial) and horizontal (lateral) loads develop permanent displacements in response to nearby pile driving; and
- (2) to assess whether or not chemical grouting of the soil surrounding the timberpile foundation of the test structures prevents or mitigates such displacements.

The secondary objectives of the test program were:

- (3) to measure the response of the test structures, their timber pile foundations, and the surrounding soil mass to nearby prototype pile driving to help explain the mechanisms governing pile driving effects, and establish relationships between pile driving parameters and observed effects;

- (4) to measure ultimate axial and lateral load capacities of single timber piles and timber pile groups in ungrouted and grouted soil; and
- (5) to assess the effects of grouting on driving resistance and lateral load capacity of steel piles.

### 1.3 ORGANIZATION OF VOLUME III

The concept of the pile driving effects test program, including the design approach, test variables, and expected performance, are discussed in Section 2. The instrumentation selected for the tests is described in Section 3. The subsurface conditions of the test area were thoroughly investigated and are discussed in Section 4. Section 5 presents a summary of the construction activities associated with the test program. Test procedures and results are discussed in Section 6 (cyclic preloading); Section 7 (prototype pile driving effects); and Section 8 (monolith load testing). A detailed evaluation of the test results was made for monolith M2 and is presented in Section 9. Results of lateral load tests on prototype piles are given in Section 10. Observations of pile condition after extraction at the end of the program are reported in Section 11.

**PHASE IV REPORT**

**VOLUME III**

**RESULTS AND INTERPRETATION OF  
PILE DRIVING EFFECTS TEST PROGRAM**

**SECTION 2  
TEST PROGRAM DESIGN**

## 2 TEST PROGRAM DESIGN

### 2.1 CONCEPT OF TEST PROGRAM

#### 2.1.1 Test Area Selection

At the onset of the project, the Government preselected four candidate test site locations for the entire foundation investigation and test program. On the basis of existing geotechnical and topographical data, it was concluded at the design stage that, although no candidate test site location exactly matched the conditions at Locks and Dam No. 26, Ellis Island was the most desirable location for this investigation and test program. This preliminary test site location was confirmed on the basis of subsurface investigations conducted at Ellis Island during the winter of 1978.

#### 2.1.2 Approach

The pile driving effects test program was designed such that the test conditions generally modelled the conditions at nearby Locks and Dam No. 26. The subsurface conditions at the test site approximately matched the conditions of Locks and Dam No. 26 (Section 4). The test structures were designed and constructed to reproduce the structural conditions of the dam to an acceptable degree of similitude.

The significant aspects of performance that needed to be measured during the tests to achieve the program objectives were selected at the design stage. These are discussed in Section 2.3. These aspects were ranked to allow first, measurement of gross performance, and second, understanding of mechanisms. By gross performance, it is meant the total, unrefined observations and measurements, free of any manipulation of data. The tests were designed to enhance the aspects of performance that had been selected as significant to the interpretation of the results.

Predictions of the outcome of the tests were made by the following process:

- (1) assessment of test conditions;
- (2) development of a simplified model for these conditions;
- (3) selection of mechanisms believed to act in the tests;
- (4) selection of a prediction method based on past experience (Section 2.3);
- (5) selection of parameters involved in the prediction method and consistent with the model developed in (2);
- (6) analysis using selected method and parameters to calculate predictions;
- (7) portrayal of the predictions to facilitate comparisons with measured test results; and

- (8) comparison between predicted and measured test results to assess reliability of prediction methods and, if necessary, improvement of these methods.

On the basis of the predicted test performance, type, location, and sensitivity of the instrumentation required to measure the significant aspects of performance were selected. Instrumentation measurement schedule during testing followed the priority ranking established for the aspects of performance, that is, first, gross performance measurement and second, mechanisms detection.

#### 2.1.3 General Description

**Description of Tests.** The concept of the tests is illustrated in Fig. 2.1. The tests involved the construction of concrete test structures (test monoliths) resting on short, instrumented timber piles installed in sand. Vertical and horizontal loads were applied to the test monoliths using vertical reaction rock anchors and pile-founded, horizontal reaction blocks. With the monolith under load, steel piles (prototype piles) were driven to rock at decreasing distances from the monoliths. The effects of the driving vibrations were measured on the monolith (vibratory movement and resulting static displacement), on the timber pile foundations (static deflections and strain redistribution) and in the soil mass immediately around and away from the monoliths (dynamic and static deformations, pore pressure changes).

Adjunctly, other tests were made during the program. They involved cyclic preloading and load testing to failure of test monoliths, measurements of driving performance of prototype piles, lateral load testing of prototype piles, and inspection of both timber and prototype piles after extraction.

**Sequence of Activities.** The pile driving effects test program included the following activities. Actual durations and detailed sequence of these activities are given in Table 2.1.

- (1) Initial subsurface investigations (winter 1977-1978);
- (2) site preparation, excavation, and installation of dewatering system (June to August 1978);
- (3) instrumentation and calibration of test timber piles (May to September 1978);
- (4) additional subsurface investigations and installation of ground instrumentation (September 1978);
- (5) installation of test timber piles, construction of test monolith, and construction of ancillary test facilities (October 1978 to January 1979);
- (6) subsurface investigations to assess effects of test timber pile installation (November 1978);
- (7) cyclic preloading of the test monoliths (December 1978 to February 1979);

- (8) grouting under two test monoliths (M3 and M7) (January and February 1979);
- (9) driving of prototype piles at various distances from vertically and horizontally loaded test monoliths (January to March 1979);
- (10) subsurface investigations to assess effects of grouting and prototype pile driving (February and March 1979);
- (11) load testing of selected test monoliths and prototype piles (January to March 1979); and
- (12) extraction of two test timber piles and four prototype piles (February 1979).

**Configuration of Test Area.** The location of the pile driving effects test area within the Ellis Island test site is shown in Fig. 2.2. The general configuration of the test area is shown in Fig. 2.3. The test area was approximately 335 ft by 300 ft in plan. The major portion of the test area (monolith trench) was excavated to approximately el 400. Subsequent crushed rock surfacing raised the grade to el 403. The area surrounding the test monoliths was excavated to el 391 to expose the top of the recent alluvial sand. The configuration of the monolith trench was modified during the course of testing; as discussed in Section 5.2.2.

The test area was ringed by a flood-protection levee constructed to el 420. A dewatering system consisting of wells connected to vacuum manifolds was installed on the perimeter of the test area to draw down and maintain groundwater at approximately el 390 in the monolith trench. In September 1978, a supplementary system of seven deep, large-diameter wells with turbine pumps was added as a precaution against river levels in excess of el 415. The performance of the dewatering systems is discussed in Section 5.2.5.

## 2.2 SELECTION OF VARIABLES

### 2.2.1 General

During formulation and design of the test program, a wide range of potential test variables and parameters were examined. In identifying potential test variables, attention was focused on providing an acceptable degree of similitude between the test and existing structures. Considerations were given to scale, pile configuration, construction details, and load levels and history on the existing structures. Other test variables examined were related to potential rehabilitation schemes such as grouting prior to pile driving, and types of pile and hammer most likely to be used. Consistent with the purpose and objectives of the pile driving effects test program stated in Section 1, only variables and parameters essential to the satisfactory performance of the program were selected. The test variables are discussed below. A summary of the test monolith variables is given in Table 2.2.

#### **2.2.2      Number of Test Monoliths**

Six monoliths were constructed and tested. Four were founded on timber pile groups; two on single timber piles. This number of test monoliths was sufficient to make the following comparisons and evaluations:

- (1) single pile vs pile groups;
- (2) effects of presence of adjacent timber piles on monolith response;
- (3) behavior of interior vs exterior timber piles;
- (4) high-level vs low-level applied loads; and
- (5) grouted vs ungrouted soil.

In addition to the six test monoliths, an uncapped control pile group, having a 2 x 3 configuration, was constructed. This control pile group was used to assess changes in soil properties induced by timber pile installation and chemical grouting, without interfering with or affecting the test monolith.

#### **2.2.3      Test Monolith Configuration and Geometry**

The dimensions of the test monoliths were selected on the basis of available budget and schedule considerations and limitations imposed by the size of the reaction structures needed to apply the test loads. The dimensions of the test monoliths are given in Table 2.2 and Fig. 2.5. The test monoliths were founded on clusters of two or three rows of four timber piles each (2 x 4 or 3 x 4 pile configurations) or on single timber piles. The long axis of monoliths founded on pile clusters coincided with the direction of applied lateral load (Fig. 2.4 and 2.5). The timber piles were embedded 2 ft into a reinforced concrete cap to approximate the fixity conditions typically found in existing navigation structures such as Locks and Dam No. 26. The caps of the pile clusters were cast 3 ft above ground surface to eliminate cap-soil interaction effects and facilitate interpretation of cap-pile-soil load transfer. The caps of the single piles were only 6 in. above ground surface.

#### **2.2.4      Adjacent and Interior Piles**

Three test monoliths were founded on a 2 x 4-pile configuration (M2, M3, and M5). In this configuration all piles were exterior piles. One test monolith (M1) was founded on a 3 x 4-pile configuration, so that the behavior of interior piles could be investigated. Monolith M1 was also surrounded by one and two rows of unloaded timber piles to model the effects of adjacent piles (Fig. 2.3). Two test monoliths were founded on single timber piles (M6 and M7).

#### **2.2.5      Timber Pile Installation**

All timber piles were jetted to a depth of approximately 30 ft below ground surface. Jetting was often accompanied by some driving to advance the piles to the jetted depth. The timber piles were then driven for another 5 ft to obtain a 35-ft embedment. This procedure generally was used in the construction of Locks and Dam No. 26, according to available records.

#### **2.2.6      Applied Load Levels**

Two different load levels were applied to the test monoliths during the pile driving effects phase of testing to assess the influence of applied load intensity on monolith response. The lower load level ( $W_1$ ) corresponded to the expected normal maximum working loads delivered by the existing Locks and Dam No. 26 structures to their foundation piles. At the working load level, the horizontal load  $H_1$  was 4 t/pile and the vertical load  $V_1$  was 15 t/pile. Monolith M5 (2 x 4) was subjected to the working load level  $W_1$ .

The higher load level ( $W_2$ ) corresponded to that for which Locks and Dam No. 26 were designed. At the design load level, the horizontal load was 6 t/pile and the vertical load  $V_2$  was 30 t/pile. Monoliths M1 (3 x 4), M2 and M3 (2 x 4) and M6 and M7 (single piles) were subjected to the design load level  $W_2$ .

#### **2.2.7      Cyclic Preloading**

All monoliths were subjected to cyclic preloading before the pile driving effects phase of testing to approximate to some degree the effects of load variations during the service life of existing structures. During cyclic preloading, the vertical load was maintained at design level ( $V_2$ ), while the horizontal load was varied between 0.1  $H_2$  and  $H_2$ , until the horizontal displacements of the monolith reached a steady-state response. This usually occurred after approximately 40 cycles.

#### **2.2.8      Grouted/Ungrounded Soil**

The soil under monoliths M3 (2 x 4) and M7 (single pile) was grouted between ground surface and a depth of 20 ft (Fig. 2.3). Grouting was done after cyclic preloading of the monoliths but before the prototype pile driving effects phase of testing. The purpose of grouting was to observe the effects of soil treatment by chemical grout injection on monolith behavior. A low-strength silicate grout (25% silicate/aluminate; Volume II) was used.

The following ungrouted and grouted soil parameters were selected at the design stage on the basis of laboratory tests and published data by Warner (1972), Woodward-Clyde Consultants (1971), Clough et al (1977), and Koenzen (1975):

<u>Parameter</u>	<u>Ungrouted Soil</u>	<u>Grouted Soil</u>
Total unit weight, $\gamma$ , lb/ft <sup>3</sup>	130	130
Angle $\phi$ , degree		
Static	40	40
Cyclic	38	-
Cohesion $c$ , lb/ft <sup>2</sup>	0	1000
Unconfined compressive strength $q_u$ , t/ft <sup>2</sup>	0	1 to 3
Friction angle on steel pile-soil interface $\delta$ , degree	28	28
Coefficient of mass permeability $k$ , cm/s	$2 \times 10^{-1}$	$10^{-3}$

**2.2.9      Prototype Piles**

The primary prototype piles driven in the vicinity of the test monoliths were H piles. The HP 14 x 73 section selected is the most likely candidate for future construction on existing or proposed navigation structures. Five pipe piles (PP 14 x 0.375) and two sheet piles (MP 102) were also driven as secondary piles.

**2.2.10     Pile Driving Hammers**

The timber piles supporting the test monoliths were driven to final penetration using a Vulcan 1 (15,000 ft-lb rated energy) single-acting, air/steam hammer. This hammer was generally used to install the timber piles supporting the existing structures.

The majority of prototype piles were driven with a Vulcan 010 (32,500 ft-lb rated energy) single-acting air/steam hammer. This hammer was selected as the primary hammer because of its relatively constant impact energy characteristics. Also, a Vulcan 010 hammer had been used successfully in a previous pile driving testing program for Locks and Dam No. 26 replacement studies (Fruco and Associates 1973).

A few prototype piles were driven with a MKT DE 70B (42,000 to 63,000 ft-lb rated energy) single acting, diesel hammer (secondary hammer). At the design stage, it was assumed that a Delmag D22-02 (39,780 ft-lb rated energy) would be used. The contractor provided the MKT hammer instead, because of local availability. Two H piles and the two sheet piles were driven with a Foster 4000 low frequency vibratory hammer. Two timber piles and four prototype piles were extracted with a Foster 40E vibratory extractor at the end of the testing program.

## 2.3 SIGNIFICANT ASPECTS OF PERFORMANCE

### 2.3.1 General

The tests were designed so that certain aspects of the monolith performance during testing could be monitored. The significant aspects of performance selected at the design stage were those that were considered necessary to meet the objectives of the tests and to extrapolate the results. Consistent with the objectives of the test program (Section 1.2), the aspects of performance that were considered of primary importance were those reflecting the gross behavior of the monoliths during pile driving. The secondary aspects of performance were those reflecting the gross behavior of the monoliths during static load testing, and those bringing to light the mechanisms governing gross behavior during both nearby pile driving and load testing.

Significant aspects of performance and corresponding measurable characteristics were identified for the pile driving effects test program for both the grouted and ungrouted cases. They are listed in order of importance and priority in Table 2.3.

### 2.3.2 Prediction Method

**Pile Driving Effects.** The present state of knowledge did not permit an analytical prediction of the magnitude of permanent displacements of test monoliths caused by nearby pile driving. A prediction was attempted on the basis of the limited amount of available pertinent information. Basically, the prediction was based on:

- (1) a study of pile driving effects on nearby soil by Lo (1977) relating pile driving hammer energy, pile driving blowcount, and induced soil particle velocity at a reference distance from a pile being driven;
- (2) a seismic wave propagation and attenuation theory by Barkan (1962) relating peak particle velocity and distance from source of vibration in a soil medium; and
- (3) data gathered by Feagin (1936) during pile driving effects tests at Dam No. 11, on the Mississippi River, which provided a benchmark case history of response of pile-founded structures.

**Pile Driving Effects on Nearby Soil.** On the basis of field measurements during driving of 16.5-in.-dia octagonal prestressed concrete piles, Lo (1977) generated a set of curves relating peak particle velocity  $V_1$  at ground surface and at a distance of 1 ft from the pile axis to rated hammer energy and pile penetration resistance expressed in blow/ft. He recommended that  $V_1$  be scaled proportionally to the cross-sectional area for other piles. Accordingly, curves for prototype 14-in. piles (HP 14 x 73 and PP 14 x 0.375) were approximated and are given in Fig. 2.6. Calculations supporting Fig. 2.6 are given in Appendix H, Volume IIIA.

**Propagation and Attenuation of Waves Through the Free-Field.** For the purpose of this investigation, it was assumed that the nature of wave propagation phenomena in the vicinity of a driven pile could be effectively characterized by peak particle velocities measured on the ground surface, at various distances from the source of vibration. The velocities reflect both the geometric and material damping effects as the waves propagate from the pile point through the soil. Geometric damping occurs because of wave energy volumetric dispersion from the source; material damping occurs because of mechanical dissipation of the energy in the soil.

Based on field observations and wave propagation theory (Barkan 1962), the peak particle velocity at a distance  $r$  from the energy source was expressed as:

$$V = V_{r_1} \left( \frac{r_1}{r} \right)^n \exp \left[ -\alpha(r-r_1) \right] \quad (\text{eq 2.1})$$

where:  $V$  = peak particle velocity at distance  $r$  from source;  
 $V_{r_1}$  = peak particle velocity at distance  $r_1$  from source;  
 $r$  = distance from source to observation point;  
 $r_1$  = distance from source to point of known amplitude;  
 $\alpha$  = coefficient of attenuation representing material damping effects;  
 $n$  = coefficient, usually 0.5 to 1.0 representing geometric damping effects.

For saturated fine-grained sand, Barkan suggested a value of  $0.03 \text{ ft}^{-1}$  for the coefficient of attenuation  $\alpha$ . Based on review of published data (for example, Lo 1977, Richart et al 1970), a value of 0.5 was selected for the coefficient  $n$  for distances  $r$  in the range of 10 ft to 100 ft. Therefore, the free-field attenuation law for the pile driving effects test area was expressed as follows:

$$V = V_1 \sqrt{\frac{1}{r}} \exp \left[ -0.03(r-1) \right] \quad (\text{eq 2.2})$$

where:  $V$  = peak particle velocity at distance  $r$  from source, in./s;  
 $V_1$  = peak particle velocity at  $r_1 = 1 \text{ ft}$  from source, obtained from Fig. 2.6, in./s; and  
 $r$  = distance from source to observation point, ft.

Whereas eq 2.2 was considered to be sufficient for a preliminary prediction of peak particle velocities at the ground surface, it could not be used to rationally predict the wave amplitude at depth, or the frequency content of the propagation waves. These two aspects were not predicted, although it was recognized that they may be important in interpreting the observed behavior of test monoliths during prototype pile driving.

**Response of Test Monoliths.** In assessing the behavior of a test monolith due to arriving waves, the complexity of the problem, including the soil-structure interaction and load redistribution effects, made it virtually impossible to predict beforehand the deformation of a soil element near the pile group in any direct way. It was, therefore, more appropriate to correlate a free-field wave propagation parameter, such as peak particle velocity at the surface, with a monolith gross movement parameter, such as permanent horizontal displacement due to propagating waves. Data collected by Feagin (1936) at Dam No. 11 are plotted in Fig. 2.7. Calculations supporting Fig. 2.7 are given in Appendix H, Volume IIIA. In Fig. 2.7a, the cumulative displacement of Feagin's monoliths ( $\delta_{H'r}$ ) at various distances  $r$  normalized with respect to cumulative displacement ( $\delta_{H'10}$ ) measured at  $r = 10$  ft for each 10 pile driving hammer blows, is plotted vs distance  $r$ . The influence factor  $I_u$  is defined as:

$$I_u = \frac{\text{Cumulative displacement at } r \text{ for 10 blows}}{\text{Cumulative displacement at } r = 10 \text{ ft for 10 blows}} = \frac{(\delta_{H'r})}{(\delta_{H'10})}$$

Considering the uncertainties involved in Feagin's data, Fig. 2.7a indicates that  $\delta_{H'r}$  data fit reasonably well the following attenuation law:

$$(\delta_{H'r}) = (\delta_{H'10}) \sqrt{\frac{10}{r}} \exp [-0.03 (r - 10)] \quad (\text{eq 2.3})$$

or more generally:

$$(\delta_{H'r}) = (\delta_{H'r_1}) \sqrt{\frac{r_1}{r}} \exp [-0.03 (r - r_1)] \quad (\text{eq 2.4})$$

Equations 2.3 and 2.4 are identical in form to eq 2.2 relating peak particle velocity  $V$  and distance  $r$ . Therefore the following relationships appear valid:

$$\frac{(V)_r}{(V)_r} = \frac{(\delta_{H'r})}{(\delta_{H'r_1})} \quad \text{or} \quad \frac{(\delta_{H'r})}{(V)_r} = \frac{(\delta_{H'r_1})}{(V)_r} \quad (\text{eq 2.5})$$

Equation 2.5 implies that the ratio of cumulative monolith displacement for 10 hammer blows to peak particle velocity at ground surface is a constant independant of  $r$ , as long as displacement and particle velocity are measured at the same distance from the source.

In Fig. 2.7b, the cumulative displacement of Feagin's monolith ( $\delta_{H'r}$ ) for each 10 hammer blows is plotted vs lateral load per pile for  $r = 10$  ft and  $r = 20$  ft. Considering the uncertainties involved in Feagin's data, Fig. 2.7b indicates that there is a reasonable relationship between  $(\delta_{H'r})$  and horizontal load per pile. The difference between Feagin's monoliths 2 and 3 could not be explained. Results from monolith 2 were used for prediction purposes in this study because they yielded larger predicted displacements.

No measurements of particle velocity were made at Dam No. 11. Particle velocities were inferred on the basis of Fig. 2.6. Since Feagin used a Vulcan 1 hammer (15,000 ft-lb) and the probable blowcount for his piles was  $B = 60$  blow/ft, Fig. 2.6 indicates that  $V_1$  was probably around 2.5 in./s. Using eq 2.2, the following particle velocities were calculated:

$$V = 0.604 \text{ in./s at } r = 10 \text{ ft}$$

$$V = 0.315 \text{ in./s at } r = 20 \text{ ft}$$

These values of  $V$  were used to normalize the data from monolith 2 in Fig. 2.7b, to obtain the curve presented in Fig. 2.8. In essence then, an assessment of the effects of nearby pile driving on the behavior of loaded monoliths can be made by:

- (1) estimating a value of reference peak particle velocity  $V_1$  from Fig. 2.6 based on the rated pile driving hammer energy  $E_{\text{ram}}$  and blowcount  $B$ ;
- (2) attenuating that value  $V_1$  to a peak particle velocity value  $V$  as a function of distance  $r$  between test monoliths and driven prototype piles using eq 2.2; and
- (3) deriving a value of cumulative horizontal displacement  $\delta_H$  of the test monolith caused by 10 hammer blows using Fig. 2.8 and the corresponding lateral load per pile.

Predictions made in accordance with the above procedure are discussed in Section 2.3.3.

**Statically Loaded Single Piles and Pile Groups.** The response of piles and pile groups to axial and lateral loads is a common problem in foundation engineering; however, experimental and field data on full-scale pile groups often are prohibitively expensive to obtain and many of the cases reported in the literature are only partially documented. The available experimental data pertinent to the pile driving effects test program were reviewed, and methods of analysis that were used to predict pile performance are discussed below.

**Experimental Data.** Feagin conducted several well documented field test programs in support of the design and construction of the existing Locks and Dam No. 26. Axial load tests were performed on individual piles within the cofferdams during construction (Feagin 1936a and 1937). Lateral load tests were performed under similar conditions, both on single piles and on several pile groups of different configurations (Feagin 1937a). Feagin (1948 and 1953) also summarized results of axial and lateral load tests on single piles and pile groups conducted at Locks and Dam No. 26 and elsewhere on the Upper Mississippi River.

#### Methods of Analysis.

**Single Pile Axial Load Capacity.** One-dimensional wave equation solutions are commonly used to predict driving performance of single piles and relate their ultimate axial load capacity  $P_{\text{ult}}$  to dynamic resistance to driving  $R_{\text{ult}}$ . The computer program Wave Equation Analysis of Piles-WEAP (Goble and Rausche 1976) was used in this instance to analyze the hammer assembly-pile-soil system for single timber piles and steel prototype piles.

**Single Pile Lateral Load Capacity.** The usual analytical approach to predict lateral capacity of a pile involves the concept of subgrade reaction. The subgrade reaction method is semi-empirical and involves a soil modulus  $E_s$ , defined by McClelland and Focht (1958), Matlock and Reese (1956), and others as:

$$E_s(z, y) = p/y = k_h D/\text{unit of length}$$

where:  $p$  = lateral soil resistance per unit length of pile, expressed as a force per unit length;  
 $z$  = depth below free ground surface;  
 $y$  = horizontal displacement of pile;  
 $k_h$  = coefficient of horizontal subgrade reaction (Terzaghi 1955); and  
 $D$  = pile diameter.

In this instance, the pile-soil system was analyzed using the computer program Beam-Column 67 described by Bogard and Matlock (1977).

**Pile Groups.** Analyses of pile group behavior under static loading conditions were made using the solution developed by O'Neill et al (1977) and the computer program GP3A. In this solution, the behavior of each pile in the group is analyzed using elemental  $p-y$  (lateral) and  $t-z$  (axial)\* representations of the load transfer behavior of the surrounding soil. The GP3A solution incorporates pile-soil-pile interaction effects.

### 2.3.3 Predicted Performance

The characteristics of the significant aspects of performance were predicted. Documentation is provided in Appendix H, Volume IIIA.

**Pile Driving Effects.** Using the method described in Section 2.3.2, an attempt was made to predict cumulative horizontal displacement of a test monolith caused by 10 hammer blows on one prototype pile. These predictions are presented in Fig. 2.9 and Fig. 2.10 for the primary hammer (Vulcan 010) and one secondary hammer (Delmag D22)\*\*, respectively. Wave equation analysis predictions of  $R_{ult}$  and  $E_{max}$  (dynamic resistance to penetration and maximum energy transferred at the pile built per hammer blow) vs blowcount, are given in Fig. 2.11.

As an example, using Fig. 2.9, it was expected that 10 blows of a Vulcan 010 hammer on a 14-in. prototype pile (HP 14 x 73 or PP 14 x 0.375), at a distance of 10 ft from a 2 x 4-pile test monolith would induce the following permanent horizontal displacements in ungrouted soil:

- 
- \*  $t$  is the axial soil resistance, expressed as a stress per unit area, and  $z$  is the settlement of the pile
  - \*\* The actual secondary hammer used during the tests was an MKT DE 70B with a rated energy of 42,000 to 63,000 ft-lb; a Delmag D22 has a rated energy of 39,780 ft-lb. The actual energy used for prediction purpose was 25,000 ft-lb at low blowcount and 39,780 ft-lb at high blowcount, to account for mechanical efficiency

<u>Load Level</u>	<u>Prototype Pile</u> <u>Penetration</u> <u>Blowcount B</u> <u>blow/ft</u>	<u>Permanent</u> <u>Displacement <math>\delta_H</math></u> <u>in.</u>
$H_1 = 32 \text{ t}$ (4 t/pile)	10	0.06
$w_1$		
$V_1 = 120 \text{ t}$ (15 t/pile)	50	0.13
$H_2 = 48 \text{ t}$ (6 t/pile)	10	0.07
$w_2$		
$V_2 = 240 \text{ t}$ (30 t/pile)	50	0.16

In essence, these data ( $\delta_H$  per 10 blows) define the slope of a curve representing cumulative displacement versus hammer blows based on Feagin's test results. It was unclear, however, from Feagin's data, what the exact conditions were during his test program. It was uncertain whether his data describe maximum slope values or average slope values during the course of nearby pile driving. The depth of penetration of the piles during driving was not reported. Thus, the meaning of the data presented by Feagin and these interpretations of his data are questionable.

The vertical and rotational displacements of the test monolith were calculated approximately (based on static analyses) by multiplying the horizontal displacement values expressed in inches by 0.12 to obtain the vertical displacement  $\delta_v$  in inches, and by 0.09 to obtain the rotational displacement  $\theta$  in degrees:

$$\delta_v = 0.12 \delta_H$$

$$\theta (\text{degrees}) = 0.09 \delta_H (\text{inches})$$

The predicted peak particle velocity  $V$  at the ground surface was estimated as a function of distance from pile driving, rated driving energy, and penetration blowcount. These predictions are presented in Fig. 2.12. For example, based on Fig. 2.12, the following predictions were made:

<u>Distance from Pile Driving r ft</u>	<u>Hammer Type</u>	<u>Penetration Blowcount blow/ft</u>	<u>Predicted Peak Velocity at Ground Surface V in./s</u>
10	Vulcan 010	10	1.6
10	Vulcan 010	50	3.4
10	Delmag D22-02*	10	0.9
10	Delmag D22-02**	50	5.2
2.4***	Vulcan 010	10	4
8	Vulcan 010	50	4
1****	Delmag D22-02*	10	4
14	Delmag D22-02**	50	4

\* At low blowcount, assumed  $E_{\text{ram}} = 25,000 \text{ ft-lb}$

\*\* At high blowcount, assumed  $E_{\text{ram}} = 39,780 \text{ ft-lb}$

\*\*\* The relationship is probably invalid for  $r < 5 \text{ ft}$

**Effects of Grouting.** Predictions of driving resistance and driving stresses for piles driven through grouted and ungrouted soil are presented in Fig. 2.13. The predictions were made using the WEAP computer program discussed in Section 2.3.2. Blowcount was expected to be twice as large in grouted soil than in ungrouted soil. Slightly higher driving stresses were also expected in grouted soil.

**Lateral Load Capacity of Steel Piles.** Load-deflection relationships for lateral load tests on H and pipe piles were predicted using the beam-column analysis discussed in Section 2.3.2. These predictions were made assuming certain stiffness characteristics for the piles. Actually, the stiffness of the test piles was significantly increased by various instrumentation protections welded to the piles. This is discussed further in Section 10. On the basis of the general predictions presented in Fig. 2.14, it was predicted that the following static lateral loads  $P_{0.25}$  would produce a pile-head displacement  $\delta_{y\text{max}}$  of 0.25 in.:

<u>Soil Conditions</u>	<u>Prototype Pile</u>	$P_{0.25}$ <u>t</u>
UngROUTed soil	HP 14 x 73 PP 14 x 0.375 (concrete-filled)	5.5 5
PregROUTed soil (Pile driven through grouted soil)	HP 14 x 73 PP 14 x 0.375 (concrete-filled)	4 3.8
PostgROUTed soil (Soil grouted after pile is driven)	HP 14 x 73 PP 14 x 0.375 (concrete-filled)	27 24

Driving the piles through pregrouted soil was expected to cancel the effects of grouting, and result in lateral load capacity similar to that in ungrouted soil. Postgrouting was expected to significantly increase lateral load capacity of the piles.

1978

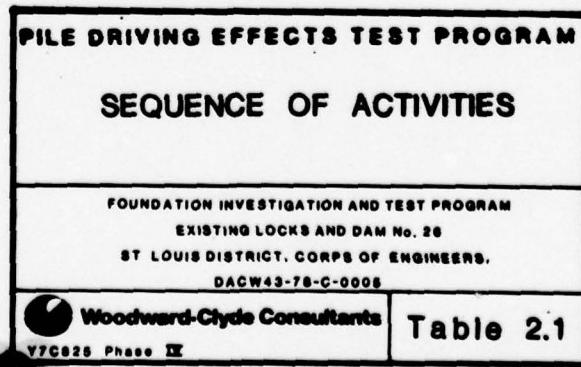
January February March April May June July Au

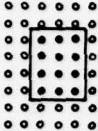
Initial subsurface investigation (1)							
Site preparation dewatering (2)							
Timber pile calibration (3)							Seattle
Instrumentation instl. In situ testing (4)							
Timber pile instl. and monolith construction (5)							
In situ testing (6)							
Monolith preloading (7)							
Grouting (8)							
Prototype pile driving (9)							
In situ testing (10)							
Load testing (11)							
Pile extraction (12)							

1979

August September October November December January February March

The figure consists of a grid of 12 columns and 10 rows. It features several horizontal black bars of varying lengths. The first bar is at the top left. Below it, the word "Alton" is written above a horizontal bar. To the right of "Alton" is a short bar. In the middle section, there is a long horizontal bar spanning approximately 8 columns. Below this long bar is a short bar. To the right of the long bar, the labels M1, M3/M7, M2/M6, and M5 are written. In the bottom section, there are two horizontal bars: one spanning approximately 6 columns and another spanning approximately 4 columns. To the right of these bars, the labels M1, M2/M6, M5, and M3/M7 are written. The bottom right corner contains a single short bar.



<u>MONOLITH NUMBER</u>	<u>TIMBER PILE<sup>(1)</sup> CONFIGURATION</u>	<u>MONOLITH DIMENSIONS, ft</u>			<u>LOAD LEVEL t/pile</u>		<u>SOIL CONDITIONS</u>
		<u>HEIGHT</u>	<u>WIDTH</u>	<u>LENGTH</u>	<u>HORIZONTAL</u>	<u>VERTICAL</u>	
M1		6	10	13	$H_2 = 6$	$V_2 = 30$	Ungrouted
	(3 x 4)						
M2		6	7	13	$H_2 = 6$	$V_2 = 30$	Ungrouted
	(2 x 4)						
M3		6	7	13	$H_2 = 6$	$V_2 = 30$	Grouted
	(2 x 3)						
M5		6	7	13	$H_1 = 4$	$H_1 = 15$	Ungrouted
	(2 x 2)						
M6 <sup>(2)</sup>		3	3	3	$H_2 = 6$	$V_2 = 30$	Ungrouted
	(single pile)						
M7 <sup>(2)</sup>		3	3	3	$H_2 = 6$	$V_2 = 30$	Grouted
	(single pile)						

Legend

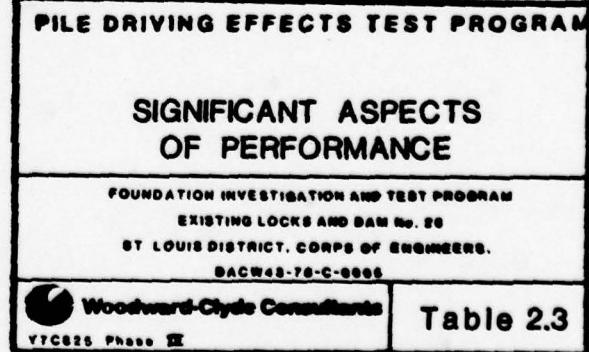
- Instrumented, loaded test timber pile
- Uninstrumented, unloaded timber pile

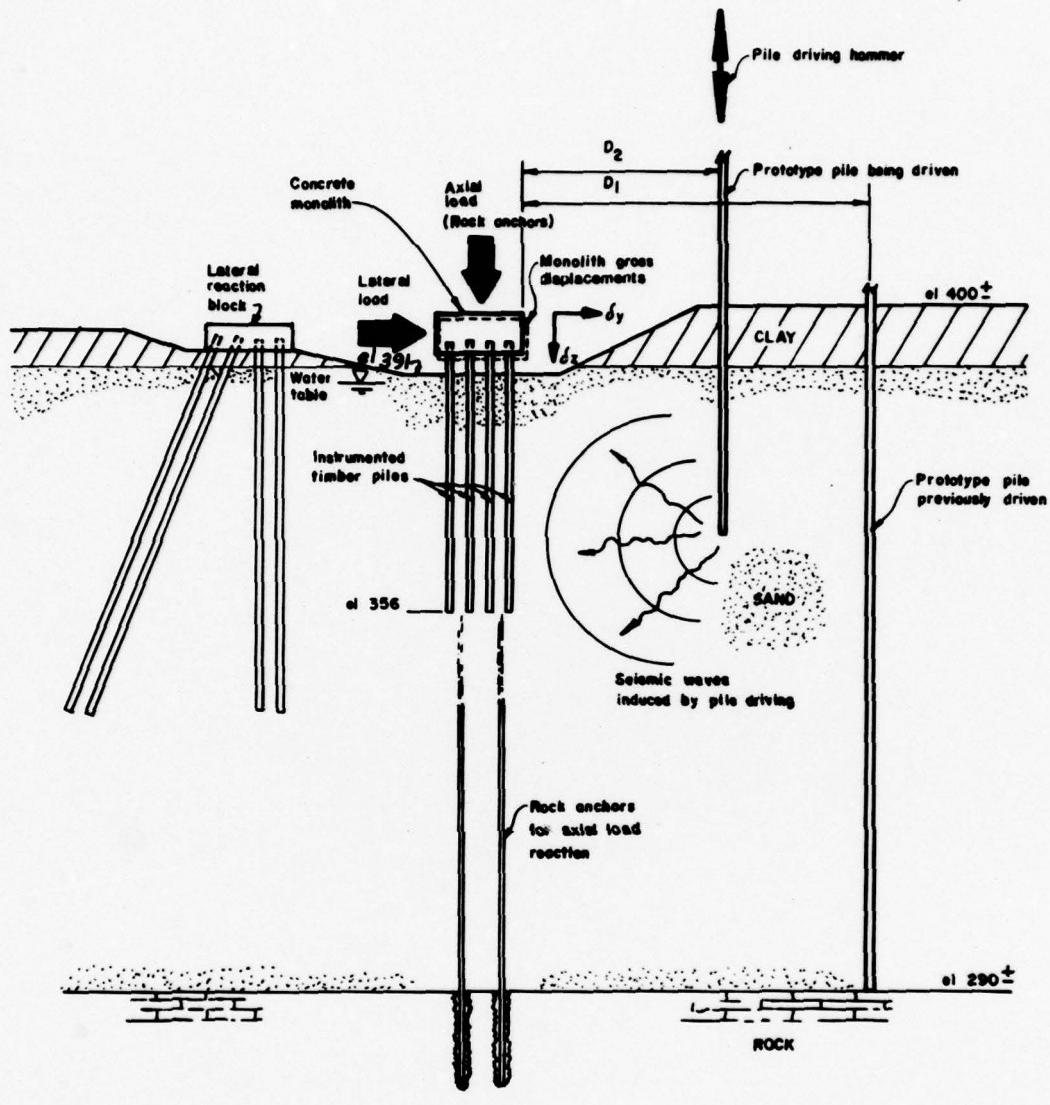
Notes

- (1) Timber piles were installed at 3-ft centers
- (2) M6 and M7 were raised 0.5 ft above ground surface; all other monoliths were raised 3 ft above ground surface

PILE DRIVING EFFECTS TEST PROGRAM	
SUMMARY OF TEST MONOLITH VARIABLES	
FOUNDATION INVESTIGATION AND TEST PROGRAM EXISTING LOCKS AND DAM NO. 26 ST LOUIS DISTRICT, CORPS OF ENGINEERS. BACW43-78-C-0006	
 Woodward-Clyde Consultants V7C825 Phase III	Table 2.2

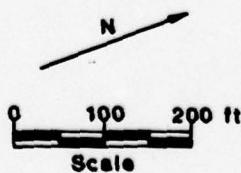
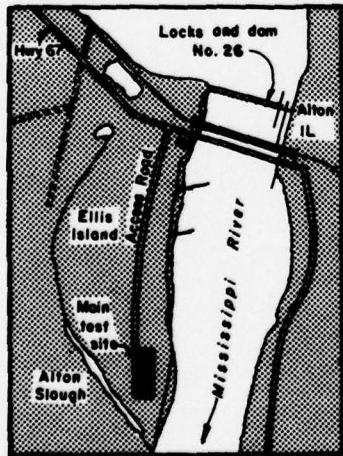
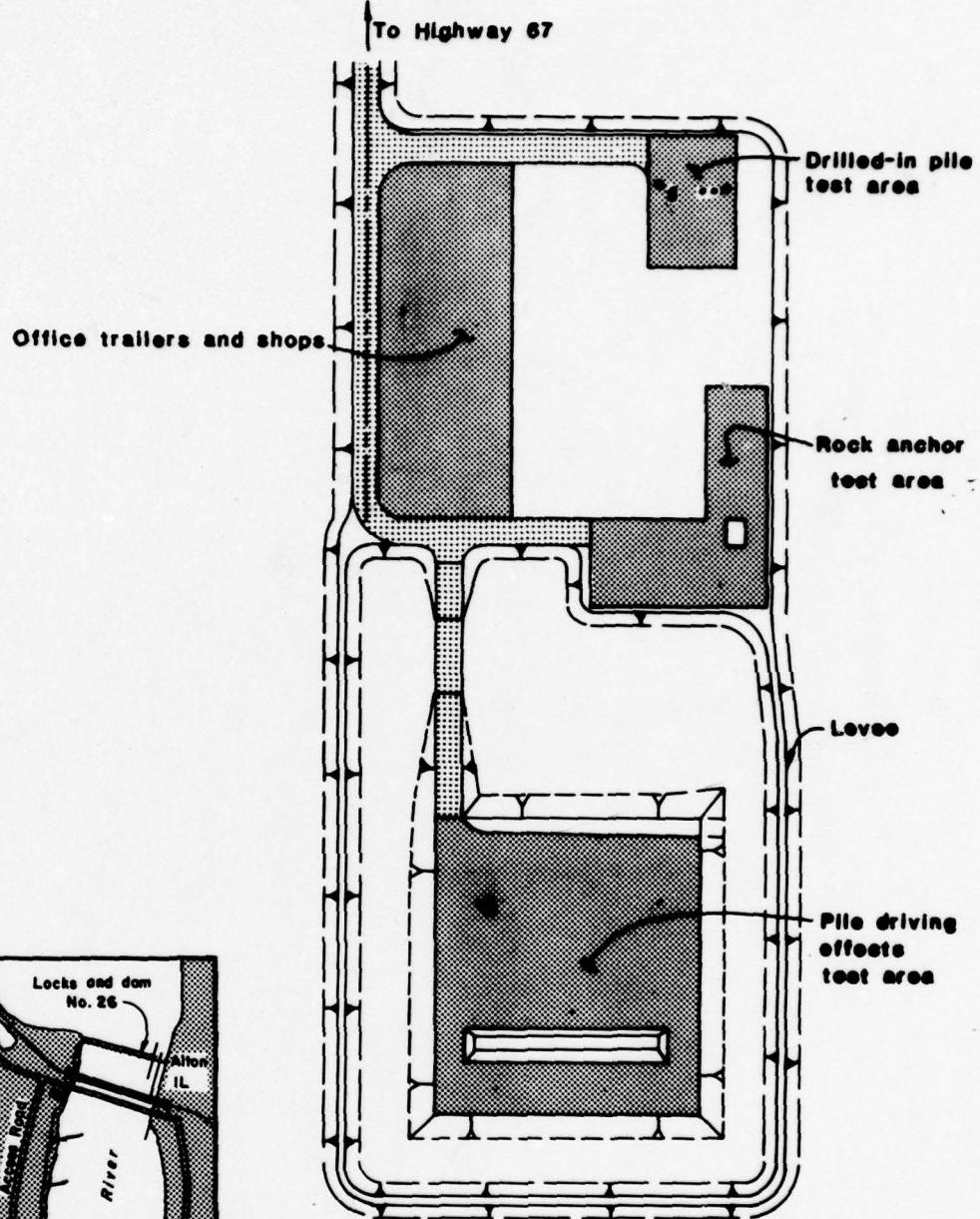
<u>Priority</u>	<u>Aspect of Performance</u>	<u>Measurable Characteristic</u>
<u>Primary</u>		
1	Response of monoliths during nearby prototype pile driving	-Permanent displacement -Applied load -Particle velocity
2	Performance of prototype piles during their driving	-Penetration resistance -Force-time history at butt -Acceleration-time history at butt
3	Wave propagation in soil	-Particle velocity at ground surface
<u>Secondary</u>		
4	Response of timber piles during nearby prototype pile driving	-Permanent pile deflection -Cap-pile-soil load transfer
5	Response of soil mass during nearby prototype pile driving	-Permanent deformation -Particle velocity at depth -Pore pressure
6	Ultimate load capacity of timber piles	-Ultimate load -Pile deflection -Cap-pile-soil load transfer
7	Performance of timber piles during their driving	-Penetration resistance -Force-time history at butt -Acceleration-time history at butt -Observation after extraction
8	Effects of grouted soil on pile driving	-Dynamic pile penetration resistance $R_{ult}$ -Dynamic stress in pile $\sigma_{max}^c$
9	Lateral load capacity of piles driven in grouted and ungrouted soil	-Ultimate load $P_{ult}$ -Pile deflection $\delta_y$





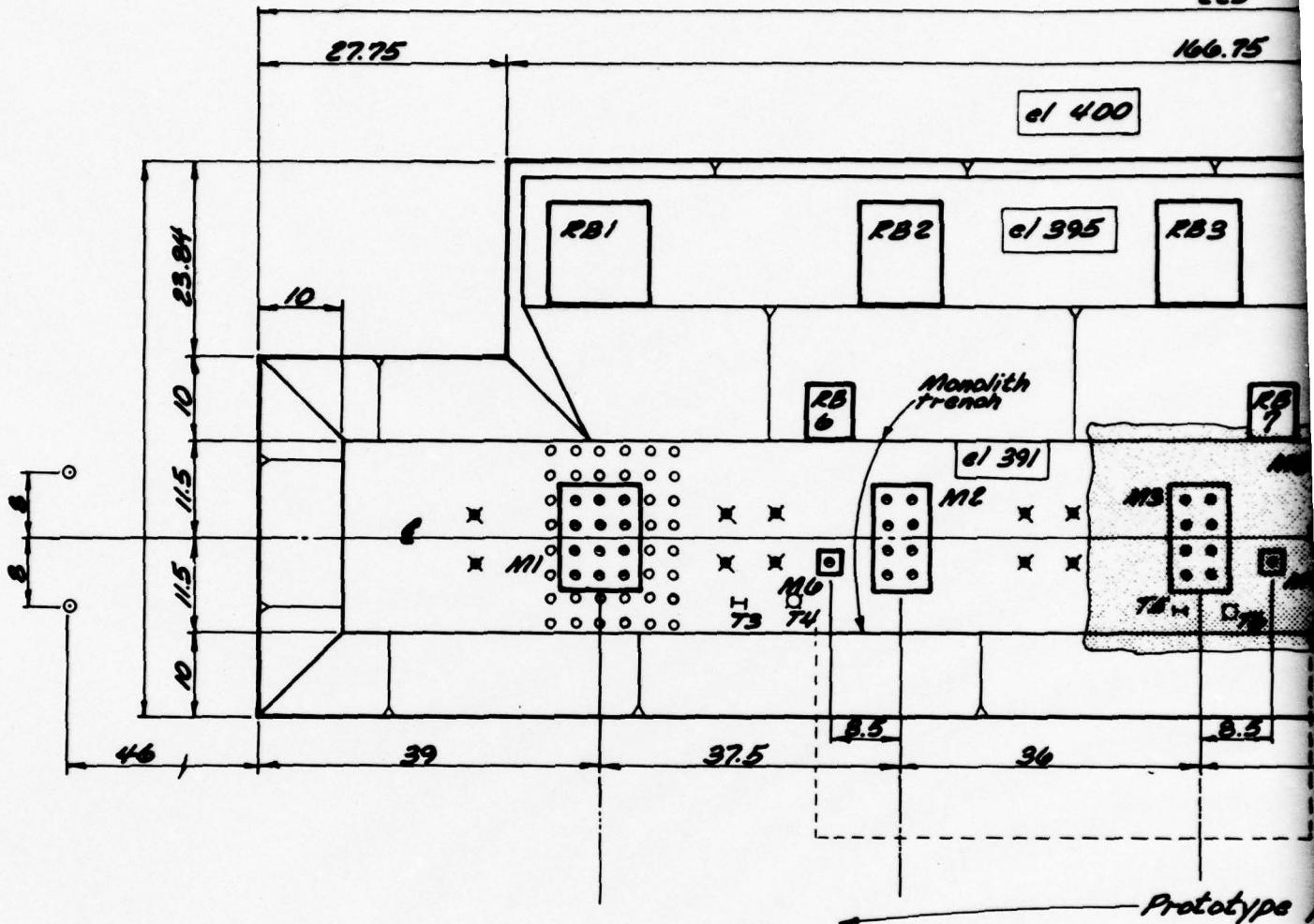
0      10      20  
Scale, ft

<b>PILE DRIVING EFFECTS TEST PROGRAM</b> <b>CONCEPT OF TESTS</b>	
<small>FOUNDATION INVESTIGATION AND TEST PROGRAM          EXISTING LOCKS AND DAM No. 26          ST LOUIS DISTRICT, CORPS OF ENGINEERS.          DACW43-78-C-0006</small>	
 Woodward-Clyde Consultants <small>Y7C825 Phase IX</small>	<b>Fig. 2.1</b>



<b>PILE DRIVING EFFECTS TEST PROGRAM</b>	
<b>LOCATION OF TEST AREA</b>	
FOUNDATION INVESTIGATION AND TEST PROGRAM	
EXISTING LOCKS AND DAM NO. 26	
ST LOUIS DISTRICT, CORPS OF ENGINEERS.	
DAGW43-78-C-0003	
Woodward-Clyde Consultants	Y7C825 Phase III
<b>Fig. 2.2</b>	

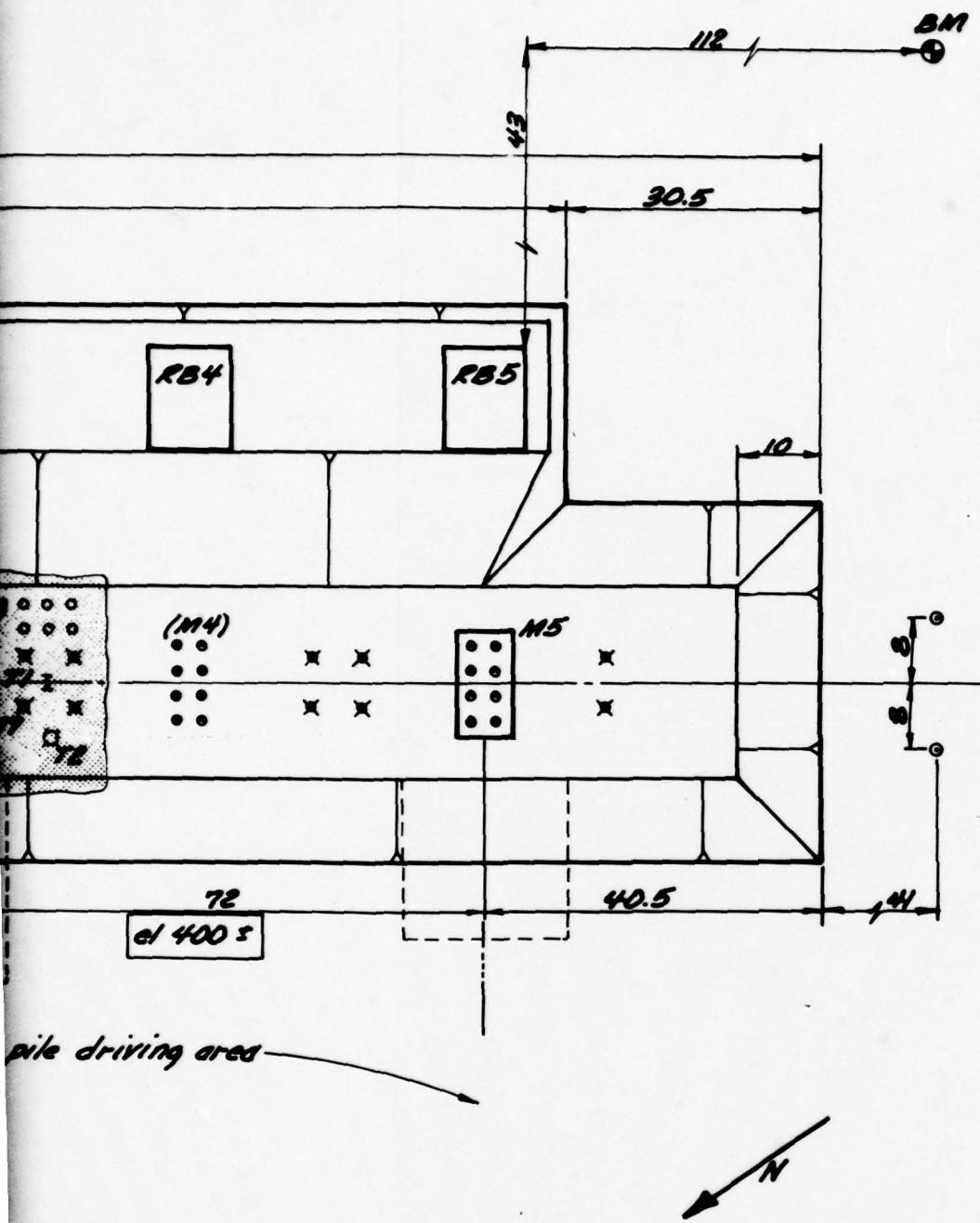
225



### Legend

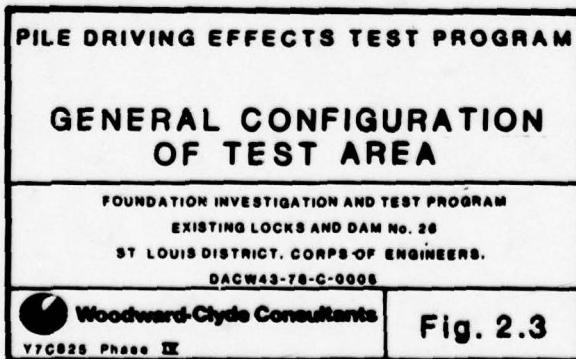
- Uninstrumented timber pile
- Instrumented timber pile
- Instrumented prototype pipe pile
- ⊖ Instrumented prototype H pile
- ✖ Vertical reaction rock anchor
- RBi Lateral reaction block
- Mi Test monolith
- ◎ Horizontal control points
- Vertical benchmark
- ▨ Horizontal limit of
- - Approximate location after cyclic preloading
- Axis of prototype pile

Note:  
All dimensions in

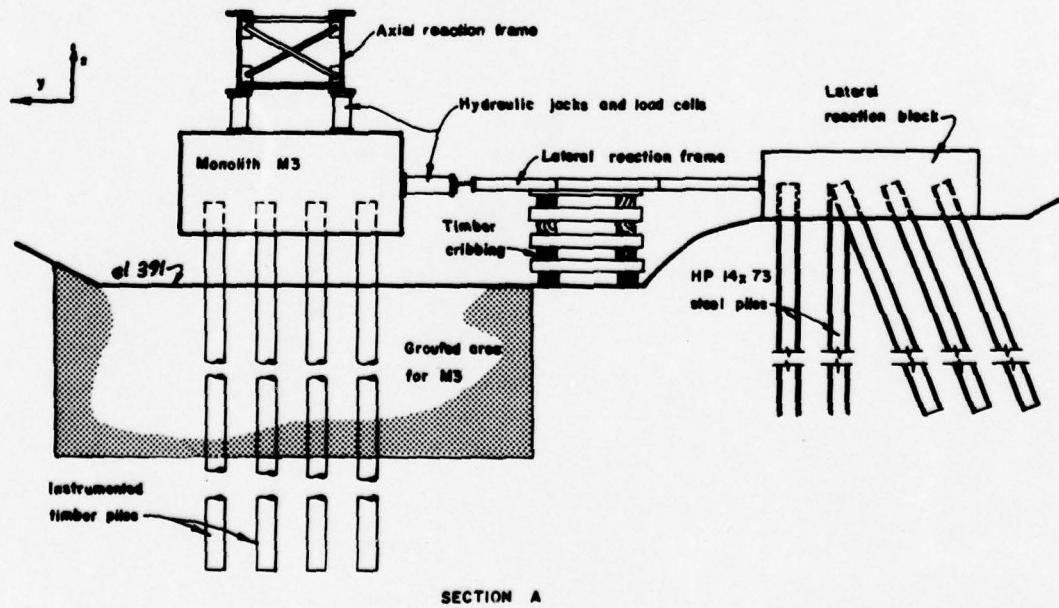
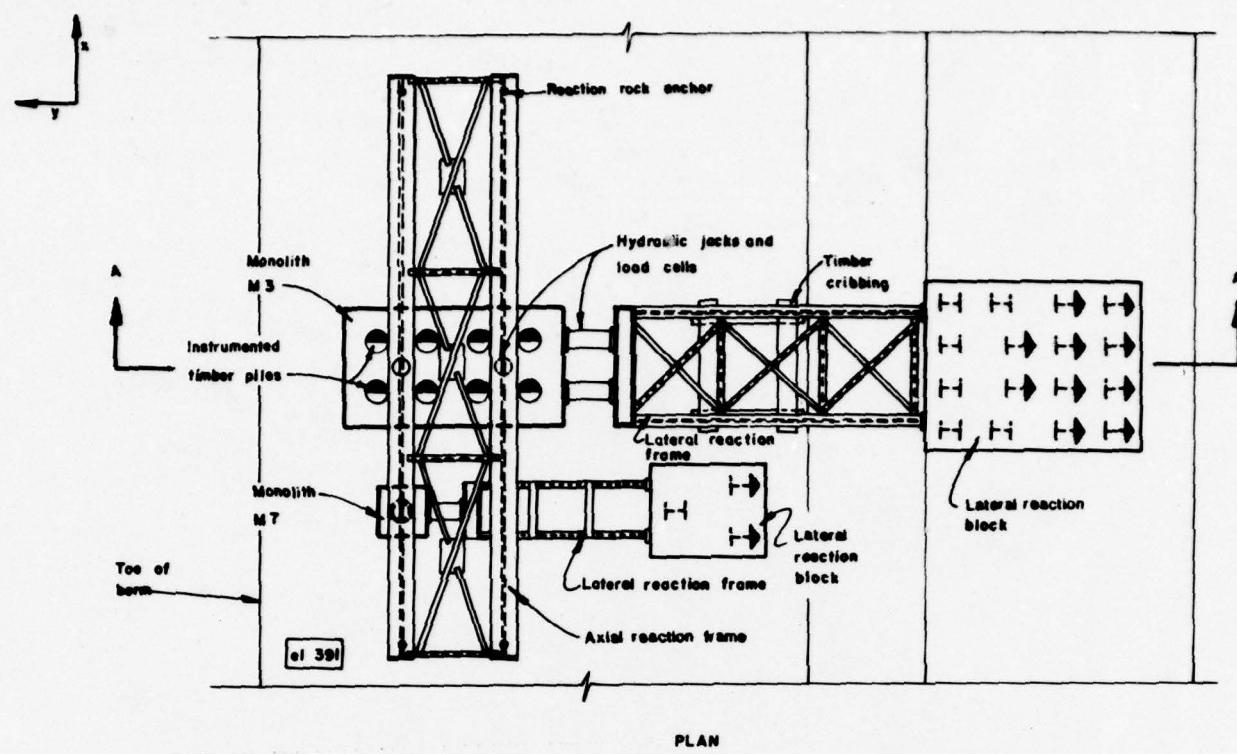


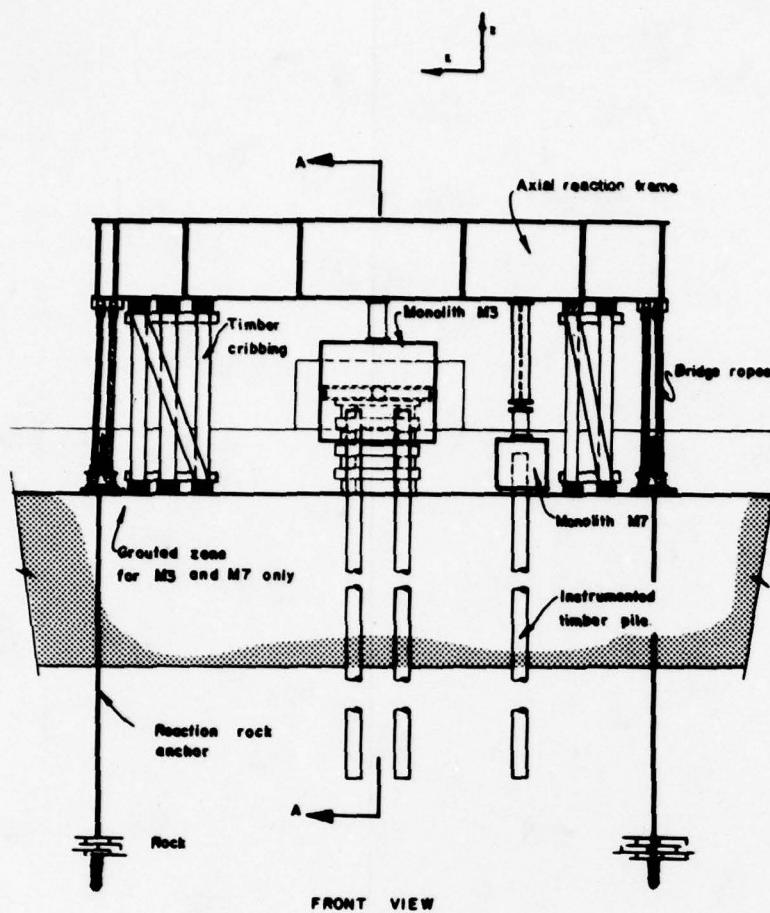
grouted zone  
n. of berm toe  
ing  
driving

feet



2



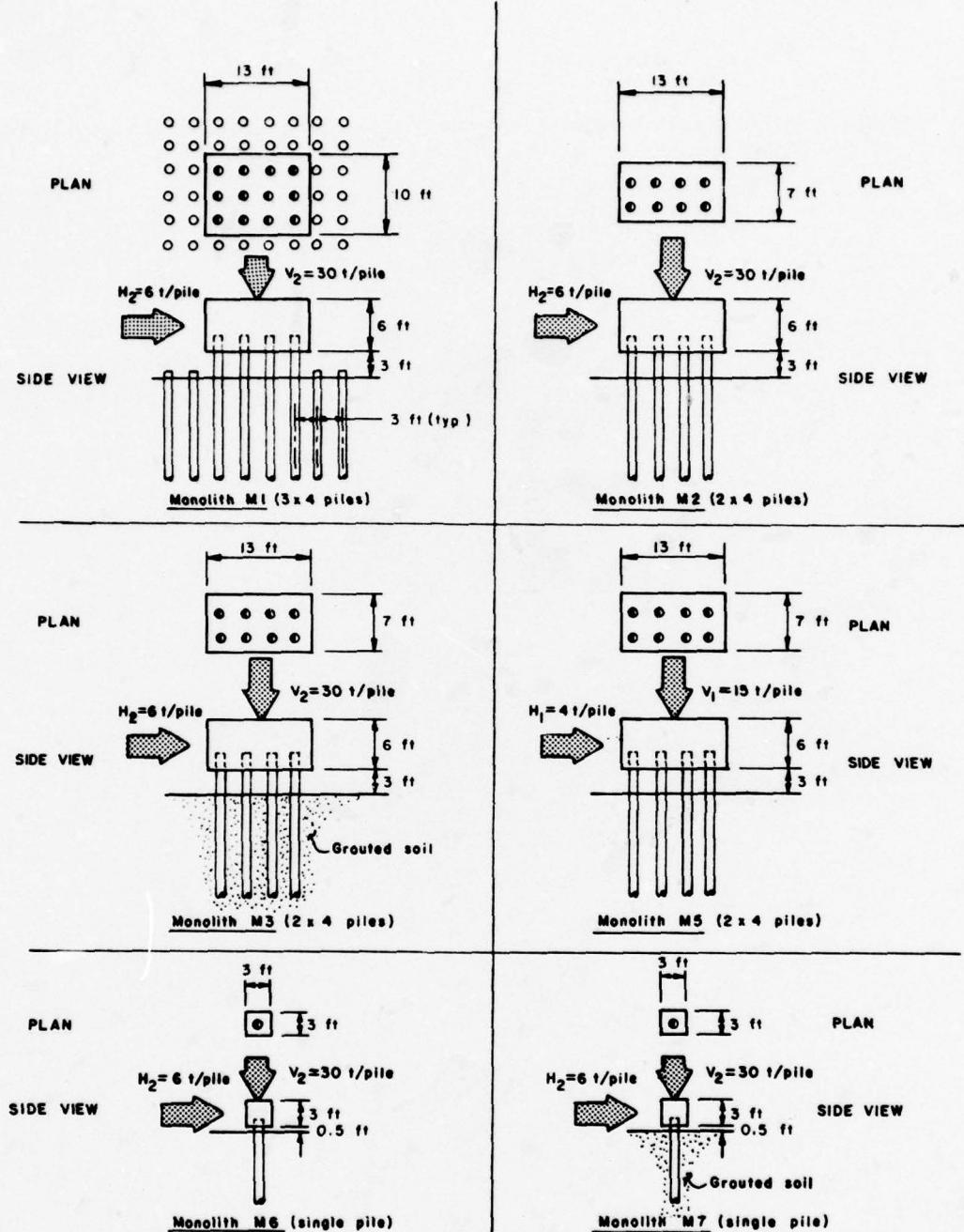


Note:

Monoliths other than  
M3 and M7 are similar  
in concept.

<b>PILE DRIVING EFFECTS TEST PROGRAM</b>	
<b>TYPICAL MONOLITH AND LOADING SETUP</b>	
FOUNDATION INVESTIGATION AND TEST PROGRAM	
EXISTING LOCKS AND DAM NO. 26	
ST LOUIS DISTRICT, CORPS OF ENGINEERS.	
DAGW43-78-C-0008	
 Woodward-Clyde Consultants Y7C828 Phase II	Fig. 2.4

2



#### Legend

- Instrumented, loaded test timber pile
- Uninstrumented, unloaded timber pile

### PILE DRIVING EFFECTS TEST PROGRAM

### MONOLITH CONFIGURATIONS

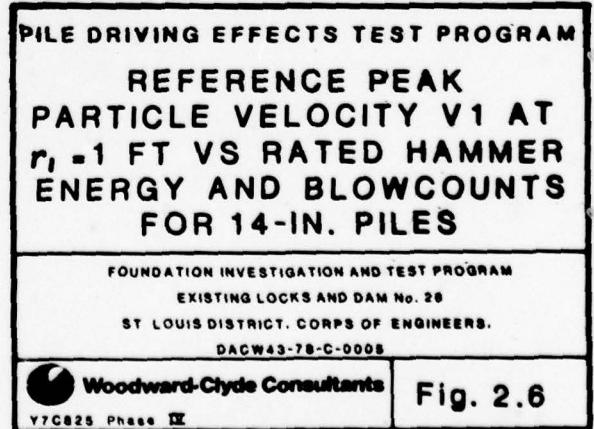
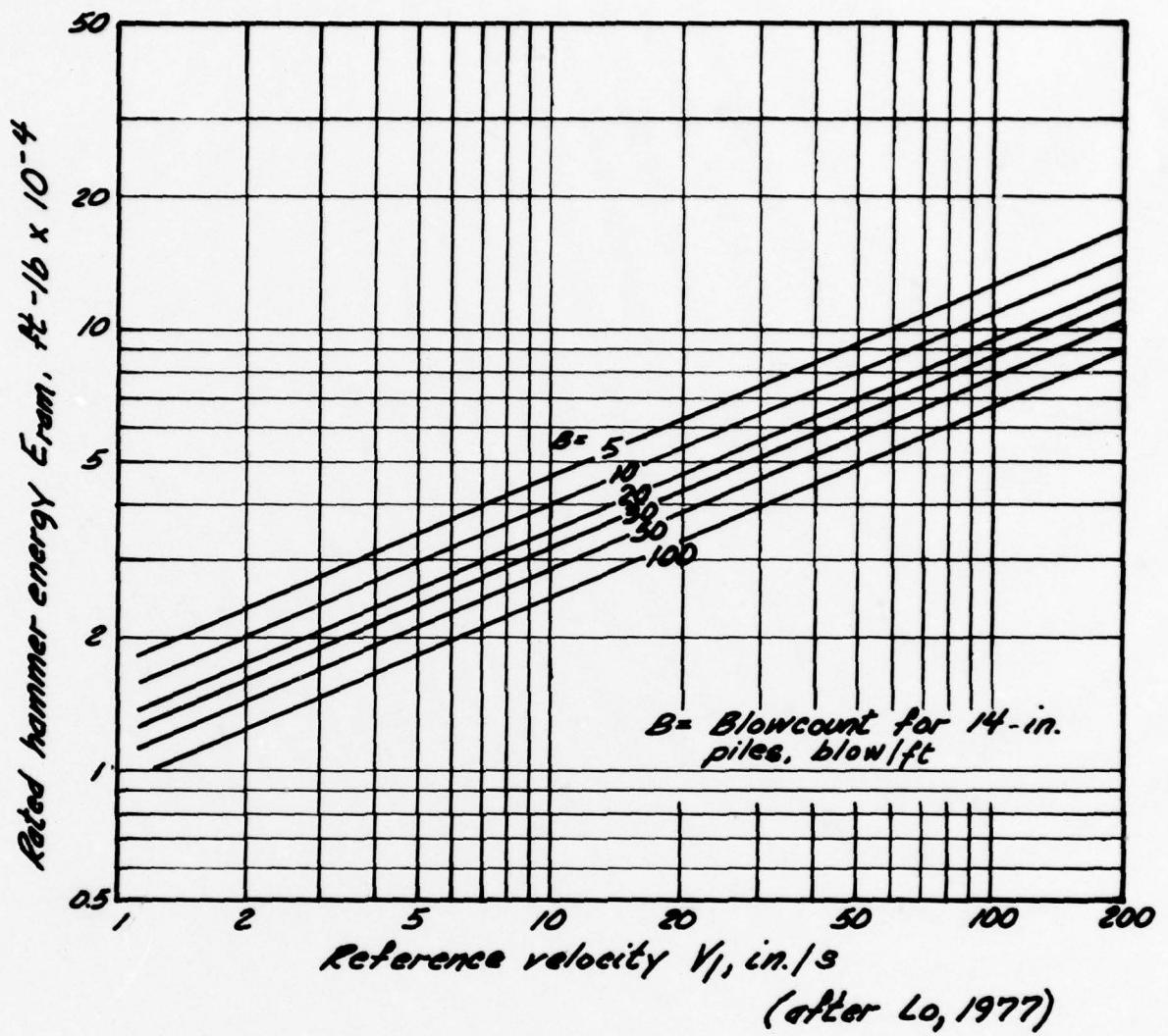
FOUNDATION INVESTIGATION AND TEST PROGRAM  
EXISTING LOCKS AND DAM No. 28  
ST LOUIS DISTRICT, CORPS OF ENGINEERS.  
DACPW43-78-C-0008

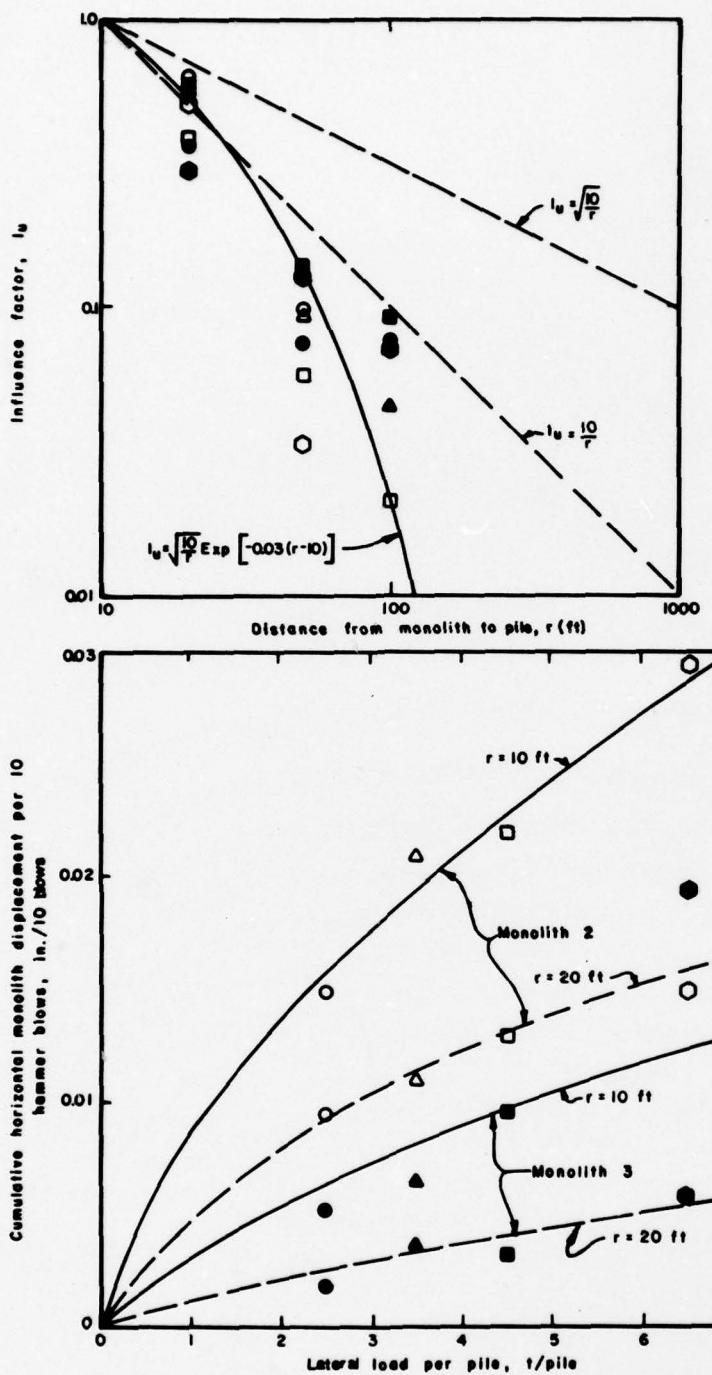


Woodward-Clyde Consultants

Y7C825 Phase III

Fig. 2.5





Legend:

- □ ○ Feagin's monolith 2
- ▲ ● Feagin's monolith 3

Note:

$I_u = \frac{\text{Cumulative displacement at } r \text{ for 10 hammer blows}}{\text{Cumulative displacement at } r = 10 \text{ ft for 10 hammer blows}}$

PILE DRIVING EFFECTS TEST PROGRAM

PILE DRIVING EFFECTS DATA  
FROM DAM NO. 11

FOUNDATION INVESTIGATION AND TEST PROGRAM

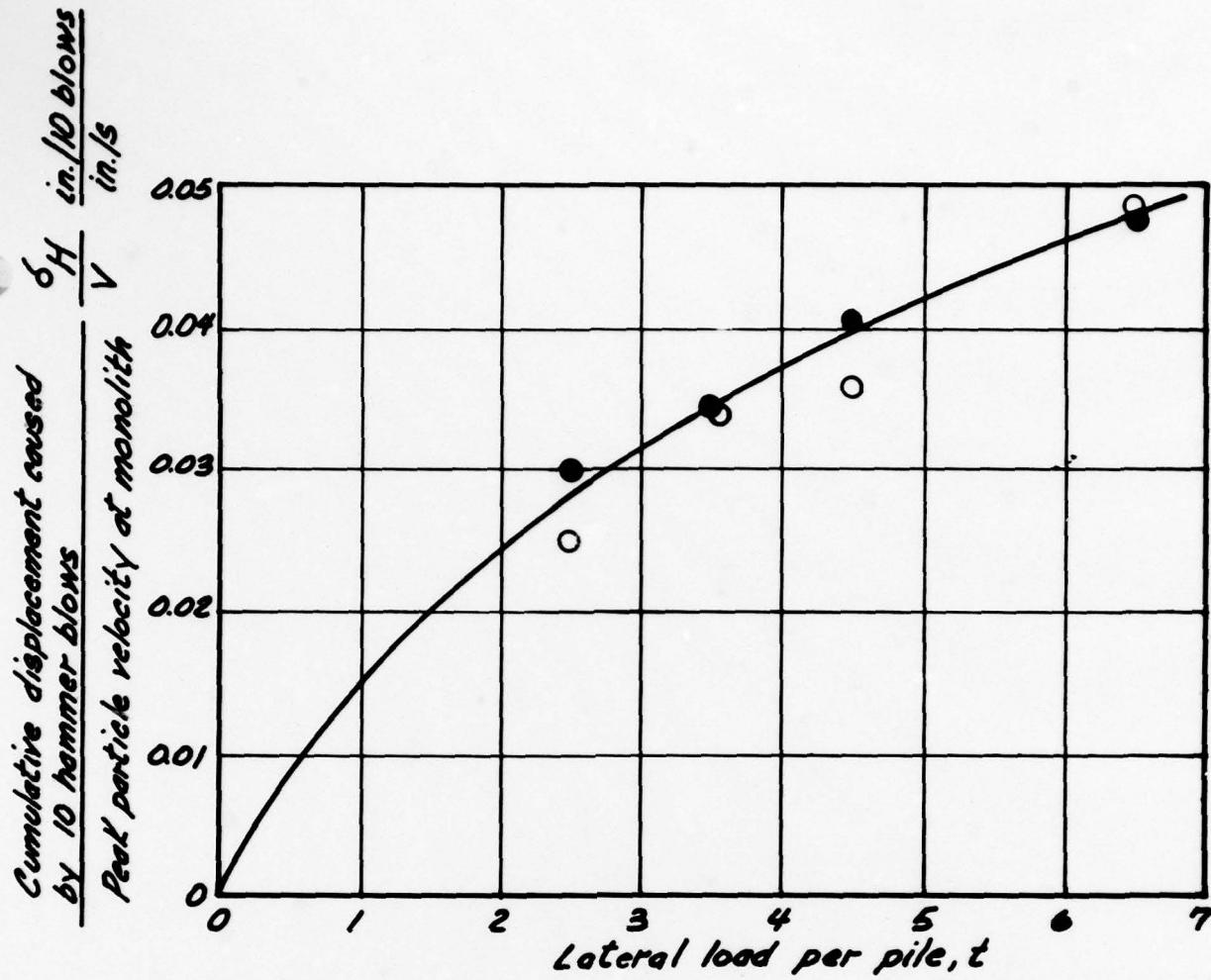
EXISTING LOCKS AND DAM NO. 26

ST LOUIS DISTRICT, CORPS OF ENGINEERS.

DACW43-78-C-0008

Woodward-Clyde Consultants  
V7C825 Phase II

Fig. 2.7



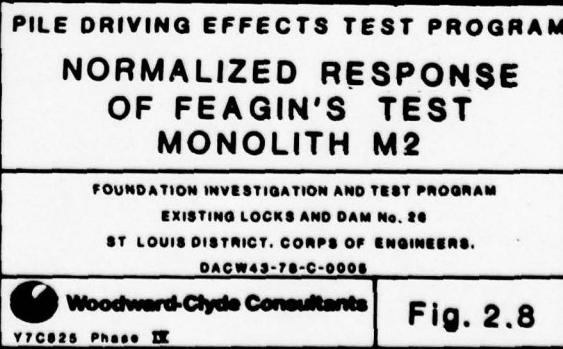
*Legend*

(After Feagin, 1936)

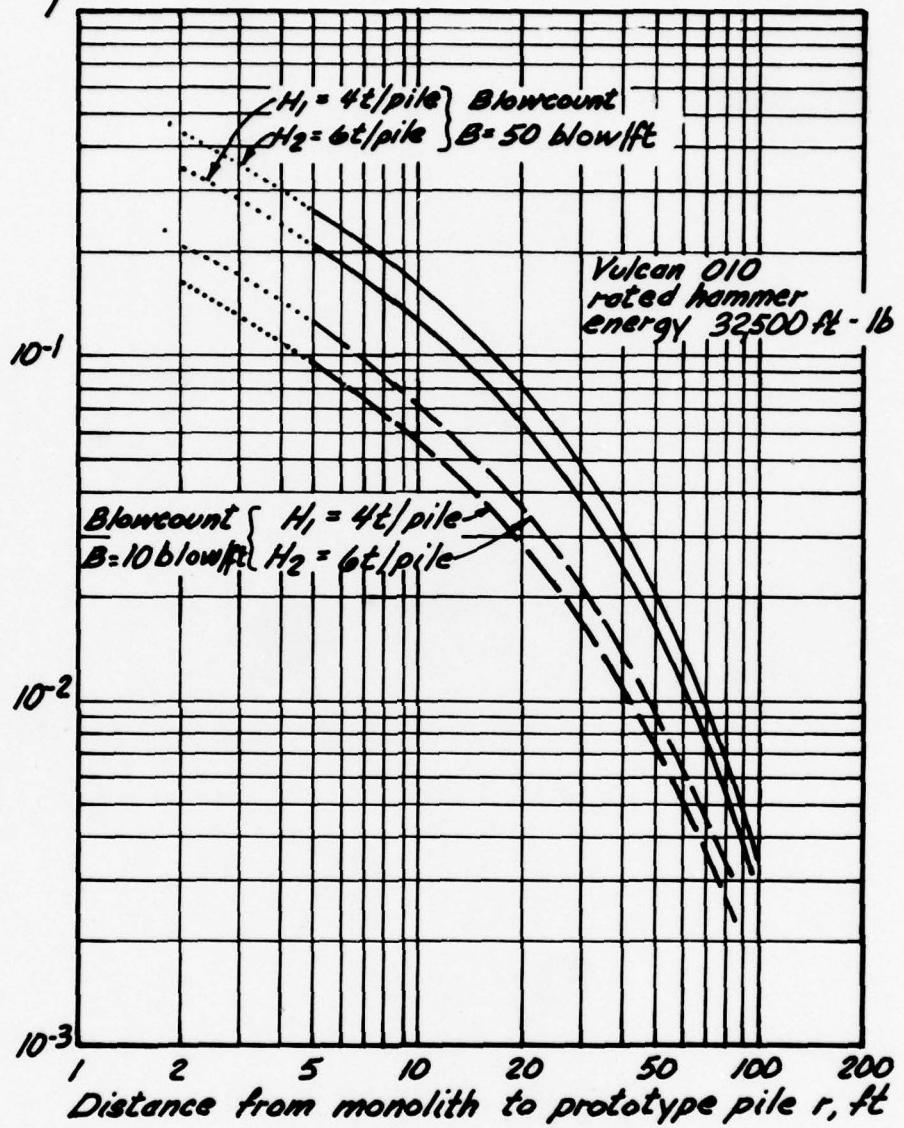
- Data from  $r = 10 \text{ ft}$
- Data from  $r = 20 \text{ ft}$

*Notes:*

- (1) Feagin's monolith No. 2 was  $3 \text{ ft} \times 3 \text{ ft} \times 6 \text{ ft}$  high, founded on two timber piles. Monolith cap was cast directly on ground surface
- (2)  $V$  was estimated on the basis of Fig. 2.6 ( $V_1 = 2.5 \text{ in./s}$  for  $B = 60 \text{ blow/ft}$  and Vulcan 1 Eram =  $15000 \text{ ft-lb}$ ) and eq 2.2



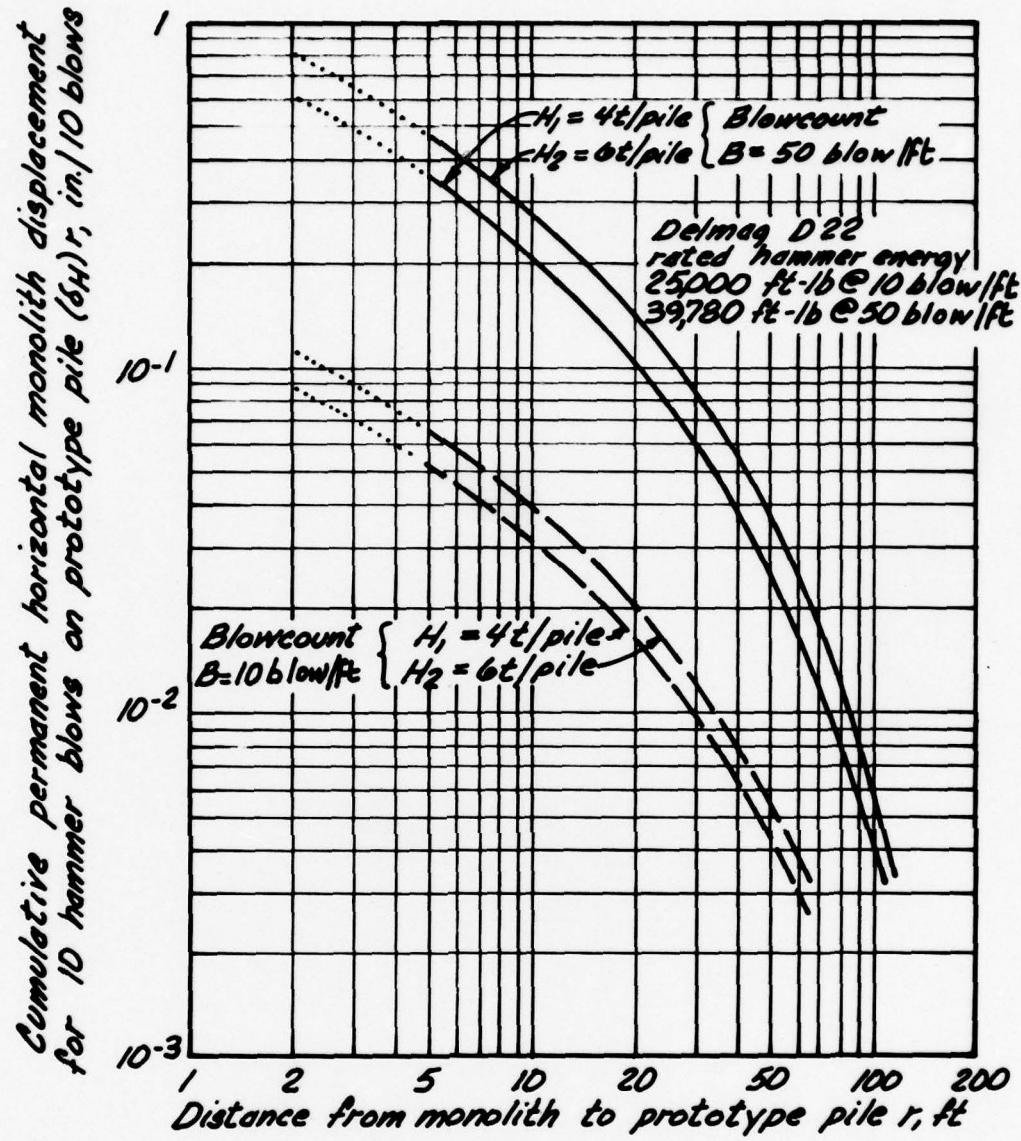
Cumulative permanent horizontal monolith displacement  
for 10 hammer blows on prototype pile ( $\delta_H$ ) $r$ , in./10 blows



Note:

$(\delta_H)r$  predicted at ground surface

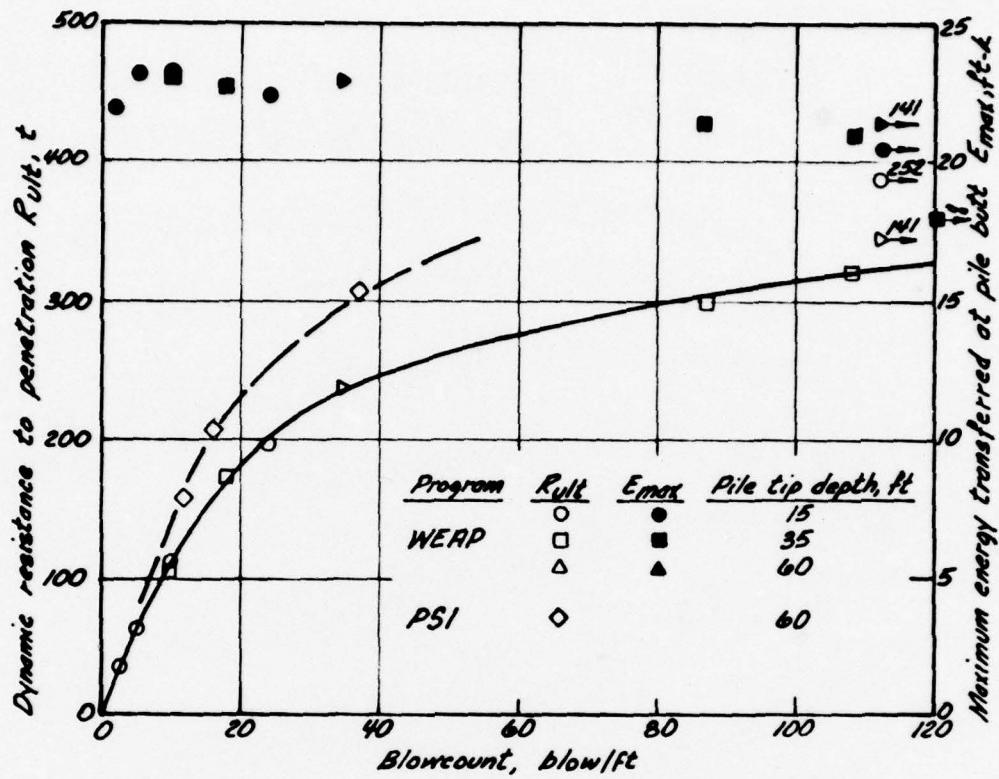
<b>PILE DRIVING EFFECTS TEST PROGRAM</b> <b>PREDICTED MONOLITH</b> <b>DISPLACEMENT CAUSED BY</b> <b>DRIVING WITH VULCAN 010</b>	
<small>FOUNDATION INVESTIGATION AND TEST PROGRAM EXISTING LOCKS AND DAM No. 26 ST LOUIS DISTRICT, CORPS OF ENGINEERS. DACPW43-78-C-0008</small>	
 Woodward-Clyde Consultants Y7C825 Phase IV	<b>Fig. 2.9</b>



Note:

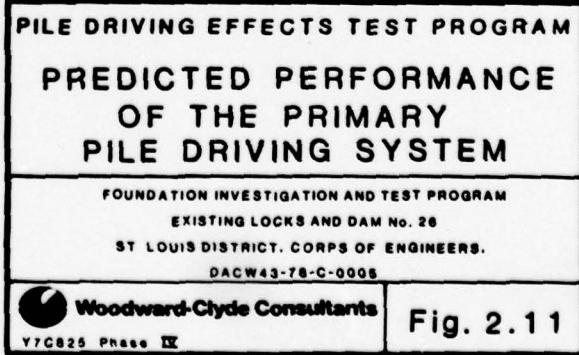
$(\delta_H)_r$  predicted at  
ground surface

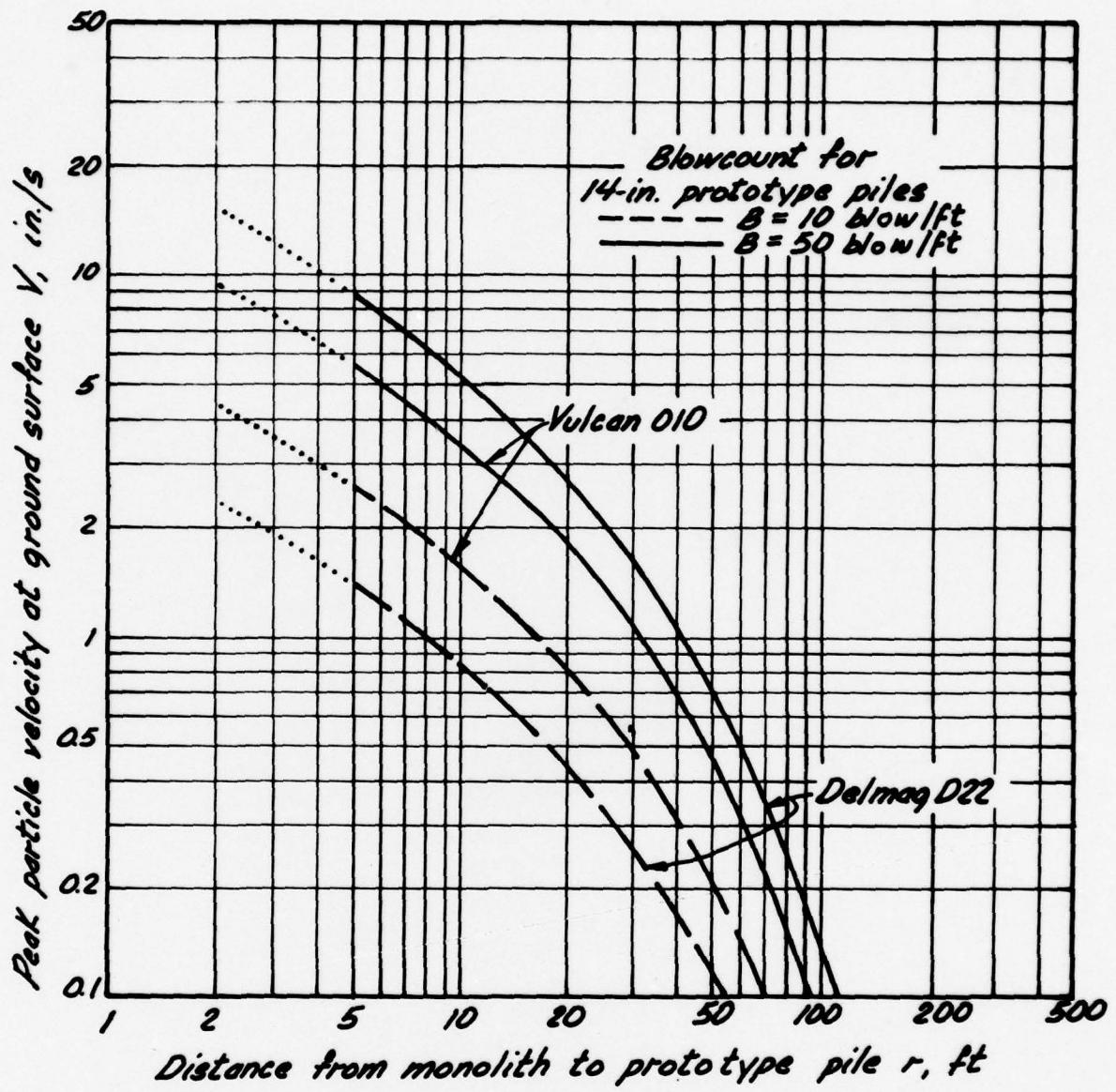
<b>PILE DRIVING EFFECTS TEST PROGRAM</b> <b>PREDICTED MONOLITH</b> <b>DISPLACEMENT CAUSED BY</b> <b>DRIVING WITH DELMAG D22</b>	
<small>FOUNDATION INVESTIGATION AND TEST PROGRAM</small> <small>EXISTING LOCKS AND DAM NO. 28</small> <small>ST LOUIS DISTRICT, CORPS OF ENGINEERS.</small> <small>DACW43-78-C-0008</small>	
 Woodward-Clyde Consultants <small>Y7C825 Phase IX</small>	<b>Fig. 2.10</b>



Note:

Primary pile driving system:  
HP 14 x 73 driven with  
Vulcan O10 hammer



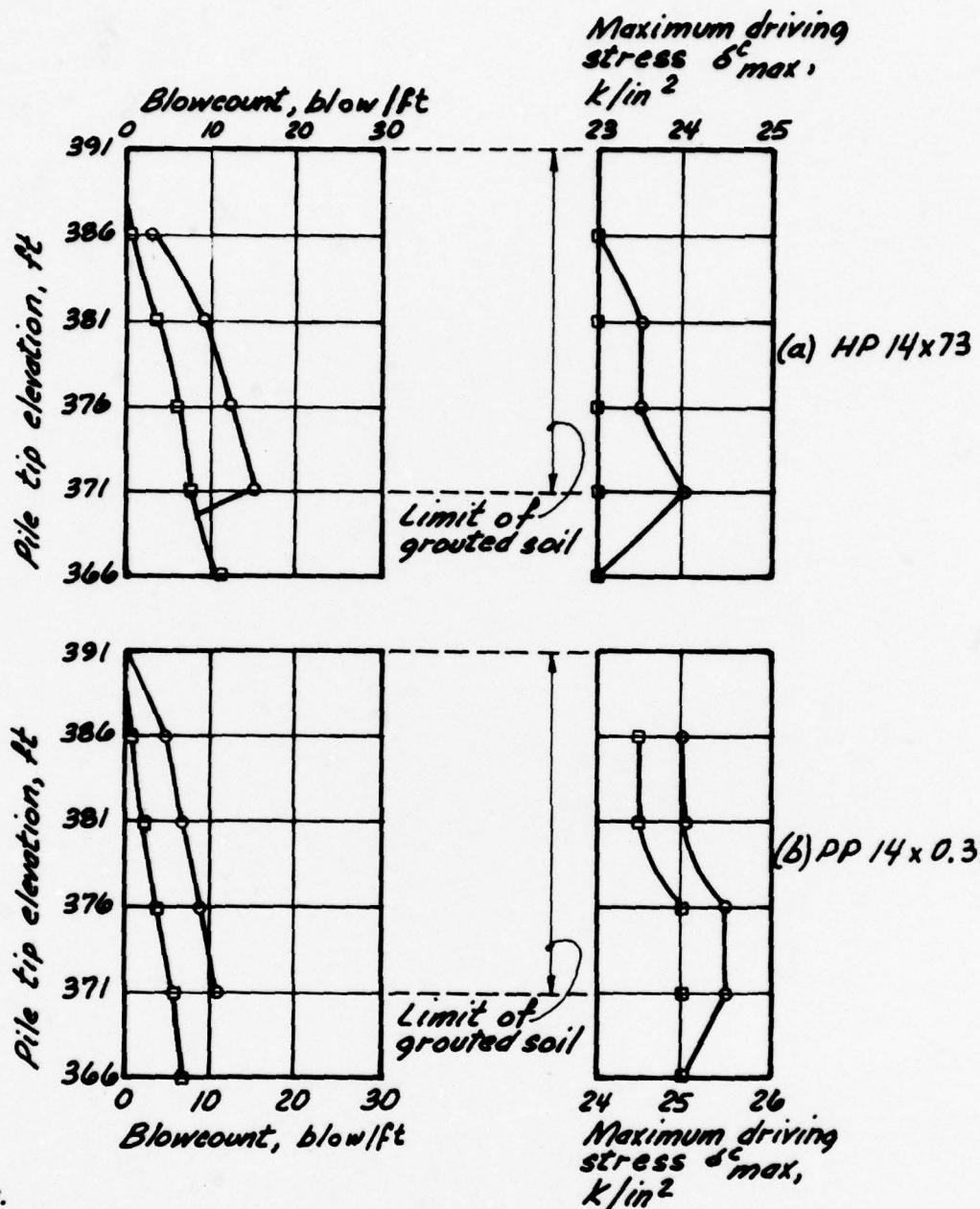


PILE DRIVING EFFECTS TEST PROGRAM  
PREDICTED PEAK  
PARTICLE VELOCITY AT  
GROUND SURFACE CAUSED  
BY PROTOTYPE PILE DRIVING

FOUNDATION INVESTIGATION AND TEST PROGRAM  
EXISTING LOCKS AND DAM No. 28  
ST. LOUIS DISTRICT, CORPS OF ENGINEERS.  
DACP43-78-C-0008

Woodward-Clyde Consultants  
Y7C825 Phase IV

Fig. 2.12

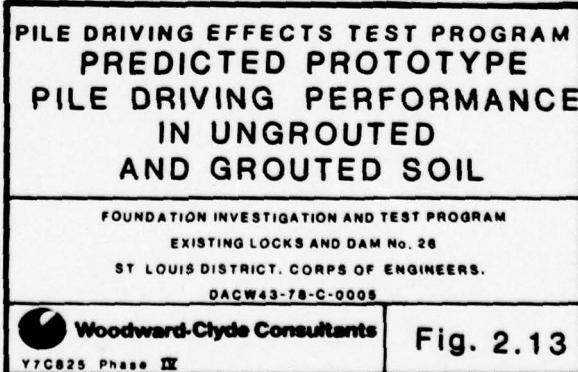


**Legend:**

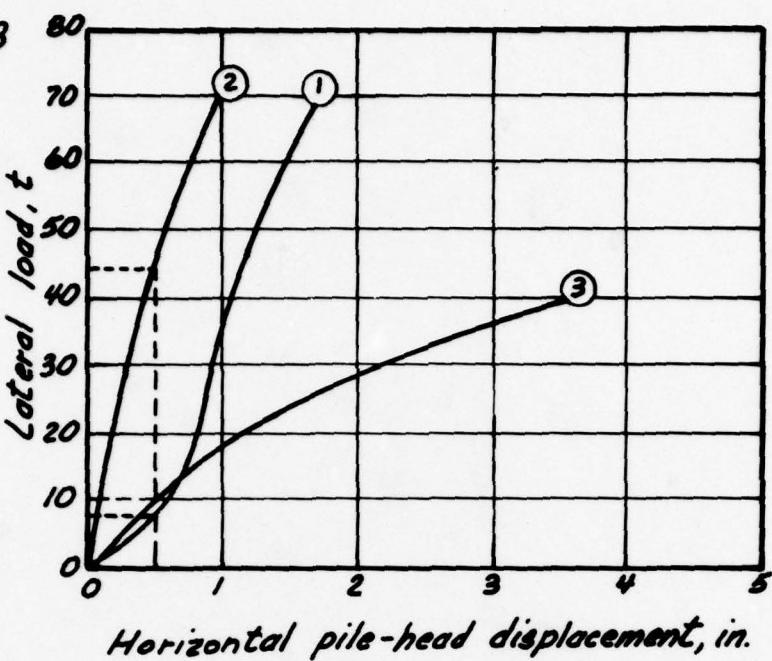
- Predicted driving resistance through grouted soil
- Predicted driving resistance and stress through ungrouted soil

**Note:**

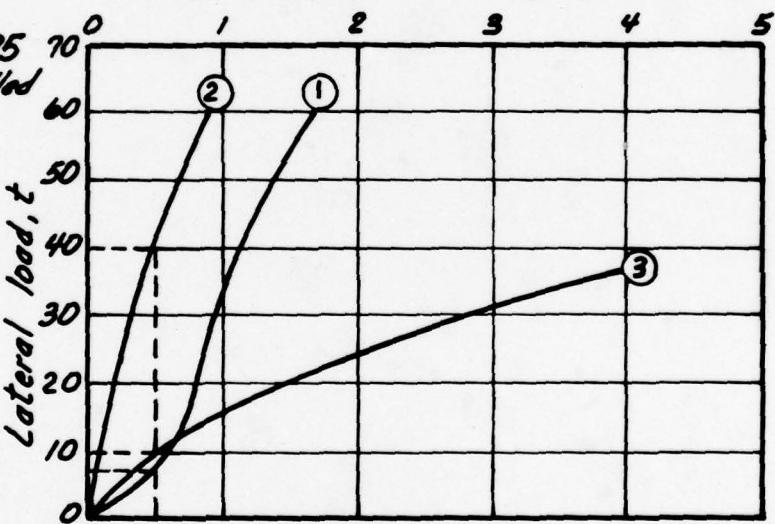
Results based on WEAP analysis



(a) HP 14x73



(b) PP 14 x 0.375  
concrete filled

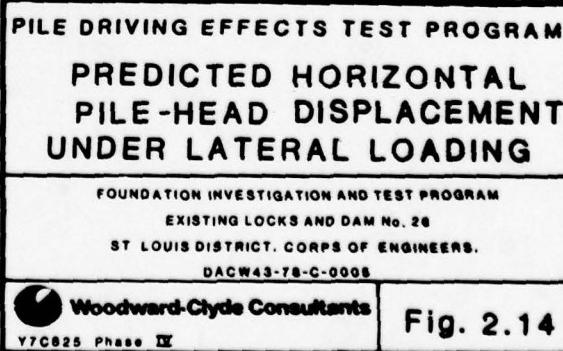


*Legend*

- ① Pregrouted soil
- ② Postgrouted soil
- ③ Ungrouted soil

*Note:*

Results based on  
beam-col 67 analysis



**PHASE IV REPORT**

**VOLUME III**

**RESULTS AND INTERPRETATION OF  
PILE DRIVING EFFECTS TEST PROGRAM**

**SECTION 3  
INSTRUMENTATION**

### 3 INSTRUMENTATION

#### 3.1 INSTRUMENTATION REQUIREMENTS

##### 3.1.1 General Requirements

The instrumentation required for the pile driving effects tests was complex and extensive. It was designed to satisfy the primary and secondary objectives of the test program by monitoring the significant aspects of performance. The instrumentation was designed to:

- (1) measure the response of the test monoliths in grouted and ungrouted soil during nearby prototype pile driving;
- (2) monitor the performance of the prototype piles during driving into ungrouted and grouted soil;
- (3) monitor the wave propagation behavior in soil during prototype pile driving;
- (4) measure the response of timber piles in grouted and ungrouted soil during nearby prototype pile driving;
- (5) measure the response of the soil mass during nearby prototype pile driving;
- (6) measure the ultimate load capacity of single timber piles and groups of timber piles in grouted and ungrouted soil;
- (7) monitor the performance of timber piles during their driving; and
- (8) measure the ultimate lateral load capacity of instrumented prototype piles driven through ungrouted and grouted soil.

The instrumentation installed and monitored during the program is listed in Table 3.1. The instrumentation is discussed in detail in the following sections.

##### 3.1.2 Response of Monoliths During Nearby Prototype Pile Driving

**Scope of Instrumentation.** During driving of prototype piles, the response of the monoliths was monitored by measuring (Fig. 3.1):

- (1) permanent displacements of the monoliths;
- (2) applied axial and lateral loads; and
- (3) transient movement of the monoliths.

**Permanent Displacements.** Permanent (static) displacements of the monoliths were measured using:

- (1) displacement gages consisting of linear potentiometers and dial gages attached to survey-controlled reference beams. The linear potenti-

ometers were read through the automatic data acquisition system (Section 3.2.6). The dial gages were read and the readings were recorded manually;

- (2) optical survey (vertical and horizontal) of the reference beams and directly of reference points installed on the monoliths; and
- (3) two-dimensional tiltmeters located on top of each monolith.

**Applied Loads.** Loads applied to the monoliths by the test jacks were monitored with load cells. Depending on the applied load level, load cells having a capacity ranging from 10 t to 350 t were used. The load cells were read both manually using a digital millivoltmeter and through the automatic data acquisition system.

**Transient Movement.** Three-dimensional velocity transducers (geophones) were installed on or near the top of the monolith. The geophones were read and the results recorded using a dynamic data acquisition system (Section 3.2.7).

### **3.1.3      Performance of Prototype Piles During Driving**

During driving of prototype piles, the pile penetration resistance was monitored in terms of blowcount expressed as hammer blows per foot of penetration. The response of the pile butt was monitored using:

- (1) one or two accelerometers mounted near the butt of each prototype pile;
- (2) one or two strain transducers mounted near the butt of each prototype pile; and
- (3) a Pile Driving Analyzer system, which included a field analog computer (analyzer), a two-channel storage oscilloscope, and a four-channel magnetic tape recorder.

This dynamic measurement and analysis system was used for evaluation of the following, for any given hammer blow:

- (1) the maximum energy ( $E_{max}$ ) transmitted to the pile;
- (2) values (maxima and time histories) of force, velocity, and acceleration at the pile butt; and
- (3) an estimated value of dynamic resistance to penetration  $R_{ult}$ .

### **3.1.4      Wave Propagation in Soil**

During driving of prototype piles, seismic waves were monitored using three-level arrays of three-dimensional geophones installed at designated locations (Fig. 3.2). The geophones were installed at approximate depths of 1 ft, 15 ft, and 50 ft below ground surface to measure soil particle velocities induced by prototype pile driving both in the free field and near the test monoliths. The geophones were

read and the results were recorded using a dynamic data acquisition system (Section 3.2.7).

### **3.1.5      Response of Timber Piles During Nearby Prototype Pile Driving**

**Scope of Instrumentation.** During driving of prototype piles, the response of timber piles supporting the test monoliths was monitored by measuring:

- (1) timber pile permanent deflection;
- (2) cap-pile-soil load transfer; and
- (3) temperature distribution along the pile shafts.

**Timber Pile Permanent Deflection.** Permanent deflection of timber piles was measured using (Fig. 3.3):

- (1) small-diameter inclinometer casings installed on the four corner piles of each monolith M1 through M5 and on the single piles of monoliths M6 and M7;
- (2) four-position rod-extensometers (telltale) attached to linear potentiometers installed on all the monolith timber piles.

These instruments were read manually at various intervals during testing.

**Cap-Pile-Soil Load Transfer.** The manner in which applied lateral and axial loads were transferred from the concrete monolith cap to each timber pile and then to the soil was measured. The required instrumentation included (Fig. 3.3):

- (1) strain gages mounted on all monolith timber piles, except for two piles under monolith M5. The strain gages were read through the automatic data acquisition system (Section 3.2.6); and
- (2) four-position rod extensometers (telltale) attached to linear potentiometers and read manually. All monolith timber piles were instrumented with telltales.

Most timber piles were instrumented with seven levels of four strain gages each. Only six of the eight piles of monolith M5 were instrumented with strain gages. Four of those six piles and the single pile under monolith M6 had eleven levels of four strain gages each for monitoring deep pile-soil load transfer during axial load testing to failure; the other two instrumented piles of monolith M5 had seven levels of strain gages.

**Temperature Distribution.** Twenty-six thermocouples were embedded in epoxy near selected strain gage locations to provide means of measuring temperature distribution along the pile shafts.

### 3.1.6 Response of Soil Mass During Nearby Prototype Pile Driving

**Scope of Instrumentation.** During driving of prototype piles, the response of the soil mass, both in the free field and in the vicinity of the monoliths, was monitored by measuring:

- (1) permanent deformation of the soil mass;
- (2) particle velocity at depth (Section 3.1.4);
- (3) porewater pressure at various depths; and
- (4) temperature.

**Permanent Deformations Within the Soil Mass.** Permanent static deformations within the soil mass were measured using (Fig. 3.2):

- (1) settlement points installed at or near the ground surface; and
- (2) three-dimensional deformation gages, consisting of inclinometer casings and magnetic settlement devices (Sondex rings) installed at various depths around the inclinometer casing.

**Porewater Pressure.** Porewater pressure in the soil mass during driving of prototype piles was measured using piezometers installed in two-unit arrays at depths of 5 ft and 15 ft below the ground surface.

**Temperature.** Up to six thermocouples were used at various times to measure near-surface ground and air temperature.

### 3.1.7 Static Load Testing of Monoliths

**Scope of Instrumentation.** During cyclic preloading and static load testing of the monoliths, the following parameters were measured:

- (1) applied loads;
- (2) monolith displacements;
- (3) timber pile deflections; and
- (4) cap-pile-soil load transfer.

**Applied Loads.** Load cells and jack gages were used to monitor applied loads during load testing (Section 3.1.2).

**Monolith Displacements.** Monolith displacements were measured as discussed in Section 3.1.2.

**Timber Pile Deflections.** Timber pile deflections were measured as discussed in Section 3.1.5.

**Cap-Pile-Soil Load Transfer.** Cap-pile-soil load transfers were measured using:

- (1) strain gages mounted on the timber piles (Section 3.1.5); and
- (2) four-position rod-extensometers and linear potentiometers (Section 3.1.5).

### 3.1.8 Driving Performance of Timber Piles

During monolith construction, driving and restriking of the timber piles were monitored in terms of blowcount. The dynamic response at the pile butt was also measured using the instrumentation system described in Section 3.1.3, that is:

- (1) one or two accelerometers;
- (2) one or two strain transducers; and
- (3) the pile driving analyzer system.

### 3.1.9 Lateral Load Tests on Prototype Piles

**Scope of Instrumentation.** During lateral load testing of six prototype piles, the performance of the piles was monitored by measuring (Fig. 11.2, Section 11):

- (1) applied load;
- (2) pile-head displacement and slope;
- (3) bending stress distribution; and
- (4) pile deflection at depth.

**Applied Loads.** A 100-t load cell was used to measure applied lateral load (Section 3.1.2).

**Pile-Head Displacement and Slope.** Pile-head displacement and slope were measured with dial gages mounted at the ground surface and 18 in. above ground surface.

**Bending Stress Distribution.** Stress distribution along the pile shaft was obtained from measurements by strain gages mounted on the prototype piles (Fig. 3.4).

**Pile Deflection at Depth.** Pile deflections were monitored using a small-diameter inclinometer attached to each prototype pile shaft (Fig. 3.4).

## 3.2 DESCRIPTION AND GENERAL EVALUATION OF INSTRUMENTATION

### 3.2.1 Optical Instrumentation and Controls

As stated in Section 2.3, the primary aspect of performance of first priority was the permanent displacements of the test monolith during prototype pile driving. Although sophisticated electrical instrumentation (linear potentiometers and automatic data acquisition system) was routinely used to track monolith displacements almost continuously, absolute displacements were always referenced to a fixed vertical benchmark or to fixed horizontal control points. This was done either by direct measurements of control points on the monolith or by indirect measurements of control points on reference beams, using a Wild NAKI self-leveling level and a Wild T2 theodolite.

**Vertical Benchmark.** An as-built sketch of the vertical benchmark used for the pile driving effects tests is shown in Fig. 3.5. The benchmark was located in the southwest corner of the test area (Fig. 2.3). Surveying rods and machinist's scales were used for the vertical surveys.

**Horizontal Control Points.** Two pairs of horizontal control points were installed at both extremities of the monolith trench (Fig. 2.3). An as-built sketch of the horizontal control points is shown in Fig. 3.6. A specially designed vernier caliper was used for the horizontal surveys.

**Reference Beams.** Two removable reference beams were used to mount linear potentiometers and dial gages used for automatic tracking of the monolith and timber pile displacements. As-built sketches of the reference beams and their foundations are shown in Fig. 3.7. The reference beams were not perfectly stationary, and their displacement was measured often during testing. These measurements were used to correct data obtained using linear potentiometers and dial gages.

### 3.2.2 Monolith Instrumentation

Several types of instruments were mounted on the monoliths or on the portion of the timber piles above ground.

**Survey Points.** Direct optical measurements were made on the monoliths during testing. Vertical survey points were 1-in.-dia steel hex-head bolts affixed to the concrete and read with a level and a machinist's scale graduated to 0.01 in. Horizontal survey points were mounted on angle or channel brackets screwed into the concrete, and protruding on the front and back of the monolith. The horizontal survey points were read using a theodolite and a specially designed vernier caliper.

**Dial Gages.** Dial gages were used to measure displacements of monoliths and timber piles in three directions:

- (1) y: direction of applied lateral load, approximately north;
- (2) z: vertical; and
- (3) x: direction perpendicular to applied lateral load, approximately east.

Starrett dial indicators were used (operating range: 2, 3, or 4 in.; graduation: 0.001 in.). The dial gages were mounted on angle brackets welded to the reference beams and bore on chromed, steel cubes screwed to the monoliths and the timber piles, as shown in Fig. 3.8. The dial gages were read and recorded manually.

**Linear Potentiometers.** Each dial gage was paired with a linear potentiometer, mounted on the same bracket and bearing on the same surface. Sinco Model 51703, spring-activated potentiometers were used (operating range: 2 or 4 in.; sensitivity: operating range  $\times 10^{-3}$ ). These potentiometers were connected to the automatic data acquisition system (Section 3.2.6) and were read very often during testing. Dial gage and linear potentiometer data compared well throughout the program.

**Tape Extensometers.** Relative displacements between monoliths were measured using two Sinco tape extensometers (operating range 100 ft; sensitivity:  $\pm 0.001$  in.). The tape extensometers were stretched between survey points mounted on monoliths and reference beams. Data obtained using the tape extensometers were affected by changes in temperature. They were also sensitive to the operator's technique.

**Tiltmeters.** The rotation of the monoliths was measured directly using a Sinco tiltmeter (operating range:  $\pm 30^\circ$  from vertical; sensitivity:  $10^{-4}$ ). The ceramic base plates on which the portable readout unit was placed for measurements were affixed by epoxy to the top surface of the monolith. Results of tiltmeter measurements did not compare very well with rotation values calculated from horizontal and vertical displacement measurements. Difficulties were often experienced with chipping and breaking of the knobs of the ceramic plates. The tiltmeters appeared to have been affected by the cold temperatures experienced during testing.

**Geophones.** Particle velocity measurements were made directly on the monoliths. One to three geophones were mounted on the monoliths during prototype pile driving. The geophones were Mark Products Model L-15B (standard frequency range: 4.5 to 40 Hz). The geophones were connected to a dynamic data acquisition system (Section 3.2.7). Geophone data were very consistent.

**Load Cells.** The axial load was applied to the  $2 \times 4$ - and  $3 \times 4$ -pile monoliths by a tandem of two hydraulic rams. A beam load cell custom-designed and built by Evergreen Weigh, Inc, Seattle, (operating range: 0 to 200 t; sensitivity: 0.05 percent of full range) was placed under each vertical ram. The load cells were provided with a Teflon skid pad and a ball and socket assembly to allow relatively free horizontal displacement. For monolith M5, which was axially loaded up to 800 t, 250-t and 360-t cylindrical load cells (Evergreen Weigh) were used under the vertical hydraulic rams. The lateral load, or the axial load of the single pile monoliths, was also applied to the monoliths by a tandem of hydraulic rams. A cylindrical load cell built by Evergreen Weigh, Inc (operating range: 0 to 10 t, 0 to 50 t, or 0 to 100 t; sensitivity: 0.5 percent of full range) and a ball and socket assembly were intercalated between the ram and the reaction frame. The load cells were read manually on a continuous basis using a digital millivoltmeter, and were also connected to the automatic data acquisition system. The load cells performed very well throughout the program.

### **3.2.3 Timber Pile Instrumentation**

The 46 timber piles supporting the six test monoliths were heavily instrumented, as shown in Fig. 3.3. The instrumentation installation was done off-site in Seattle. The instruments were installed in longitudinal grooves in the piles and sealed with epoxy (Sikadur Hi-Mod HV).

**Strain Gages.** The strain gages used were Micromeasurements Model CEA-06-125UW-350 (nominal resistance:  $350\ \Omega$ ; strain range:  $30,000\ \mu\epsilon$ ; sensitivity: 2 to 4  $\mu\epsilon$ ) constantan on foil with polyamide backing. From the results of a

pilot test program (Section 3.3.1), it was determined that the best method of strain gage installation was to mount the gages on 3/8-in.-dia aluminum tubing and embed the tubes in the grooves with epoxy. Four gages were installed at each gaging level. Generally, seven gaging levels were located in the upper 20 ft of the timber piles (Fig. 3.3). For four piles under monolith M5 and for the single pile of monolith M6, eleven gaging levels were used along the entire length of the piles to detect complete strain distribution during axial load testing to failure. The strain gages were connected to the automatic data acquisition system (Section 3.2.6). The performance of the timber pile strain gages is discussed in Section 3.3.

**Telltale.** Axial deflections of the timber piles during testing were measured using telltales embedded in epoxy-filled grooves in the piles. The telltales consisted of rod-extensometers anchored at four different levels along the piles, and attached to linear potentiometers connected to the top of the piles. The extensometers consisted of a 1/4-in.-dia, stainless steel inner rod, sheathed with a 1/2-in.-dia PVC tubing. The potentiometers (similar to those described in Section 3.2.2) were read manually using a Sinco digital extensometer indicator. Although the telltales appeared to have performed generally well, they were not very sensitive ( $1 \mu\epsilon = 6 \times 10^{-5}$  in. for a 5 ft gage length) and were affected by temperature variation.

**Inclinometer Casings.** Horizontal deflections of the timber piles during testing were monitored using an inclinometer casing embedded in an epoxy-filled groove in the piles. The four corner piles of the 2 x 4 monoliths (M2, M3, and M5), six piles of monolith M1 (3 x 4), and the single piles under monoliths M6 and M7 were instrumented with 1.9-in.-od, 1.5-in.-id, flush coupled, ABS plastic inclinometer casings, supplied by Sinco. The casings were surveyed manually with Sinco Model 50325 inclinometer probe attached to Sinco Model 50309 digitilt indicator (operating range: 0 to 30° from vertical; sensitivity:  $\pm 0.005$  ft/100 ft of casing). Pile inclinometers performed well throughout the program. The inclinometers mounted on the single timber piles of monoliths M6 and M7 were rendered inoperable during concrete cap construction due to excessive bending of the casing to install steel reinforcement.

**Thermocouples.** Temperature measurements were made using Type T copper-constantan thermocouples manufactured by Medtherm Corp. The thermocouples were read using a portable, calibrated, digital millivoltmeter. They performed well throughout the program.

### 3.2.4 Ground Instrumentation

The following instruments were installed in the ground to measure soil mass response during prototype pile driving.

Type of Instrument	Number of Instruments	Comments
Surface reference point	28	Rebar installed 2 ft below ground surface
3-D deformation gage	18	Inclinometer casings fitted with Sondex rings
Piezometer	29	Pneumatic pore pressure transducers installed at various elevations
3-D geophone	38	Installed at various elevations
Casing for shear wave velocity measurements	12	50-ft-long, 4-in.-dia PVC or steel casings grouted with cement in boreholes

**Surface Reference Points.** The surface reference points consisted of a No. 6 reinforcing steel bar with a diagonal saw cut at the top. An as-built sketch is shown in Fig. 3.9.

**3-D Deformation Gages.** The three-dimensional (3-D) deformation gages consisted of Sondex rings attached to a PVC inclinometer casing (Sinc 2.75-in.-od casing). The Sondex rings were placed 5 ft to 10 ft apart along the casing. They consisted of stainless steel wire loops, attached to 12-in.-long segments of thin, corrugated polyethylene casing. The segments of polyethylene casing were attached to the PVC casings using plastic tape. A bentonite paste was inserted between the two casings to reduce friction. This installation method was developed in the field on the basis of observations made earlier during the chemical grouting test program (Section 8, Volume II). An as-built sketch of a 3-D deformation gage is shown in Fig. 3.10. Measurements were made using an inclinometer readout (Section 3.2.4) and a Sinc Model 50812 Sondex settlement probe (operating range: 250 ft; sensitivity: 0.01 in.). The reliability of horizontal displacement measurements using the inclinometers was satisfactory. All inclinometers functioned reliably. The accuracy of the instrumentation appeared to be about 0.01 ft. The reliability of settlement measurements using the Sondex rings was greatly improved from that experienced in the chemical grouting test program (Section 8.2.3, Volume II). Frequency of readings was low due to the long time required for a complete set of readings. Therefore, data base was too small to allow meaningful interpretation. The system accuracy appeared to be larger than 0.005 ft.

**Piezometers.** Porewater pressure was measured during testing using Sinc Model 51481 pneumatic pore pressure transducers and a Sinc Model 51411 precision indicator (operating range: 0.60 lb/in<sup>2</sup>; sensitivity: 0.006 lb/in<sup>2</sup>). A typical as-built sketch of a piezometer installation is shown in Fig. 3.11. In some cases, two pore pressure transducers or one pore pressure transducer and two geophones were installed in the same borehole. In all cases, biodegradable drilling fluid

(Revert) was used for piezometer installation. The piezometer leads were fed into a manifold system that enabled reading several instruments at the same time from a sheltered, remote location. The accuracy of the piezometers was approximately 0.5 lb/in<sup>2</sup> or about 1 ft of water. The piezometers reflected well the static groundwater level. They did not detect any pore pressure changes; however, such transient changes were not expected to be of sufficient magnitude to affect response of the test structures.

**Geophones.** A typical installation of ground geophones is shown in Fig. 3.12. Two materials were used to backfill the installation boreholes: low-strength plastic grout and pea gravel. Geophone data indicate that the instrument response did not appear to be affected by the backfilling material. Movable surface geophones were installed 1 ft below ground surface at various locations during testing. The instruments were similar to those described in Section 3.2.2. All geophones performed well throughout the program.

**Shear Wave Velocity Casings.** Cross-hole shear wave velocity measurements were made at several stages of testing. The measurements were made using permanent casings installed in boreholes. The equipment used was developed by WCC and is manufactured by Bison Instruments (Mirafuente et al 1975). The energy signal source consisted of a down-hole hammer jacked against the wall of a 5-in.-dia steel casing grouted with cement in a 6-7/8-in.-dia borehole (PD-S3 and PD-S8, Fig. 3.10). The down-hole hammer is designed such that an uniaxial impact is imparted along the axis of the borehole. The direction of impact, however, can be either upward or downward, providing for symmetrical reversal of impact motion. The polarity of the first arrival shear wave can be reversed by reversal of impact motion. The shear wave motions detected along the vertical axis of the source are uniquely reversed with source reversal, while other seismic waves generated have constant polarity independent of source impact direction. The signal generated by the hammer was detected in four sets of boreholes (for example, PD-S1 and PD-S2) using pairs of vertical geophones placed at the same depth as the hammer in two adjacent boreholes. The geophones were housed in PVC capsules containing both a geophone and a pneumatic bladder that was inflated to couple the capsule firmly to a 3-in.-dia PVC casing. Seismic wave data detected by the geophones were fed to a storage oscilloscope and a multi-channel signal enhancement seismograph, where trace and arrival time were displayed. Polaroid photographs of the screen displays were taken for each recording. Shear wave velocity was calculated from arrival times and distances between boreholes. Borehole inclinometer measurements were made in each of the ten shear wave boreholes to determine the precise distances between source and receiver at any depth.

### **3.2.5      Steel Pile Instrumentation**

Three H piles (HP 14 x 73) and three pipe piles (PP 14 x 0.375) were instrumented and used for lateral load tests (Section 10). The instrumentation consisted of strain gages and inclinometer casings. The strain gages were similar to those described in Section 3.2.3, except that they were mounted on steel shim stock, which was in turn welded to the steel pile surface. The inclinometer casings were similar to those described in Section 3.2.3. The inclinometers performed well

throughout the program. The performance of the strain gages is discussed in Section 3.4.

### 3.2.6 Automatic Data Acquisition System (Cyber II)

Load cells, strain gages on the timber piles, and linear potentiometers used to track monolith and timber pile displacements were connected to an automatic data acquisition system. The automatic data acquisition system was a microcomputer designed and programmed to acquire, process, or playback data from voltage- or bridge-type transducers. The equipment consisted of a 320-channel Cyber II system manufactured by Cyber Systems, Inc plus linkage cables, connectors and junction boxes between the sensors and the measurement and recording components.

The automatic data acquisition system performed remarkably well. The presence of a full-time service engineer, completely familiar with system hardware and software, made the Cyber II system very reliable. Use of the system for instrumented timber pile recalibration at the site (Section 3.3.4), not only expedited that effort, but also provided an opportunity to establish efficient hardware and software usage and troubleshooting procedures. During actual testing, the interactive software-oriented features of the system made the operation particularly flexible. The microcomputer calculation capabilities made possible immediate on-line evaluation of primary test results, which provided savings in time and manpower. Most of the difficulties experienced with the system were related to connectors, cables, and junction boxes exposed to a difficult field environment. Detailed description of Cyber II is given in Appendix I, Volume IIIA.

### 3.2.7 Dynamic Data Acquisition System (Geophones)

Geophones were connected to a dynamic data acquisition system designed to accommodate simultaneous signals from 54 channels (that is, eighteen 3-D geophones) on three paper-strip-chart recorders, thus providing full geophone monitoring capability during any one pile driving effects test step. Additional features allowed simultaneous recording of peak vectorial particle velocity for any four of the eighteen 3-D geophones, and simultaneous recording of data from 12 of the 54 channels on two analog magnetic tape recorders. Detailed description of the dynamic data acquisition system is given in Appendix I, Volume IIIA.

The geophone data collection system proved to be highly reliable in terms of performance, and the agreement between results recorded by each system component was found to be very good. Operation of the equipment during a test required personnel thoroughly familiar with system usage due to the large volume of data being generated. System calibration, maintenance, and data documentation efforts produced a complete record of the vibrations monitored during the test. Digitization of analog magnetic tape records was accomplished on site successfully, providing processed data for more rigorous analyses of the observed vibration characteristics.

### **3.2.8      Pile Driving Analyzer System**

Driving of every timber and a number of prototype piles was monitored using a pile driving analyzer system. The system consisted of one or two accelerometers and strain transducers attached near the top of the pile to be driven and of an analyzer (field analog computer) manufactured by Pile Dynamics, Inc. Auxiliary equipment included a two-channel storage oscilloscope and a four-channel analog magnetic tape recorder. Detailed description of the pile driving analyzer is given in Appendix I, Volume IIIA.

The pile driving analyzer system performed very well during timber pile installation operations; however, during the course of prototype pile driving, a number of factors rendered the system partially or completely inoperable at times. Difficulties generally involved damage to transducers, cable connections, and the transmission cable, which resulted from the vulnerability of these components to handling by the pile driving crew. For timber pile driving measurements, the transducers were installed after the piles were jetted and seated, generally within a few feet of final penetration, whereas continuous monitoring of prototype pile driving was attempted from beginning of driving to refusal. Nevertheless, documentation of the pile driving system's performance was sufficiently complete for the test program purposes so that significant trends could be established, as discussed in Section 7.3.1.

### **3.2.9      Details of Instrumentation for Monolith M2**

Most detailed analyses of test data presented in this report pertain to monolith M2. The instrumentation associated with this monolith is described in detail in Fig. 3.13. Instrumentation for other monoliths was very similar.

## **3.3            CALIBRATION OF INSTRUMENTED TIMBER PILES**

### **3.3.1      General**

The calibration of the timber piles consisted of three different phases. The first phase was primarily a pilot evaluation of different methods of installing strain gages on the timber piles. As part of this pilot program, a calibration method for the strain gages was developed and used in subsequent phases.

The second phase of the pile calibration was performed during the instrumentation of the piles in Seattle, Washington. After each pile was instrumented and curing of all adhesives had taken place, the strain gages were calibrated to relate bending stress to observed strain.

The third phase took place at the test site. This was a repeat of the work performed in Seattle, with supplemental studies.

### **3.3.2      Pilot Test Program**

The primary purpose of this program was to evaluate different methods of installing strain gages on timber piles. At the same time, methods for installing inclinometer casings and telltales were tested.

Three different methods of installing the strain gages were evaluated on two oak piles:

- (1) the gages were mounted on a thin epoxy coating bonded directly to the wood surface;
- (2) the gages were mounted on stainless steel shim stock strips 0.001 in. and 0.003 in. thick and 6 in. long. The strips were then attached to the wood with wood screws; or
- (3) the gages were mounted on 3/8-in.-dia aluminum tubing having a wall thickness of 0.035 in. The tubing was then embedded in epoxy-filled grooves cut in the pile.

In addition, vibrating-wire gages were mounted on the test piles. The installation procedure was to attach the gage with epoxy and four small nails. The exciter/pickup sensor was then placed over the vibrating wire and fixed to the pile with wires and nails. The entire system was then protected by encapsulating it in epoxy.

Load tests were then performed on the instrumented piles to check the performance of all the strain gages in place and to calibrate them. In this operation, the two piles were placed on a bench and were tied together 9 ft from the butt with a cable. The tips were separated by a rigid strut. A hydraulic jack and load cell were placed horizontally between the piles 1.5 ft from the butt. The piles were jacked apart. Strain readings were taken at different jack loads and compared to the theoretical strains computed using engineering mechanics.

From these calibration tests, it was determined that the strain gages mounted directly on the pile and those on the stainless steel strips did not perform satisfactorily. Only the vibrating-wire gages and those mounted on the aluminum tubes performed reliably and predictably.

As part of the pilot test program, the two oak piles were driven near Everett, Washington, in March 1978. After driving, the strain gages were checked to evaluate their survival performance. Most gages mounted on aluminum tubes survived the driving. Vibrating-wire gages and other gages installed by different methods did not perform as well. The two test piles were loaded laterally by jacking them apart, and the strain gage performance checked again. The two piles were extracted several months later in August 1978 to observe gage survival after long-term submergence. The gages mounted on aluminum tubes were generally still operative after extraction.

On the basis of the pilot test program, it was concluded that the best strain gage installation procedure would be to mount the gages on aluminum tubes and embed the instrumented tubes in epoxy-filled grooves cut in the piles. Similarly, telltale assemblies and small-diameter inclinometer casings would be installed in epoxy-filled grooves.

Various types of epoxy were tested during this pilot test program. Sikadur Hi-Mod HV was found to be the most appropriate for the purpose of the testing program. It was found that the uneven shape of the oak piles used in the pilot program seriously complicated grooving and instrumentation installation. The decision was then made to use Douglas fir timber for the piles to be instrumented for the actual tests. Douglas fir piles are straight and have a relatively circular cross section.

### 3.3.3 Initial Calibration in Seattle

After each pile was instrumented and the epoxy cured, the strain gages were calibrated to relate bending stress to observed strain. Although the setup for the calibration was similar to that in the pilot program, its performance was much more rigorous. Prior to testing, careful measurements were made of pile diameter, depth of gage below pile surface, and dimensions and locations of the grooves so that a pile moment of inertia and distance of gages from neutral axis could be accurately computed for each gage.

Each pile was placed in the calibration setup. Details of the setup are given in Fig. 3.14. The straps, jack, and load cell were positioned next. The position of the jacks and straps was selected so that the resulting moment distribution would be similar to that expected during the pile driving effects tests. The pile was aligned so that one pair of diametrically opposed grooves containing strain gages was in the same plane as the jack. These were the gages to be calibrated. The first jack position selected resulted in strain measurements for some gages that obviously were in error. After study, it was concluded that the jack was causing a local stress concentration on the pile surface. As a result, the jack was moved to another location, as shown in Fig. 3.15a. For the piles instrumented with eleven levels of gages (monoliths M5 and M6), the position of the jack and straps was changed to calibrate the lower four gage levels, as shown in Fig. 3.15b.

The first step of pile calibration was to precondition the pile and gages. Preconditioning consisted of cyclically loading the pile four or five times up to the maximum calibration load. Preconditioning was necessary to set the gages and pile. If this were not done, the gages would demonstrate non-linear behavior and show significant zero shifts.

After preconditioning, final adjustments to the calibration setup were made and the strain gages were connected to the readout devices. The readout instrumentation consisted of Vishay SB-1 switch and balance units connected to a Vishay VS-20 strain indicator. The pile was loaded and unloaded in five increments to the maximum calibration load. The maximum load was selected so that the maximum bending stress in the pile was approximately  $6 \text{ k/in}^2$  or about 80 percent of the ultimate strength of the wood. Strain readings were taken at each load from each gage as the pile was being loaded and unloaded. Readings were taken for two load-unload cycles.

After calibration of one set of diametrically opposed gages, the pile was rotated 90 degrees so that the other pair of strain gage grooves was placed in the jack plane. Preconditioning was carried out followed by calibration using two load-unload cycles. A pile was completely calibrated when each gage had been calibrated in both tension and compression.

After all gages had been tested, the strain values were related to the theoretical stress values obtained from engineering mechanics. A linear regression analysis was used to obtain an effective or gage modulus. Separate modulus values were obtained for tension and compression. These modulus values were intended to be used subsequently as multiplier constants in the Cyber II system programs during actual testing. Actually, modulus values obtained during subsequent recalibration of the piles at the site were used.

### **3.3.4 Recalibration of Timber Piles at Test Site**

At the test site, a limited recalibration effort was anticipated. The purpose of this effort was to determine if the modulus values obtained in Seattle significantly changed during transit to the site. The modulus values would change if the water content of the piles was reduced below the fiber saturation point. This became a real concern when the first shipment of piles arrived, having not been continuously soaked since their departure from Seattle because of a breakdown of the watering system installed on the truck. After unloading at the site, these piles were stacked, covered with burlap, and soaked by a spray system. The site spray system was not kept in continuous operation because of difficulties with water supply and contractor staffing over weekends. Eventually, soaking of the piles was done on a continuous basis. The second shipment was kept soaked during transit and was stacked with the first shipment at the site.

The recalibration was carried out using the same equipment and following the same procedure as in Seattle with two exceptions:

- (1) most of the strain gage readings were made using the Cyber II automatic data acquisition system instead of the manual system used in Seattle. This permitted simultaneous reading of all gages on two piles; and
- (2) different load cells were used to measure the load applied by the jack. In the first calibration effort in Seattle, a load cell furnished by Shannon & Wilson, Inc was used. For the calibrations at the test site, load cells purchased from Evergreen Weigh, Inc (Section 3.2.2) were used.

As the recalibration effort proceeded, the results were found to differ significantly from those obtained in Seattle. The modulus values obtained during recalibration were typically 35 percent lower than those obtained during initial calibration. The differences could be due to many factors; among them are load cell calibration and changes in timber properties due to changes in water content. The uncertainties were such that it was decided to recalibrate all the instrumented timber piles at the site.

Initially, the maximum recalibration loads applied to the piles were the same as those used in Seattle. However, during recalibration of pile No. 37, the pile was broken prior to reaching the maximum load. Because of the speed at which the failure took place, it was not possible to reconstruct the conditions leading up to the failure. To reduce the possibility of a recurrence of this incident, the maximum load was limited to 80 percent of that applied in Seattle. At the end of the testing program, pile No. 37 was sliced transversely at the location of the failure. It was found that the growth rings of the timber were eccentric. This weakness may explain the premature failure during calibration.

In addition to the regular calibration tests, two additional studies on gage response were simultaneously undertaken at the site. One study was to determine if the gages would creep under sustained loads. Two piles were positioned in the calibration setup as for a calibration test and loaded to the maximum calibration test load. This load was maintained for approximately two days. Strain gage and thermocouple readings were taken hourly. When the strain gage readings were corrected for temperature effects, it became apparent that the gages or piles did not creep under sustained loads producing up to 800  $\mu\text{in./in.}$  of strain.

The other study was concerned with temperature effects. The strain gages were installed on the piles as quarter-bridges for which temperature compensation was not possible. To study temperature effects, a pile was exposed to the sun for one day. During that day, the thermocouples and the strain gages closest to the thermocouples were read at regular time intervals. It was found that the gages showed an apparent average tensile strain of  $5 \mu\text{in./in.}$  per degree Fahrenheit of temperature increase.

### 3.3.5 Summary of Calibration Results

From the calibration tests performed at the site, modulus values were obtained for all operating strain gages. It was expected that, if the gages were complying with the strains in the wood, the gage modulus would be close to the elastic modulus of wood. Upon examination of the data, it was found that some gages were responding poorly. The response of other gages was questionable. Therefore, a ranking system was initiated to reflect confidence in strain measurements obtained from the gages.

Confidence in strain measurement was based on factors that could affect the gage response. The ranking method consisted of assigning a point value to each factor, and the sum of the points was taken as the rank of the gage. The greater the rank, the greater the confidence in the strain readings from that gage. A rank of zero indicated a useless gage. For each factor, an acceptability criterion was established. These criteria reflected the expected variation and were sufficiently sensitive to render the ranking meaningful. Based on previous experience, general practice, and observations during the calibration efforts, the following five criteria were established.

**Absolute Value of Modulus.** The moduli of the instrumented timber piles were dependent on several factors. The average modulus for Douglas fir is approximately  $1.6 \times 10^6$  lb/in<sup>2</sup> with a coefficient of variation of about 25 percent. This value is for tests on clear, standard-sized specimens under controlled moisture and temperature conditions. For the piles, the coefficient of variation was expected to be larger. The modulus values obtained during calibration averaged  $2 \times 10^6$  lb/in<sup>2</sup>. This higher modulus value was believed to be due to the composite transducer-wood system and the relatively high quality of the piles selected for the test. The criterion of gage acceptance for modulus was selected as  $2 \times 10^6$  lb/in<sup>2</sup>  $\pm 25$  percent or  $1.5 \times 10^6$  to  $2.5 \times 10^6$  lb/in<sup>2</sup>.

**Repeatability.** Repeatability of gage readings is dependent on strain level, accuracy of repeated readings, hysteresis characteristics of the composite system, and gage stability. The criterion of gage acceptance for repeatability was selected such that the difference between strain readings at the highest load level for the two calibration cycles did not exceed 5 percent of the lower reading.

**Resistance to Ground.** The criterion for gage acceptance was that the gage resistance to ground must be at least 50 megohms.

**Linearity.** The linearity of the gages was characterized by the correlation coefficient from the regression analysis used to obtain the gage modulus (Section 3.3.3). To be consistent with the above repeatability criteria, the criterion of gage acceptance for linearity was selected as a correlation coefficient of 0.95 or greater.

**Gage Resistance.** Significant changes in gage resistance after installation would indicate problems with the gage. The criterion of gage acceptance for gage resistance was such that changes in resistance greater than 2 percent were not acceptable.

**Final Ranking.** Using this system, all recalibrated gages were ranked (a few gages were not recalibrated at the site; all these were gages at gaging levels 8 through 11 for piles under monoliths M5 and M6). Seventy percent of the gages had a rank of 5, which was the highest possible. Twenty-two percent of the gages had a rank of 4, and the remaining eight percent, a rank of 3, 2, 1, or 0.

The modulus values obtained from recalibration of the gages having ranks of 4 and 5 were used to calculate stress values with the Cyber II system programs during actual testing. The gages having ranks lower than 4 were not used for data processing.

### **3.3.6      Detailed Calibration Results for Piles Under Monolith M2**

The modulus values in tension and compression and ranks for the gages on timber piles installed under monolith M2 are presented in Appendix J, Volume IIIA.

### **3.4 CALIBRATION OF INSTRUMENTED PROTOTYPE PILES**

#### **3.4.1 Calibration Procedures**

Six prototype piles (three H and three pipe piles) were instrumented and calibrated prior to driving. The calibration set up was similar to that used for timber pile calibration (Section 3.3). Two prototype piles were calibrated at the same time by jacking them apart. Details of the calibration procedures are given in Appendix S, Volume IIIA.

#### **3.4.2 Summary of Calibration Results**

Gage modulus values were calculated from strain gage readings during calibration, using a least-square regression method. Except for eight malfunctioning gages, the gage modulus values ranged from  $29 \times 10^6$  to  $31 \times 10^6$  lb/in<sup>2</sup>. These values were subsequently used for processing test data.

### **3.5 MEASUREMENT PRIORITIES**

The data to be obtained during the various testing phases were ranked in terms of primary and secondary aspects of performance (Section 2.3.1). In a similar fashion, test measurements to be made during prototype pile driving were ranked as follows to be consistent with the test program objectives.

<u>Aspect of Performance</u>	<u>Measurement Number and Rank</u>	<u>Measured Characteristic</u>	<u>Instrumentation Item in Table 3.1</u>
<b><u>Primary (P)</u></b>			
Structural response of monolith	1	-Displacement	1,2,3
	2	-Applied load	4
	3	-Transient motion	5
Prototype pile behavior during driving	4	-Dynamic measurements at pile butt	6,7,8
	5	-Blowcount	-
Wave propagation in soil	6	-Particle velocity	5
<b><u>Secondary (S)</u></b>			
Response of timber piles	7	-Dynamic measurements during their driving	6,7,8
	8	-Blowcount	-
	9	-Horizontal deflection vs depth	9
	10	-Axial and bending strains	10,11
	14	-Temperature	15
Response of soil mass	11	-Surface settlement	12
	12	-3-D deformation at depth	13
	13	-Pore pressure	14
	14	-Temperature	15

The selection of frequency and timing of measurements was based on both the reliability of the results under given conditions (for example, optical survey data were of questionable value during a blizzard) and the relative changes between measurements (for example, pile inclinometers were not measured, a time consuming activity, unless the incremental monolith displacement from the last pile inclinometer measurement exceeded 0.1 to 0.2 in.).

A computer program included in the Cyber II system software was used to compute immediately rigid-body displacements of the monolith relative to the reference system using linear potentiometer data. Periodic surveys were made to monitor reference system displacements and correct the data acquired automatically. A programmable calculator (Hewlett-Packard HP 67 or HP 97) was used to reduce manually acquired linear potentiometer dial gage data to rigid-body displacements using the same basic algorithm as the Cyber II system.

ITEM NO.	INSTRUMENT	NO. OF UNITS USED	MEASUREMENT	ASPECT OF PERFORMANCE
1	Displacement gage rod-extensometer, linear potentiometer, and dial gage	60	Permanent monolith and timber pile displacement	Structural response during nearby pile driving and static load testing
2	Optical survey with level and theodolite	N/A	Same as above	Same as above
3	Two-dimensional tiltmeter	6	Permanent monolith rotation	Same as above
4	Load cell	4	Lateral loads on M6 and M7	Same as above
		8	Axial loads, preloading and dynamic testing, M6 and M7	
		8	Axial loads, preloading and dynamic testing, M1 through M5	Same as above
			Lateral loads, preloading and dynamic testing, M1 through M5	
			Axial loads, static load testing, M6 and M7	
		2	Axial loads, static load testing, M1, M2, and M3	Same as above
			Lateral loads, static load testing, M1, M2, and M3	
5	Geophone	38	Particle velocity on monolith	Response of monolith during nearby pile driving
			Particle velocity at ground surface and at depth	Response of soil mass during nearby pile driving
6	Accelerometer	2	Impact acceleration at pile butt	Driving performance of prototype piles and timber piles
7	Strain transducer	2	Impact strains at pile butt	Same as above
8	Pile Driving Analyzer System	1	Maximum energy and force transferred at pile butt	Same as above
9	Small diameter inclinometer	22	Permanent horizontal deflection of timber piles	Response of timber piles during nearby pile driving and static load testing
10	Four-position rod-extensometer with linear potentiometer	38	Permanent vertical deflection of timber piles	Same as above
11	Thermocouple	26	Temperature distribution along pile shaft	Same as above
12	Strain gage	1344	Strain along timber pile	Response of timber piles during nearby pile driving and static load testing Cap-pile-soil load transfer
13	Surface settlement points	39	Settlement	Response of soil mass during nearby pile driving and static load testing
14	Three-dimensional deformation gage	18	Deformation within soil mass	Same as above
15	Piezometer	29	Pore Pressure	Same as above

PILE DRIVING EFFECTS TEST PROGRAM	
LIST OF INSTRUMENTATION	
FOUNDATION INVESTIGATION AND TEST PROGRAM EXISTING LOCKS AND DAM No. 20 ST. LOUIS DISTRICT, CORPS OF ENGINEERS. BACW43-FB-C-0000	
Woodward-Clyde Consultants VTC826 Phase II	Table 3.1

AD-A076 093 WOODWARD-CLYDE CONSULTANTS CHICAGO IL  
RESULTS AND INTERPRETATION OF PILE DRIVING EFFECTS TEST PROGRAM--ETC(I)  
JUL 79 J PEREZ , D M HOLLOWAY

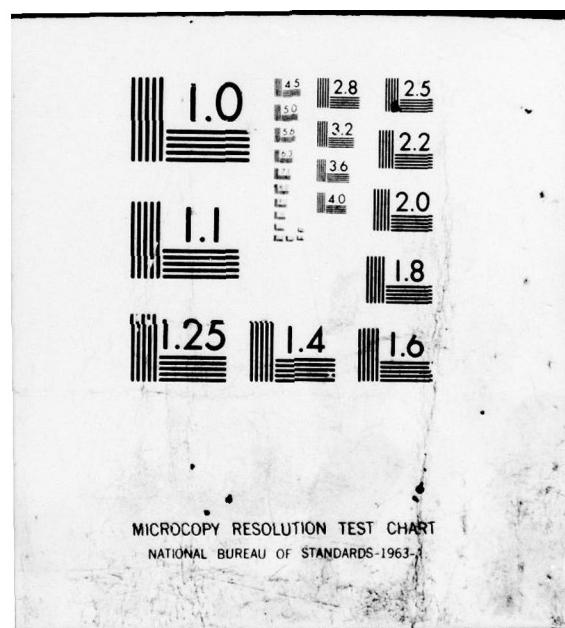
F/G 13/2  
DACP43-78-C-0005

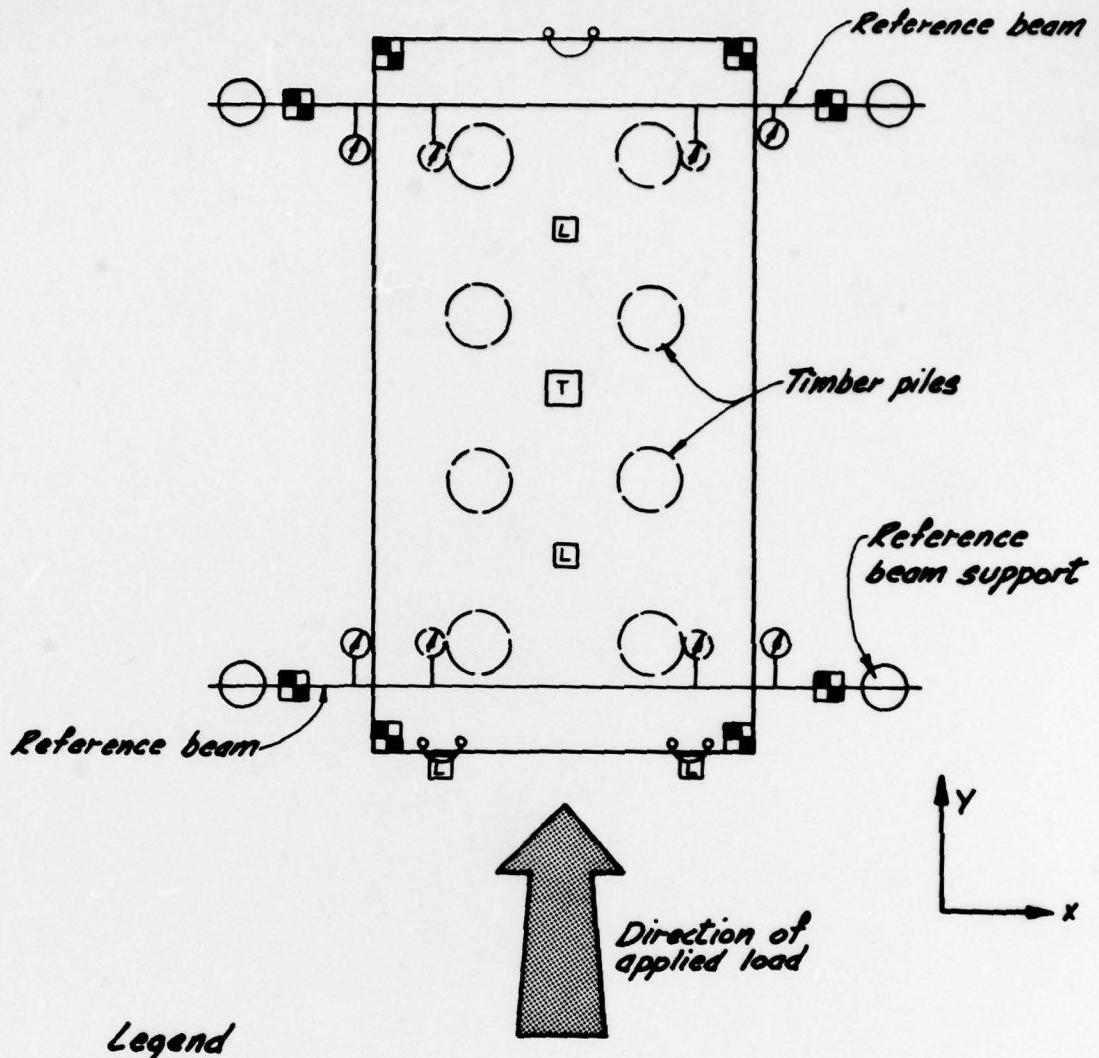
NL

UNCLASSIFIED

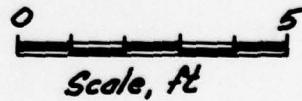
2 OF 5  
AD  
A076093



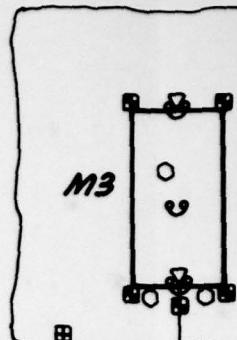
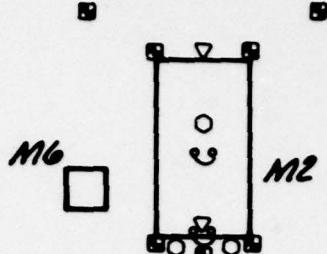
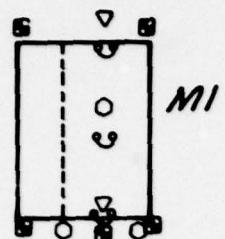




- Legend**
- Surface reference point on monolith or reference beam
  - ① 3-D ( $x, y, z$ ) displacement gages (linear potentiometer and dial gages) on monolith
  - ② 3-D ( $x, y, z$ ) displacement gages (linear potentiometer and dial gages) on timber piles
  - 3-D geophone
  - Load cell
  - Tiltmeter



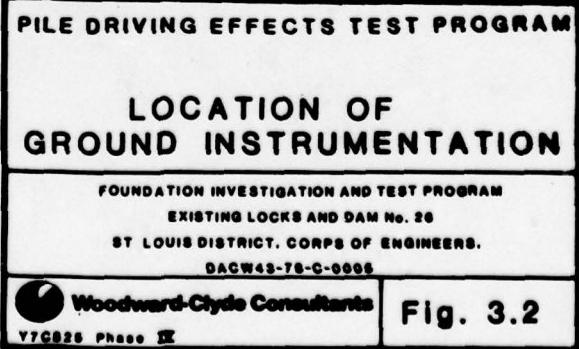
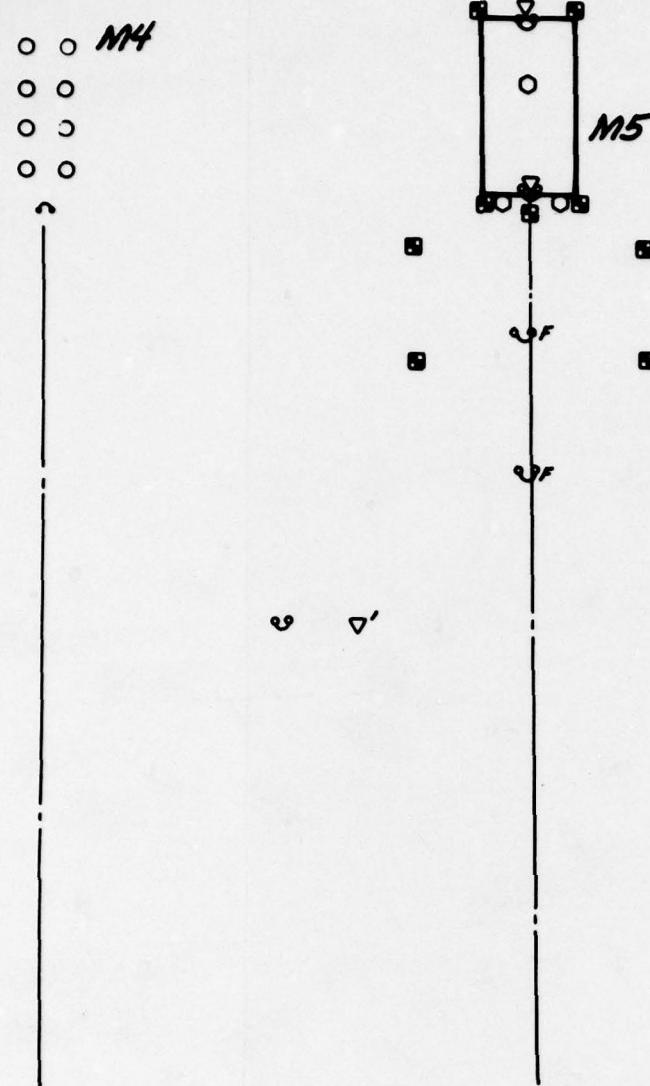
PILE DRIVING EFFECTS TEST PROGRAM	
TYPICAL MONOLITH INSTRUMENTATION	
FOUNDATION INVESTIGATION AND TEST PROGRAM EXISTING LOCKS AND DAM NO. 26 ST. LOUIS DISTRICT, CORPS OF ENGINEERS. DAGW43-78-C-0008	
Woodward-Clyde Consultants V7C826 Phase III	Fig. 3.1



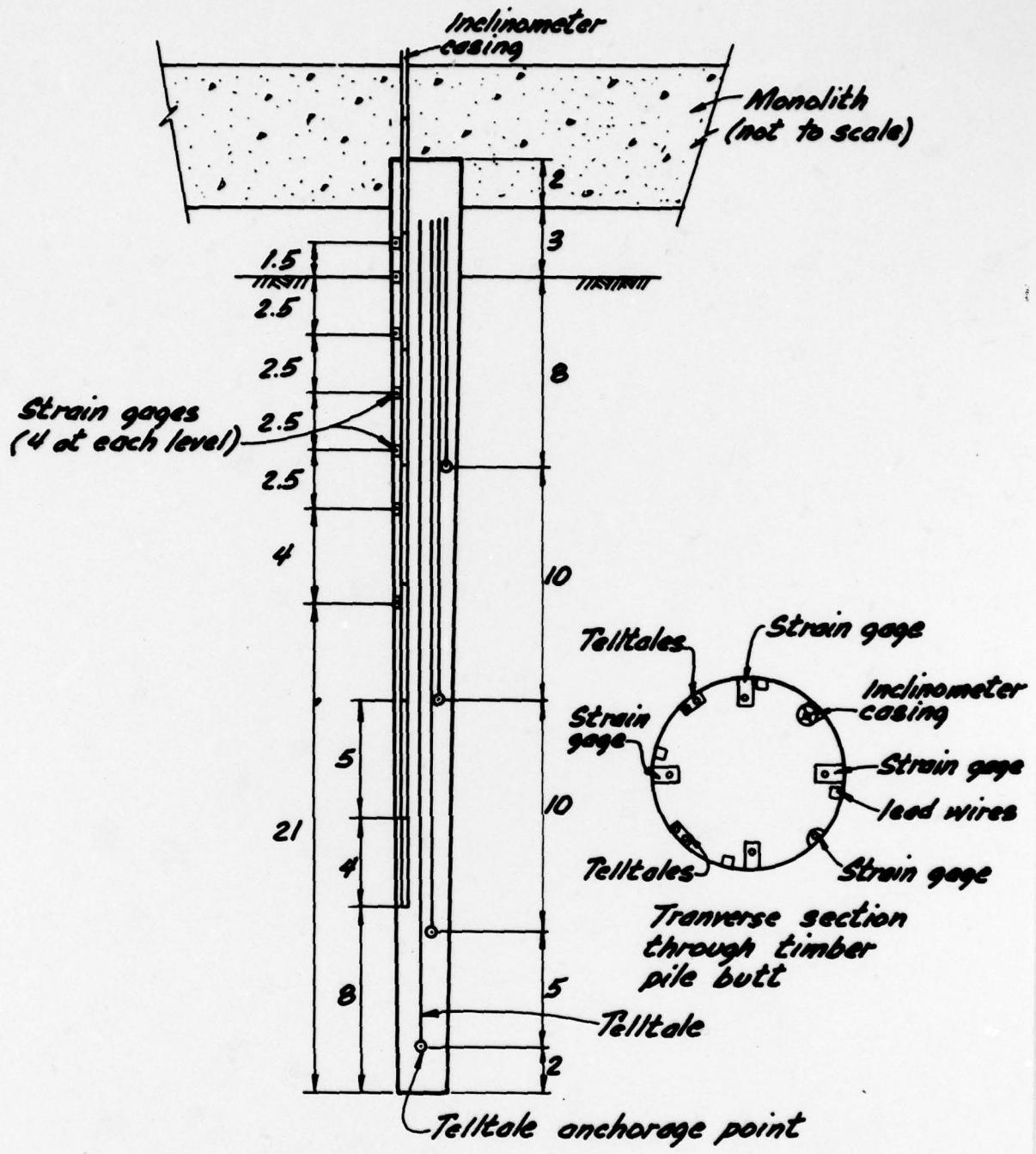
#### Legend

- ▽ Single level piezometer
- Surface reference point in soil
- ▽ 2-level piezometer array
- 3-level, 3-D geophone
- ▽ Single level 3-D geophone
- 3-D deformation gage

117

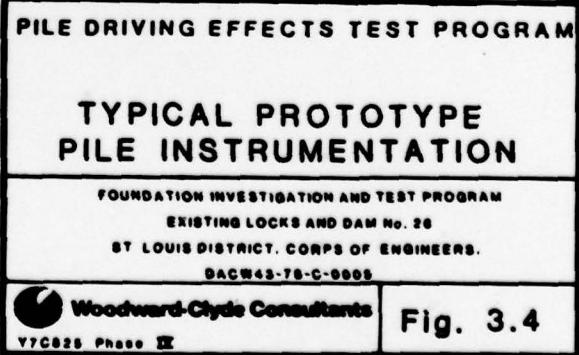
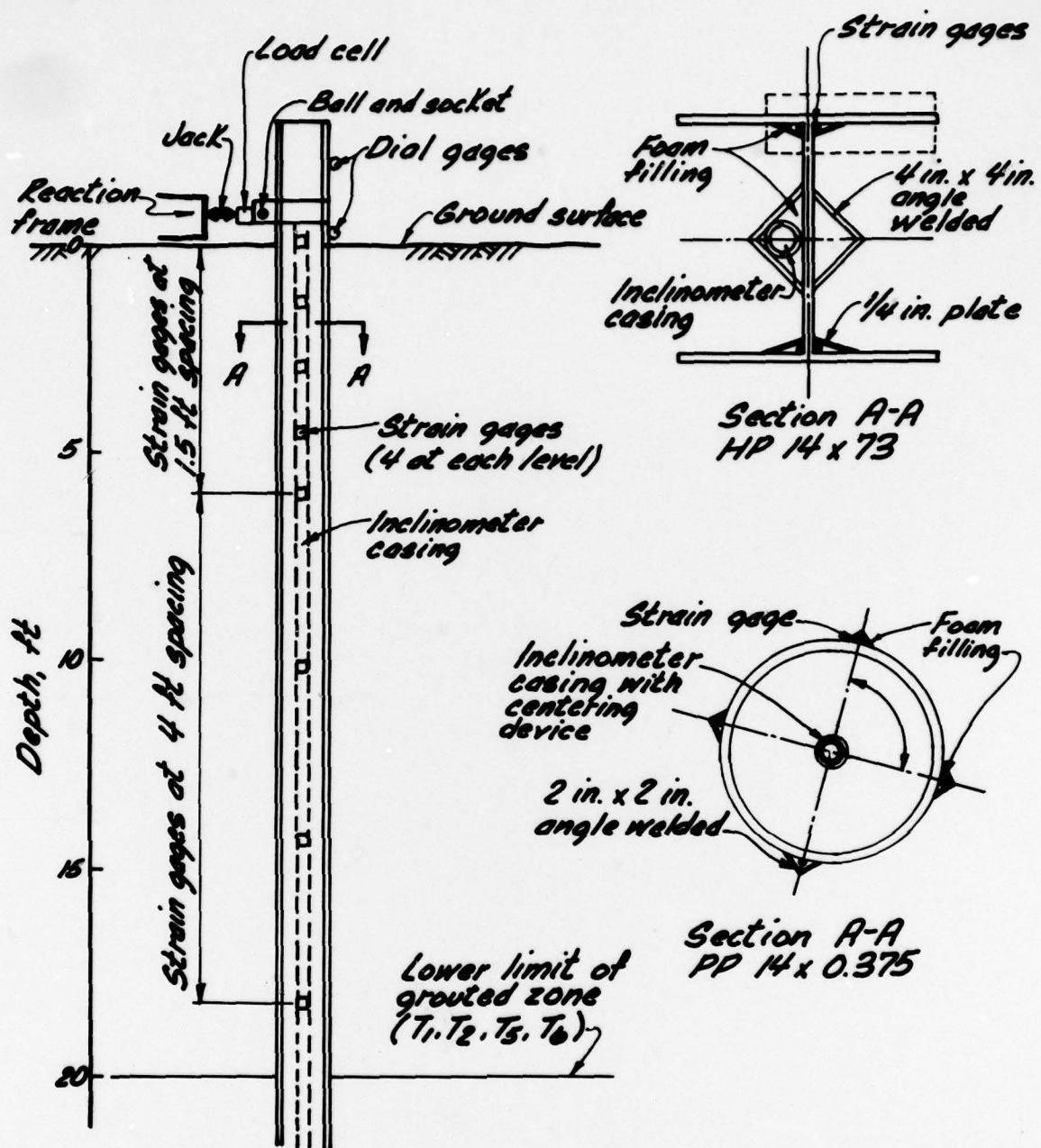


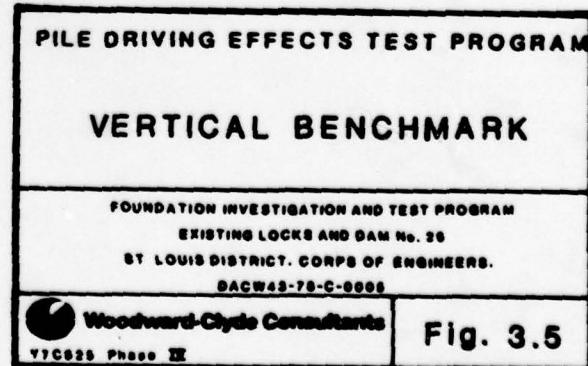
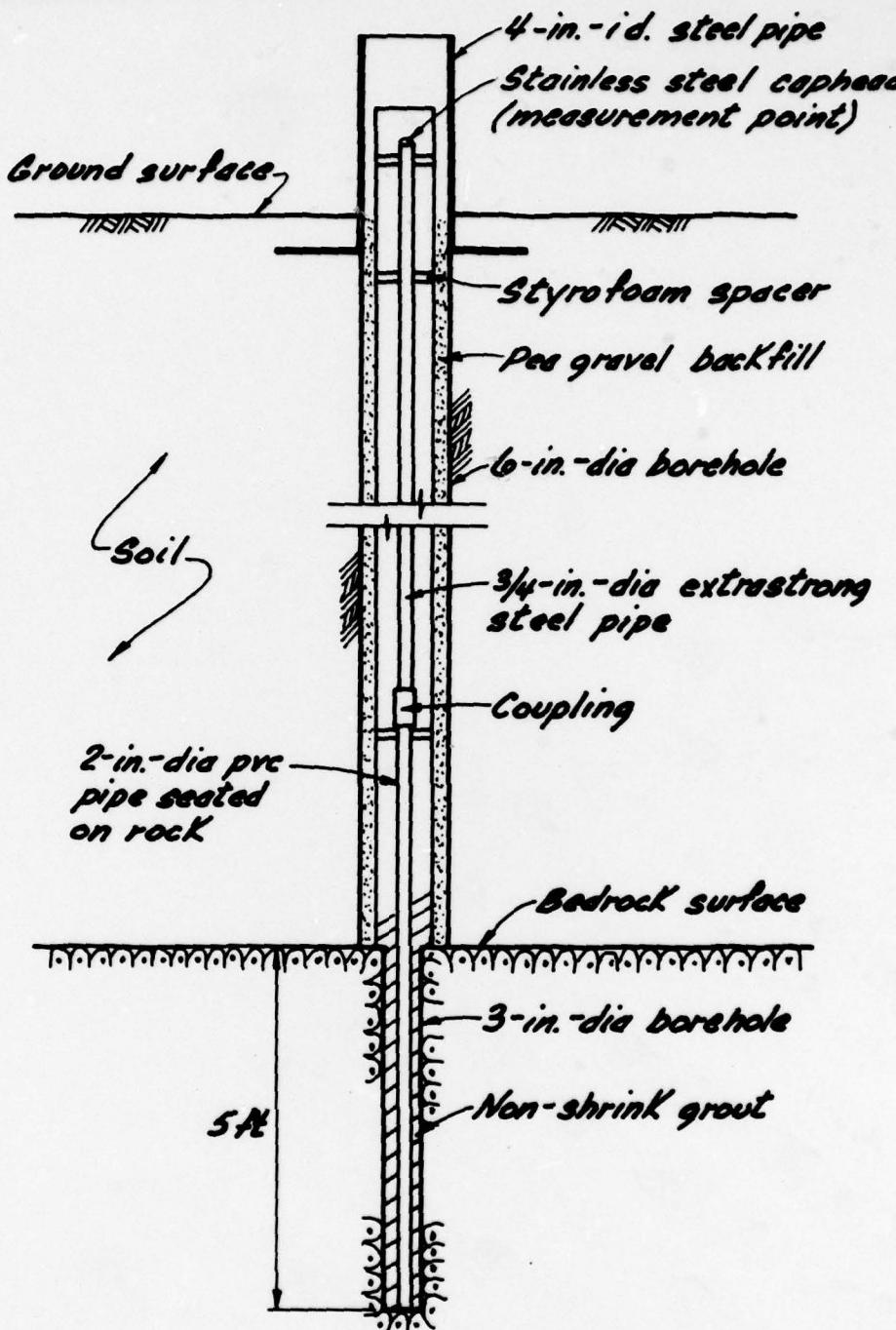
2

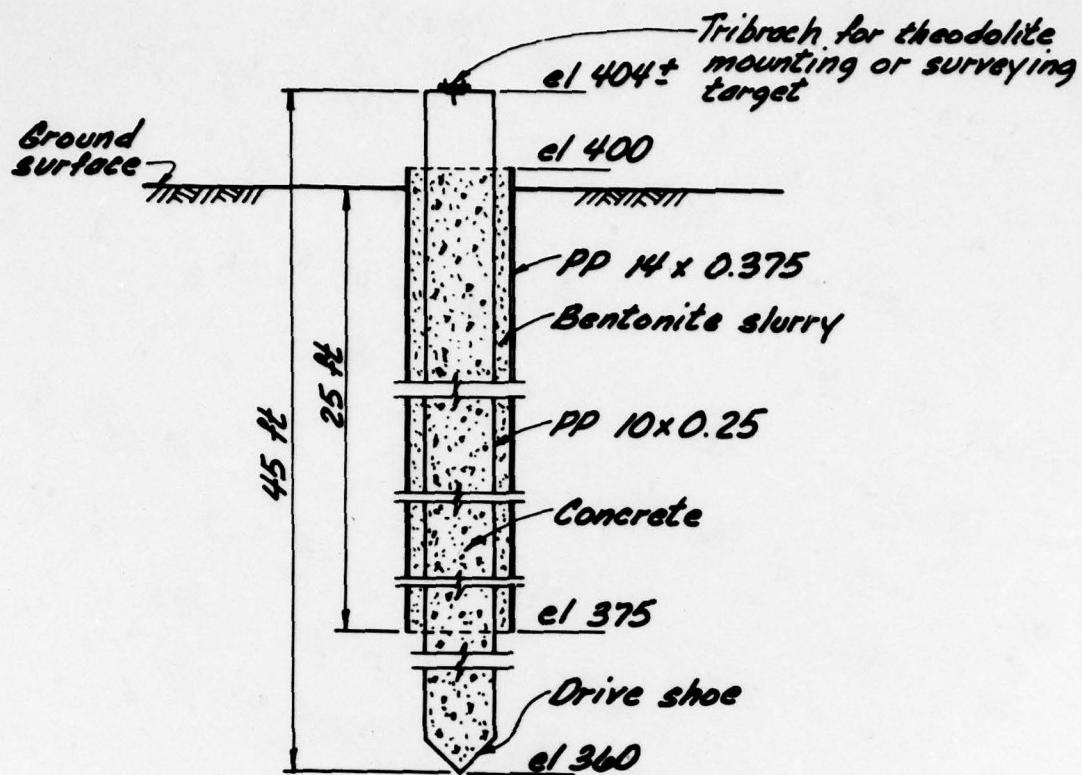


Note:  
All dimensions are in feet

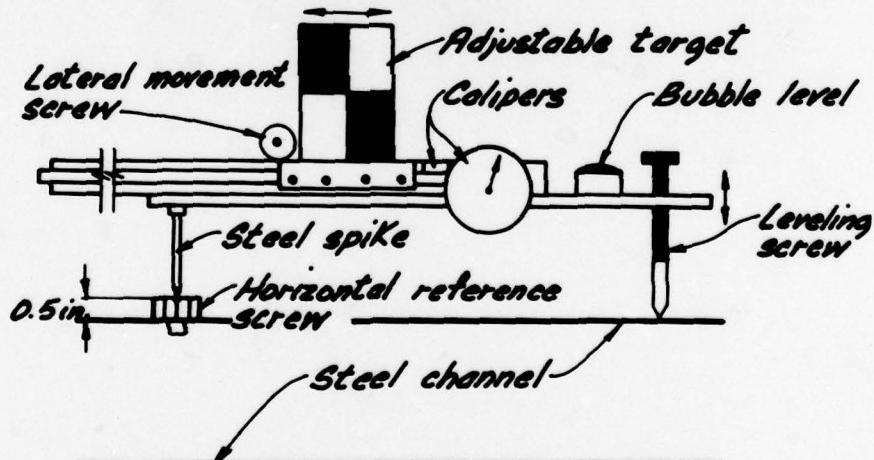




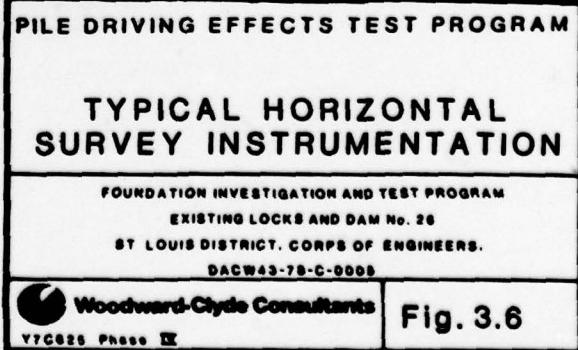


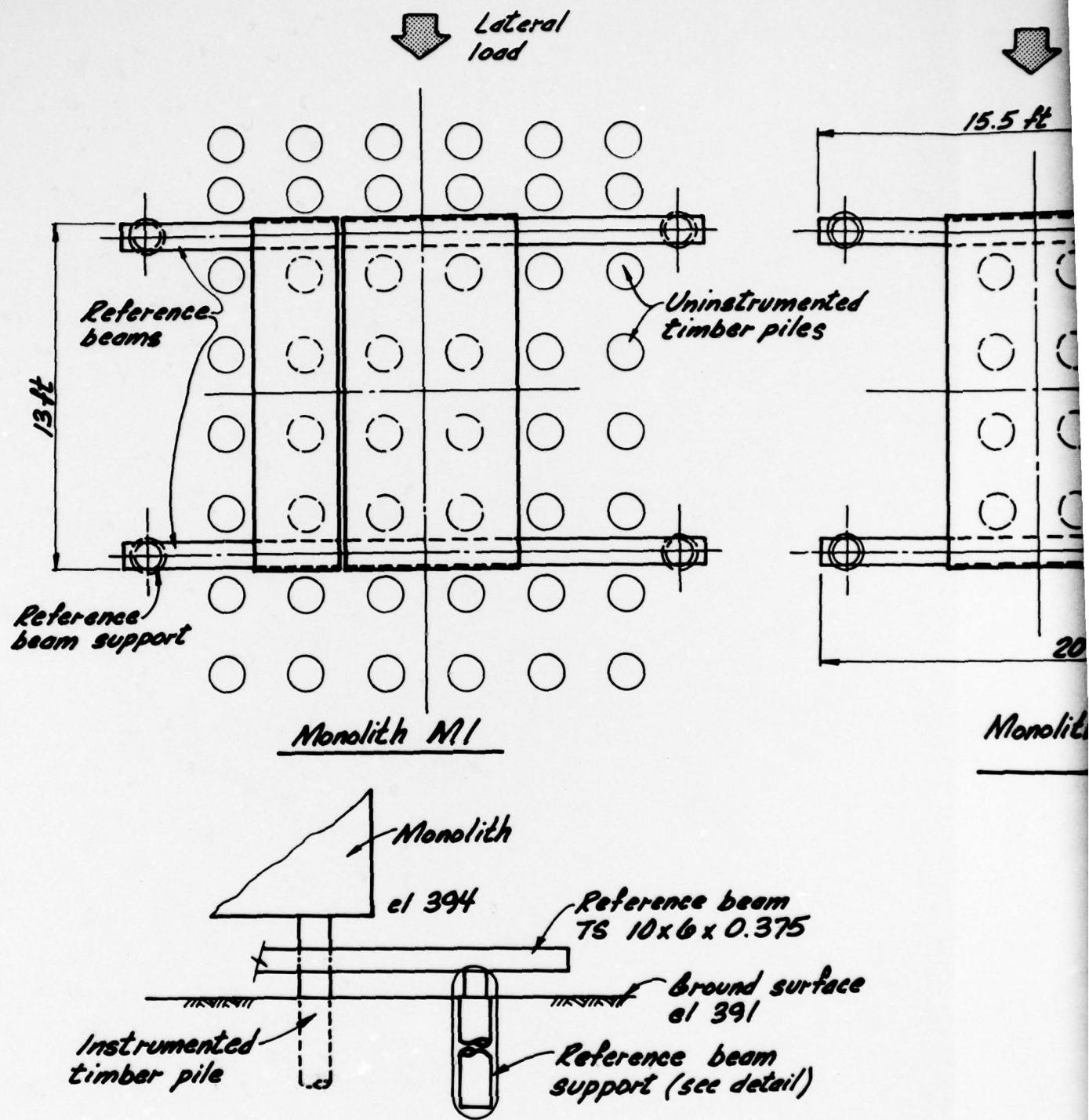


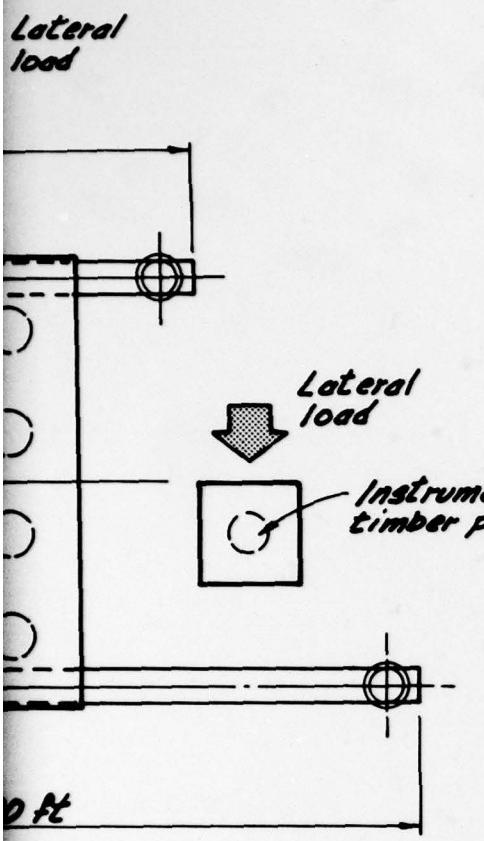
(a) Typical horizontal control point



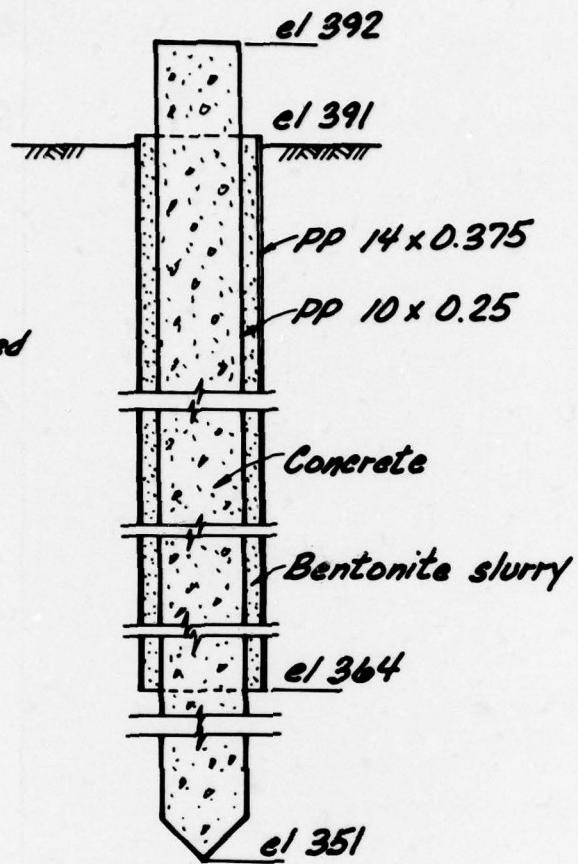
(b) Vernier caliper



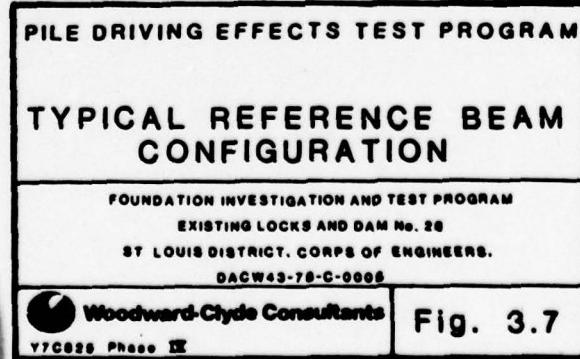




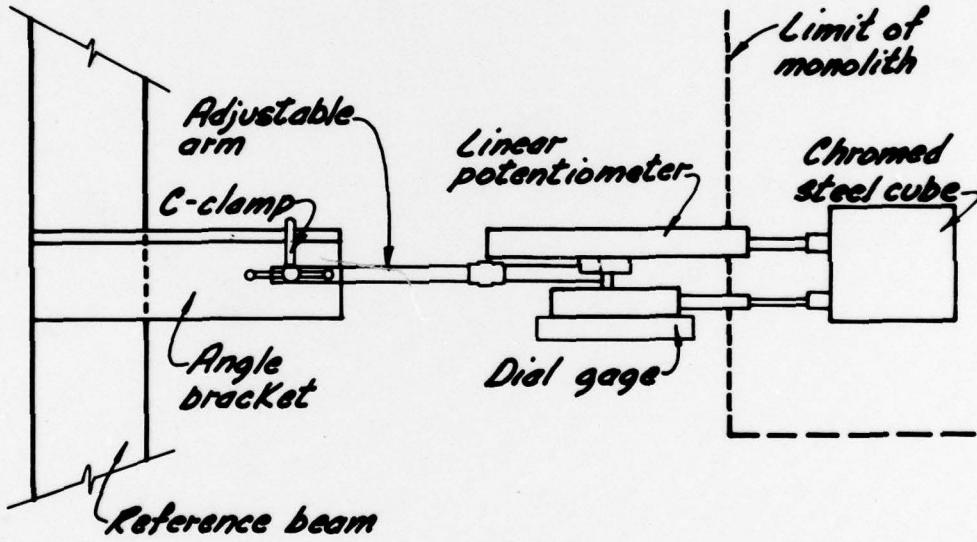
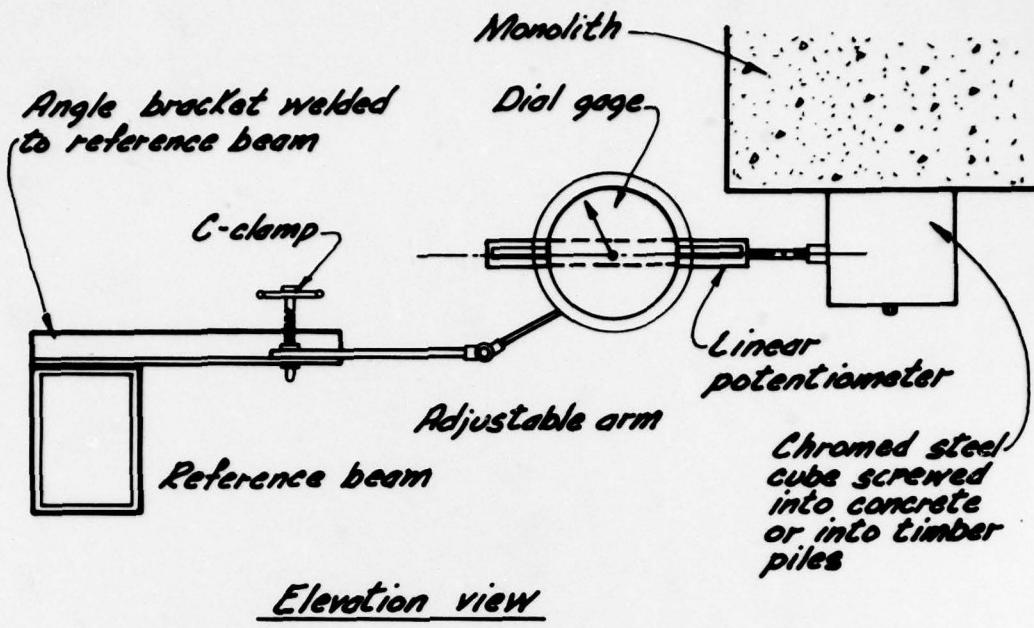
lhs M2/M6  
M3/M7



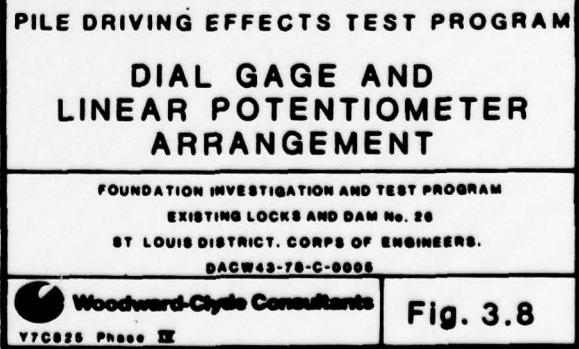
Detail of reference  
beam support

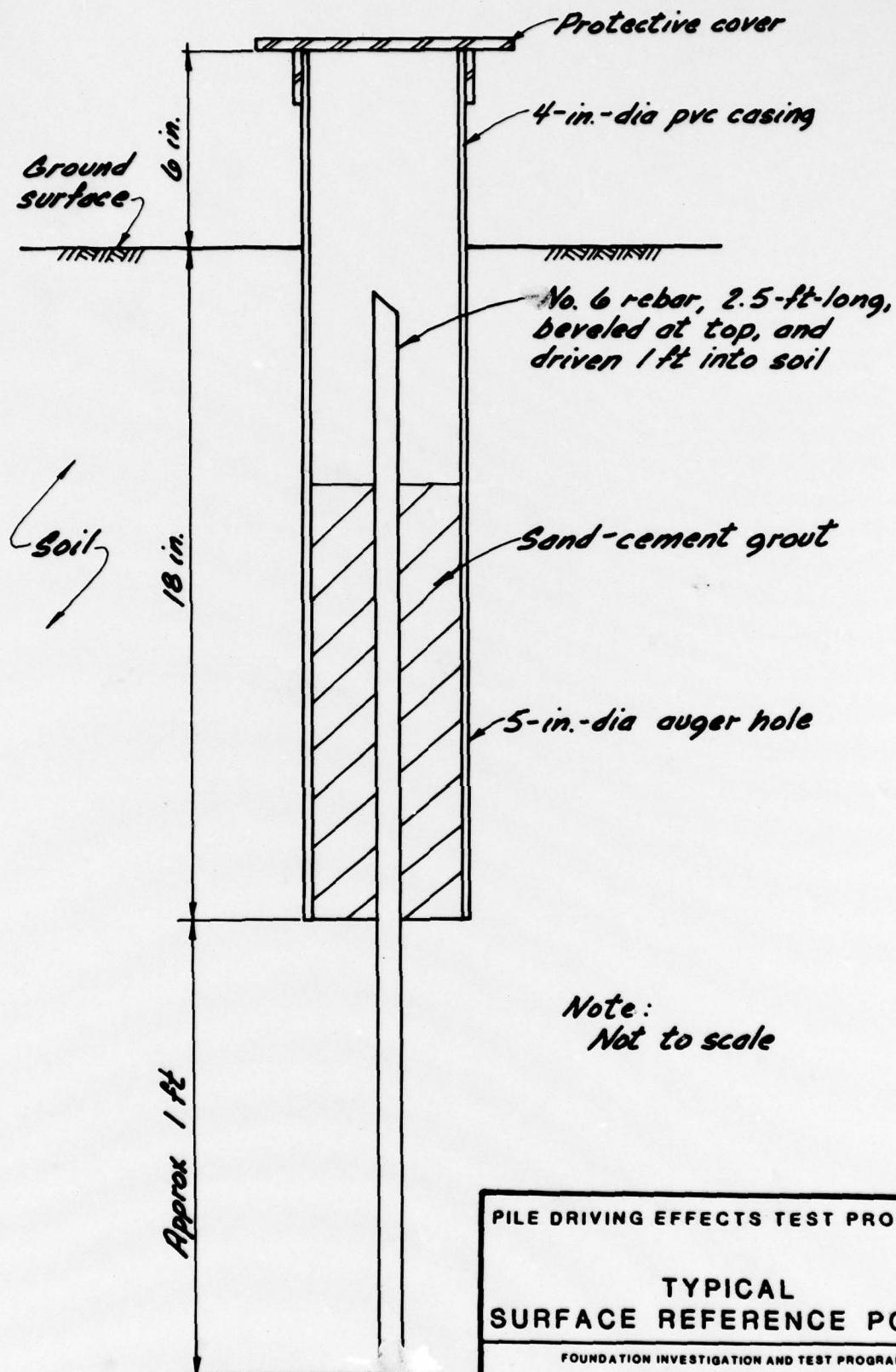


2

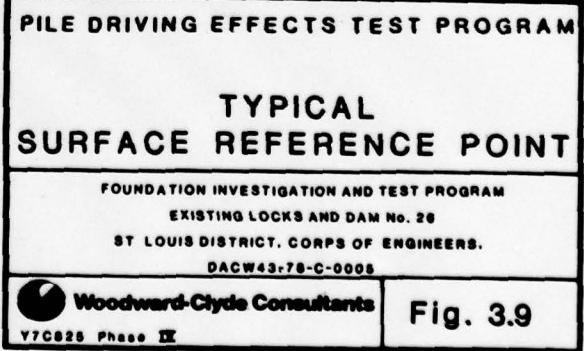


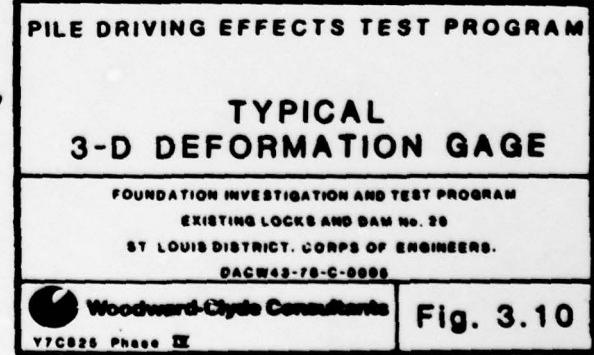
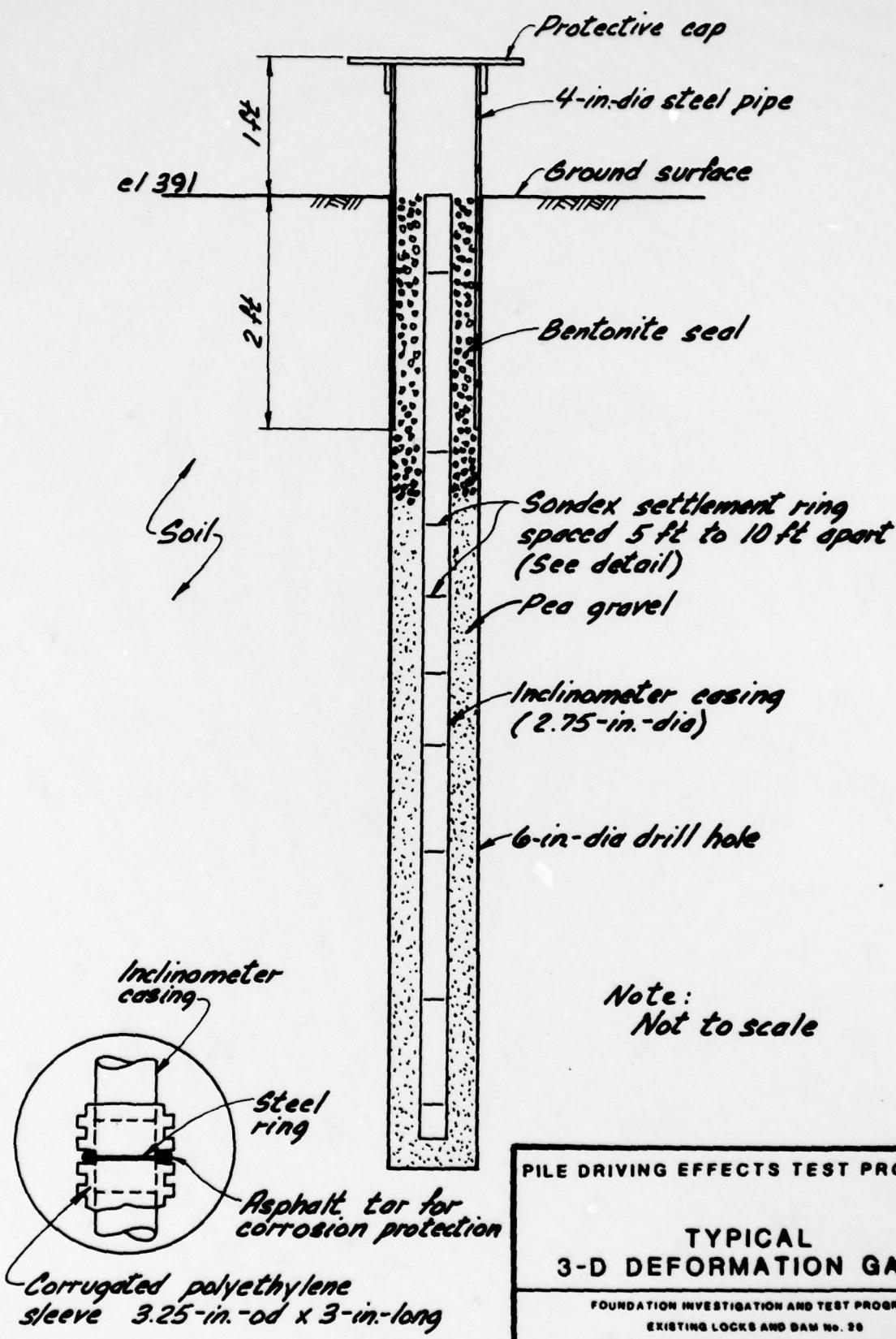
Plan view

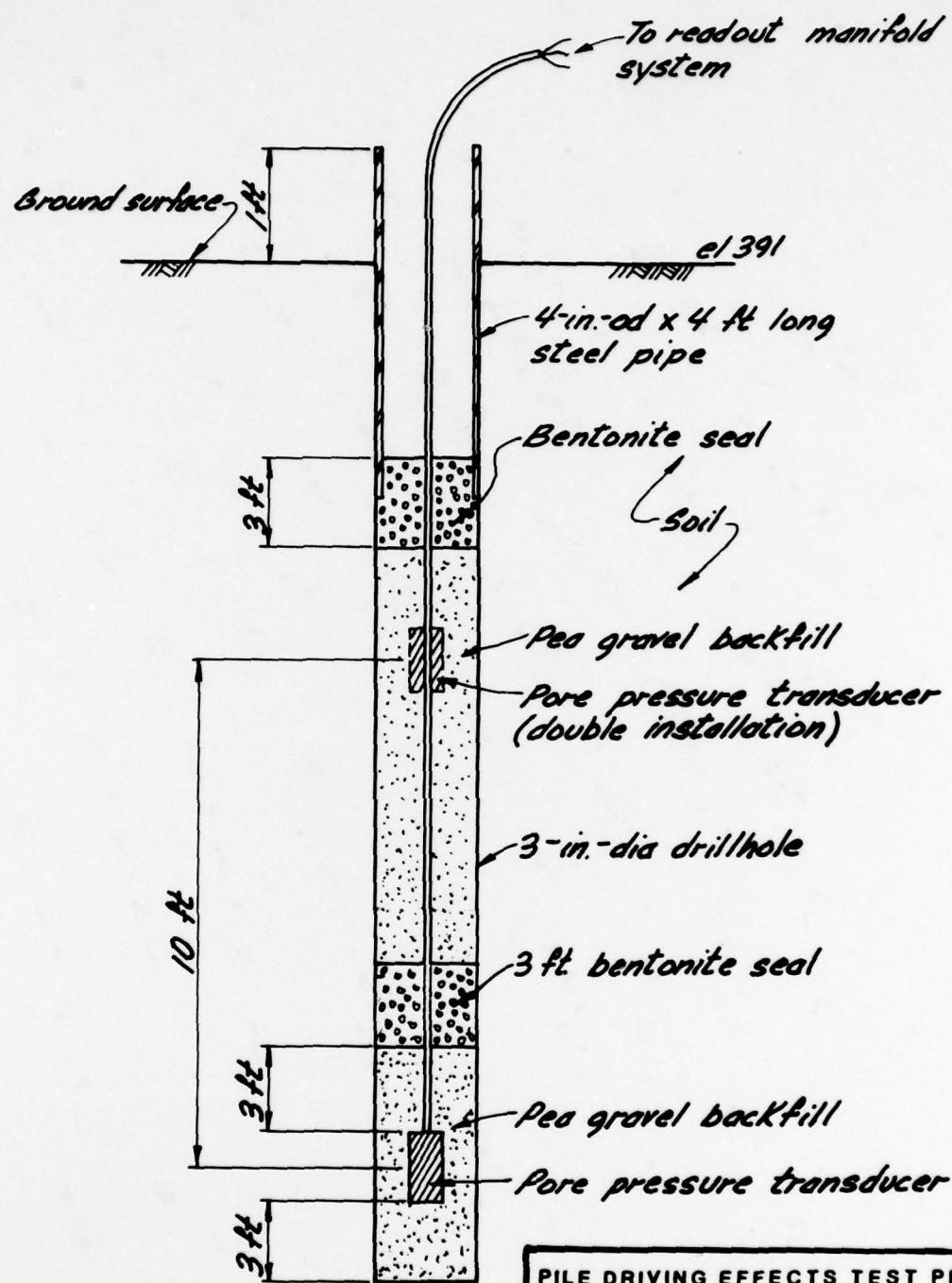




Note:  
Not to scale







Note:  
Not to scale

PILE DRIVING EFFECTS TEST PROGRAM	
TYPICAL PNEUMATIC PIEZOMETER INSTALLATION	
FOUNDATION INVESTIGATION AND TEST PROGRAM	
EXISTING LOCKS AND DAM NO. 26	
ST. LOUIS DISTRICT, CORPS OF ENGINEERS.	
DACPW43-78-C-0005	
Woodward-Clyde Consultants V7C826 Phase II	Fig. 3.11

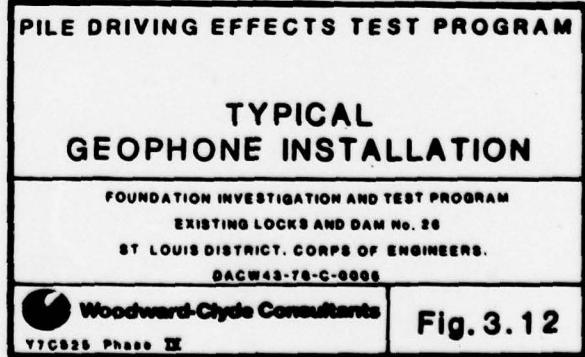
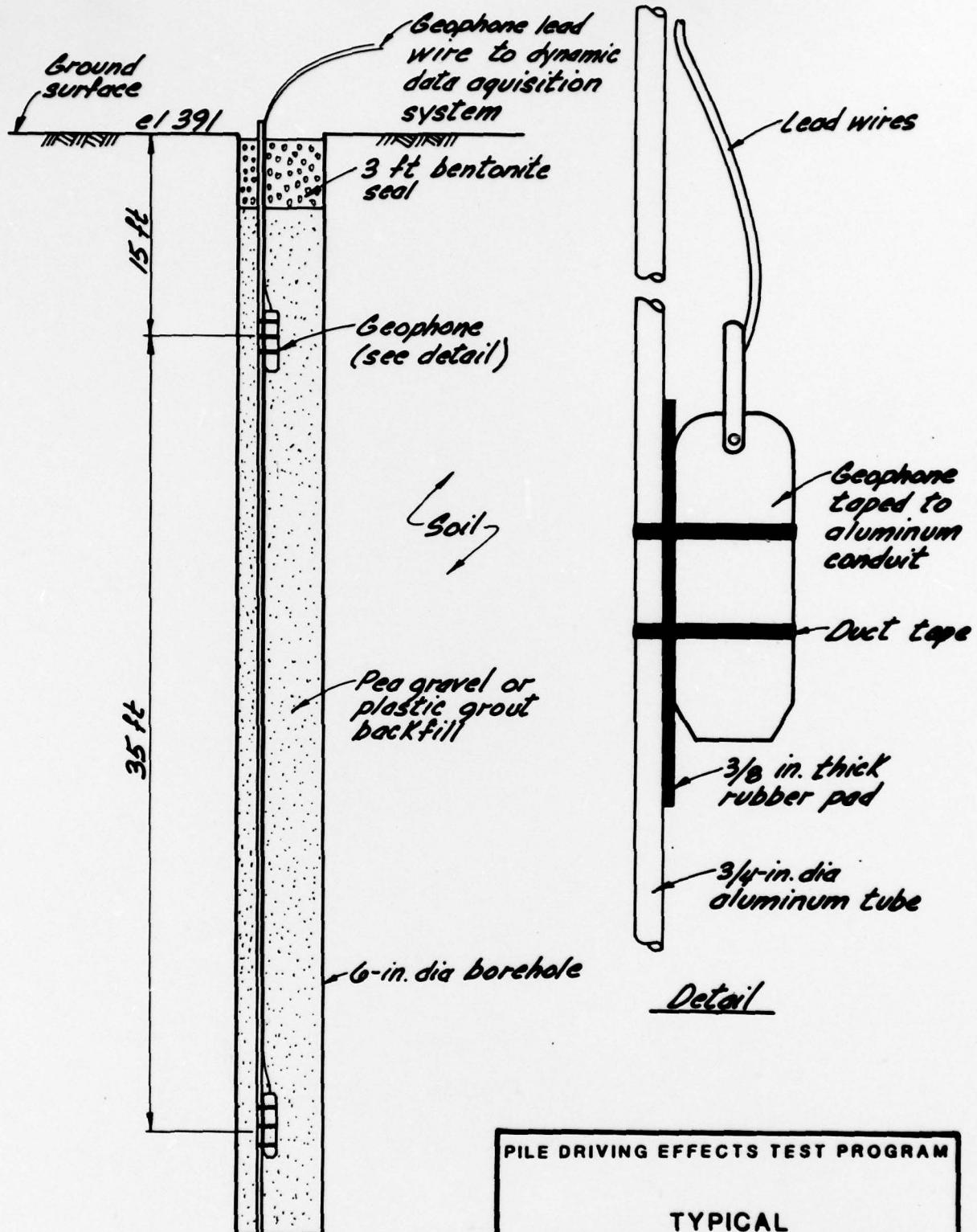
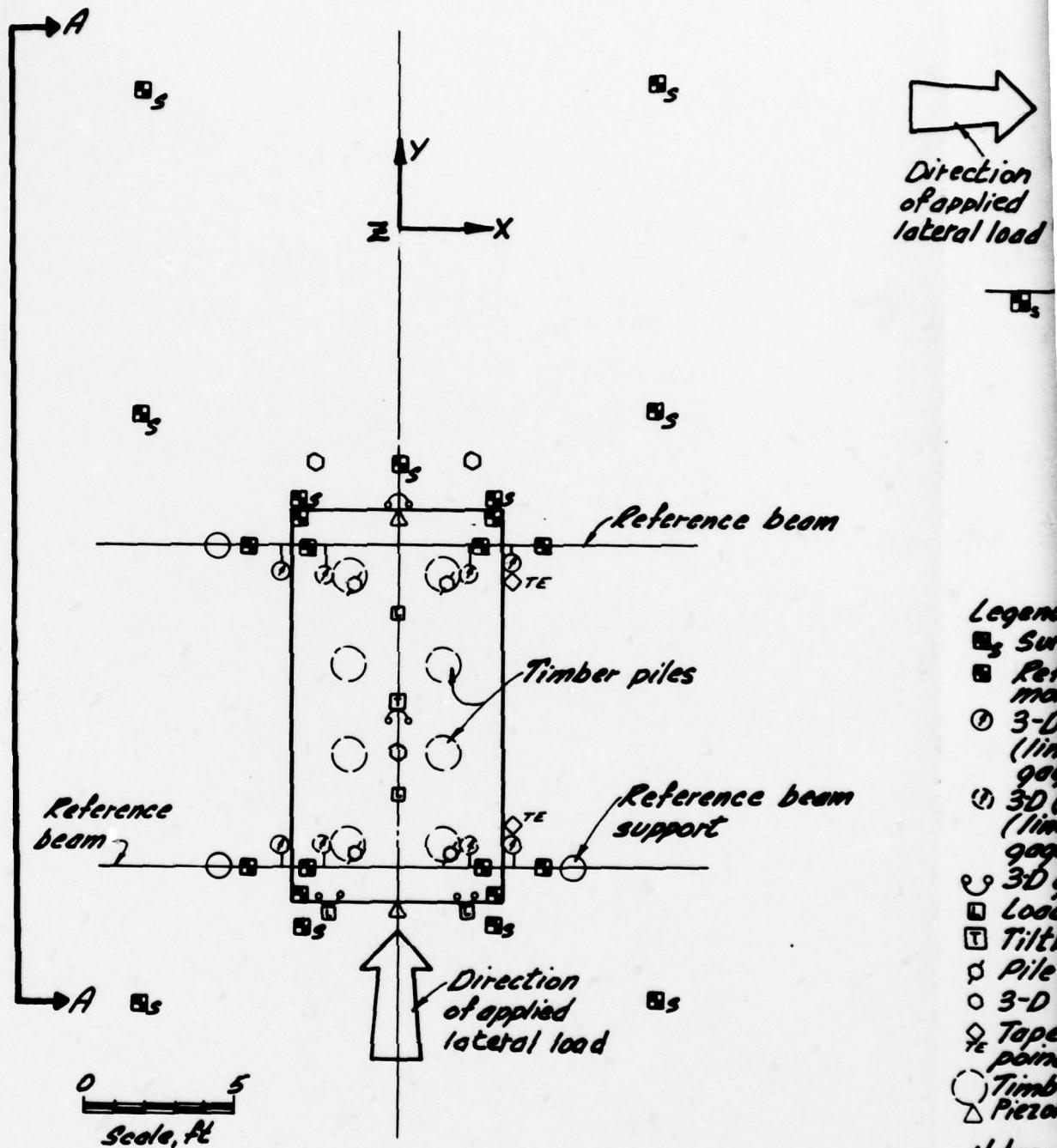


Fig. 3.12

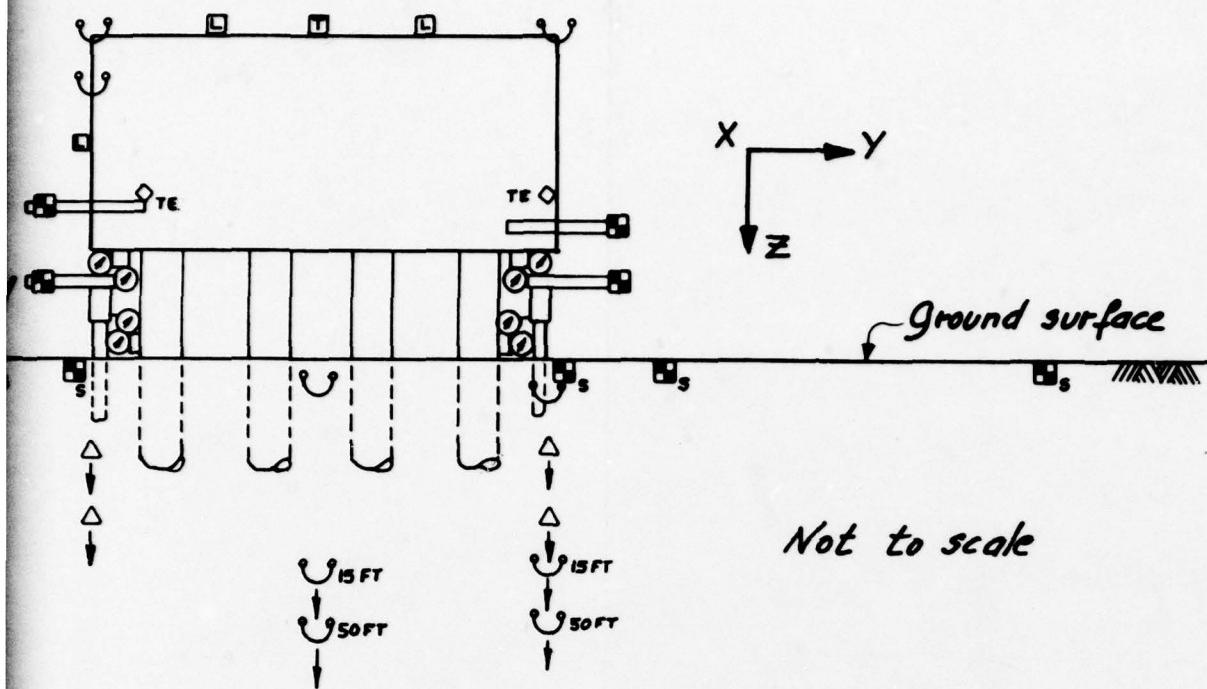
Plan view



Notes:

- (1) Timber not shown
- (2) Strain piles not shown

Section A-A

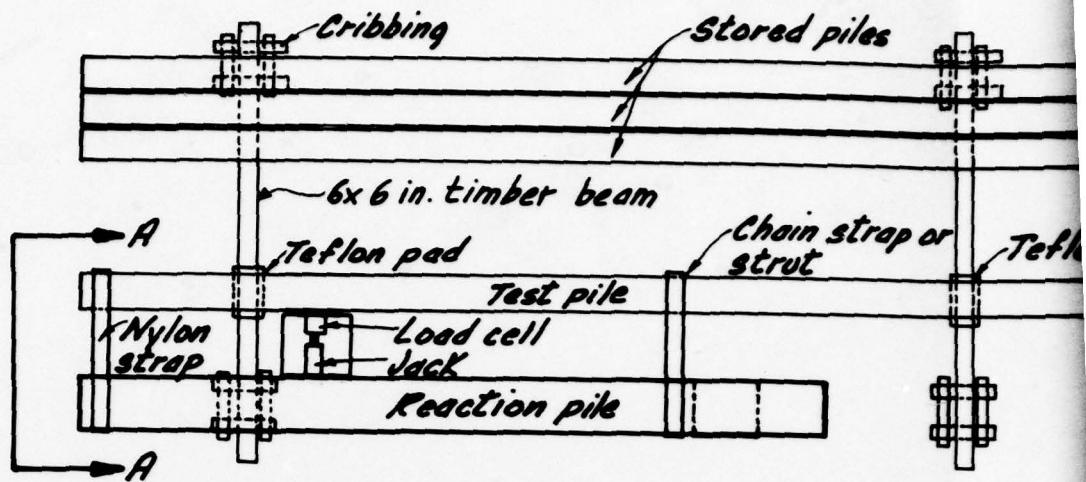


ad  
 surface reference point  
 reference point ( $y_B$ ) on  
 monolith or reference beam  
 $D(x,y,z)$  set of displacement gages  
 linear potentiometer and dial  
 gages) on monolith  
 $(x,y,z)$  set of displacement gages  
 linear potentiometer and dial  
 gages) on timber piles

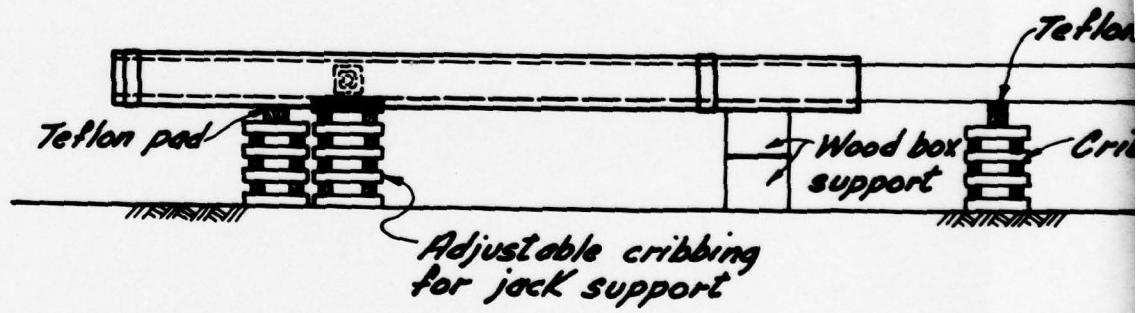
geophone  
 ed cell  
 meter  
 inclinometer  
 deformation gage  
 extensometer reference  
 $z(x)$   
 bar pile  
 meter

ber pile and ground inclinometers  
 own in Section  
 in gages and telltales on timber  
 not shown

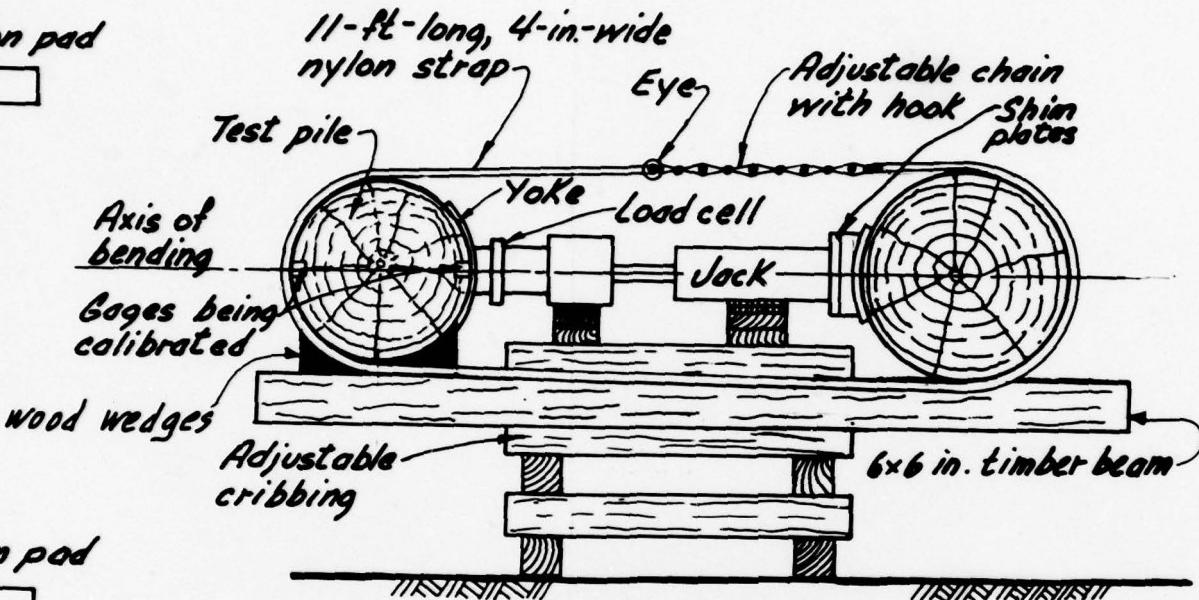
<b>PILE DRIVING EFFECTS TEST PROGRAM</b> <b>DETAILS</b> <b>OF INSTRUMENTATION</b> <b>FOR MONOLITH M2</b>	
<small>FOUNDATION INVESTIGATION AND TEST PROGRAM</small> <small>EXISTING LOCKS AND DAM NO. 26</small> <small>ST. LOUIS DISTRICT, CORPS OF ENGINEERS.</small> <small>DAEW43-78-C-0008</small>	
 Woodward-Clyde Consultants <small>VTC828 Phase III</small>	<b>Fig. 3.13</b>



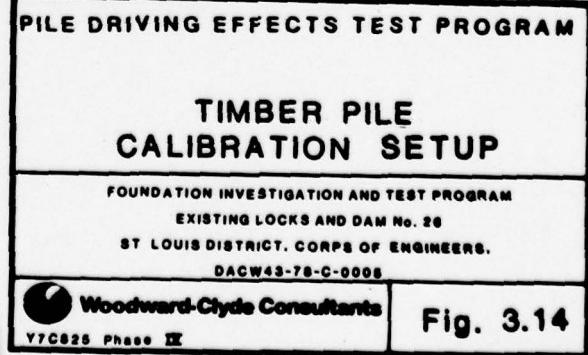
Plan



Elevation

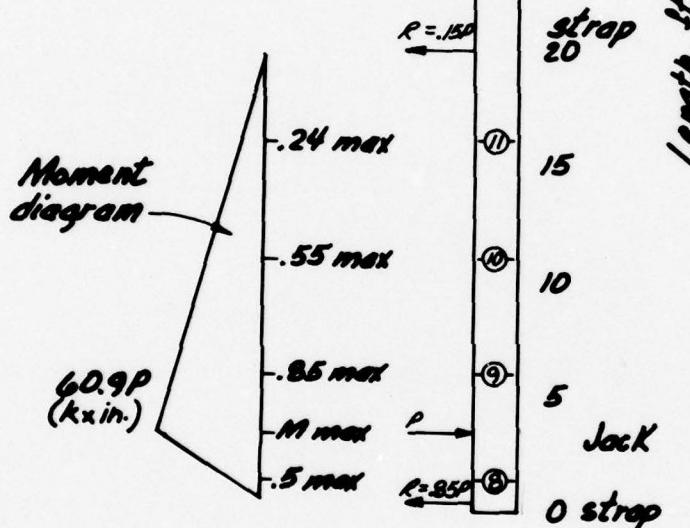


Section A-A

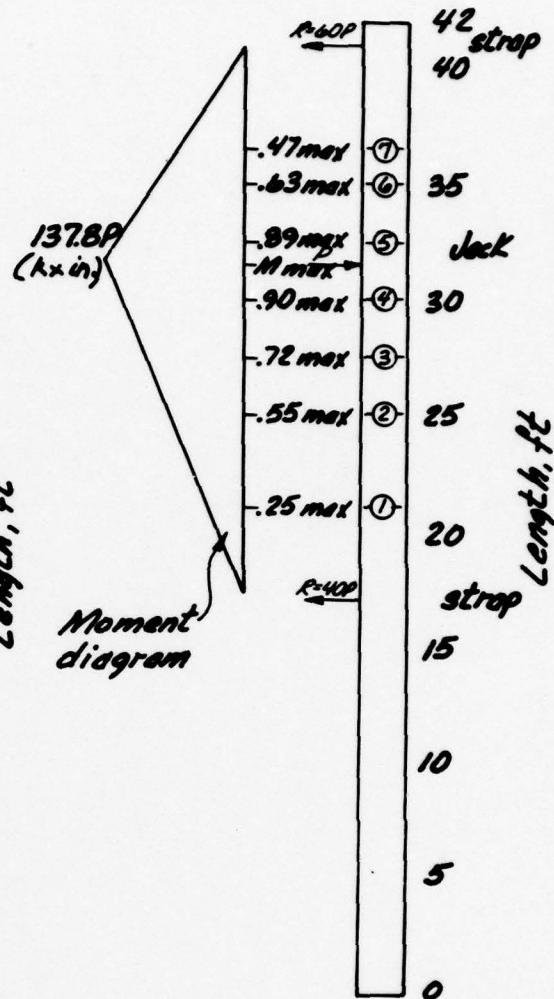


(b) Jack load applied between gages 8 and 9

Load applied to piles 25, 37, 39, 42 and 44 (piles with 11 levels of strain gages)



(a) Jack load applied between gages 4 and 5



*Note:*  
Recalibration loading  
applied to all 45 piles  
except piles No. 45  
and 46

PILE DRIVING EFFECTS TEST PROGRAM	
JACK POSITION FOR TIMBER PILE CALIBRATION	
FOUNDATION INVESTIGATION AND TEST PROGRAM EXISTING LOCKS AND DAM NO. 26 ST LOUIS DISTRICT, CORPS OF ENGINEERS. DACPW43-76-C-0006	
Woodward-Clyde Consultants Y7G826 PHASE II	Fig. 3.15

**PHASE IV REPORT**

**VOLUME III**

**RESULTS AND INTERPRETATION OF  
PILE DRIVING EFFECTS TEST PROGRAM**

**SECTION 4  
TEST AREA SUBSURFACE CONDITIONS**

#### 4 TEST AREA SUBSURFACE CONDITIONS

##### 4.1 SUBSURFACE INVESTIGATIONS

###### 4.1.1 Purpose and Scope

A program of subsurface explorations, and in situ and laboratory tests was performed at the test area to assess the initial soil properties prior to any pile driving. In January and February 1978, several borings were made to obtain disturbed and undisturbed samples and measure standard penetration resistances. In October 1978, at the conclusion of test area preparation activities, an intensive program of borings, sampling, and in situ testing was accomplished.

Boreholes were drilled at locations shown in Fig. 4.1. In situ testing performed in these boreholes included: static cone penetration test soundings near the center of monoliths M1, M2, M3, M5, and M8; seven static cone penetration test soundings in the prototype pile driving area; four pressuremeter borings with standard penetration tests near monoliths M2, M3, M5, and M8; shear wave velocity measurements in two arrays near monoliths M2 and M3; and three series of borehole permeability tests near monoliths M4, M5, and M8. Laboratory testing included: grain-size analyses on disturbed and undisturbed borehole samples; triaxial compression tests on undisturbed borehole and laboratory reconstituted samples. Subsurface exploration, in situ testing, and laboratory testing provided data for characterization of the following soil properties: stratigraphic profile; grain-size distribution of various strata; in situ stress state; in situ unit weight and relative density; stiffness; shear strength; and permeability.

###### 4.1.2 Soil Sampling

Undisturbed and disturbed samples were obtained for laboratory index and strength property determination. Undisturbed samples were obtained in borings D-1, D-2, D-5, and D-6 using Osterberg and Denison samplers. Sample recoveries of 65 to 97 percent were obtained with these samplers in the upper sand deposits. Laboratory tests performed on these samples included: mechanical sieve analyses, maximum-minimum density determination, and triaxial compression tests.

Disturbed soil specimens were obtained in conjunction with penetration tests. Visual classification of these samples provided information regarding the subsurface stratigraphic profile. Laboratory grain-size analyses were performed on samples from borings C-5, C-9, D-1, D-2, D-5, D-6, PD-PM1, PD-PM2, PD-PM3, PD-PM4, PD-K1, PD-K2, PD-K3, and PD2-SP1. For the pressuremeter borings (PD-PM) or the permeability borings (PD-K), dynamic penetration test samples enabled a visual classification of the soil involved in the pressuremeter or permeability tests.

#### **4.1.3      Dynamic Penetration Testing**

These tests consisted of driving a split-spoon into the soil. Two split-spoons were used: standard 2-in.-od spoon driven with a 140-lb hammer falling 30 in. (standard penetration test, ASTM D1586-67), and a 3-in.-od spoon driven with a 350-lb hammer falling 18 in. (a procedure commonly used by the St Louis District in alluvial deposits). The dynamic penetration resistance was recorded as the number of hammer blows  $N$  or  $N_3$  required to drive the 2-in. or 3-in. spoon, respectively, 12 in. into the soil.

Dynamic penetration tests using the 3-in. split spoon were made in borings C-5, C-9, D-1, and D-2. The non-standard, larger spoon was used to provide a correlation with prior borings made by the St Louis District.

Standard penetration tests were made in borings D-5, D-6, PD-PM1, PD-PM2, PD-PM3, PD-PM4, PD-K1, PD-K2, PD-K3, and PD2-SP1. N-values from the permeability borings were disregarded because these holes were advanced by driving casing and washing with clean water. Without bentonite drilling fluid, washing was probably ineffective in removing coarse sand and gravel, which caused erroneous N-values. Standard penetration resistances obtained before and after pile monolith trench excavation are plotted on Fig. 4.2. Above el 358, N-values obtained after excavation averaged 30 to 50 percent less than N-values before excavation. Below el 358, N-values remained unchanged. This is in good agreement with the decrease suggested by the results presented by Gibbs and Holtz (1953) relating N-value, vertical effective stress, and relative density.

#### **4.1.4      Static Cone Penetration Testing**

Static cone penetration tests were made in borings PD-C1, C2, C3, C5, C6, C7, C8, C10, C11, C13, and C14. The cone system used was developed by WCC. The cone has a 10-cm<sup>2</sup> cross sectional area, and an angle of 60°. The load applied on the cone to push it into the soil at a constant rate of penetration of 4 ft/min was measured by a load cell and was recorded on a strip chart. Continuous cone penetration profiles were obtained by alternately pushing the cone 5 ft to 10 ft into the soil at the bottom of the borehole, and reaming the borehole after each cone run by rotary drilling.

A profile of static cone resistance for borings PD-C13, C10, C7, and C1, which were made along the prototype pile driving centerline for monolith M1, is presented in Fig. 4.3. The results of other soundings in the prototype pile driving area are given in Appendix K, Volume IIIA. Static cone penetration resistance for borings PD-C1, C2, C3, C5, and C6 that were made in the center of monoliths M1, M2, M3, M5, and M8, respectively, are presented in Fig. 4.2. The ratio between cone point resistance and standard penetration resistance  $q_c/N$  generally varied between 5 and 6 for the upper 50 ft of alluvium in the pile driving effects test area. However, when gravel was encountered, the ratio increased to 7 to 11; when clay was encountered, the ratio decreased to 3.5.

#### 4.1.5 Pressuremeter Testing

Pressuremeter tests were made in borings PD-PM1, PM2, PM3, and PM4 which were drilled after monolith trench excavation. The Menard-type GAM pressuremeter used for the measurements consisted of a BX-size probe that was expanded at the bottom of a borehole. The volume change of the probe was measured as a function of the applied pressure. The data were used to obtain elastic deformation and failure characteristics of the soil. The boreholes were carefully prepared by slow drilling with a drag bit and thick Revert drilling fluid.

An idealized pressuremeter volume-change vs applied pressure curve is shown in Fig. 4.4. At the beginning of the test, the probe begins to expand through the drilling fluid with little lateral restraint, until it makes contact with the borehole walls. This corresponds to the steep initial portion of the volume change curve. As the probe continues to expand, the soil resistance is mobilized and the volume-change curve is linear (pseudo-elastic response). At higher pressure, plastic deformation occurs. The soil then sustains large deformations for small pressure increases. The asymptote of the volume-change vs pressure curve corresponds to the ultimate strength of the soil (or limit pressure).

Results of actual pressuremeter tests performed in borings PD-PM1, PM2, PM3, and PM4 are presented in Appendix K, Volume IIIA.

#### 4.1.6 Cross-Hole Shear Wave Velocity Measurements

Cross-hole seismic shear wave velocity measurements were made in two arrays in the test area shortly before pile driving started (October 1978) (Section 3.2.4). One array was near the future location of monolith M3 in an area to be chemically grouted (boreholes PD-S6 through S10; see Fig. 4.1); the other array was near monolith M2 (boreholes PD-S1 through S5).

Results of the shear wave velocity measurements before pile driving for the two sets of arrays are presented in Fig. 4.5. Source-to-receiver hole velocities were not used because of equipment difficulties with instrument triggering and a high background noise environment caused by nearby construction activities. Since two receiver holes were used with each source hole, the difference in arrival times ( $\Delta t$ ) for the two receiver holes was used to calculate shear wave velocity. Background noise also hampered identification of shear wave arrivals to some extent. Some scatter of data is apparent as the velocities fall within a range of 450 to 800 ft/sec. The low velocity at a depth of 20 ft in array S-6 and 7 corresponds to a layer of clay that was not encountered in arrays S-9 and 10 and S-4 and 5. The wide range of shear wave velocities measured in array S-1 and 2 was probably due to interference from a rock anchor erroneously installed near borehole S-2 and in the path of the seismic waves incoming from source hole S-3. The average shear wave velocity in the upper 50 ft below ground surface was 650 ft/s before any pile installation.

#### **4.1.7      Borehole Permeability Testing**

Falling-head permeability tests were performed in borings PD-K1, K2, and K3. The tests were conducted by driving an NX-size, flush joint casing into the soil to the desired testing depths, cleaning out the soil with a rotary drill bit and circulating water, and flushing the casing with clean water to remove bottom sediment. The casing was filled with water and the elevation of the water surface in the casing was measured as a function of time.

The coefficients of permeability obtained from these tests are given in Fig. 4.6, together with results from permeability tests performed in borings throughout the site prior to site preparation. In general, the results before and after excavation agree fairly well. However, two tests were not carried out for a time sufficient to allow for accurate determination of the permeability, and an early test in boring PD-K1 had insufficient casing stickup to provide adequate hydraulic head for the test. The water table was only 1 ft below ground surface and at least 5 ft of head would have been needed for reliable results. Insufficient test duration and casing stickup resulted in underprediction of permeability for these tests.

#### **4.1.8      Laboratory Testing**

Grain-size analyses were made on disturbed split-spoon samples and undisturbed Osterberg and Denison samples obtained in borings D-1, D-2, D-5, D-6, and PD2-SP1. Grain-size distribution curves for these samples are presented in Appendix K, Volume IIIA.

Maximum and minimum unit weights were measured in the laboratory on undisturbed Osterberg samples obtained in borings D-1 and D-2. The maximum density was determined by the modified Providence method using an electromagnetic jack hammer instead of the standard ASTM hammer. Minimum densities were determined using the tube method developed by Lucks (1970), funnel method on 0.1 ft<sup>3</sup> mold (ASTM), and small 432 cm<sup>3</sup> mold, and cylinder tilt method (Kolbuszewski 1948). Test results are discussed in Section 4.3.4.

Consolidated drained and undrained triaxial compression tests were performed on undisturbed Osterberg samples from borings D-1 and D-2. A consolidated drained triaxial compression test series was also performed on laboratory reconstituted specimens obtained using the 3-in.-od split spoon. The samples were reconstituted to a relative density of 70 percent. Confining stresses and strain rates for these tests are given below.

<u>Boring</u>	<u>Sample Type</u>	<u>Test Type</u>	<u>Confining Stress</u>	<u>Strain Rate</u>
D-1	Osterberg	CIU	0.85, 1.73, 3.49 t/ft <sup>2</sup>	0.05 percent/min
D-2	Osterberg	CID	0.72, 1.45, 2.17 t/ft <sup>2</sup>	0.05 percent/min
D-25	3-in. split spoon	CID	1.0, 2.0, 4.0 t/ft <sup>2</sup>	0.5 percent/min

Triaxial test results are presented in Appendix K, Volume IIIA.

#### 4.2 STRATIGRAPHY

##### 4.2.1 General Geology

The pile driving effects test area is located within the Mississippi River flood plain near Alton, Illinois, at the southwestern border of the Central Lowland physiographic province. In the vicinity of Locks and Dam No. 26, the flood plain surface is generally flat at el 410 to el 420. High bluffs, approximately 240 ft above the flood plain, lie northeast of Locks and Dam No. 26 on the left bank of the Mississippi River.

The area is part of a monocline that dips northeast into the Illinois basin from the northwest flank of the Ozark uplift. The monoclinal structure is interrupted by several anticlines and synclines trending northwest. The Cap au Gres faulted flexure extends from central Missouri to central Illinois through the area.

In the vicinity of Locks and Dam No. 26, bedrock rises uniformly from el 270 on the Missouri side to el 330 on the Illinois side. The bedrock is overlain by soil deposits of glacial, alluvial, and colluvial origin. Five soil strata and one bedrock unit have been identified; see Fig. 4.7. The strata are, in descending order, flood plain deposits, recent alluvium, alluvial outwash (reworked alluvium), Wisconsinan outwash, and Illinoian ice contact deposits. Occasionally, glacial till pockets are intercalated with the ice contact deposits and bedrock surface. Till was not present at the test area location. The rock units underlying the soil consist of Mississippian limestone of the Meramecian (Valmeyer) Series. The upper formation is the St Genevieve. The following is a description of each soil deposit and rock unit.

##### 4.2.2 Flood Plain Deposits

Flood plain deposits were removed from the pile driving effects monolith trench, but remained in part in the prototype pile driving area. They consist primarily of high to low plasticity clay, and varying amounts of silt, fine sand, and organic material. The clay is very soft to firm, and the sand very loose to loose. The source of the flood plain deposits is the active and abandoned channels, back swamps, and flood basin areas of the Mississippi River flood plain. The river materials, mainly silt and clay, are deposited in relatively quiescent waters, and new material is carried in during river flood stages or forms as colluvial deposits.

##### 4.2.3 Recent Alluvium

The recent alluvium was the surficial material in the monolith trench. It was mapped during the chemical grouting test program excavation, in an area approximately 1 mile north of the pile driving effects test area.

The recent alluvium originated during aggrading and meandering of the Mississippi River across its flood plain during post-Wisconsinan (Holocene to Recent) time. The recent alluvium is a relatively uniform deposit because of a

common depositional environment and history, and because of the large scale of the Mississippi-Missouri fluvial system. It is uniform in such characteristics as composition, grain size, roundness, sorting, distribution and orientation of primary depositional structures, and abundance and distribution of carbonaceous material. The strata range in grain size from coarse silt to fine gravel, but are predominantly fine to medium sand. These sediments are characteristically clean, well-sorted (poorly graded) sand composed of at least 70 percent, and frequently more than 80 percent, quartz grains. They also contain abundant concentrations of carbonaceous material including wood, charcoal, and lignite, which range in size from coarse silt to large tree trunks. Fresh water shells are also abundant. All the sediments are pervasively and consistently cross bedded; the majority of the cross beds dip generally N to NE at an angle of 5 to 35 degrees. These cross beds are broad and continuous, and they occur in sets from several inches to a few feet thick. Associations of contiguous beds having similar grain size and sorting characteristics comprise the sheet and shoestring sands that make up the recent alluvium of the valley. Laterally extensive sand sheets were deposited as a result of continuous lateral migration of fluvial channels. Narrow elongate sand shoestrings were deposited as a result of occasional, discontinuous channel shifts or jumps, and subsequent infilling of the resulting abandoned channel. These associations of cross-bed sets extend laterally as distinct geologic units. Contacts between these geologic units are somewhat irregular, but are generally horizontal to gently dipping. These contacts are either abrupt or gradational, and they are usually fairly well defined by subtle discontinuities in grain size across the contact.

#### **4.2.4      Alluvial Outwash**

The alluvial outwash consists of medium- to fine-grained, poorly graded sand, with some silty sand and gravel zones. Occasional cobble or boulder zones are interspersed. The alluvial outwash is considered to be an intergrading of recent alluvium and the underlying Wisconsinan outwash. It may have formed contemporaneously with Wisconsin glaciation. The major portion of this alluvial outwash deposit, however, is believed to have formed during the *in situ* reworking of glacial outwash in post-Wisconsin to Recent time. Variations in stream flow, channel form and width, and obstructions easily led to renewed scouring of previously deposited sediment (Wisconsinan outwash) and redeposition elsewhere.

#### **4.2.5      Wisconsinan Outwash**

The Wisconsinan outwash consists of coarse- to medium-grained, poorly graded sand, silty sand, and gravel. The Wisconsinan outwash was deposited in the Mississippi Valley during the Wisconsin glacial advance into areas west, north, and east of the St Louis area. Major streams that carried outwash material included the Illinois and Missouri Rivers, as well as the Mississippi River.

#### **4.2.6      Illinoian Ice Contact Deposits**

The Illinoian ice contact deposits consist generally of fine- to coarse-grained, poorly graded sand, with numerous boulder, cobble, gravel, and occasional silty sand zones. The ice contact deposits are generally dense. They formed immediately adjacent to the glacial ice front, resulting in an extremely variable

particle size. The deposits are discontinuous and may not be undisturbed glacial deposits. Large particles from upstream glacial materials, along with alluvium, may have been placed in some areas as channel lag deposits. Till-like material (flow till) resulting from superglacial mud or debris flows are often found in the ice contact deposits.

#### 4.2.7 Limestone: St Genevieve Formation

The St Genevieve Formation is a light-colored, sandy, oolitic, cross-bedded calcarenite. The upper beds are often separated by thin, shaly limestone and thin shale partings. On the bluffs north of Alton, portions of the St Genevieve massive cross-bedded oolite are abruptly replaced by thin-bedded shaly or slabby oolitic limestone. Small faults and some solution activity have been noted in the limestone on the bluffs.

#### 4.2.8 Upper Stratigraphic Units

Nine distinct stratigraphic units have been identified in the upper 50 ft of the subsurface sand profile. This 50-ft-thick zone was thought to be the zone of primary influence for the pile driving effects tests. The overlying flood plain deposits were excavated. A subsurface profile (A-A) along the centerline of the pile driving effects test monolith trench was developed based on borehole sampling, in situ testing, and information obtained during the chemical grouting test program (Volume II). On this profile, Fig. 4.8, the contacts between various stratigraphic units have been inferred. Results and locations of in situ tests performed prior to pile driving are also shown in this figure. These units are described in order of stratigraphic position from highest to lowest.

**Unit A.** Unit A is a 1-ft-thick layer of fill that was placed at a few locations in the monolith trench after the flood plain clay was removed to bring the subgrade elevation to el 391. No fill was placed under or immediately adjacent to the test monoliths. The fill consisted of a loose to medium-dense gray-brown fine sand, which was occasionally infiltrated with cement grout, drilling mud, and other materials from drilling and surface preparation activities. No specific compactive effort was used in addition to the movement of a small front-end loader during placement.

**Unit B.** Unit B is the highest layer of natural recent alluvial sands. It is a medium-dense, gray-brown, fine to medium sand with a trace of silt and trace of fine gravel (SP). Grains are generally rounded to subrounded and uniform in size.

**Unit C.** Unit C is also a recent alluvial deposit. It is medium dense to dense, gray, fine to medium sand with a trace of silt and trace of fine gravel (SP). It is rounded to subangular, generally poorly graded sand, having occasional well-graded cross beds of coarser material.

**Unit D.** Unit D is medium-dense, gray, fine to coarse sand with a trace of silt and trace of angular fine gravel (SP). Generally, this recent alluvial sand is rounded to subangular and poorly graded. This unit is very similar to Unit C,

except that it is better graded, coarser grained, and contains local concentrations of fine gravel.

**Unit E.** Within the recent alluvium, a 1-ft- to 3-ft-thick layer of firm, gray, silty clay with a trace of fine sand (CL) was encountered. This clay is of medium to low plasticity. This layer was deposited in a quiescent environment between major depositional periods similar to that existing during deposition of the flood plain deposits.

**Unit F.** Unit F was deposited during the same period as Unit E. It is a very stiff, gray, fine sandy silt (SM-ML) grading into a dense, silty fine sand. This layer is discontinuous throughout the site, having differing thicknesses and amounts of silt and fine sand.

**Unit G.** Unit G is the alluvial outwash deposit. It consists of medium-dense, gray, fine to coarse sand with a trace of silt and trace of fine gravel (SP). Occasional shell, rock, and lignite fragments are also found. This unit is easily identified by the wide variety of its particle mineral types.

**Unit H.** At the top of the Wisconsinan outwash deposit is a layer of medium-dense to dense, gray, fine to medium sand with a trace of silt and trace to some fine gravel (SP). Occasional coarse sand layers 1 ft to 3 ft thick are found in this unit. Unit H is poorly graded and contains subrounded to subangular particles. Significant concentrations of black basaltic minerals were observed in the sand particle matrix.

**Unit L.** The intermittent fine to coarse zones become more continuous in the underlying Unit L. This unit is a medium-dense to dense, gray, fine to coarse sand with a trace of silt and trace to some fine gravel (SP). Unit I is poorly graded and contains subrounded to subangular particles.

#### 4.3 SOIL PROPERTIES

##### 4.3.1 General

The initial properties of the soil prior to pile driving were evaluated on the basis of in situ and laboratory tests. Grain-size distribution, in situ stresses, relative density, stiffness, shear strength, and permeability were assessed.

##### 4.3.2 Grain-Size Distribution

The grain-size distributions were evaluated in light of the stratigraphic profile. The ranges of grain-size distributions for Units A through D, and F through I are given in Fig. 4.9.

##### 4.3.3 Stresses

The in situ state of stress was evaluated from pressuremeter test results, groundwater level measurements, and observations of site preparation

excavation. The excavation of the monolith trench resulted in removal of 22.5 ft of flood plain clay and drawdown of the groundwater table to approximately el 390 by the dewatering system. This activity caused a reduction of vertical effective stress and induced overconsolidation. The degree of overconsolidation due to excavation can be expressed by an overconsolidation ratio OCR, that is:

$$\text{OCR} = \frac{\bar{\sigma}_{v\max}}{\bar{\sigma}_{vo}}$$

where:  $\bar{\sigma}_{v\max}$  = maximum past vertical effective stress; and  
 $\bar{\sigma}_{vo}$  = present in situ vertical effective stress.

In this case, the maximum past stress equals the present stress plus the excavation stress reduction. A plot of OCR vs elevation is given in Fig. 4.10.

The in situ horizontal total stress was measured during pressuremeter testing as the cell pressure at which the undisturbed elastic resistance of the soil was mobilized; that is, the stress at which the pressure-volume change curve becomes linear. The horizontal effective stress was obtained by subtracting the static pore pressure because the tests are assumed to be fully drained. The inferred horizontal effective stress profile before pile driving from borings PD-PM1, PM2, PM3, and PM4 is presented in Fig. 4.11. Superimposed on these stress measurements are profiles of stresses that correspond to certain values of  $K_o$ . The coefficient of earth pressure at rest  $K_o$  is the ratio of horizontal to vertical effective stress. The influence of the actual monolith trench configuration on vertical effective stress is included in this evaluation.

A profile of stress corresponding to a  $K_o$  derived from excavation-induced overconsolidation ratio is also shown in Fig. 4.11. The following equation was developed by Schmertmann (1976) based on sand-tank tests:

$$K_o = (1 - \sin \phi) (\text{OCR})^{0.42}$$

where:  $K_o$  = coefficient of earth pressure at rest;  
 $\phi$  = drained angle of internal friction; and  
OCR = overconsolidation ratio.

The in situ stress conditions derived from the pressuremeter test results are in excellent agreement with stresses calculated on the basis of overconsolidation induced by excavation of the monolith trench.

#### 4.3.4 Relative Density

Relative density profiles were derived from the results of static cone penetration tests and standard penetration tests. Relative density was calculated from static cone penetration resistance using an empirical correlation between

relative density, cone point resistance, and effective overburden stress. This correlation developed by Schmertmann (1976) was based on usage of an electrical cone (similar to WCC cone) in normally consolidated fine to medium sand (SP). It is necessary to reduce the measured cone penetration resistance  $q'_c$  to account for overconsolidation by a factor  $F$ , suggested by Schmertmann on the basis of sand-tank tests:

$$q'_c = F q_c$$

$$F = \frac{1}{1 + 0.75 (\text{OCR}^{0.42} - 1)}$$

where:  $q'_c$  = reduced cone point resistance;  
 $F$  = reduction factor;  
 $q_c$  = measured cone point resistance; and  
 $\text{OCR}$  = overconsolidation ratio.

The reduced  $q'_c$  was used with Schmertmann's correlation for normally consolidated sand. Relative density profiles calculated from cone penetration test soundings PD-Ca, C2, C3, C5, and C6 are given in Fig. 4.12.

Standard penetration resistances were related to relative density using Gibbs and Holtz' (1953) correlation, chosen because the sands tested in that study were similar to Ellis Island sand. The effect of vertical effective stress is also considered in this empirical correlation. The effect of overconsolidation can be considered by multiplying the vertical effective stress by a factor  $K_o/0.4$ . For normally consolidated sand, that factor is one. The Gibbs and Holtz relationship corrected for overconsolidation is closely approximated by the following equation:

$$D_r = 30 \frac{10N}{\bar{\sigma}_v \left( \frac{K_o}{0.4} \right) \left( \frac{2000}{144} \right) + 10}$$

where:  $D_r$  = relative density  
 $N$  = standard penetration resistance (N-value) blow/ft;  
 $\bar{\sigma}_v$  = vertical effective stress, t/ft<sup>2</sup>;  
 $K_o$  = coefficient of earth pressure at rest.

Relative densities calculated from N-values using the above equation for borings PD-PM1, PD-PM2, PD-PM3, PD-PM4, and PD2-SP1 are plotted in Fig. 4.12.

Comparisons of relative densities derived from N-values and static cone resistance show excellent agreement throughout the profile. Above el 365, an average relative density ranges from 50 to 60 percent. Below el 365, standard penetration resistance indicates a relative density of 70 to 80 percent and cone

penetration resistance indicates a relative density of 70 to 90 percent. The larger cone-derived densities are probably influenced by thin gravel layers, which increased cone point resistance. This is illustrated by the series of sharp peaks at el 373 and below el 365 on the cone profile. Review of grain-size distribution of samples obtained in strata exhibiting large cone resistance indicates the presence of coarse sand and fine gravel.

Maximum and minimum dry unit weights were determined on Osterberg samples in the laboratory using the modified Providence, funnel, tube, and cylinder tilt methods. Results of these laboratory tests are presented in Fig. 4.13.

#### 4.3.5 Stiffness

Soil stiffness is characterized by the soil elastic deformation modulus, which relates the stress-strain response of the soil up to a stress level where the shear strength of the soil is exceeded. The elastic deformation modulus (Young's modulus) was inferred from the results of static cone penetration tests, pressuremeter tests, laboratory consolidated drained triaxial compression tests, and cross-hole shear wave velocity measurements. Each of these moduli represent a drained modulus; however, the strain amplitude and plane of deformation were different for each test.

**Static Cone Modulus.** Elastic deformation modulus values can be determined from the static cone penetration test by using a strictly empirical correlation first suggested by Vesic (1970) for normally consolidated sand:

$$E_s = 2(1 + D_r^2) q_c$$

where:  $D_r$  = relative density; and  
 $q_c$  = cone penetration resistance.

A modification of this equation for overconsolidated sand was used. Derivation of the equation is given in Appendix K, Volume IIIA.

$$E_{s_{oc}} = \alpha_3 \cdot E_{s_{nc}}$$

$$\alpha_3 = \frac{1 + 2(1 - \sin\phi)}{1 + 2(1 - \sin\phi)} (OCR^{0.42})$$

where:  $E_{s_{oc}}$  = modulus in overconsolidated sand;  
 $E_{s_{nc}}$  = modulus in normally consolidated sand;  
 $\alpha_3$  = modulus correction;  
 $\phi$  = drained angle of internal friction; and  
 $OCR$  = overconsolidation ratio.

Modulus values calculated from static cone penetration tests in borings PD-C1, C2, C3, C5, and C6 are presented in Fig. 4.14.

**Pressuremeter Modulus.** Elastic deformation modulus values were calculated from pressuremeter tests using the slope of the linear pseudo-elastic portion of the volume-change vs pressure curve. An equation for cylindrical cavity expansion of a linearly elastic material under conditions of axial symmetry and plane strain was used:

$$E_s = 2V_0 (1+v) \Delta P / \Delta V$$

where:  $V_0$  = initial volume of measuring cell;  
 $v$  = Poisson's ratio;  
 $\Delta P$  = pressure increment; and  
 $\Delta V$  = volume increment resulting from  $\Delta P$

Modulus values calculated from pressuremeter tests in borings PD-PM1, PM2, PM3, and PM4 are presented in Fig. 4.15.

**Laboratory Modulus.** Elastic deformation modulus values were calculated from laboratory CID triaxial compression tests on undisturbed borehole samples and laboratory reconstituted samples. Initial tangent modulus and secant modulus at peak deviator stress (failure) were obtained from stress-strain curves. These moduli are plotted on Fig. 4.15 at a depth corresponding to a stratigraphic unit similar to that at which the sample was obtained.

**Shear Wave Modulus.** Elastic deformation modulus values can be determined from cross-hole shear wave velocity measurements using:

$$G = \rho V_s^2 \quad \text{and} \quad E = 2(1+v) G$$

where:  $G$  = shear modulus;  
 $\rho$  = mass density of soil;  
 $V_s$  = shear wave velocity; and  
 $v$  = Poisson's ratio.

Arrays PD-S-6, 7, 8, and PD-S-8, 9, 10 yielded the most reliable shear wave velocities; therefore, modulus values calculated from measurements in these arrays are plotted on Fig. 4.16.

**Comparison of Modulus Values.** Modulus values derived from cone penetration tests suggest that stiffness is relatively constant to approximately el 365, then increases sharply to a rather high value with large deviations from this value. The pressuremeter modulus values corroborate this trend, although the modulus

increase below el 365 is smaller. The shear wave modulus values increase gradually with depth, except at el 370 where the clay layer was encountered. A reasonable low average profile of cone-derived modulus is shown on Fig. 4.15. For most of the tests made at the test site, the cone modulus exceeds the pressuremeter modulus by 1 to 2 times due to differences in principal stress direction, stress duration, and strain amplitude. Secant modulus at failure from laboratory tests appears to agree with the pressuremeter modulus. The initial tangent modulus agrees fairly well with the cone modulus, except when the cone results are affected by the presence of coarse particles.

#### 4.3.6      Shear Strength

The shear strength of the subsurface sand can be characterized by the Mohr-Coulomb failure criterion:

$$\tau_f = \bar{c} + \bar{\sigma}_f \tan\phi$$

where:  $\tau_f$  = shear strength;  
 $\bar{c}$  = cohesion;  
 $\bar{\sigma}_f$  = effective stress on failure plane at failure; and  
 $\phi$  = drained angle of internal friction.

Results of laboratory triaxial tests from which these parameters can be derived are presented in Appendix K, Volume IIIA. Results indicate that the sand is cohesionless and develops its shear strength from the frictional component between sand grains. The drained angle of internal friction derived from these tests on undisturbed borehole samples and laboratory reconstituted samples is 39.5 degrees.

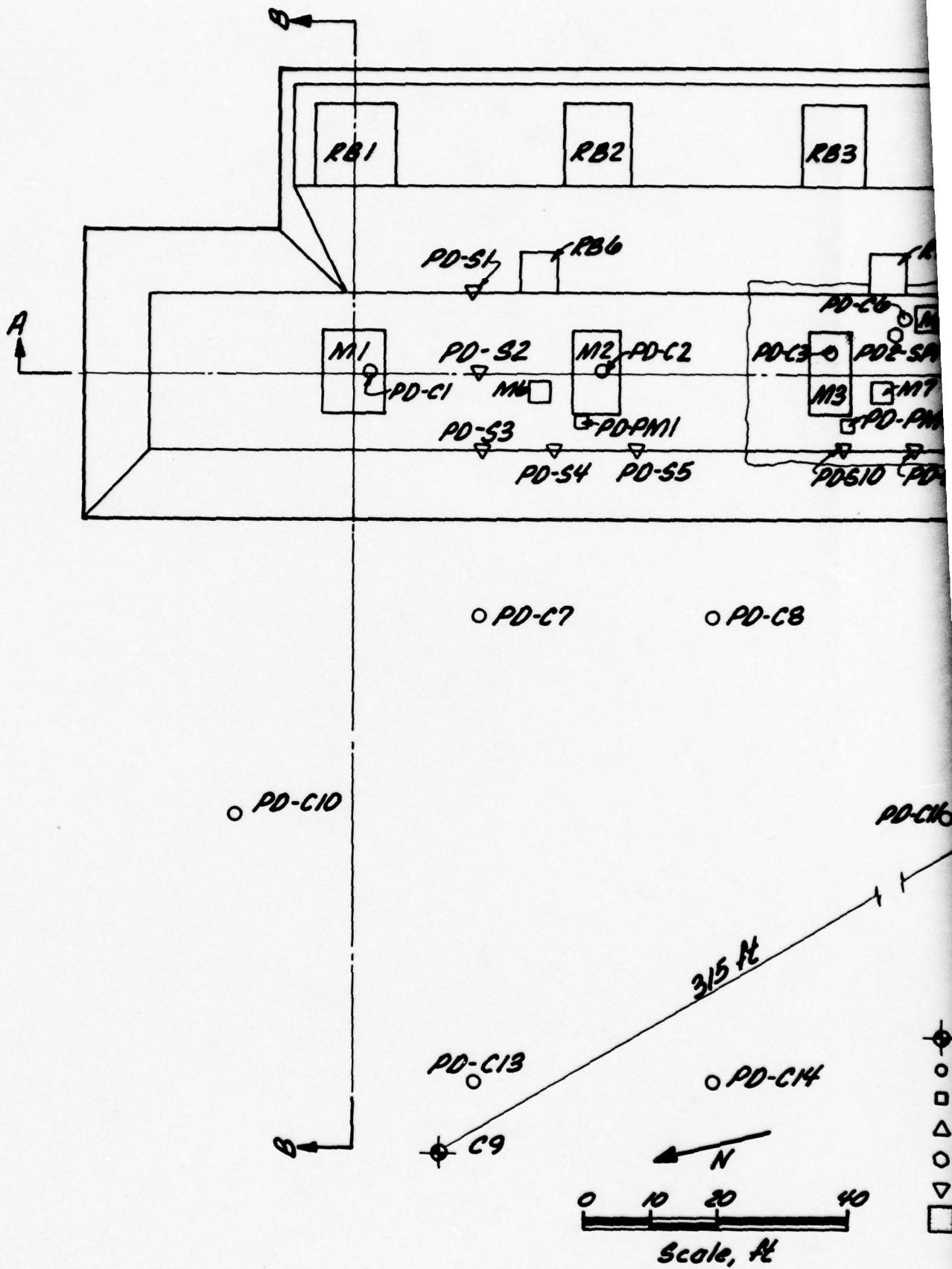
The drained angle of internal friction was derived from the results of static cone penetration and pressuremeter tests. Static cone penetration resistance was correlated to friction angle  $\phi$  using an empirical chart developed by Meyerhoff (1974). This correlation is independent of the in situ stress conditions. Friction angles calculated from the cone point resistance are plotted with depth in Fig. 4.17. The drained angle of internal friction was also determined from pressuremeter tests using a method developed by Hughes et al (1977). Friction angles calculated using this method are plotted on Fig. 4.17.

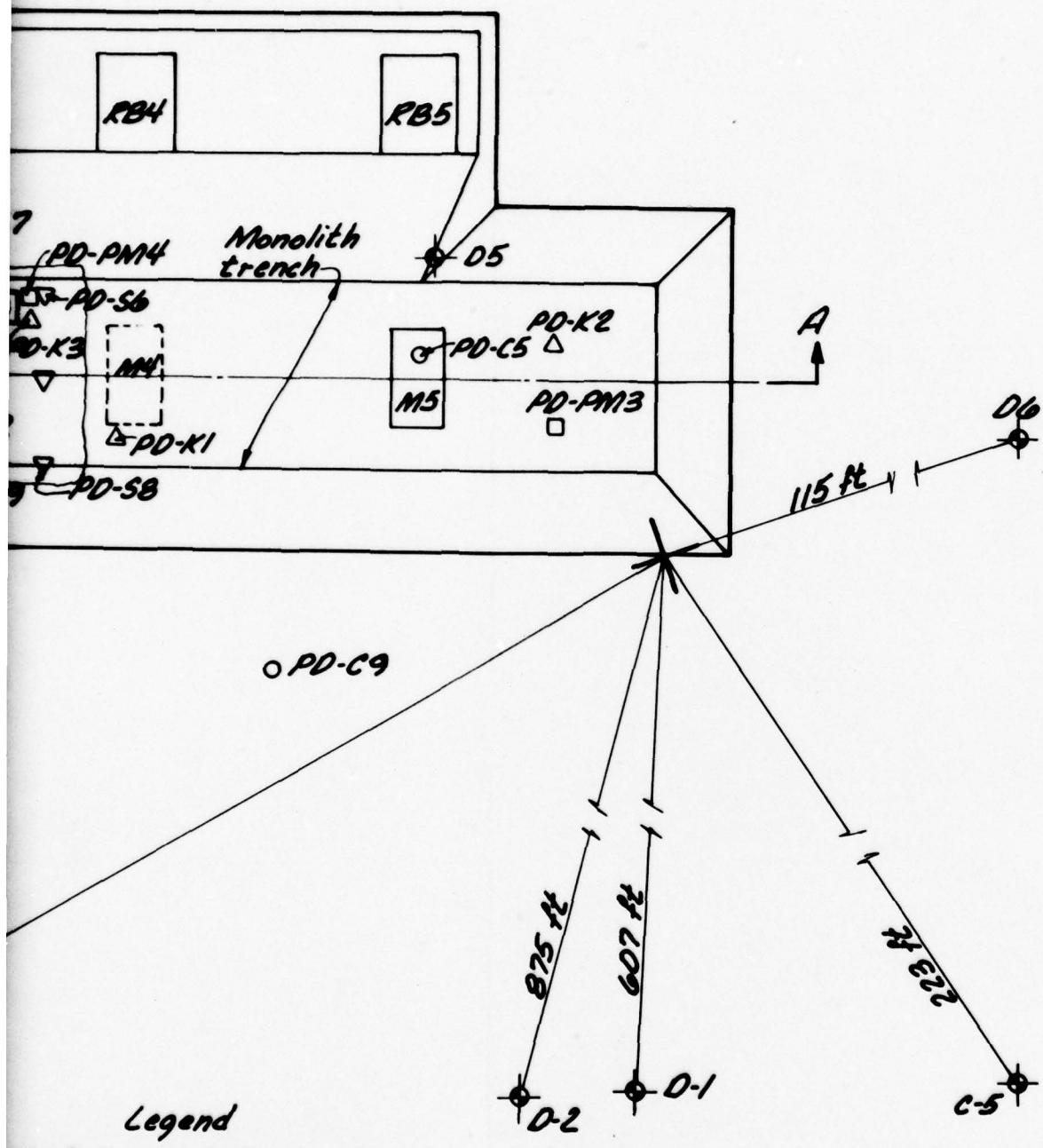
Above el 378, the cone indicated a lower value of friction angle than the pressuremeter. The pressuremeter indicated a relatively constant friction angle value with depth, ranging from 38 to 42 degrees. Below el 378, both cone and pressuremeter yielded an average angle of 40 degrees. The low value of  $\phi$  derived from the cone above el 365 may indicate an effect of overconsolidation, which is not accounted for in the empirical correlation. As discussed in the previous section, the increase at el 365 may be due to the influence of coarse particles in the outwash deposits; however, cone-derived angles in these lower deposits matched the laboratory-derived friction angle of about 40 degrees.

**Pressuremeter Limit Pressure.** The pressuremeter limit pressure (asymptote to which the volume-change vs pressure curve tends at large strains) has been used in design of shallow and deep foundations as representative of ultimate soil strength. The limit pressure has been related theoretically to shear strength in cohesive soils and friction angle in sands, but most often directly to ultimate bearing capacity. For this program, however, it provided an index to ultimate strength. Pressuremeter limit pressures from borings PD-PM1, PM2, PM3, and PM4 are plotted in Fig. 4.18. The pressuremeter limit pressure profile indicates a gradual increase in bearing capacity and ultimate shear strength with depth.

#### 4.3.7 Permeability

Borehole permeability testing in boreholes PD-K1, K2, and K3 provided a profile of permeability coefficient with depth before pile driving, as shown in Fig. 4.6. Also shown on this figure are permeability test results obtained in borings before site preparation throughout the main test site. In spite of the wide scatter of data, the latter tests fall within the range of values obtained before excavation of the test area. A significant increase in permeability is noted around el 360 to el 365, which corresponds to the stratigraphic contact between alluvial outwash and underlying glacial outwash deposits. In the coarser outwash deposits, permeabilities ranged from  $6 \times 10^{-1}$  to  $6 \times 10^{-4}$  cm/s, whereas in recent alluvium, permeabilities ranged from  $3 \times 10^{-2}$  to  $1.6 \times 10^{-4}$  cm/s. On the average, the glacial deposits were approximately ten times more pervious than the recent alluvium.

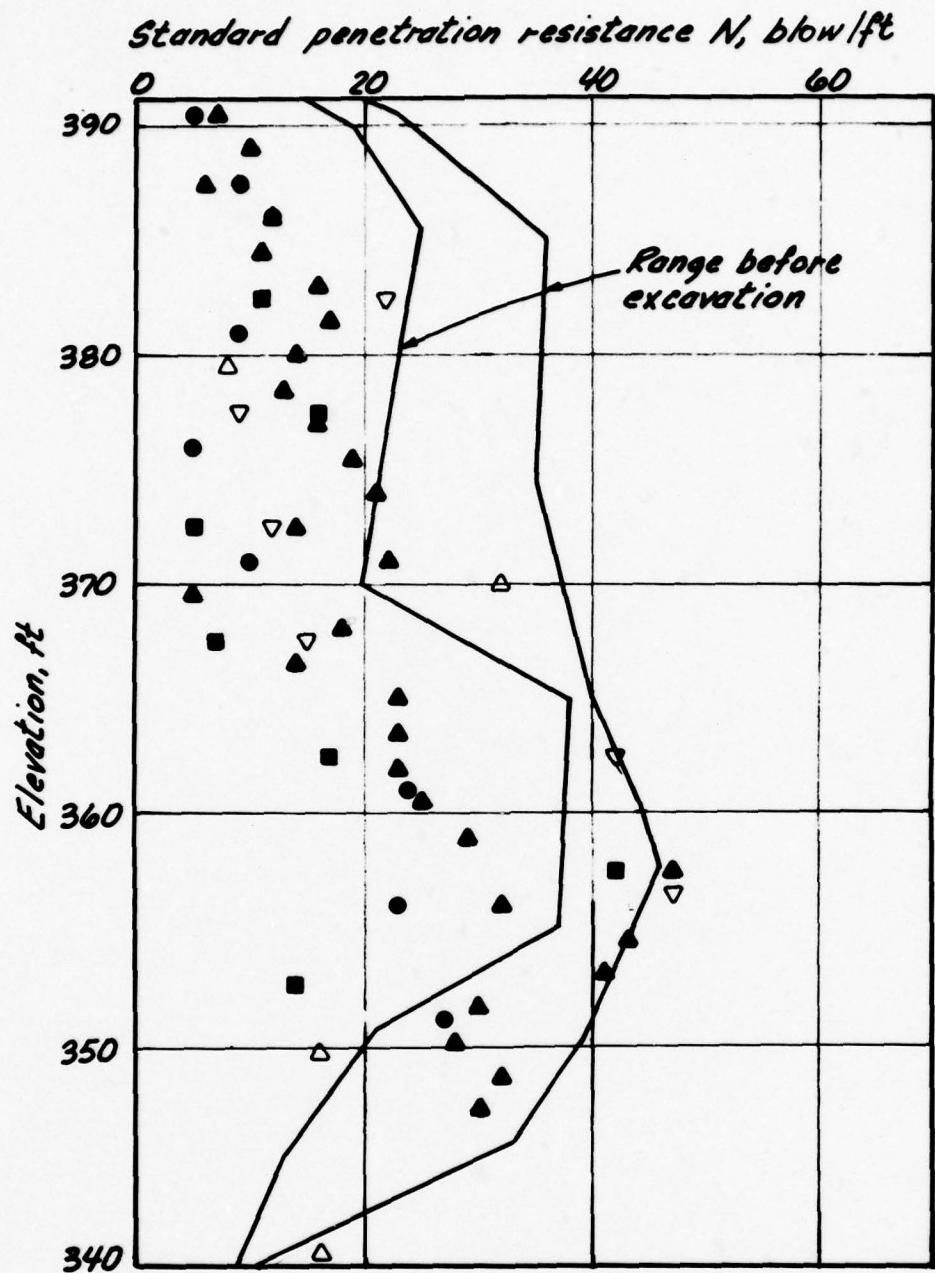




Before excavation boring  
 Cone penetration sounding  
 Pressuremeter boring  
 Permeability boring  
 Continuous SPT boring  
 Shear wave casing  
 Horizontal limit of grouted zone

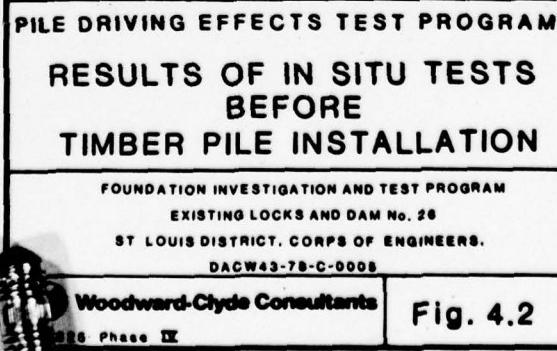
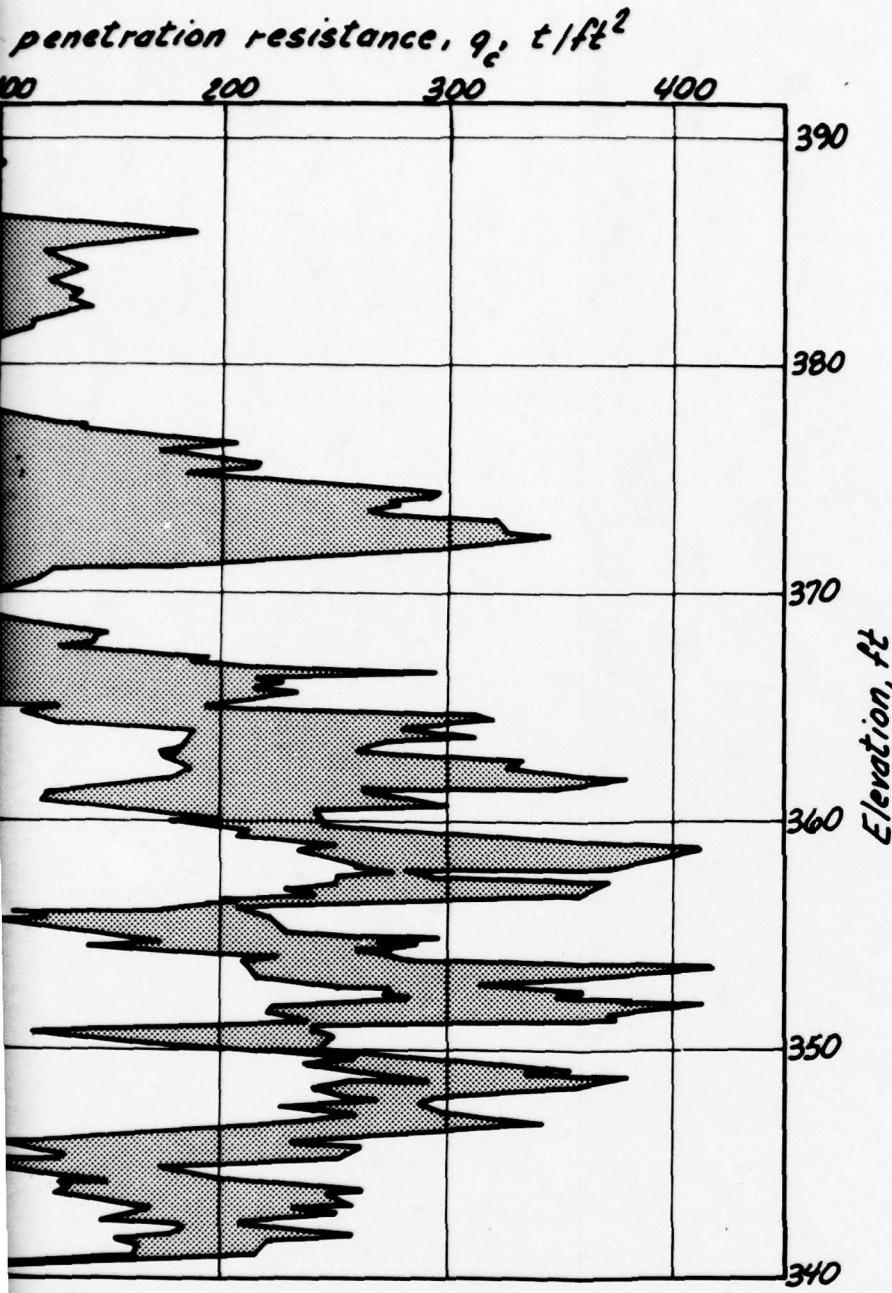
<b>PILE DRIVING EFFECTS TEST PROGRAM</b> <b>LOCATION OF</b> <b>SUBSURFACE INVESTIGATIONS</b> <b>BEFORE</b> <b>TIMBER PILE INSTALLATION</b>	
FOUNDATION INVESTIGATION AND TEST PROGRAM EXISTING LOCKS AND DAM NO. 26 ST LOUIS DISTRICT, CORPS OF ENGINEERS. DACW43-78-C-0008	
Woodward-Clyde Consultants Phase IV	Fig. 4.1

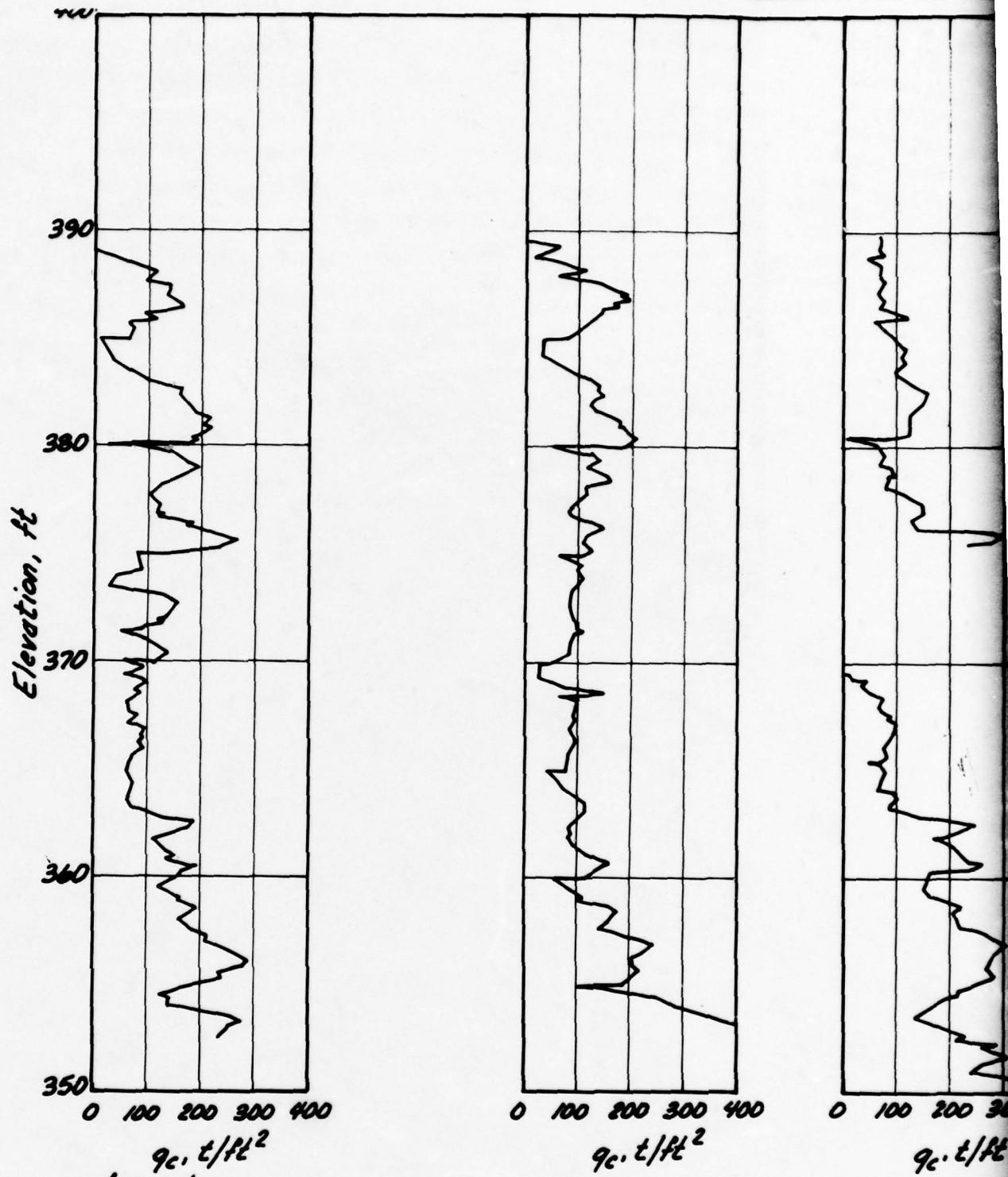
2



#### Legend

- $\nabla$  Boring PD-PM1
- $\circ$  Boring PD-PM2
- $\triangle$  Boring PD-PM3
- $\blacksquare$  Boring PD-PM4
- $\blacktriangle$  Boring PD2-SP1 (after timber pile installation, but outside zone of installation influence)
- $\blacksquare$  Range of static cone penetration resistance PD-C1, PD-C2, PD-C3, PD-C5, and PD-C6



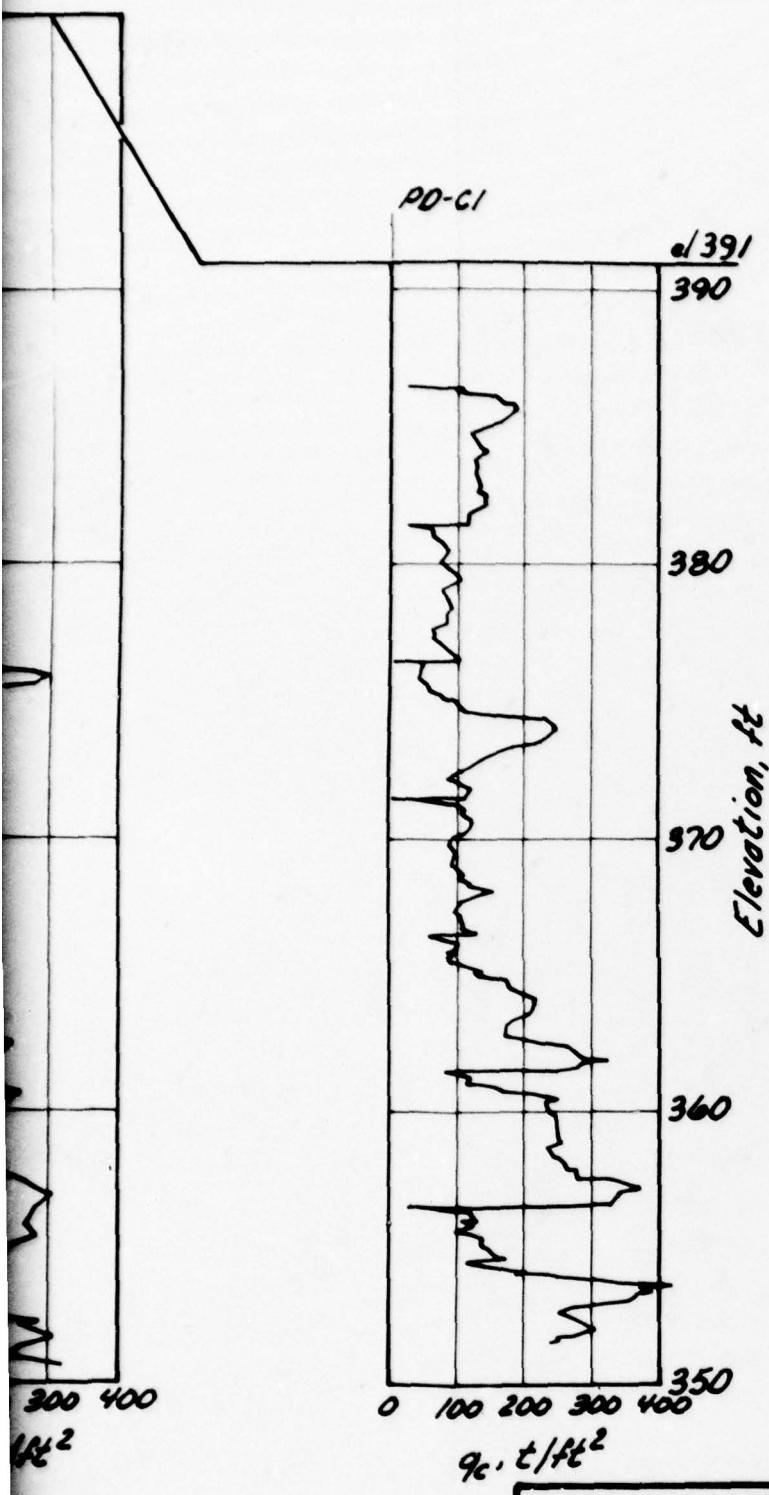


Legend

$q_c$  = Static cone penetration resistance

Note:

Profile made along section B-B Figure 4.1



**PILE DRIVING EFFECTS TEST PROGRAM  
RESULTS OF  
CONE PENETRATION SOUNDINGS  
IN  
PROTOTYPE PILE DRIVING AREA**

FOUNDATION INVESTIGATION AND TEST PROGRAM  
EXISTING LOCKS AND DAM NO. 20  
BY LOUIS DISTRICT, CORPS OF ENGINEERS.  
DACEW43-78-C-0000

Woodward-Clyde Consultants  
1982 Phase II

Fig. 4.3

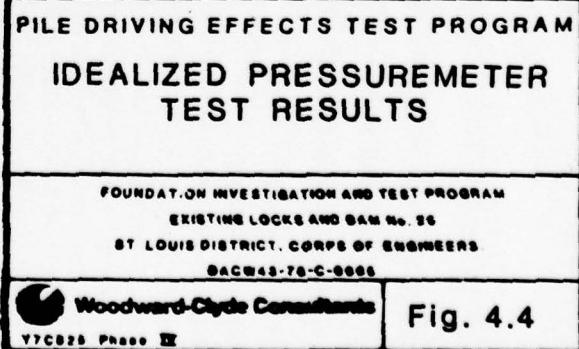
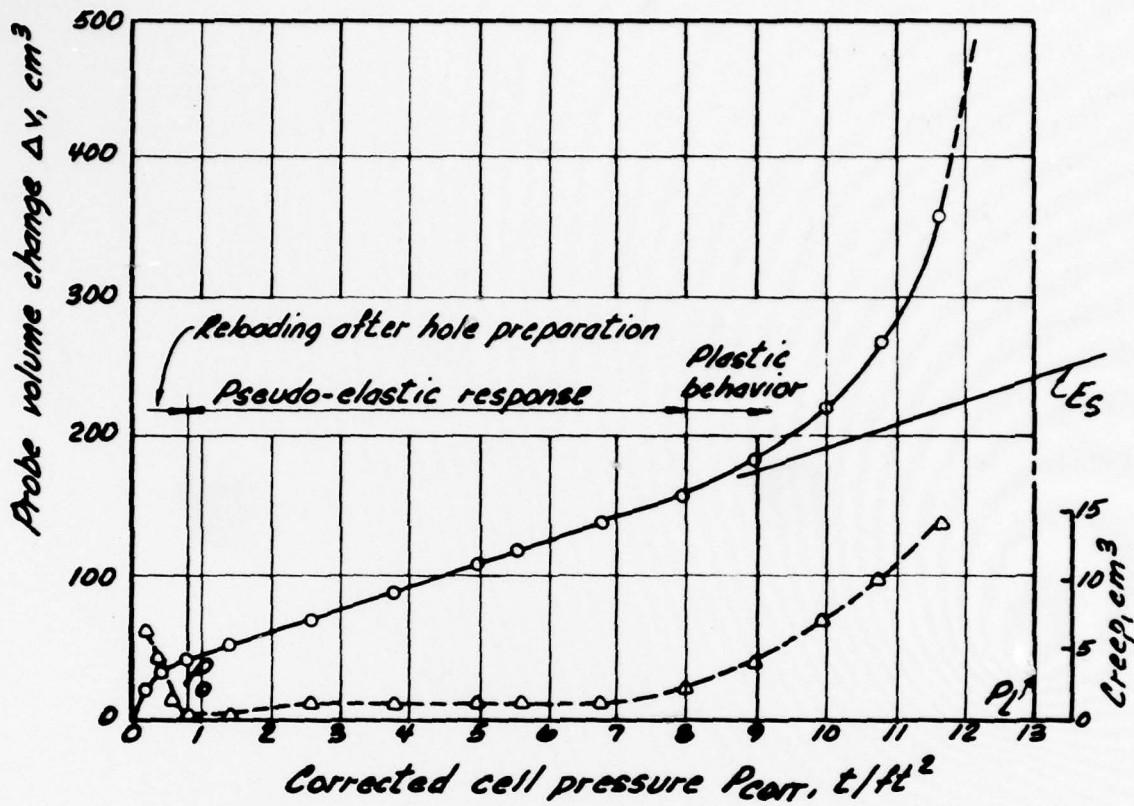
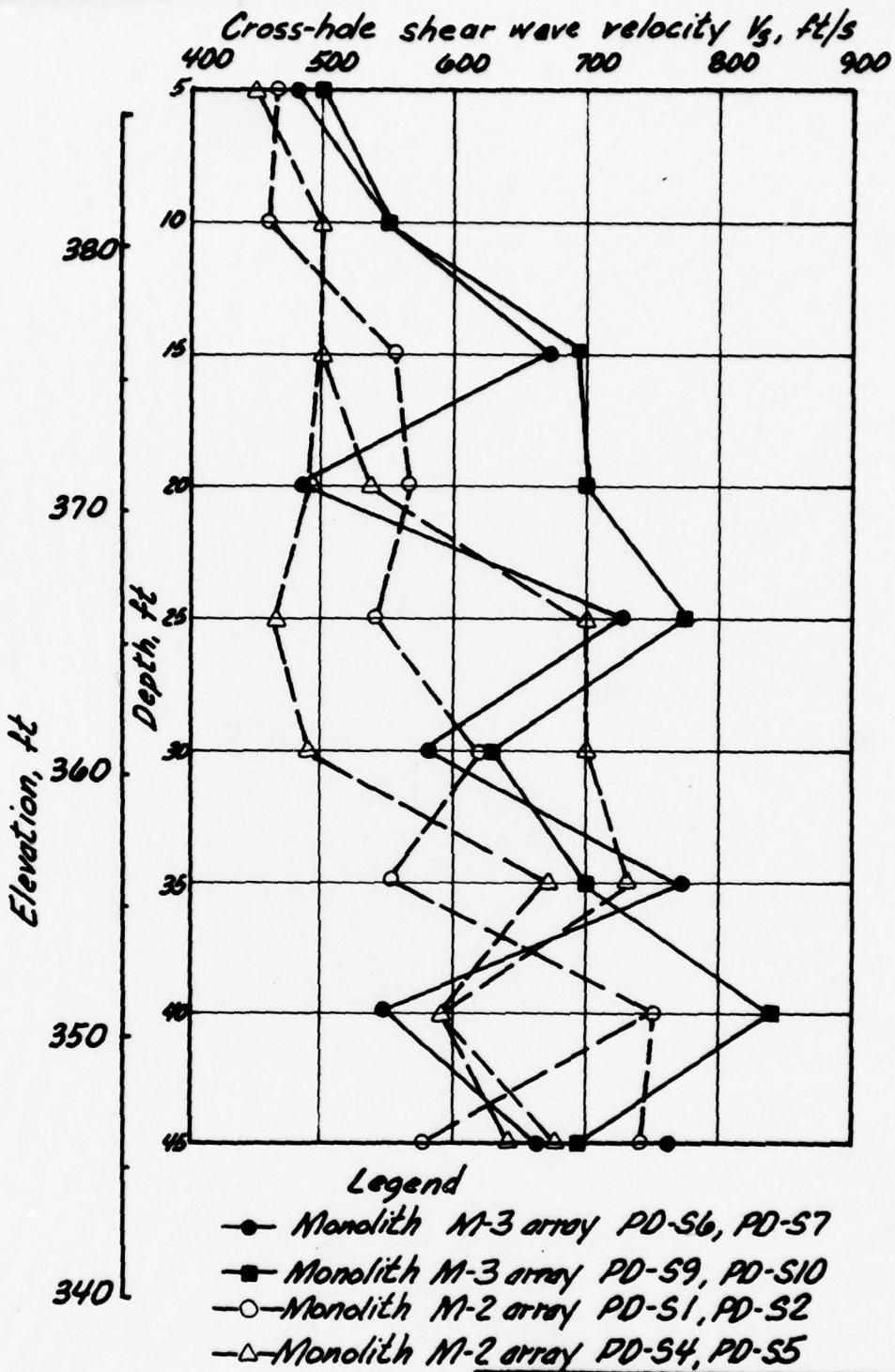
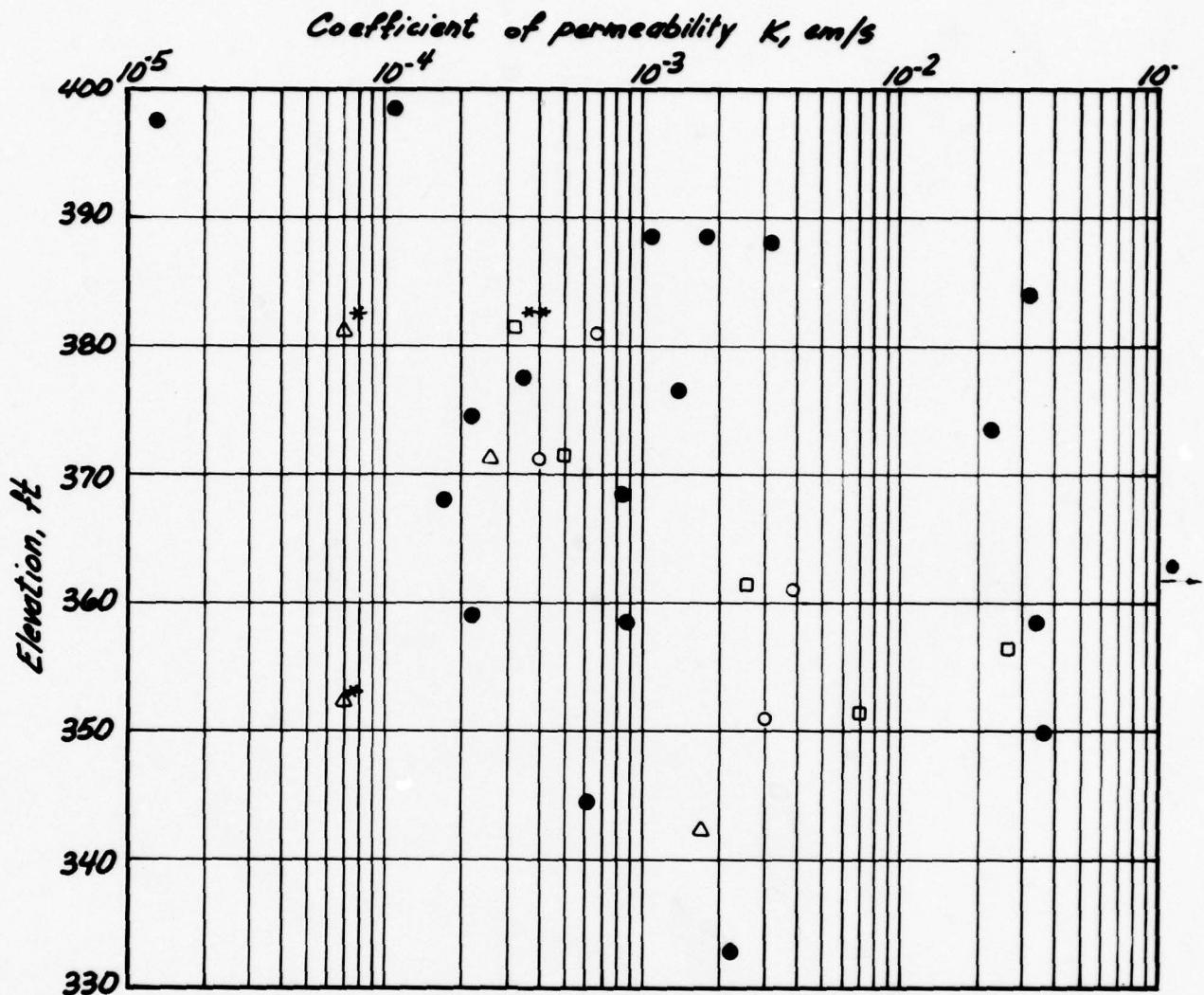


Fig. 4.4



**PILE DRIVING EFFECTS TEST PROGRAM**  
**SHEAR WAVE VELOCITIES**  
**BEFORE**  
**TIMBER PILE INSTALLATION**

FOUNDATION INVESTIGATION AND TEST PROGRAM EXISTING LOCKS AND DAM No. 28 ST. LOUIS DISTRICT, CORPS OF ENGINEERS. DACW43-78-C-0008
Woodward-Clyde Consultants <small>Y7C825 Phase II</small>
<b>Fig. 4.5</b>



### *Legend*

- Boring before excavation
  - Boring PD-K1
  - △ Boring PD-K2
  - Boring PD-K3
  - \* Insufficient time
  - \*\* Insufficient head

#### **PILE DRIVING EFFECTS TEST PROGRAM**

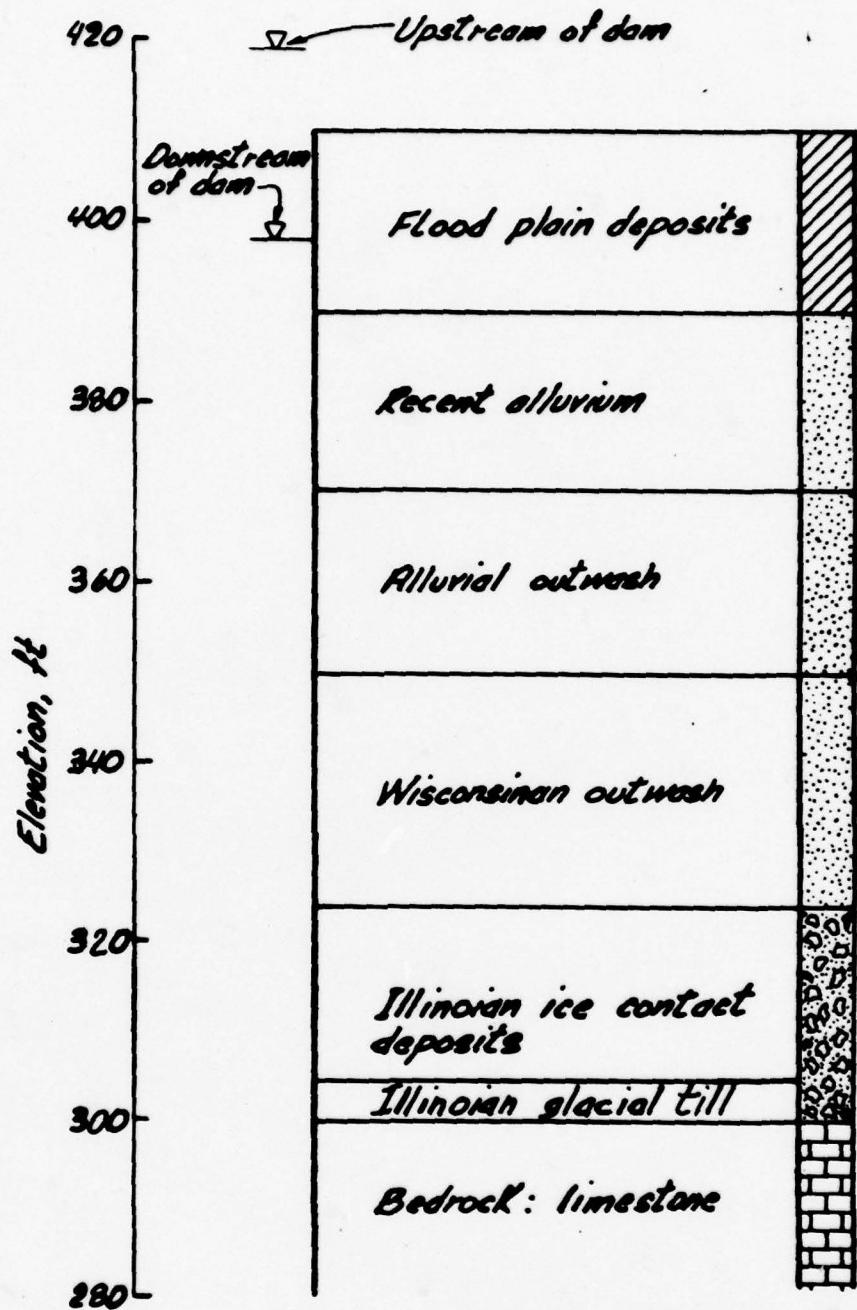
**PERMEABILITY TEST RESULTS  
BEFORE  
TIMBER PILE INSTALLATION**

**FOUNDATION INVESTIGATION AND TEST PROGRAM  
EXISTING LOCKS AND DAM NO. 20  
ST LOUIS DISTRICT, CORPS OF ENGINEERS.**



Woodward-Clyde Consultants  
V7C625 Phase II

**Fig. 4.6**



PILE DRIVING EFFECTS TEST PROGRAM

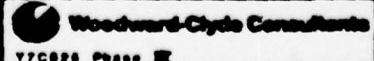
**GENERALIZED  
SUBSURFACE PROFILE  
IN VICINITY OF TEST AREA**

FOUNDATION INVESTIGATION AND TEST PROGRAM

EXISTING LOCKS AND DAM NO. 20

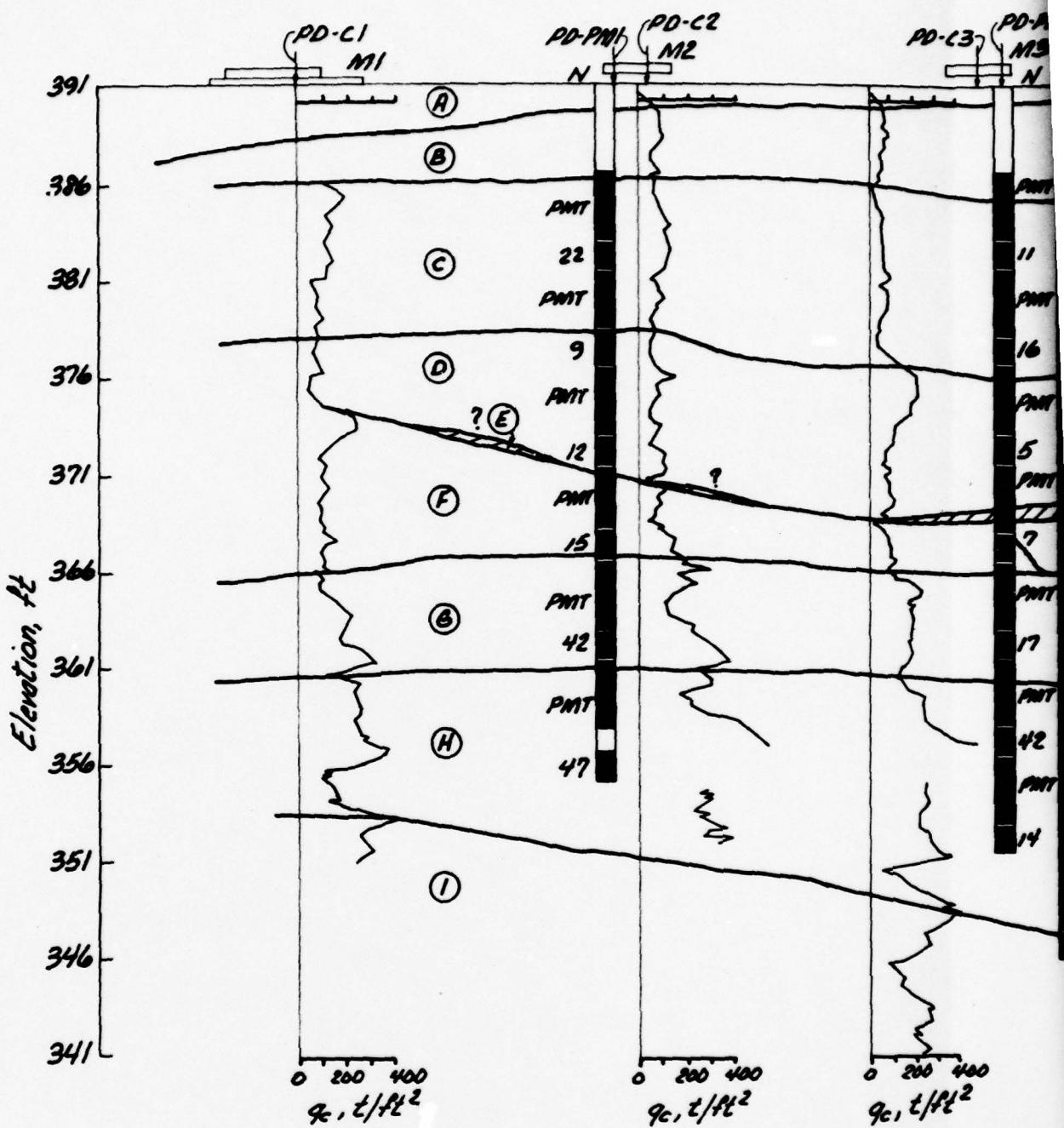
BY LOUIS DISTRICT, CORPS OF ENGINEERS.

DAGW43-70-6-0000



Y7C925 PHASE II

Fig. 4.7



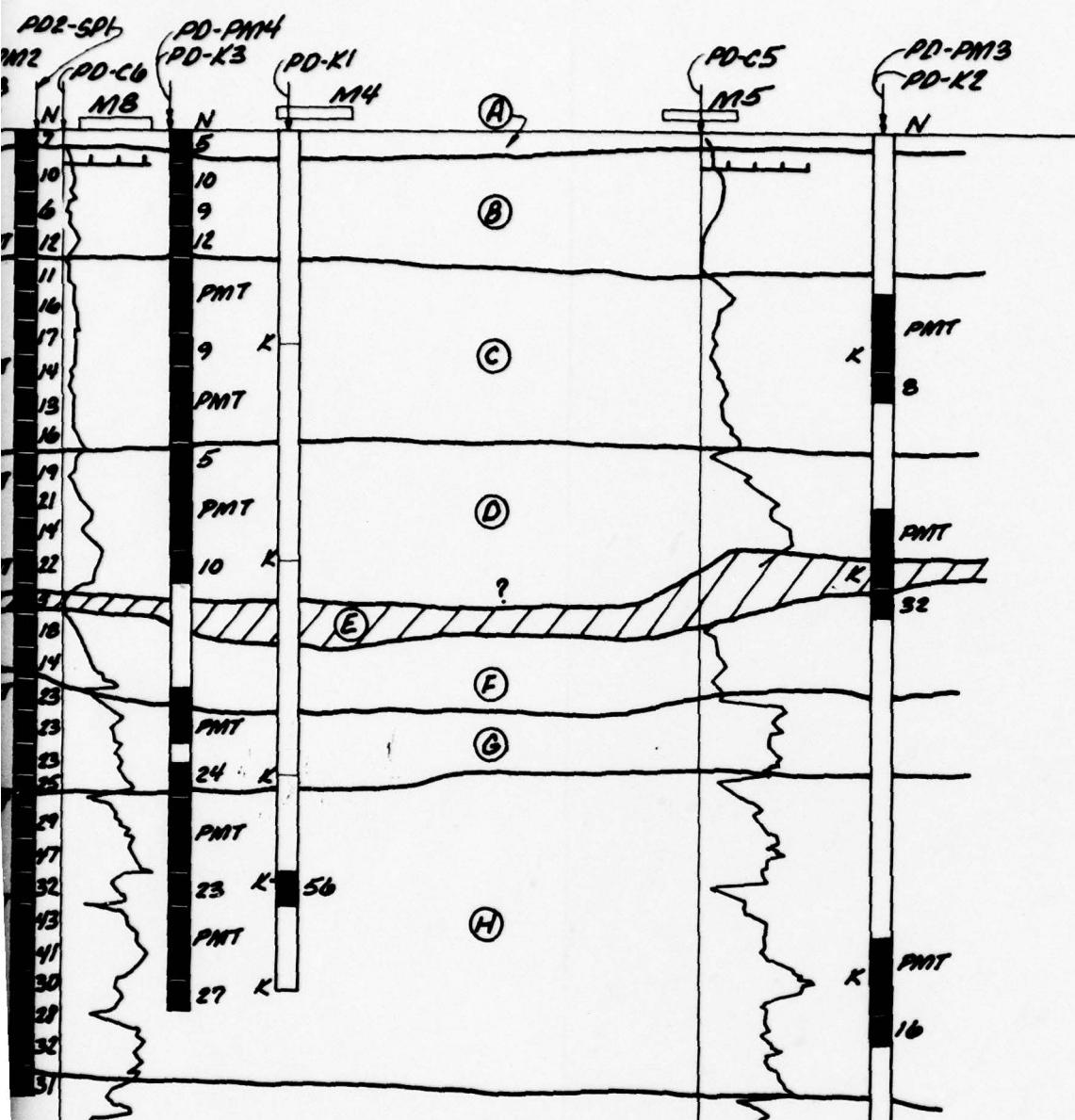
#### STRATIGRAPHY

- (A) Loose to medium dense grey-brown fine SAND w/occ lenses of cement grout (fill)
- (B) Medium dense grey-brown fine to medium SAND, trace of silt, trace fine gravel (SP)
- (C) Medium dense grey fine to medium SAND, trace silt, trace fine gravel, occasionally grading with coarse sand (SP)
- (D) Medium dense grey fine to coarse SAND, trace silt, trace angular fine gravel (SP)

- (E) Firm grey silty CLAY, trace fine sand (CL)
- (F) Very stiff grey fine sandy SILT (SM-ML)
- (G) Medium dense grey fine to coarse SAND, ALLUVIAL OUTWASH
- (H) Medium dense to dense grey fine to medium some fine gravel, occasionally grading with coarse sand (SP)
- (I) Medium dense to dense grey fine to coarse fine gravel (SP)

Note:

For location of profile A-A refer to Fig. 4.1



#### Legend

$q_c$ : Static cone penetration resistance

PMT: Pressuremeter test

N: Standard penetration resistance, blowcount

K: Falling head permeability test

$q_c, t/ft^2$

$0 \quad 200 \quad 400$

$q_c, t/ft^2$

$K$

PMT

$K$

PMT

(1)

#### PILE DRIVING EFFECTS TEST PROGRAM

#### SUBSURFACE PROFILE A-A

FOUNDATION INVESTIGATION AND TEST PROGRAM

EXISTING LOCKS AND DAM NO. 26

ST LOUIS DISTRICT, CORPS OF ENGINEERS.

DACW43-78-C-0008

Woodward-Clyde Consultants

V7C625 Phase IV

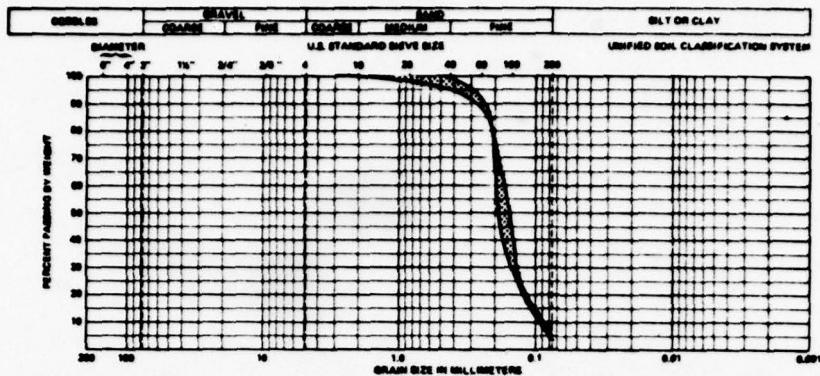
Fig. 4.8

WISCONSINAN  
OUTWASH

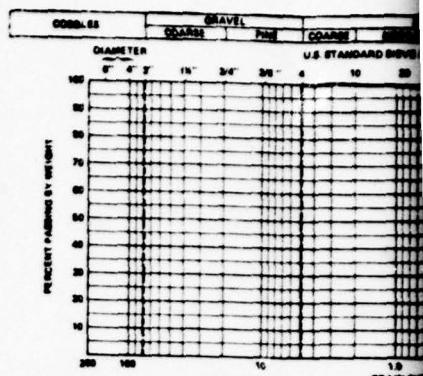
trace silt, trace fine gravel (SP)

SAND, trace of silt, trace to coarse sand (SP)

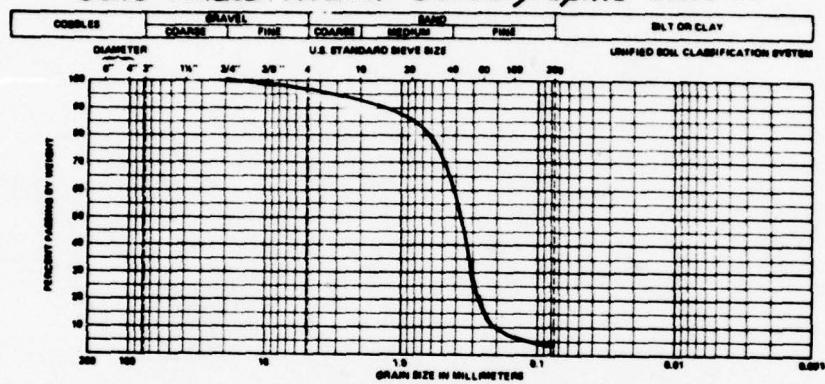
SAND, trace silt, trace to some



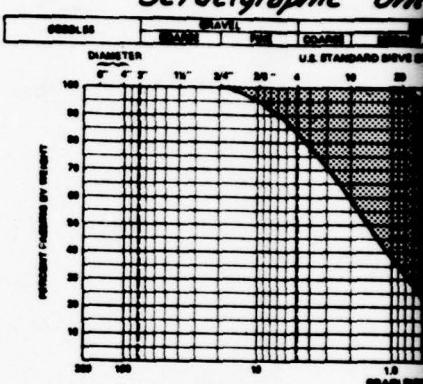
*Sand lenses within Stratigraphic unit A*



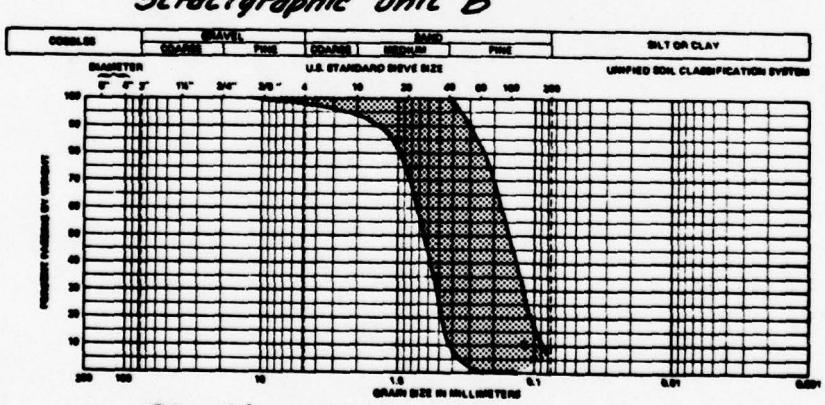
*Stratigraphic unit B*



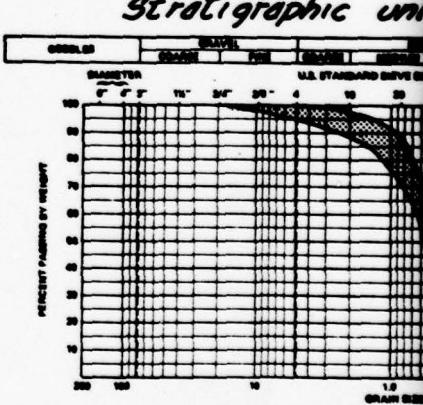
*Stratigraphic unit C*



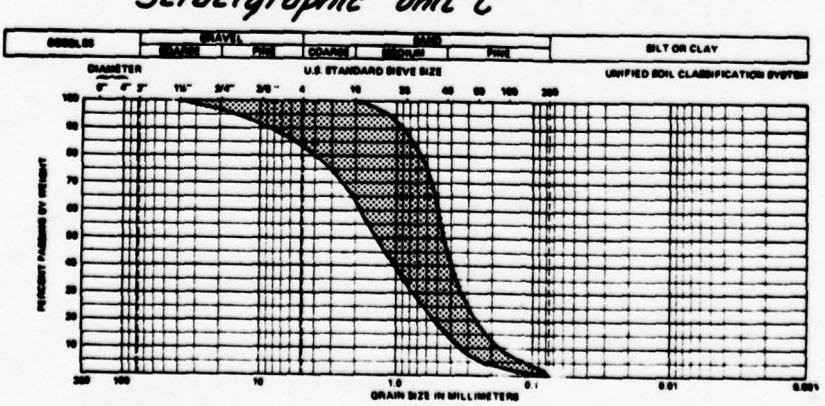
*Stratigraphic unit D*



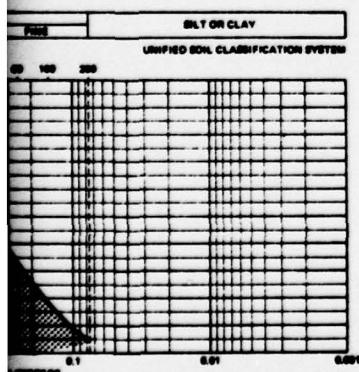
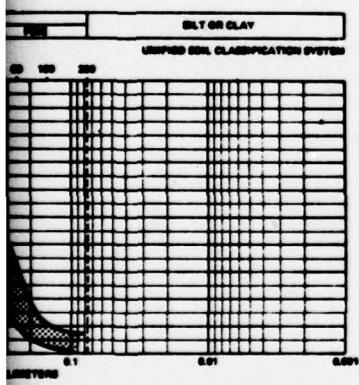
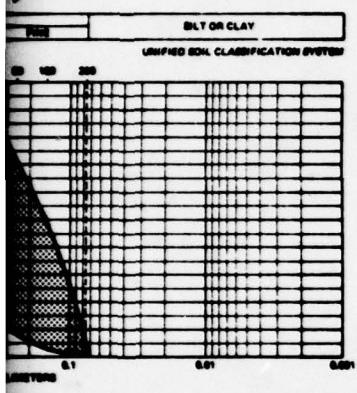
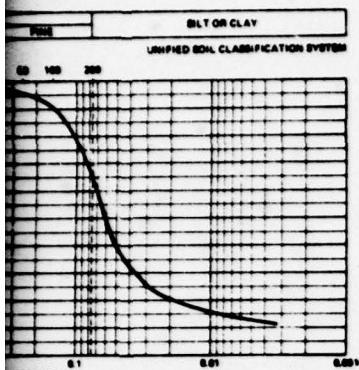
*Stratigraphic unit E*

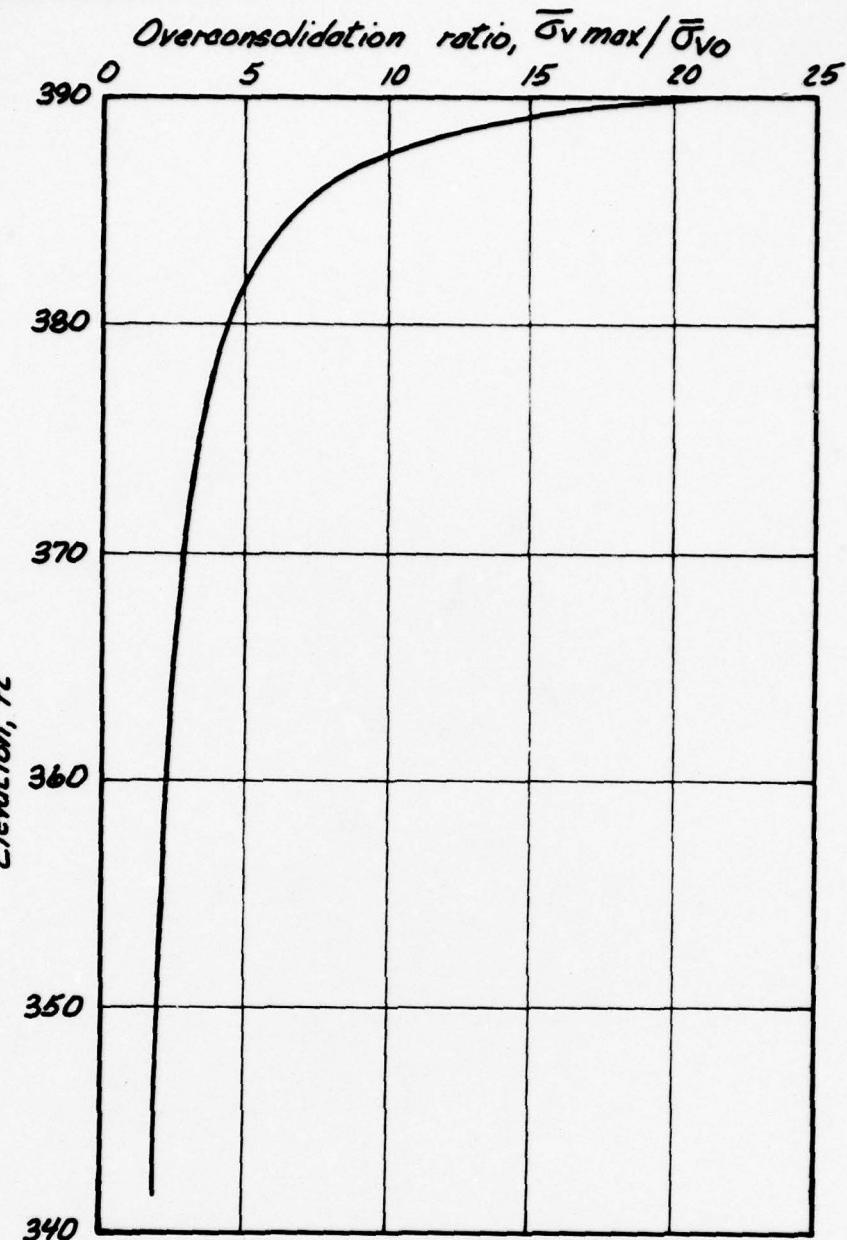


*Stratigraphic unit F*



*Stratigraphic unit G*





### Legend

$\bar{\sigma}_v \text{ max}$  = Maximum post vertical effective stress

$\bar{\sigma}_{v0}$  = Present in situ vertical effective stress

### Notes:

- (1) Overconsolidation caused by excavation of monolith trench
- (2) Reduction in stress estimated from measured density

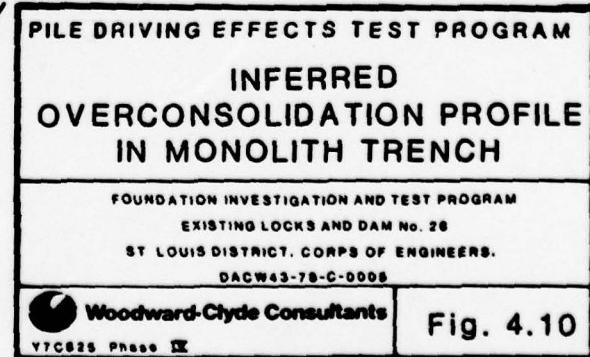
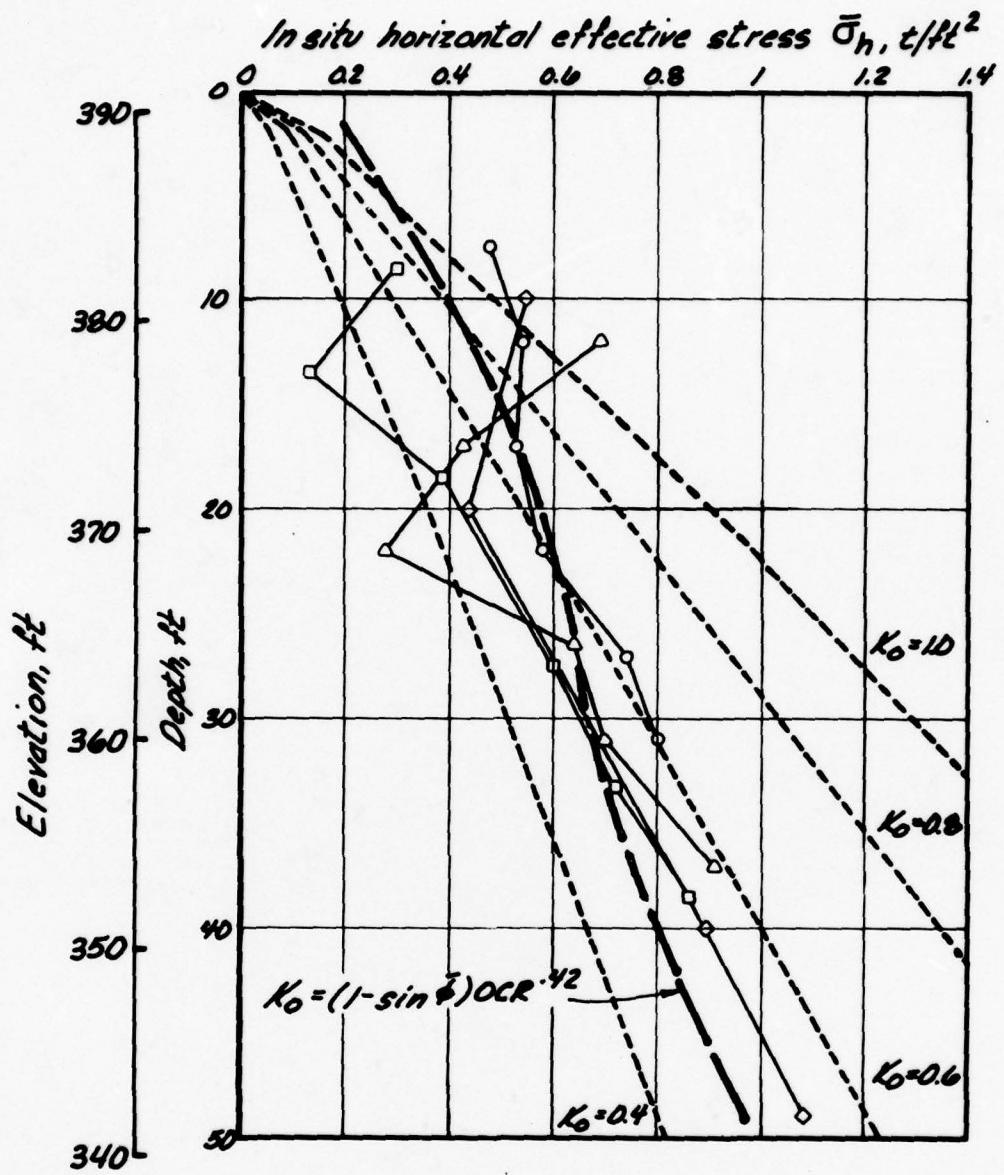


Fig. 4.10

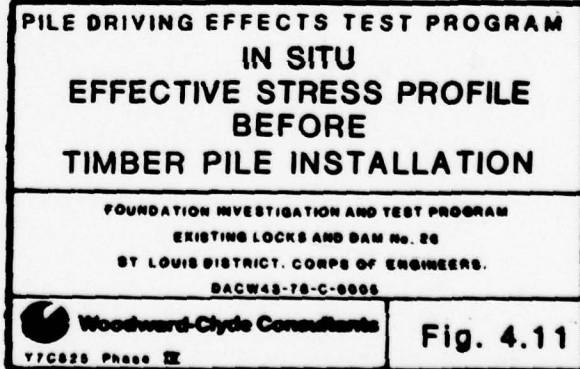


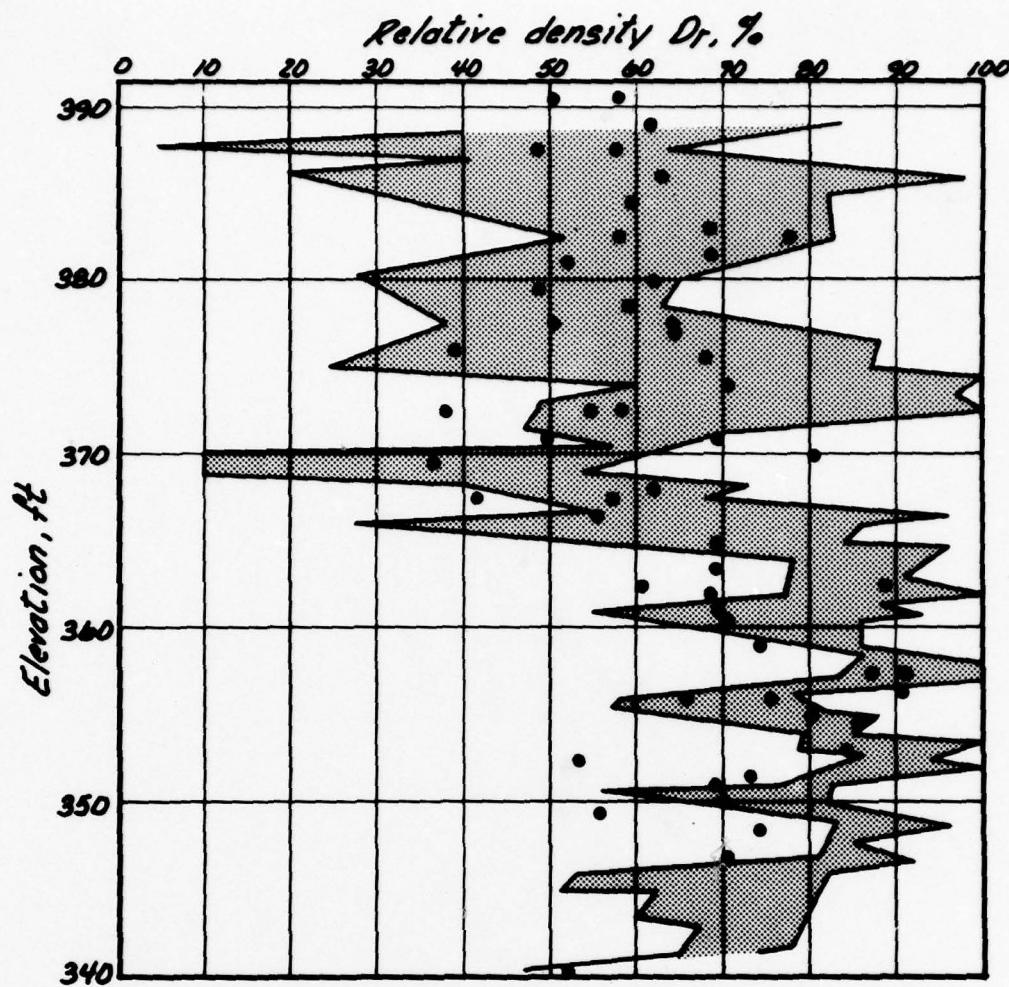
Legend

- PD-PM1
- △— PD-PM2
- ◇— PD-PM3
- PD-PM4
- $K_o = \bar{\sigma}_h / \bar{\sigma}_v$

Note:

Horizontal stress measured  
in pressure meter test  
 $K_o$  calculated from excavation  
induced overconsolidation



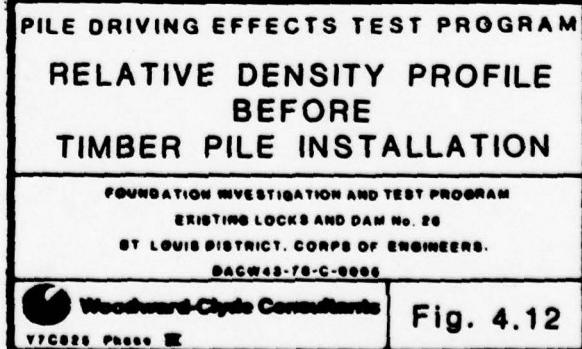


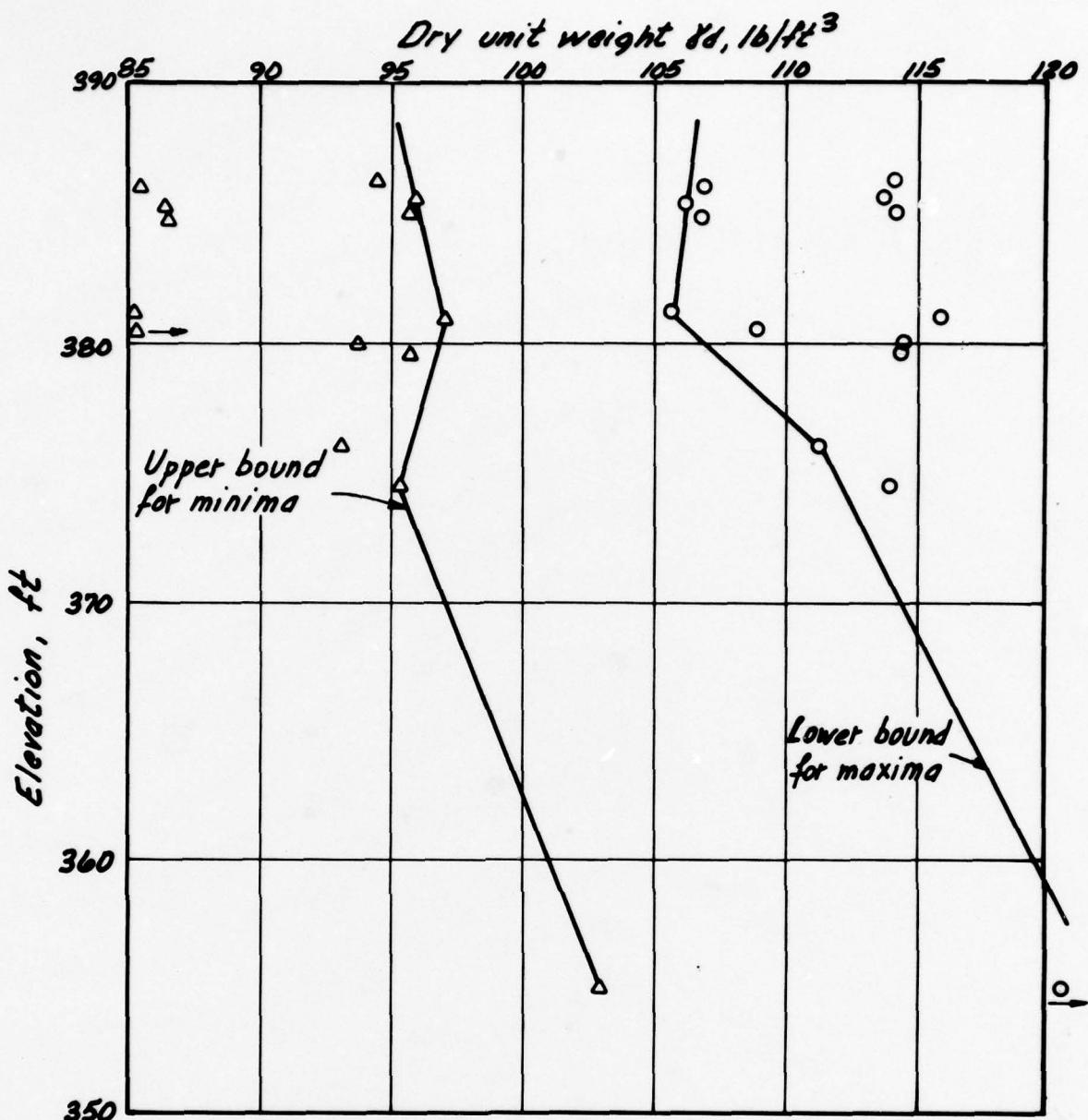
### Legend

- Range for cone soundings PD-C1, PD-C2, PD-C3, PD-C5, and PD-C6
- From standard penetration resistance tests, borings PD-PM1, PD-PM2, PD-PM3, PD-PM4 and PD2-SPI

### Notes:

- (1) Gibbs and Holtz (1953) correlation used for standard penetration tests
- (2) Schmertmann (1976) correlation used for static cone penetration tests



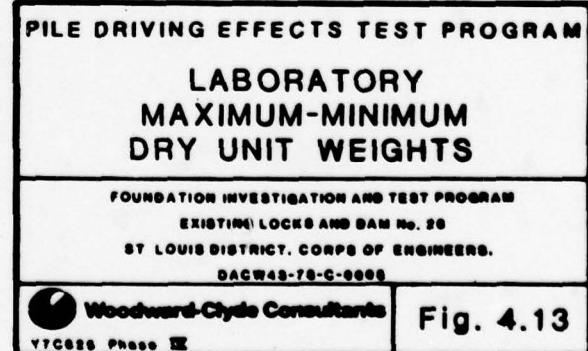


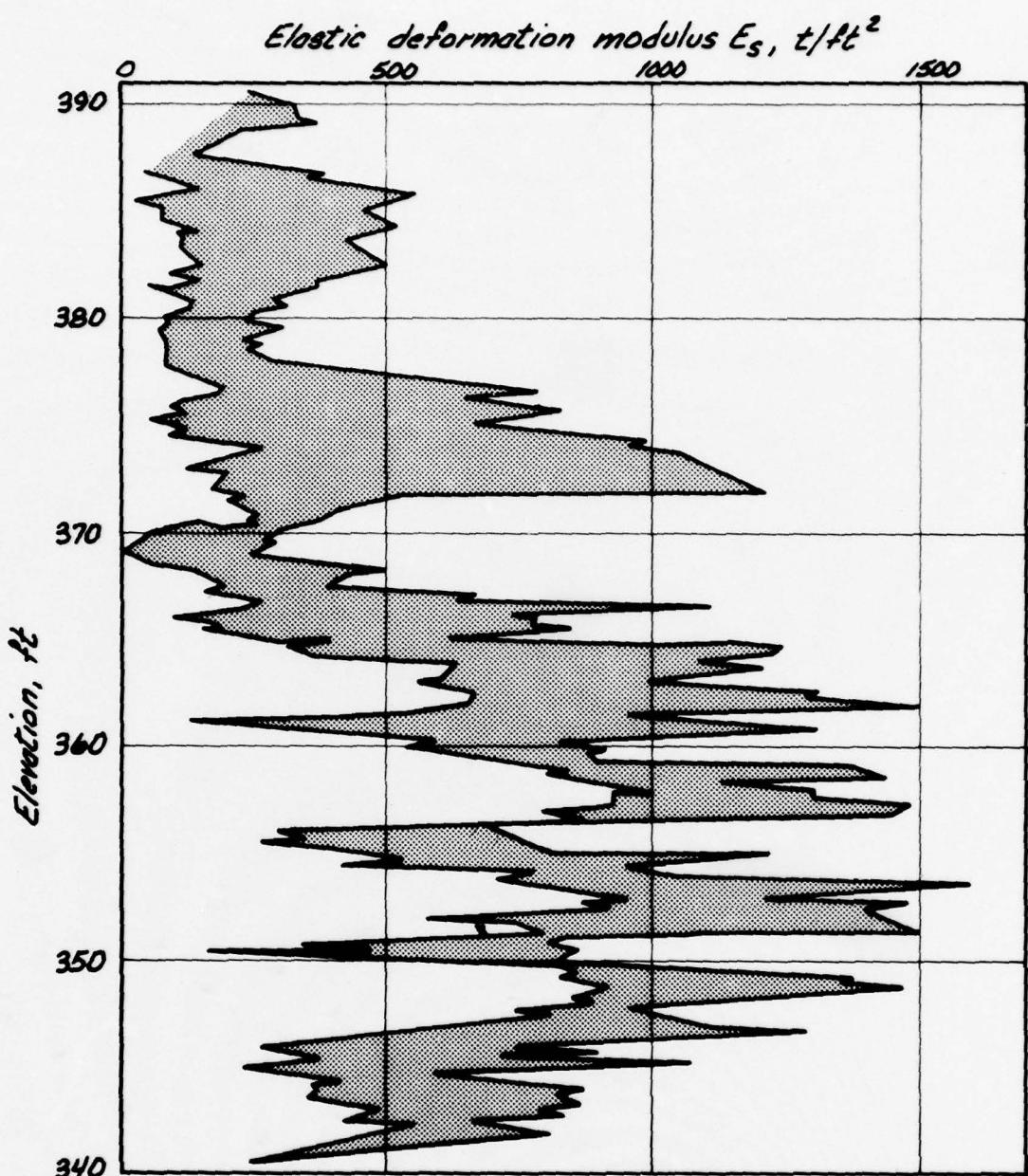
### Legend

- Maximum dry unit weight
- △ Minimum dry unit weight

### Note:

Maximum and minimum dry unit weights determined on Osterberg samples using the modified Providence, funnel, tube, and cylinder tilt methods





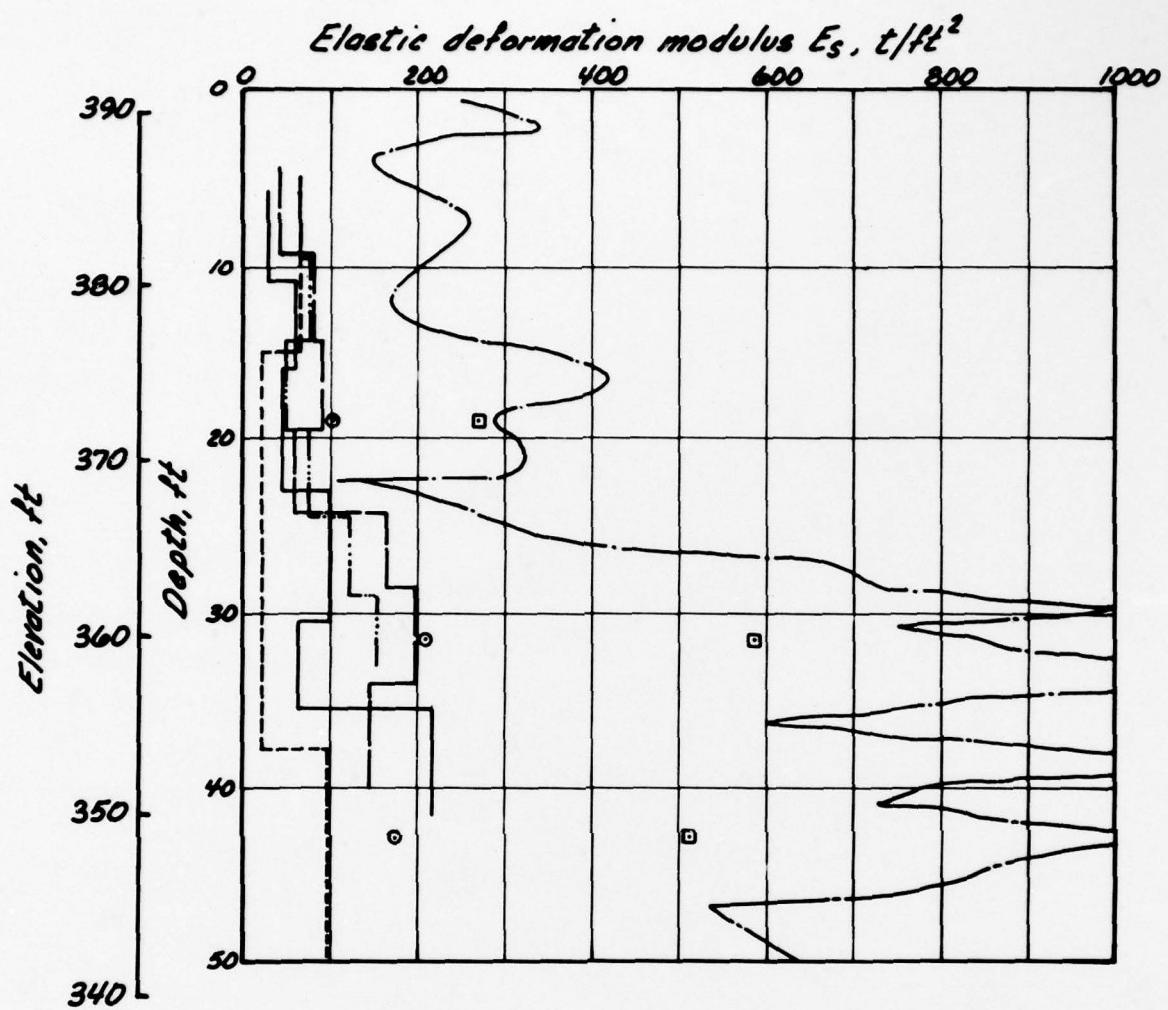
**Legend**

■ Elastic deformation modulus range for static cone penetration tests, PD-C1, PD-C2, PD-C3, PD-C5 and PD-C6

**Note:**

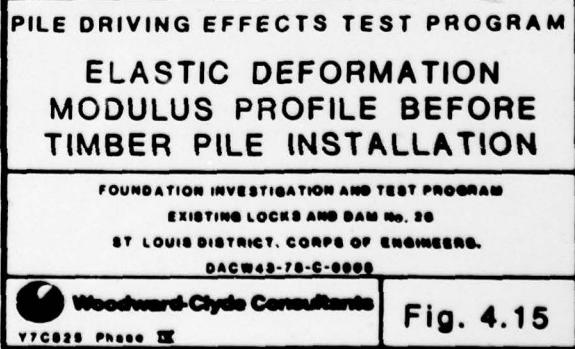
Static cone modulus determinations made with Vesic's correlation (1970) corrected for overconsolidation

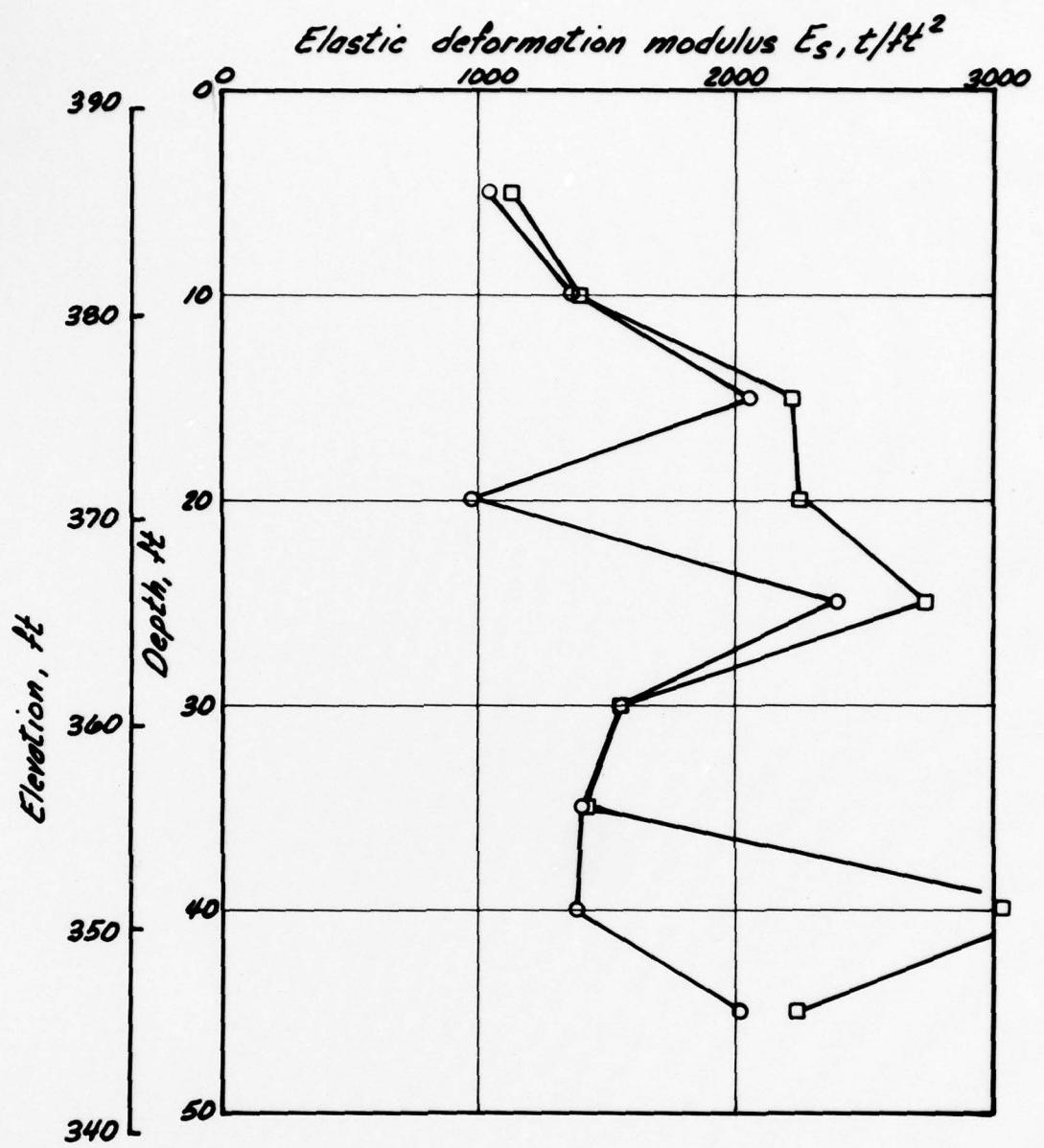
<b>PILE DRIVING EFFECTS TEST PROGRAM</b> <b>ELASTIC DEFORMATION MODULUS</b> <b>DERIVED FROM STATIC CONE</b> <b>PENETRATION TESTS</b>	
<small>FOUNDATION INVESTIGATION AND TEST PROGRAM EXISTING LOCKS AND DAM No. 26 ST LOUIS DISTRICT, CORPS OF ENGINEERS. DACPW43-78-C-0008</small>	
 Woodward-Clyde Consultants VTCB25 Phase III	<b>Fig. 4.14</b>



### Legend

- Boring PD-PM1
  - Boring PD-PM2
  - - - Boring PD-PM3
  - - - Boring PD-PM4
  - Average cone penetration test sounding
  - Second modulus at failure
  - Initial tangent modulus
- } CTD triaxial tests





*Legend*

- Array PD-56  
PD-57  
PD-58
- Array PD-58  
PD-59  
PD-610

PILE DRIVING EFFECTS TEST PROGRAM

ELASTIC DEFORMATION  
MODULUS FROM CROSS-HOLE  
SHEAR WAVE VELOCITY  
MEASUREMENTS BEFORE  
TIMBER PILE INSTALLATION

FOUNDATION INVESTIGATION AND TEST PROGRAM

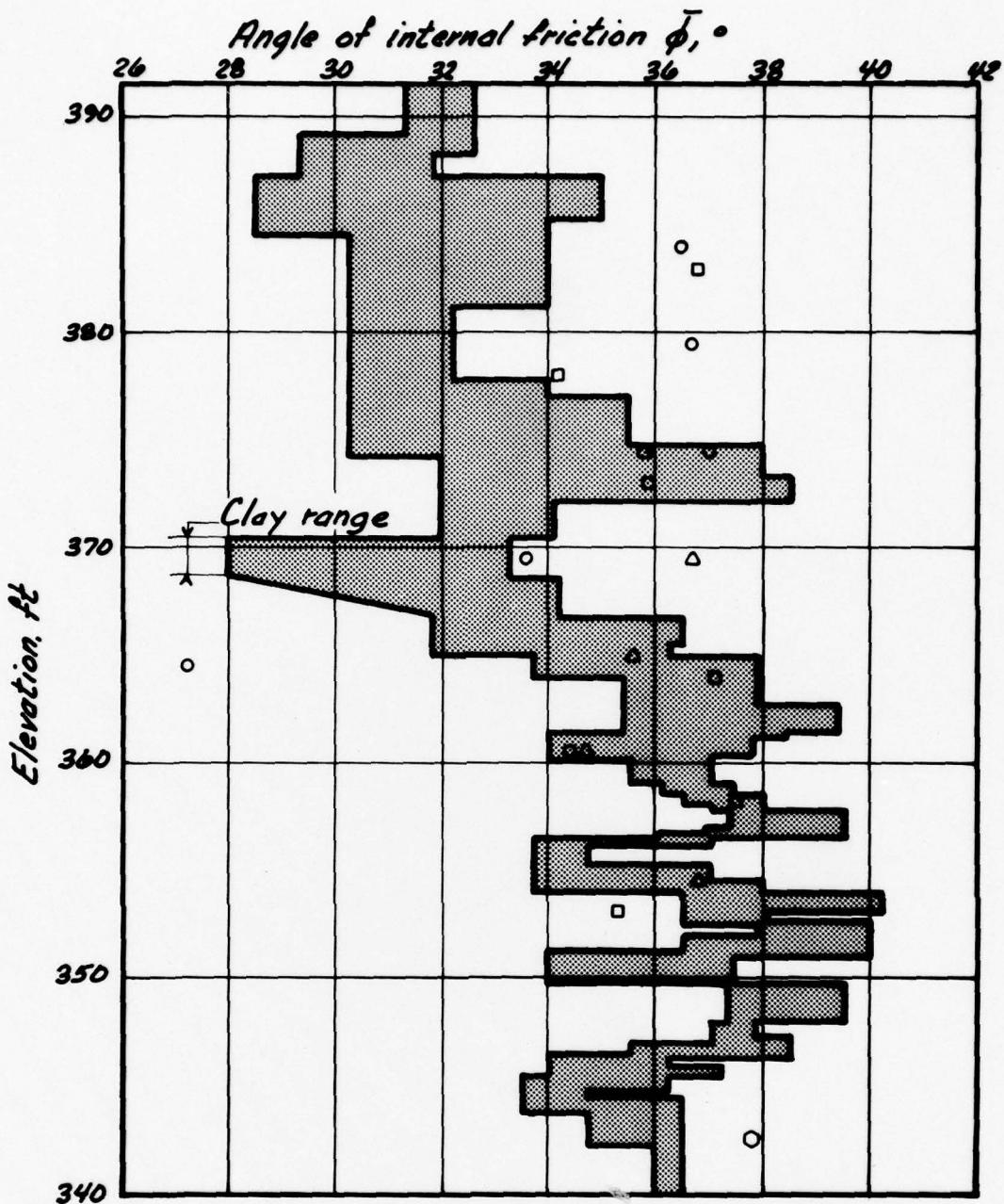
EXISTING LOCKS AND DAM No. 26  
ST LOUIS DISTRICT, CORPS OF ENGINEERS.  
DACPW63-78-C-0008



Woodward-Clyde Consultants

V7C828 Phase IX

Fig. 4.16



### Legend

■ Range from static cone penetration tests  
PD-C1, PD-C2, PD-C3, PD-C5, and PD-C6 using Meyerhof (1974)

- Boring PD-PM 1
- △ Boring PD-PM 2
- Boring PD-PM 3
- Boring PD-PM 4

Pressuremeter test results using Hughes et al(1977)

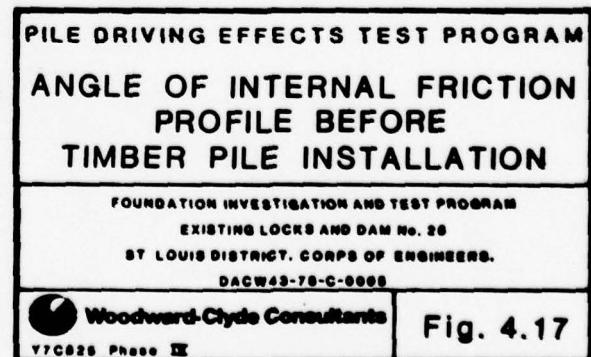
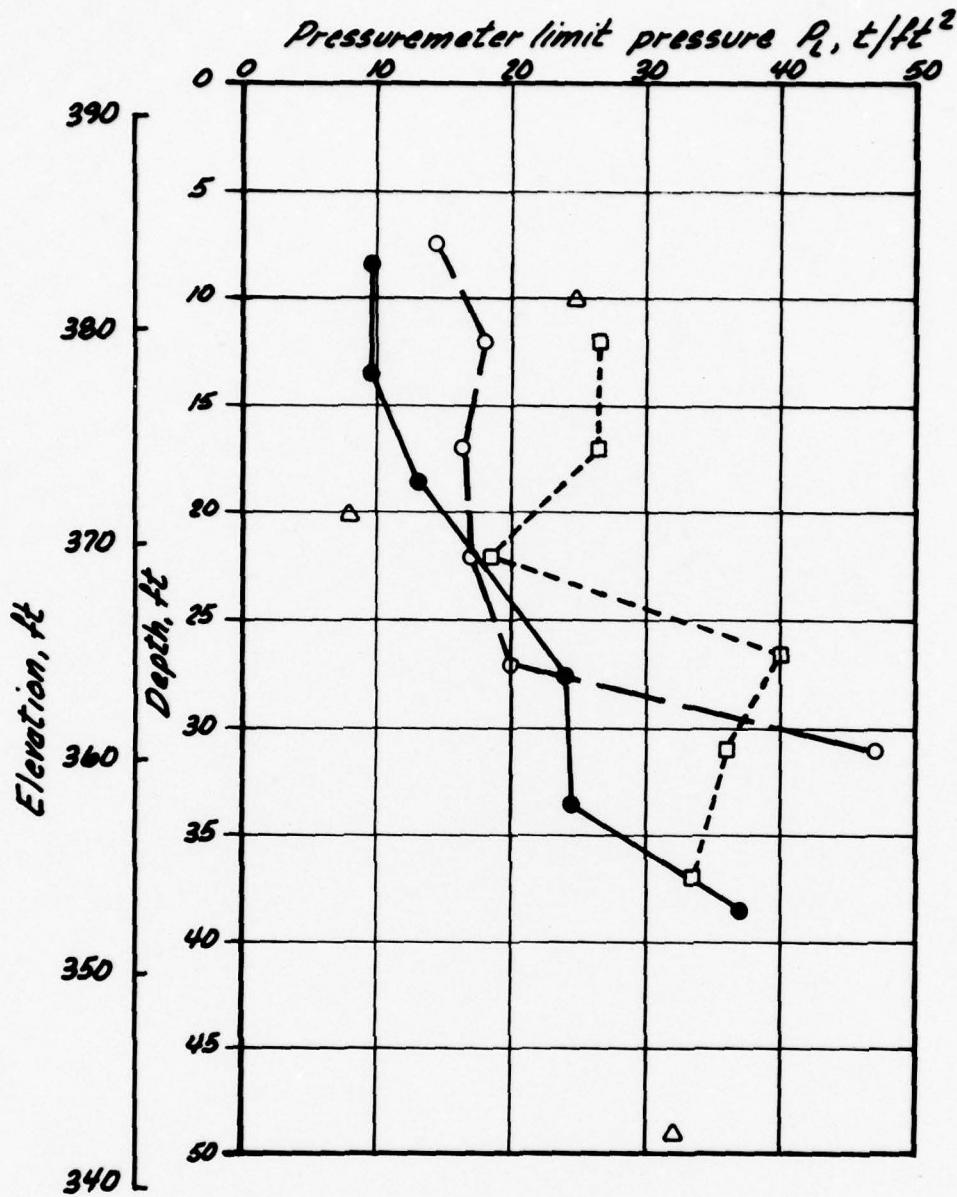


Fig. 4.17



### Legend

- Boring PD-PM1
- Boring PD-PM2
- △- Boring PD-PM3
- Boring PD-PM4



**PHASE IV REPORT**

**VOLUME III**

**RESULTS AND INTERPRETATION OF  
PILE DRIVING EFFECTS TEST PROGRAM**

**SECTION 5  
CONSTRUCTION OF TEST FACILITIES**

## 5 CONSTRUCTION OF TEST FACILITIES

### 5.1 GENERAL TEST REQUIREMENTS

#### 5.1.1 Test Area

The general requirements and selection criteria for the main test site are discussed in Volume I. The specific requirements for the pile driving effects test area were:

- (1) the test monoliths and their timber pile foundations must be constructed in the same stratigraphic units as the foundations for Locks and Dam No. 26;
- (2) the groundwater level at the location of the test monoliths must be maintained very close to the ground surface;
- (3) the test area, and particularly the portion of the area where the test monoliths were to be constructed, must be isolated from extraneous vibrations due to construction equipment, traffic, and other testing activities;
- (4) the test area must be protected from flooding during the expected duration of the tests; and
- (5) a stable working platform must be provided and maintained to accommodate heavy construction equipment throughout the test program.

#### 5.1.2 Reaction Structures

The conduct of the pile driving effects tests required design and construction of appropriate reaction structures and systems capable of delivering large horizontal and vertical loads to the test monoliths. The size and capacity of these reaction structures were important factors in the selection of the scale and configuration of the test monoliths. The maximum loads expected during the tests were as follows:

	Monolith Number and Timber Pile Configuration						
	M1 (3x4)	M2 (2x4)	M3 (2x4)	M4* (2x4)	M5 (2x4)	M6 (single)	M7 (single)
Sustained loads during pile driving effects tests, t	H 72 V 360	48 240	48 240	32 120	32 120	6 30	6 30
Maximum expected loads during lateral load tests, t	H 252 V 360	168 240	168 240	- -	- -	21 30	21 30
Maximum expected loads during axial load tests, t	H 0 V 720	0 480	0 480	- -	0 1000**	0 125	0 60

\* Monolith M4 was cancelled later in the program

\*\* Axial load testing of monolith M5 was added to the program after design was completed. Reaction structures were modified accordingly

### 5.1.3 Test Monolith Construction

The requirements set forth for construction of the test monoliths have been presented in Section 2.2 discussing the selection of the test variables.

### 5.1.4 Chemical Grouting

One of the primary objectives of the pile driving effects test program was to assess whether or not injection of chemical grout into the soil surrounding the timber pile foundations would prevent or mitigate displacements of the test monoliths when subjected to the effects of nearby pile driving. The program also aimed at assessing the effects of grouting on the lateral load capacity of steel and timber piles.

On the basis of predictions (Section 2.3.3) that indicated that the monolith displacements due to pile driving would be primarily lateral, it was decided to grout only the upper 20 ft of soil beneath monoliths M3 and M7\*. Grouting more than 20 ft of soil under existing structures was considered to be prohibitively expensive and would not constitute a potentially feasible rehabilitation scheme. Grouting only the upper 10 ft would not produce the desired grouted product due to lack of confinement.

\* Initially, grouting was also planned under monolith M4. Testing of monolith M4, including chemical grouting was cancelled in November 1978; the objectives of the tests scheduled for M4 were considered of secondary importance

Ideally, the strength of the grouted soil should be such that:

- (1) it would prevent rearrangement or movement of soil particles due to pile driving vibrations (that is, grouting would increase cohesion of the soil, and increase the internal stability of the sand mass);
- (2) it would not significantly increase soil resistance to prototype pile penetration during driving, as some of the rehabilitation piles may have to be driven through grouted soil; and
- (3) it would increase the lateral load capacity of steel and timber piles.

## 5.2 TEST AREA PREPARATION AND DEWATERING

### 5.2.1 Location of Test Area Within Main Test Site

The pile driving effects test area was located at the extreme southern end of the main test site. With this configuration, the test monoliths were as far away as possible from the other test locations and from general traffic.

### 5.2.2 Excavations

**Monolith Trench.** To approximate the foundation conditions at Locks and Dam No. 26, it was necessary to excavate the surficial flood plain deposits and expose the underlying Recent alluvium over the portion of the test area where the tests monoliths were to be constructed (monolith trench). At the design stage, it had been expected that the alluvial sand would be found below el 395. However, the test area location was shifted riverward after the initial design was completed to afford savings in site preparation cost. At the new location, the Recent alluvial sand was slightly deeper, requiring excavation of the monolith trench to el 391, approximately 24 ft below the surrounding natural ground surface. The general configuration of the monolith trench is depicted in Fig. 2.3. Initially, the toe of the excavation was 5 ft to 8 ft away from the front end of the test monolith. During the course of the program, the monolith trench was widened in front of monoliths M2, M3, and M5 such that the toe of the excavation was 25 ft from the front end of these monoliths. This was done to minimize the confining effects of the berm leading from the bottom of the monolith trench at el 391 to the surface of the general excavation at el 400 to el 403.

The excavation of the monolith trench was done using a backhoe. Careful control was exercised to ensure that the subgrade under and immediately adjacent to the future test monoliths was not disturbed below el 391. Elsewhere in the monolith trench, local portions were overexcavated. These portions were later backfilled with Mississippi River sand similar to the natural Recent alluvial sand (stratigraphic unit A, Section 4.3.8).

**General Excavation.** The portion of the pile driving effects test area surrounding the monolith trench was excavated to el 400. The clayey flood plain deposits were not entirely removed in the general excavation. Over the course of the program, the grade of the general excavation was gradually raised up to el 403 at some locations by adding crushed rock for surface maintenance (Section 5.2.4).

#### 5.2.3 Levees

Downstream of the dam, the minimum water level is at el 395. The Mississippi River is known, however, to rise, sometimes very quickly, to as high as el 432 (April 1973). It was, therefore, decided to protect the pile driving effects test area by a system of levees and a permanent dewatering system.

Considering the time of year during which the test activities were scheduled (July to November), it appeared adequate to protect the area from Mississippi flood stages up to el 418. The likelihood of exceeding this river stage was very low during that period. The levees ringing the pile driving effects test area were designed and constructed to el 420, to provide a 2-ft free-board above design river stage. The levees were 3 ft to 9 ft high, and had slopes of 2(hor) to 1(vert). They were constructed from clayey flood plain deposits from the general excavation.

#### 5.2.4 Surfacing

The bottom of the general excavation at el 400 was initially surfaced with 6 in. to 12 in. of crushed rock. Portions of that area were subjected to heavy equipment traffic during construction of the test facilities and actual testing. Large quantities of additional crushed rock were spread over the area to maintain the working platform. In October 1978, it was decided to stabilize the worst portions of the excavation bottom with a geotextile. Approximately 30,000 ft<sup>2</sup> of Mirafi 500x (a polypropylene slit-film, woven fabric) were spread on top of the previously placed mud-contaminated crushed rock. A 1-ft- to 2-ft-thick layer of crushed rock was spread over the geotextile. Very little additional surface maintenance was needed thereafter. These surfacing activities progressively raised the bottom of the general excavation to el 403 in some places.

#### 5.2.5 Dewatering System

The purpose of the dewatering system was to maintain the groundwater surface at el 390 ± 0.5 within the monolith trench excavated to el 391. Adjunctly, the system was also intended to maintain the groundwater surface at or below el 397 in the general excavation. The system was initially designed to drawdown and maintain groundwater at el 394 in the monolith trench. The monolith trench was eventually excavated deeper (Section 5.2.2) and a supplementary system was installed to provide sufficient dewatering capacity for this 4-ft additional drawdown at high river stages.

**Original Dewatering System.** The original dewatering system consisted of approximately 90 wells connected to vacuum manifolds. The wells were 6-in.-dia screens installed by jetting in 16-in.-dia holes. The wells were installed from el 410 on the periphery of the general excavation (Fig. 5.1). They were 61 ft deep. The top of the gravel filter was at el 387, such that the upper portion of the wells was sealed. The wells were individually connected to a 24-in.-dia header consisting of two branches, each branch servicing the wells on two sides of the rectangular excavation. The headers were maintained under vacuum by a battery of seven pumps located adjacent to the access ramp to the pile driving effects test area. That location was chosen to minimize vibrations at the monolith trench. Depending on river stages, four to seven pumps were kept in operation. The total capacity of this system was theoretically rated at approximately 20,000 gal/min by the dewatering contractor. However, at high river stages, the actual pumping capacity was much less. During most of the testing period, the original system was sufficient, pumping generally some 8,000 to 10,000 gal/min for river stages at el 405 or below.

**Supplementary Dewatering System.** In September 1978, when it became apparent that the monolith trench had to be excavated to el 391 instead of el 394, a supplementary dewatering system was designed. The original dewatering system could not maintain the groundwater surface at el 390.5 for river stages in excess of el 407. The supplementary system was designed to handle approximately 18,000 gal/min, bringing the actual total capacity of the combined systems to over 20,000 gal/min\*.

### 5.3 REACTION STRUCTURES

#### 5.3.1 Horizontal Reaction Blocks

Each test monolith was provided with companion horizontal reaction block designed to deliver the maximum anticipated horizontal load (Section 5.1.2). The reaction blocks were 4-ft-high concrete blocks, cast at el 394, and supported by vertical and batter HP 14 x 73 piles (Fig. 2.4 and 2.5). The piles were driven to a tip elevation of 350. The horizontal reaction blocks performed very well during testing.

#### 5.3.2 Reaction Rock Anchors

The vertical load applied to each test monolith was reacted by four vertical rock anchors, two on each side of the monoliths. Monoliths M2 and M6, and M3 and M7 used the same reaction rock anchors. The anchors were of the VSL type, similar to those tested in the rock anchor test program (Volume V). Their design capacity varied from 500 k/anchor at monolith M5 to 60 k/anchor at monolith M4 (which was not tested). The design anchorage length in rock varied from 15.5 ft to 10 ft. The free length above rock was approximately 100 ft.

---

\* The operation of the supplementary dewatering system reduced the volume of water flowing into the original system

The anchor holes were very difficult to drill. Various equipment was used, ranging from a heavy-duty Drilltech rig using ODEX tools (Volume V) to a Mobile Drill B61 soil boring rig using rotary techniques. Air tracks were also used. The lengthy reaction rock anchor installation seriously affected the overall testing schedule and may have disturbed the surrounding soil. After installation, the reaction rock anchors performed well during testing.

After installation, the reaction rock anchors were tested to 120 percent of their design capacity and locked off at about 10 to 20 percent of that load. The anchor heads were attached to special chairs and bridge ropes connected to the vertical reaction frames (Section 5.3.3).

#### 5.3.3 Reaction Frames

Horizontal and vertical loads were delivered to the test monoliths by steel reaction frames bearing on the reaction blocks and connected to the reaction rock anchors. Two horizontal and two vertical reaction frames were built offsite to accommodate the range of loads during testing. Typical frames are shown in Fig. 2.4. The single pile monoliths (M6 and M7) were loaded by H beam assemblies designed and constructed at the site as needed. The reaction frames were supported with heavy timber cribbing.

Several modifications had to be implemented in the field to adjust the vertical load frames because the reaction rock anchors were not installed exactly as shown on the construction drawings. Notwithstanding these time-consuming modifications, the reaction frames performed well during testing.

Load frames were also used to jack apart the three pairs of prototype piles tested under lateral loads. These load frames are described in detail in Section 10.

#### 5.3.4 Jacking System

The test monoliths were loaded with hydraulic jacks placed between the monoliths and the reaction frames. Tandems of two jacks were used to apply horizontal and vertical loads. The jack controls were centralized in a shed located on top of the horizontal reaction block for monolith M3. During simultaneous testing of monoliths M2 and M6, and M3 and M7, six jacks (four for M2 or M6; two for M3 or M7) were used at the same time. The system was set up such that the jack operator could monitor the load on any one jack using the jack gages and a multi-channel millivoltmeter to read the load cell output, and was in constant communication with the operator of the automatic data acquisition system through an interphone.

Several difficulties were experienced with the jacking system. Most of the difficulties were directly attributable to cold weather and freezing of the hydraulic lines between control shed and jacks. The nitrogen-activated jack pumps were sometimes too slow, particularly during quick load changes in the cyclic preloading activities; but generally, the system functioned well.

#### 5.4 TEST MONOLITH CONSTRUCTION

##### 5.4.1 Timber Pile Installation

**Equipment.** The timber piles were installed by jetting and driving to a prescribed tip elevation. This installation method was used during construction of Locks and Dam No. 26 in the 1930's. The jetting equipment consisted of a 2-in.-od jet pipe with a 1-in.-dia nozzle connected by a 2-in.-dia rubber hose to a Peerless variable-speed, multi-stage pump. Jetting water was tapped from the dewatering system discharge and stored in a 6000-gal tank. The pump pressure and rate of flow were varied within large limits depending on the jetting and driving results.

Driving accompanying and following jetting was done with a Vulcan 1 single-acting air hammer. Details of the Vulcan 1 hammer assembly are given below.

Rated Energy, ft-lb	15,000
Rated Speed, blow/min	60
Air Pressure at Hammer, lb/in <sup>2</sup>	80
Weight of Ram, lb	5,000
Capblock material*	Duracush**
(Mississippi Valley Equipment Co, St Louis)	
Capblock Thickness, in.	3 to 4

\* During driving of timber piles at monolith M1, 3-in.-thick plywood disks were used as cushion; subsequent driving was done with Duracush disks

\*\* A 3/4-in.-thick plywood disk was included in the capblock to retain the Duracush disks

The crane leads used for timber pile installation were fixed at ground surface by stabbing them into the soil and on the crane platform with outriggers. This was done to minimize shifting of the piles as they were jetted and driven. This measure proved to be moderately successful. Restriking of the piles (discussed below) was done with swing leads (outriggers detached from the crane).

Dynamic measurements of strain and acceleration at each timber pile butt were made using the pile driving analyzer system described in Section 3.2.8 to monitor timber pile behavior during driving. Prior to driving, sonic wave speed measurements along the pile shaft were made for each timber pile to obtain elastic parameters used in the analyzer calculations.

**Procedures.** The uninstrumented timber piles surrounding monolith M1 were installed first to establish optimal jetting and driving combination required to reach a final pile tip penetration of 35 ft (el 356) with minimal soil disturbance and within acceptable position tolerances. For the hundreds of timber piles under Locks and Dam No. 26, the aggregate effects of position deviation and installation technique tended to average out; however, for the small pile groups supporting the

test monoliths, commonly accepted position tolerances or variations in installation technique would have large effects on test results.

*Monolith M1.* The timber piles (12 instrumented, 36 uninstrumented) at monolith M1 were installed starting at the southwest corner of the group and moving northward along the north-south row of outer, uninstrumented piles. This sequence was repeated for the second north-south row of uninstrumented piles, and for the remaining rows of either instrumented or uninstrumented piles. This installation sequence afforded the opportunity to experiment with depth and duration of prejetting, jetting pressure and rate of flow, and relative position of jet pipe and pile for several uninstrumented piles before installing the timber piles supporting monolith M1. It was originally intended to jet the piles to a depth of 30 ft and drive them for another 5 ft, attaining a final blowcount of 50 blow/ft.

*Actual Installation Procedure* On the basis of observations during installation of the first few timber piles at monolith M1, the following procedures were developed and generally followed for installing the remaining timber piles:

- (1) prejet at a pile location to a depth of approximately 25 ft;
- (2) lower the timber pile into the prejetted hole and tap it with the Vulcan 1 hammer to seat it;
- (3) begin driving; if driving resistance becomes too high (that is, more than 40 to 50 blow/ft), assist pile penetration by additional jetting, but keeping the jet pipe no deeper than el 356;
- (4) mount the strain transducers and accelerometer on the pile when pile tip is at el  $361 \pm 2$ ;
- (5) continue driving until prescribed tip elevation; and
- (6) restrike each pile one to several days after initial driving after having remounted the pile driving analyzer transducers to assess relaxation and group installation effects.

The installation sequence for piles other than those of M1 was reversed. These piles were installed in east-west rows of two piles, starting at the southern row and proceeding northward. The sequence was altered after M1 to minimize effects of asymmetric installation relative to the north-south axis of lateral monolith loading.

#### Summary of Observations

*Jetting.* The presence of occasional clayey seams, particularly at about el 370, disrupted jetting operations. Jetting water return to the ground surface completely ceased at times. Elsewhere, the jet pipe could not be lowered to the desired depth despite repeated attempts. In a few cases, these occurrences made timber pile installation very difficult. Nevertheless, every timber pile was successfully installed to within 3 in. of design penetration, with the exception of monolith M5; a surveying error resulted in these piles being installed to a tip elevation of 355.5.

**Driving.** A summary of pertinent timber pile installation data, including depth of jetting, blowcount and pile driving analyzer results, is given in Table 5.1. This table should be used in conjunction with Fig. 5.2 showing as-built location and identification number for each timber pile. Complete field logs for these piles are included in Appendices L through Q, Volume IIIA.

In general, hard driving with the Vulcan 1 hammer was needed to reach design tip elevation; blowcount commonly exceeded the intended 50 blow/ft. This was of concern because of potential for damaging the timber piles (Section 11). The restrike blowcount was generally much higher than that experienced at the end of initial driving; this may be an indication of significant increase in soil resistance caused by pile group effects and/or soil setup, or less efficient hammer operation. A comparison between maximum transferred energy at the pile butt  $E_{max}$  during initial and restrike driving indicates that the restrike values averaged 2.5 k-ft less than the initial values (a 21 percent decrease). The decrease may have been the result of misalignment between driven pile and hammer (swinging leads were used for restriking the piles) and equipment warmup difficulties. The lower  $E_{max}$  values during restrike are consistent with the higher blowcount experienced.

Static pile capacities derived from pile driving analyzer results do not show a uniform trend between initial and restrike values. The mean timber pile axial capacity after restriking was 146 k which was about 7 percent larger than the initial value. The capacity increase from initial driving to restriking was marked for monolith M5 and slight for monolith M1. Monoliths M2 and M3 showed a slight decrease. These variations illustrate the complex effects of jetting and driving piles in closely-spaced groups and the influence of installation details.

#### **5.4.2      Concrete Work**

The test monoliths were lightly-reinforced concrete structures. High early strength Portland cement, Type III, was used to provide a minimum compressive strength of 4000 lb/in<sup>2</sup> at seven days. The timber piles were embedded 2 ft into the concrete. Forming was done by constructing a 3-ft-high box around the timber piles and filling the box with sand. In that manner, no complicated forms were needed to cast the bottom of the 2 x 4- and 3 x 4- pile monoliths 3 ft above ground (Section 2.2.3). The concrete forms were then constructed on top of the sand-filled box. After setting of the concrete, the forms and sand boxes were removed. The sand fill was shoveled and washed out from under the monoliths. The single pile monoliths (M6 and M7) did not require sand-filled boxes because they were cast 6 in. above ground.

Monolith M1 was cast as two separate blocks, 3 in. apart. Initially, it was proposed to test monolith M1 as a 3 x 4- pile group during cyclic preloading by connecting the two blocks using shims and stressed Dywidag thread bars. During

pile driving effects testing, the two blocks would be disconnected and only the 2 x 4-pile portion of M1 would be tested. Then, for final load testing, the two blocks would be reconnected, this time using both shims and Dywidag bars, and epoxy to fill the gap between the two blocks. During testing, this procedure was not followed. Monolith M1 remained as 3 x 4-pile group throughout testing because it was realized that the amount of work required to connect and disconnect the two blocks would not permit adherence to the testing schedule, which was seriously delayed. Cyclic preloading was done with the two blocks held together with the shims and Dywidag bars. Immediately after cyclic preloading, the epoxy (Sikadur Grout Pack) was placed in the gap. The connection performed very well throughout the tests.

#### 5.4.3 Effects of Timber Pile Installation on Soil Properties

In situ soil testing was performed between the six (2 x 3) timber piles of control group M8 (Section 2.2.2) and within the 2 x 4-pile group of monolith M4\* to evaluate the influence of timber pile installation on the properties of the natural sand. In situ soil testing included: a continuous standard penetration test boring PD2-SP1 near M8; static cone penetration test soundings PD2-C1 and C2 within M8 and M4, respectively; two pressuremeter borings PD2-PM1 and PM2 in M8, also including standard penetration tests; cross-hole shear wave velocity measurements near M8, M3, and M4; and a falling-head permeability boring PD-K1 in M8. The locations of these borings are shown in Fig. 5.3. Results obtained after timber pile installation are compared with results obtained before pile installation (Section 4) in the following sections.

**Standard Penetration Tests.** Standard penetration test results (expressed as N-values, Section 4.1.3) from borings PD2-PM1 and PM2 are compared to results from boring PD-PM4 and PD2-SP1 in Fig. 5.4. Boring PD2-SP1 was located 4 ft from the nearest pile and was, therefore, influenced to a much lesser extent by the driving and jetting activities than borings made within M8. Figure 5.4 indicates some increase in N-values in the upper 20 ft in boring PD2-SP1, but data is well within the scatter experienced before driving. Results from borings PD2-PM1 and PM2 show additional increase in N-values in the upper 20 ft. Below el 370, all N-values agree reasonably well. The increase in N-value in the upper 20 ft would suggest an increase in relative density of 20 to 30 percent due to timber pile installation; this apparent increase, however, may be due in part to change in in situ stress conditions.

---

\* After plans for testing monolith M4 were cancelled, M4 was used for this purpose because its timber piles had already been installed

**Static Cone Penetration Tests.** Static cone penetration resistance profiles after timber pile installation from borings PD2-C1 and C2 are compared in Fig. 5.5 to the profile from boring PD-C6 made before pile installation. Above the clay layer located at el 380, there was a significant increase in cone penetration resistance due to timber pile installation. Boring PD2-C2 was performed in monolith M4 and shows the same increase from measurements before timber pile installation. Below the clay layer, the after-installation cone resistances from boring PD2-C1 and C2 are slightly larger down to el 357 than those obtained before installation in sounding PD-C6. Below el 357, the after-installation cone resistances are somewhat lower than those before installation, especially in boring PD2-C1. Increases in cone resistance usually indicate increases in relative density, stiffness, and shear strength; the small decreases below el 357 may indicate some loosening. In the upper 20 ft, the cone resistances would suggest an increase in relative density of 20 to 40 percent; this apparent increase, however, may be due in part to change in in situ stress conditions.

**Pressuremeter Testing.** In situ horizontal stress, elastic deformation modulus, angle of internal friction, and limit pressure were derived after timber pile installation from pressuremeter tests in borings PD2-PM1 and PD2-PM2. Pressuremeter test curves for PD2 series borings are presented in Appendix K, Volume IIIA. Results of pressuremeter tests in the upper 35 ft of boring PD2-PM1, located between piles 91 and 92, indicate extremely low soil strength and stiffness. These results could be attributed to a void around the piles or inadequate hole preparation (this hole was drilled with bentonite). Below the tip of the piles, however, pressuremeter test results indicated normal soil stiffness and strength. For boring PD2-PM2, Revert drilling fluid was used and good quality test results were obtained. These test results indicate normal stiffness and strength properties and give no indication of a void around the pile. In fact, in all other in situ tests near timber piles, no void-like response was encountered. It is, therefore, believed that the pressuremeter results from boring PD2-PM1 were influenced by hole preparation method.

**In Situ Stress.** Pressuremeter tests results from boring PD2-PM2 were used to infer the in situ horizontal effective stress profile shown in Fig. 5.6. Comparing these stresses with stresses measured before timber pile installation in boring PD-PM4, there appears to be an increase in stress in the upper 20 ft and a decrease below that level. Stresses below the clay layer at 20 ft decreased to a normally consolidated stress level, indicating that jetting and driving may have obliterated the effects of overconsolidation (Section 4.3.3).

Observations during the jetting operations revealed that below the clay layer return of the jetting water was often poor. The clay acted as a cutoff and resulted in a concentration of jetting water action in the sand below the clay. The increased jetting activity may have resulted in an increase in pore pressure, decrease in effective stress, and possible liquefaction of the soil some distance

away from the jet pipe. After jetting, the excess pore pressure dissipated and the sand consolidated under overburden weight. This explains the measurement of stresses indicative of a normally consolidated sand. Above the clay layer, the jetting action was confined to a smaller area surrounding the pile. Pile driving following jetting created dynamic shear stresses and densification, which increased lateral stresses. Effects of driving apparently dominated above the clay; effects of jetting dominated below the clay.

**Modulus.** Elastic deformation modulus values were also derived from the pressuremeter tests in boring PD2-PM2 and are shown in Fig. 5.7 with the values from boring PD-PM4. These results indicate an increase in stiffness due to timber pile installation. The modulus increase may have resulted from pile driving-induced densification and a confining effect due to adjacent timber piles. As the pressuremeter probe expanded, the zone of stressed soil surrounding the probe increased, until it extended to the stiffer pile.

**Friction Angle.** A value of drained angle of internal friction was calculated from the failure portion of the pressuremeter curves for boring PD2-PM2. These test results are plotted vs depth in Fig 5.8 and compared with friction angles determined before timber pile installation. Pressuremeter results from boring PD2-PM2 indicate a slight decrease in friction angle due to timber pile installation, but this decrease is almost insignificant.

**Limit Pressure.** Pressuremeter limit pressure is a measure of the ultimate shear strength of the soil. Limit pressures measured in boring PD2-PM2 are plotted vs depth in Fig. 5.9 and compared with pressuremeter results before timber pile installation. Above the clay layer, a significant increase in limit pressure was observed, probably caused by pile driving-induced densification. Below the clay layer, the limit pressure remained practically unchanged from before pile installation, suggesting that the influences of loosening due to jetting and timber pile confinement may have cancelled each other.

**Shear Wave Velocity Measurements.** Results of cross-hole shear wave velocity measurements made in arrays PD-S6, 7, 8, and PD-S8, 9, 10 after timber pile installation are shown in Fig. 5.10. Both arrays indicate a large increase in velocity above the clay layer in comparison with velocity measured before timber pile installation; the largest increase was noted near the piles of M8. Below the clay, shear wave velocities also increased, but by a smaller amount. These measurements would suggest increases in stiffness and density some distance from the jetted and driven timber piles.

**Borehole Permeability Tests.** The results of falling-head permeability tests performed in boring PD2-K1 are compared in Fig. 5.11 with test results from borings PD2-K1 and K3 made before timber pile installation. Both borings PD-K3 and PD2-K1 were located in control group M8; PD-K1 was located near monolith M4. The higher permeabilities measured in boring PD-K1 are representative of the scatter inherent in the alluvial deposit. Results indicate that permeability after timber pile installation increased by almost an order of magnitude above the level of prejetting and did not change below that level.

## 5.5 CHEMICAL GROUTING

### 5.5.1 Sequence of Activities

Grout pipes were installed in October 1978. Monoliths M3 and M7 were cyclically preloaded in January 1979. After preloading, the area surrounding the two monoliths was prepared for grouting (pea gravel roof and sand surcharge, Section 5.5.3). Grouting started a few days later and was completed in mid-February. The sand surcharge and pea gravel roof were removed and the area regraded at el 391. Monoliths M3 and M7 were reloaded and the pile driving effects phase of testing proceeded.

### 5.5.2 Grouting Method and Equipment

**Grout Pipes.** Injection was done through sleeve pipes in three, and sometimes four grouting stages. This grouting method (Method S<sub>3</sub>) is described in detail in Section 2, Volume II. The sleeve pipes consisted of 1.5-in.-dia steel pipes having openings every 13 in. The openings were covered with rubber sleeves. The sleeve pipes were installed by driving and air-flushing a casing with an air-track, filling the casing with a cement-bentonite grout (sleeve-grout), inserting the sleeve-pipes into the grout-filled casing, and withdrawing the casing. Air-flushing the soil inside the air-track casing, at times, produced air bubbles escaping from the surrounding ground surface. This phenomenon may have had a disturbing effect on the soil.

Injection of silicate grout was done by inserting a double packer inside the sleeve-pipe and positioning the packer assembly so it straddled one sleeve. Grout was pumped from the plant into the packer assembly under sufficient pressure to force the rubber sleeve to expand and crack the surrounding cement-bentonite sleeve grout. The silicate grout flowed through the sleeve and into the soil. After a predetermined volume of grout had been injected at one sleeve level, the packer was positioned on the next sleeve (above or below depending on the injection stage), and the process repeated.

**Grouting Plant.** The grouting plant was of the proportioning type. It is schematically shown in Fig. 5.12. This grouting plant was basically different than the batching type plant used for the chemical grouting test program, described in Section 4, Volume II; theoretically, both plants should be equally adequate. Compared to the batching plant, the proportioning plant did not perform as well. The major reasons appeared to be:

- (1) more fragile plant components (pumps, flow meters, valves, pressure gages, and pressure recorders);
- (2) the proportioning plant was more under the control of local operators having little or no training or experience in chemical grouting;

- (3) the working conditions were much more difficult during winter than during spring when the batching was used; and
- (4) various incidents, such as sand thrown into the mixing tanks which jammed the flow meters, were experienced during operation of the proportioning plant.

The chemical grout components (sodium silicate and sodium aluminate) were proportioned and diluted with water in two separate tanks. Both diluted grout components were pumped and metered separately into two hoses merging into a Y just before entering the grout pipe inserted in the sleeve pipe. The grout components flowed together into the Y and grout pipe where they mixed, before being injected through the sleeve and into the soil. Four sets of two pumps were used to inject a maximum of four grout holes at a time. Generally, only two to three sets of pumps were in simultaneous operation. Theoretically, the flow in each hose could be regulated by needle valves to modify grout composition. In fact, metering difficulties due to clogging of the flowmeters did not allow perfect control of the grout composition at the beginning of the operation. In time, equipment difficulties and operator inexperience were resolved.

Overall, despite these difficulties, grouting during the pile driving effects test program appeared to have been accomplished satisfactorily, in a manner which is probably more representative of production work than the earlier, more controlled chemical grouting tests. Further evaluation of grouting effectiveness is given in Section 5.5.5.

### 5.5.3 Pattern and Sequence of Grouting.

On the basis of the results of the chemical grouting test program, (Volume II), a 4-ft spacing between grout holes was selected. The location of the grout holes in relation to the test structures is shown in Fig. 5.13.

The major difficulty faced in injecting grout into the upper 20 ft of soil under the monoliths was the lack of confinement. To reduce losses due to upward seepage of grout, the area to be grouted was covered with a 8-in.- to 12-in.-thick layer of pea gravel. The pea gravel was flooded with a slow-setting silicate grout with the intent of creating an impervious layer or roof. It was hoped that the grout would not only permeate the pea gravel, but also seep down several inches into the underlying natural sand. Subsequent observations indicated that this did occur.

A 3-ft-thick layer of sand was then placed on top of the grouted pea gravel to provide nominal confinement. The first stage of grouting consisted of injecting 28 gal of grout through each sleeve located between el 391 and el 385. This was done starting at the upper sleeves and proceeding downward. The rate of pumping was kept below 2 gal/min. Grouting pressure varied between 20 and 120 lb/in<sup>2</sup>. A short grout setting time on the order of 10 min was used. Subsequent grouting stages did not start until the previous stage was substantially completed in the entire area to be grouted. The sequence of injection was such that grouting proceeded from the east end towards the west end of the area.

In the second stage of grouting, grout was injected starting at the bottom of the sleeve-pipes (el 371) and proceeding upward to el 391. Between el 371 and el 385, a maximum of 37.5 gal of grout were injected through each sleeve. Between el 385 and el 391, a maximum of 19 gal of grout were injected through each sleeve. The rate of pumping was maintained at 2 gal/min or slightly less. Grouting pressure varied from 20 to 120 lb/in<sup>2</sup>.

In the third stage of grouting, grout was again injected starting at the bottom of the sleeve-pipes and proceeding upward. Between el 371 and el 385, a maximum of 19 gal of grout were injected through each sleeve. Between el 385 and el 391, a maximum of 9.5 gal were injected through each sleeve. The rate of pumping was kept at about 1.5 gal/min. Grouting pressure varied from 20 to 150 lb/in<sup>2</sup>.

A fourth stage of grouting was implemented in some grout holes at selected levels where low grout take or leaks had been observed in the previous stages. Some grout holes received much less than the intended volume of grout because of leaks. Grout take, pumping pressure, and rate of grout flow for every grout hole are given in Appendix K, Volume IIIA.

#### 5.5.4 Grout

On the basis of the chemical grouting test program results (Volume II), a low-strength silicate/aluminate grout was selected. This grout was chosen because results of in situ tests and visual observation during the chemical grouting test program indicated that this was the only grout in which pile driving would be feasible; an increase in soil properties was also measured by in situ and laboratory tests.

The grout used to saturate the pea gravel layer and upper soil had the following composition:

sodium silicate (grade 40) (70°F):	30 gal
dry sodium aluminate (NALCO) (68°F):	12 to 13 lb
water (55°F):	70 gal

The setting time of this grout at an ambient air temperature of 35°F to 25°F varied from 1 hr to 6 hr. A total of 3800 gal of this grout was pumped into the pea gravel layer.

The remainder of the grout injected through the sleeve-pipes had the following composition:

sodium silicate (Grade 40) (70°F to 80°F):	25 gal
dry sodium aluminate (NALCO) (68°F):	15 to 18 lb
water (55°F):	75 gal

The setting time of this grout at an ambient air temperature of 40°F to 0°F varied from 7 min to 60 min. The setting time was constantly adjusted as a function of components and air temperatures and somewhat erratic operation of the proportioning mechanisms of the grouting plant.

#### 5.5.5 Evaluation of Grouting

**Grout Take.** A total of 61,700 gal of 25% silicate/aluminate grout were injected in the grouted area. In addition, approximately 3800 gal of 30% silicate/aluminate grout were used to saturate the pea gravel roof. The theoretical volume of soil to be grouted was 22,400 ft<sup>3</sup> or 167,500 gal. The average grout take was 37 percent. Actually, the grout take was somewhat less because of losses by leakage. Leakage up to the top of sand surcharge was often experienced. This was to be expected considering the small overburden confinement on the area to be grouted. When a leak was noticed, injection was discontinued for several minutes to allow setting of the grout. If leakage persisted when injection was restarted, the packer was moved to another sleeve. The sleeve which produced the leak was generally reinjected in a later grouting stage.

Significant leakage was observed around monolith M3, and several grout pipes extending through the monolith became obstructed after early grouting stages and could not be completely injected. Leakage is attributed to conduits forming around the piles. Once a conduit formed, the grout strength was insufficient to prevent further leakage. Leakage and obstructed grout pipes resulted in poorly grouted zones near ground surface under monolith M3.

Grouting was done in January and February often in subzero temperatures, particularly during night shift work. Grout lines had to be protected from freezing with tarps and forced-air heaters. Setting time of the grout was difficult to control, requiring numerous adjustments in grout composition.

**Grouted Soil Properties.** A program of in situ testing was performed after grouting to evaluate the properties of the grouted soil mass. These properties were used to evaluate behavior of monoliths M3 and M7, and prototype piles T1, T2, T5, and T6. In situ testing included: two static cone penetration test soundings in control group M8 (PD3-C1) and near pile T2 (PD3-C2); three pressuremeter test borings with standard penetration tests in M8 (PD3-PM1), near pile T2 (PD3-PM2), and near pile T1 (PD3-PM3); one falling-head permeability test boring PD3-K1 in M8; and cross-hole shear wave velocity measurements in arrays PD-S6, 7, 8, and PD-S8, 9, and 10. Locations of these borings are given in Fig. 5.14.

**Standard Penetration Tests.** Results of standard penetration tests performed in borings PD3-PM1, PM2, and PM3 are compared to the range of results before grouting in Fig. 5.15. Grouting increased standard penetration resistances. Standard penetration resistances increased slightly more inside the timber pile group than outside. Disturbed samples obtained during standard penetration tests indicated that grout extended beyond the theoretical lower limit (el 371) of the grouted zone to at least el 369.5.

**Static Cone Penetration Tests.** Static cone penetration resistance profiles from borings PD3-C1 and PD3-C2 are compared in Fig. 5.16 to results from boring PD2-C1 obtained before grouting. In boring PD3-C1 which was located within M8, there was a significant increase in cone resistance in the grouted zone. In boring PD3-C2 outside M8, the cone resistance after grouting was lower than that measured before grouting in M8 in the upper 10 ft of the grouted zone. Boring PD3-C1 did, however, indicate higher cone resistances than measured before timber pile installation. The higher resistances in boring PD3-C1 illustrate the influence of adjacent pile driving and the confining effect of the piles which tended to concentrate grout penetration in the area bounded by the piles. The resistance measured below el 380 indicates a thoroughly grouted soil mass; this conclusion is based on results of similar tests and visual observations during the chemical grouting test program. Below the grouted zone and the clay layer at el 370, a significant decrease in cone resistance was noted after grouting. For boring PD3-C2, this decrease could be explained by disturbance due to installation of reaction rock anchors. For boring PD3-C1, this decrease followed the decreasing trend established after timber pile installation. Below the tip elevation of the timber piles, cone resistances from boring PD2-C1 and PD3-C1 matched fairly well.

**Pressuremeter Tests.** In situ horizontal stress, elastic deformation modulus, and limit pressure were determined from pressuremeter tests in borings PD3-PM1, PD3-PM2, and PD3-PM3. Pressuremeter test curves from PD3 series borings are presented in Appendix K, Volume IIIA. In situ horizontal effective stresses measured after grouting are compared in Fig. 5.17 to stresses measured before grouting in borings PD2-PM2 and PD-PM4. All three borings indicate a significant increase in horizontal stress due to grouting. Below the grouted zone, the stresses tend back toward the pregrouted level.

Elastic deformation modulus values determined from pressuremeter tests in borings PD3-PM1, PM2, and PM3 are presented in Fig. 5.18, along with modulus values measured before grouting. In pile group M8, boring PD3-PM1 showed an increase in modulus due to grouting. This increase is not large and indicates that grouting did not significantly increase soil stiffness near this boring. Modulus values from boring PD3-PM2 must be compared with measurements before timber pile installation (boring PD-PM4) because this boring is outside the zone influenced by timber pile installation. Grouting also increased soil stiffness near this boring. Below the grouted zone, modulus values equivalent to those obtained before grouting were measured.

Pressuremeter limit pressure measured in borings PD3-PM1 and PD3-PM2 are compared to results obtained before grouting in Fig. 5.19. Both borings indicate an increase in limit pressure due to grouting. Results from boring

PD3-PM2 must be again compared to results from boring PD-PM4. Grouting generally increased limit pressure. The shape of volume-change vs pressure curves for tests in boring PD3-PM1 are indicative of a strain-hardening behavior of the grouted soil, as it yielded to the expanding pressuremeter probe. The ultimate strength (limit pressure) derived from these curves is overpredicted. The strain-hardening behavior was observed in laboratory tests in support of the chemical grouting test program. It is probably due to the ductile nature of the low-strength grout, coupled with the confining effects of nearby timber piles. The grouted soil around the expanding probe yielded to a point above which it could not accommodate any further stress. The increasing stresses were transferred farther from the probe, increasing the radius of the deformed soil zone until it extended to the adjacent piles. The stiff piles did not yield, thus stabilizing the soil deformation and increasing the apparent limit pressure. Below the grouted zone, limit pressures measured before and after grouting were identical.

*Cross-Hole Shear Wave Velocity Measurements.* Shear wave velocities measured in arrays PD-S6, 7, 8 and PD-S8, 9, 10 after grouting are compared with measurements made before grouting. In the grouted zone, the average shear wave velocity increased by an average of 62 percent due to grouting. Increases in shear wave velocity are indicative of increased soil stiffness and density, but are also influenced by grouting effectiveness between the source and geophone. The increase measured here indicates a thoroughly grouted soil. A 50 percent increase in shear wave velocity was measured for the same grout in the chemical grouting test program.

*Borehole Permeability Tests.* The results of falling-head permeability tests in boring PD3-K1 revealed a significant artesian head in the grouted zone. Instead of the water level falling during the test, water flowed out of the casing. Subsequent measurements of pore pressure using a pneumatic piezometer in monolith M3 indicated a pressure head equivalent to 5 ft above groundwater level. It is not known whether or not the piezometer was still functioning properly after grouting; however, the excess head detected using the piezometer agreed well with the observed head during the permeability tests. The excess pore pressure developed during grouting because the grouted pea gravel roof, created to eliminate vertical grout leakage, effectively locked-in the pressure while water flow was cut off horizontally by the previously grouted perimeter. During pile driving effects testing of M3, no such artesian head could be detected.

Monolith	Timber Pile No.	Maximum Jetting Depth, ft	Blowcount, bl/ft		$E_{max}$ <sup>(1)</sup> , ft-k		$R_{ult}$ <sup>(2)</sup> , k	
			Initial <sup>(3)</sup>	Restrike <sup>(3)</sup>	Initial	Restrike	Initial	Restrike
M1	12	15	62	220	1.9	2.6	85	160
	4	22	55	72	1.0	2.5	90	170
	7	31	50	112	2.3	2.0	120	135
	22	20	60	86	5.5	3.8	190	190
	11	35	156	128	4.0	3.9	165	200
	18	25	80	116	4.0	2.4	155	135
	5	33	42	148	4.0	2.0	160	155
	2	31	60	98	4.0	2.1	160	160
	27	28	11	88	2.3	2.5	125	135
	23	28	95	110	2.5	3.3	140	165
	26	29	102	80	2.3	2.6	130	150
M2	1	34	209	114	1.9	2.2	140	160
	14	31	64	114	2.8	1.7	140	140
	30	27	25	148	2.6	1.3	130	120
	17	27	100	334	2.6	1.7	170	130
	9	28	66	198	2.5	1.5	150	155
	8	28	117	332	2.2	1.6	190	145
	46	27	135	222	1.8	1.3	120	120
	10	31	71	156	3.8	2.8	210	175
	20	27	70	136	2.3	1.9	145	148
M3	3	26	84	220	4.4	1.7	180	155
	28	27	79	314	4.1	1.0	170	145
	16	27	60	176	4.4	2.4	205	180
	15	27	100	296	2.8	1.3	130	125
	24	27	62	184	3.2	1.9	185	145
	6	27	66	140	1.8	1.1	115	120
	13	30	76	114	2.5	1.8	110	130
	19	35	48	116	3.1	1.4	130	120
	44	27	40	122	2.5	3.0	70	160
M5	43	29	36	104	2.9	3.1	95	140
	42	27	65	125	1.5	1.5	95	115
	41	25	75	72	2.0	3.6	95	125
	40	27	107	146	1.4	1.5	90	130
	39	28	69	80	1.4	1.8	75	115
	38	29	77	82	2.5	2.7	115	125
	37	31	56	60	2.9	3.8	105	150
M6	25	29	60	114	3.3	1.4	135	140
M7	45	28	65	165	3.2	1.8	135	190
Mean		28			2.8	2.2	136	146
Std Dev		4			1.0	0.8	37	22

Notes

- (1)  $E_{max}$  is the maximum transferred energy at the pile butt
- (2)  $R_{ult}$  is the estimated pile capacity using the Pile Driving Analyzer
- (3) "Initial" describes values at the end of initial driving; "Restrike" describes values at the final tip penetration elevation

PILE DRIVING EFFECTS TEST PROGRAM

SUMMARY OF  
TIMBER PILE INSTALLATION  
FOR LOADED TEST MONOLITHS

FOUNDATION INVESTIGATION AND TEST PROGRAM

EXISTING LOCKS AND DAM NO. 26

BY LOUIS DISTRICT, CORPS OF ENGINEERS.

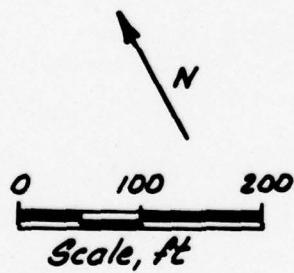
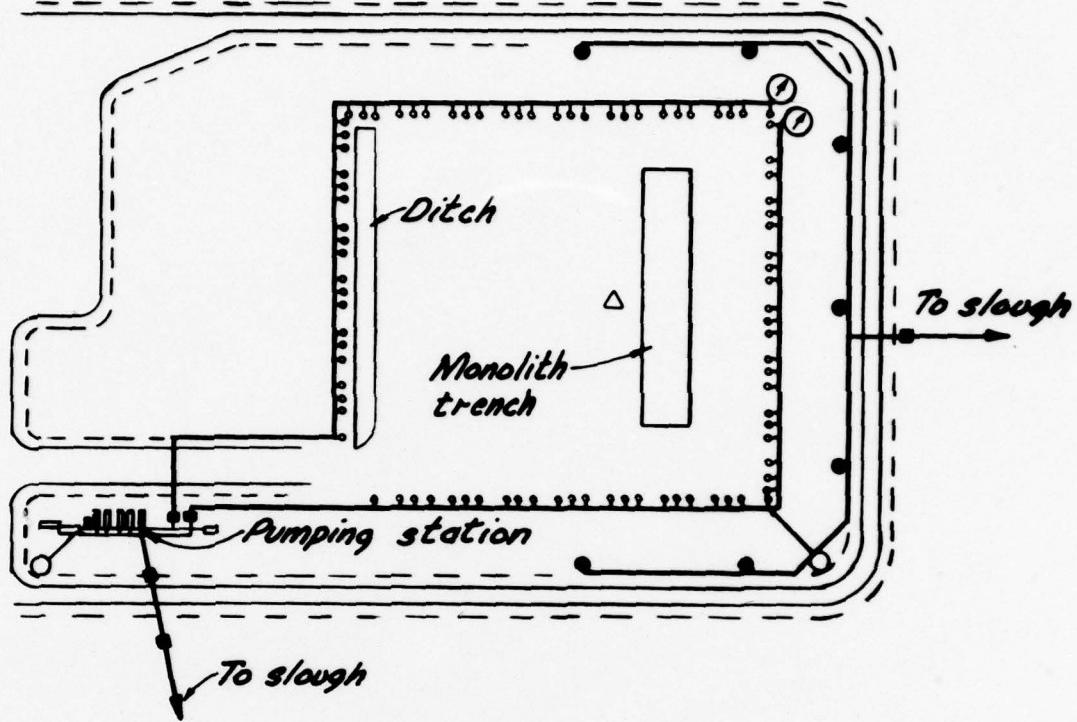
DACW43-76-C-0006



Woodward-Clyde Consultants

VFC825 Phase II

Table 5.1



### Legend

- 6-in-dia primary dewatering well
- 16-in-dia supplementary dewatering well
- ① Vacuum gage
- △ Piezometer
- Vacuum manifold

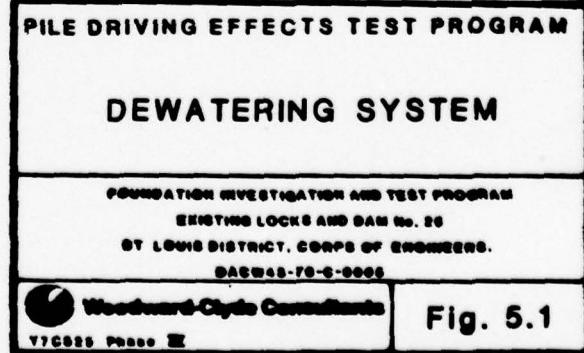
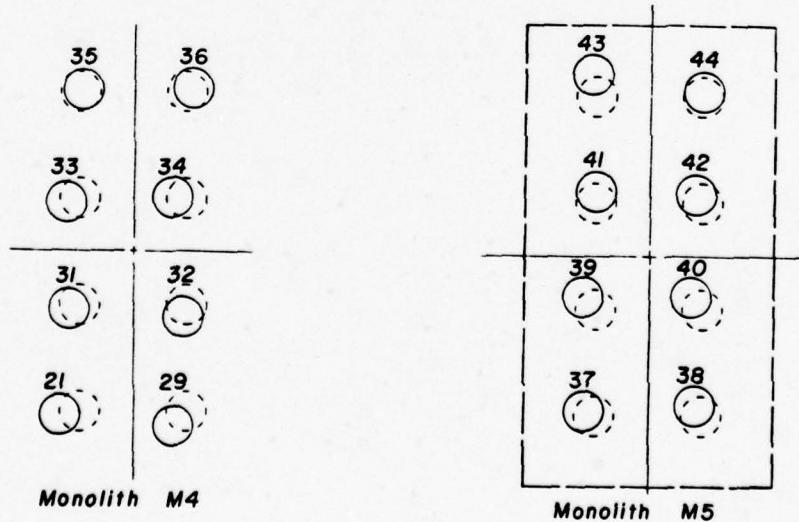
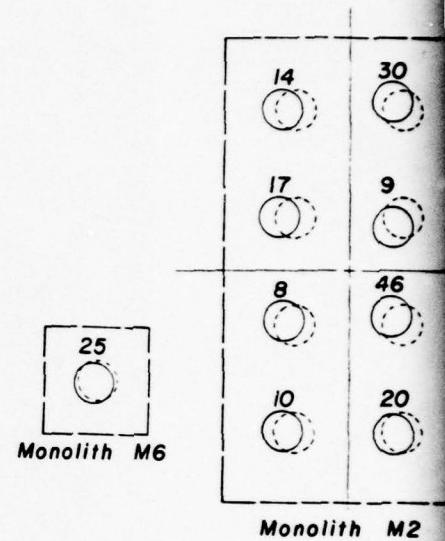
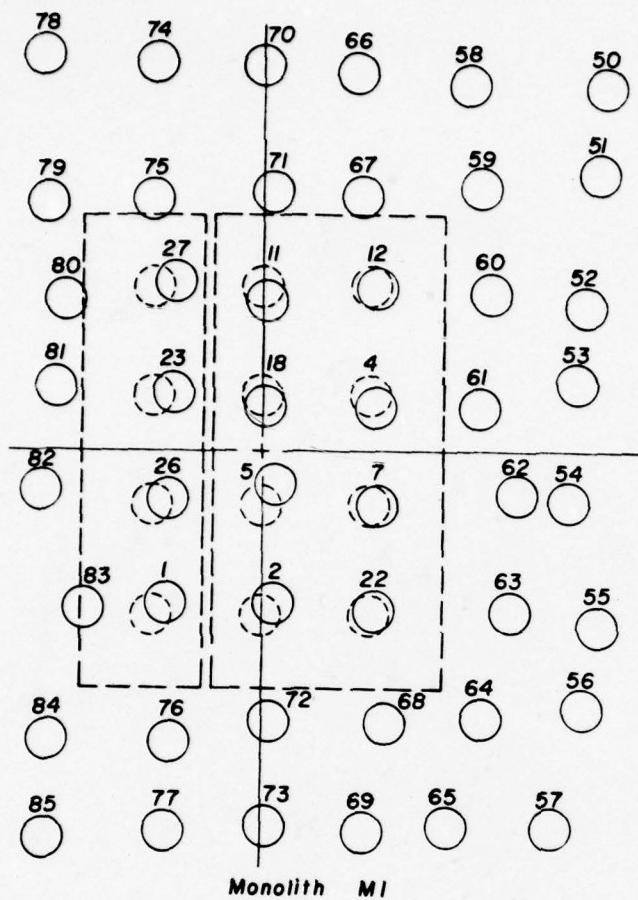
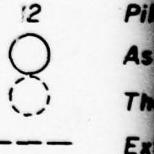


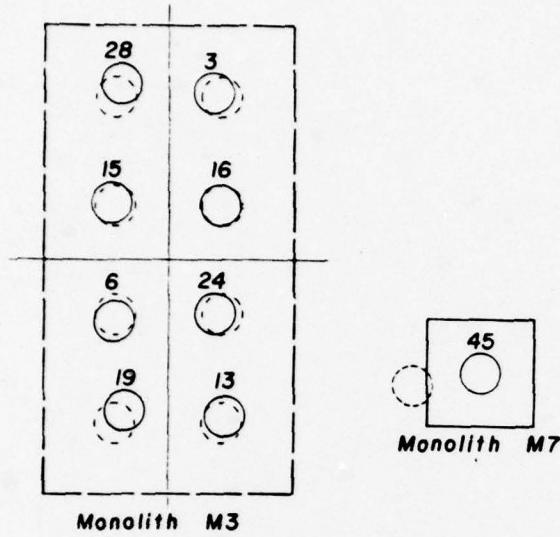
Fig. 5.1



Legend:

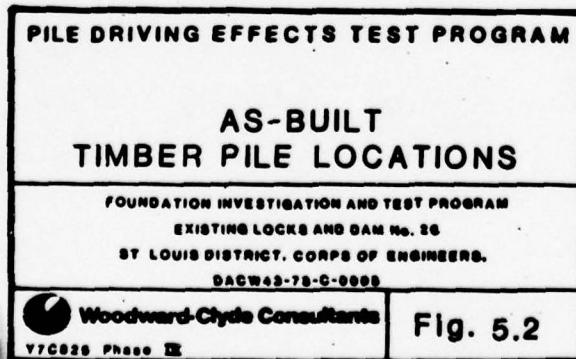


0



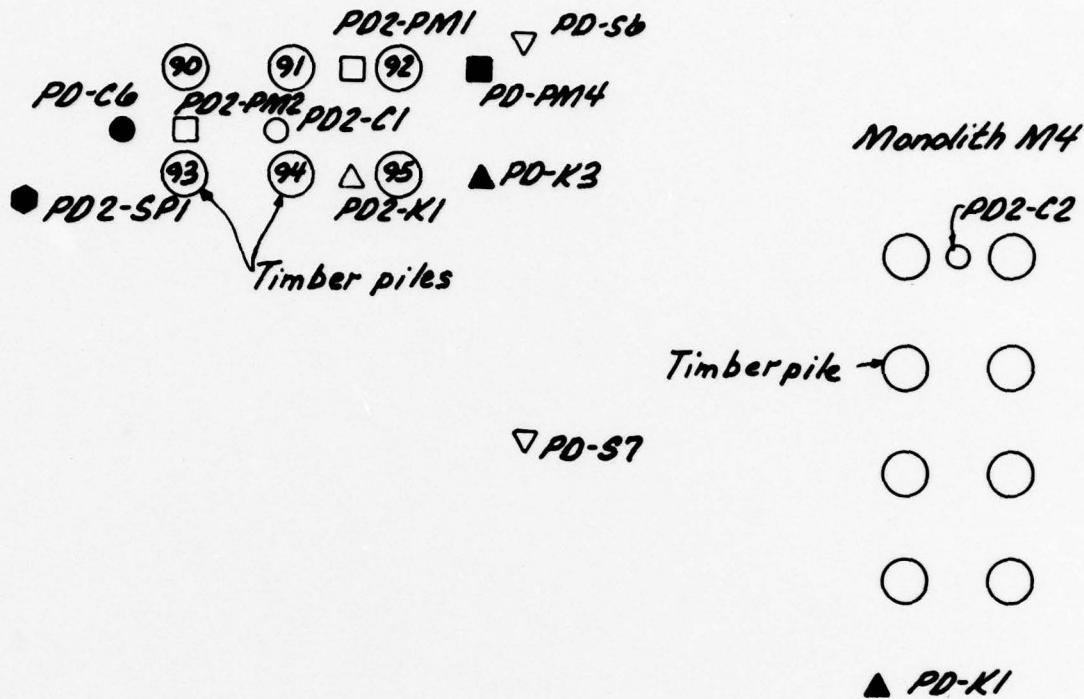
*ile number*  
*s built pile location*  
*heoretical pile location*  
*xtent of monolith*

5              10 ft  
Scale

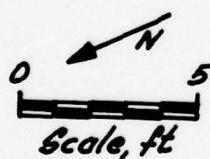


J

Control group M8



▽ PD-58



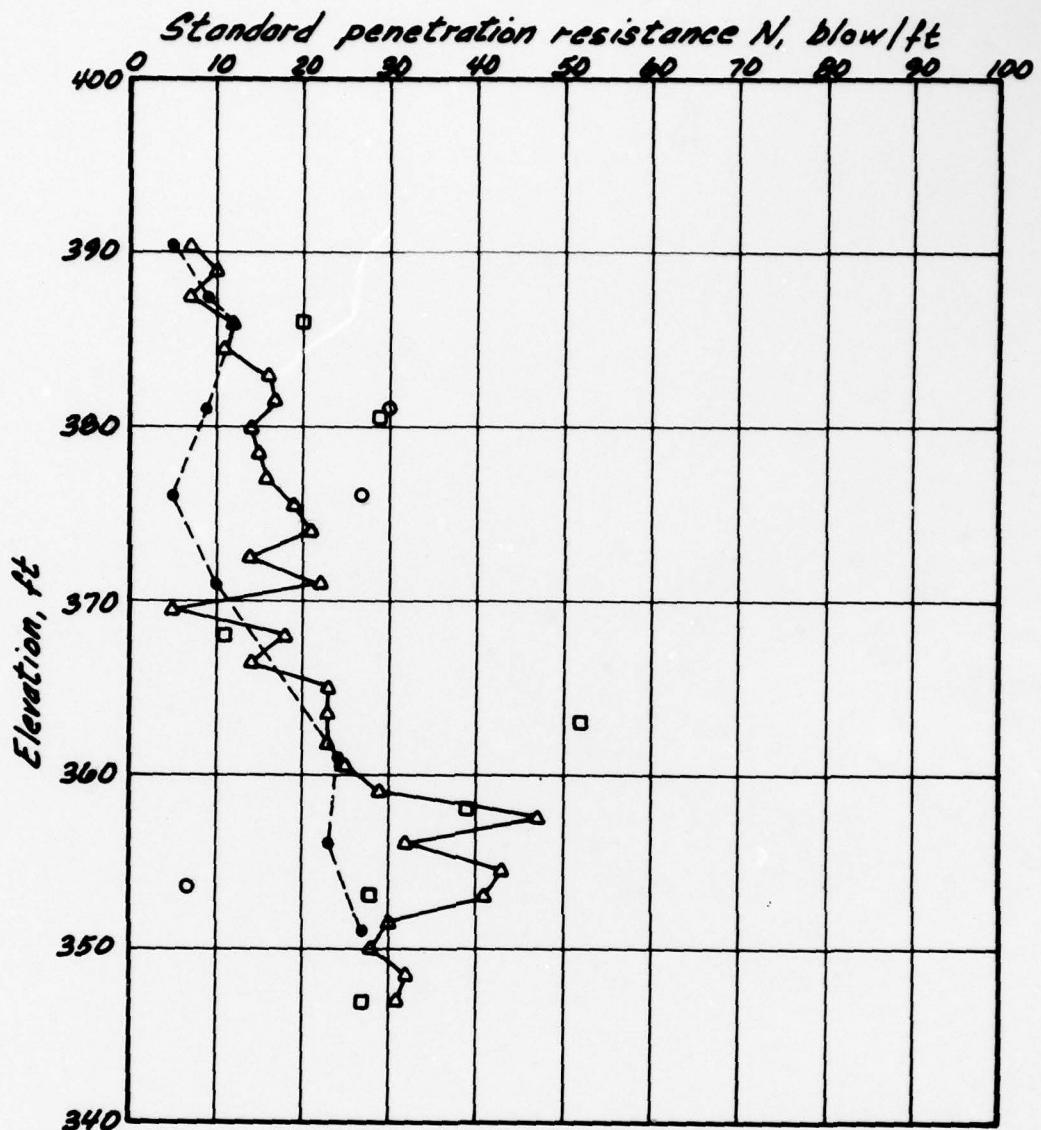
**Legend**

- Cone penetration test sounding
- Pressuremeter test boring
- Continuous SPT boring
- △ Permeability test boring
- ▽ Shear-wave casing

**Note:**

Borings made before timber pile installation are shown by dark symbols

PILE DRIVING EFFECTS TEST PROGRAM	
BORING LOCATION PLAN AFTER TIMBER PILE INSTALLATION	
FOUNDATION INVESTIGATION AND TEST PROGRAM EXISTING LOCKS AND DAM NO. 26 ST. LOUIS DISTRICT, CORPS OF ENGINEERS. DACPW43-78-C-0005	
Woodward-Clyde Consultants V7C825 Phase II	Fig. 5.3



### Legend

Before timber pile installation

--○-- Boring PD-PM4

After timber pile installation

-○- Boring PD2-SP1(near M8)

□ Boring PD2-PM1(in M8)

○ Boring PD2-PM2(in M8)

### PILE DRIVING EFFECTS TEST PROGRAM

### STANDARD PENETRATION RESISTANCE PROFILES AFTER TIMBER PILE INSTALLATION

FOUNDATION INVESTIGATION AND TEST PROGRAM

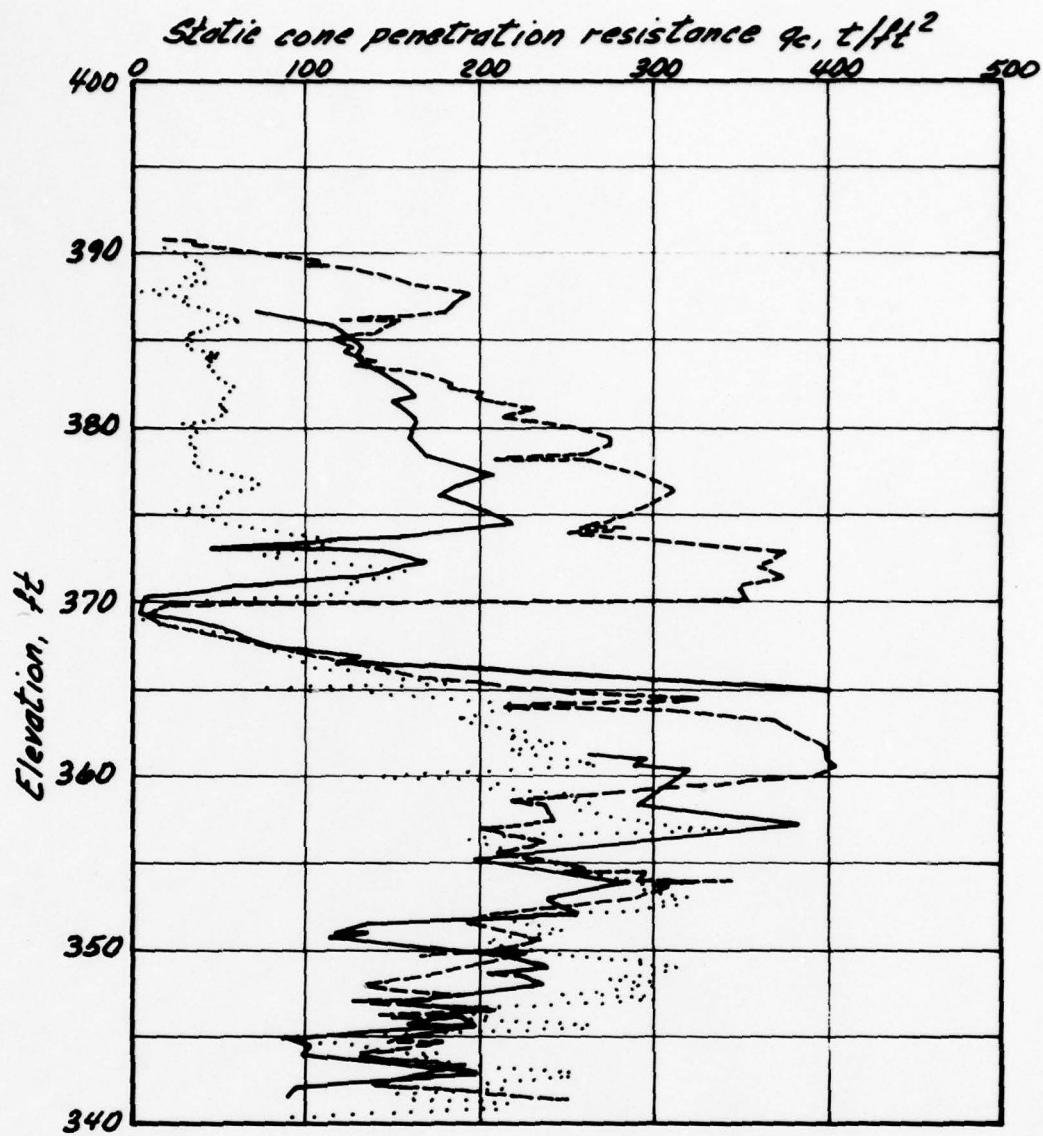
EXISTING LOCKS AND DAM No. 28

ST LOUIS DISTRICT, CORPS OF ENGINEERS.

DACW43-78-C-0008

Woodward-Clyde Consultants  
Y7C825 Phase IX

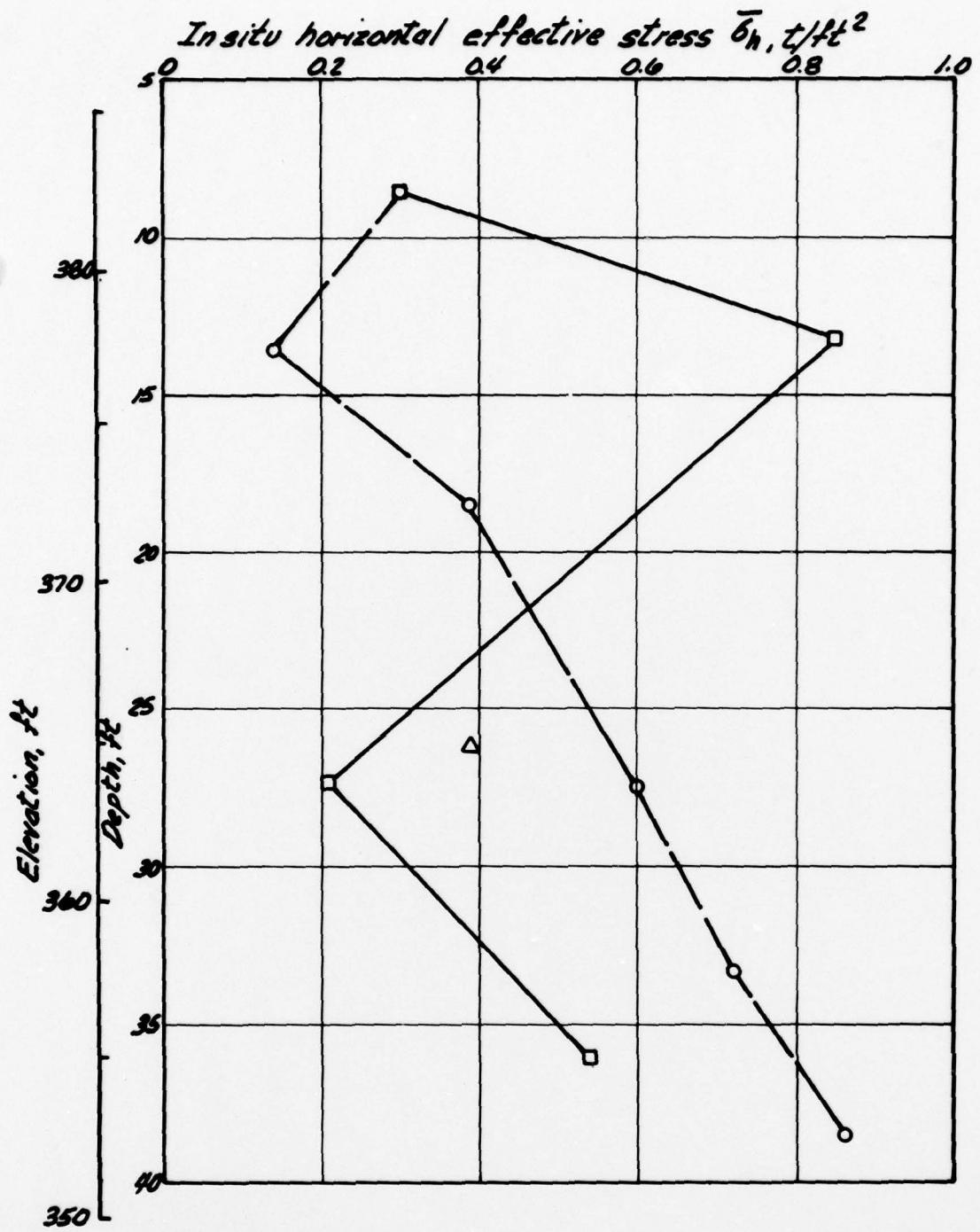
Fig. 5.4



*Legend*

- Before timber pile installation  
 ..... Boring PD-C6  
 After timber pile installation  
 ---- Boring PD2-C1  
 ——— Boring PD2-C2

<b>PILE DRIVING EFFECTS TEST PROGRAM</b> <b>STATIC CONE PENETRATION</b> <b>RESISTANCE PROFILES AFTER</b> <b>TIMBER PILE INSTALLATION</b>	
<small>FOUNDATION INVESTIGATION AND TEST PROGRAM          EXISTING LOCKS AND DAM NO. 28          ST. LOUIS DISTRICT, CORPS OF ENGINEERS.          DACW43-78-C-0008</small>	
 Woodward-Clyde Consultants <small>YTCS25 Phase II</small>	<b>Fig. 5.5</b>



*Legend*

Before timber pile installation

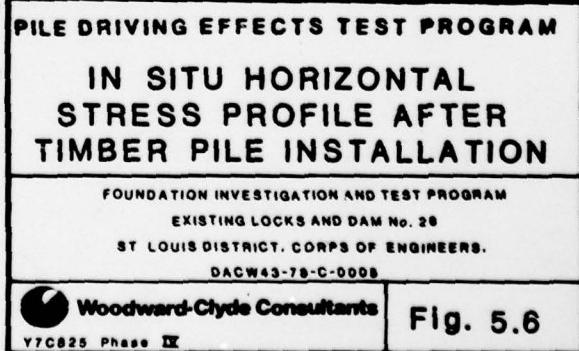
- Boring PD-PM4

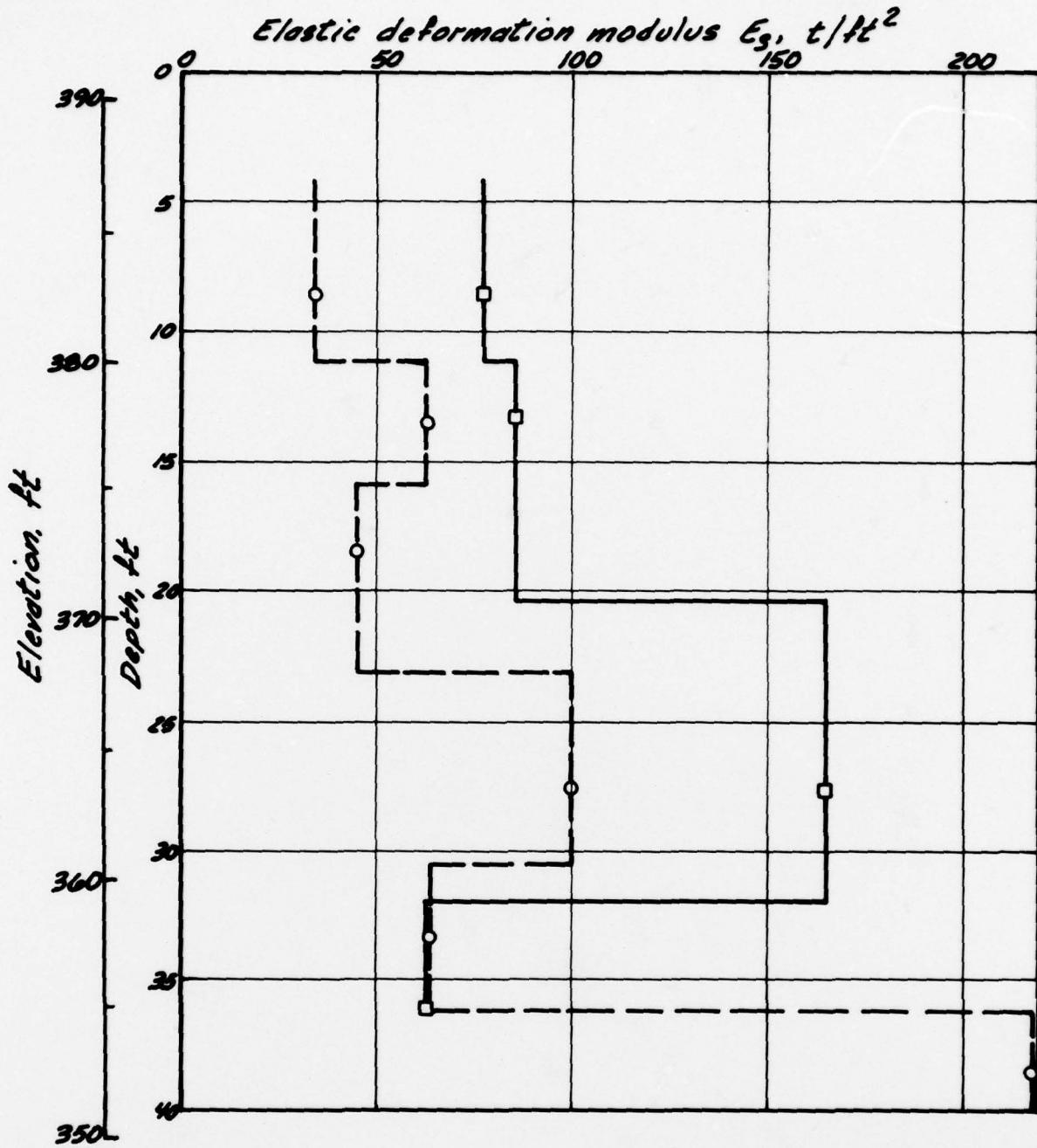
After timber pile installation

- △ Boring PD2-PM1
- Boring PD2-PM2

*Note:*

Horizontal in situ effective  
stress inferred from  
pressuremeter tests



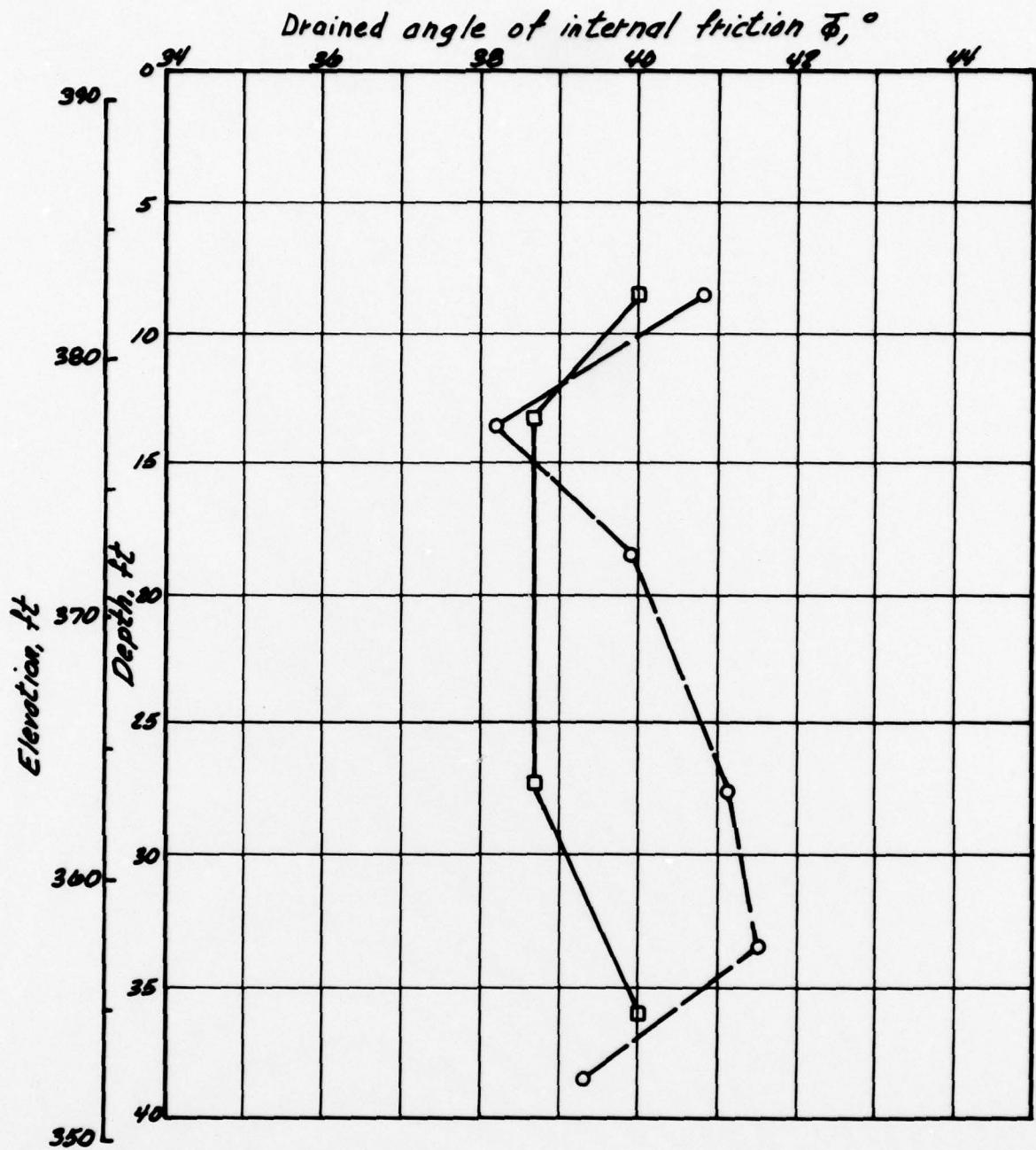


*Legend*

- Boring PD-PM4  
(before timber pile installation)
- Boring PD2-PM2  
(after timber pile installation)

*Note: Modulus derived from pressuremeter tests*

<b>PILE DRIVING EFFECTS TEST PROGRAM</b> <b>ELASTIC DEFORMATION</b> <b>MODULUS PROFILE AFTER</b> <b>TIMBER PILE INSTALLATION</b>	
<small>FOUNDATION INVESTIGATION AND TEST PROGRAM</small> <small>EXISTING LOCKS AND DAM NO. 26</small> <small>ST. LOUIS DISTRICT, CORPS OF ENGINEERS.</small> <small>DACW43-78-C-0008</small>	
 Woodward-Clyde Consultants <small>Y7C825 Phase IV</small>	<b>Fig. 5.7</b>



*Legend*

- Before timber pile installation
- Boring PD-PM14  
After timber pile installation
- Boring PD2-PM2

*Note:*

Drained angle of internal friction derived using Hughes et al (1977) procedure

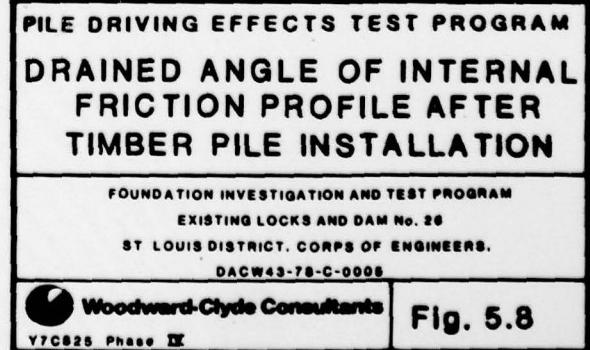
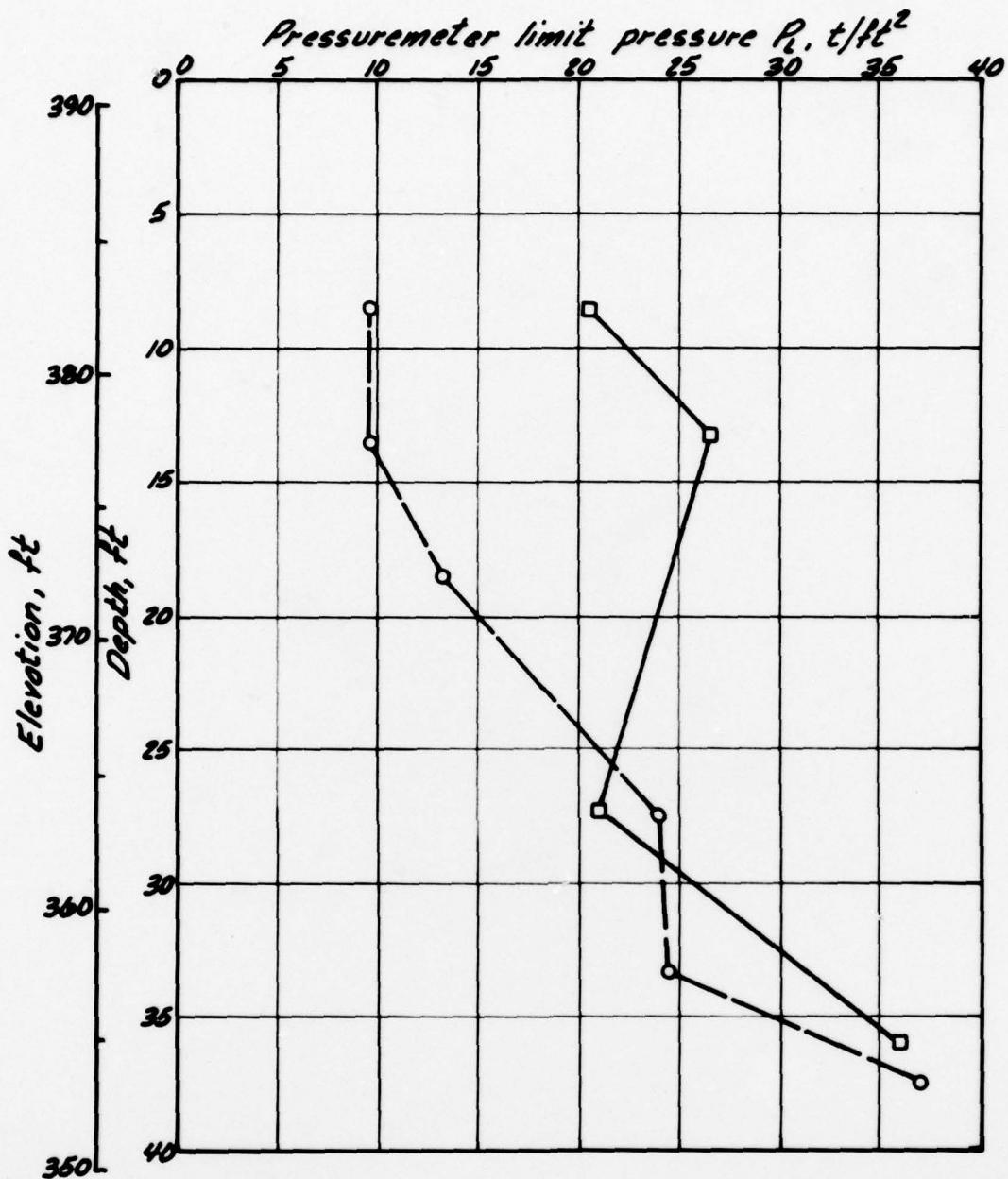


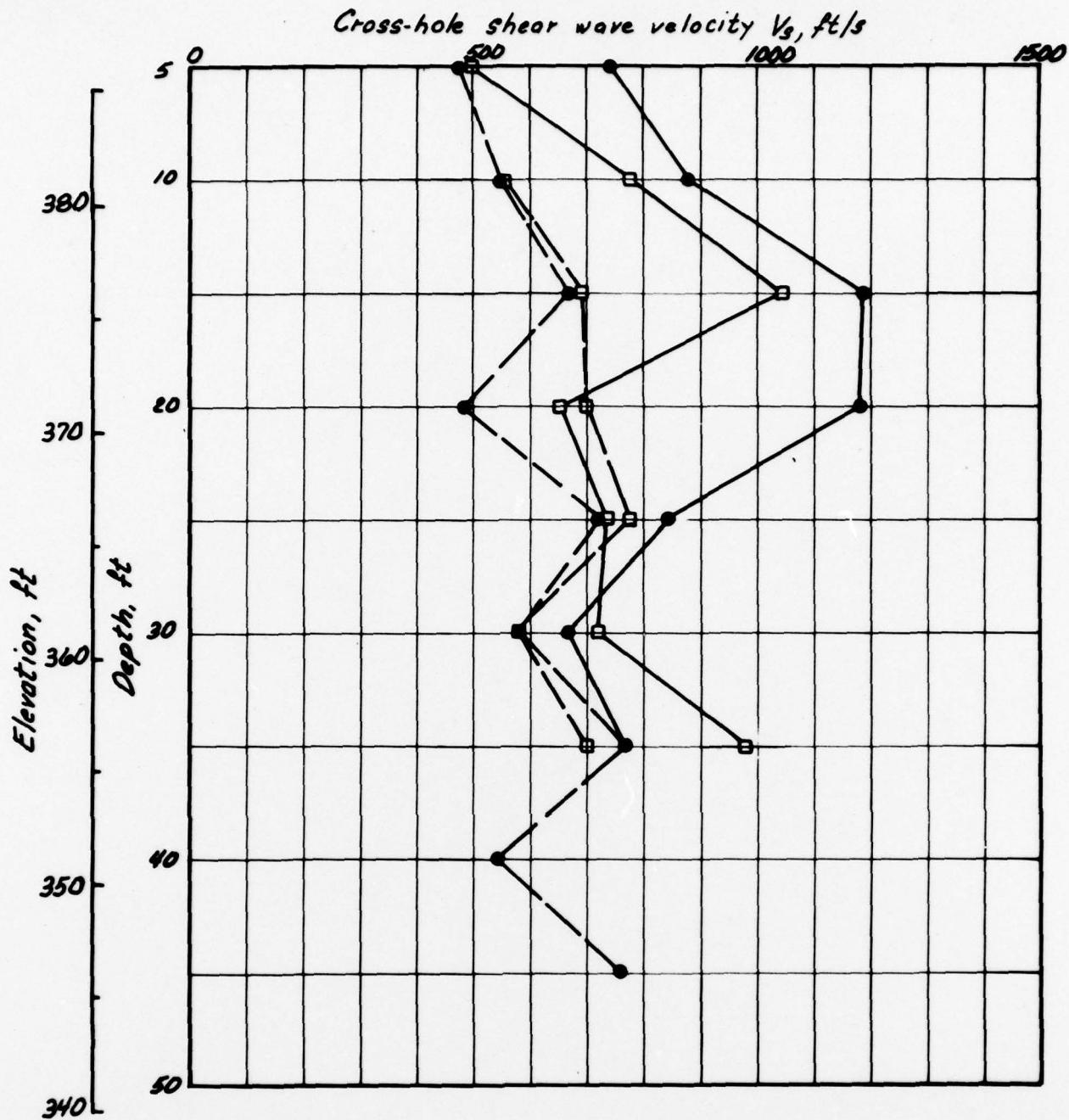
**Fig. 5.8**



*Legend*

- Boring PD-PM4  
(before timber pile installation)
- Boring PD2-PM2  
(after timber pile installation)

PILE DRIVING EFFECTS TEST PROGRAM	
PRESSUREMETER LIMIT PRESSURE PROFILE AFTER TIMBER PILE INSTALLATION	
FOUNDATION INVESTIGATION AND TEST PROGRAM EXISTING LOCKS AND DAM NO. 26 ST. LOUIS DISTRICT, CORPS OF ENGINEERS. DACPW43-78-C-0008	
Woodward-Clyde Consultants Y7C825 Phase IX	Fig. 5.9



### Legend

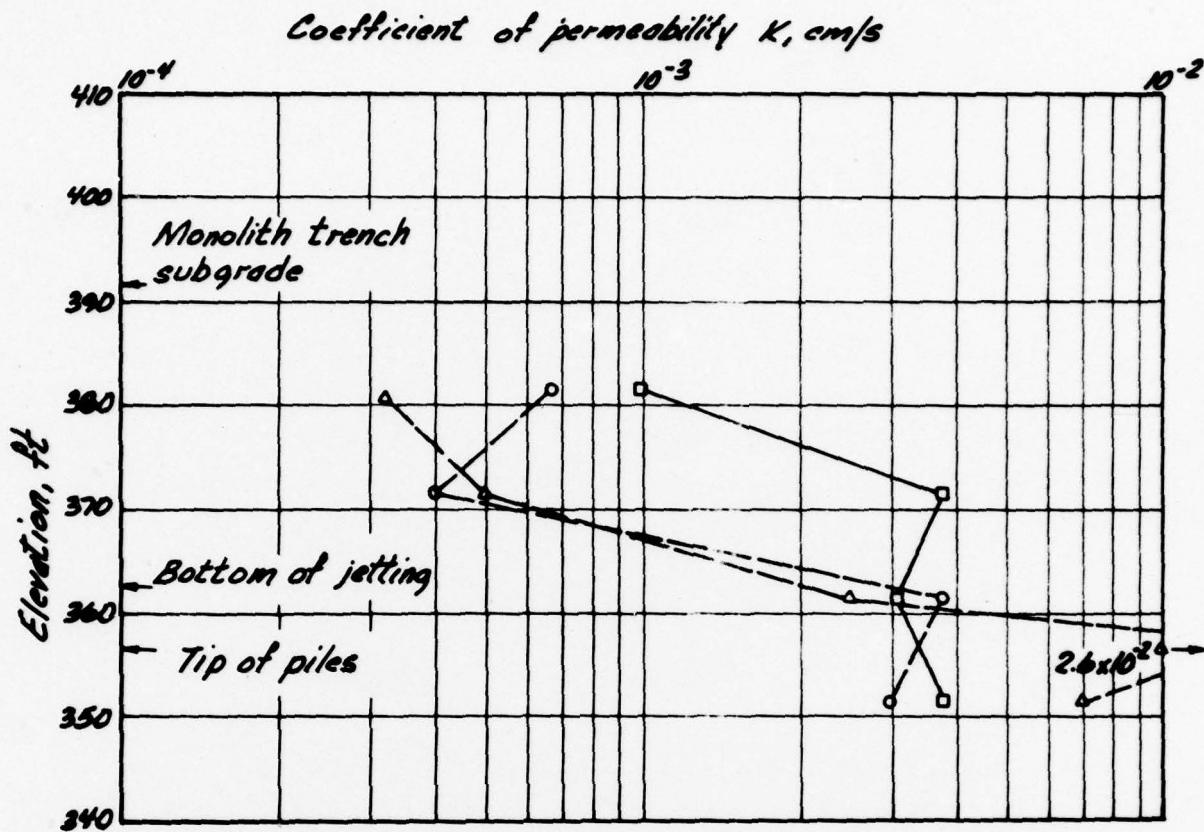
- Array PD-S6, PD-S7, and PD-S8
- Array PD-S8, PD-S9 and PD-S10
- Before timber pile installation
- After timber pile installation

**PILE DRIVING EFFECTS TEST PROGRAM  
CROSS-HOLE  
SHEAR WAVE VELOCITIES  
AFTER  
TIMBER PILE INSTALLATION**

FOUNDATION INVESTIGATION AND TEST PROGRAM  
EXISTING LOCKS AND DAM NO. 20  
ST. LOUIS DISTRICT, CORPS OF ENGINEERS.  
DAGW42-70-C-0000

Woodward-Clyde Consultants  
VTC025 Phase II

Fig. 5.10



*Legend*

- Before timber pile installation
- Boring PD-K3 (M8)
- △-- Boring PD-K1 (M4)
- After timber pile installation
- Boring PD2-K1 (M8)

**PILE DRIVING EFFECTS TEST PROGRAM  
PERMEABILITY TEST RESULTS  
AFTER  
TIMBER PILE INSTALLATION**

FOUNDATION INVESTIGATION AND TEST PROGRAM  
EXISTING LOCKS AND DAM NO. 26  
BY LOUIS DISTRICT, CORPS OF ENGINEERS.

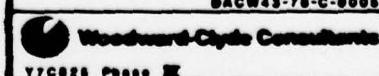
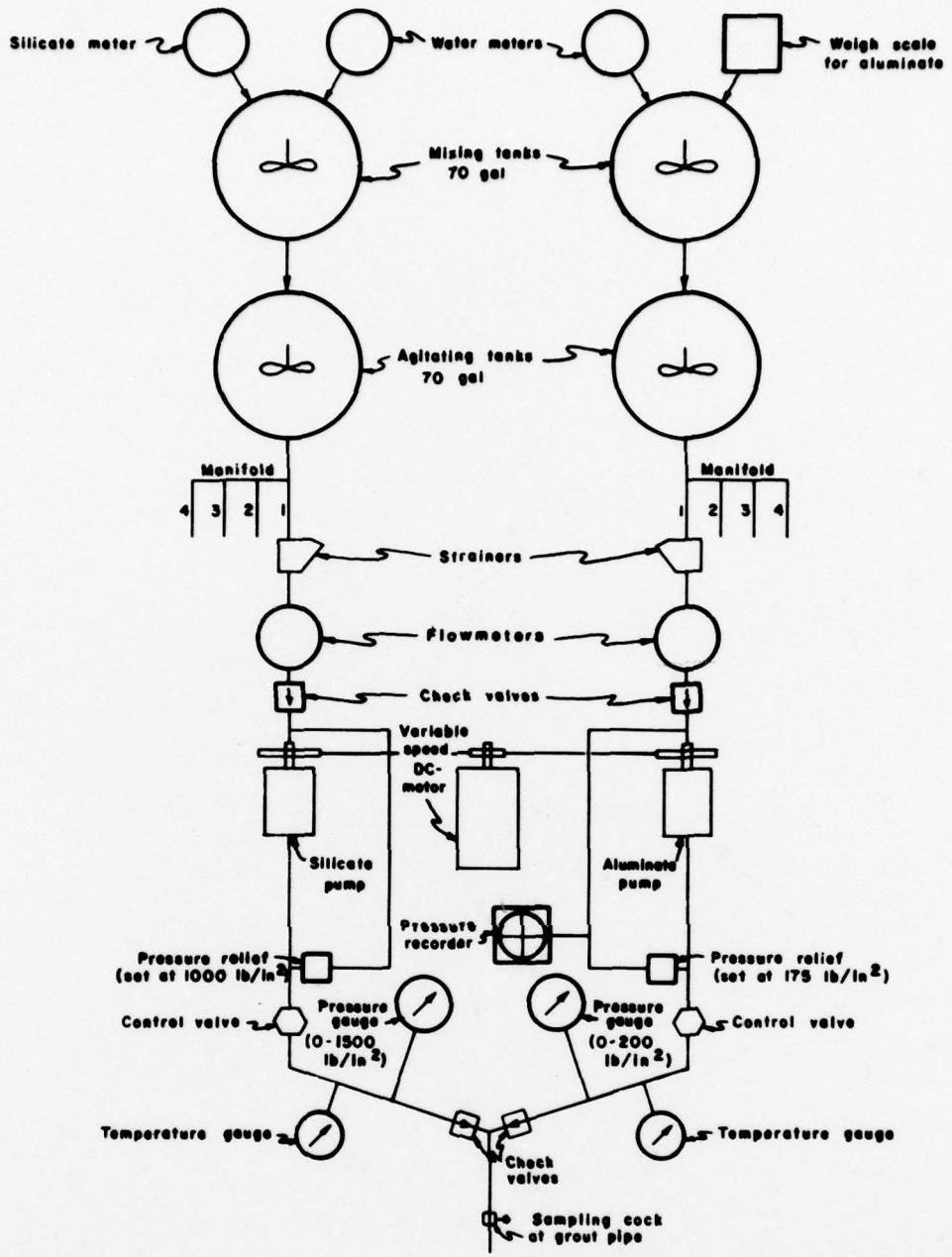


Fig. 5.11

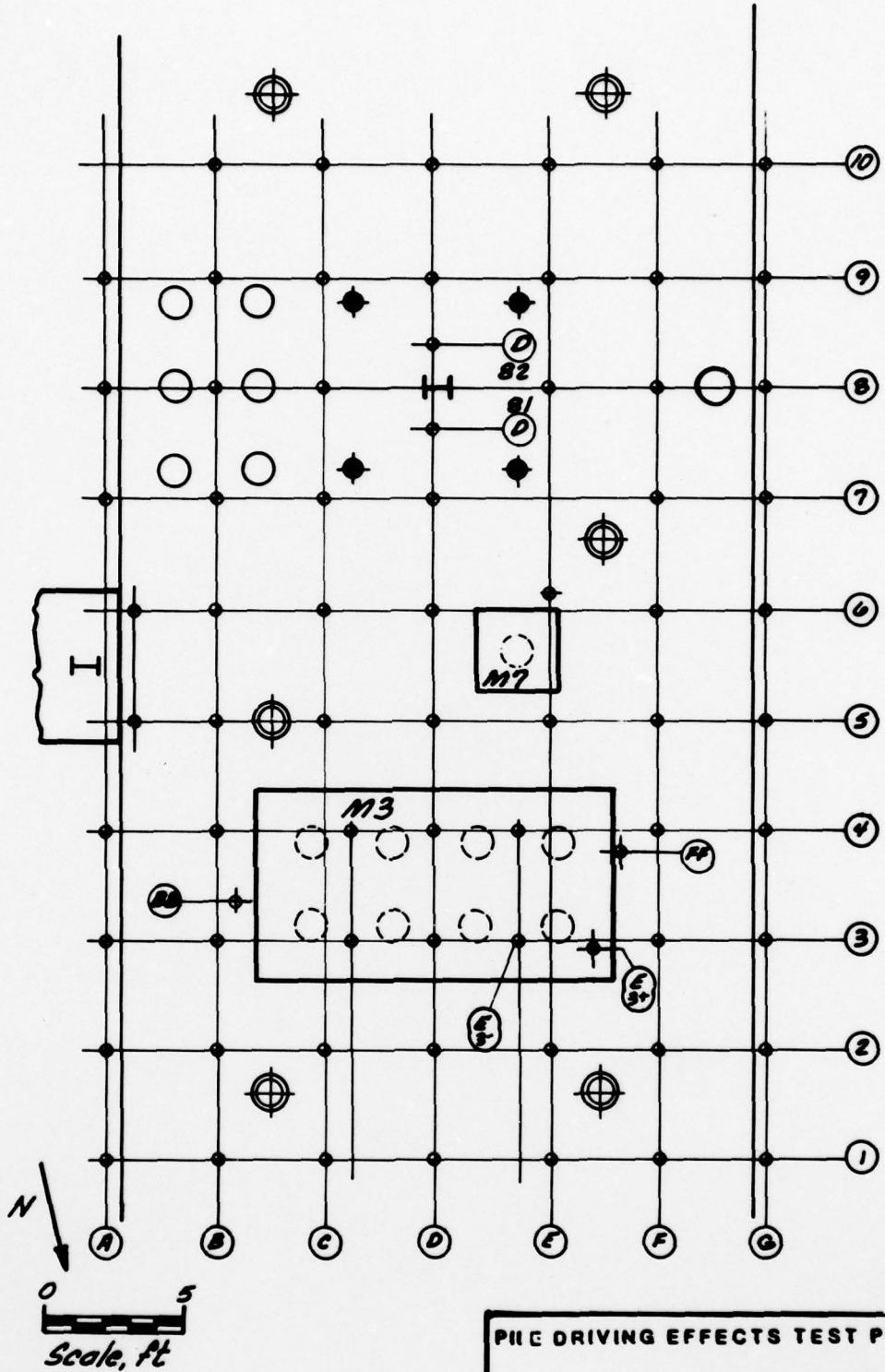


**PILE DRIVING EFFECTS TEST PROGRAM**  
**SCHEMATIC**  
**OF**  
**GROUTING PLANT**

FOUNDATION INVESTIGATION AND TEST PROGRAM  
 EXISTING LOCKS AND DAM NO. 20  
 BY LOUIS DISTRICT CORPS OF ENGINEERS.  
 DASW45-78-C-0000

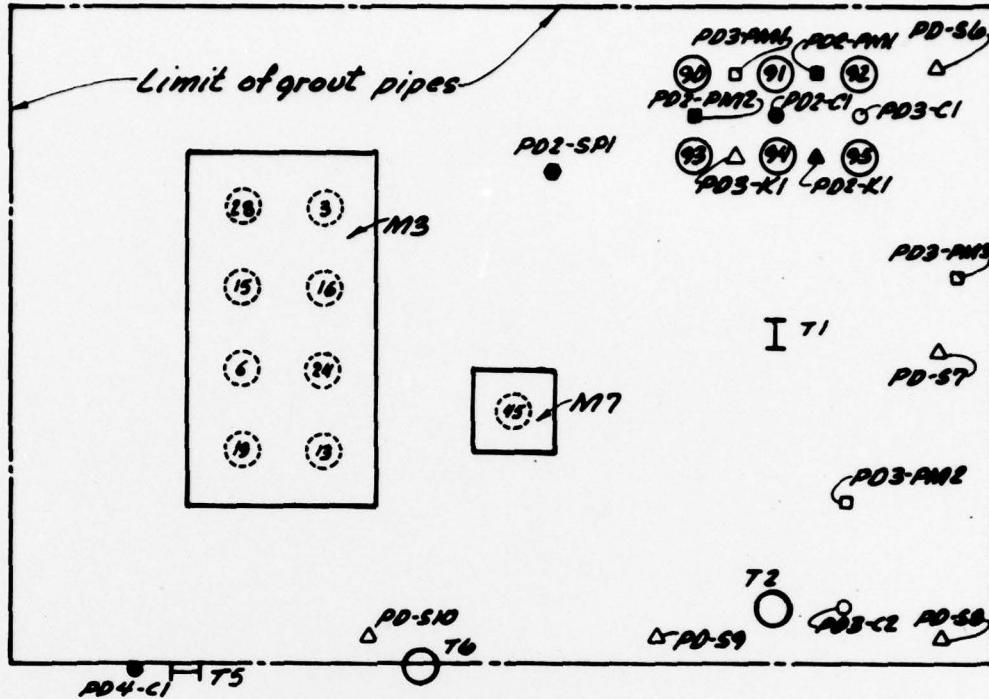
Woodward-Clyde Consultants  
 77C826 Phase II

**Fig. 5.12**



<b>PILE DRIVING EFFECTS TEST PROGRAM</b>	
<b>LAYOUT OF GROUT HOLES</b>	
FOUNDATION INVESTIGATION AND TEST PROGRAM	
EXISTING LOCKS AND DAM NO. 26	
ST LOUIS DISTRICT, CORPS OF ENGINEERS.	
DAGW43-78-C-0008	
	Woodward-Clyde Consultants
YTCB25 Phase IX	

Fig. 5.13



### Legend

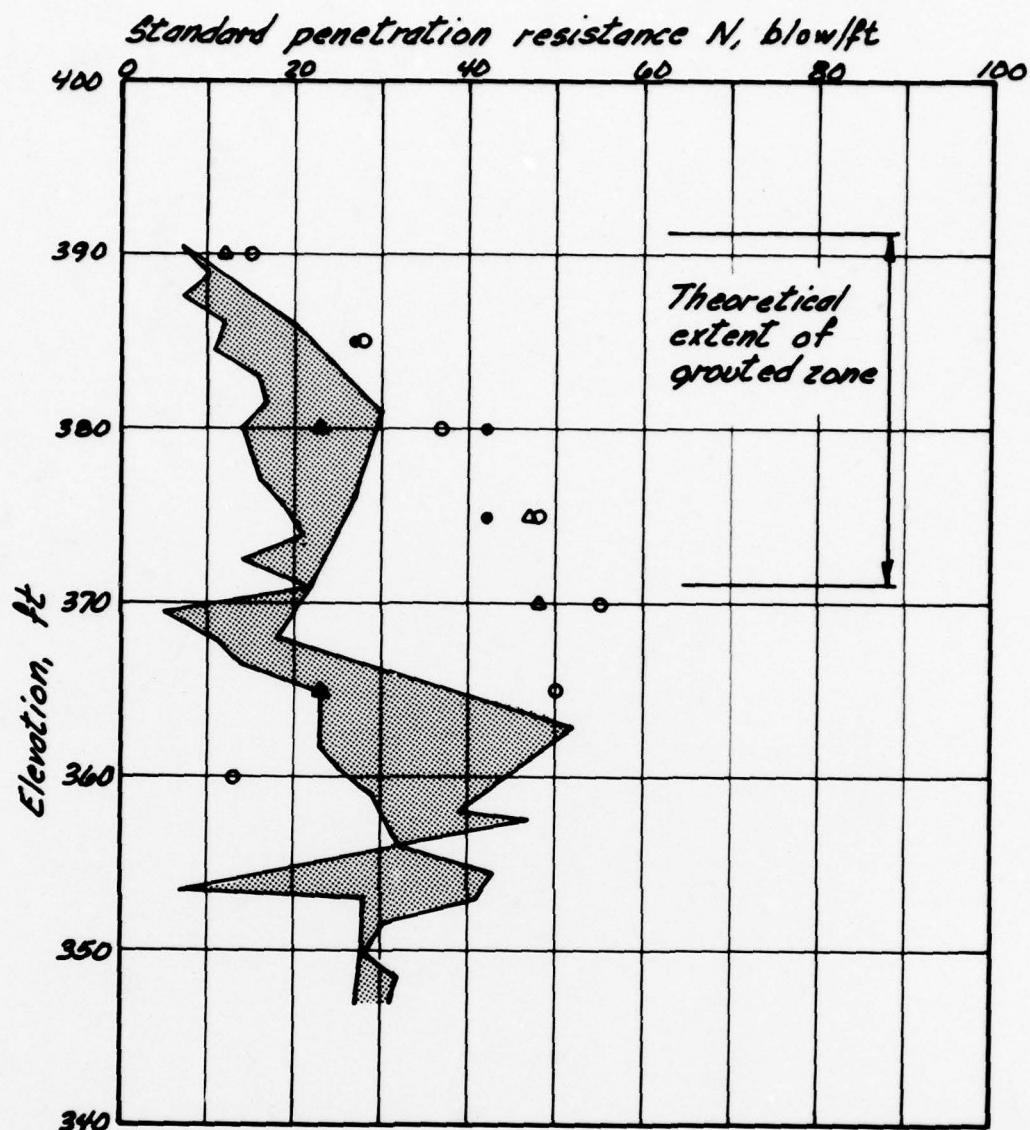
- Cone penetration test sounding
- Pressuremeter test boring
- △ Permeability test boring
- Continuous SPT boring
- ▽ Shear-wave Casing

- I Steel prototype H-pile
- Steel prototype pipe pile
- □ Timber piles

### Note:

Borings made before grouting  
are shown by dark symbols

PILE DRIVING EFFECTS TEST PROGRAM	
<b>BORING LOCATION PLAN AFTER GROUTING</b>	
FOUNDATION INVESTIGATION AND TEST PROGRAM	
EXISTING LOCKS AND DAM NO. 20	
ST LOUIS DISTRICT, CORPS OF ENGINEERS.	
BACW43-70-C-0006	
	Woodward-Clyde Consultants
VTC826 Phase II	Fig. 5.14

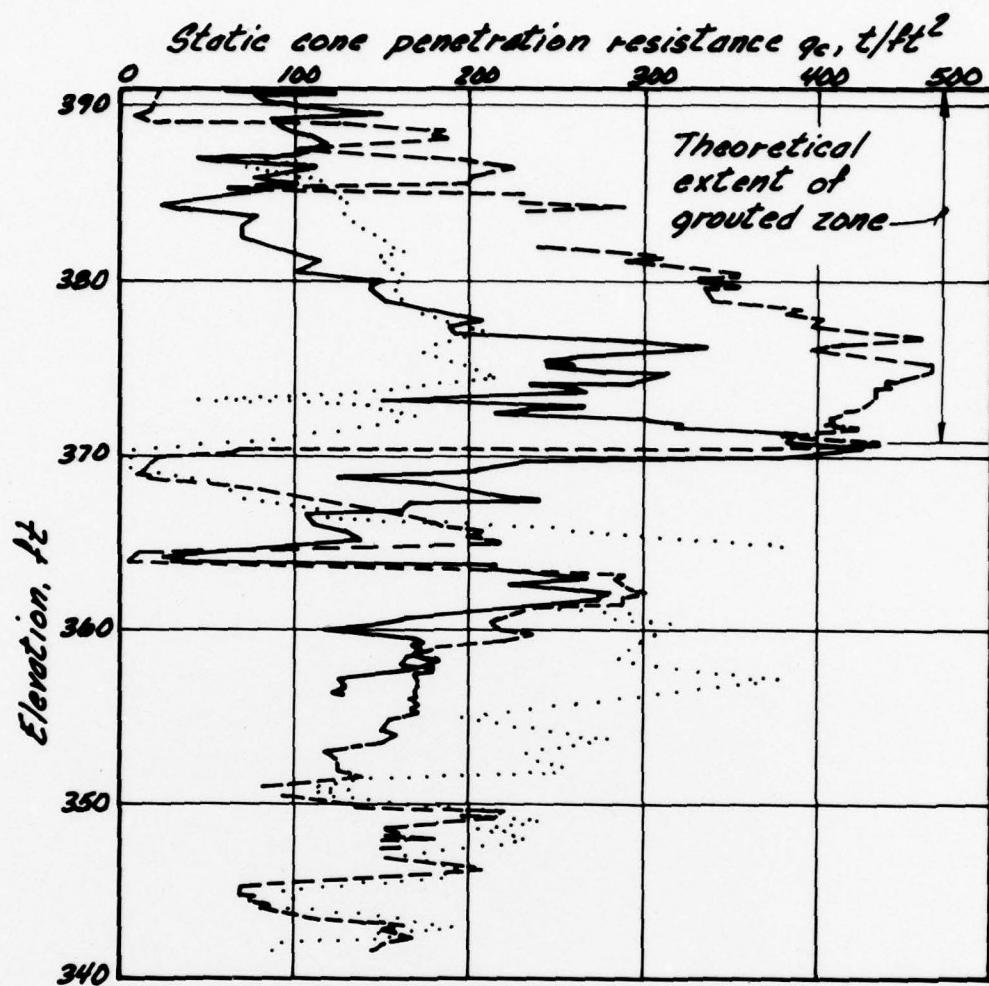


### Legend

- █ Before grouting  
Range for  
borings PD2-SP1,  
PD2-PM1, PD2-PM2
- After grouting  
Boring PD3-PM1
- △ Boring PD3-PM2
- Boring PD3-PM3

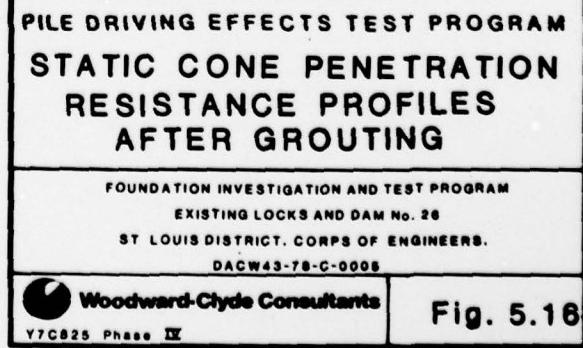


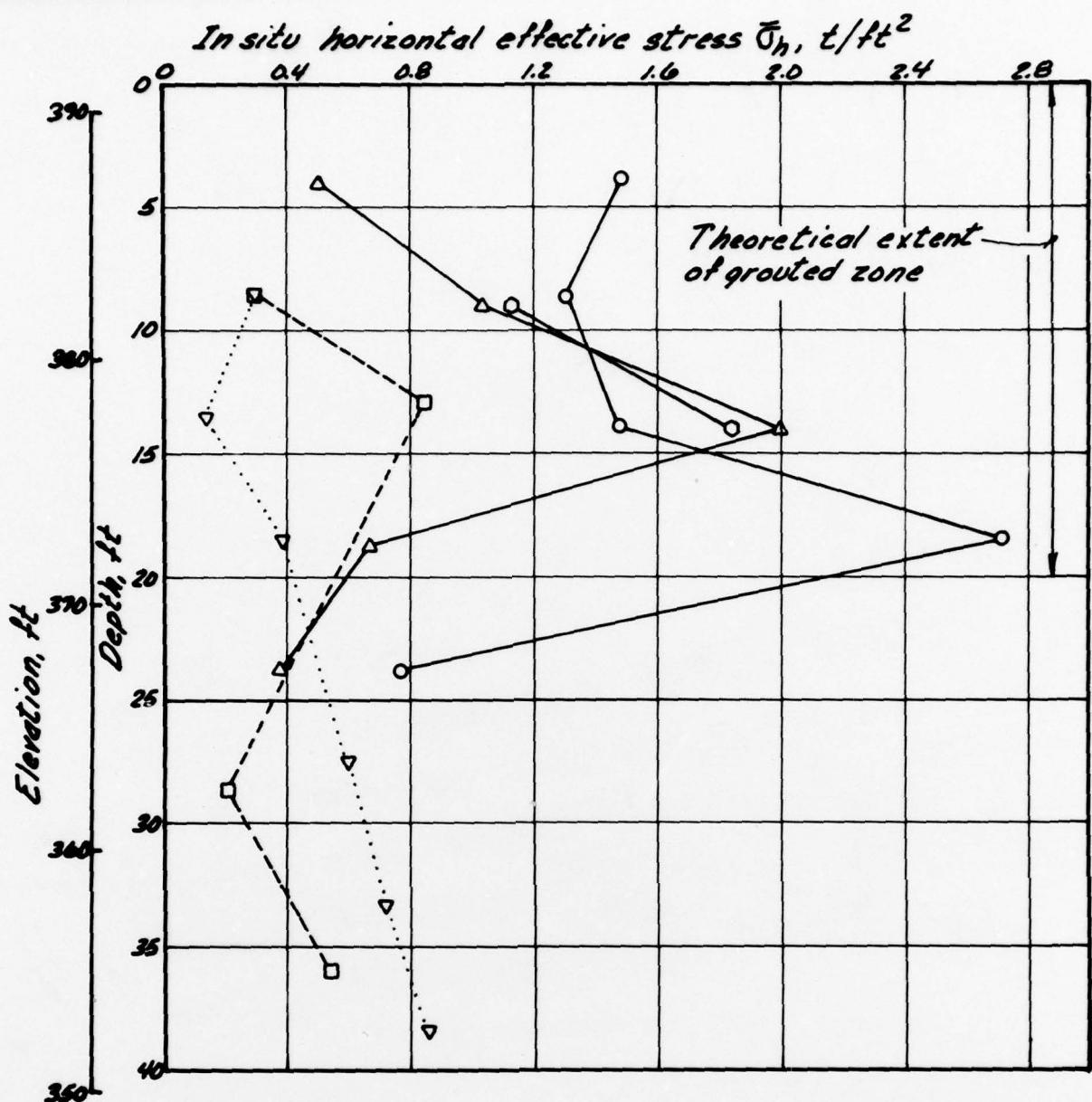
Fig. 5.15



*Legend*

- Before grouting
- ..... Boring PD2-C1
- After grouting
- Boring PD3-C1
- - Boring PD3-C2



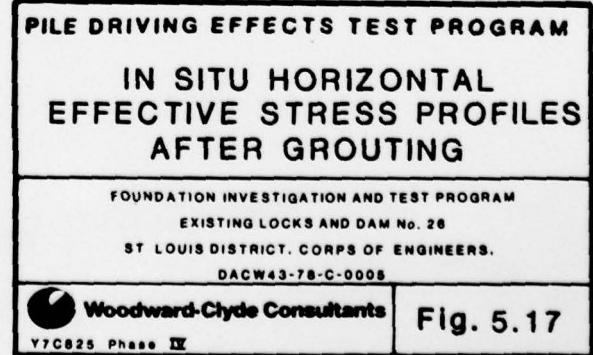


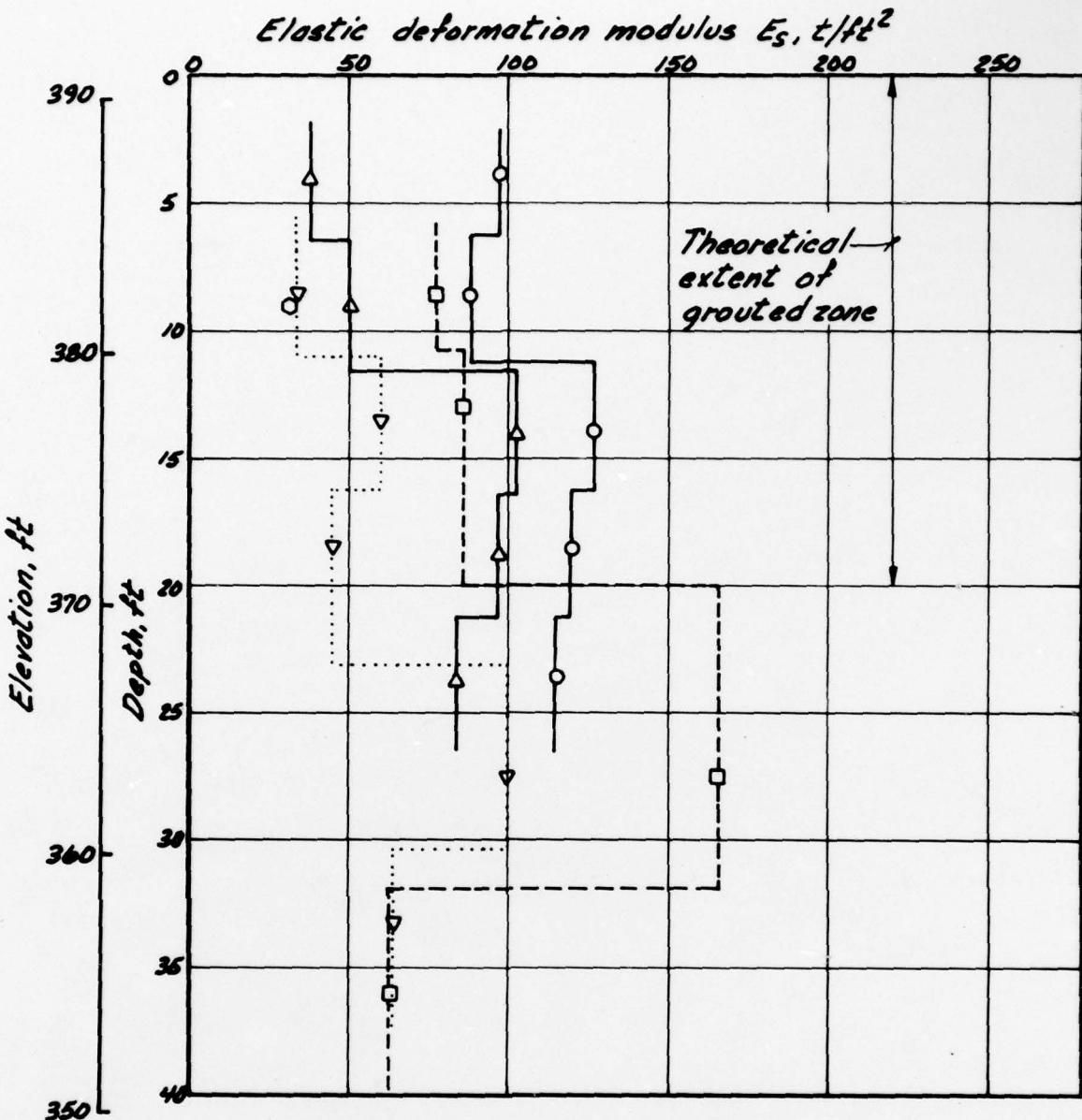
### Legend

- Before timber pile installation
- ...▽... Boring PD-PM4
- Before grouting
- Boring PD2-PM2 (MB)
- After grouting
- Boring PD3-PM1 (MB)
- △— Boring PD3-PM2
- Boring PD3-PM3

### Note:

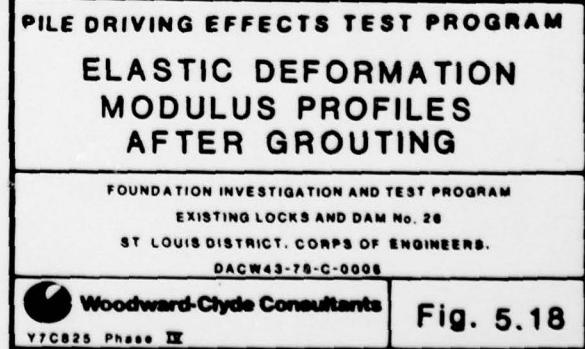
In situ horizontal effective stress inferred from pressuremeter tests





*Legend*

- Before timber pile installation
- ...▽... Boring PD-PM4
- Before grouting
- Boring PD2-PM2(MB)
- After grouting
- Boring PD3-PM1(MB)
- Boring PD3-PM2
- Boring PD3-PM3



AD-A076 093

WOODWARD-CLYDE CONSULTANTS CHICAGO IL

F/G 13/2

RESULTS AND INTERPRETATION OF PILE DRIVING EFFECTS TEST PROGRAM--ETCIL

DACW43-78-C-0005

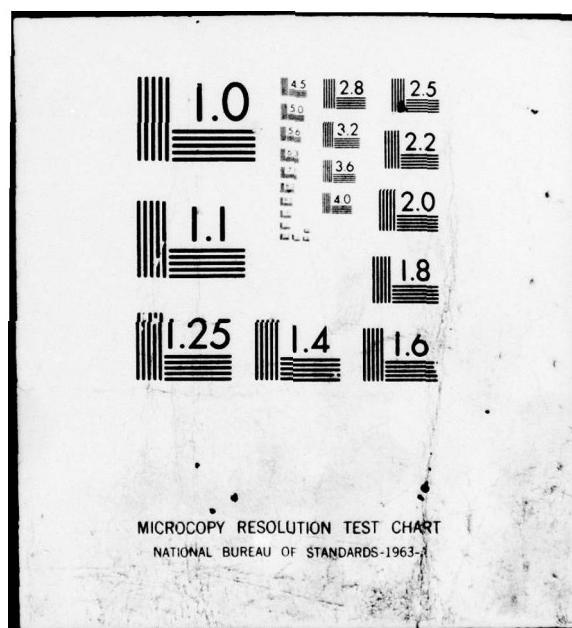
JUL 79 J PEREZ , D M HOLLOWAY

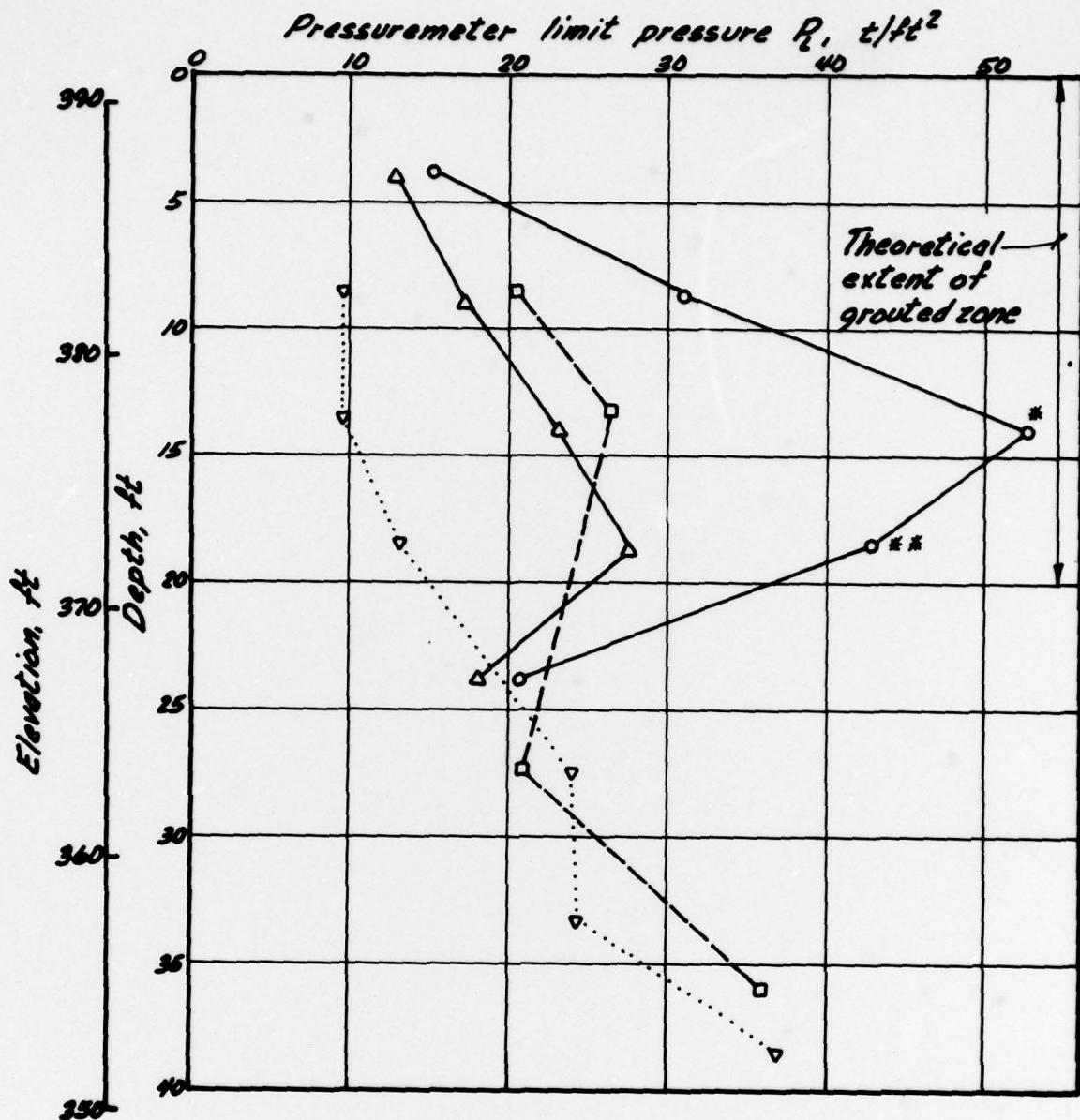
NL

UNCLASSIFIED

3 of 5  
AD  
A076093







#### Legend

- Before timber pile installation
- ...▽... Boring PD-PM4
- Before grouting
- Boring PD2-PM2(MB)
- After grouting
- Boring PD3-PM1(MB)
- Boring PD3-PM2

\* Influenced by strain hardening  
\*\* Test not carried to full limit pressure

**PILE DRIVING EFFECTS TEST PROGRAM**  
**PRESSUREMETER**  
**LIMIT PRESSURE PROFILES**  
**AFTER GROUTING**

FOUNDATION INVESTIGATION AND TEST PROGRAM  
EXISTING LOCKS AND DAM No. 26  
ST LOUIS DISTRICT, CORPS OF ENGINEERS.  
DACPW43-78-C-0008

Woodward-Clyde Consultants  
VTC625 Phase III

Fig. 5.19

**PHASE IV REPORT**

**VOLUME III**

**RESULTS AND INTERPRETATION OF  
PILE DRIVING EFFECTS TEST PROGRAM**

**SECTION 6  
MONOLITH PRELOADING**

## 6 MONOLITH PRELOADING

### 6.1 SCOPE OF TESTS

Each test monolith was laterally loaded and unloaded for a number of cycles prior to any other tests. The cyclic lateral preloading of the test monoliths was more a preconditioning than a test, done to approximate the effects of the load history on an existing navigation structure, such as Locks and Dam No. 26. It was believed that without this preconditioning, the test monoliths would creep under sustained test loads making interpretation of pile driving effects tests difficult.

Each test monolith was first axially loaded to  $V_2$  load level (30 t/pile). The axial load was maintained constant throughout the cyclic preloading activities. After initial application, the lateral load was slowly varied from  $H_2$  (6 t/pile) to 0.1  $H_2$  (0.6 t/pile) for a number of cycles. The number of loading cycles was based on the observed response of each monolith. The cyclic preloading was halted when the lateral displacement of the monolith under full lateral load remained essentially unchanged for each successive cycle; that is, when the monolith load-displacement behavior reached a steady state.

Scheduling of monolith preloading activities incorporated timing of other test events. Monolith M1 was preloaded first, followed immediately by monoliths M3 and M7 to afford sufficient time for the chemical grouting operations around these two test structures. The pile driving effects tests were then made on M1. The remaining monoliths (M2, M5, and M6) were tested sequentially from cyclic preloading through pile driving effects and, finally, load testing to failure. Monoliths M3 and M7 were subjected to pile driving effects and were load tested to failure last.

### 6.2 TEST PROCEDURES

#### 6.2.1 General

General test procedures had been established at the design stage and were essentially followed in the field. Detailed test procedures, measurement techniques, and instrumentation reading frequency and schedule were developed on the basis of the experience gained during cyclic preloading of monolith M1. Actual field procedures remained consistent with the objectives of the tests and with the priority ranking of significant aspects of performance established in Section 2.3.1.

The lateral load was applied using a tandem of two hydraulic jacks, actuated and adjusted independently using direct load cell measurements. As a result, the prescribed load levels were achieved with reasonable accuracy throughout the preloading and subsequent test operations. The duration of sustained maximum and minimum loads for most cycles was brief, normally less than 5 min,

providing only enough time to acquire data with the automatic system. Sustained load cycles, during which selected primary and secondary measurements were made, were 1 to 3 hr in duration.

#### **6.2.2 Test Setup and Instrumentation**

The monoliths were generally cyclically preloaded individually, although the test setups were common for monoliths M2 and M6. Monoliths M3 and M7 were simultaneously preloaded. The loading schemes are described in Section 5.3. Only the instrumentation related to static structural response of the monoliths, response of the timber piles, and response of the soil mass (Sections 3.1.6 and 3.1.7) was utilized during cyclic preloading, consistent with the measurement priorities established in Section 3.5.

The configuration of the monolith trench was essentially the same during cyclic preloading of all monoliths (that is, the toe of the berm was 5 ft to 8 ft from the north edge of the monolith). The berm was modified only after cyclic preloading (Section 5.2.2).

#### **6.2.3 Sequence of Operations**

The general procedures used in cyclic preloading of each monolith are given below. Minor deviations from these procedures are described within the presentation of results for a particular monolith.

- (1) Make initial static primary and secondary measurements (load cells, linear potentiometers and dial gages, optical surveys, tiltmeters, tape extensometers, ground and pile inclinometers, telltales, strain gages, and thermocouples);
- (2) apply an axial load equivalent to 30 t/pile (that is, 360 t for M1; 240 t for M2, M3, and M5; and 30 t for M6 and M7); make periodic measurements using the automatic data acquisition system (load cells and linear potentiometers) as the axial load is slowly applied, and at full axial load until settlement of the monolith stabilized to less than 0.01 in./hr;
- (3) make selected automatic and manual measurements (dial gages, optical surveys, inclinometers, telltales);
- (4) apply a lateral load equivalent to 6 t/pile (that is, 72 t for M1; 48 t for M2, M3, and M5; and 6 t for M6 and M7); make periodic measurements using the automatic data acquisition system (load cells and linear potentiometers) as the lateral load was slowly applied, and at full lateral load until the lateral displacement of the monolith stabilized to less than 0.01 in./hr.
- (5) repeat step (3);
- (6) decrease lateral load to a level equivalent to 0.6 t/pile (that is, 36 t for M1; 24 t for M2, M3, and M5; and 0.6 t for M6 and M7); make selected automatic and manual measurements;

- (7) repeat steps (4) to (6), making only automatic measurements (load cells and linear potentiometers) at maximum and minimum lateral load levels and make selected manual measurements every five to twenty cycles (the frequency of these measurements varied from monolith to monolith); continue step (7) until load-unload cycles resulted in negligible change in observed displacements, in general, less than 0.01 in. in 5 cycles;
- (8) repeat all static primary and secondary measurements made in step (1) at full lateral load;
- (9) remove lateral load; make all primary and selected secondary automatic and manual measurements; and
- (10) remove axial load from monoliths M1, M3, and M7. Axial loads on monoliths M2, M5, and M6 were not removed. These monoliths were immediately tested for prototype pile driving effects.

The original test procedures called for a relatively complete set of measurements to be taken every tenth load cycle. This procedure was somewhat modified during cyclic preloading of monolith M1 to document only relatively large changes in monolith displacement vs cycle number. Manual data acquisition was more frequent in early cycles when rapid changes in displacement occurred, and less frequent in later cycles when stable behavior was approaching. A summary log of manually acquired data is given as part of the measurement details for each monolith in Appendices L through P, Volume IIIA.

### 6.3 TEST RESULTS

#### 6.3.1 General

A description of monolith displacements vs number of load cycles follows for each monolith. Raw linear potentiometer data (uncorrected for reference beam movement) form the basis for the figures illustrating the results; optical survey measurements are shown separately. A summary of cyclic preloading results is also given in Table 6.1. In general, the displacement of the reference beams was small and only minor or no corrections to the linear potentiometer data were required.

#### 6.3.2 Monolith M1

Results of cyclic preloading of monolith M1 are presented in Fig. 6.1. Uncorrected linear potentiometer data agree closely with reference point survey data, obtained only for cycles 1, 10, 30, and 40. The small differences between the two types of measurements are attributed to reference beam displacement and to tilting of the monolith, as discussed in Section 7.3.4.

Deviations from the planned sequence of operations involved complete lateral unloading at cycle 3 due to jacking difficulties; removal of wooden wedges

inadvertently left between the monolith and the cribbing supporting the axial load reaction frame (Section 5.3.3); and complete axial and lateral unloading after cycle 10 to rebalance the strain gage channels of the automatic data acquisition system.

Stabilized load-displacement behavior was reached after 40 cycles. From cycle 30 through cycle 40, the horizontal displacement of the monolith under maximum lateral load  $H_2$  was 1.26 in. and did not change by more than  $\pm 0.02$  in. Cyclic displacement from maximum to minimum lateral load levels was reasonably constant throughout most cycles (0.53 in.). The residual horizontal displacement after complete axial and lateral unloading was 0.53 in. During early load cycles, the horizontal monolith displacement stabilized after 2 to 3 hr both at maximum and minimum lateral load levels. During these periods of time, the displacement changed by approximately 0.05 in and the jacks were adjusted to maintain constant lateral load. For late load cycles, monolith stabilization occurred almost immediately after load change, requiring less jack load adjustment.

### 6.3.3 Monolith M2

It was originally intended to cyclically preload monoliths M2 (2 x 4 timber piles) and M6 (single timber pile) simultaneously. After full axial and maximum lateral loads were applied to the two monoliths for a period of about 2 hr, the three axial jacks (two for M2 and one for M6, Fig. 2.4) suddenly slipped out of position, resulting in complete axial unloading of both monoliths. This incident occurred on a Saturday night during a severe snow storm. Testing operations were halted. The lateral loads, probably seriously affected by the sudden axial unloading, remained applied to both monoliths for the next 36 hr. The exact cause of the incident is unknown; it may have been the result of eccentric positioning of the axial reaction frame with respect to reaction rock anchors and monoliths. It was decided to proceed with cyclic preloading of monolith M2 alone. Monolith M6 was preloaded later. As a result of these events, the trend of displacement vs load-unload cycle for monolith M2 and M6 deviates from that observed for the other monoliths. Because the primary objective of cyclic preloading was to precondition the pile-soil system, it is not believed that deviation from the preestablished sequence of operations at this stage would influence subsequent monolith response to prototype pile driving effects and load testing to failure; however, comparison with the detailed preloading displacement history of other monoliths is less meaningful.

Results of cyclic preloading of monolith M2 are presented in Fig. 6.2. The maximum horizontal displacement after 29 cycles was approximately 1.07 in. under maximum lateral load. The maximum displacement did not change by more than 0.02 in. during the last 10 cycles. Cyclic displacement from maximum to minimum lateral load levels ranged from 0.48 to 0.52 in. Following cyclic preloading, monolith M2 was unloaded laterally only; the full axial load was maintained to minimize difficulties in applying axial load on monolith M6 using the same axial reaction frame. Residual monolith horizontal displacement was 0.49 in. The pile driving effects tests were conducted immediately following preloading of M6.

#### 6.3.4 Monolith M3

Cyclic preloading of monolith M3 was done prior to chemical grouting. No major difficulty was experienced. Results of cyclic preloading of monolith M3 are presented in Fig. 6.3. Maximum horizontal displacement of the monolith after 47 cycles was approximately 1.32 in. Cyclic displacement from maximum to minimum lateral load levels ranged from 0.47 to 0.52 in. Upon complete lateral and axial unloading, the residual monolith horizontal displacement was 0.6 in. The loading setup was disassembled and moved to monolith M2. The pile driving effects tests were conducted later, following grouting.

#### 6.3.5 Monolith M5

No major difficulty was experienced during cyclic preloading of monolith M5. Results are presented in Fig. 6.4. Maximum horizontal displacement of the monolith after 40 cycles was approximately 1.05 in. Cyclic displacement from maximum to minimum load levels ranged from 0.49 to 0.56 in. For this monolith, the minimum lateral load level was approximately 3.5 t or slightly more than 0.4 t/pile, as compared to about 0.6 t/pile for the other monoliths. The maximum lateral load level was 48 t, or 6 t/pile. Upon complete lateral unloading, the residual monolith horizontal displacement was 0.45 in. The pile driving effects tests were conducted immediately following preloading.

#### 6.3.6 Monolith M6

Comments concerning difficulties experienced during cyclic preloading of monolith M6 are given in Section 6.3.3. Results are presented in Fig. 6.5. Maximum horizontal displacement of the monolith after 23 cycles was 0.91 in. Cyclic displacement from maximum to minimum load levels was 0.16 in. Upon lateral unloading (axial load was maintained upon completion of cyclic preloading), the residual monolith horizontal displacement was 0.42 in. The pile driving effects tests were conducted immediately following preloading.

#### 6.3.7 Monolith M7

Cyclic preloading of monolith M7 was done prior to chemical grouting, simultaneously with preloading of monolith M3. Results are presented in Fig. 6.6. Maximum horizontal displacement of the monolith after 47 cycles was approximately 0.85 in. Cyclic displacement from maximum to minimum lateral load levels ranged from 0.34 to 0.38 in. Upon complete lateral and axial unloading, the residual monolith horizontal displacement was 0.25 in. The loading setup, common to monolith M3 and M7, was disassembled and moved to M2 and M6. The pile driving effects tests were conducted later.

### 6.4 EVALUATION OF TEST RESULTS

#### 6.4.1 Evaluation of Predictions

Predictions of timber pile group behavior under lateral loads were made at the design stage (Section 2.3.2). These predictions were representative of virgin

and repeated loading conditions, which were the case for the first and last preloading cycles. Therefore, the prediction must be compared to the results of initial cyclic lateral load application, and not to final monolith load tests discussed in Section 8.

A comparison between predicted and measured horizontal monolith displacement is given in Table 6.1. The differences between predicted and measured results are discussed in the following sections.

#### 6.4.2 Monolith M1

For monolith M1, the predicted horizontal displacement under the first lateral load application was 2.1 in. The measured value was 0.74 in. or less than one-half the prediction. Part of this difference is attributed to the low soil and timber pile modulus values assumed for prediction purposes (GP3A). Part of this difference is also attributed to the effects of the timber piles installed around the monolith (Section 2.2.4). These piles stiffened the soil medium in front of the monolith.

Another condition which probably had a stiffening effect was the berm in front of the monolith. The effects of a berm had not been included in the predictions. The berm induced horizontal stresses in the soil, which increased the lateral soil resistance. The magnitude of the stress increase due to the berm depends on geometry (distance to toe, slope, height) and unit weight of soil constituting the berm. It is estimated that the berm increased the lateral soil resistance by 15 to 30 percent.

At the end of cyclic preloading, the horizontal monolith displacement was 1.26 in., compared to a predicted value of 2.1 in. The reasons for the difference are the same as for the virgin loading case.

#### 6.4.3 Monoliths M2, M3, and M5

These monoliths were identical and were cyclically preloaded under essentially the same conditions. Their horizontal displacements under the first lateral load application were almost the same: 0.92 in. for M2, 0.9 in. for M3, and 0.7 in. for M5. During the last cycles of preloading, the respective displacements were 1.07 in., 1.32 in., and 1.05 in. These results are less than the predicted value of 1.66 in. The assumed p-y behavior was too soft. The berm probably also had an influence, as discussed above.

The displacement predictions were made using a semi-empirical method (O'Neill et al 1977) developed for driven piles. The fact that the method overpredicted displacement implies that jetting followed by driving did not reduce lateral soil resistance. This is consistent with the increased soil properties discussed in Section 5.4.3.

Monolith M3 required a larger number of cycles to reach stable cyclic response than M2 or M5. This result may be due in part to the effects of grout pipe installation around and within M3, and difficult reaction rock anchor installation at nearby monolith M5. Repeated air-flushing of the grout holes may have loosened the soil in the general area (Section 5.5.2).

**6.4.4      Monoliths M6 and M7**

Monoliths M6 and M7 were identical and were cyclically preloaded under essentially the same conditions. Their behavior under cyclic preloading was generally comparable, well within expected soil property and structural variability; however, monolith M7 required a larger number of preloading cycles than M6. The reason may be the same as for M3 (Section 6.4.3).

	<u>M1</u>	<u>M2</u>	<u>M3</u>	<u>M5</u>	<u>M6</u>	<u>M7</u>
Observed displacement <sup>(1)</sup> on first application of full lateral load, in.	0.74	0.92	0.90	0.7	0.78	0.66
Predicted displacement <sup>(1)</sup> on first application of full lateral load <sup>(2)</sup> , in.	2.10	1.66	1.66	1.66	-	-
Observed displacement <sup>(1)</sup> at end of cyclic loading with full lateral load, in.	1.26	1.07	1.32	1.05	0.91	0.85
Predicted displacement <sup>(1)</sup> at end of cyclic loading with full lateral load <sup>(2)</sup> , in.	2.10	1.70	1.70	1.7	-	-
Total number of load cycles applied	40	29	47	40	23	47
Residual horizontal displacement after unloading <sup>(4)</sup> , in.	0.53	0.49 <sup>(3)</sup>	0.60	0.45	0.42 <sup>(3)</sup>	0.25

#### Notes

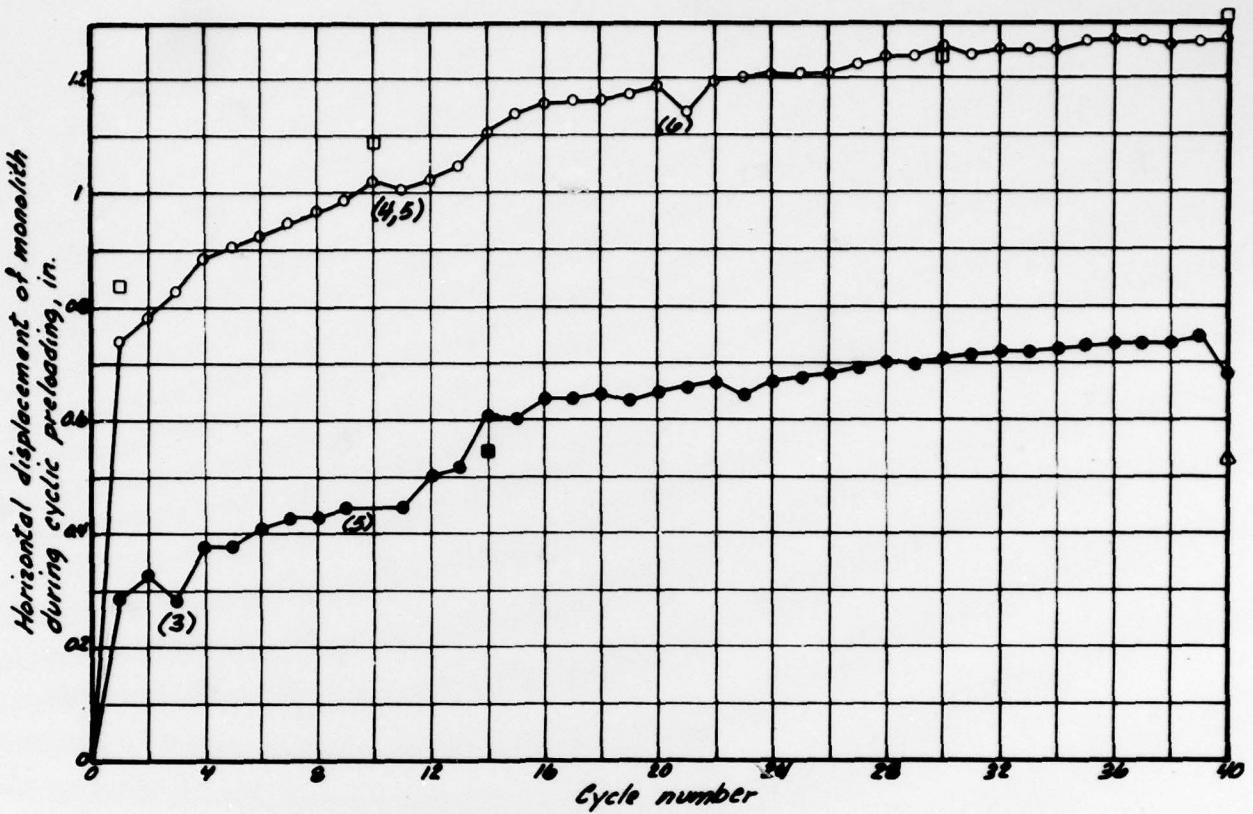
- (1) Horizontal displacement measured at 3 ft above ground surface
- (2) Toe of berm was 5 ft to 8 ft in front of monoliths during preloading; berm height and slope were about 9 ft and 1 on 1, respectively; effect of berm not considered in predictions
- (3) Horizontal displacement measured with V, load only, prior to prototype pile driving
- (4) Monoliths M1, M3, M5, and M7 axially and laterally unloaded; monoliths M2 and M6 only laterally unloaded

**PILE DRIVING EFFECTS TEST PROGRAM**

**SUMMARY OF  
MONOLITH DISPLACEMENT  
DURING PRELOADING**

FOUNDATION INVESTIGATION AND TEST PROGRAM  
EXISTING LOCKS AND DAM NO. 20  
ST LOUIS DISTRICT, CORPS OF ENGINEERS.  
BACW45-70-6-0005

 Woodward-Clyde Consultants VFC626 Page 22	<b>Table 6.1</b>
---	------------------



*Legend*

- Reference point data for lateral load of 72t
- Uncorrected linear potentiometer data for lateral load of 72t
- Reference point data for lateral load of 7.2t
- Uncorrected linear potentiometer data for lateral load of 7.2t
- △ Residual horizontal displacement after complete unloading (axial and lateral) (reference point data)

*Notes:*

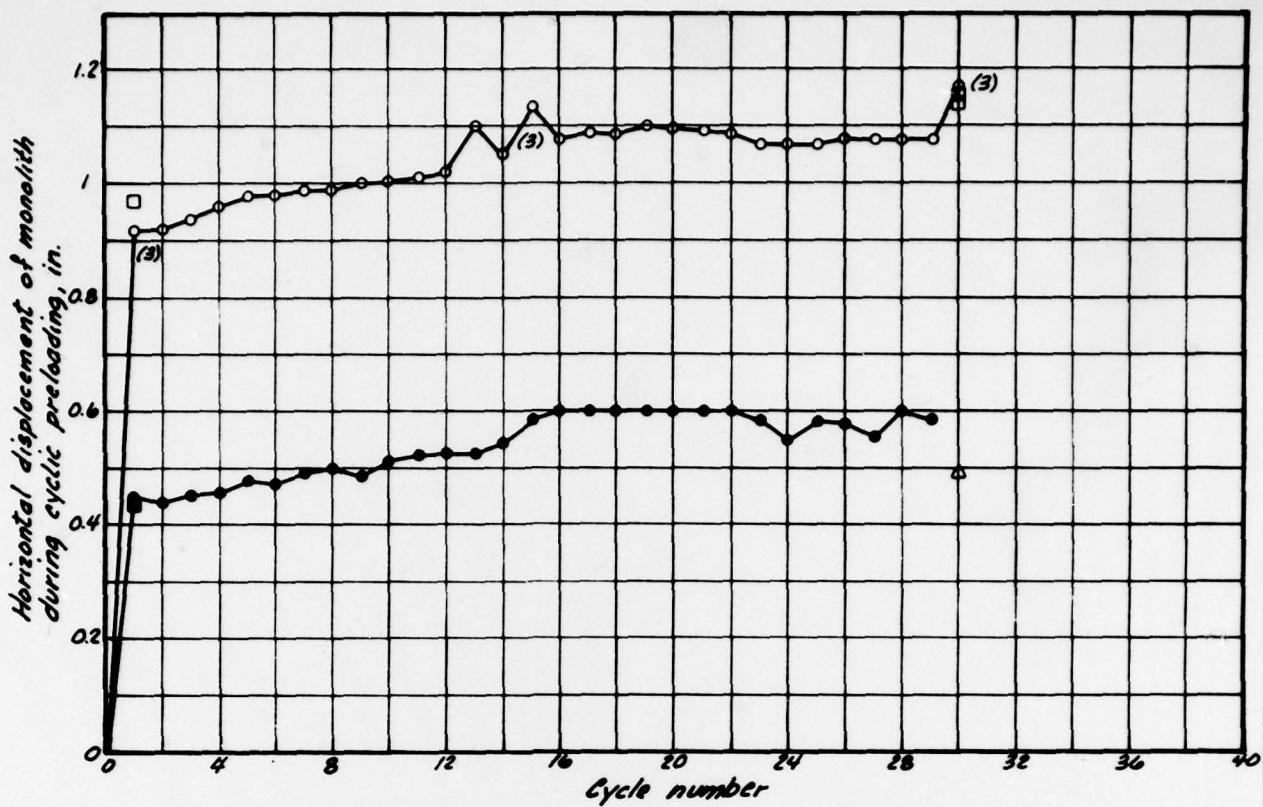
- (1) Axial load during test was 360t
- (2) Maximum and minimum lateral loads were generally maintained for 5 min
- (3) Difficulty with jacking system
- (4) Maximum lateral load was maintained for 3 hr
- (5) At the end of cycle 10, monolith was completely unloaded (axially and laterally)
- (6) Maximum lateral in. = 62t

**PILE DRIVING EFFECTS TEST PROGRAM  
HORIZONTAL DISPLACEMENT  
OF MONOLITH M1  
DURING CYCLIC PRELOADING**

FOUNDATION INVESTIGATION AND TEST PROGRAM  
EXISTING LOCKS AND DAM No. 20  
ST LOUIS DISTRICT, CORPS OF ENGINEERS.  
DACPW43-78-C-0008

Woodward-Clyde Consultants  
Y7C82B Phase II

Fig. 6.1



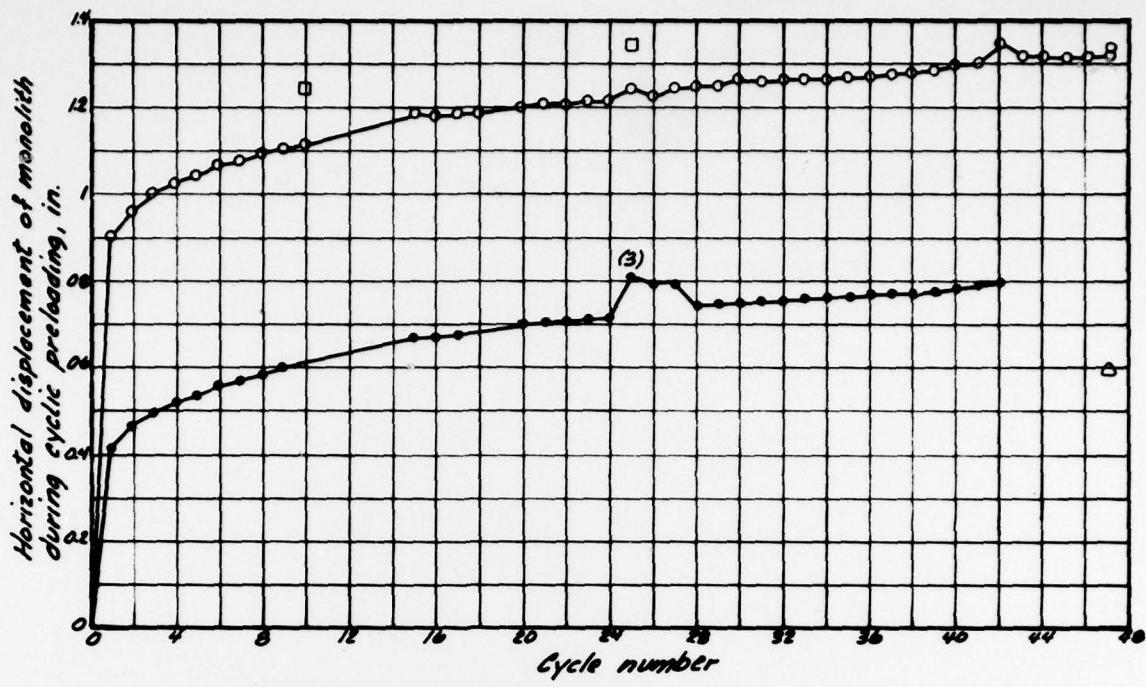
#### Legend

- Reference point data for lateral load of 48t
- Uncorrected linear potentiometer data for lateral load of 48t
- Reference point data for lateral load of 4.8t
- Uncorrected linear potentiometer data for lateral load of 4.8t
- △ Residual horizontal displacement after lateral unloading (under full axial load)  
(corrected linear potentiometer data, prior to prototype pile driving)

#### Notes:

- (1) Axial load during test was 240t
- (2) Maximum and minimum lateral loads were generally maintained for 5 min
- (3) Maximum lateral load was maintained for 6 hr for cycles 1 and 15, for 16 hr for cycle 30

<b>PILE DRIVING EFFECTS TEST PROGRAM</b> <b>HORIZONTAL DISPLACEMENT</b> <b>OF MONOLITH M2</b> <b>DURING CYCLIC PRELOADING</b>	
<small>FOUNDATION INVESTIGATION AND TEST PROGRAM          EXISTING LOCKS AND DAM NO. 20          ST LOUIS DISTRICT, CORPS OF ENGINEERS.          DACW43-78-C-0008</small>	
 Woodward-Clyde Consultants <small>Y7CB25 Phase II</small>	<b>Fig. 6.2</b>



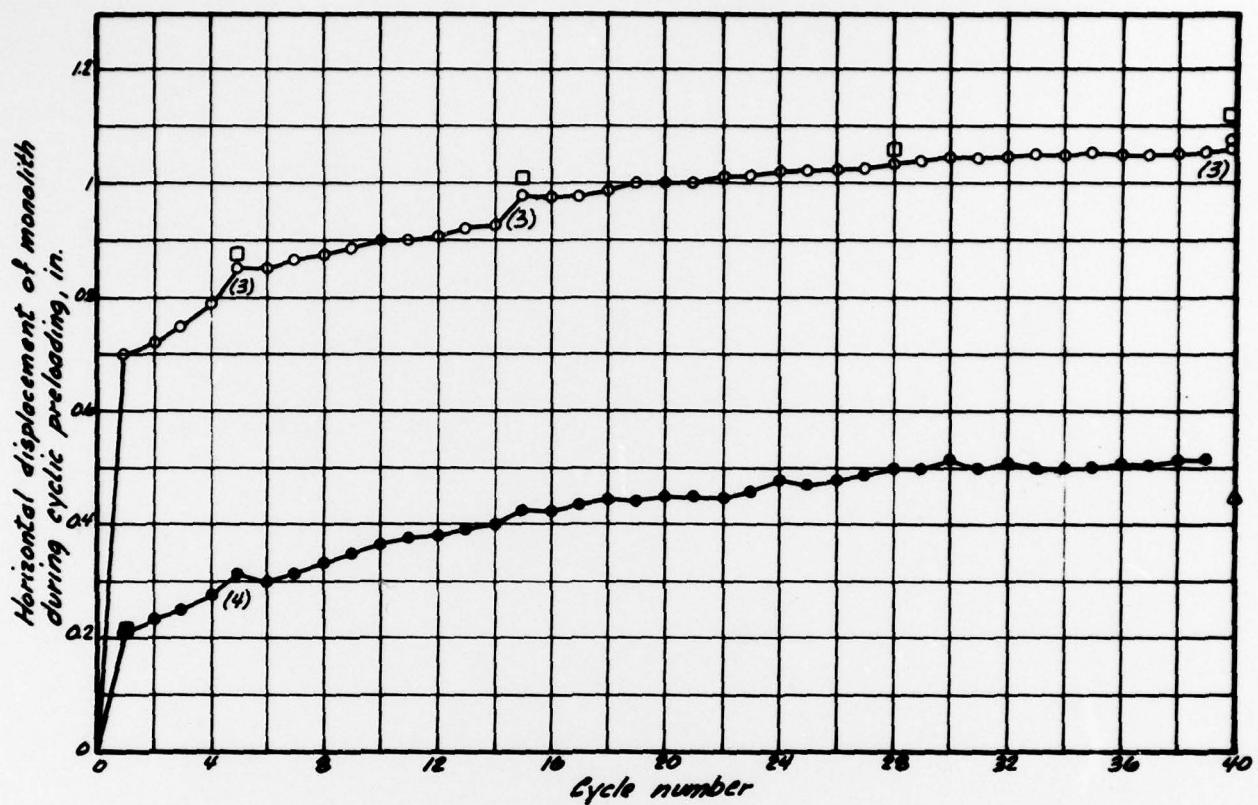
*Legend*

- Reference point data for lateral load of 48t
- Uncorrected linear potentiometer data for lateral load of 48t
- Uncorrected linear potentiometer data for lateral load of 4.8t
- △ Residual horizontal displacement after complete unloading (axial and lateral) (uncorrected linear potentiometer data)

*Notes:*

- (1) Axial load during test was 240t
- (2) Maximum and minimum lateral loads were generally maintained for 5 min
- (3) Load cell difficulties

<b>PILE DRIVING EFFECTS TEST PROGRAM</b> <b>HORIZONTAL DISPLACEMENT</b> <b>OF MONOLITH M3</b> <b>DURING CYCLIC PRELOADING</b>	
<small>FOUNDATION INVESTIGATION AND TEST PROGRAM            EXISTING LOCKS AND DAM NO. 26            ST LOUIS DISTRICT, CORPS OF ENGINEERS.            DACW43-78-C-0008</small>	
 Woodward-Clyde Consultants <small>V7C826 Phase III</small>	<b>Fig. 6.3</b>

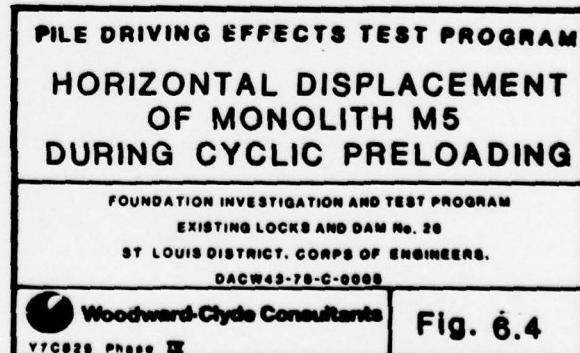


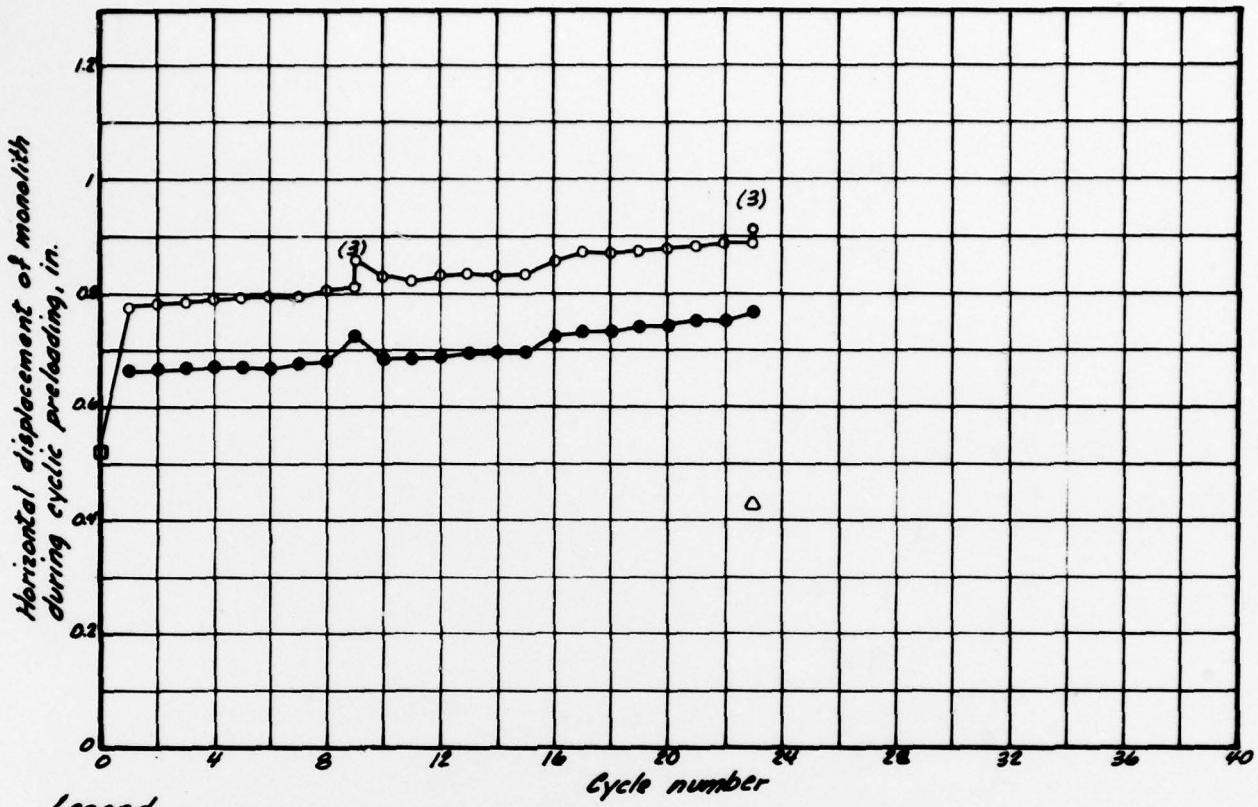
*Legend*

- (1) Reference point data for lateral load of 48t
- (2) Uncorrected linear potentiometer data for lateral load of 48t
- (3) Reference point data for lateral load of 3.5t
- (4) Uncorrected linear potentiometer data for lateral load of 3.5t
- △ Residual horizontal displacement after complete unloading (axial and lateral) (uncorrected linear potentiometer data)

*Notes:*

- (1) Axial load during test was 240t
- (2) Maximum and minimum lateral loads were generally maintained for 5 min
- (3) Maximum lateral load was maintained for 4 hr for cycles 5 and 15, for 6 hr for cycle 40
- (4) Minimum lateral load was maintained for 30 min for cycle 5





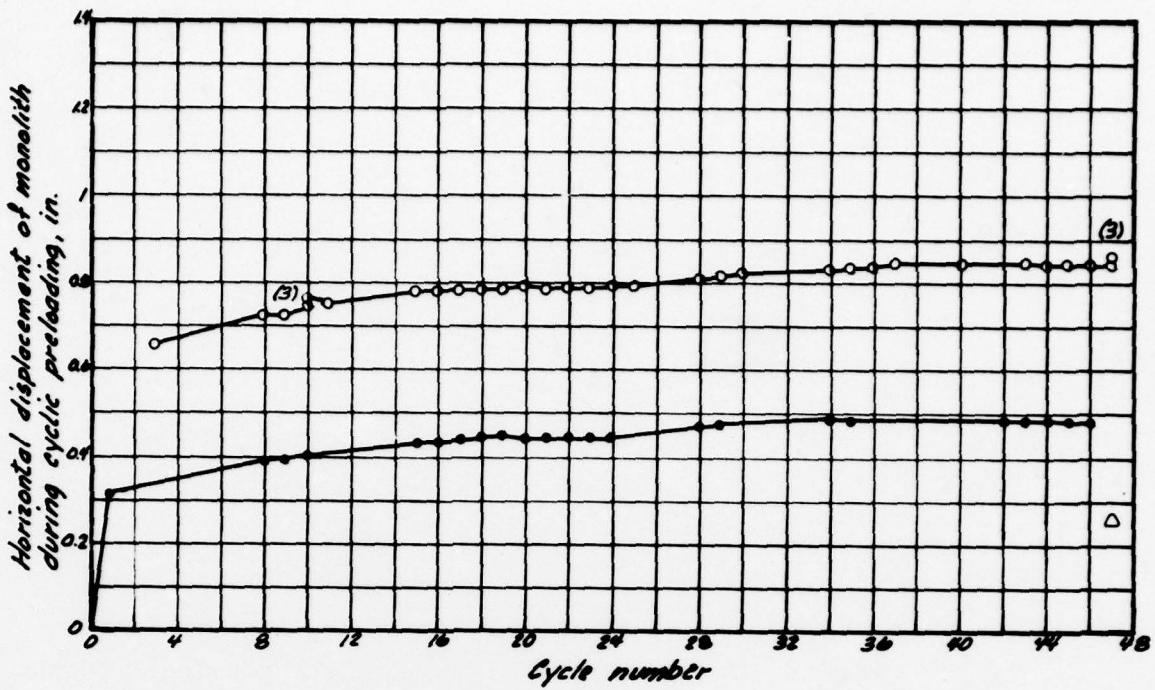
#### Legend

- Horizontal displacement of monolith, prior to cyclic preloading, under axial load only (uncorrected linear potentiometer data)
- △ Residual horizontal displacement after lateral unloading, under full axial load (corrected linear potentiometer data prior to prototype pile driving)
- Uncorrected linear potentiometer data for lateral load of 6t
- Uncorrected linear potentiometer data for lateral load of 0.6t

#### Notes:

- (1) Axial load during test was 30t
- (2) Maximum and minimum lateral loads were generally maintained for 5 min
- (3) Maximum lateral load was maintained for 1 hr for cycle 9 and for 3 hr for cycle 23
- (4) Horizontal displacement of monolith was measured at 33 in. above ground surface.
- (5) Lateral load was applied at 28 in. above ground surface

PILE DRIVING EFFECTS TEST PROGRAM	
HORIZONTAL DISPLACEMENT OF MONOLITH M6 DURING CYCLIC PRELOADING	
FOUNDATION INVESTIGATION AND TEST PROGRAM EXISTING LOCKS AND DAM NO. 26 ST LOUIS DISTRICT, CORPS OF ENGINEERS. DACPW43-78-C-0008	
Woodward-Clyde Consultants VTC020 Phase IX	Fig. 6.5



*Legend*

- Uncorrected linear potentiometer data for lateral load of 1.6t
- Uncorrected linear potentiometer data for lateral load of 0.6t
- △ Residual horizontal displacement after complete unloading (axial and lateral)  
(uncorrected linear potentiometer data)

*Notes:*

- (1) Axial load during test was 30t
- (2) Maximum and minimum lateral loads were generally maintained for 5 min
- (3) Maximum lateral load was maintained for several hours for cycles 10 and 47
- (4) Horizontal displacement of monolith was measured at 31 in. above ground surface
- (5) Lateral load was applied at 37.5 in. above ground surface

<b>PILE DRIVING EFFECTS TEST PROGRAM</b> <b>HORIZONTAL DISPLACEMENT</b> <b>OF MONOLITH M7</b> <b>DURING CYCLIC PRELOADING</b>	
FOUNDATION INVESTIGATION AND TEST PROGRAM EXISTING LOCKS AND DAM NO. 20 ST LOUIS DISTRICT, CORPS OF ENGINEERS. DACW43-78-C-0005	
 Woodward-Clyde Consultants V7C025 Phase II	<b>Fig. 6.6</b>

**PHASE IV REPORT**

**VOLUME III**

**RESULTS AND INTERPRETATION OF  
PILE DRIVING EFFECTS TEST PROGRAM**

**SECTION 7  
PILE DRIVING EFFECTS TESTING**

## 7 PILE DRIVING EFFECTS TESTING

### 7.1 SCOPE OF TESTS

The objectives of the prototype pile driving effects phase of the tests were to examine the factors affecting the response of axially and laterally loaded test monoliths to nearby prototype pile driving operations. The test variables were selected such that monolith M2 represented a reference case on which to base the comparisons discussed in Section 2.2.2.

The great majority of the prototype piles were HP 14 x 73 driven using a Vulcan 010 single-acting, air hammer. This pile-hammer combination was referred to as the primary driving system. A few secondary piles (pipe piles PP 14 x 0.375 and sheet piles MP 102) and two secondary hammers (MKT DE 70B single-acting, diesel and Foster 4000 vibratory) were used as secondary driving systems, for comparison with the primary system.

The six test monoliths (M1, M2, M3, M5, M6, and M7) were successively tested. Only the monolith or monoliths being tested were loaded when prototype piles were driven. The others were unloaded to minimize the effects of pile driving. Pile driving effects testing generally followed cyclic preloading to minimize setup delays. This was not done for monoliths M3 and M7. The soil surrounding these two monoliths was grouted after they were cyclically preloaded. The reaction frames were dismantled at the end of preloading and reinstalled later for the pile driving effects and load testing phases which took place after completion of grouting.

### 7.2 TEST PROCEDURES

#### 7.2.1 General

General test procedures had been established at the design stage and were essentially followed in the field. As was done for the cyclic preloading phase (Section 6), detailed procedures, measurement techniques, and instrumentation reading frequency and schedule were developed during pile driving effects testing of monolith M1. Actual field procedures remained consistent with the objectives of the tests and with the priority ranking of significant aspects of performance established in Section 2.3.1. Deviations from initial procedures generally resulted from unexpected performance or from weather-induced difficulties, as discussed below.

**Reference System.** Frequent checking of the position of the reference beams became necessary and measurements were made more often when it became apparent, early in monolith M1 testing, that the reference beam supports were moving under the effects of pile driving and resulting timber pile deflection. Frequent optical surveys of the reference beams were incorporated to the routine test procedures to correct displacement data obtained by the automatic data

acquisition system (linear potentiometers) and quickly calculate actual monolith displacement values needed to select the next test stage.

**Weather-Induced Difficulties.** The cold weather which was experienced during the test program resulted in various difficulties. The following example illustrates how an adjustment made to accommodate one constraint introduced other difficulties. Heating the instrumentation (linear potentiometers and dial gages) and ground surface beneath and surrounding the test monoliths became necessary when subfreezing (and often subzero) temperatures were experienced. The heat, in turn, produced temperature fluctuations in upper strain gage levels mounted on the timber piles and in the reference beams. The heat waves distorted the optical line of sight and reduced the accuracy of monolith and reference beam displacement measurements using the theodolite.

Another example is the manner by which loads were maintained and adjusted. The large changes in temperature often resulted in slight jack overloads of approximately 10 percent or less. Sluggish response of the jacks caused by extreme cold did not permit an immediate correction of the overloads. The overloads usually produced small increases in monolith displacement, typically of as much as 0.01 in. to 0.02 in. As discussed later in this section, this amount of displacement is of the same order as that observed during pile driving at a distance of 50 ft or more from the monolith.

**Test Area Configuration.** The additional 4-ft-deep excavation required for the monolith trench (Section 5.2.2) resulted in a considerable berm approximately 8 ft from the north edge of the monoliths. The berm was approximately 9 ft to 10 ft high and was at a slope of 1 to 1 or steeper. A brief analysis indicated that the presence of the berm would reduce the magnitude of monolith displacement by about 20 percent. As a result, prior to pile driving effects testing of all monoliths after M1, the berm was excavated such that its toe was at least 25 ft away from the monoliths. The berm excavation was done only after cyclic preloading of each monolith to replicate the conditions under which monolith M1 was preconditioned.

## 7.2.2 Test Setup and Instrumentation

**Test Monoliths.** The monoliths were tested individually (M1 and M5) or in pairs (M2 and M6, M3 and M7). Only the monolith(s) being tested were loaded. The loading scheme is described in Section 5.3. The instrumentation described in Sections 3.1.2 and 3.1.5 was utilized during the tests, consistent with the measurement priorities established in Section 3.5.

**Soil Mass.** The instrumentation described in Sections 3.1.4 and 3.1.6 was utilized during the tests.

**Prototype Piles.** Prototype steel piles were generally driven to refusal (120 blow/ft) at approximately a tip elevation of 295. They consisted of 50-ft to 55-ft-long steel sections spliced by butt-welding. A few piles were driven as single

55-ft sections. In all, 42 prototype piles were driven using a Vulcan 010 single-acting, air hammer (31 HP 14 x 73 H piles and 3 PP 14 x 0.375 pipe piles), an MKT DE 70B single-acting, diesel hammer (3 HP 14 x 73 and 1 PP 14 x 0.375), and a Foster 4000 vibratory hammer (2 HP 14 x 73 and 2 MP 102 sheet piles). Pertinent information regarding the three types of piles and the three types of hammers are given in Table 7.1. All the prototype piles driven with the Vulcan and MKT hammers were installed with swinging leads freely suspended on a crane line. Driving operations were frequently halted to permit monolith and ground instrumentation measurements.

Throughout prototype pile driving operations, measurements were made. Complete blowcount measurements were supplemented with dynamic measurements of force and acceleration at the pile butt. Dynamic measurements were recorded on analog magnetic tape and simultaneously processed using a pile driving analyzer system (Section 3.2.8). The analyzer system provided a direct output of two parameters: maximum transferred energy  $E_{max}$  and maximum compression force at the pile butt  $F_{max}$ . The energy was computed by the analyzer by integration as a function of time of the product force times velocity. The maximum compression force  $F_{max}$  was obtained using strain transducers. The velocity was obtained by integration of accelerometer measurements.

### 7.2.3 Sequence of Operations

The general sequence of operations is given below; minor variations did occur. The notation P indicates a primary measurement, S indicates a secondary measurement, and the measurement number, for example P(1,2), refers to measurement number in Table 3.1.

- (1) Make initial static primary and secondary measurements (zero readings);
- (2) apply first axial load, then lateral load and maintain both loads at  $W_1$  or  $W_2$  levels, depending on monolith; make measurements P(1,2) until monolith displacement has stabilized;

On several occasions, interruptions of testing operations required the loads be left unattended for extended periods, such as a two-day holiday. During these periods, the hydraulic lines between the pumps and jacks were closed at the prescribed load level. Usually, the decrease in load was small, rarely exceeding 10 percent of the load in any one jack. Upon resumption of the tests, the jacks were readjusted and resulting monolith displacements were allowed to stabilize before beginning prototype pile driving operations.

- (3) make static primary and secondary measurements after full load application; these measurements constituted the initial readings to which subsequent measurements of pile driving effects were compared;

- (4) drive a prototype pile using the primary driving system, beginning at a distance of 200 ft for monolith M1, 50 ft for monoliths M2/M6, and 40 ft for monoliths M3/M7 and M5; during pile driving, make dynamic measurements P(3,4,5); stop driving and make static measurements P(1,2) at selected pile penetration intervals (10 ft to 25 ft); adjust applied loads as needed;
- (5) while splicing a prototype pile half-way through driving and upon reaching refusal, make a complete set of primary static measurements P(1,2) and selected secondary static measurements S(9 through 14);

During testing of monolith M2, displacement measurements P(1,2) were also made on unloaded monolith M1; no significant displacement was observed. Monolith M1 settled approximately 0.1 in. and moved laterally less than 0.05 in. The selection of secondary measurements was based on the magnitude of observed monolith displacement. Time-consuming secondary measurements were made only after significant primary measurement changes were detected (for example, pile inclinometers were measured only if incremental displacement exceeded 0.1 in.).

- (6) move pile driver closer to monolith(s) and repeat step (4);

For monolith M1, the first pile was driven at a distance of 200 ft from the monolith; the next piles were driven at 150 ft, 125 ft, 75 ft, and 50 ft, repeating steps (4) and (5). The objective of this procedure was to define the distance at which the gross monolith displacement would begin to increase at a faster rate. Such increase was observed at a distance of 30 ft for monolith M1. A second pile was driven at 30 ft to assess the trend of incremental monolith displacement per pile. For the remainder of monolith M1 testing and for all subsequent monoliths, the distance at which several piles were successively driven to assess the displacement trend was 20 ft.

- (7) continue driving piles at closer distances from the monoliths, repeating steps (4) and (5).

For monoliths M1, M2, and M3, the secondary pile driving systems were used after completion of testing with the primary pile driving system.

### 7.3 TEST RESULTS

#### 7.3.1 General

Plan and elevation views of each pile driving effects series for monoliths M1, M2/M6, M3/M7, and M5 are shown in Fig. 7.1 through 7.4, respectively. Also summarized on these figures are the location and type of prototype piles driven, location of geophones, and the type of hammer used.

The observations reported in this section characterize the different components of an extremely complex interaction problem. The results form the data base from which the influence of various test variables (grouted vs ungrouted soil, high-level vs low-level load, single pile vs group, 2 x 4-pile group vs 3 x 4-pile group, and primary vs secondary pile driving systems) can be examined. As stated previously, monolith M2 constituted a reference case to which other monoliths were compared. More detailed considerations of both primary and secondary aspects of performance for monolith M2 are given in Section 9.

#### 7.3.2 Prototype Pile Driving

**General.** A summary of available dynamic prototype pile driving measurement data is shown in Table 7.2. Difficulties with field handling of the pile driving analyzer transducers and connectors (Section 3.2.8) limited the amount of data collected; however, sufficient data were obtained to make pertinent observations. Complete driving records of all prototype piles driven with impact hammers are included in Appendices L through P, Volume IIIA.

Blowcount vs pile tip elevation are shown in Fig. 7.5 through 7.8 for monoliths M1, M2/M6, M3/M7, and M5, respectively. Blowcount increased slowly from ground surface to approximately el 310. Below el 310, blowcount increased sharply as bedrock surface was approached and reached at approximately el 295. A decreasing or constant blowcount trend was noted between el 350 and el 330; this can be explained by the presence of a softer soil stratum generally encountered at these elevations. Blowcount data for the primary pile driving system, shown within the shaded areas, indicates consistent performance.

**Primary Pile Driving System.** Maximum transferred energy  $E_{max}$  and maximum compression force  $F_{max}$  at the pile butt, obtained using the pile driving analyzer system, are shown vs pile tip elevation in Fig. 7.9 through 7.12. Predictions based on wave equation analyses, made assuming an 80 percent hammer efficiency, yielded  $E_{max}$  approximately equal to 23 ft-k and  $F_{max}$  approximately equal to 500 k. Actual measurements show significantly lower values resulting from lower hammer assembly efficiency. Factors tending to decrease the hammer assembly efficiency and, therefore, the maximum force on the pile, included losses due to:

- (1) mechanical deficiencies of the compressor and/or hammer;
- (2) deterioration of the capblock material between ram and pile helmet; and
- (3) misalignment between hammer and pile.

In addition, the discontinuous nature of the pile driving operations in extremely cold weather did not permit the equipment to warm up to normal operating conditions. This is particularly noticeable for the first pile driven at the beginning of a prototype pile driving series (for example, prototype pile 1 at monolith M1; Fig. 7.5 and 7.9).

Several steps were taken to improve the pile driving system performance. The contractor was asked to replace the compressor several times and to maintain both compressor and hammer more frequently. Oak capblocks, used early in the tests, were replaced by Conbest capblocks (an asbestos composite material sold by Connaco Inc, Kansas City, Kansas) for the remaining tests. The improvement was noticeable as shown in Fig. 7.9 and 7.12 for prototype pile 3 at monolith M1 when the capblock was switched from oak to Conbest midway through pile driving during splicing.

The persistently low  $E_{max}$  values, however, were no doubt related to mechanical inefficiencies of the hammer. The Vulcan hammer did not reach its rated speed of 50 blow/min until the pile reached bedrock. Above bedrock, the hammer speed was consistently 42 to 45 blow/min. At shallow pile penetration, the hammer would lift off the pile butt when the air pressure exceeded 90 lb/in<sup>2</sup> at the compressor.

Careful attention to these conditions did, however, produce a remarkably consistent excitation input from the primary pile driving system to all the monoliths; this relatively constant input made comparisons between the different monoliths responses more meaningful.

**Secondary Pile Driving System.** Maximum transferred energy  $E_{max}$  and maximum compression force  $F_{max}$  at the pile butt are shown vs pile tip elevation in Fig. 7.13 for prototype pipe piles 12 (open-ended) and 13 (close-ended). These piles were driven with the Vulcan 010 hammer in front of monolith M1. The combination Vulcan 010-open-ended pipe pile showed little change in blowcount (Fig. 7.5) from the primary pile driving system, although  $E_{max}$  and  $F_{max}$  were somewhat lower for the secondary system (Fig. 7.13). The close-ended pipe pile drove somewhat harder than the open-ended pile at shallow depth and again below el 310, due to point displacement. The observed increase in  $F_{max}$  coincident with the decrease in  $E_{max}$  for the close-ended pipe pile cannot be explained at this time.

$E_{max}$  and  $F_{max}$  are also shown vs pile tip elevation in Fig. 7.14 for instrumented prototype piles 13 (H pile) and 14 (pipe pile). These piles were driven with the MKT diesel hammer in front of monoliths M2 and M6. The relatively large blowcount required to drive these two piles may be explained by two factors:

- (1) diesel hammers do not operate efficiently under easy driving conditions, as was the case above el 310 at the test site; the hammer stroke increases with increasing pile penetration resistance, as demonstrated by the trend of measured forces in Fig. 7.14; and

- (2) the hammer behaved somewhat erratically during testing due to warm-up and fuel pump difficulties; this is also clearly demonstrated in Fig. 7.14.

The performance of the Foster 4000 vibratory hammer in driving two H piles (prototype piles 9 and 10) and two sheet piles (prototype piles 11 and 12) in front of monoliths M2 and M6 is illustrated in Fig. 7.15. The cumulative time duration of driving is plotted vs pile tip elevation. These data were affected by the operator's procedure, which actually controlled the rate of pile penetration.

**Pile Driving Through Grouted Soil** Prototype piles 7 (instrumented H pile T5) and 8 (instrumented pipe pile T6) were driven through grouted soil in front of monolith M3. The pile driving blowcount records for these piles are shown in Fig. 7.7, along with the range of blowcounts obtained for prototype piles 1 through 6 driven through ungrouted soil. Pile driving resistance through grouted soil penetration was larger (4 to 15 blow/ft) than through ungrouted soil (2 to 10 blow/ft), with the largest increase corresponding to the open-ended pipe pile. These results are consistent with the increase in dynamic and static cone penetration resistance measured during in situ testing in the grouted soil (Section 5.4.5).

### 7.3.3 Ground Vibration

**General** Analysis of pile driving records suggests that, during driving of the prototype piles (Section 7.3.2), only a minor portion of the energy transmitted from the hammer to the pile butt  $E_{max}$  was spent to overcome friction resistance along the pile shaft. The major portion of the energy was required to overcome the soil resistance at the pile tip. The amount of energy which is reflected back from the soil into a pile depends on the relative impedance to motion of the soil and pile driving system (hammer assembly plus pile). During easy driving, that amount is minor. For hard driving, that amount increases. The soil adjacent to the driven piles receives the pile driving energy from the pile and dissipates it by two related mechanisms: (1) permanent soil deformation dissipating energy directly, and (2) elastic vibration dispersing energy into the surrounding soil mass.

Emphasis was placed on examination of peak vectorial particle velocity measured using 3-D geophones (Sections 3.2.1 and 3.2.4) at various locations in the soil mass and on the test monoliths, as a primary index to vibration effects. Peak velocities for pure shear waves are directly proportional to the peak shear strains induced in the soil by propagating shear waves. The prototype pile tips constituted buried point sources acting along vertical axes and, not unlike the shear wave hammer described in Section 3.2.4, the seismic waves they generated are expected to have been predominantly shear waves. Therefore, the history of peak particle velocities recorded by the ground geophones may also represent an approximation of the history of peak shear strains within the soil mass.

Particular attention was given to the peak vectorial particle velocity data obtained from the near-surface geophones installed 1 ft below ground surface,

immediately north of each monolith, adjacent to the timber piles. As shown in Fig. 7.1 through 7.4, these geophones were G3-1, G5-1, G7-1, and G15-1 for monoliths M1, M2, M3, and M5, respectively. These geophone data (near-surface peak velocities) were selected for detailed analysis because they characterize the transient movement of the soil in the zone expected to control the lateral displacement of the monolith caused by prototype pile driving.

**Primary Pile Driving System.** Near-surface peak velocity recorded during prototype pile driving using the primary pile driving system are shown in Fig. 7.16 through 7.19 vs pile tip elevation for monoliths M1, M2, M3, and M5, respectively. The data in these figures is arranged by distances between monolith and prototype piles. When more than one pile was driven at one distance, the data is shown as a range of values.

Three observations can be made on the basis of the data in these figures:

- (1) the magnitude of near-surface peak velocity generally increased with decreasing distance between monolith and prototype pile; this is consistent with the law of geometric or spatial attenuation (Section 2.3.2), although test area geometry and soil stratigraphy complicate the relationship;
- (2) as the distance between prototype pile and monolith increased, the velocity data tended to become more uniform with depth, because the waves were filtered by complicated reflections and refractions, and because the distance from pile tip to geophone did not vary much with pile penetration for large distances;
- (3) the data obtained from various piles driven at the same distance are very consistent, corroborating the consistency observed in prototype pile driving measurements (Section 7.3.2) and monolith displacement measurements (Section 7.3.4).

**Influence of Pile Tip Elevation.** A closer examination of the near-surface peak velocity data in Fig. 7.16 through 7.19 suggests three discernible pile tip elevation ranges worthy of further comment. The following discussion refers principally to results obtained from prototype piles driven 20 ft from the monoliths (shaded areas in the figures).

- (1) At shallow pile tip elevation (approximately el 391 to el 375), the near-surface peak velocities were generally larger than at lower elevations. This was probably caused by surface waves propagating from the shallow point source (pile tip). The point source is closer at shallow depth and these waves decay less with distance than body waves.
- (2) for pile tip elevation between el 375 and el 310, approximately the near-surface peak velocity remained relatively constant, in spite of increasing distance between pile tip and geophone. The small increase in blowcount (Fig. 7.5 through 7.8) experienced within that elevation range probably contributed to offset the attenuation caused by increasing

distance. Further discussion of these effects is provided in Section 9.3 in regard to the detailed evaluation of monolith M2 behavior;

- (3) for pile tip elevation approximately below el 310, the near-surface peak velocities decreased, although the blowcount (Fig. 7.5 through 7.8) increased sharply. An explanation of this phenomenon may be that the energy emanating from the pile tip produced elastic waves which propagated primarily through the stiff, deeper soil and underlying bedrock, minimizing the upward propagating body waves which dominated at shallower depth in less stiff soil. Some reflection of the driving energy from the soil back into the pile may have contributed also to the observed peak velocity decrease.

The peak velocity decrease at depth is a particularly important observation. Previous investigations (Section 2.3.2) have related peak velocity and blowcount. The results obtained here indicate that, within the soil mass, where body waves predominate, the trend of blowcount and peak velocity were similar (an increase in blowcount corresponds to an increase in peak velocity and vice versa). This trend was reversed when the pile tip approached a stiff bearing stratum.

**Cumulative Effects of Vibration.** The deformations of granular soil under cyclic loading are related to both maximum strain level and number of strain cycles (strain history). It appears desirable to consider the cumulative effects of pile driving vibrations when attempting to quantify the relative intensity of a given pile driving episode. One way of characterizing the cumulative vibration effects is to calculate the product of peak vectorial velocity observed during each unit length of pile penetration times the blowcount (number of hammer blows per unit length), and accumulate the sum of these products with increasing depth. This was done to obtain Fig. 7.20(a) through (d) for the respective monoliths. The trend of the product velocity times blowcount is very similar for prototype piles driven 40 ft to 15 ft from the monoliths. Results from prototype piles driven at 50 ft (monolith M2) and 8 ft (monolith M1) deviate from the others. This approach is discussed further in Section 9.3 in regard to the detailed evaluation of monolith M2 performance.

**Secondary Pile Driving Systems.** Near-surface peak velocity vs pile tip elevation is shown in Fig. 7.21 for prototype piles 11 (H pile), 12 (open-ended pipe), and 13 (close-ended pipe) driven with the Vulcan 010 hammer 7 ft to 8 ft away from monolith M1. The close-ended pipe pile 13 generated large peak velocities for the first 40 ft of penetration. This was to be expected with a point-displacement pile. The decrease in peak velocity associated with pile 13 below el 360 can be explained by the presence of a softer soil stratum generally encountered at this elevation. Below el 350, the effects of pile 13 are more difficult to explain on the basis of peak vectorial particle velocities alone. A complete study would involve examination of components of the vectorial velocity, similar to what has been done for monolith M2 in Section 9; this study has not been attempted for M1.

The velocities induced by open-ended pipe pile 12 closely matched those induced by H pile 11 driven at similar distance from the monolith, for the first 60 ft of penetration. Below el 330, the open-ended pipe pile induced larger peak velocity than the H pile. This phenomenon was not explained.

Near-surface peak velocity vs pile tip elevation is shown in Fig. 7.22 for prototype piles driven with the Foster 4000 vibratory hammer in front of monolith M2. Prototype piles 9 and 10 were H piles; prototype piles 11 and 12 were MP 102 flat-web sheet piles. When the pile tips were above el 370, results from H pile 10 agree reasonably well with results from the two sheet piles driven at the same distance of 15 ft from the monolith. Below el 370, the two H piles produced similar peak velocities, although H pile 9 was 21 ft from the monolith; the two sheet piles produced considerably larger velocities. One proposed explanation is that these larger velocities were the results of more intense surface waves induced by eccentric driving on the extremely flexible sheet piles. The sheet piles were driven with the webs oriented east-west, normal to the monolith load application direction.

Near-surface peak velocity vs pile tip elevation is shown in Fig. 7.23 for prototype piles 7, 8, 13, and 14 driven in front of monolith M2. Prototype piles 7, 8, and 13 were H piles; prototype pile 14 was an open-ended pipe pile. All were driven using the MKT diesel hammer. Prototype piles 13 and 14 were instrumented piles (referred to as T3 and T4 in Section 10) and therefore were somewhat stiffer than uninstrumented piles due to additional steel used to protect the instrumentation. The velocity data for these piles fall within a relatively narrow band.

Near-surface peak velocity vs pile tip elevation is shown in Fig. 7.24 for prototype piles 7 and 8 driven approximately 5 ft from monolith M3 using the Vulcan 010 air hammer. These piles were instrumented and are referred to as T5 and T6 in Section 10. The piles were driven through grouted soil. H pile 7 (T5) induced large peak velocities (up to 1.8 in./s) as it was driven through the grouted soil which theoretically extended to el 371. In fact, the peak velocity remained large down to el 360. These results should be compared to those obtained with prototype H pile 11 at monolith M1 (Fig. 7.21) driven through ungrouted soil at a comparable distance. Peak velocities for the latter pile were about half of the values induced by pile 7 at M3. Pipe pile 8 (T6) also induced large peak velocities (up to 1.5 in./s) as it was driven open-ended through the grouted soil. These values are about 50 percent larger than those induced by open-ended pipe pile 12 driven through ungrouted soil 7 ft from monolith M1. The relative increase in velocity for pipe pile 8 relative to H pile 7 at monolith M3 was not observed at M1. This could be due, in part, to formation of a soil plug at the bottom of the pipe pile as it was driven through the 20 ft of grouted soil (Section 10.2.2).

#### 7.3.4 Monolith Displacements

**General.** Gross monolith displacements constituted the primary aspect of performance of highest priority for the pile driving effects tests. The cumulative displacements of a monolith during prototype pile driving refers to total displacements with respect to position of the monolith at the beginning of pile

driving and after application of the full lateral and axial loads prescribed for that monolith ( $W_1$  or  $W_2$ ). Unless otherwise stated, the horizontal cumulative displacement is either the arithmetic average of the horizontal displacement values measured by the four corner linear potentiometers corrected for reference beam displacement, or the arithmetic average of the horizontal displacement values measured directly by optical survey of the four corner reference points installed on the monolith. The north-end cumulative settlement of a monolith is either the arithmetic average of the two northern linear potentiometer data corrected for reference beam settlement, or the arithmetic average of the two northern reference point survey data. A similar definition applies to the south-end cumulative settlement of a monolith.

The incremental displacements of a monolith due to the driving of each prototype pile were obtained by subtracting the cumulative displacements at the beginning of the given prototype pile driving from that at the end of driving. Incremental and cumulative displacements of each monolith due to prototype pile driving are summarized in Tables 7.3 through 7.8. These values are based on corrected linear potentiometer data. The displacement monitoring system was redundant. It was used to describe the displacements of relatively rigid concrete monoliths from independent measurements at four corners. A statistical assessment of displacement data scatter was made as described in Appendix R, Volume IIIA. Standard deviations for the displacement data are also shown in Tables 7.3 through 7.8.

#### **Monolith Horizontal Displacement.**

**Cumulative Horizontal Displacement.** The cumulative horizontal displacement of each monolith as a function of the number of prototype piles driven is shown in Fig. 7.25a through 7.30a. The displacement values plotted are both corrected linear potentiometer and reference point data, except for monoliths M6 and M7 (Fig. 7.29a and 7.30a, respectively), which did not have reference points. The numbers along the abscissa in these figures represent the prototype pile numbers, and the abscissa length above each prototype pile number is proportional to the final prototype pile penetration depth (for example, for monolith M1, Fig. 7.25a, pile No. 1 was driven to a final depth of about 50 ft, whereas pile No. 2 was driven to a final depth of about 100 ft; the abscissa length for pile No. 1 is about one-half that for pile No. 2). Tables 7.3 through 7.8 give cumulative horizontal displacement values for all cases.

There is a good agreement between corrected linear potentiometer and reference point data. The slight difference observed during driving of the closest prototype piles can be explained by the rotation of the monoliths. The reference points were installed a few feet above the linear potentiometers. There is evidence that the monoliths tilted northward, inducing a larger apparent horizontal displacement at the reference point level than at the linear potentiometer level. The difference between the two instrumental results increased with monolith tilt. Results from monolith M7 (Fig. 7.30a) were affected by difficulties experienced with tilting and readjustment of the axial jack.

Two observations can be made from Fig. 7.25a through Fig. 7.30a:

- (1) the horizontal displacement increased with the number of prototype piles driven and as the distance between driven prototype pile and monolith decreased; and
- (2) larger horizontal displacements were generally induced by driving the second half of the 100-ft-long prototype piles (from a depth of 50 ft to 100 ft) than the first half (from ground surface to a depth of 50 ft). This observation is consistent with the trend shown by particle velocity data (Section 7.3.3).

*Incremental Horizontal Displacement.* Incremental horizontal displacement of the monoliths due to each prototype pile vs distance between prototype pile and monolith are shown in Fig. 7.31a through 7.36a, for monoliths M1, M2, M3, M6, and M7, respectively. These figures are based on corrected linear potentiometer data for the primary pile driving system. Tables 7.3 through 7.8 give incremental horizontal displacement values for all cases. For monolith M1, M2, M3, and M5 (Fig. 7.31a through 7.34a), standard deviations calculated for the data are also shown. Inasmuch as twice the standard deviation averages 0.05 in., any incremental horizontal displacement less than 0.05 in. should be considered unreliable.

The incremental horizontal displacement data for the 3 x 4- and 2 x 4-pile monoliths (M1, M2, M3, and M5) are combined in Fig. 7.37a. From this figure, it can be concluded that a detectable monolith horizontal displacement occurred when a prototype pile was driven at a distance of 50 ft or less from a monolith. At distances greater than 50 ft, the measured horizontal displacement was less than the accuracy of the measurements.

*Stability of Horizontal Displacement.* Several prototype piles were driven at a distance of 20 ft from each monolith to assess the stability of the monolith horizontal displacement under repeated pile driving at a constant distance. In addition, two piles were driven at 30 ft from monolith M1 and two piles were driven at 15 ft from monolith M5. In all cases of repeated prototype pile driving, the primary pile driving system was used. The data from these repeated driving tests are presented in Fig. 7.38a through 7.45a.

It is apparent in these figures that evaluation of the displacement stability cannot be made if less than three prototype piles were driven at the same distance. For example, for monolith M5, two piles were driven at 15 ft. On the basis of measured displacement (Fig. 7.43a), it would be concluded that monolith M5 showed a stable response because the second prototype pile caused less horizontal displacement than the first. The same conclusion would be drawn on the basis of the response of monolith M2 during driving of the first two piles at 20 ft (Fig. 7.40a). However, the third and fourth prototype piles driven at 20 ft from monolith M2 invalidate this conclusion, as they induced larger displacements than the second piles.

On the basis of the data presented in Fig. 7.38a through 7.45a, it can be concluded that, when as many as four prototype piles were successively driven at the same distance from a given monolith, the horizontal incremental monolith displacement of the monolith due to each pile generally did not show a decreasing trend. It is also clear in these figures that, as stated earlier, larger horizontal displacements were induced during driving of the prototype piles from a depth of 50 ft to 100 ft, than from ground surface to a depth of 50 ft.

#### Monolith Settlement.

**Cumulative Settlement.** The cumulative settlement of the north end (opposite end with respect to lateral load application) and south end of each monolith as a function of the number of prototype piles driven is shown in Fig. 7.25b through 7.30b. These figures are similar to those depicting cumulative horizontal displacement (Fig. 7.25a through 7.30a). Unlike the cumulative horizontal displacement data, there is no geometric reason for the difference between corrected linear potentiometer and reference point settlement data. In this case, the small difference may be explained only by the accuracy of measurements. Results for monoliths M3 (Fig. 7.27b) and M7 (Fig. 7.30b) were affected by difficulties experienced with tilting and readjustment of the axial jacks.

Three observations can be made from Fig. 7.25b through 7.30b:

- (1) the north end of the monoliths settled more than the south end, which was the end on which the lateral load was applied; the cumulative monolith tilt was approximately 0.2 to 0.3 degrees for all monoliths;
- (2) the monolith settlement increased with the number of prototype piles driven and as the distance between driven prototype pile and monolith decreased;
- (3) larger settlements were generally induced by driving the second half of the 100-ft-long prototype piles (from a depth of 50 ft to 100 ft) than the first half (from ground surface to a depth of 50 ft); this trend is especially clear for prototype pile 11 at monolith M1 (Fig. 7.25b), and for prototype pile 9 at monoliths M2 (Fig. 7.26b) and M6 (Fig. 7.29b).

**Incremental Settlement.** Incremental monolith settlement due to driving of each prototype pile vs distance between prototype pile and monolith is shown in Fig. 7.31b through 7.36b, for monoliths M1, M2, M3, M5, M6, and M7, respectively. These figures are similar to those depicting incremental horizontal displacement (Fig. 7.31a through 7.36a). Monolith settlement values for all cases, including data from secondary pile driving systems, are given in Tables 7.3 through 7.8. Standard deviations for the settlement data differ more from monolith to monolith than the standard deviations calculated for horizontal displacement data.

The incremental settlement data for the 3 x 4- and 2 x 4-pile monoliths (M1, M2, M3, and M5) are combined in Fig. 7.37b. From this figure, it can be concluded that detectable monolith settlement occurred when a prototype pile was driven at a distance of 50 ft or less from a monolith. At distances greater than 50 ft, the measured settlement was less than the accuracy of the measurements.

**Stability of Settlement.** The data from repeated prototype pile driving at a constant distance are presented in Fig. 7.38b through 7.45b. As was the case with horizontal displacement data, it is impossible to evaluate the settlement stability if less than three prototype piles were driven at the same distance. When as many as four prototype piles were successively driven at the same distance from a given monolith, the incremental settlement of the monolith due to each prototype pile generally did not show a stabilizing trend. In fact, for monoliths M2 and M6 settlement increased progressively when four prototype piles were successively driven 20 ft away (Fig. 7.40b and 7.44b). Monoliths M2 and M6 exhibited unstable behavior with respect to settlement caused by repeated pile driving at a constant distance.

## 7.4 INFLUENCE OF TEST VARIABLES

### 7.4.1 General

The results of the pile driving effects tests were discussed with respect to the primary aspects of performance in the preceding sections. The influence of the test variables (grouted vs ungrouted soil, high load-level vs low load-level, timber pile configuration, and pile driving systems) on observed monolith behavior is reviewed in the following sections. Monolith M2 is used as the reference case on which the comparisons are based. In particular, emphasis is placed on results obtained from prototype piles (H piles) driven using the primary pile driving system at a distance of 20 ft from the monoliths. Test results obtained from prototype piles 2 through 4 driven with the primary pile driving system approximately 20 ft from monolith M2 are referred to as M2 standard case hereafter. A fourth prototype pile (pile 5) was also driven at 20 ft from M2. That pile is not used for comparison purposes because no more than three prototype piles were driven for the other monoliths.

Few piles were driven with the secondary pile driving system and data on which to base comparisons for this variable are limited. Comparison between monolith M1 and other monoliths is complicated by the fact that the berm was left at 8 ft from M1, whereas it was removed to 25 ft from the others, and M1 was surrounded by unloaded timber piles. Additional comparisons and evaluation of test data are provided in Section 9.

### 7.4.2 Influence of Grouting

The influence of grouting is evaluated by comparing test results obtained from prototype piles 3 through 5 (H piles) driven with the primary pile driving system 20 ft from monolith M3 (referred to as M3 grouted case hereafter) with M2 standard results.

**Ground Vibrations.** Near-surface peak vectorial particle velocities recorded at M2 and M3 are shown in Fig. 7.46. The velocity data are from the two near-surface geophones located immediately north of the two monoliths. The velocity range for M3 grouted case is clearly lower than that for M2 standard case. The grouted soil surrounding M3 probably reflected back and filtered incoming vibratory waves, thus reducing observed peak particle velocity. From this results,

it is concluded that grouting significantly reduced near-surface peak particle velocity induced by prototype pile driving.

**Monolith Displacements.** Horizontal displacement and settlement of monoliths M2 and M3 are compared in Fig. 7.47. For the first three prototype H piles driven at both monoliths, the results are similar. Horizontal displacement for M3 grouted case is slightly less than for M2 standard case. The reverse is true for settlement. The apparent discrepancy at the end of the third prototype pile is believed to have been caused by difficulties experienced at that time with surveys, axial jacks, and load cells during testing of M3. From these results, it is concluded that grouting had only a small influence on monolith displacement caused by prototype pile driving.

Grouting under and around monoliths M3 and M7 (Section 5.5) was very difficult due to the lack of confinement (small overburden) and incipient grout travel paths along the jetted timber piles. Grout leakage was generally experienced during grouting. Considering these difficulties, grout coverage beneath monolith M3 was as good as could be attained, but was probably not sufficient to reduce monolith displacements.

#### 7.4.3 Influence of Load Level

The influence of load level is evaluated by comparing test results obtained from prototype piles 3 through 5 (H piles) driven with the primary pile driving system 20 ft from monolith M5 (referred to as M5 low-load case hereafter) with M2 standard results. Monolith M5 was loaded to the  $W_1^1$  load level ( $V_1 = 15$  t/pile;  $H_1 = 4$  t/pile); monolith M2 was loaded to the  $W_2^1$  load level ( $V_2 = 30$  t/pile;  $H_2 = 6$  t/pile).

**Ground Vibrations.** Near-surface peak vectorial particle velocities recorded at M2 and M5 are shown in Fig. 7.48. As expected, the velocity ranges for M2 standard and M5 low-load cases are very similar. The monolith load level did not influence level of ground vibration caused by prototype pile driving.

**Monolith Displacements.** Horizontal displacement and settlement of monoliths M2 and M5 are compared in Fig. 7.49. Horizontal displacement for M5 low-load case was about one-half that for M2 standard case. Settlement for M5 low-load case was slightly smaller than for M2 standard case. From these results, it is concluded that horizontal displacement of the monolith was reduced by about 50 percent, and settlement of the monolith was reduced by about 30 percent when the load level was reduced from 6 t/pile to 4 t/pile laterally, and 30 t/pile to 15 t/pile axially. These results are highly dependent on the marked increase of monolith M2 horizontal displacement during driving of prototype pile 2.

#### 7.4.4 Influence of Timber Pile Configuration

The influence of timber pile configuration is evaluated by comparing monolith M1 (3 x 4-pile configuration and adjacent unloaded timber piles) with monolith M2 (2 x 4-pile configuration), and monolith M6 (single pile) with monolith M2. The first comparison is based on results obtained from prototype piles 8 through 10 driven 20 ft from monolith M1 using the primary pile driving system (referred to as M1 3 x 4 case). The second comparison is based on results obtained from prototype piles 2 through 5 driven 20 ft from monolith M6 also using the

primary pile driving system (referred to as M6 single case). The comparison between M1 3 x 4 and M2 standard cases is complicated by the monolith trench berm configuration discussed in Section 5.2.2 and the surrounding timber piles. The comparison between M6 single and M2 standard cases could be made also for all prototype piles driven because both monoliths were tested simultaneously; the overall comparison will be addressed.

**Ground Vibrations.** Near-surface peak vectorial particle velocity data recorded at M1 and M2 are shown in Fig. 7.50. The velocity range for M1 3 x 4 case is lower than that for M2 standard case, except for the first 10 ft of prototype pile penetration. From these results, it is concluded that the unloaded timber piles adjacent to monolith M1 contributed to reduce the level of vibration; the proximity of the berm probably also contributed to the reduction.

Monoliths M2 and M6 shared the same geophone system during their simultaneous testing. No comparison can be made.

#### Monolith Displacements.

**M1 (3 x 4) vs M2 (2 x 4).** Horizontal displacement and settlement of monoliths M1 and M2 are compared in Fig. 7.51. Horizontal displacement for M1 3 x 4 case was approximately 35 percent lower than that for M2 standard case; most of that difference is attributable to prototype pile 2 at monolith M2. Cumulative settlement after three prototype piles driven at 20 ft was almost identical for both cases; incremental settlement for M1 was larger than that of M2 for the first piles, and smaller for the second piles. From these results, it is concluded that the larger monolith moved less horizontally than the smaller monolith; this is believed to be partly a result of the presence of the monolith trench berm which was closer to M1 (8 ft) than to M2 (25 ft). There was no difference in settlement for the two monoliths.

**M2 (2 x 4) vs M6 (Single).** Horizontal displacement and settlement of monoliths M2 and M6 are compared in Fig. 7.52. Both monoliths moved essentially in unison. This result is somewhat unexpected because:

- (1) timber pile configurations were different (2 x 4 vs single);
- (2) the pile-head for M6 was almost completely free, whereas the pile heads for M2 were essentially fixed;
- (3) the soil stress bulb associated with M6 was much smaller than that associated with M2; and
- (4) the single pile under M6 was much closer to the prototype piles than the average pile under M2; only the north-end piles of M2 were at comparable distance.

From these results, it is concluded that the single timber pile and the 8-pile group were affected to the same extent by nearby prototype pile driving.

#### **7.4.5 Influence of Pile Driving System**

The influence of pile driving system on ground vibrations is discussed in Section 7.3.3. The influence of pile driving system on prototype pile driving behavior is discussed in Section 7.3.2. The influence of pile driving system on displacement of the monoliths is evaluated by comparing results obtained for monoliths M1, M2, and M3. In making these comparisons, it should be noted that the effects of prior prototype pile driving and prior monolith displacements are likely to have had an influence on the results obtained for any given single prototype pile; comparisons based on incremental displacements must be qualitative, because it is not possible to eliminate or account for these prior influences.

Table 7.9 summarizes pertinent data for monoliths M1, M2, and M3. The following observations are made on the basis of the data in Table 7.9.

- (1) Prototype H pile 11 induced a larger horizontal displacement of monolith M1 than any of the two pipe piles driven at similar distance (7 to 8 ft) with the same hammer (Vulcan). The H pile was driven first and at very close distance from the monolith; this fact may account for the difference. The displacement of monolith M1 caused by close-ended pipe pile 13 differ from the trend observed with other piles; it increased linearly with pile penetration. For other piles, the displacement was much larger during prototype pile driving from a depth of 50 ft to 100 ft than from ground surface to 50 ft (Section 7.3.4). The displacement associated with the close-ended pipe pile was larger than that caused by the open-ended pipe pile 12. These differences are attributed to the point-displacement nature of the close-ended pipe pile;
- (2) the diesel hammer-H pile combination induced somewhat smaller horizontal displacement of monolith M2 than the primary system (Vulcan-H pile). The settlement induced by both combinations is very similar;
- (3) the vibratory hammer-H pile combination resulted in much larger displacements of monolith M2 than either Vulcan- or diesel-H pile combinations at 15 ft and especially 20 ft; however, settlement induced at 15 ft by the vibratory hammer-H pile combination was comparable to that induced by the primary pile driving system. The displacements of monolith M2 induced by the vibratory hammer are larger at 20 ft than at 15 ft; this may be explained by the fact that the vibratory hammer was first tried at 20 ft. The monolith may have moved so much under the influence of the hammer at 20 ft, that effects of subsequent use of the equipment were lessened;
- (4) the vibratory hammer-sheet pile combination induced much less displacements of monolith M2 than the vibratory-H pile combination, even when consideration is given to the fact that the sheet piles were driven only to a depth of 50 ft. It is possible that the very large displacements caused by prior H pile driving with the vibratory hammer may have desensitized the monolith to the effects of sheet pile driving. In any case, driving the two sheet piles did produce over 6.04 in. horizontal displacement and 0.05 in. settlement. These values are less, but of the same order of magnitude as values obtained with H piles driven at a distance of 20 ft from the monolith; and

- (5) the instrumented H pile driven with the Vulcan hammer approximately 5 ft from monolith M3 induced less displacements of the monolith than its companion instrumented open-ended pipe pile at the same distance. The H pile was driven first. The comment made in item 1 above regarding the influence of driving sequence of prototype piles 11 and 12 at monolith M1 may also apply here.

### IMPACT HAMMER ASSEMBLY DETAILS

<u>Vulcan 010</u>		<u>MKT DE 70B</u>
<u>Hammer Characteristics</u>		
Hammer type	single-acting, air	single-acting, diesel
Maximum rated energy, ft-lb	32,500	42,000 to 63,000
Rated speed, blow/min	50	40 to 50
Air pressure at hammer, lb/in <sup>2</sup>	105	N/A
Weight of ram, lb	10,000	7,000
<u>Helmet/Capblock</u>		
Weight, lb	1645	unknown
Capblock material	oak <sup>(1)</sup> , conbest <sup>(2)</sup>	oak <sup>(1)</sup>
Capblock thickness, in: oak conbest	2 to 4 in. <sup>(1)</sup> 5 to 6.5 in. <sup>(2)</sup>	2 to 4 in. <sup>(1)</sup>

### VIBRATORY HAMMER DETAILS

Hammer type	Foster 4000 (hydraulic)
Eccentric moment	4000 in.-lb
Frequency range (variable pump speed)	0 to 1400 rpm
Driving force at maximum steady-state frequency	223 k
Driving amplitude range	5/16 to 1-1/4 in.
Suspended weight	18,800 lb

### CHARACTERISTICS OF PROTOTYPE PILES

	<u>H Piles</u>	<u>Pipe Piles</u>	<u>Sheet Piles</u>
Type	HP 14 x 73	PP 14 x 0.375	MP102
Weight, lb/ft	73	54.6	40
Minimum perimeter <sup>(3)</sup> , in.	57	44	N/A
Web thickness, in.	0.506	N/A	0.375
Cross-sectional area <sup>(3)</sup> , in <sup>2</sup>	21.46	16.05	N/A

#### Notes:

- (1) Oak capblock used for all prototype piles at M1 and diesel-driven piles thereafter; compression parallel to the grain
- (2) Conbest discs used for all prototype piles driven with Vulcan 010
- (3) Steel piles used for lateral load testing were instrumented with inclinometers and strain gages, with protective steel covers added to the net pile section. Refer to Section 10 for details

### PILE DRIVING EFFECTS TEST PROGRAM

#### CHARACTERISTICS OF PROTOTYPE PILES AND HAMMERS

FOUNDATION INVESTIGATION AND TEST PROGRAM  
EXISTING LOCKS AND DAM NO. 26  
ST. LOUIS DISTRICT, CORPS OF ENGINEERS.  
DAMW43-78-C-0005

Woodward-Clyde Consultants  
V7CB25 Phase II

Table 7.1

<u>MONOLITH NO.</u>	<u>HAMMER-PILE<sup>(1)</sup> COMBINATION</u>	<u>DATA AVAILABLE FOR PILE NO.</u>	<u>DEPTH RANGE<sup>(2)</sup> FOR WHICH E<sub>max</sub> IS AVAILABLE ft</u>	<u>DEPTH RANGE<sup>(3)</sup> FOR WHICH F<sub>max</sub> IS AVAILABLE ft</u>
M1	1	1	>12	>12
		3	13 to 22 28 to 32 35 to 42 45 to 55 58 to 65 68 to 70 72 to 81 83 to 102	14 to 15 17 to 22 28 to 32 35 to 42 44 to 55 58 to 65 68 to 70 72 to 81 83 to 103
		4	54 to 57 >60	54 to 84
		5	>47	>12
		6	11 to 60 64 to 65 71 to 92	12 to 92 >94
		7	>58	>58
		9	46 to 51 >53	46 to 51 >53
		10	11 to 51 >53	11 to 30 32 to 44 46 to 49 53 to 59 61 to 72 74 to 77 79 to 82 84 to 85 89 to 90 92 to 93 >97
		11	6 to 9 >16	6 to 9 >16
	2	12	7 to 77 >79	>7
	3	13	11 to 51 >54	11 to 51 >54
M2	1	1	>11	>11
		2	>61	>61
		3	57 to 66	57 to 66
	4	7	>62	>62
		8	14 to 47	14 to 47 49 to 80 82 to 90 >94
		13	>8	>8
	5	14	>8	>8
M3	1	5	6 to 12 >16	6 to 12 16 to 62 >64
		6	5 to 48 >53	5 to 37 39 to 48 >53
M5	1	1	none	2 to 47
		2	>54	>54
		7	>53	>53

Notes

- (1) Hammer-pile combinations:
  - 1 = Vulcan 010 - HP 14 x 73
  - 2 = Vulcan 010 - PP 14 x 0.375, open-ended
  - 3 = Vulcan 010 - PP 14 x 0.375, close-ended
  - 4 = MKT DE 70B - HP 14 x 73
  - 5 = MKT DE 70B - PP 14 x 0.375
- (2)  $E_{max}$  = maximum energy transferred at pile butt
- (3)  $F_{max}$  = Maximum compression force at pile butt

**PILE DRIVING EFFECTS TEST PROGRAM**

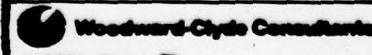
**SUMMARY OF AVAILABLE  
DYNAMIC PILE DRIVING DATA**

FOUNDATION INVESTIGATION AND TEST PROGRAM

EXISTING LOCKS AND DAM NO. 20

ST LOUIS DISTRICT, CORPS OF ENGINEERS.

BACW48-78-C-0006



V7C826 Phase II

**Table 7.2**

Prototype Pile No. <sup>(1)</sup>	Distance From Prototype Pile To Monolith, ft	Horizontal Displacement, in.		Settlement, in. <sup>(2)(3)</sup>	
		Incremental	Cumulative <sup>(2)</sup>	Incremental	Cumulative <sup>(2)(3)</sup>
1	200	0.000	0.000	0.000	0.000
2	150	-0.008	-0.005	-0.014	-0.014
3	125	0.019	0.035	-0.017	0.013
4	75	0.038	0.084	-0.013	0.025
5	50	0.005	0.093	-0.014	0.006
6	30	0.044	0.136	0.043	0.056
7	30	0.065	0.199	0.031	0.102
8	20	0.078	0.280	0.046	0.154
9	20	0.121	0.404	0.031	0.177
10	20	0.054	0.459	0.081	0.256
11	8	0.483	0.968	0.391	0.656
12	7	0.181	1.141	0.280	0.955
13	7	0.357	1.517	0.354	1.329

Standard Deviation

Cumulative Horizontal Displacement	0.015 in.
Incremental Horizontal Displacement	0.022 in.
Cumulative Settlement	0.019 in.
Incremental Settlement	0.026 in.

Notes

- (1) Location and type of prototype pile given in Fig. 7.1
- (2) Cumulative displacement is not exact sum of incremental values because it reflects small displacements occurring between driving of each pile
- (3) Settlement is average of settlements at north and south end of monolith

**PILE DRIVING EFFECTS TEST PROGRAM**

**DISPLACEMENTS OF  
MONOLITH M1 DUE TO  
PROTOTYPE PILE DRIVING**

FOUNDATION INVESTIGATION AND TEST PROGRAM

EXISTING LOCKS AND DAM NO. 26

ST LOUIS DISTRICT, CORPS OF ENGINEERS.

DACW43-78-C-0005

Woodward-Clyde Consultants  
77C826 Phase II

Table 7.3

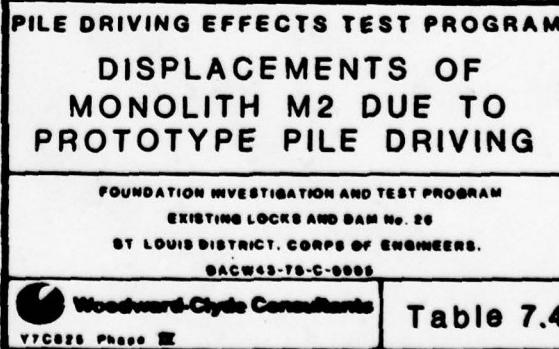
Prototype <sup>(1)</sup> Pile No.	Distance From Prototype Pile To Monolith, ft	Horizontal Displacement, in.		Settlement, in.	
		Incremental	Cumulative <sup>(2)</sup>	Incremental	Cumulative <sup>(2)(3)</sup>
1	50	0.019	0.019	0.033	0.033
2	21	0.153	0.160	0.037	0.085
3	20.6	0.076	0.238	0.050	0.147
4	21.1	0.149	0.387	0.087	0.223
5	20.8	0.159	0.545	0.112	0.338
6	14.8	0.176	0.725	0.115	0.465
7	20.6	0.126	0.850	0.079	0.544
8	14.9	0.139	0.986	0.103	0.644
9	20.6	0.302	1.289	0.215	0.859
10	15.4	0.253	1.543	0.114	0.981
11	15	0.042 <sup>(4)</sup>	1.622 <sup>(4)</sup>	0.050 <sup>(4)</sup>	1.066 <sup>(4)</sup>
12	15				
13	10.4	0.085	1.698	0.007	1.058
14	11.65	0.168	1.870	0.033	1.093

#### Standard Deviation

Cumulative Horizontal Displacement                    0.022 in.  
 Incremental Horizontal Displacement                0.031 in.  
 Cumulative Settlement                                  0.003 in.  
 Incremental Settlement                                0.004 in.

#### Notes

- (1) Location and type of prototype pile given in Fig. 7.2
- (2) Cumulative displacement is not exact sum of incremental values because it reflects small displacements occurring between driving of each pile
- (3) Settlement is average of settlements at north and south ends of monolith
- (4) Total incremental displacement due to driving of both sheet piles



Prototype Pile No. <sup>(1)</sup>	Distance From Prototype Pile To Monolith, ft	Horizontal Displacement, in.		Settlement, in.	
		Incremental	Cumulative <sup>(2)</sup>	Incremental	Cumulative <sup>(2)(3)</sup>
1	40.5	0.155	0.155	0.061	0.061
2	24.3	0.011	0.176	0.043	0.106
3	20	0.136	0.313	0.064	0.171
4	20	0.105	0.421	0.072	0.243
5	20	0.118	0.540	0.040	0.284
6	15	0.166	0.703	0.134	0.418
7	5.5	0.233	0.936	0.111	0.532
8	4.8	0.178	1.118	-0.031	0.558

Standard Deviation

Cumulative Horizontal Displacement	0.020 in.
Incremental Horizontal Displacement	0.028 in.
Cumulative Settlement	0.011 in.
Incremental Settlement	0.015 in.

**PILE DRIVING EFFECTS TEST PROGRAM**

**DISPLACEMENTS OF  
MONOLITH M3 DUE TO  
PROTOTYPE PILE DRIVING**

<small>FOUNDATION INVESTIGATION AND TEST PROGRAM EXISTING LOCKS AND DAM NO. 26 ST LOUIS DISTRICT, CORPS OF ENGINEERS. DAMW43-78-C-0008</small>
 Woodward-Clyde Consultants V7C825 Phase III
<b>Table 7.5</b>

Notes

- (1) Location and type of prototype pile given in Fig. 7.3
- (2) Cumulative displacement is not exact sum of incremental values because it reflects small displacements occurring between driving of each pile
- (3) Settlement is average of settlements at north and south end of monolith

Prototype <sup>(1)</sup> Pile No.	Distance From Prototype Pile To Monolith, ft	Horizontal Displacement, in.		Settlement, in. <sup>(2)(3)</sup>	
		Incremental	Cumulative <sup>(2)</sup>	Incremental	Cumulative
1	39.5	0.030	0.030	0.008	0.008
2	23	0.059	0.094	0.022	0.054
3	19.7	0.061	0.160	0.034	0.069
4	20	0.044	0.202	0.022	0.089
5	20	0.110	0.314	0.057	0.147
6	14.6	0.201	0.516	0.176	0.292
7	14.8	0.155	0.672	0.0	0.386

Standard Deviation

Cumulative Horizontal Displacement	0.014 in.
Incremental Horizontal Displacement	0.020 in.
Cumulative Settlement	0.003 in.
Incremental Settlement	0.003 in.

Notes

- (1) Location and type of prototype pile given in Fig. 7.4
- (2) Cumulative displacement is not exact sum of incremental values because it reflects small displacements occurring between driving of each pile
- (3) Settlement is average of settlements at north and south end of monolith

**PILE DRIVING EFFECTS TEST PROGRAM**

**DISPLACEMENTS OF  
MONOLITH M5 DUE TO  
PROTOTYPE PILE DRIVING**

FOUNDATION INVESTIGATION AND TEST PROGRAM  
EXISTING LOCKS AND DAM NO. 20  
ST. LOUIS DISTRICT, CORPS OF ENGINEERS.  
DAGW43-TB-C-0006

 Woodward-Clyde Consultants  
VTC825 Phase II

Table 7.6

Prototype Pile No. <sup>(1)</sup>	Distance From Prototype Pile To Monolith, ft	Horizontal Displacement, in.		Settlement, in. <sup>(2)</sup>	
		Incremental	Cumulative <sup>(2)</sup>	Incremental	Cumulative <sup>(2)</sup>
1	50	0.062	0.062	0.047	0.047
2	21	0.132	0.194	0.065	0.112
3	20.6	0.101	0.295	0.043	0.155
4	21.1	0.142	0.437	0.140	0.295
5	20.8	0.140	0.577	0.120	0.415
6	14.8	0.223	0.800	0.151	0.566
7	20.6	0.107	0.907	0.092	0.658
8	14.9	0.124	1.031	0.132	0.790
9	20.6	0.318	1.349	0.301	1.091
10	15.4	0.230	1.579	0.162	1.253
11	15	0.067 <sup>(3)</sup>	1.646 <sup>(3)</sup>	0.213 <sup>(3)</sup>	1.466 <sup>(3)</sup>
12	15				
13	10.4	0.154	1.788	0.006	1.384
14	11.65	0.206	1.994	0.095	1.479

Notes

- (1) Location and type of prototype pile given in Fig. 7.2
- (2) Cumulative displacement is not exact sum of incremental values because it reflects small displacements occurring between driving of each pile
- (3) Total incremental displacement due to driving of both sheet piles

**PILE DRIVING EFFECTS TEST PROGRAM**

**DISPLACEMENTS OF  
MONOLITH M6 DUE TO  
PROTOTYPE PILE DRIVING**

FOUNDATION INVESTIGATION AND TEST PROGRAM  
EXISTING LOCKS AND DAM NO. 20  
BY LOUIS DISTRICT, CORPS OF ENGINEERS.  
BACW62-70-C-8005

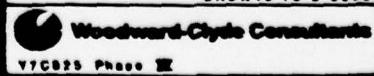


Table 7.7

Prototype <sup>(1)</sup> Pile No.	Distance From Prototype Pile To Monolith, ft	Horizontal Displacement, in.		Settlement, in.	
		Incremental	Cumulative <sup>(2)</sup>	Incremental	Cumulative <sup>(2)</sup>
1	40.5	0.105	0.105	0.003	0.003
2	24.3	0.101	0.206	0.113	0.116
3	20	0.637	0.843	0.267	0.383
4	20	0.140	0.983	0.053	0.436
5	20	0.432	1.415	0.242	0.678
6	15	0.236	1.651	0.113	0.791
7	5.5	0.418	2.069	0.315	1.106
8	4.8	0.263	2.332	0.154	0.952

Notes

- (1) Location and type of prototype pile given in Fig. 7.3
- (2) Cumulative displacement is not exact sum of incremental values because it reflects small displacements occurring between driving of each pile
- (3) Total incremental displacement due to driving of both sheet piles

PILE DRIVING EFFECTS TEST PROGRAM	
DISPLACEMENTS OF MONOLITH M7 DUE TO PROTOTYPE PILE DRIVING	
FOUNDATION INVESTIGATION AND TEST PROGRAM EXISTING LOCKS AND DAM NO. 26 ST LOUIS DISTRICT, CORPS OF ENGINEERS. BACW48-78-C-0005	
 Woodward-Clyde Consultants V7C025 Phase II	Table 7.8

MONOLITH NO.	PROTOTYPE PILE NO.	DISTANCE ft	INCREMENTAL DISPLACEMENT in.		HAMMER-PILE COMBINATION
			HORIZONTAL	VERTICAL (SETTLEMENT)	
M1	11	7-8	0.483	-0.391	Vulcan - H Pile
M1	12	7-8	0.181	-0.281	Vulcan - Open-Ended Pipe Pile
M1	13	7-8	0.354	-0.354	Vulcan - Close-Ended Pipe Pile
M2	2, 3, 4, 5 average	20	0.134	-0.071	Vulcan - H Pile
M2	7	20	0.126	-0.079	MKT - H Pile
M2	9	20	0.302	-0.215	Vibratory - H Pile
M2	6	15	0.176	-0.115	Vulcan - H Pile
M2	8	15	0.139	-0.103	Diesel - H Pile
M2	10	15	0.253	-0.114	Vibratory - H Pile
M2	11, 12 average	15	0.021	-0.025	Vibratory - Sheet Pile
M3	7	5	0.233	-0.110	Vulcan - Instrumented H Pile
M3	8	5	0.178	-0.031	Vulcan - Instrumented Open-Ended Pipe Pile

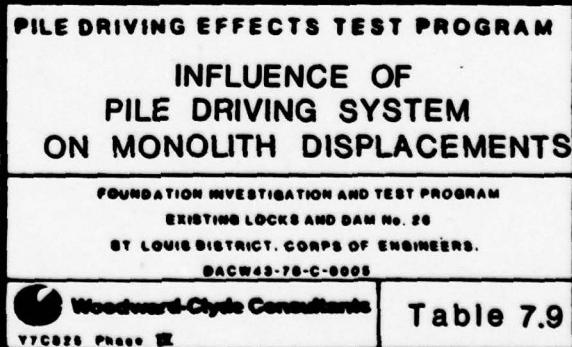
Notes

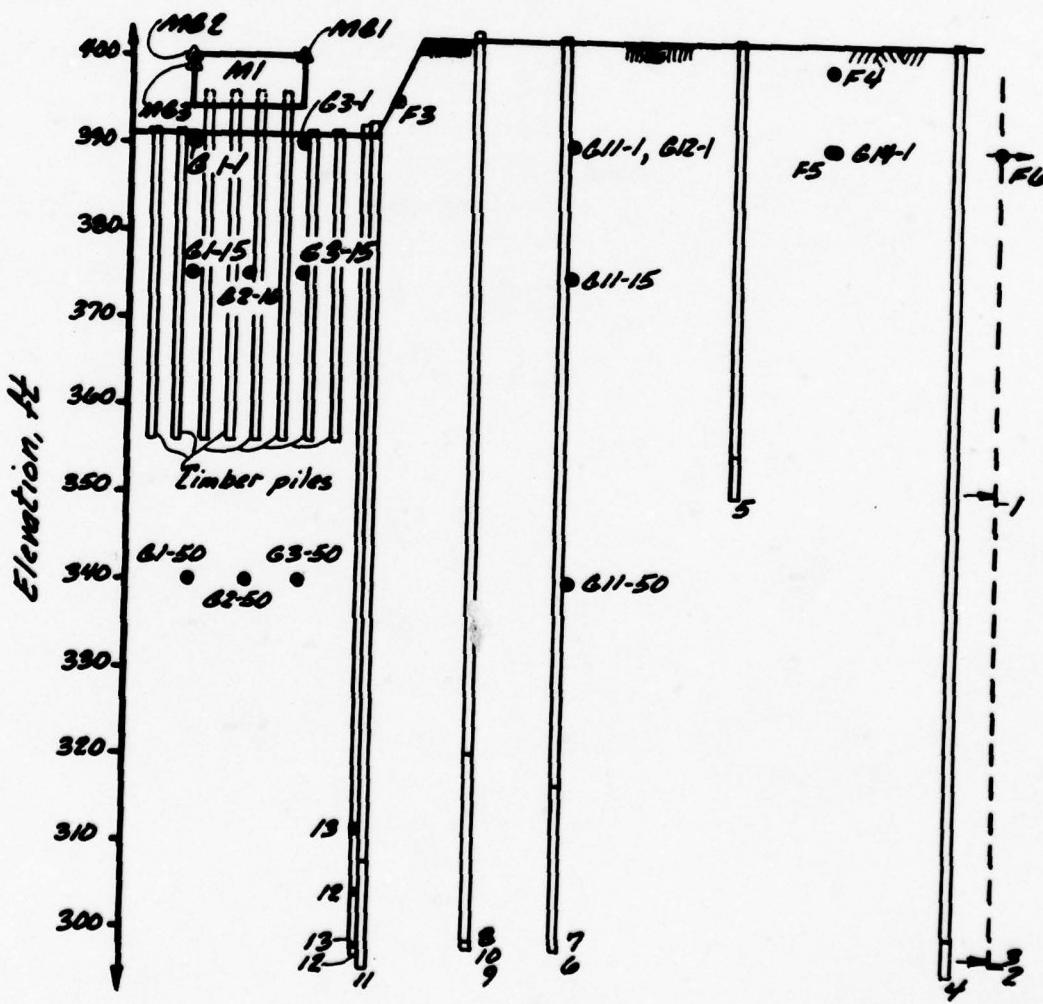
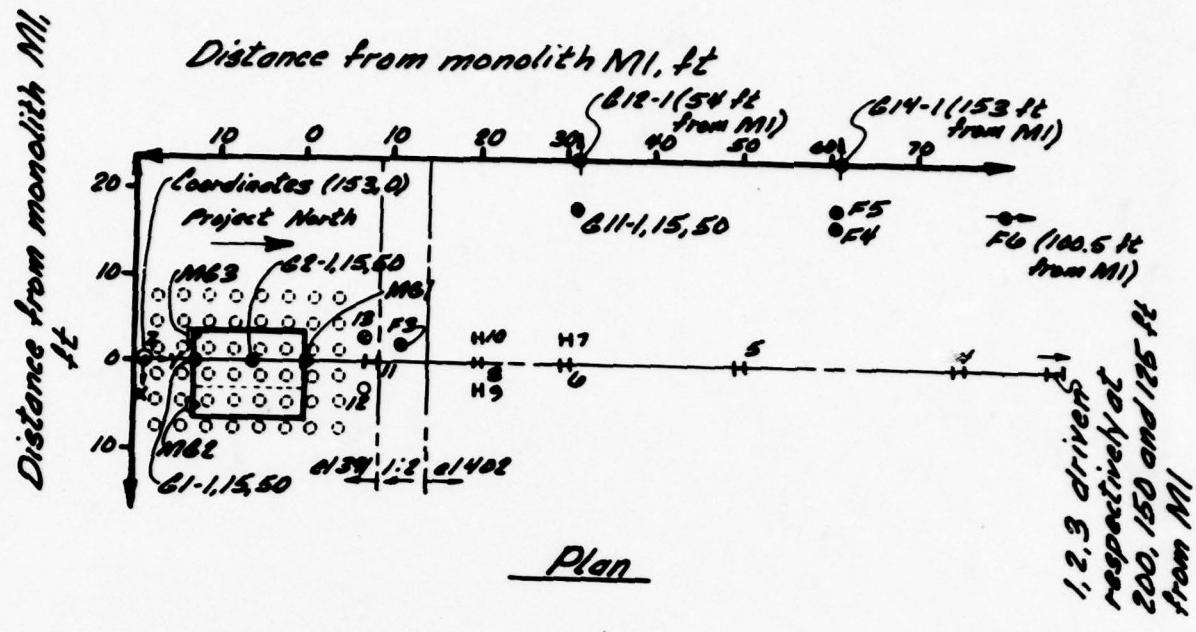
Hammers:

Vulcan: Vulcan 010 single-acting air hammer  
 MKT: MKT DE 70B single-acting diesel hammer  
 Vibratory: Foster 4000 Vibratory hammer

Prototype Piles:

H Pile: HP 14 x 73, 100 ft long  
 Pipe Pile: PP 14 x 0.375, 100 ft long  
 Instrumented H Pile: HP 14 x 73 with instrumentation protection, 55 ft long  
 Instrumented Pipe Pile: PP 14 x 0.375 with instrumentation protection, 55 ft long  
 Sheet Pile: MP 102, 50 ft long



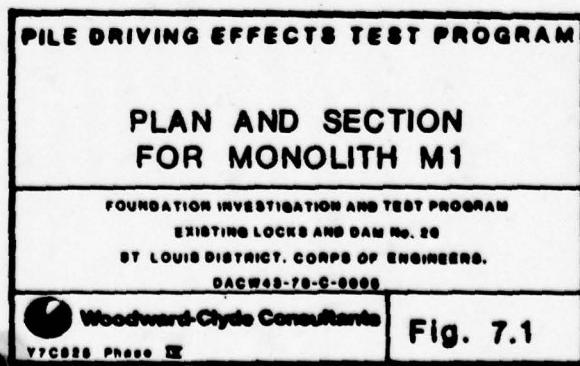


Leg  
•  
△  
○  
H  
○  
●

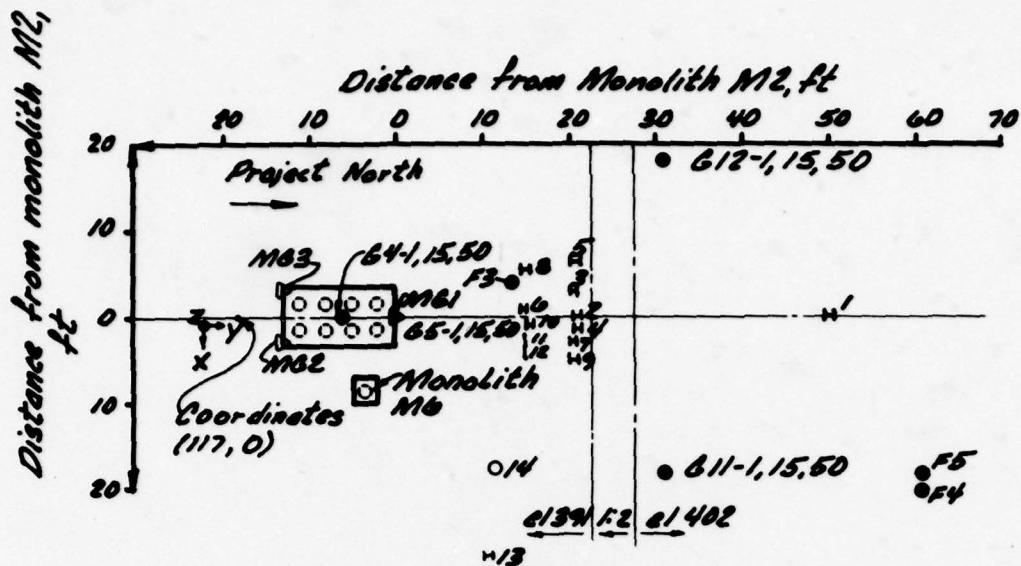
## MONOLITH M1

<u>Prototype Pile No.</u>	<u>Distance Between Prototype Pile And Monolith ft</u>	<u>Prototype Pile Type</u>	<u>Hammer Type</u>	<u>Final Tip Elevation ft</u>
1	200	HP 14x73	Vulcan 010	350
2	150	"	"	297
3	125	"	"	297.3
4	75	"	"	295.5
5	50	"	"	350
6	30	"	"	297.9
7	30	"	"	298
8	20	"	"	299
9	20	"	"	298
10	20	"	"	298.3
11	8	"	"	295.6
12	7	PP 14x0.375 (open-ended)	"	296.9
13	7	PP 14x0.375 (close-ended)	"	298

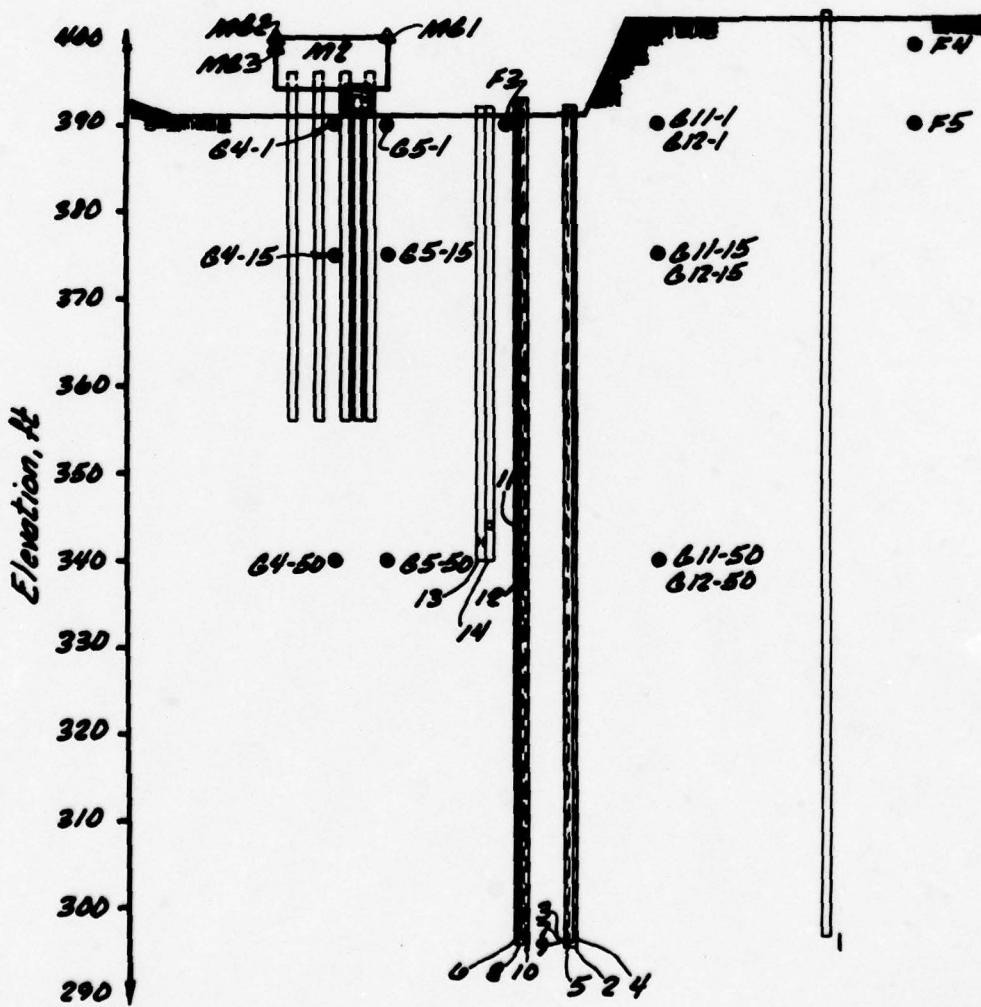
Ground geophone  
 Monolith geophone  
 Timber pile  
 HP 14x73  
 PP 14x0.375 (open-ended)  
 PP 14x0.375 (close-ended)



2



## Plan



## Section

*Legend*

- GI
- △ MI
- Tim
- H HAB
- PP
- PPD
- MP

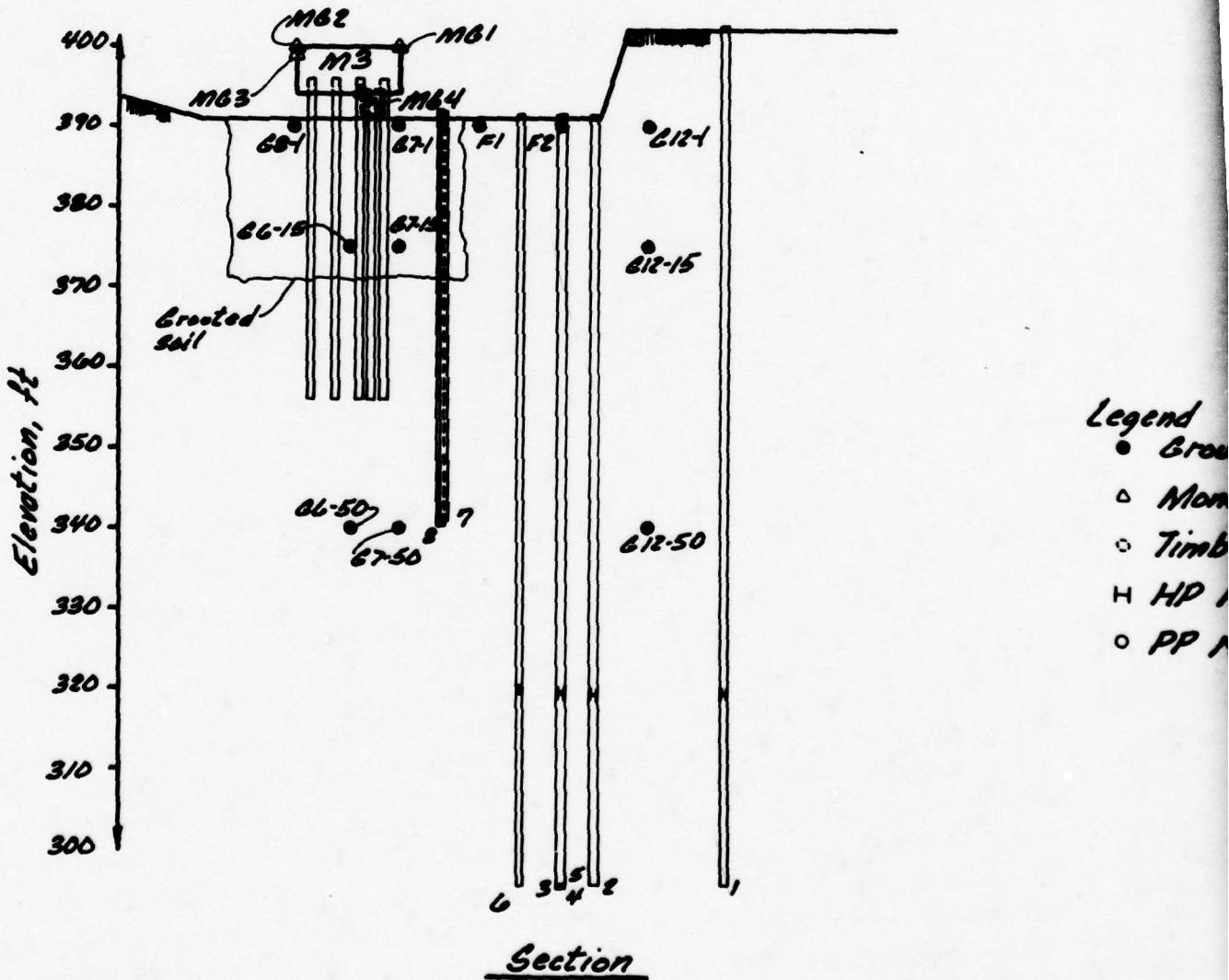
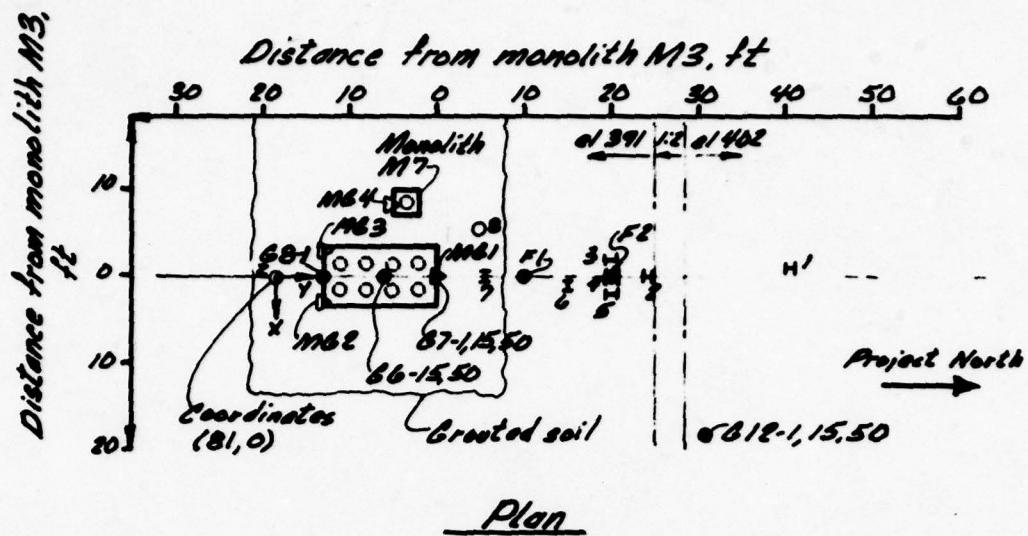
## MONOLITHS M2 AND M6

Prototype Pile No.	Distance Between Prototype Pile And Monolith ft			Final Tip Elevation ft
		Prototype Pile Type	Hammer Type	
1	50	HP 14x73	Vulcan 010	296.8
2	21	"	"	295
3	20.6	"	"	295.9
4	21.1	"	"	295.6
5	20.8	"	"	295.4
6	14.8	"	"	296
7	20.6	"	MKT DE 70B	296.1
8	14.9	"	"	296.1
9	20.6	"	Foster 4000	296
10	15.4	"	"	296.5
11	15	MP 102	"	344
12	15	"	"	337.3
13	10.4	HP 14x73 (Instrumented T3)	MKT DE 70B	340
14	11.7	PP 14x0.375 (open-ended) (Instrumented T4)	"	340

round geophone  
 monolith geophone  
 timber pile  
 P 14x73  
 P 14x0.375 (open-ended)  
 P 14x0.375 (close-ended)  
 102

<b>PILE DRIVING EFFECTS TEST PROGRAM</b>	
<b>PLAN AND SECTION FOR MONOLITHS M2 AND M6</b>	
<small>FOUNDATION INVESTIGATION AND TEST PROGRAM EXISTING LOCKS AND DAM No. 20 ST LOUIS DISTRICT, CORPS OF ENGINEERS. DAGW48-78-C-0000</small>	
 Woodward-Clyde Consultants V7C828 Phase II	<b>Fig. 7.2</b>

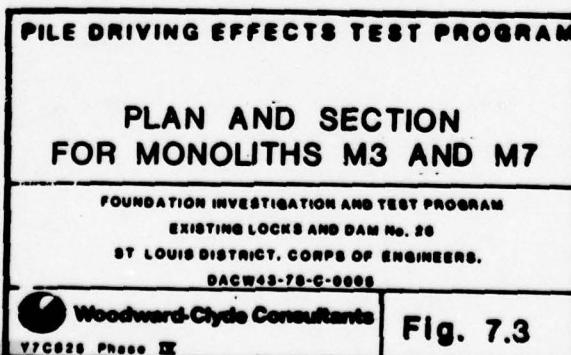
2



MONOLITHS M3 AND M7

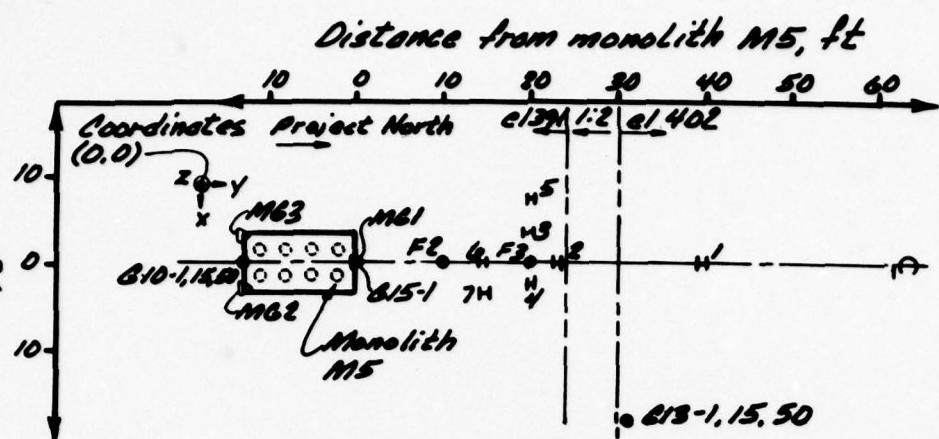
Prototype Pile No.	Distance Between Prototype Pile And Monolith ft	Prototype Pile Type	Hammer Type	Final Tip Elevation ft
1	40.5	HP 14x73	Vulcan 010	295.4
2	24.3	"	"	295.4
3	20	"	"	295.3
4	20	"	"	294.9
5	20	"	"	295.4
6	15	"	"	295.5
7	5.5	HP 14x73 (Instrumented T5)	"	340.8
8	4.8	PP 14x0.375 (open-ended) (Instrumented T6)	"	340.3

und. geophone  
monolith geophone  
per pile  
14x73  
4x0.375 (open-ended)

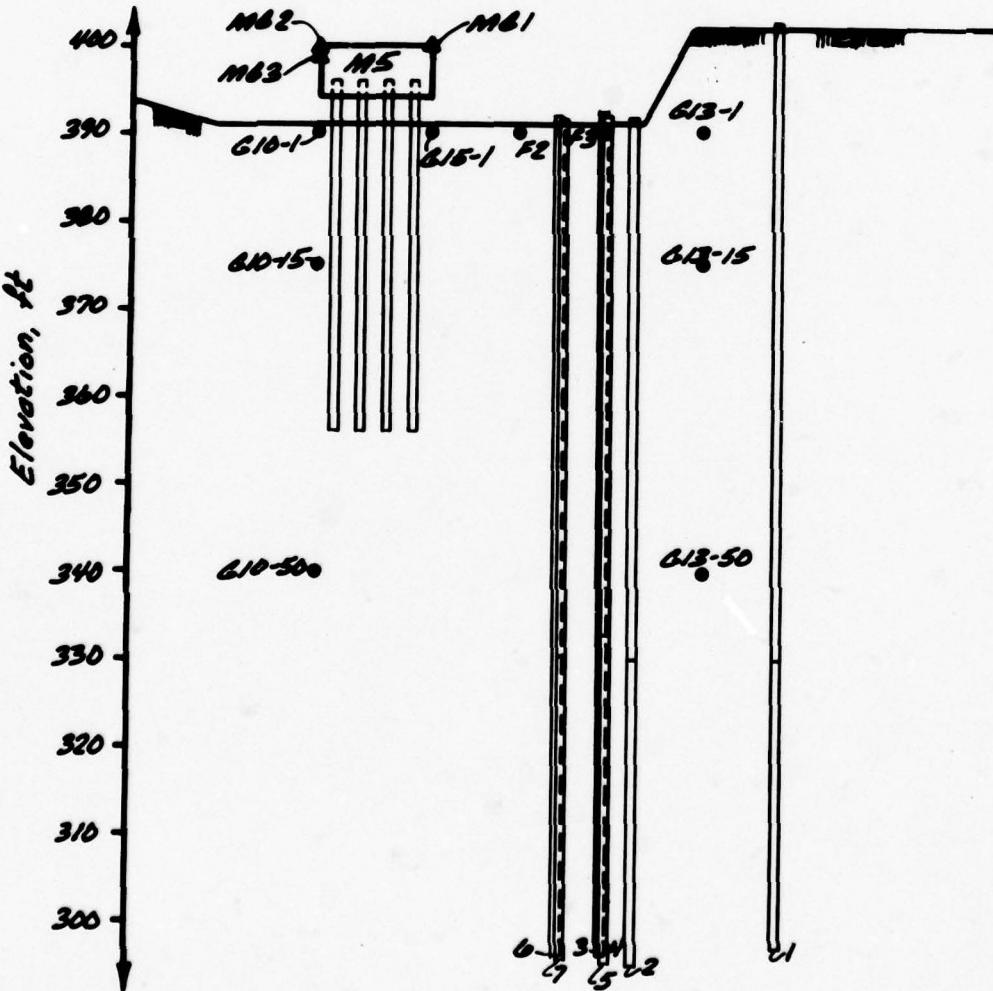


21

Distance from monolith M5



Plan

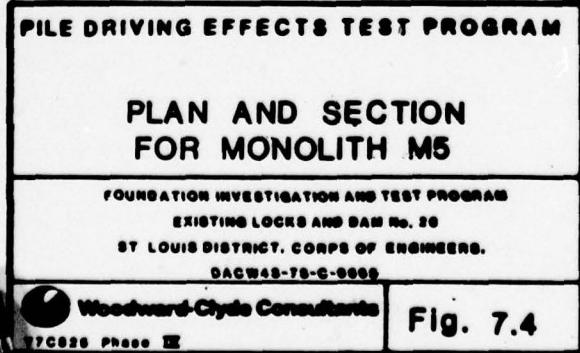


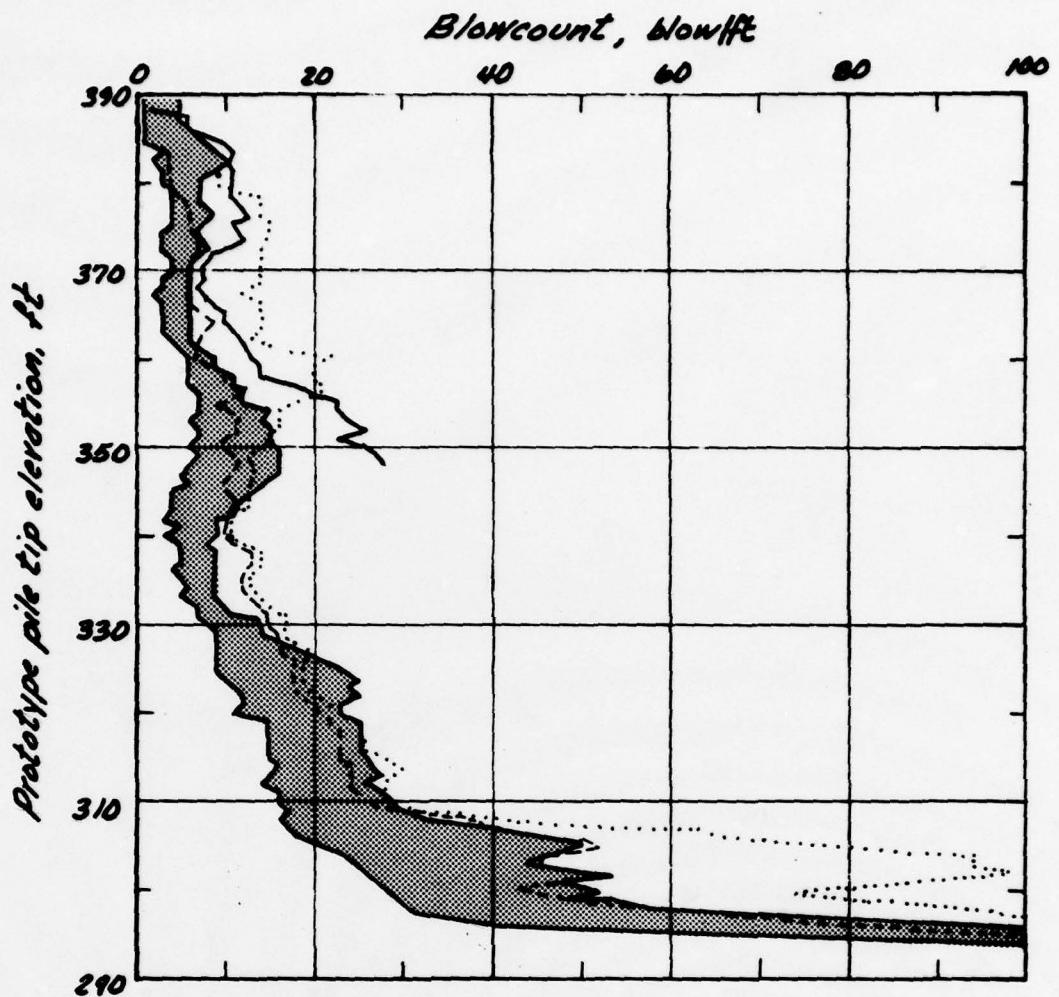
Section

- Legend
- Ground.
  - △ Monolith
  - Timber,
  - H HD 14x

## MONOLITH M5

Distance Between Prototype Pile And Monolith <u>ft</u>	Prototype <u>Pile Type</u>	Hammer <u>Type</u>	Final Tip Elevation <u>ft</u>
39.5	HP 14x73	Vulcan 010	297
23	"	"	295
19.7	"	"	296
20	"	"	296.3
20	"	"	295.8
14.6	"	"	296.5
14.8	"	"	296.4





*Legend*

<u>Prototype pile No.</u>	<u>Prototype pile type</u>	<u>Hammer type</u>
1	HP 14x73	
2 through 11	HP 14x73	
12	PP 14x0.375 (open-ended)	Vulcan OIO
13	PP 14x0.375 (close-ended)	

PILE DRIVING EFFECTS TEST PROGRAM

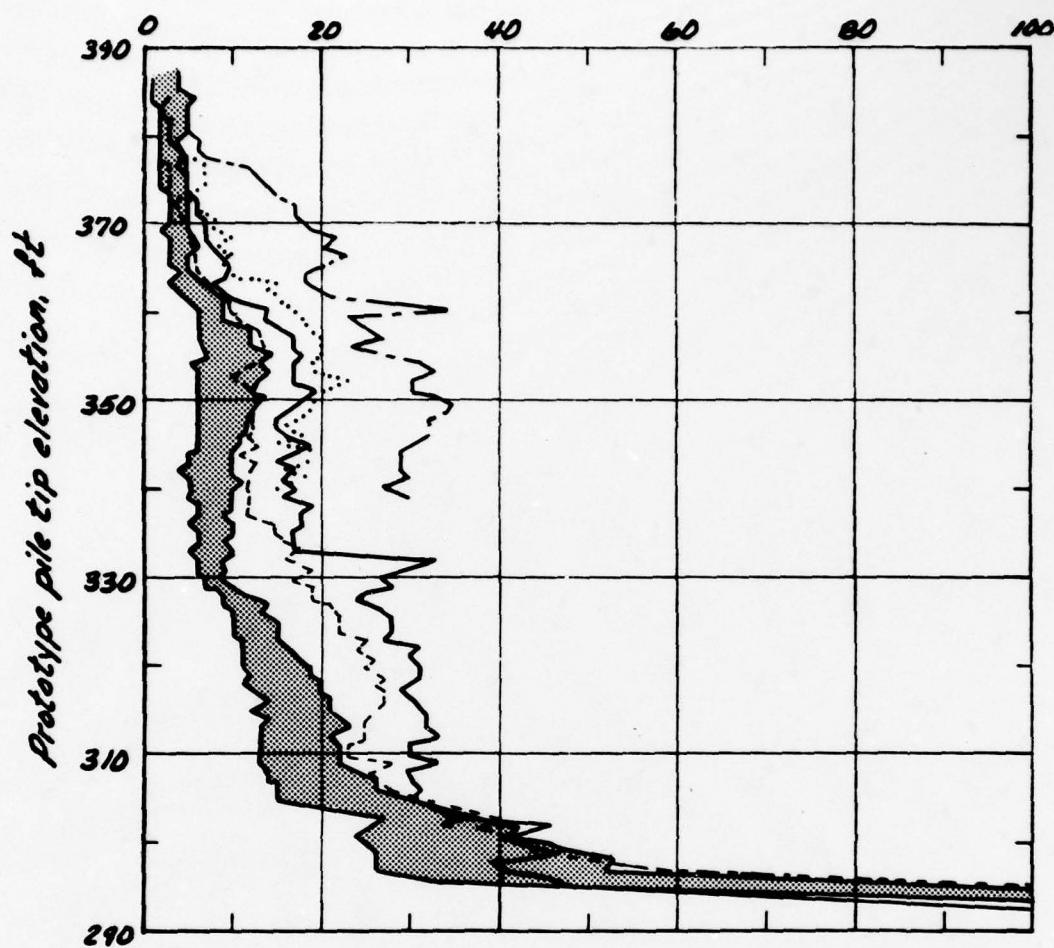
BLOWCOUNT DATA,  
PROTOTYPE PILE DRIVING,  
MONOLITH M1

FOUNDATION INVESTIGATION AND TEST PROGRAM  
EXISTING LOCKS AND DAM NO. 28  
ST. LOUIS DISTRICT, CORPS OF ENGINEERS.  
DACW49-78-C-0008

Woodward-Clyde Consultants  
TTCB25 Phase II

Fig. 7.5

*Blowcount, blow/ft*



*Legend*

<u>Prototype pile No.</u>	<u>Prototype pile TYPE</u>	<u>Hammer TYPE</u>
1 through 6	HPMx73	Vulcan 010
7	HPMx73	MKT DE 70B
8	HPMx73	MKT DE 70B
13	HPMx73	MKT DE 70B
14	PP Mx0.375 (open-ended)	MKT DE 70B

**PILE DRIVING EFFECTS TEST PROGRAM**

**BLOWCOUNT DATA,  
PROTOTYPE PILE DRIVING,  
MONOLITHS M2 AND M6**

FOUNDATION INVESTIGATION AND TEST PROGRAM

EXISTING LOCKS AND DAM NO. 26

ST LOUIS DISTRICT, CORPS OF ENGINEERS.

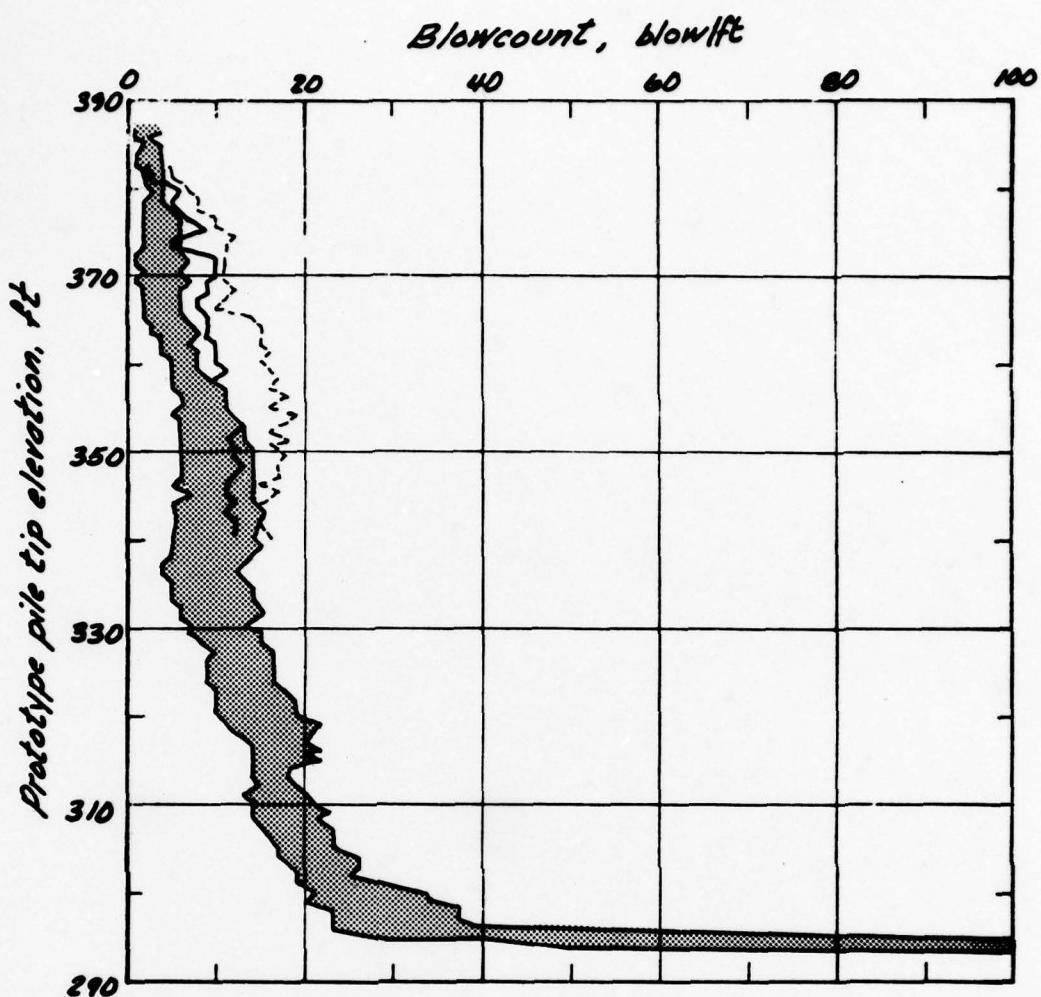
DACW43-78-C-0005



Woodward-Clyde Consultants

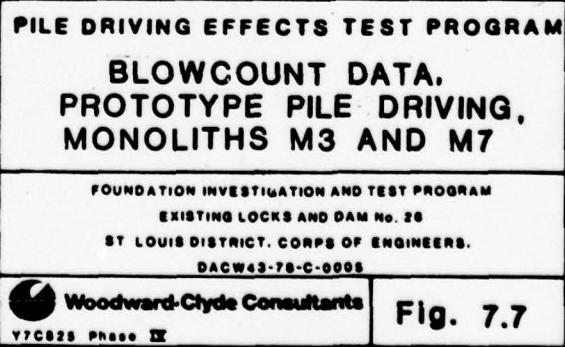
Y7C825 Phase II

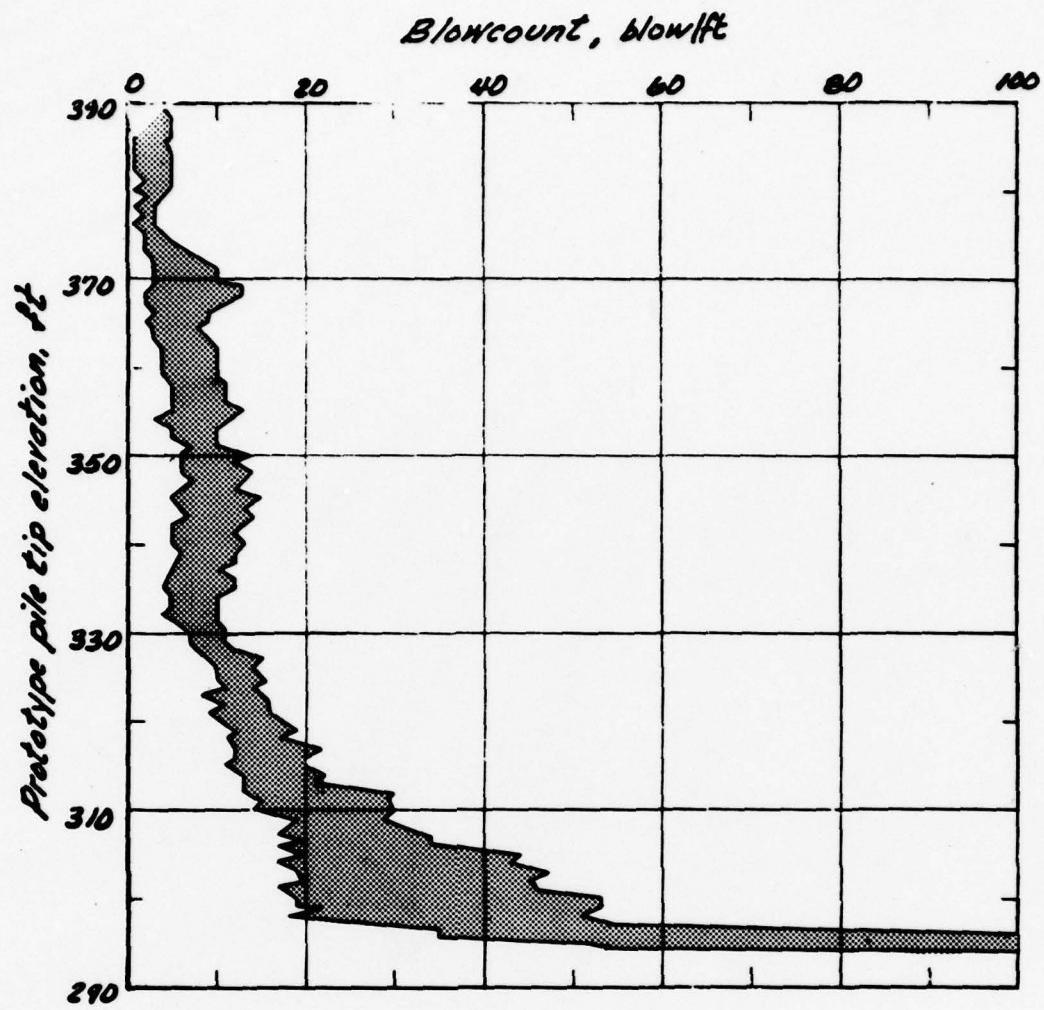
**Fig. 7.6**



*Legend*

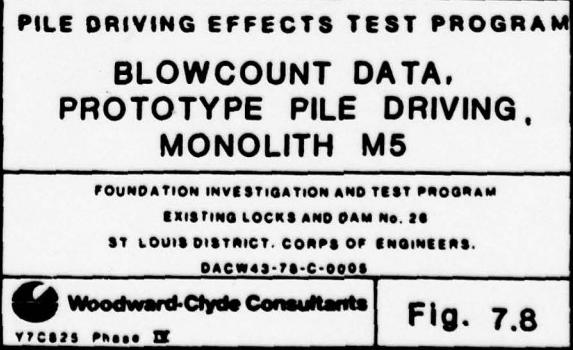
<u>Prototype pile No.</u>	<u>Prototype pile type</u>	<u>Hammer type</u>
1 through 6	HP 14x73	
7	HP 14x73	Vulcan 010
8	PP 14x0.375 (open-ended)	

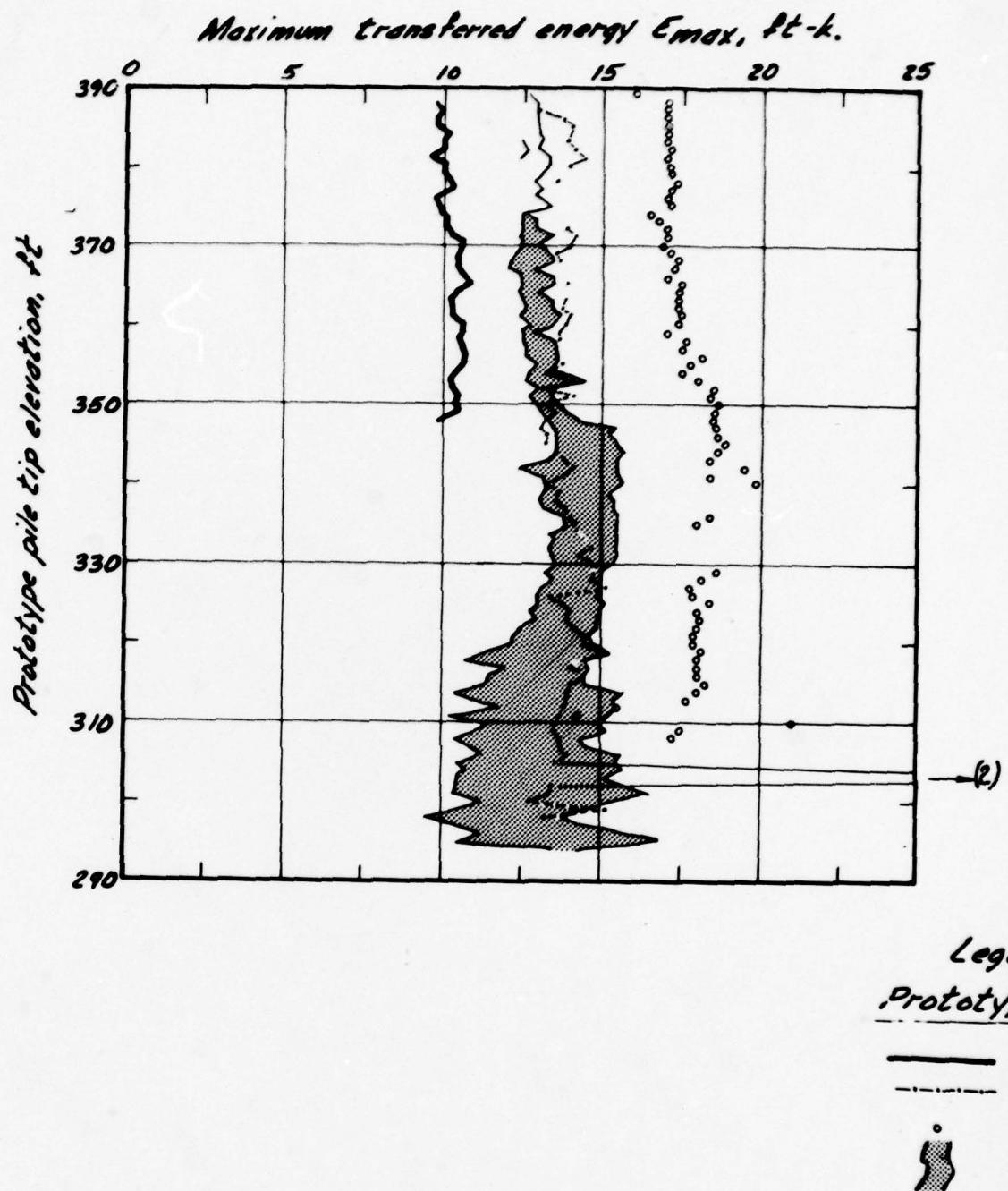




Legend

<u>Prototype</u>	<u>Prototype</u>	<u>Hammer</u>
<u>pile No.</u>	<u>pile type</u>	<u>TYPE</u>
■ 1 through 7	HP14x73	Vulcan O10

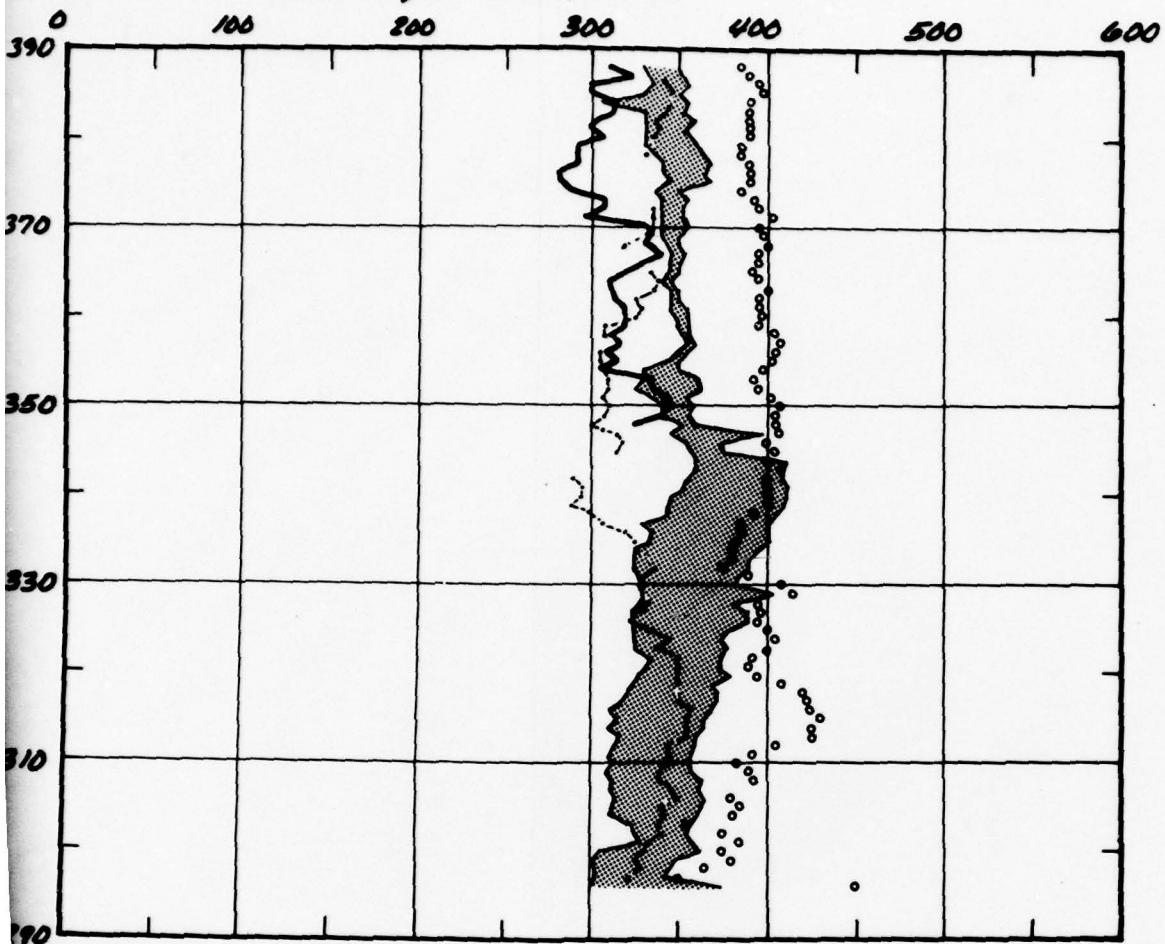




*Notes:*

- (1) Driving of prototype piles by the same driving system (Vulcan)
- (2) Questionable data

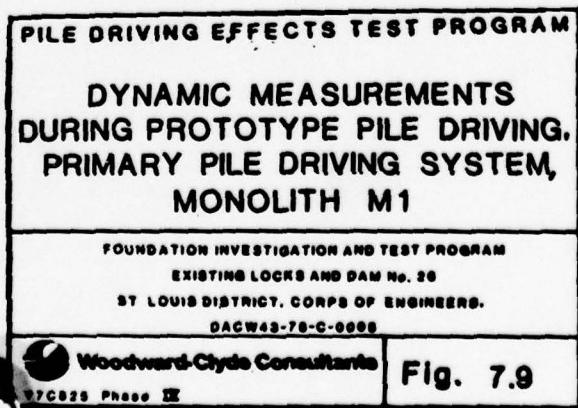
Maximum compression force  $F_{max}$   
at the pile butt, ft-k.



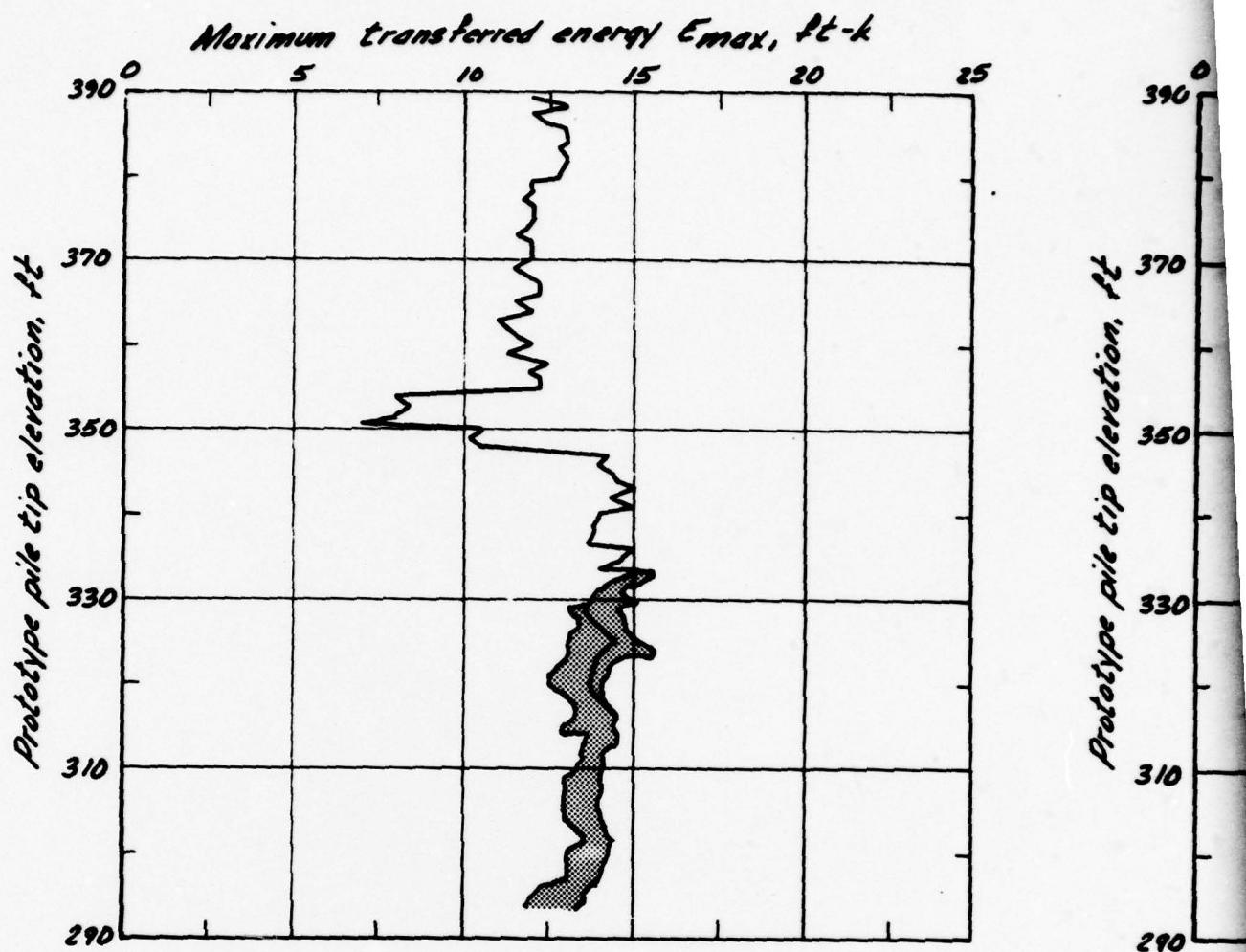
pile No.

9,10,11

les using the primary pile  
(# 010 - HP 14 x 73)



2

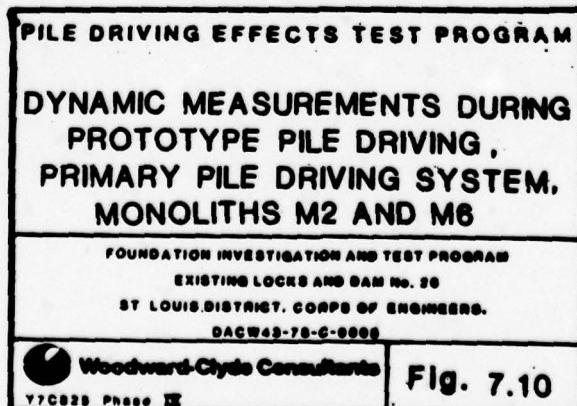
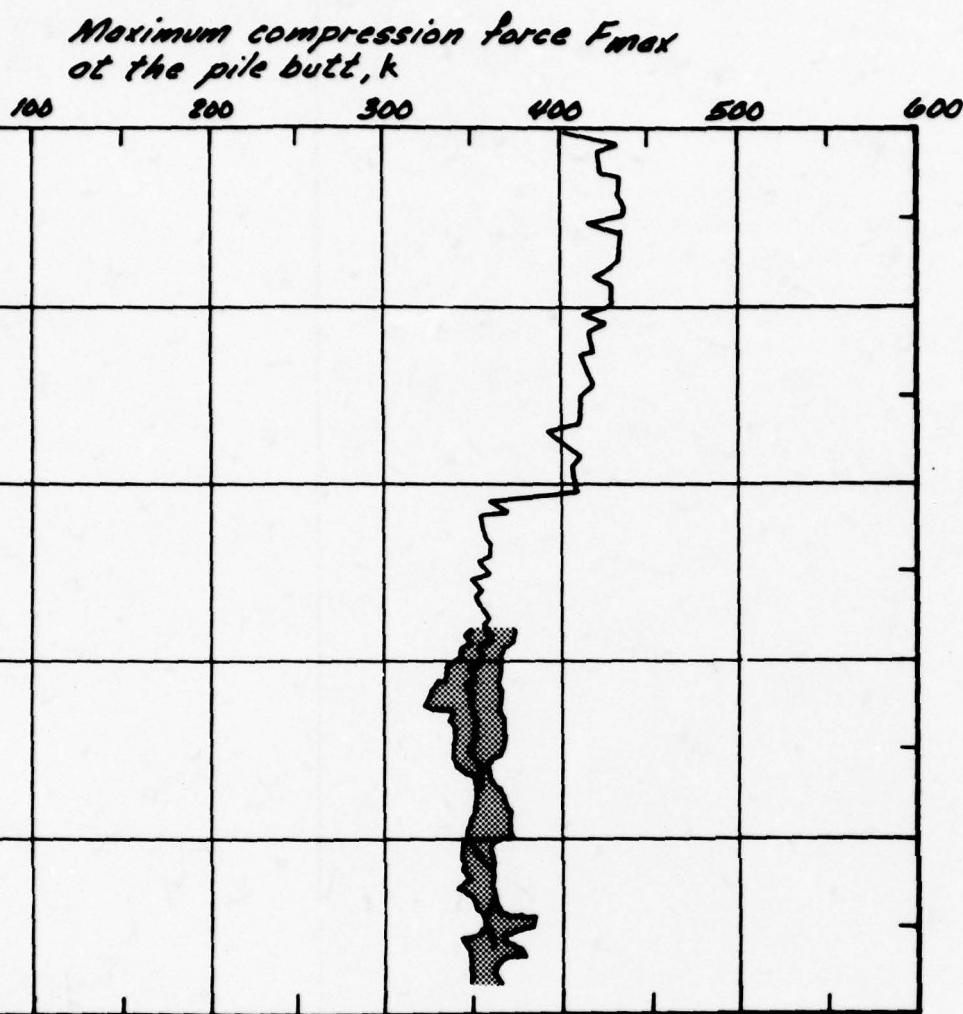


*Legend*  
Prototype pile No.

— 1  
■ 1 through 4

*Note:*

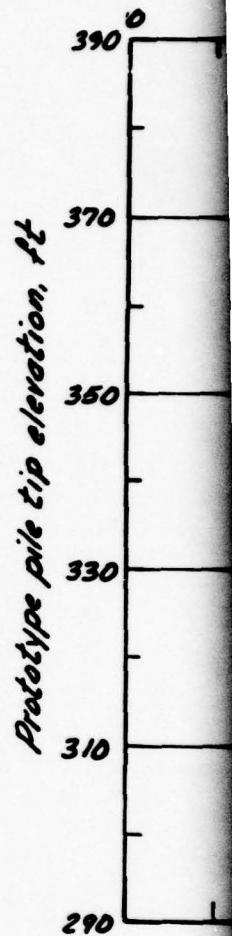
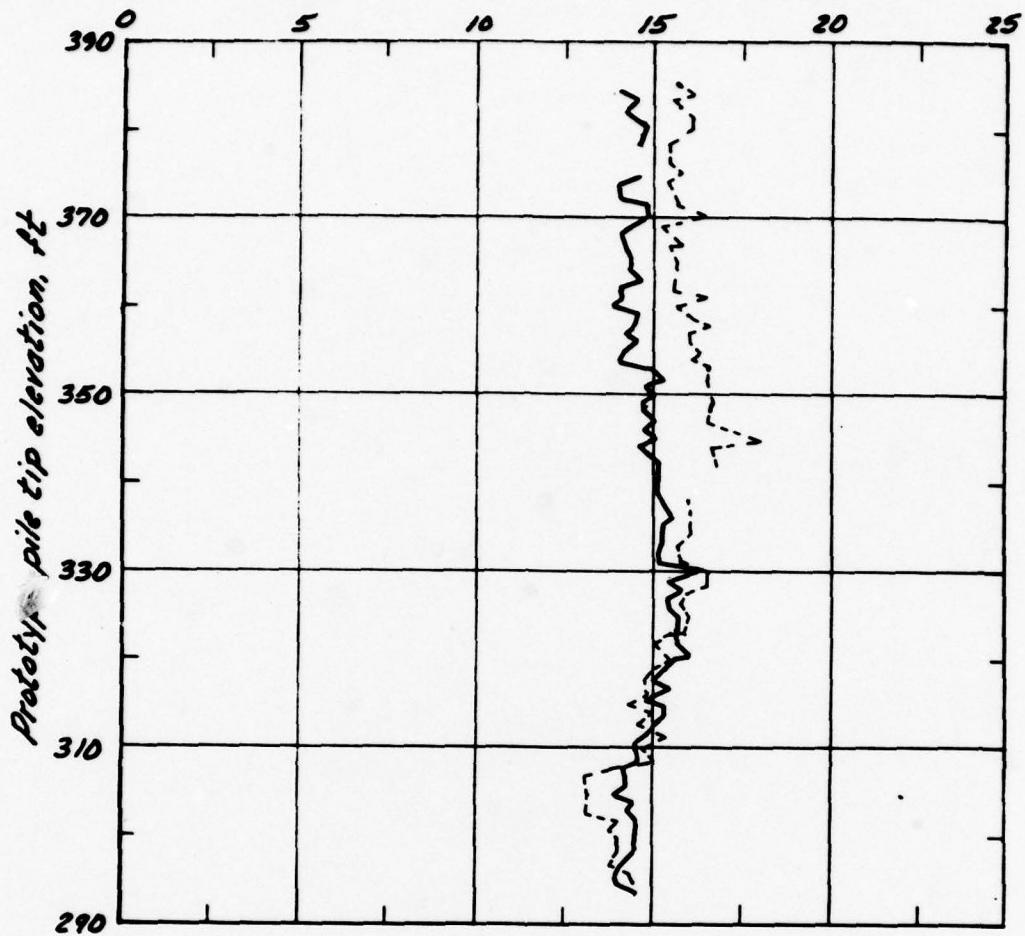
Driving of prototype piles using  
driving system (Vulcan O10 -)



the primary pile  
(HP 14 x 73)

2

Maximum transferred energy  $E_{max}$ , ft-k

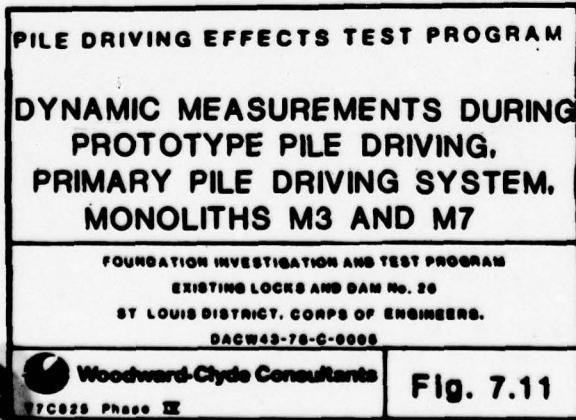
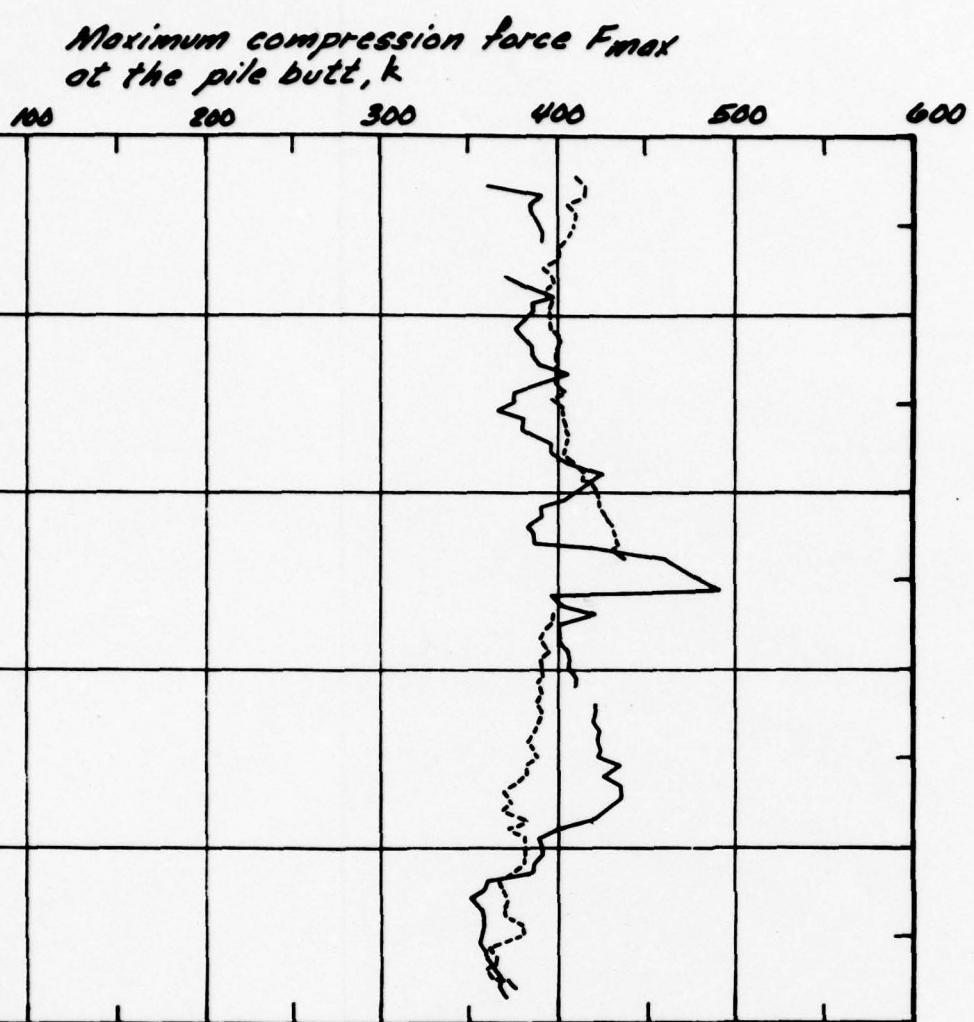


Legend  
Prototype pile No.

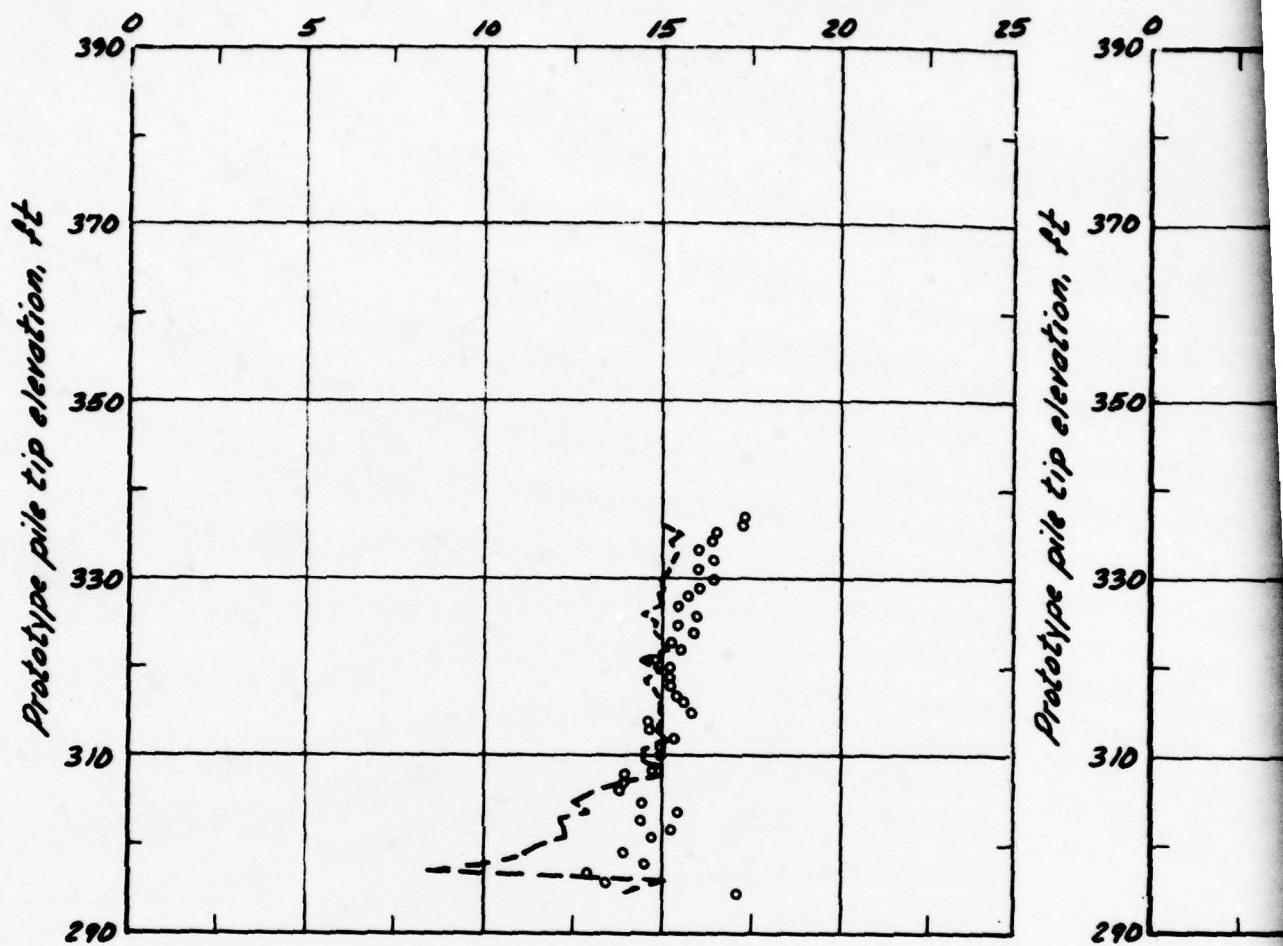
— 5  
--- 6

Note:

Driving of prototype piles using the  
driving system (Vulcan O10-HP)



Maximum transferred energy  $E_{max}$ , ft-lb.



Legend

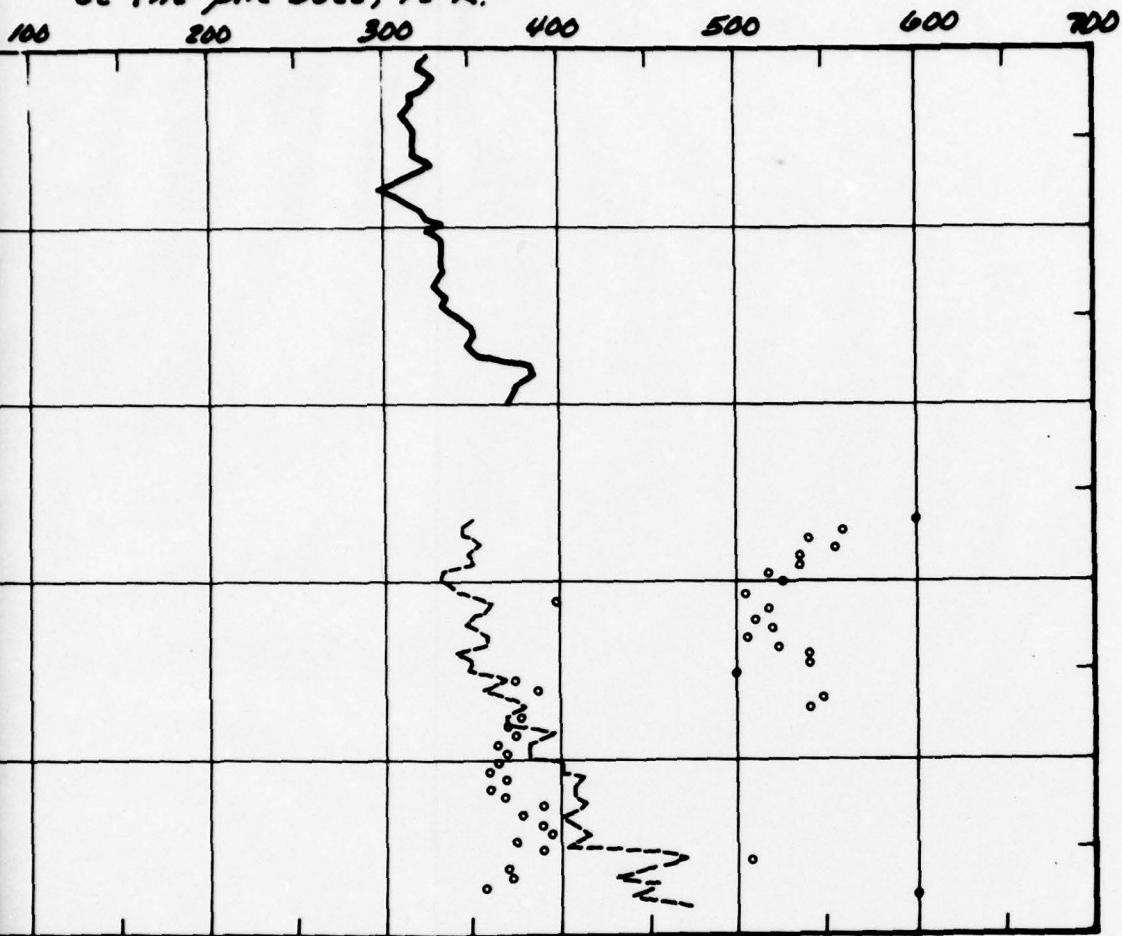
Prototype pile M

— 1  
- - - 2  
° 7

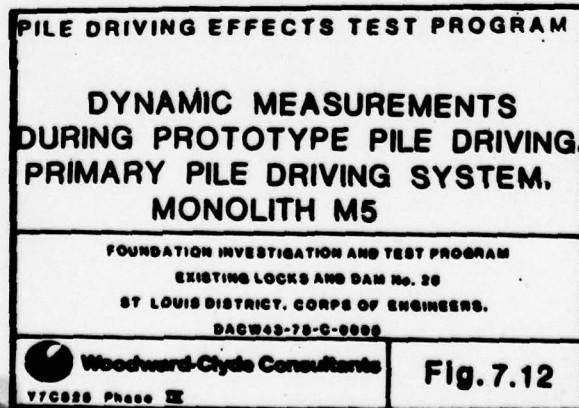
Note:

Driving of prototype piles vs  
driving system (Vulcan OI)

Maximum compression force  $F_{max}$   
at the pile butt, ft-k.

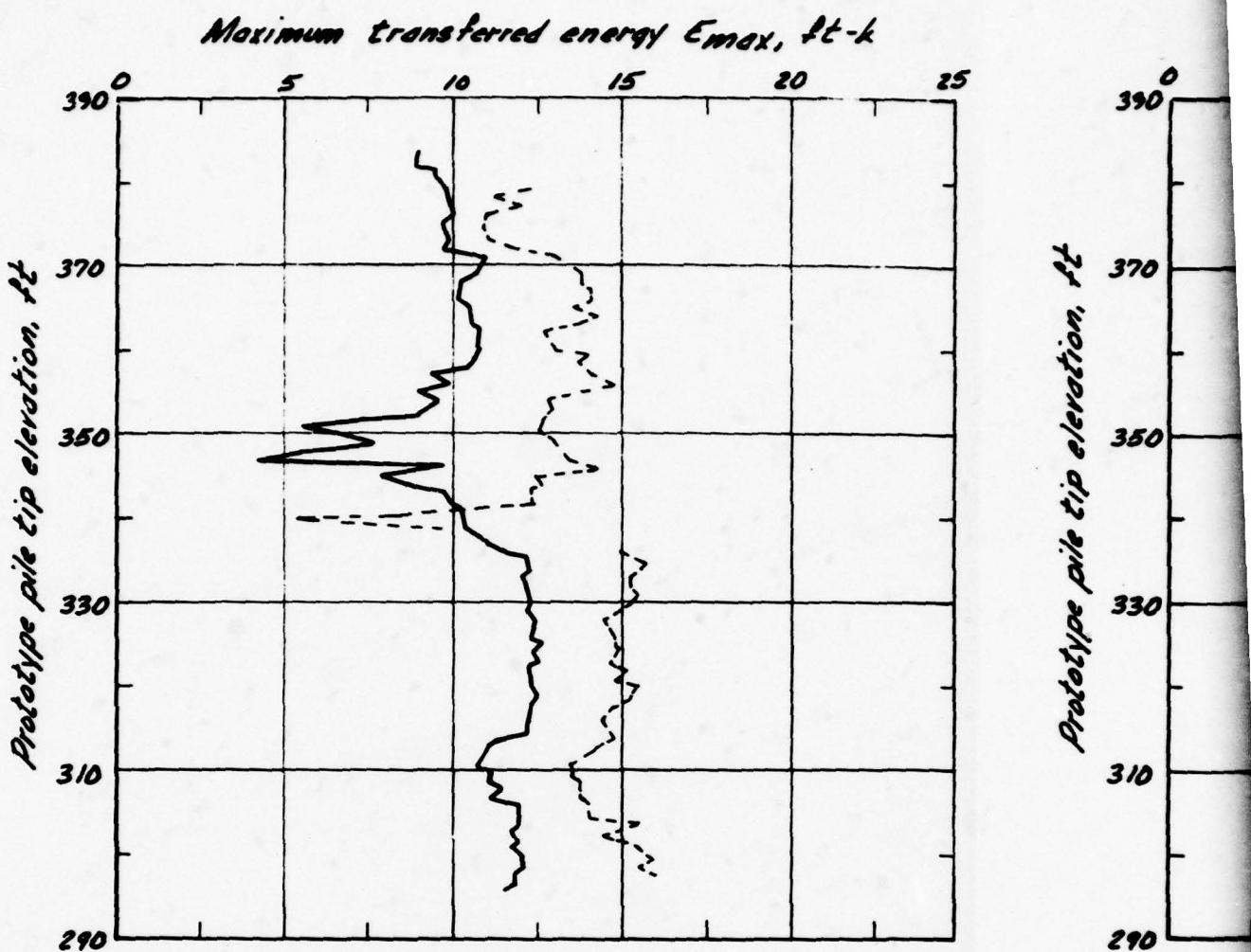


6.



ing the primary pile  
(-HP 14 x 73)

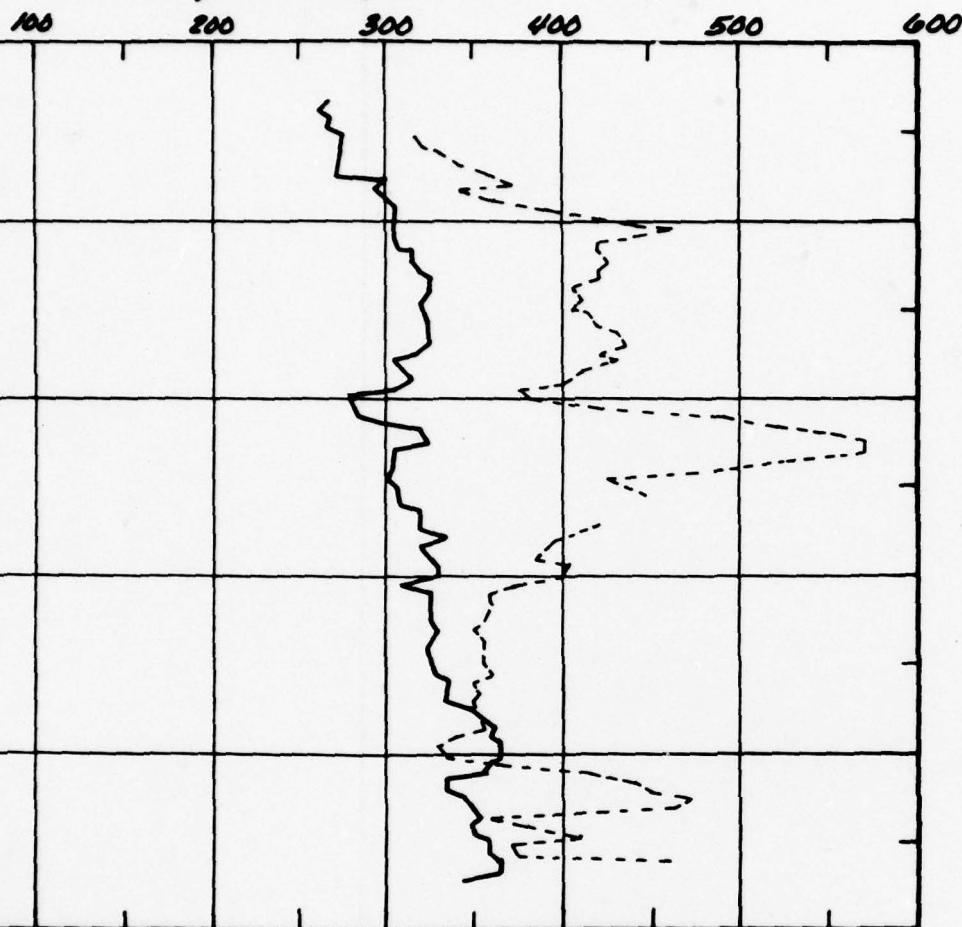
2



*Legend*

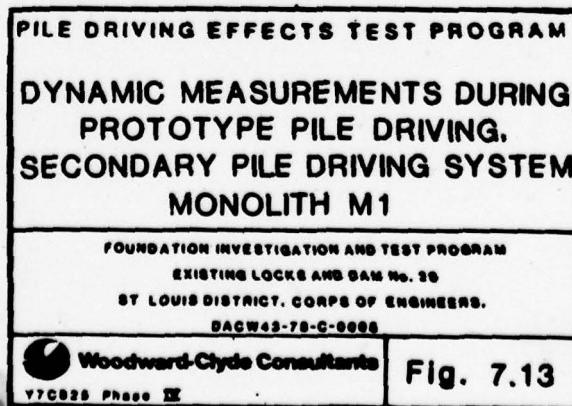
<u>Prototype pile No.</u>	<u>Prototype pile type</u>	<u>Ham- mer typ</u>
— 12	PP 14 x 0.375 (open-ended)	Vul-
--- 13	PP 14 x 0.375 (close-ended)	Vul-

Maximum compression force  $F_{max}$   
at the pile butt, k



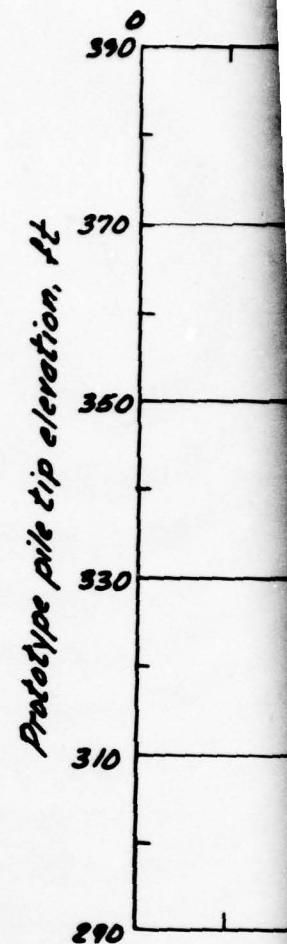
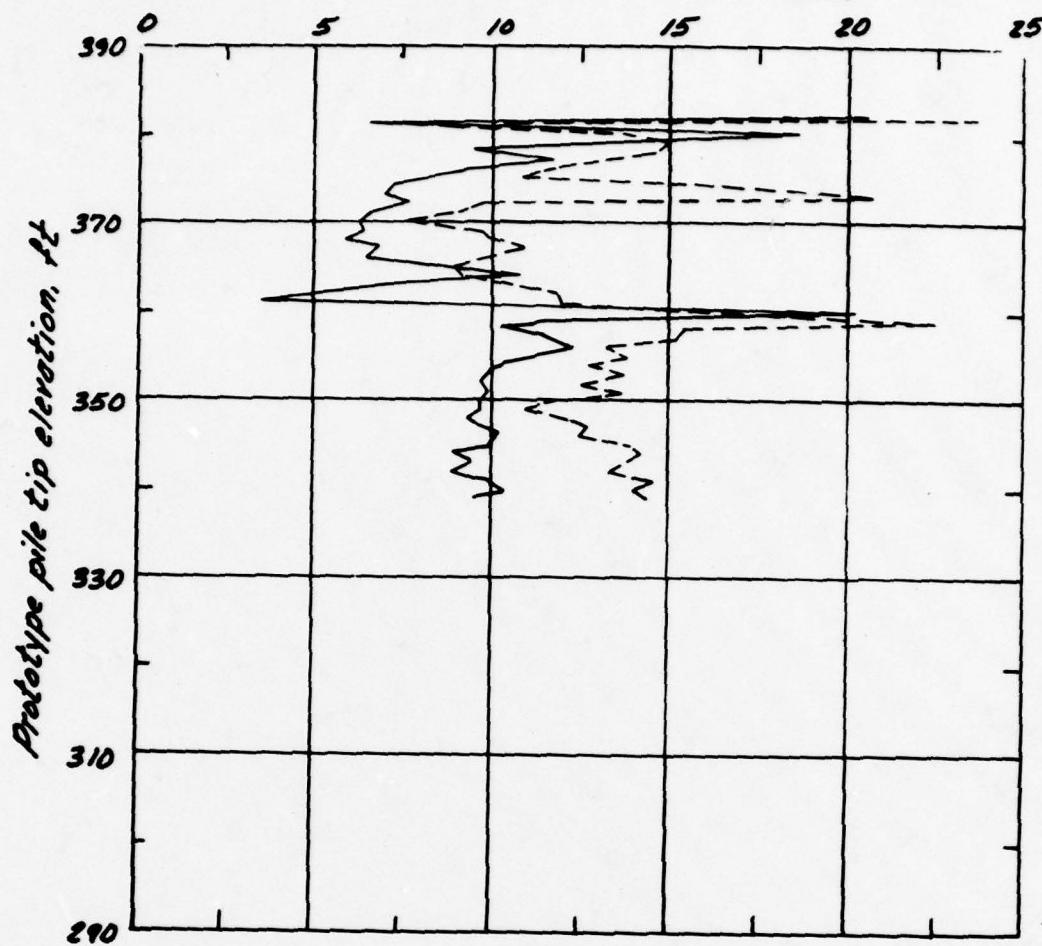
ummer  
ype  
ulcan O10

lcan O10



J

Maximum transferred energy  $E_{max}$ , ft-lb

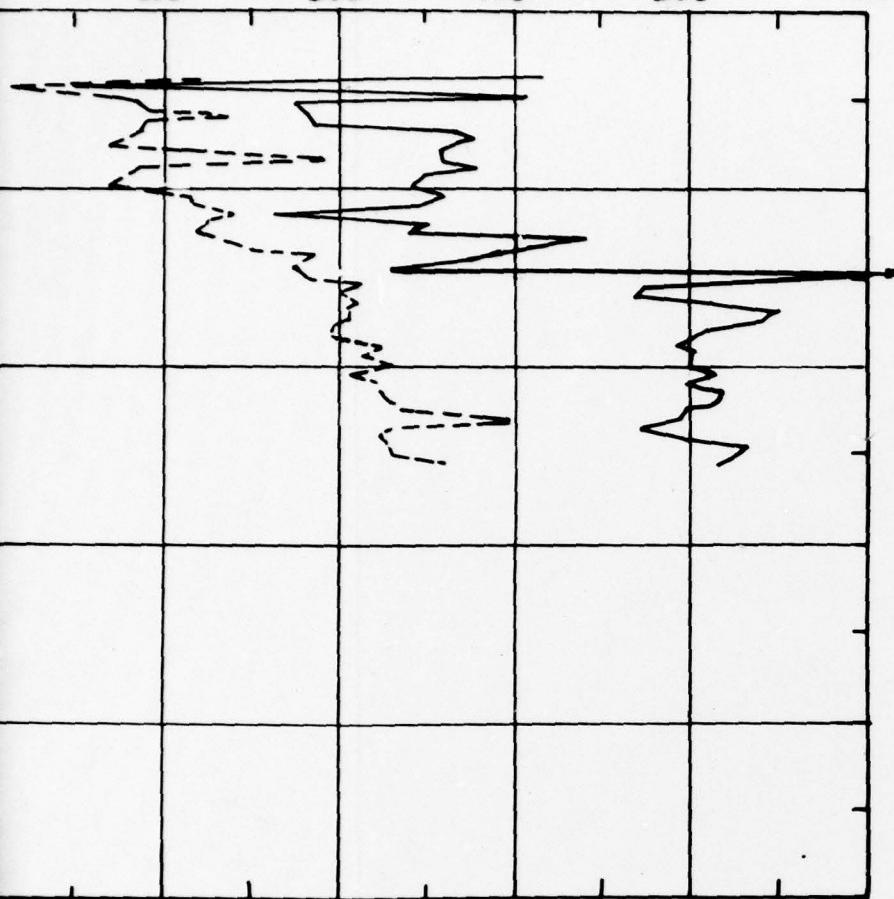


Legend

<u>Prototype pile No.</u>	<u>Prototype pile type</u>	<u>Hammer type</u>
— 13	HP 14x73	MKT DE
--- 14	PP 14x0.375 MKT DE (open-ended)	

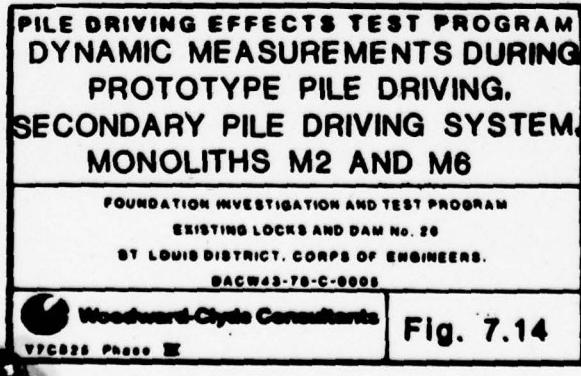
Maximum compression force  $F_{max}$   
at the pile butt, k

200 300 400 500 600

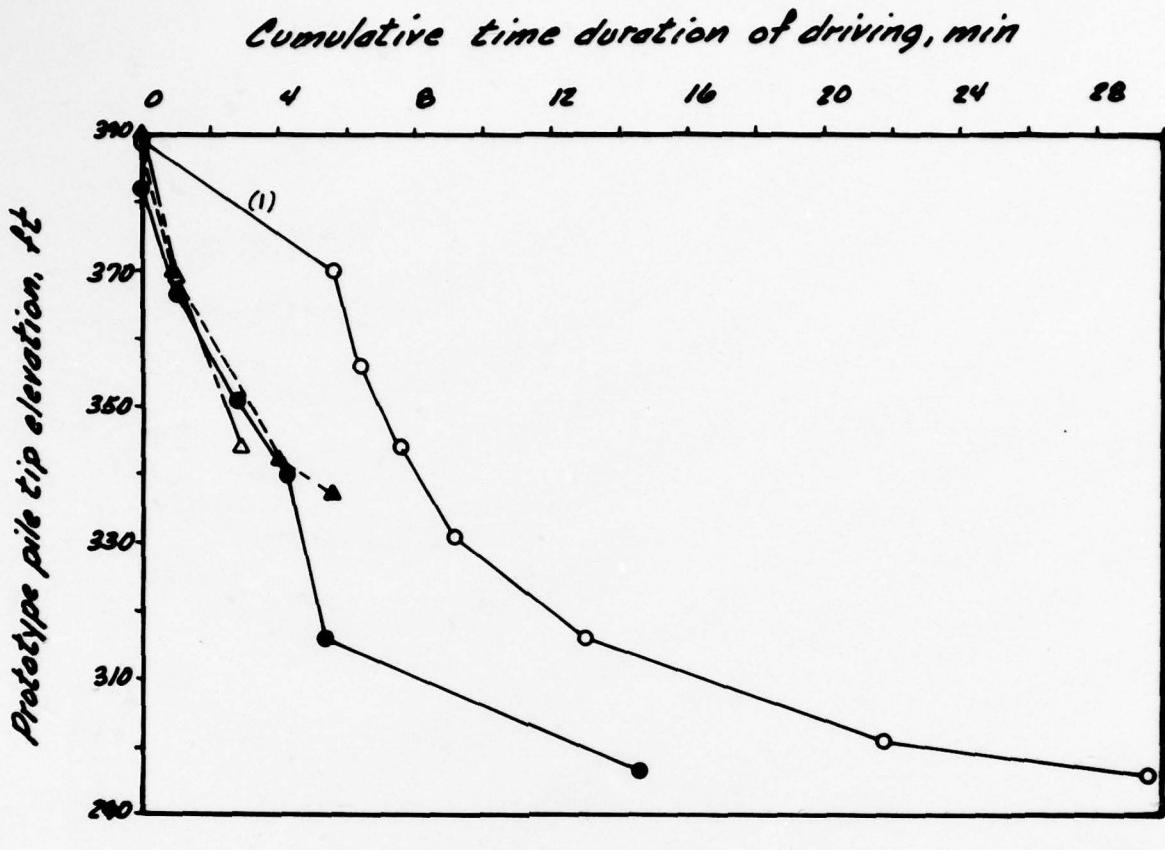


70B

70B



2

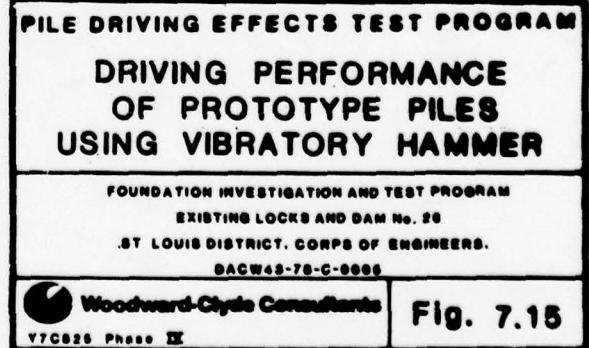


*Legend*

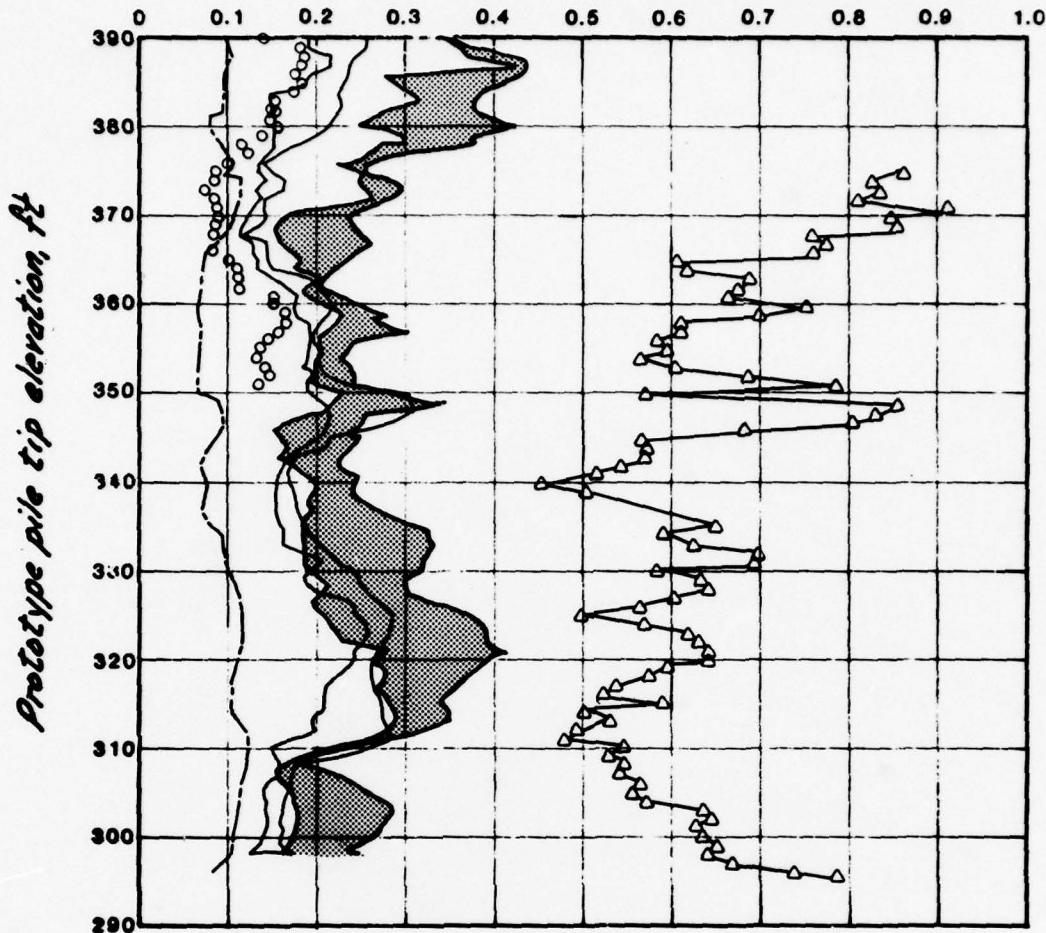
<u>Prototype pile No.</u>	<u>Prototype pile type</u>	<u>Hammer type</u>
-○- 9	HP14x73	
-●- 10	HP14x73	
-△- 11	MP 102	Faster 4000 vibratory
-◆- 12	MP 102	

*Notes:*

- (1) Long time duration of driving due to hammer-pile alignment difficulties
- (2) Prototype piles driven in front of monoliths M2 and M6



Near-surface peak vectorial particle velocity, in./s



Distance between  
prototype pile  
and monolith, ft

75	4
50	5
30	6,7
20	8,9,10
8	11

Notes:

(1) Peak vectorial particle velocity values from prototype piles No. 1, 2, 3, all at distances greater than 75 ft from monolith M1, are lower than those of prototype pile No. 4 and are not plotted.

(2) Primary pile driving system was a combination of Vulcan O10 and LJD 14 x 72.

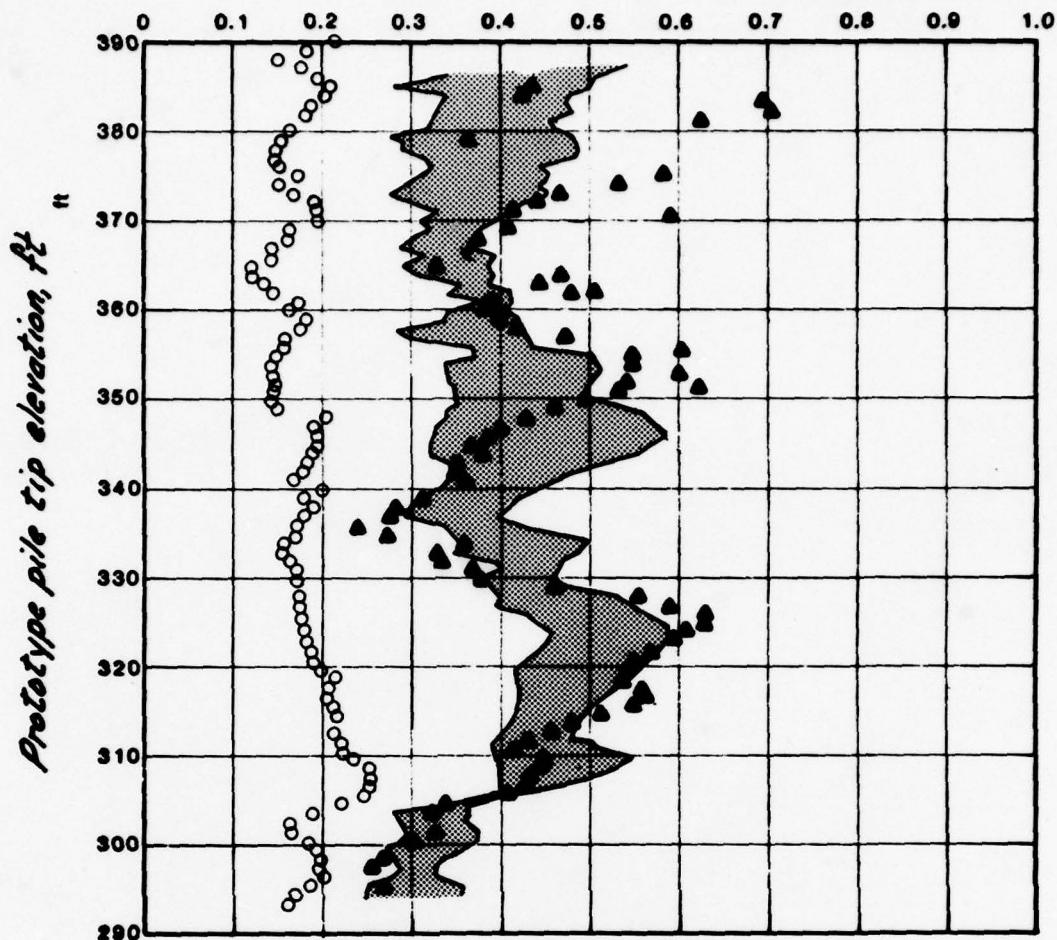
PILE DRIVING EFFECTS TEST PROGRAM  
PRIMARY PILE DRIVING SYSTEM,  
NEAR-SURFACE PARTICLE VELOCITY  
AT MONOLITH M1

FOUNDATION INVESTIGATION AND TEST PROGRAM  
EXISTING LOCKS AND DAM NO. 26  
ST. LOUIS DISTRICT, CORPS OF ENGINEERS.  
DAMW43-78-C-0008

Woodward-Clyde Consultants  
Y7C825 Phase III

Fig. 7.16

Near-surface peak vectorial particle velocity, in./s



Distance between prototype pile and monolith, ft

○	50	1
▨	21	2,3,4,5
▲	15	6

Note:

Primary pile driving system was a combination of Vulcan O10 and HP 14x73

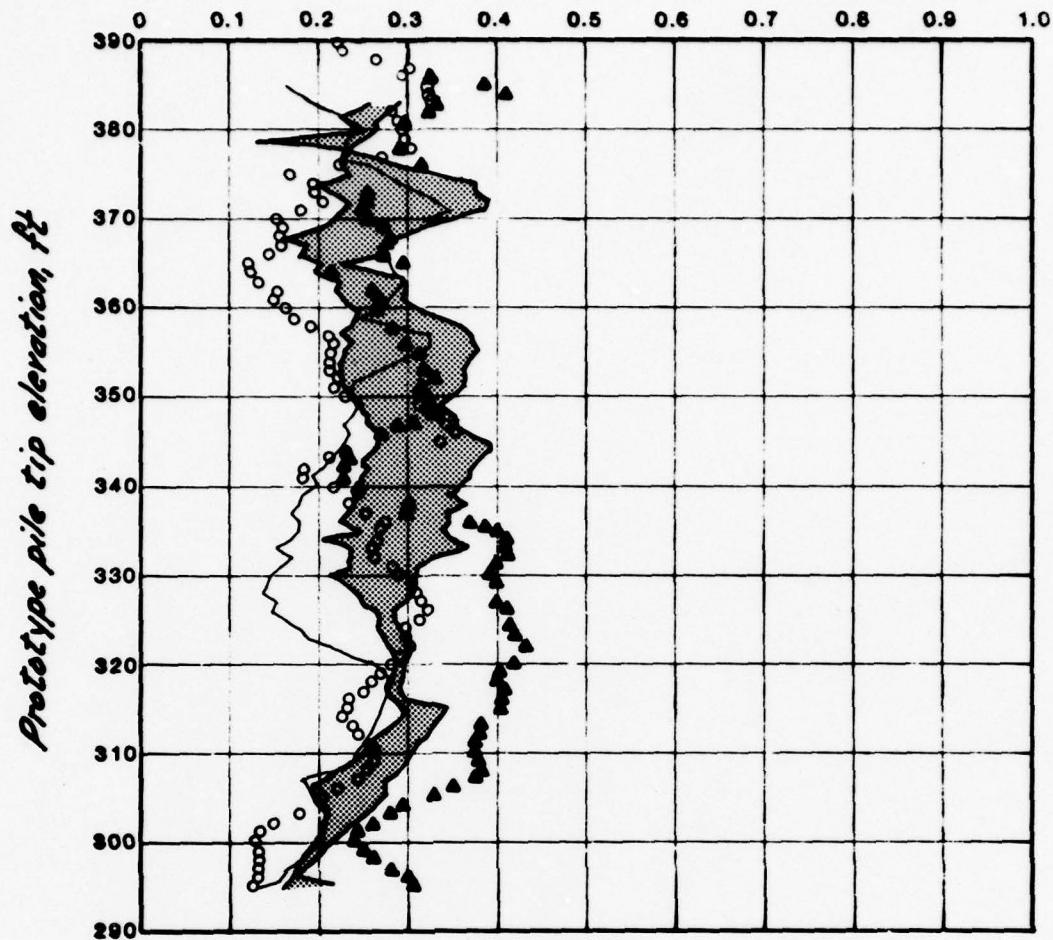
PILE DRIVING EFFECTS TEST PROGRAM  
PRIMARY PILE DRIVING SYSTEM,  
NEAR-SURFACE PARTICLE VELOCITY  
AT MONOLITH M2

FOUNDATION INVESTIGATION AND TEST PROGRAM  
EXISTING LOCKS AND DAM NO. 26  
ST LOUIS DISTRICT, CORPS OF ENGINEERS.  
DAGW63-78-C-0000

Woodward-Clyde Consultants  
V7C825 Phase II

Fig. 7.17

Near-surface peak vectorial particle velocity, in./s



Distance between  
prototype pile  
and monolith, ft

○	40.5	1
○	24.3	2
▨	20	3,4,5
▲	15	6

Notes:

- (1) Prototype pile No. 6 was driven perpendicular to monolith axis
- (2) Primary pile driving system was a combination of Vulcan O10 and HP 14x73

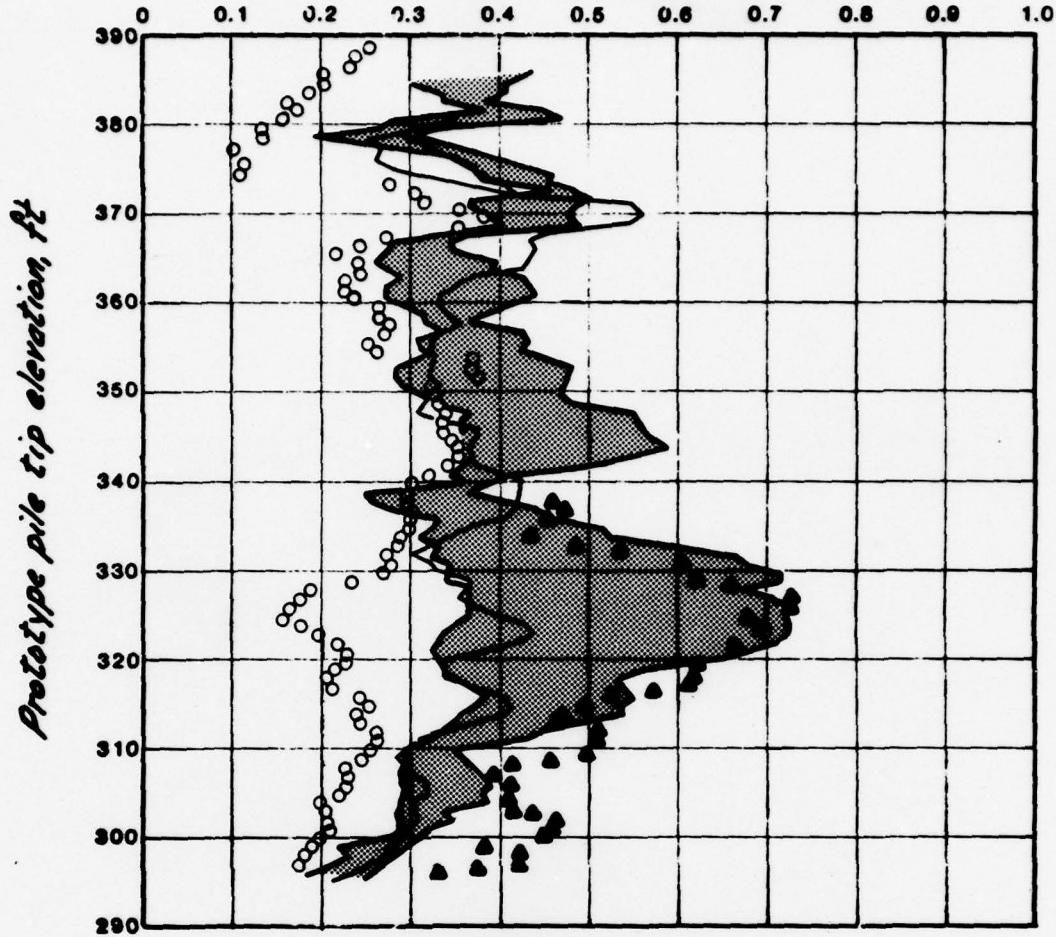
PILE DRIVING EFFECTS TEST PROGRAM  
PRIMARY PILE DRIVING SYSTEM,  
NEAR-SURFACE PARTICLE VELOCITY  
AT MONOLITH M3

FOUNDATION INVESTIGATION AND TEST PROGRAM  
EXISTING LOCKS AND DAM NO. 26  
ST. LOUIS DISTRICT, CORPS OF ENGINEERS.  
BACW43-78-C-0005

Woodward-Clyde Consultants  
Y7C825 Phase II

Fig. 7.18

Near-surface peak vectorial particle velocity, in./s

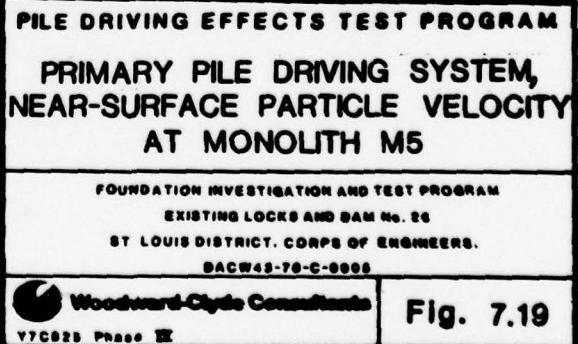


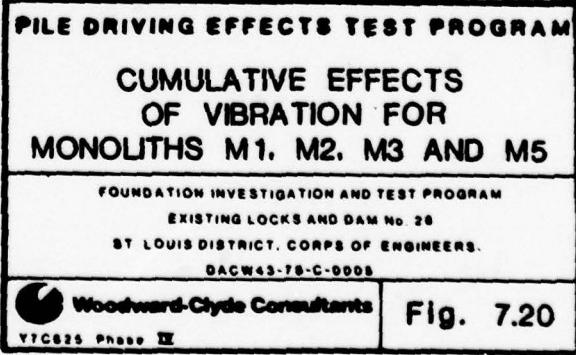
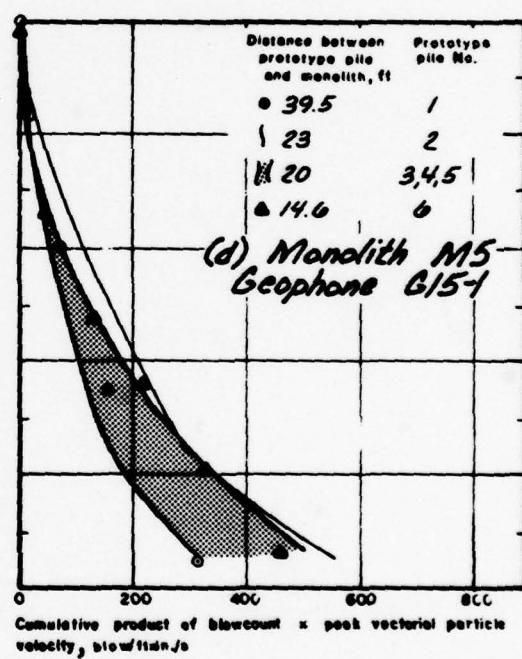
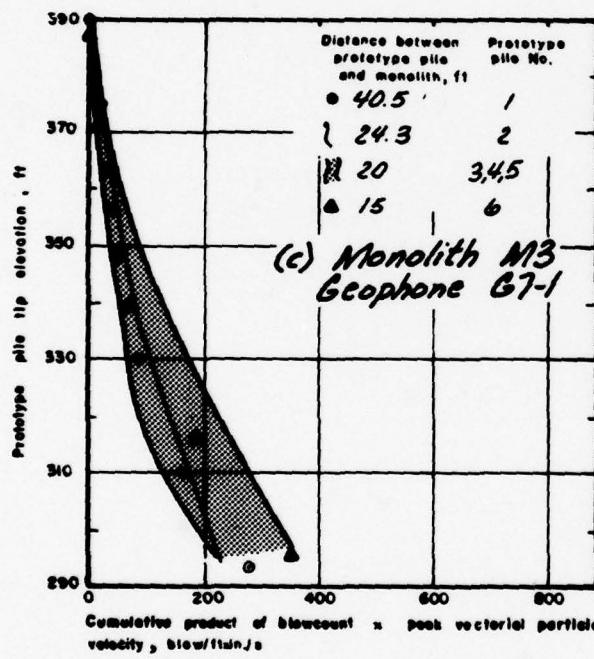
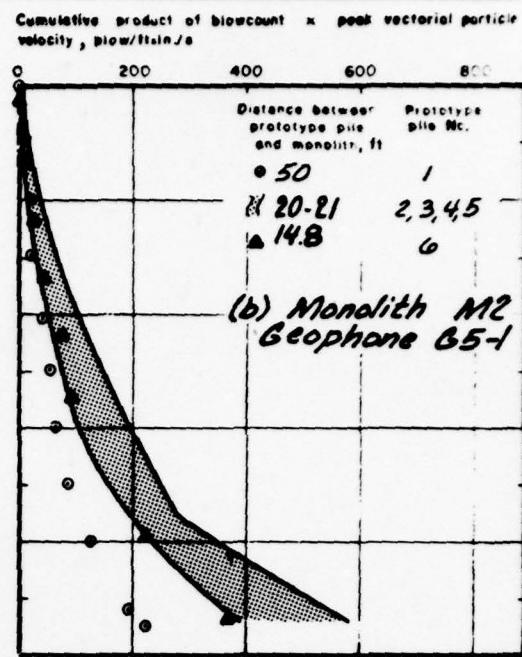
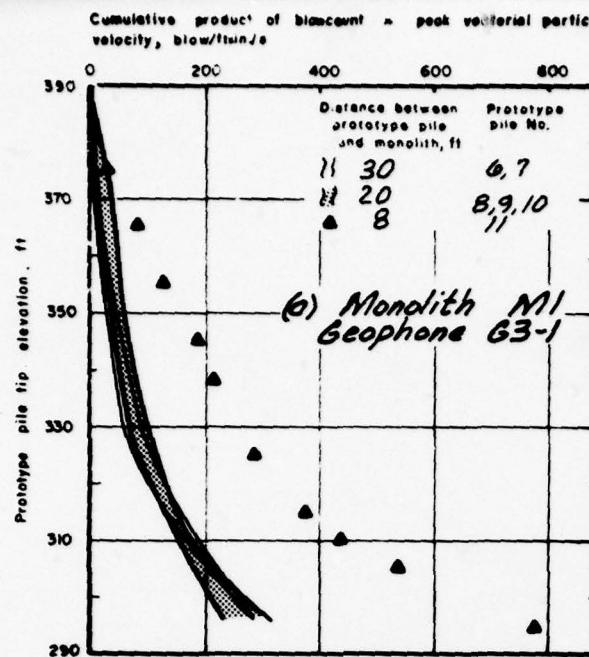
Distance between  
prototype pile  
and monolith, ft

○	39.5	1
△	23	2
✗	20	3,4,5
▲	14.8	?

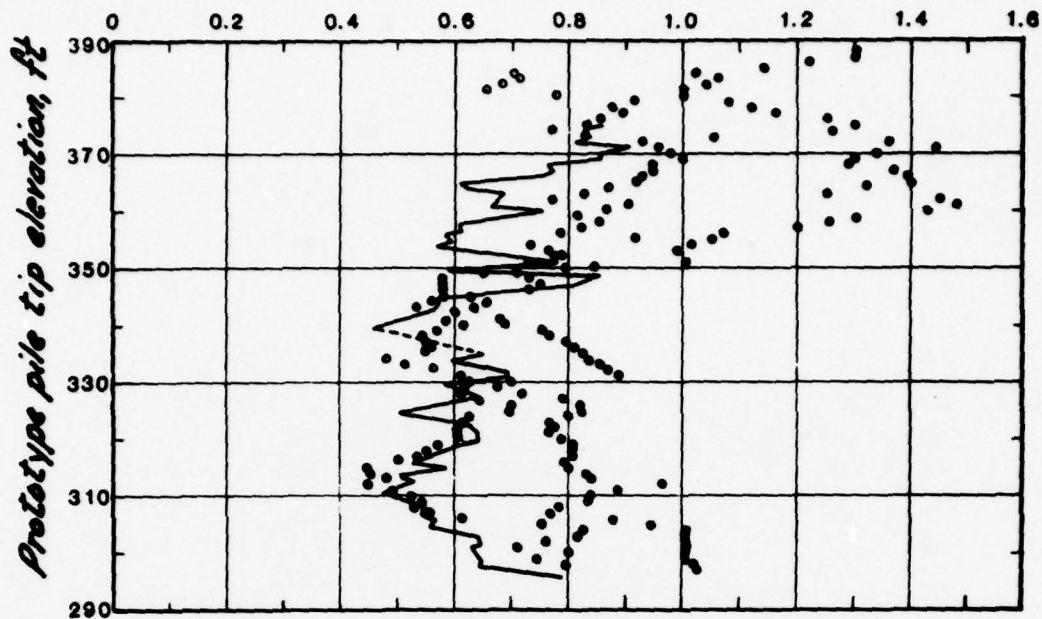
Note:

Primary pile driving system  
was a combination of  
Vulcan 010 and HP 14x73





Near-surface peak vectorial particle velocity, in./s



*Vulcan O10 (air hammer)*

Distance between      Prototype      Pile type  
prototype pile      pile No.  
and monolith, ft

- |   |    |                       |
|---|----|-----------------------|
| 8 | 11 | H pile                |
| 7 | 12 | Open-ended pipe pile  |
| 7 | 13 | Close-ended pipe pile |

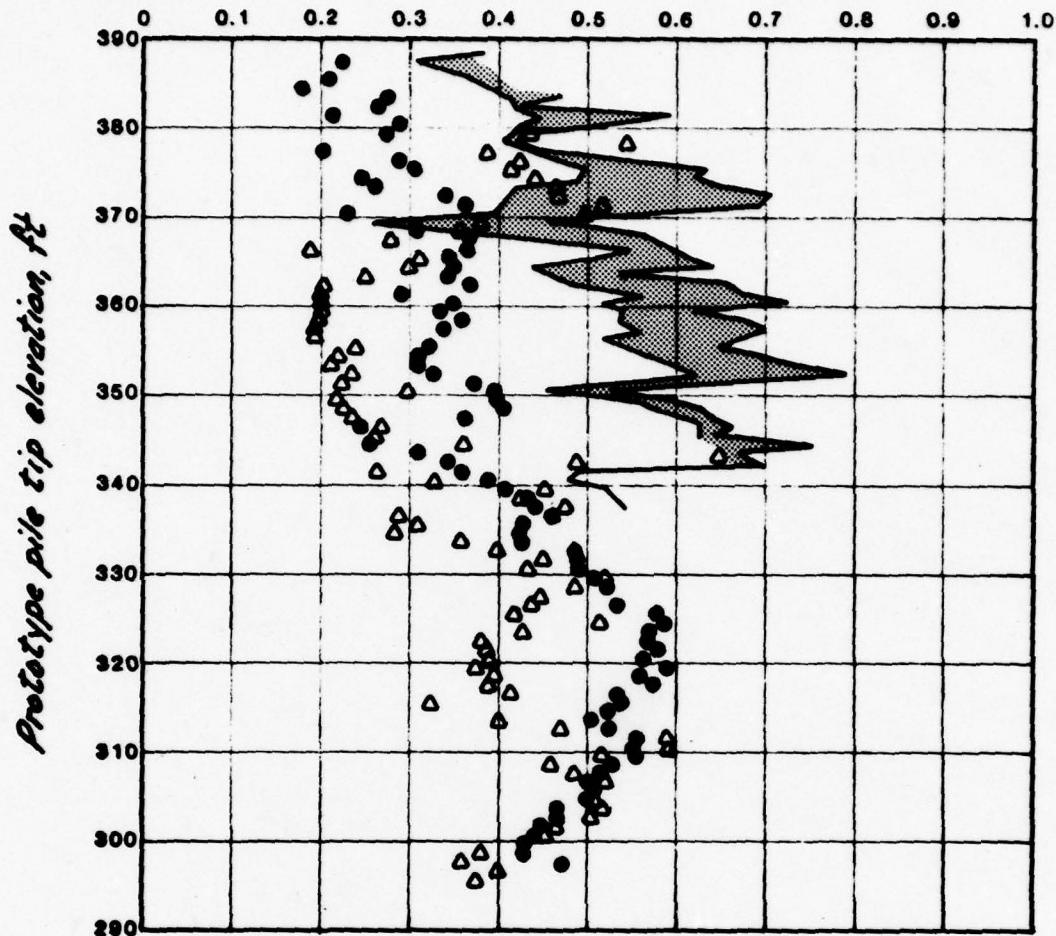
PILE DRIVING EFFECTS TEST PROGRAM  
SECONDARY PILE DRIVING SYSTEM,  
NEAR-SURFACE PARTICLE VELOCITY  
AT MONOLITH M1,  
AIR HAMMER

FOUNDATION INVESTIGATION AND TEST PROGRAM  
EXISTING LOCKS AND DAM NO. 28  
ST. LOUIS DISTRICT, CORPS OF ENGINEERS.  
DACP43-78-C-0000

Woodward-Clyde Consultants  
Y7C826 Phase II

Fig. 7.21

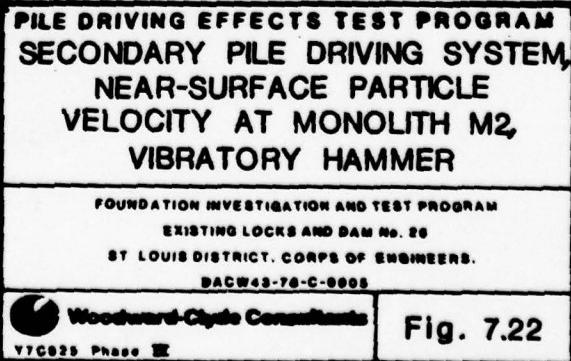
Near-surface peak vectorial particle velocity, in./s

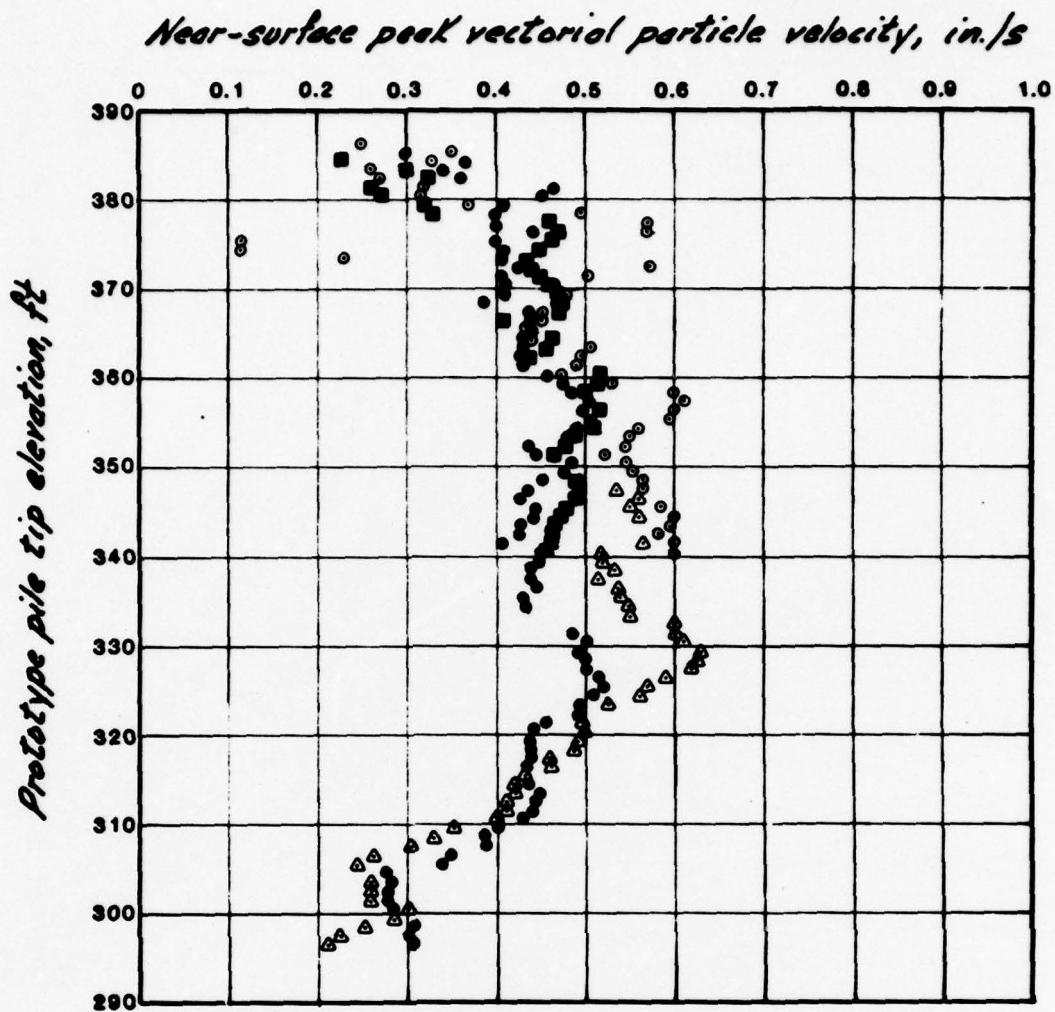


Foster 4000 (vibratory hammer)

Distance between prototype pile and monolith, ft	Prototype pile No.	Pile type
--	-----------------------	-----------

● 20.6	9	H pile
△ 15.4	10	H pile
■ 15	11,12	Sheet pile MPI02

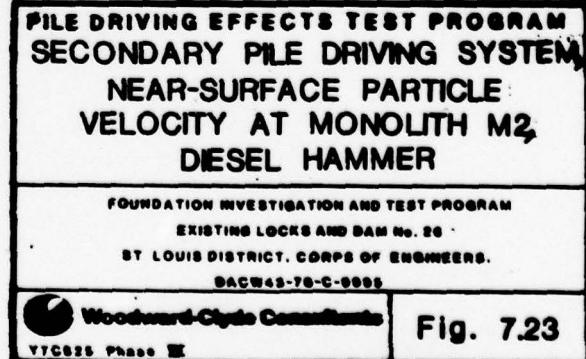




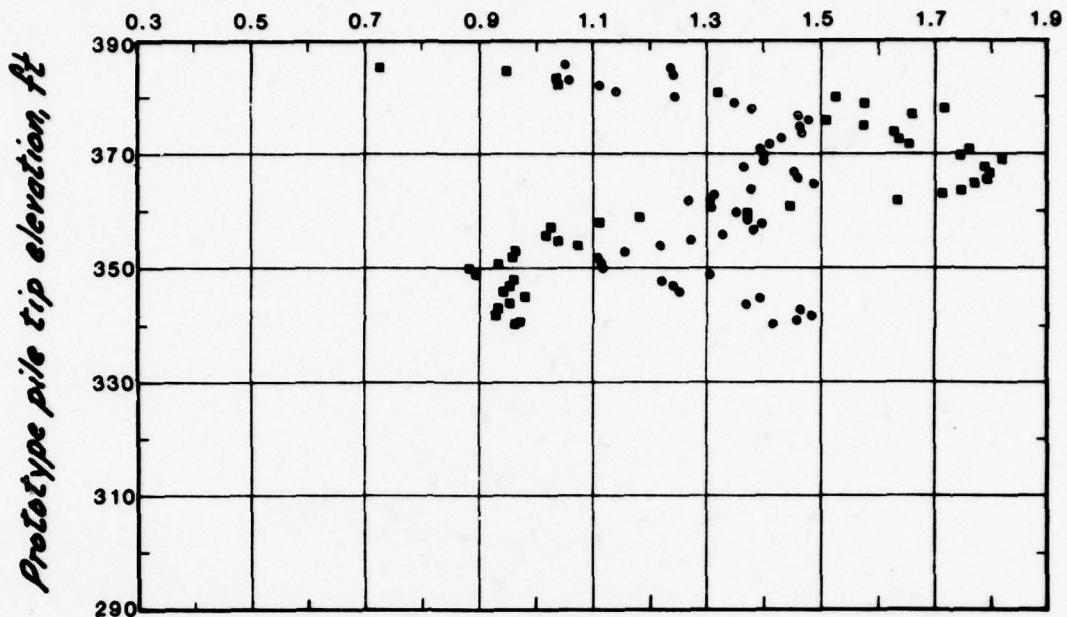
### MKT DE 70B (diesel hammer)

Distance between prototype pile and monolith, ft	Prototype pile No.	Pile type
--	-----------------------	-----------

- 20.6              7        H pile
- △ 14.9              8        H pile
- 10.4              13(T3)   H pile
- 11.7              14(T4)   Open-ended  
                        pipe pile



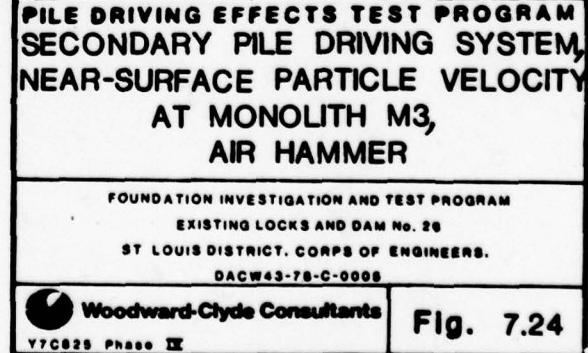
Near-surface peak vectorial particle velocity, in./s



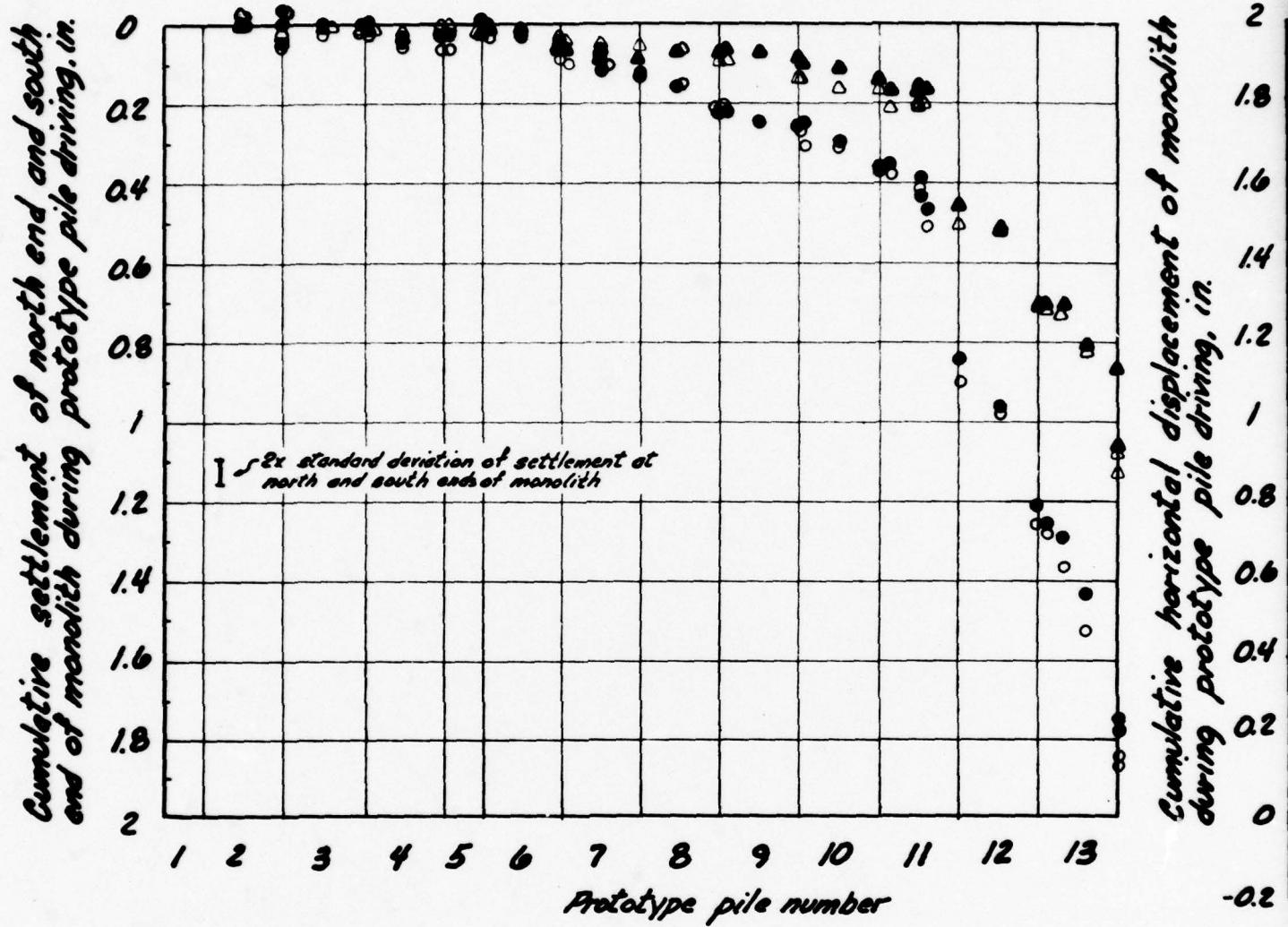
Vulcan O10 (air hammer)

Distance between prototype pile and monolith, ft      Prototype pile No.      Pile type

- 5.5      7(T5)      H pile
- 4.8      8(T6)      Open-ended pipe pile



(b) Cumulative settlement



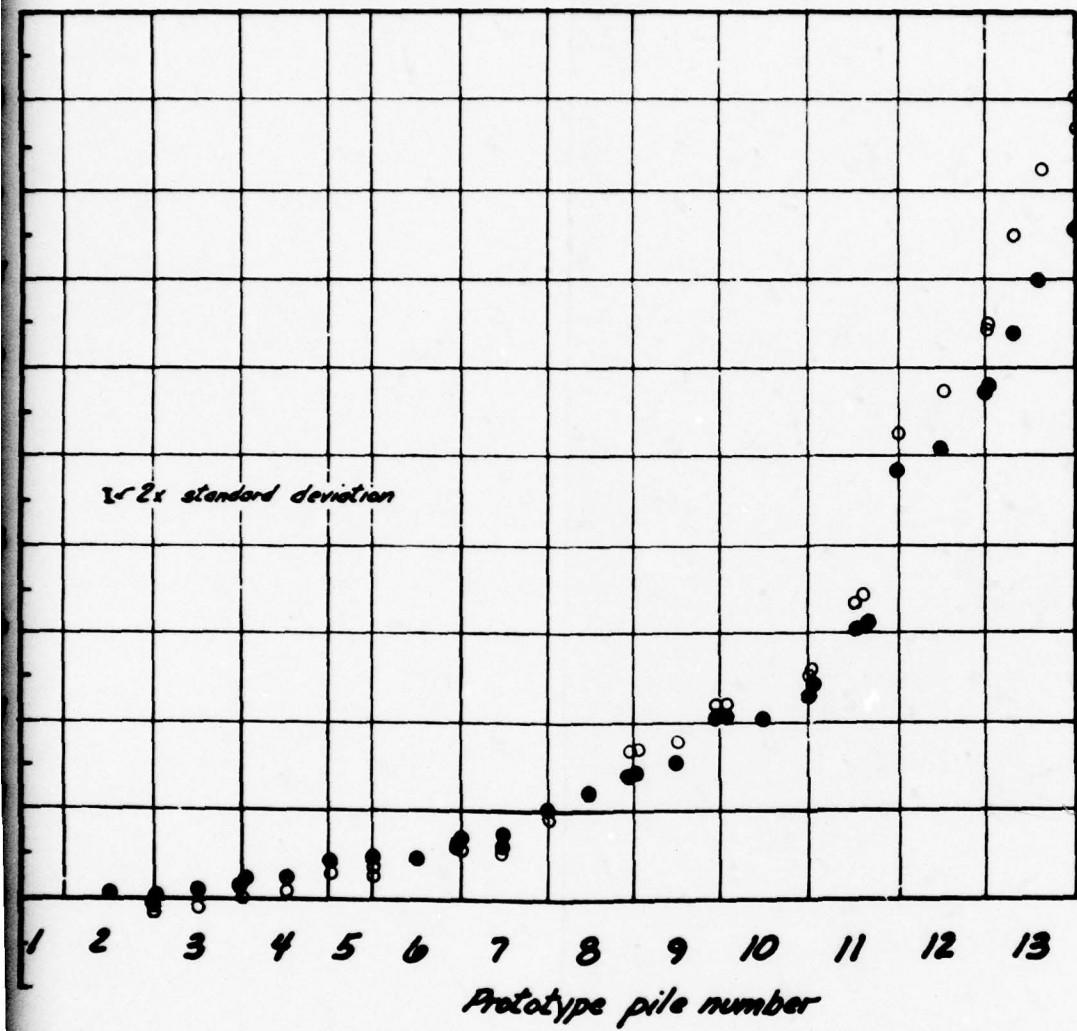
Legend

- Reference point data at north end of monolith
- Corrected linear potentiometer data at north end of monolith
- △ Reference point data at south end of monolith
- ▲ Corrected linear potentiometer data at south end of monolith

Note:

Location and type of prototype p system used are given in Fig. 7.1

(a) Cumulative horizontal displacement



Legend

- Reference point data
- Corrected linear potentiometer data

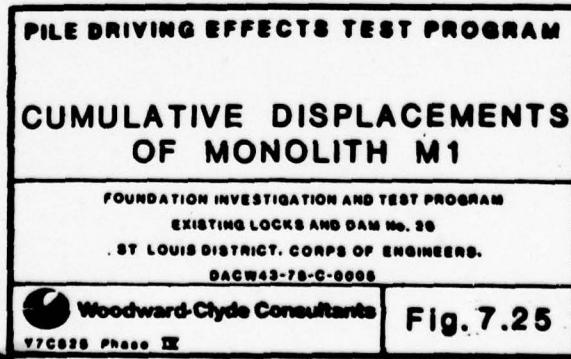
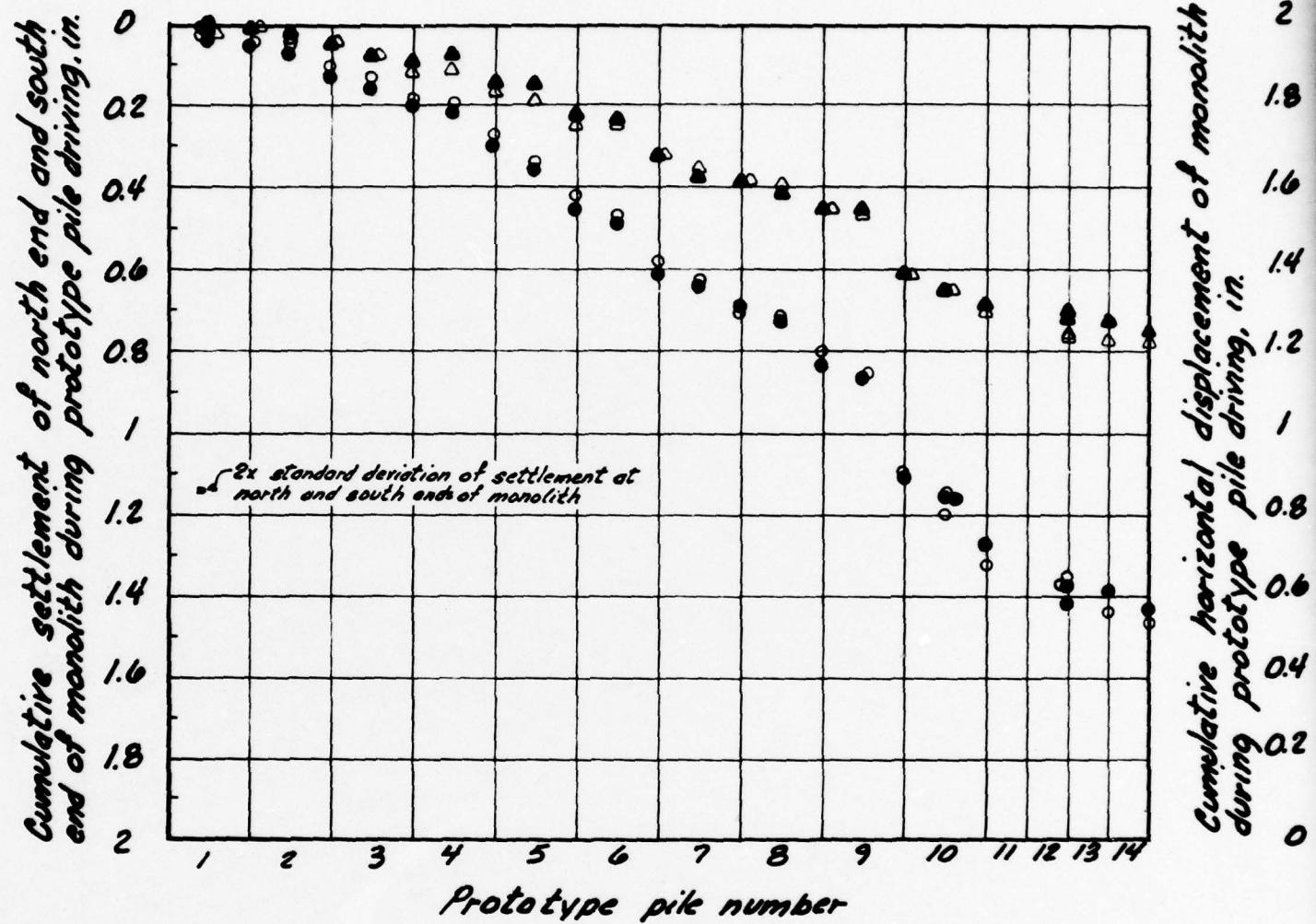


Fig. 7.25

pile, and pile driving

2

(b) Cumulative settlement



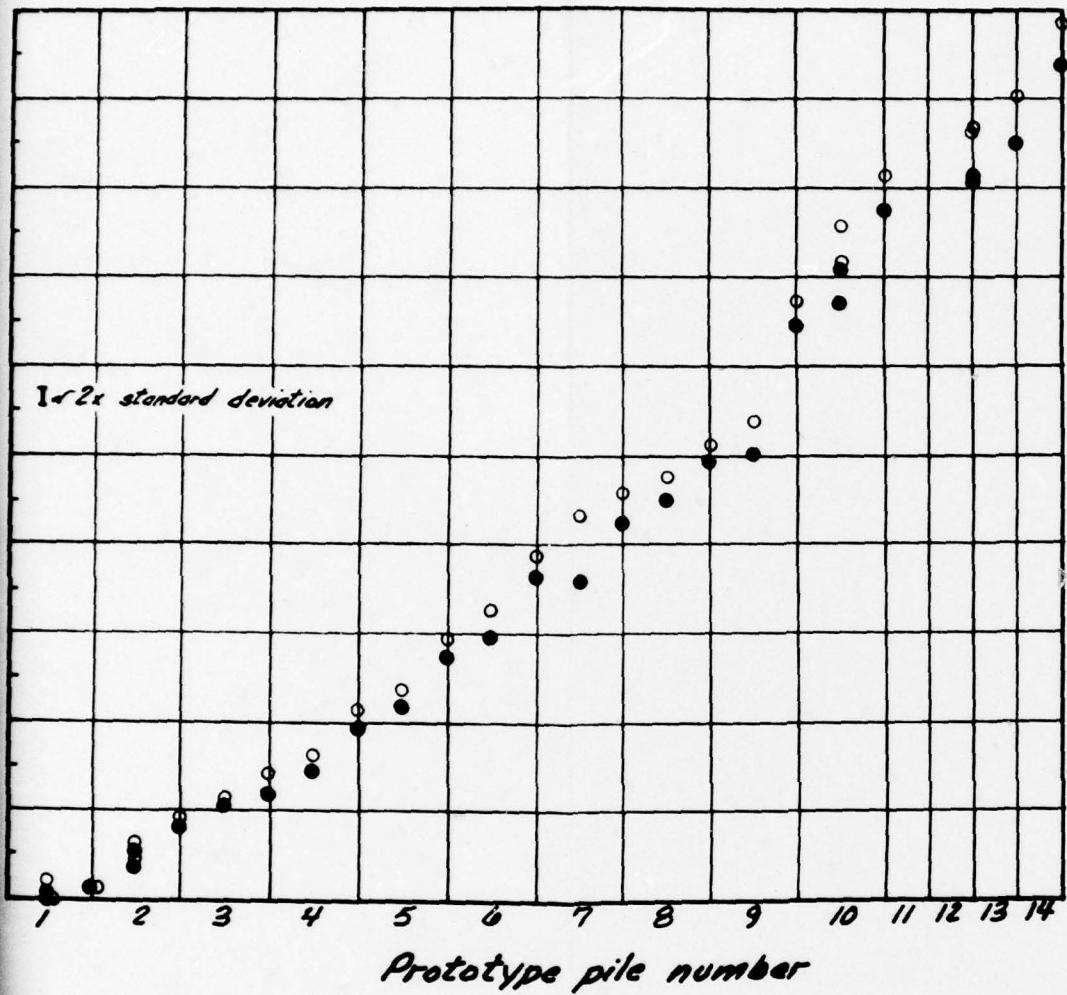
Legend

- Reference point data at north end of monolith
- Corrected linear potentiometer data at north end of monolith
- △ Reference point data at south end of monolith
- ▲ Corrected linear potentiometer data at south end of monolith

Note:

Location and type of prototype system used are given in Fig. 7.

(a) Cumulative horizontal displacement



Legend

- Reference point data
- Corrected linear potentiometer data

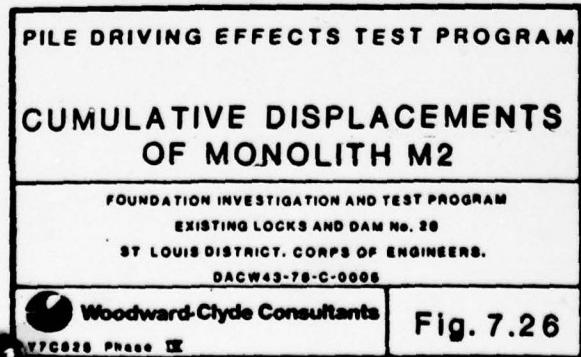


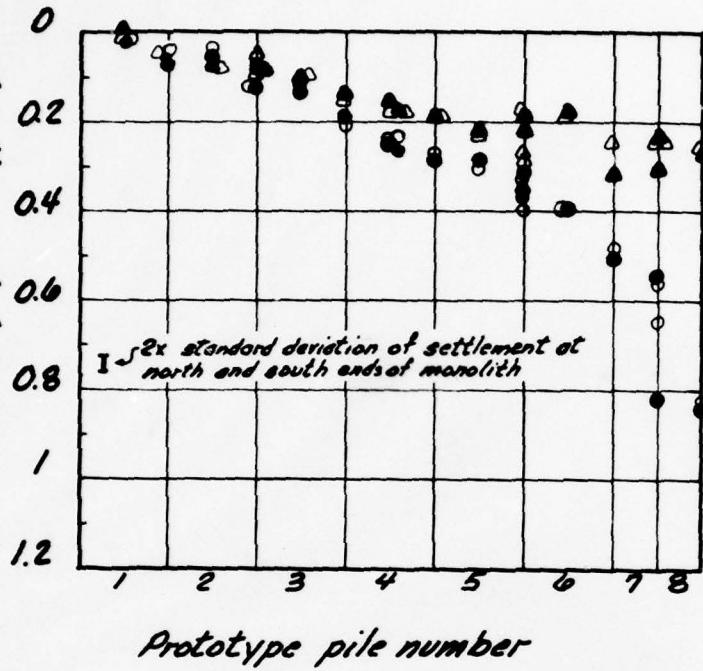
Fig. 7.26

pile, and pile driving

2

Cumulative settlement of north end and south end of monolith during prototype pile driving, in.

(b) Cumulative settlement



Legend

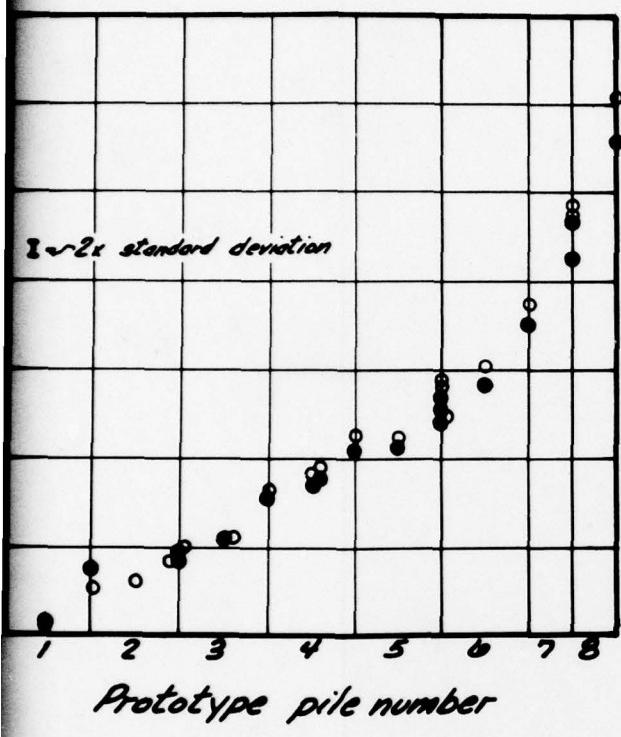
- Reference point data at north end of monolith
- Corrected linear potentiometer data at north end of monolith
- △ Reference point data at south end of monolith
- ▲ Corrected linear potentiometer data at south end of monolith

Note:

Location and type of prototype pile, and system used are given in Fig. 7.3

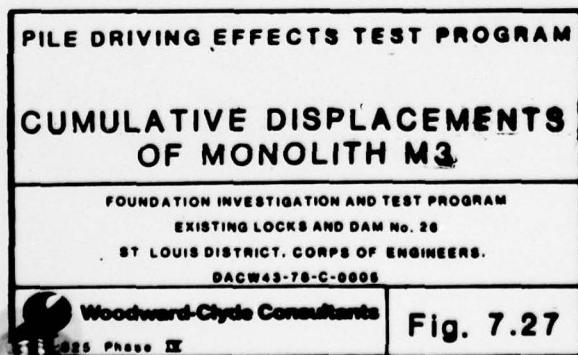
Cumulative horizontal displacement of monolith during prototype pile driving, in.

## Cumulative horizontal displacement



### Legend

- Reference point data
- Corrected linear potentiometer data



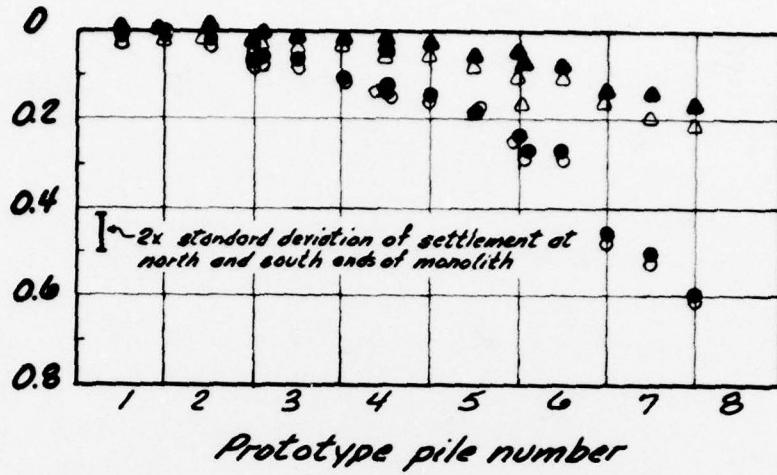
pile driving

2

Cumulative horizontal displacement of monolith during prototype pile driving, in.

(b) Cumulative settlement

Cumulative settlement of north end and south end of monolith during prototype pile driving, in.



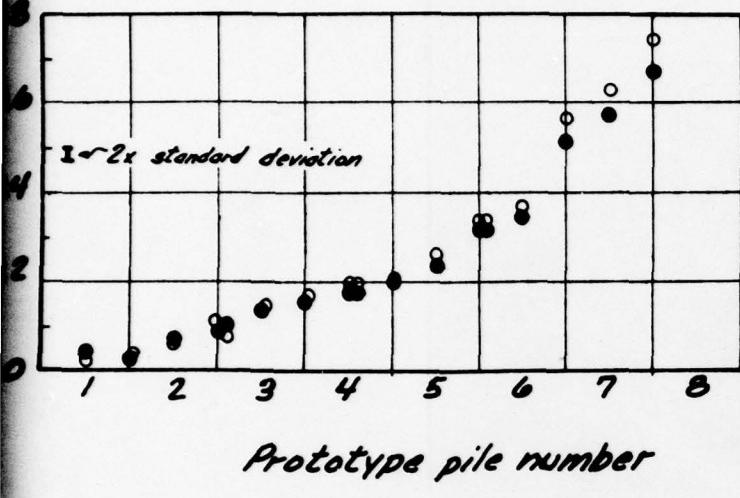
Legend

- Reference point data at north end of monolith
- Corrected linear potentiometer data at north end of monolith
- △ Reference point data at south end of monolith
- ▲ Corrected linear potentiometer data at south end of monolith

Note:

Location and type of prototype pile system used are given in Fig. 7.4

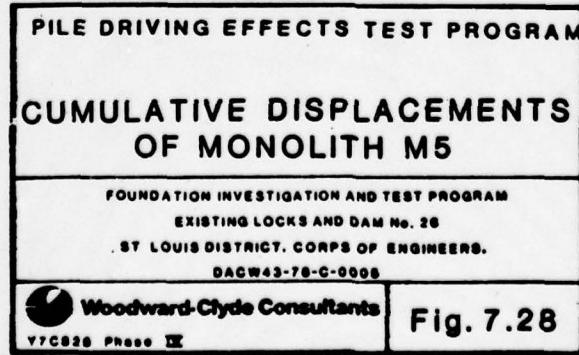
(a) Cumulative horizontal displacement



Prototype pile number

Legend

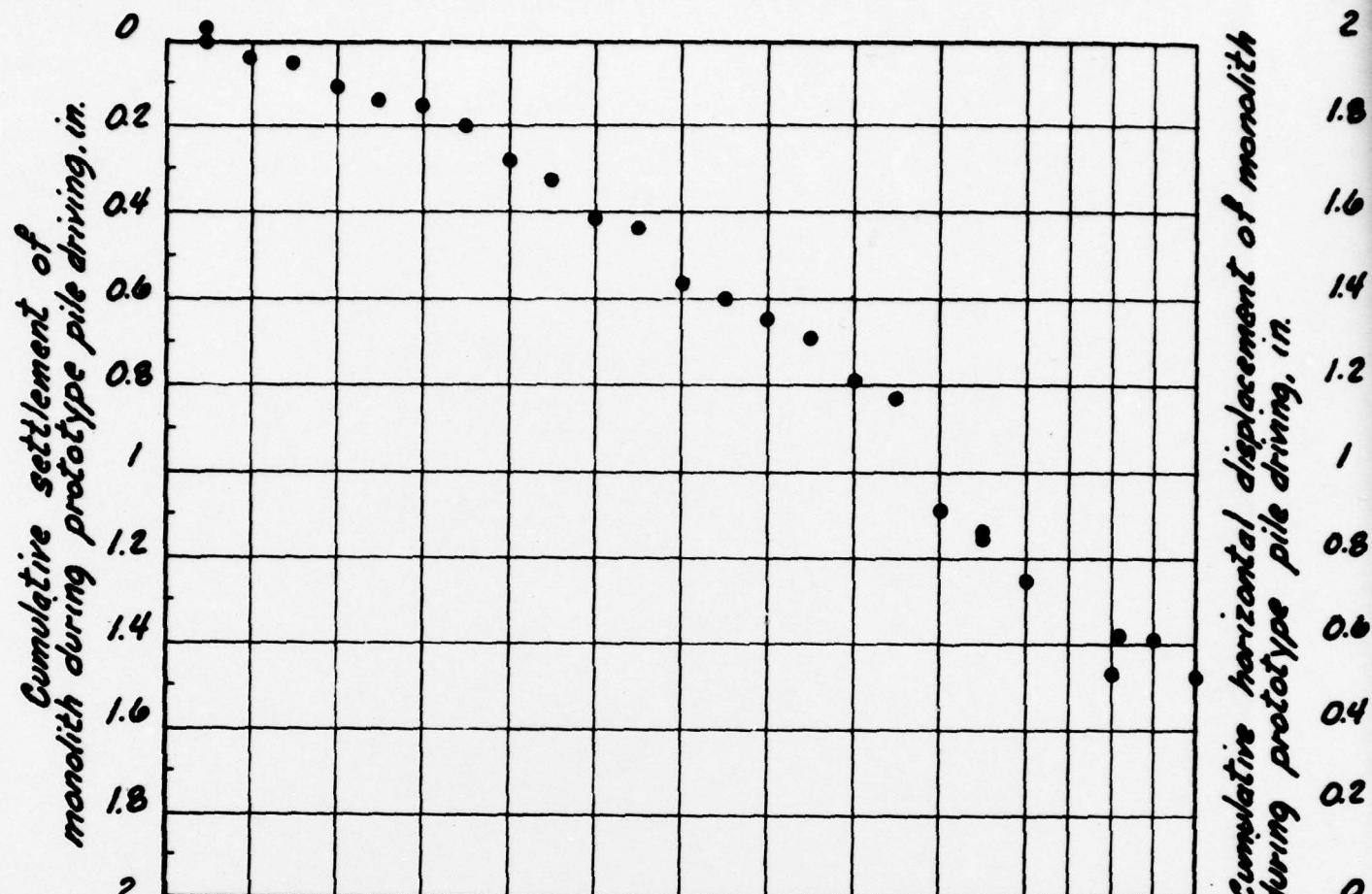
- Reference point data
- Corrected linear potentiometer data



and pile driving

Z

(b) Cumulative settlement

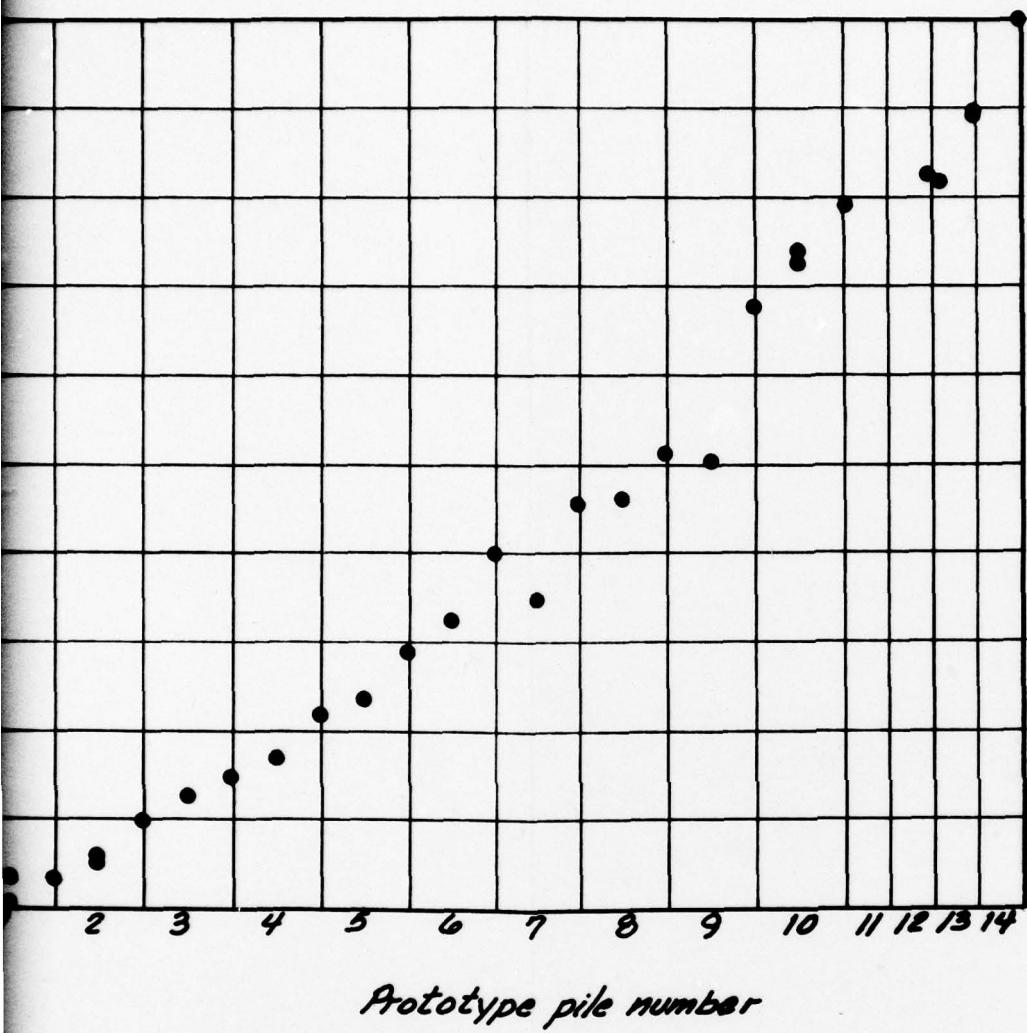


Legend  
• Corrected linear potentiometer data

Notes:

- (1) Horizontal displacement measured at 33 in. above ground surface
- (2) Settlement measured at 33 in. above ground surface
- (3) Location and type of prototype pile, and pile driving system used are given in Fig. 7.

(a) Cumulative horizontal displacement



Prototype pile number

Legend

• Corrected linear potentiometer  
data

measured  
distance  
13 in.

prototype  
item

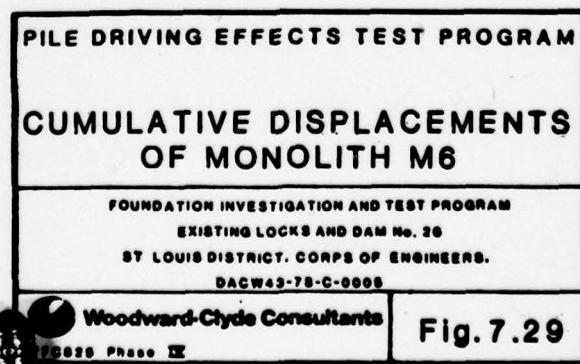
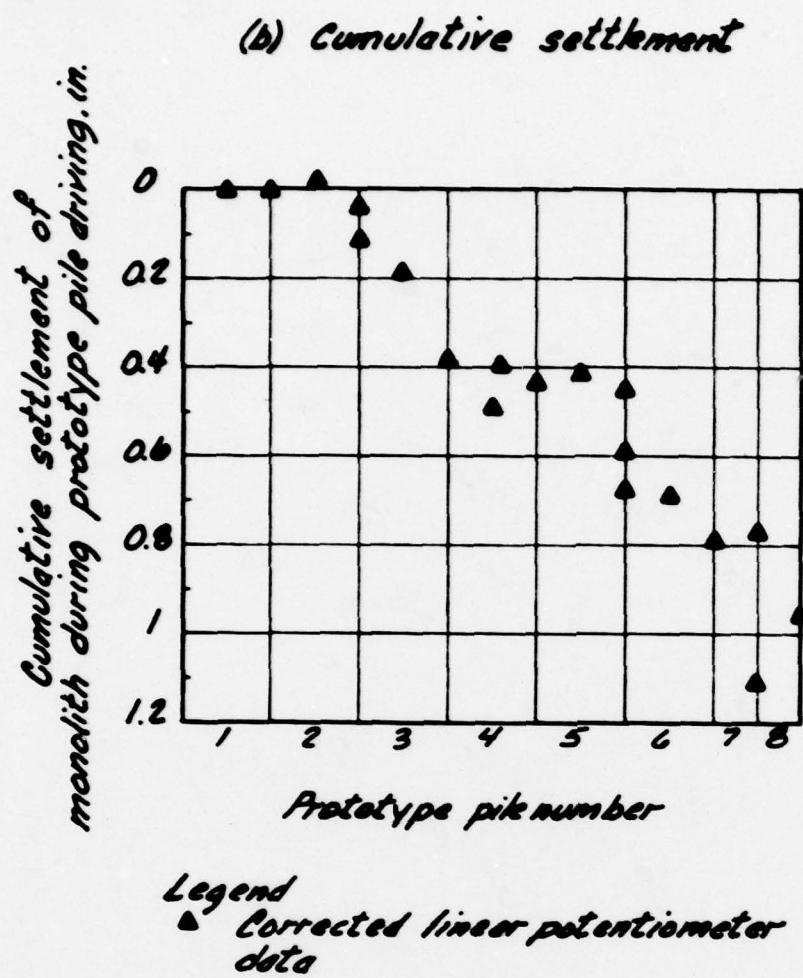


Fig. 7.29

2

Cumulative horizontal displacement of monolith during prototype pile driving. in.

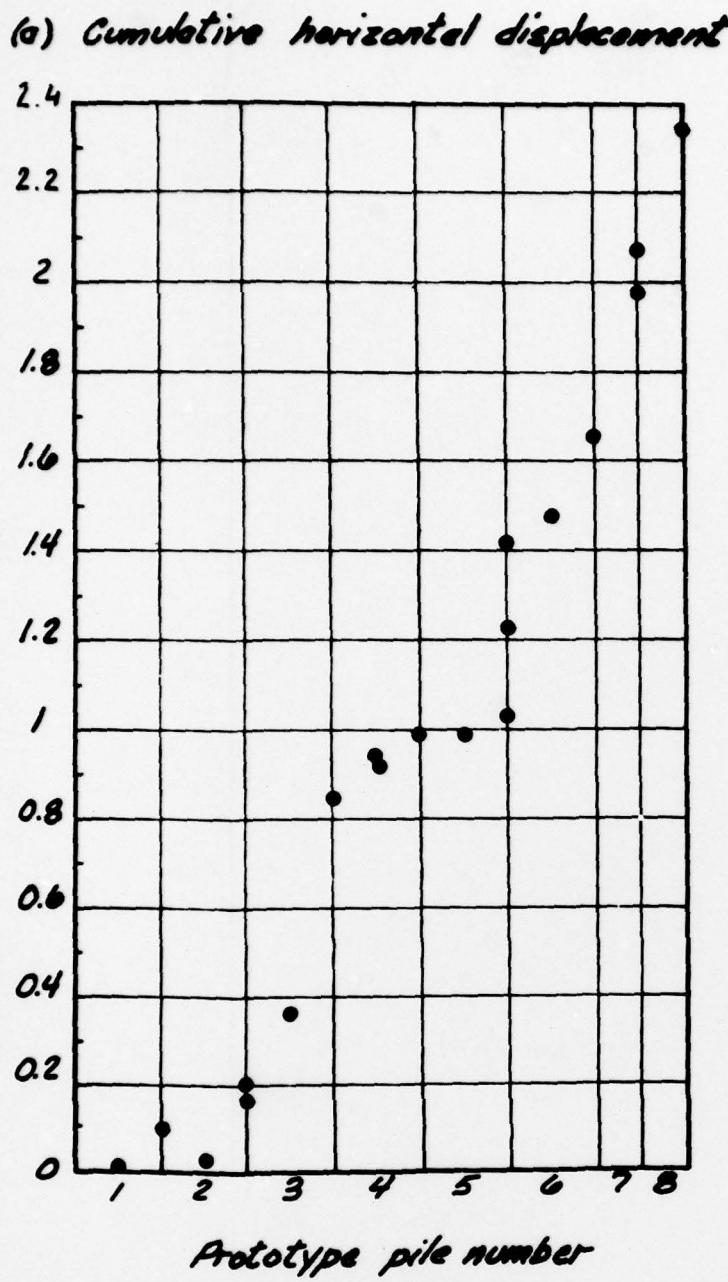


Legend  
▲ Corrected linear potentiometer data

Notes:

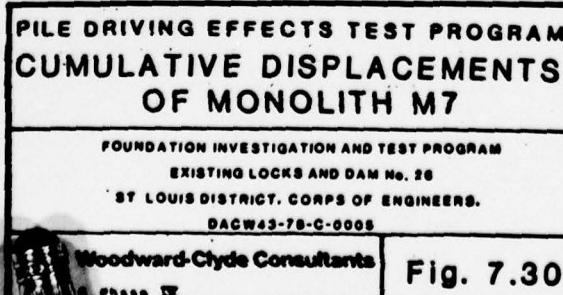
- (1) Horizontal displacement measured at 31 in. above ground surface
- (2) Settlement measured at 7 in. above ground surface
- (3) Location and type of prototype pile, and pile driving system used are given in Fig. 7.3

*Cumulative horizontal displacement or monolith  
during prototype pile driving, in.*

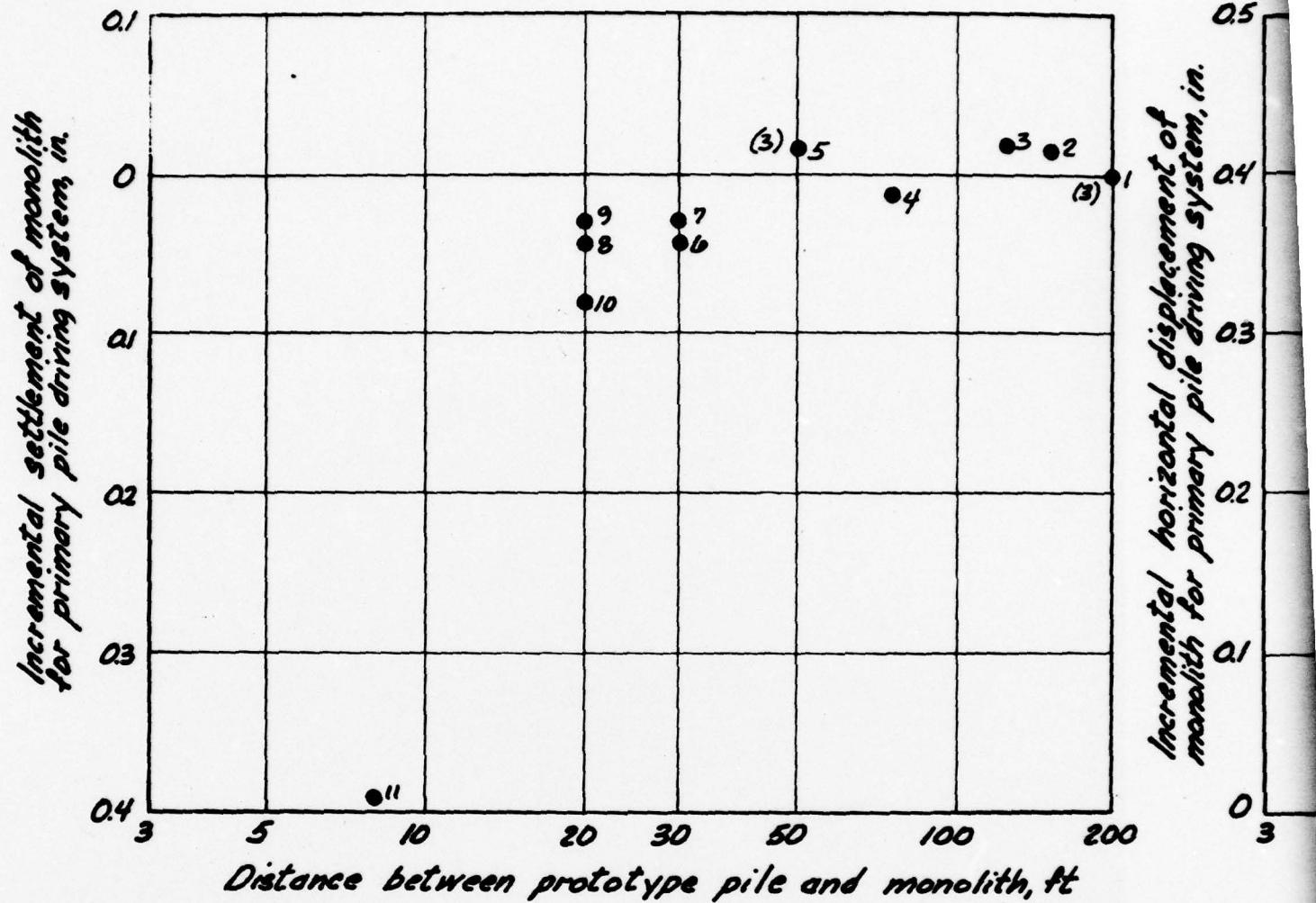


Legend

- Corrected linear potentiometer data



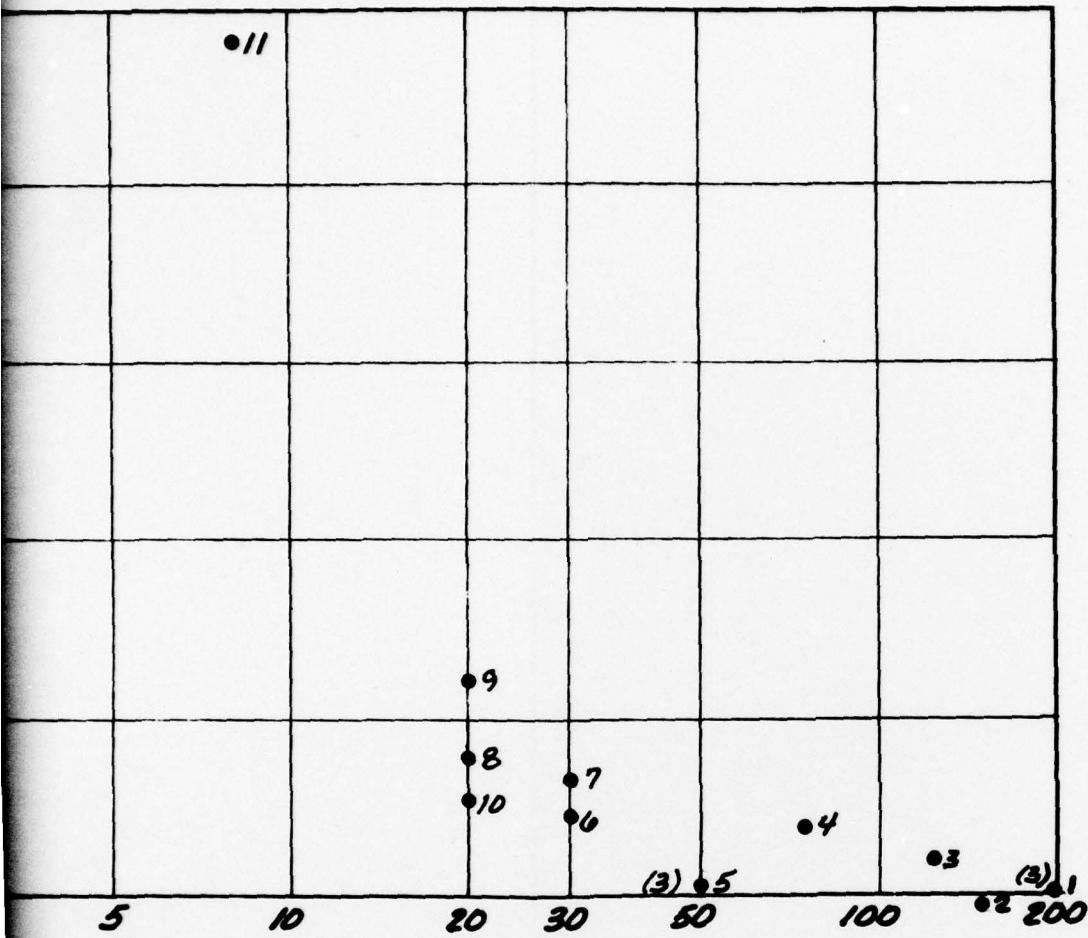
(b) Incremental settlement



Notes:

- (1) Incremental displacements of monolith on corrected linear potential
- (2) Primary pile driving system was a combination of Vulcan O10 and H
- (3) Prototype pile driven to a depth of
- (4) Number on right side of symbol represents pile number

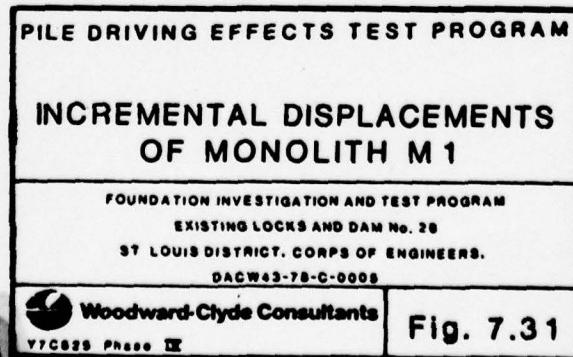
(a) Incremental horizontal displacement



Distance between prototype pile and monolith, ft

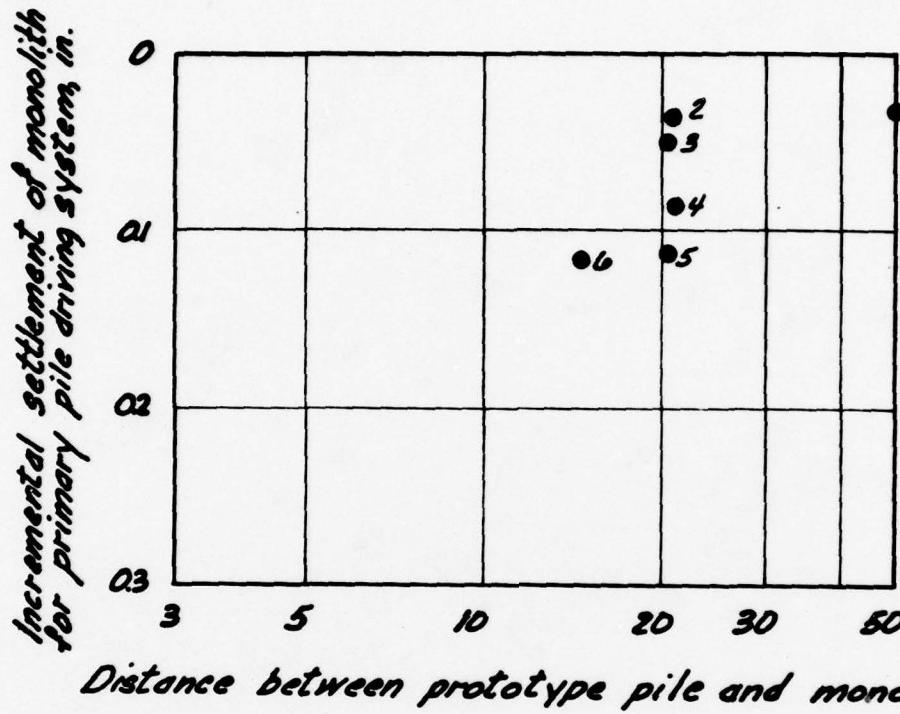
monolith are based  
meter data

HP 14x73  
at 50 ft approximately  
represents prototype



2

(b) Incremental settlement

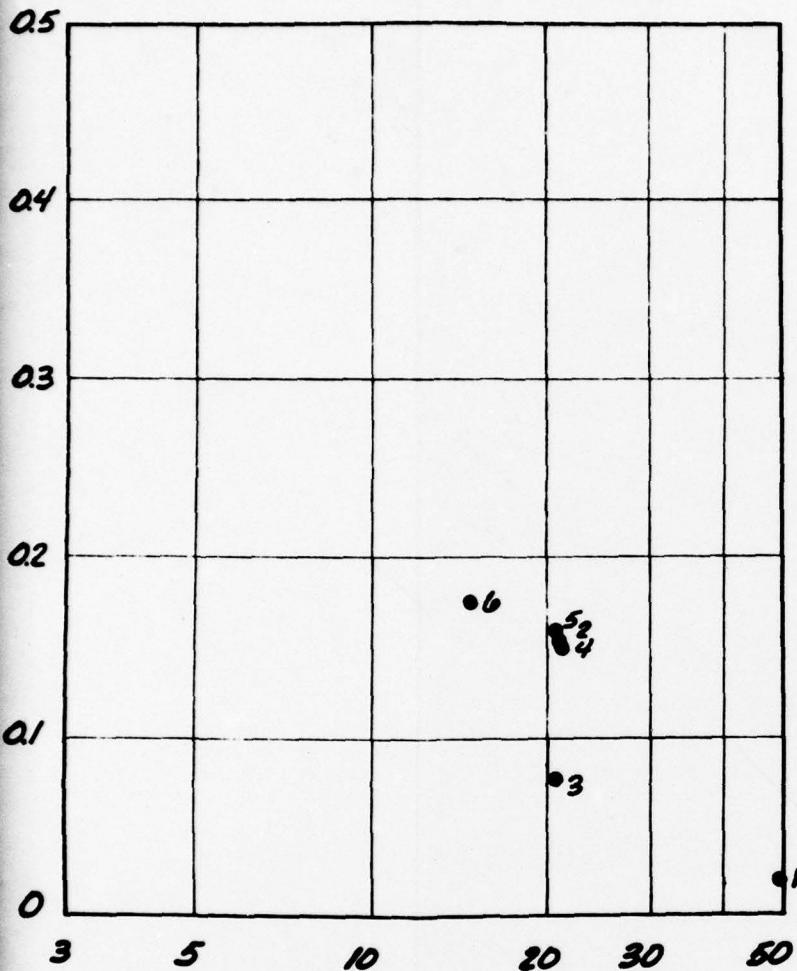


Incremental horizontal displacement of  
monolith for primary pile driving system, in.

Notes:

- (1) Incremental displacements of monolith on corrected linear potentiometer
- (2) Primary pile driving system was a combination of Vulcan O10 and HD 14
- (3) Number on right side of symbol represents prototype pile number

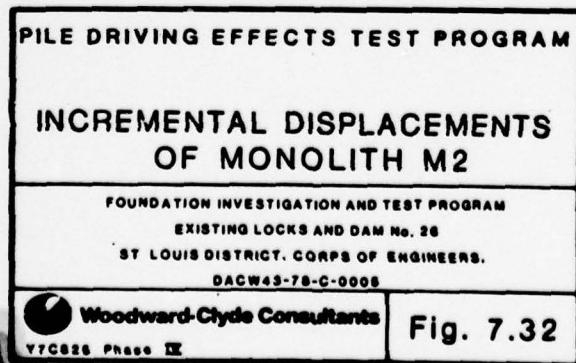
(a) Incremental horizontal displacement



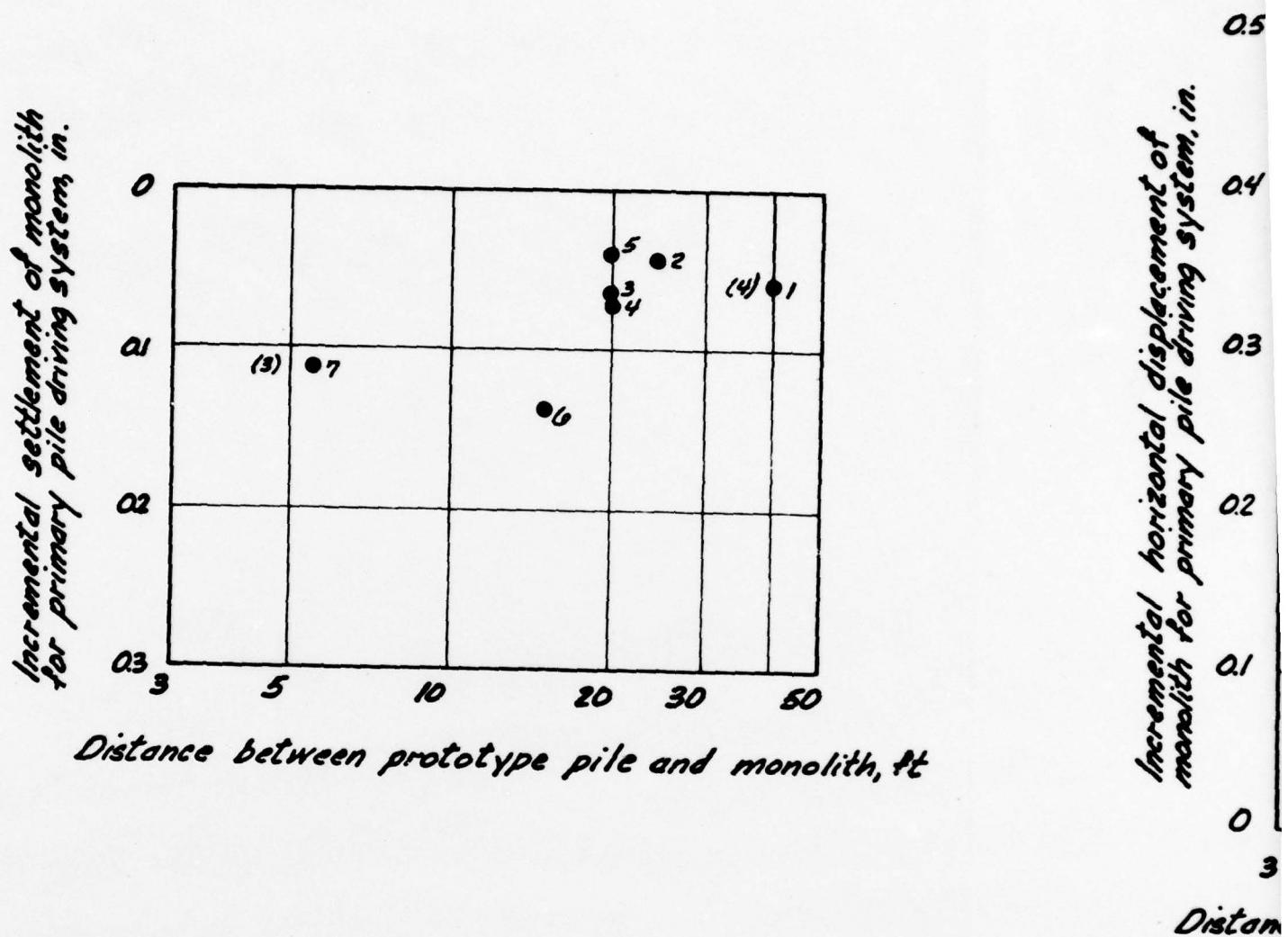
istance between prototype pile and monolith, ft

ith are based  
data

'x73  
ent's



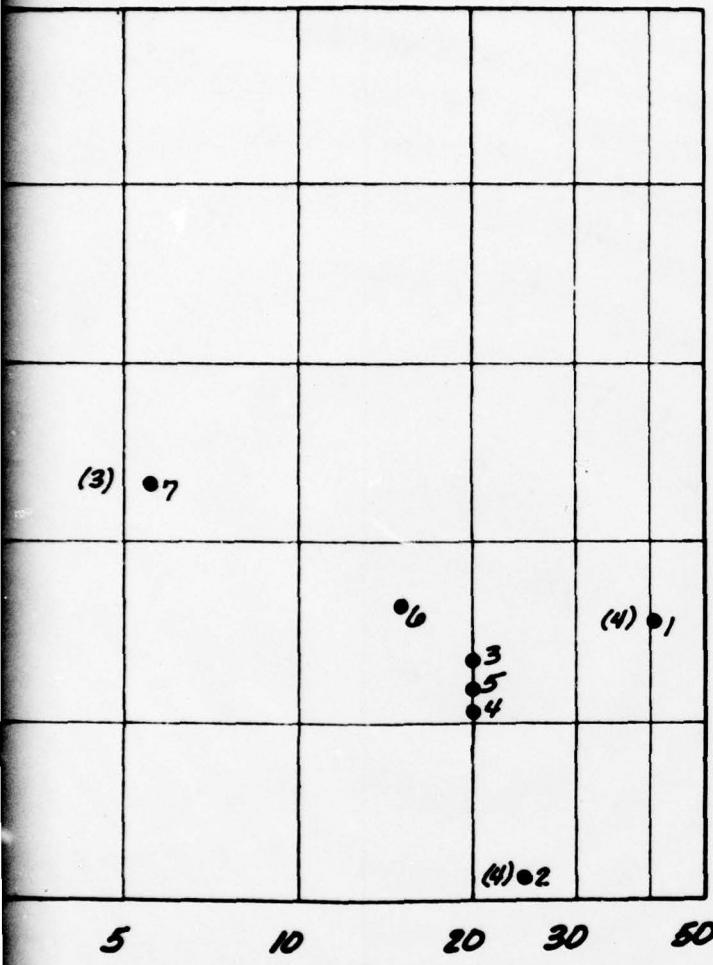
(b) Incremental settlement



Notes:

- (1) Incremental displacements of monolith on corrected linear potentiometer
- (2) Primary pile driving system was a combination of Vulcan O10 and HP 14X
- (3) Prototype pile driven to a depth of 50 ft
- (4) Questionable data
- (5) Number on right side of symbol represents prototype pile number

## Incremental horizontal displacement

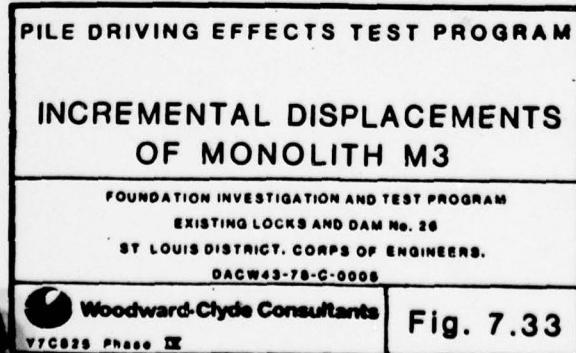


displacement between prototype pile and monolith, ft

are based  
to

3  
approximately

ments



2

AD-A076 093

WOODWARD-CLYDE CONSULTANTS CHICAGO IL

F/G 13/2

RESULTS AND INTERPRETATION OF PILE DRIVING EFFECTS TEST PROGRAM--ETCIL

DACW43-78-C-0005

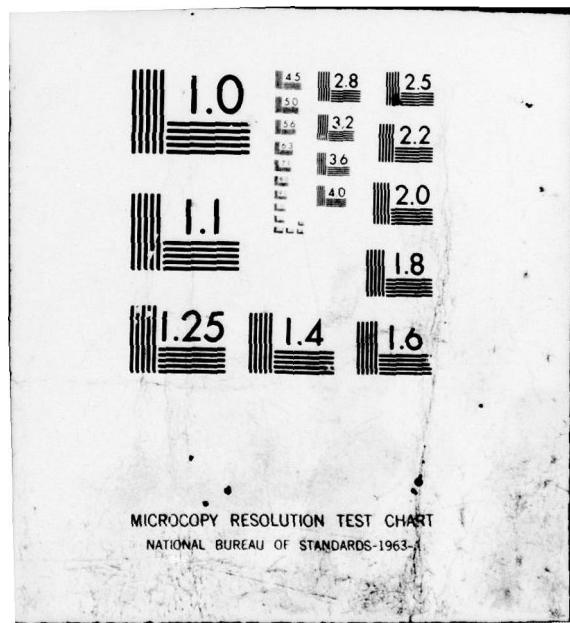
JUL 79 J PEREZ , D M HOLLOWAY

NL

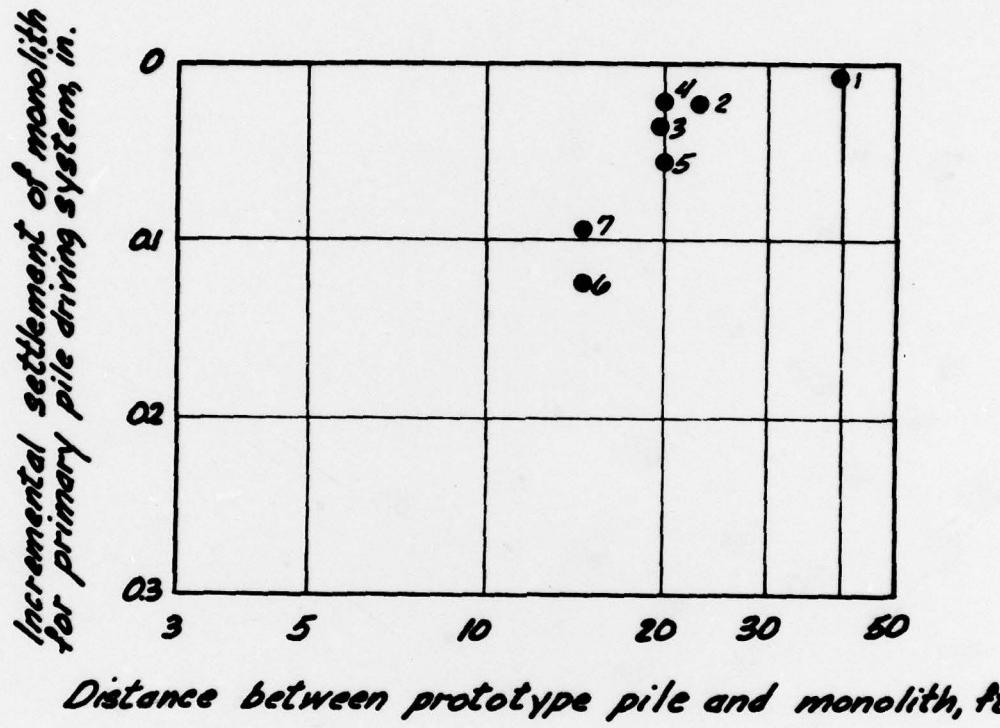
UNCLASSIFIED

4 OF 5  
AD  
A076093





(b) Incremental settlement

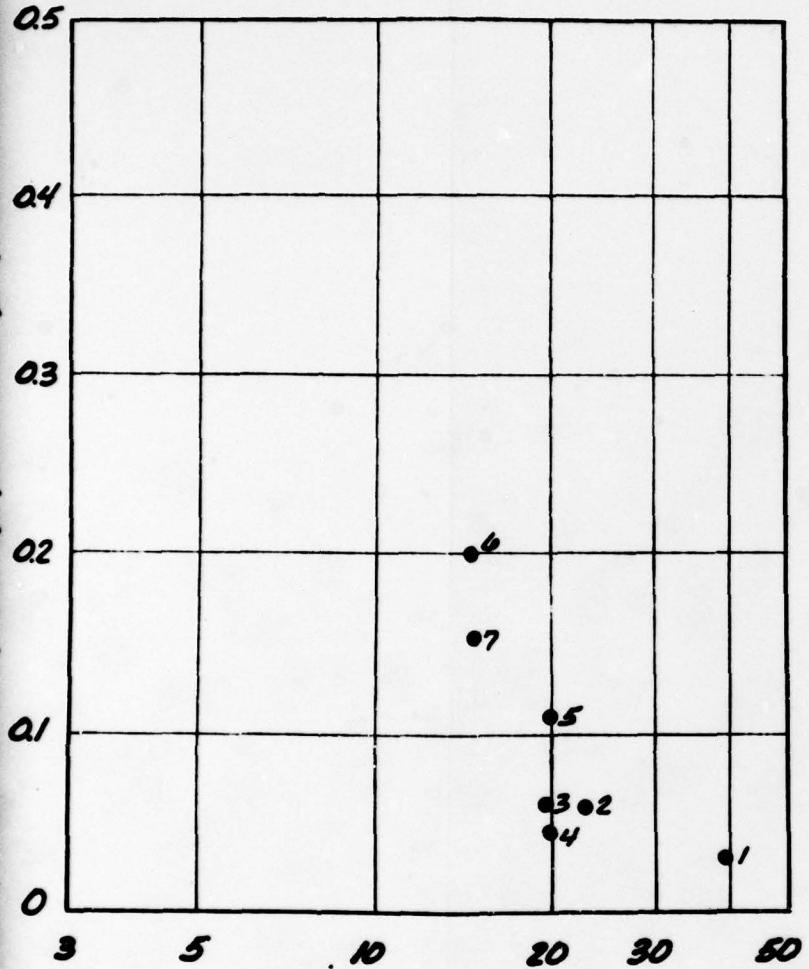


Notes:

- (1) Incremental displacements of monolith on corrected linear potentiometer
- (2) Primary pile driving system was a combination of Vulcan O10 and HD 10
- (3) Number on right side of symbol represents prototype pile number

Incremental horizontal displacement of monolith for primary pile driving system:

(a) Incremental horizontal displacement

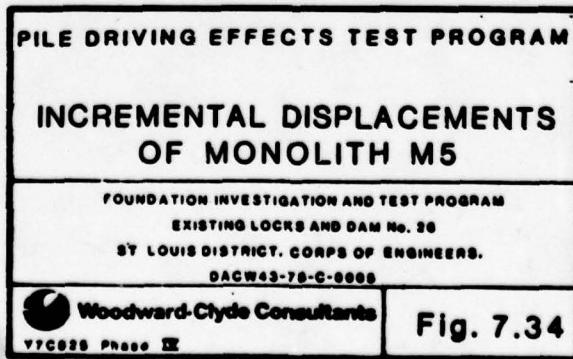


Distance between prototype pile and monolith, ft

lith are based  
or data

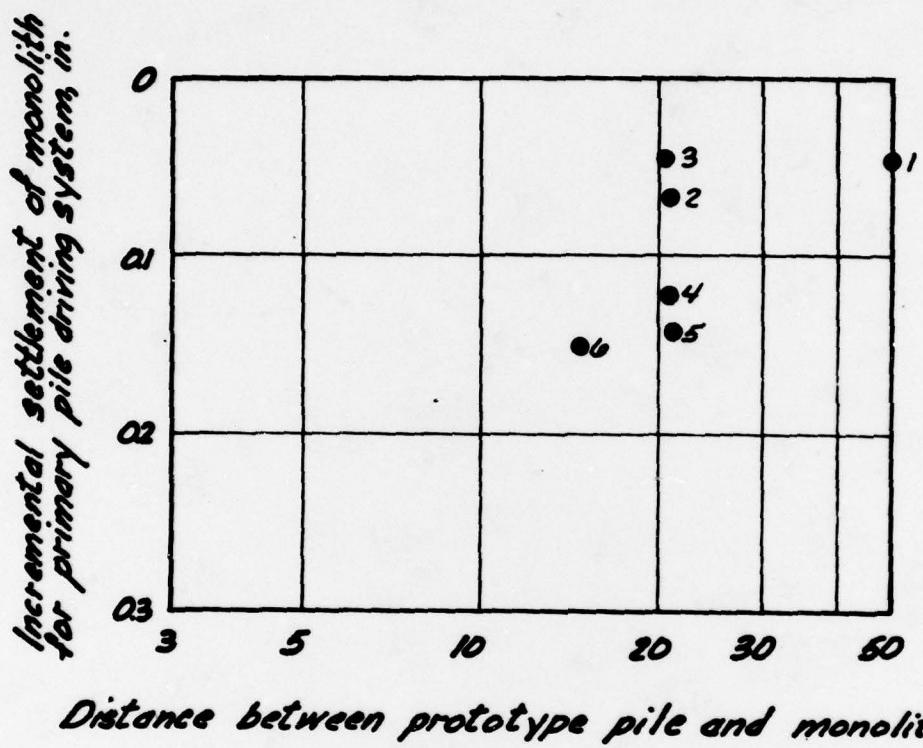
4x73

recent's



J

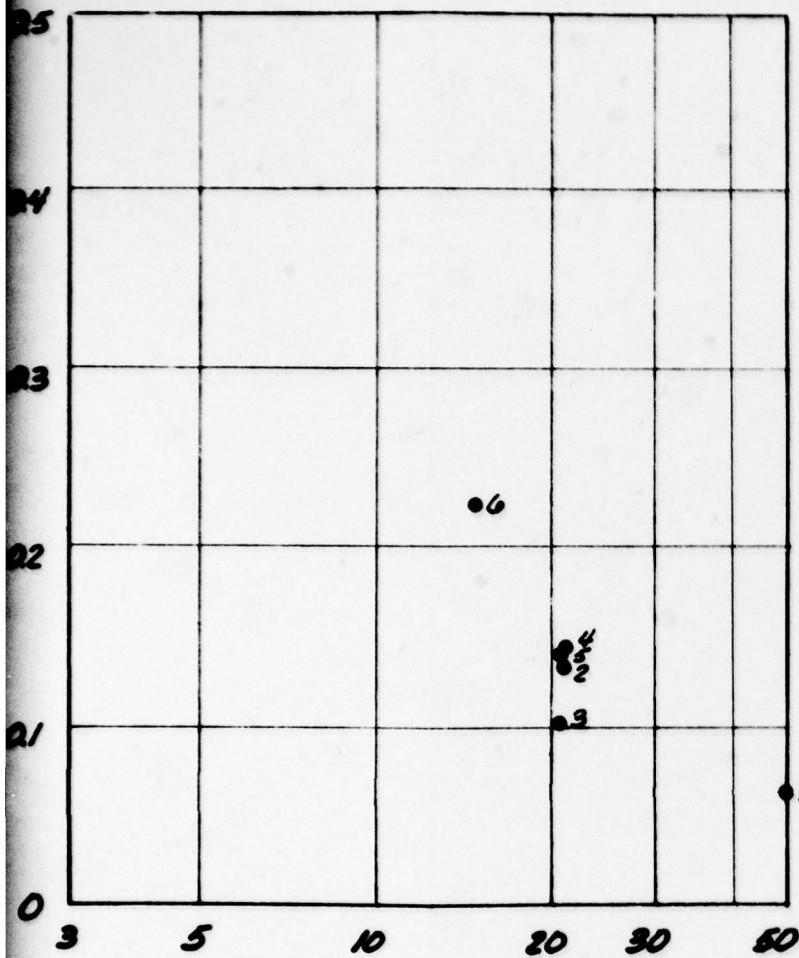
(b) Incremental settlement



Notes:

- (1) Incremental displacements of monoliths measured on corrected linear potentiometer
- (2) Primary pile driving system was a combination of Vulcan O10 and HP M
- (3) Number on right side of symbol represents prototype pile number

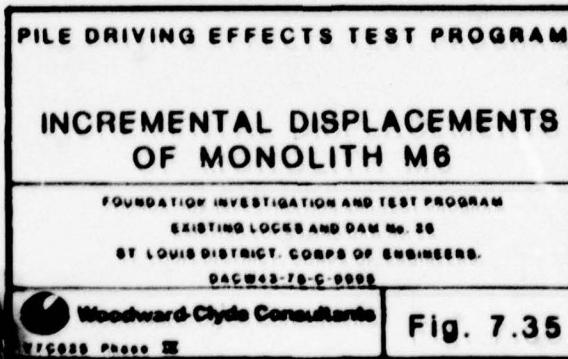
(a) Incremental horizontal displacement



istance between prototype pile and monolith, ft

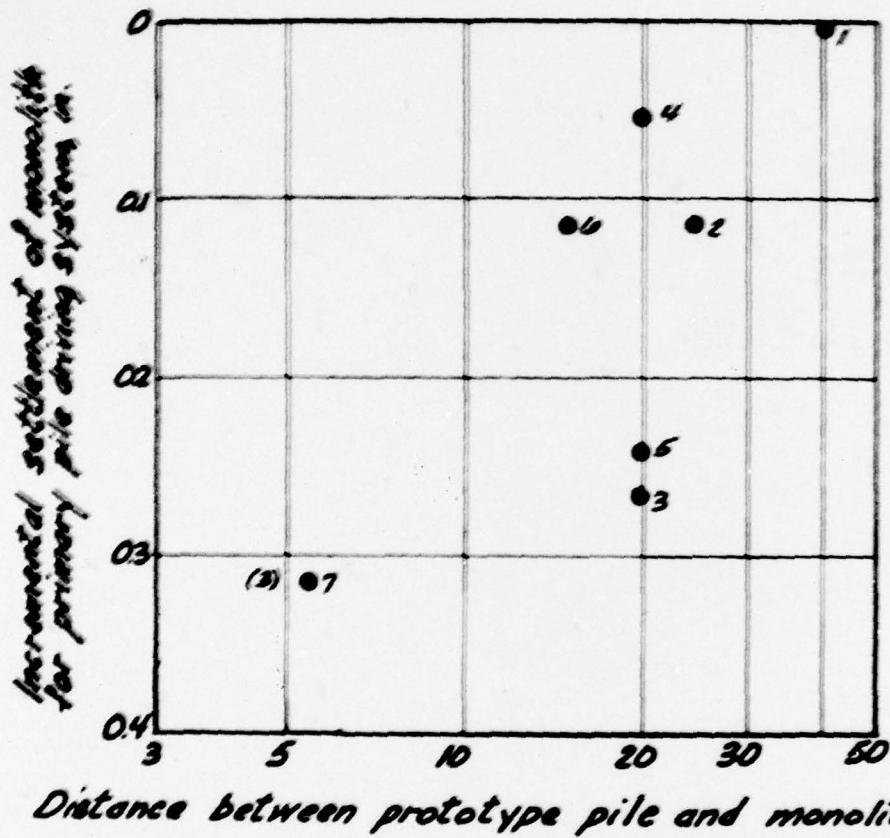
monolith are based  
for data

14x73  
recently



2

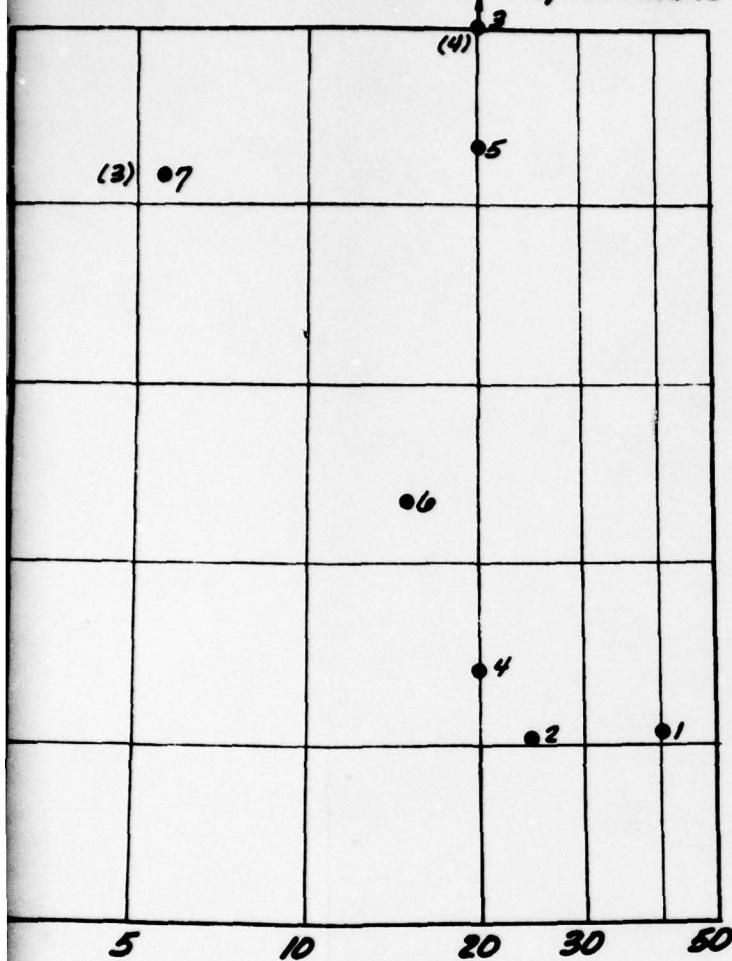
(b) Incremental settlement



Notes:

- (1) Incremental displacements of monolith on corrected linear potentiometer
- (2) Primary pile driving system was a combination of Vulcan O10 and HP 14x7
- (3) Prototype pile driven to a depth of 50 ft
- (4) Questionable data
- (5) Number on right side of symbol represents prototype pile number

6) Incremental horizontal displacement

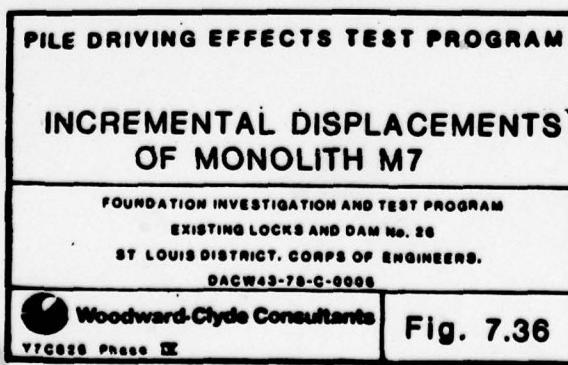


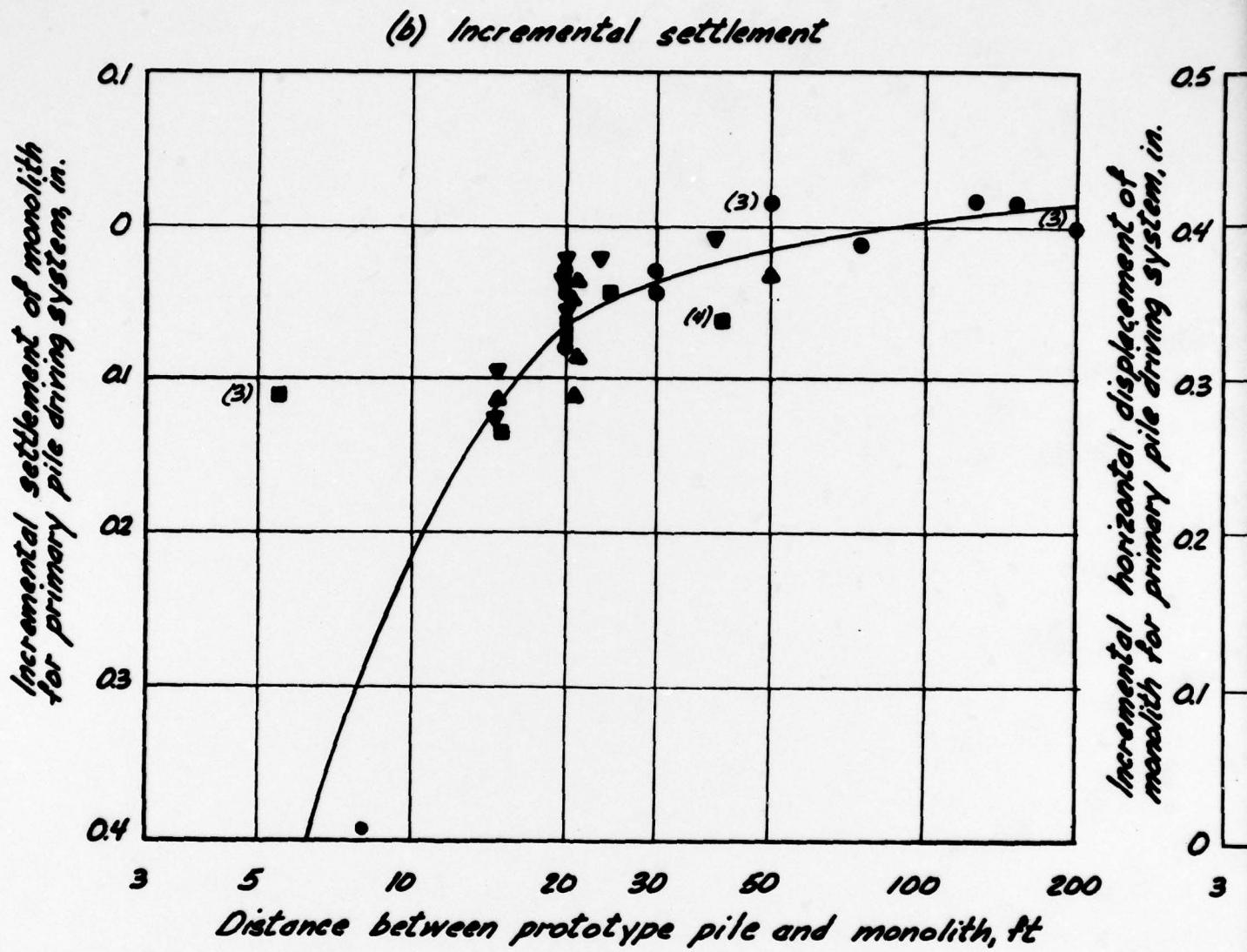
se between prototype pile and monolith, At

are based  
to

3  
approximately

sents

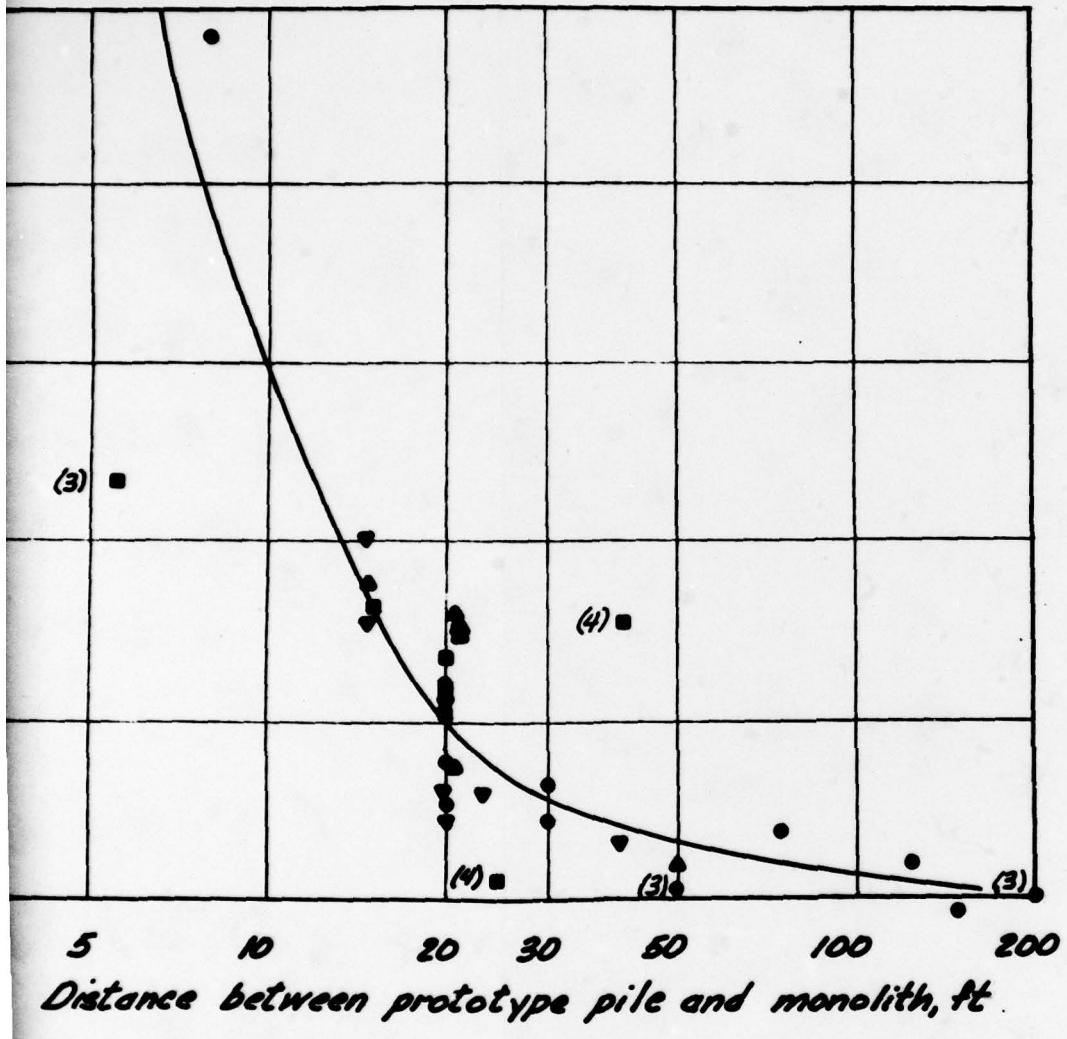




Notes:

- (1) Incremental displacements of a  
on corrected linear potential
- (2) Primary pile driving system was a  
combination of Vulcan 010 and
- (3) Prototype pile driven to a depth of
- (4) Questionable data

(a) Incremental horizontal displacement

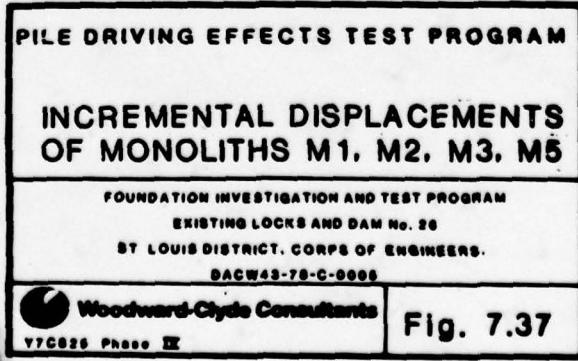


Distance between prototype pile and monolith, ft.

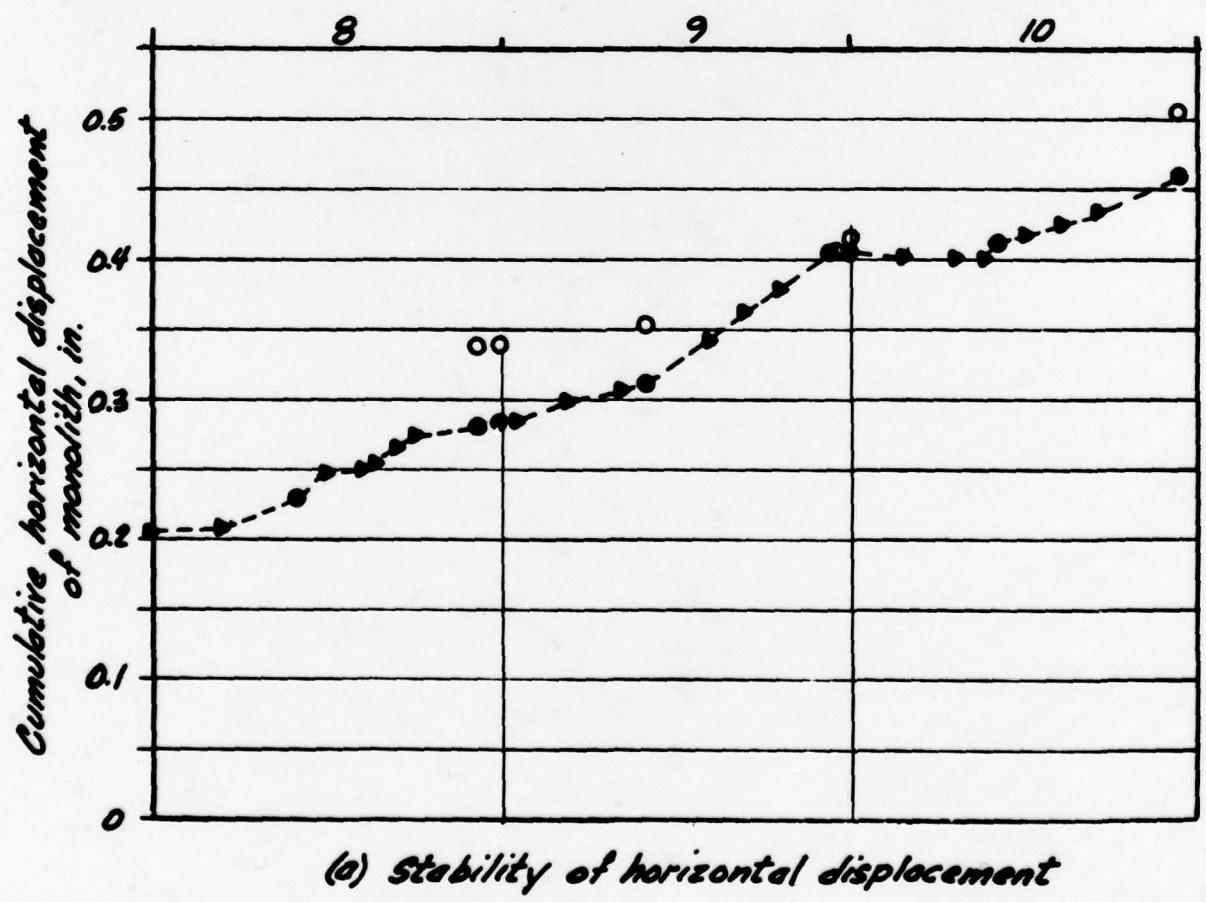
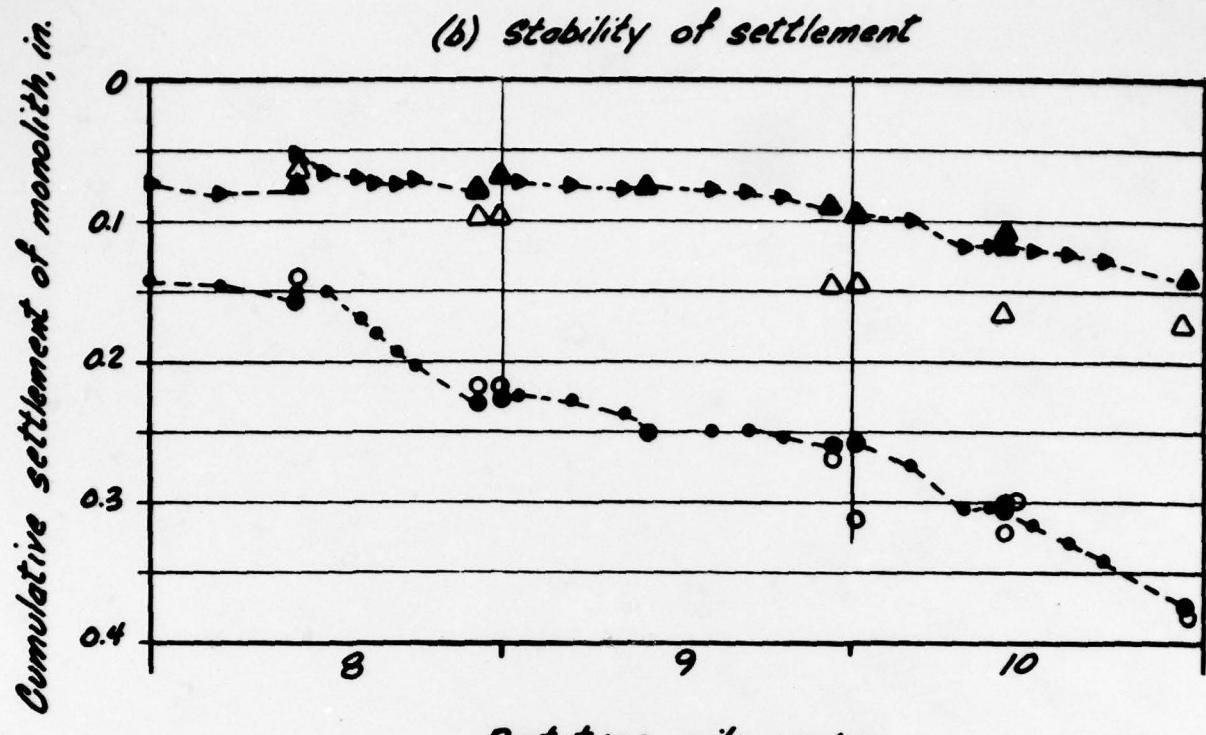
monolith are based  
meter data

HP 14x73

of 50 ft approximately



2



(c) Stability of horizontal displacement

Note:  
Successive piles  
from a  
pile driver  
(Vulcan)

arth end  
monolith

Legend

At south end  
of monolith

- Reference point data
- Linear potentiometer data corrected for measured reference beam displacement
- Linear potentiometer data corrected for interpolated reference beam displacement

△

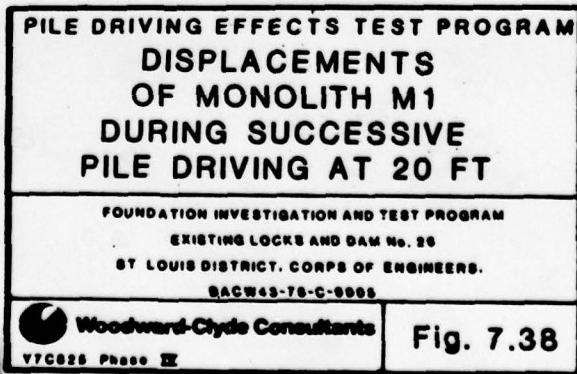
▲

►

Legend

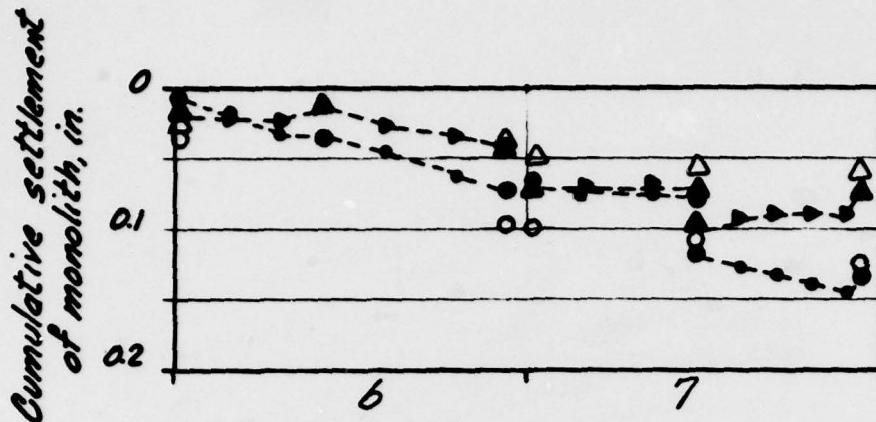
- Reference point data
- Linear potentiometer data corrected for measured reference beam displacement
- Linear potentiometer data corrected for interpolated reference beam displacement

cessive driving of prototype  
at a distance of 20 ft  
monolith, using the primary  
driving system  
(on O10 - HP 14 x 73 pile)



2

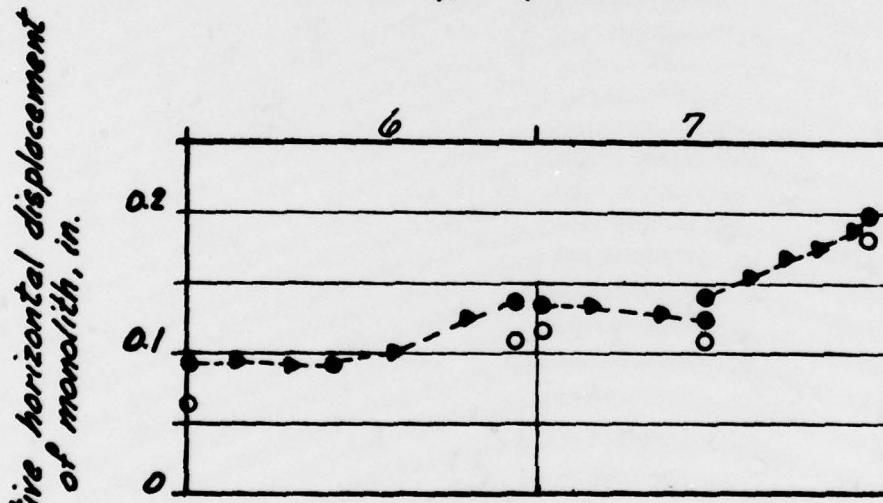
### (b) Stability of settlement



At north end  
of monolith

• 10 •

*Prototype pile number*



### (a) Stability of horizontal displacement

*Note:*

Successive driving of prototype piles at a distance of 30 ft from monolith, using the primary pile driving system (Vulcan O10 - HP 14 x 73 pile)

*Legend*

*At south end  
of monolith*

*Reference point data*



*Linear potentiometer data  
corrected for measured  
reference beam displacement*



*Linear potentiometer data  
corrected for interpolated  
reference beam displacement*



*Legend*

- *Reference point data*
- *Linear potentiometer data corrected  
for measured reference beam displacement*
- *Linear potentiometer data corrected for  
interpolated reference beam displacement*

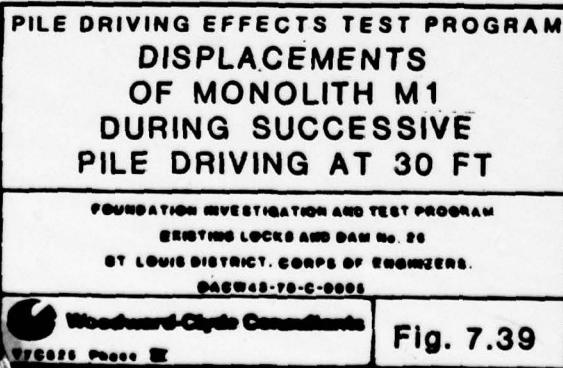
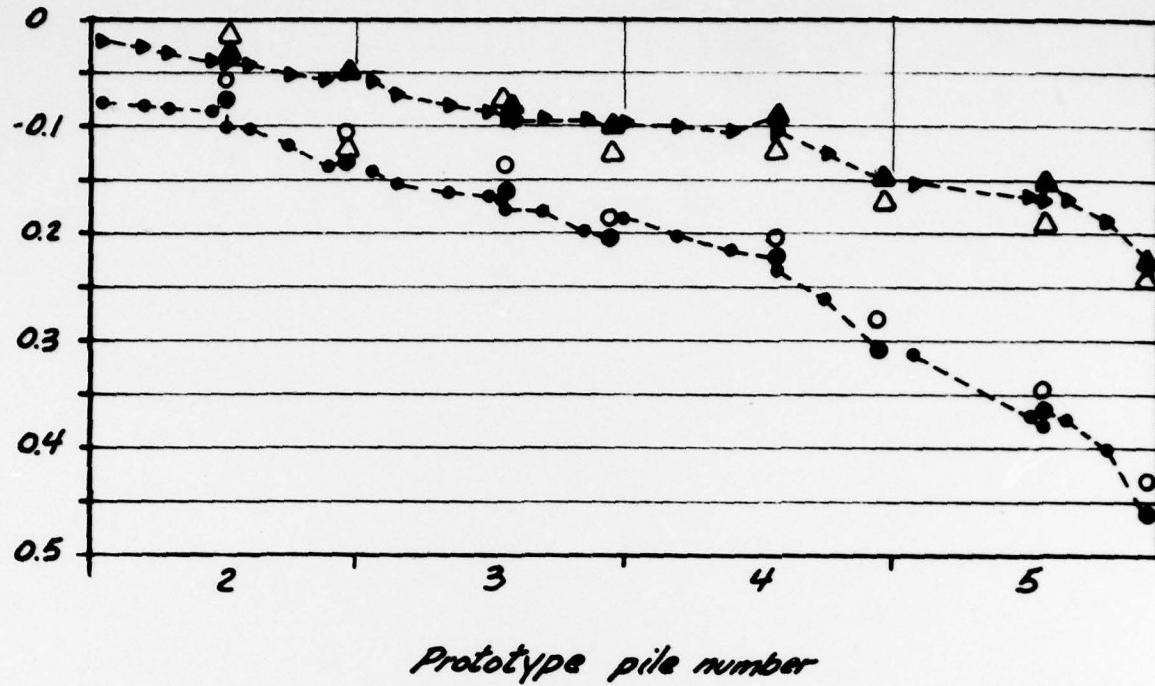


Fig. 7.39

Cumulative settlement of monolith, in.

(b) Stability of settlement

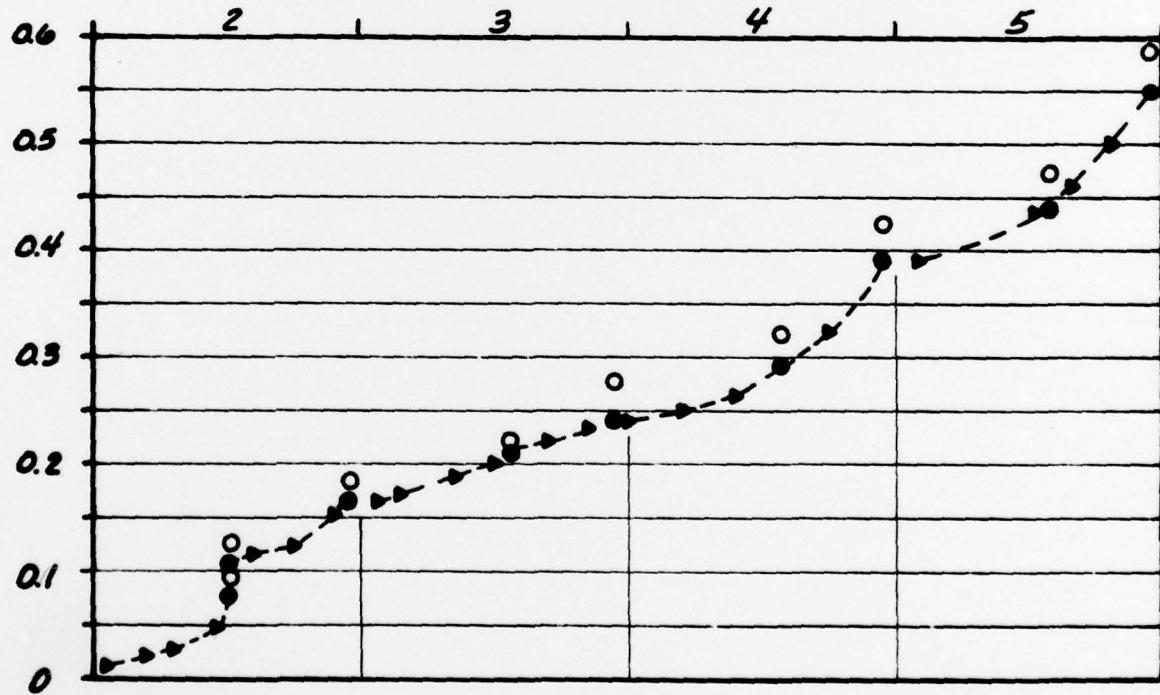


Cumulative horizontal displacement of monolith, in.

(c) Stability of horizontal displacement

At no  
of mon

Note:  
Suc  
piles  
from  
pile o  
(Vulca



north end  
monolith

Legend

At south end  
of monolith

- Reference point data
- Linear potentiometer data corrected for measured reference beam displacement
- Linear potentiometer data corrected for interpolated reference beam displacement



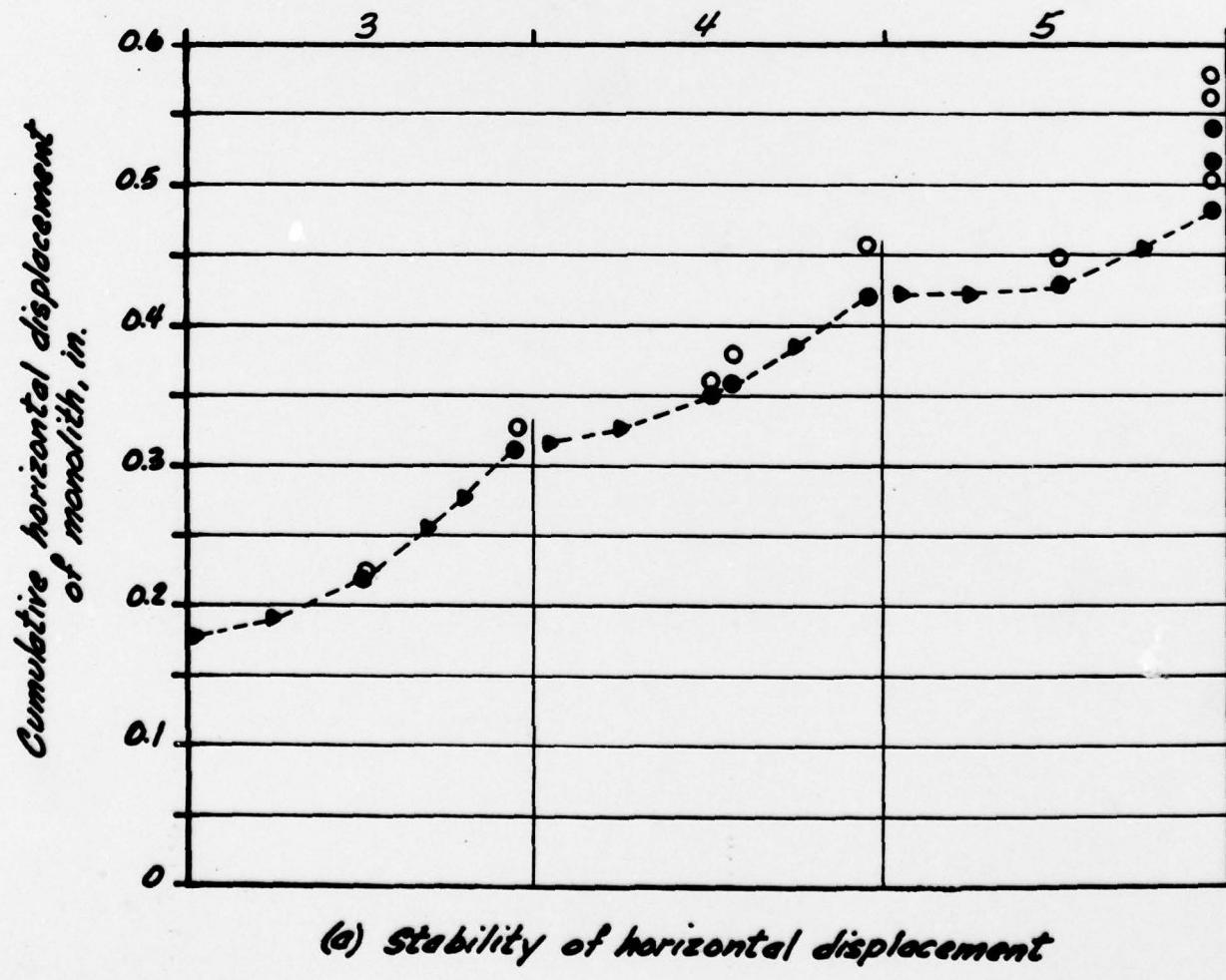
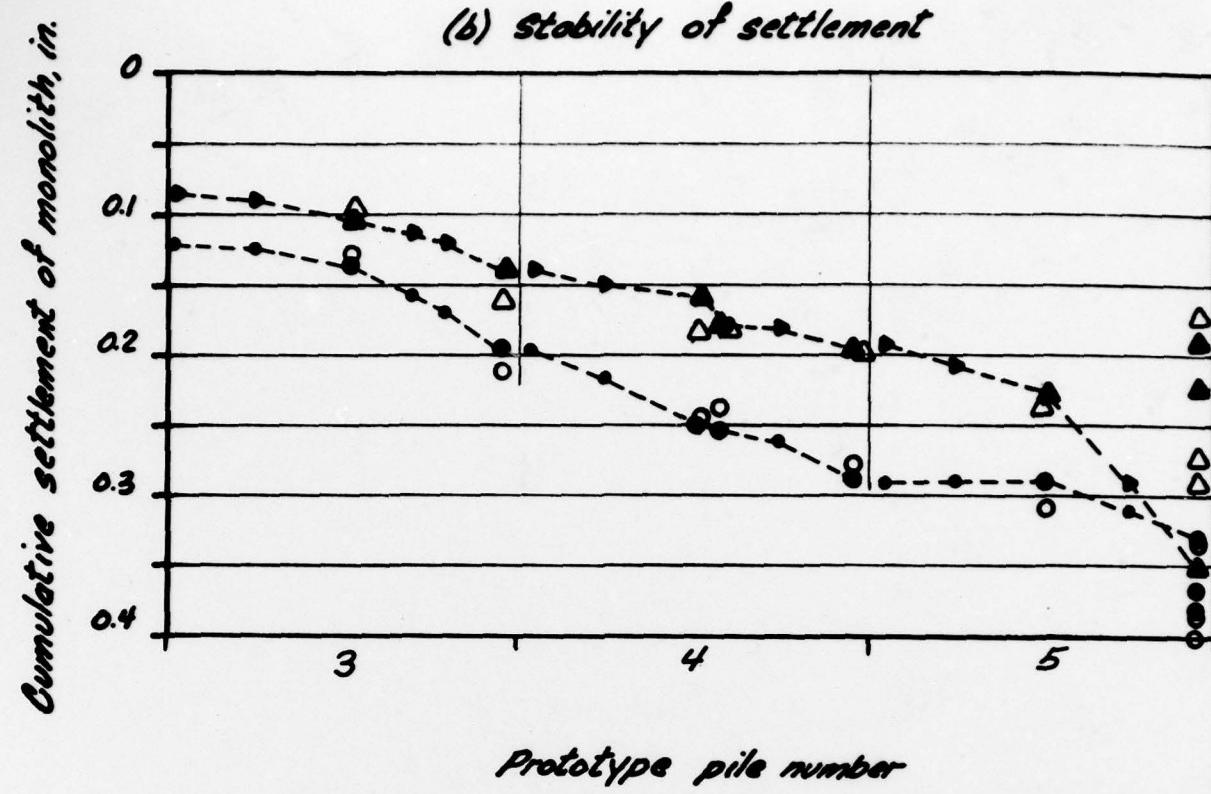
Legend

- Reference point data
- Linear potentiometer data corrected for measured reference beam displacement
- Linear potentiometer data corrected for interpolated reference beam displacement

Successive driving of prototype  
is at a distance of 20 ft  
on monolith, using the primary  
driving system  
(con 010 - HP 14 x 73 pile)

PILE DRIVING EFFECTS TEST PROGRAM DISPLACEMENTS OF MONOLITH M2 DURING SUCCESSIVE PILE DRIVING AT 20 FT	
FOUNDATION INVESTIGATION AND TEST PROGRAM EXISTING LOCKS AND DAM No. 28 ST. LOUIS DISTRICT, CORPS OF ENGINEERS. DACPW43-78-C-0008	
Woodward-Clyde Consultants YTC625 Phase IV	Fig. 7.40

2



Note:  
Successive piles from pile 3 (Vulcan)

North end  
monolith

Legend

At south end  
of monolith

- Reference point data
- Linear potentiometer data corrected for measured reference beam displacement
- Linear potentiometer data corrected for interpolated reference beam displacement



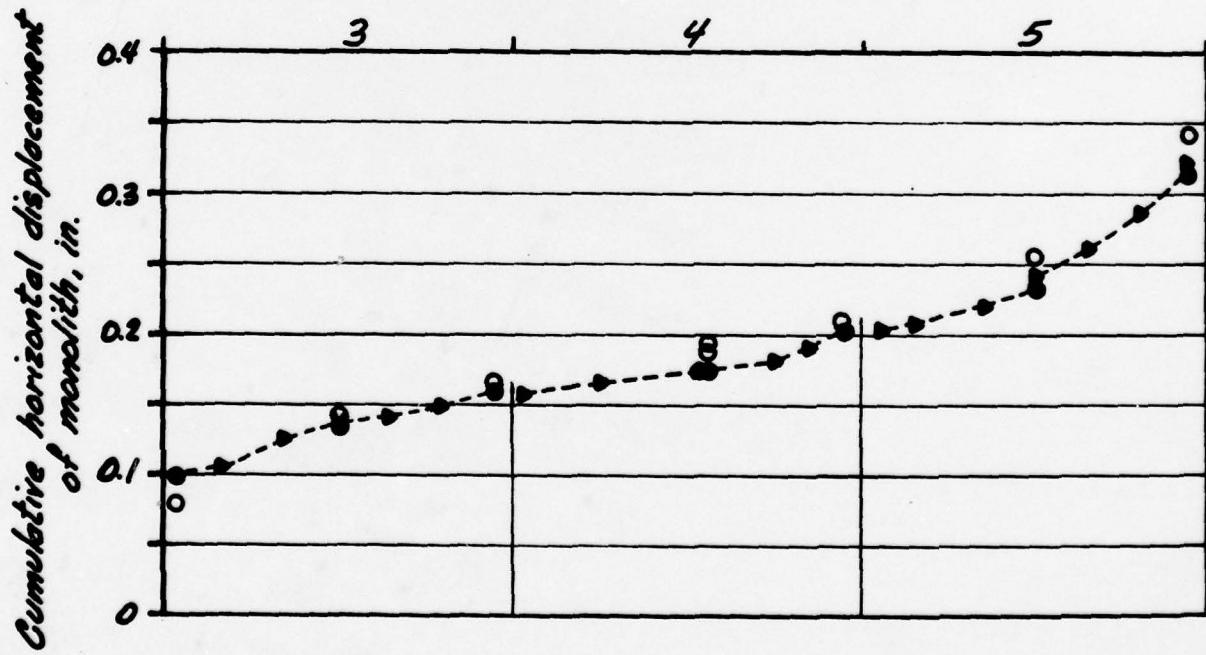
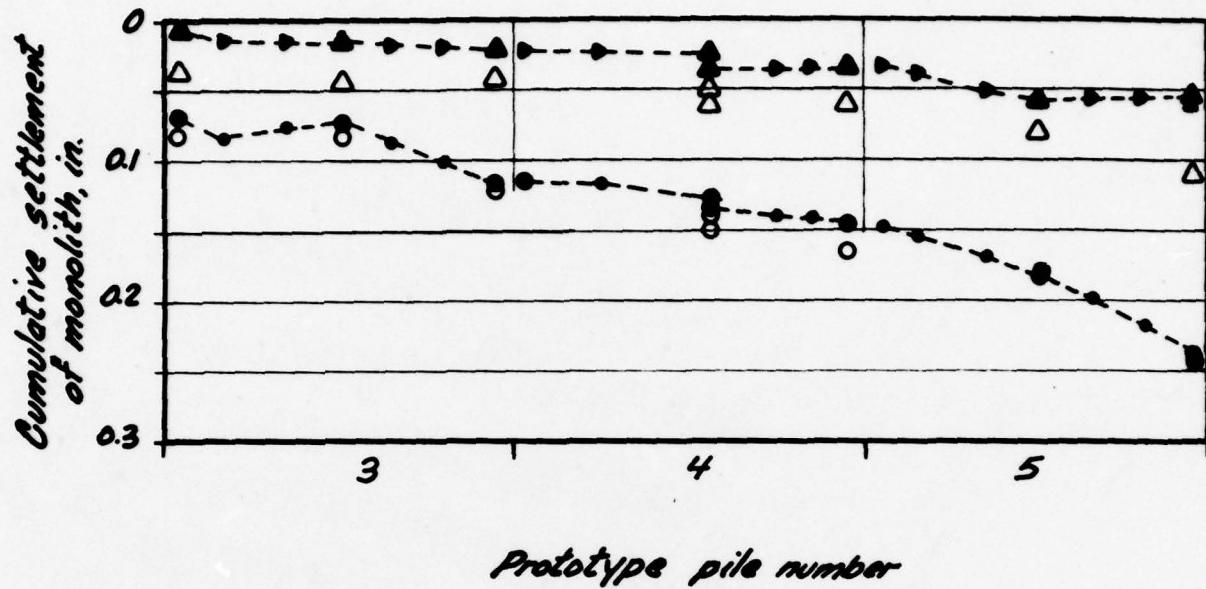
Legend

- Reference point data
- Linear potentiometer data corrected for measured reference beam displacement
- Linear potentiometer data corrected for interpolated reference beam displacement

Excessive driving of prototype  
pile at a distance of 20 ft  
in monolith, using the primary  
driving system  
(on O10 - HP 14 x 73 pile)

PILE DRIVING EFFECTS TEST PROGRAM DISPLACEMENTS OF MONOLITH M3 DURING SUCCESSIVE PILE DRIVING AT 20 FT	
FOUNDATION INVESTIGATION AND TEST PROGRAM EXISTING LOCKS AND DAM No. 28 ST LOUIS DISTRICT, CORPS OF ENGINEERS. DACPW43-78-C-0008	
Woodward-Clyde Consultants V7C826 Phase II	Fig. 7.41

(b) Stability of settlement



(c) Stability of horizontal displacement

at north end  
monolith

Legend

At south end  
of monolith

- Reference point data
- Linear potentiometer data corrected for measured reference beam displacement
- Linear potentiometer data corrected for interpolated reference beam displacement

△

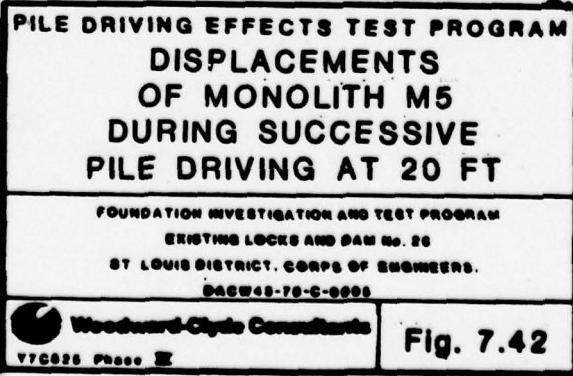
▲

●

Legend

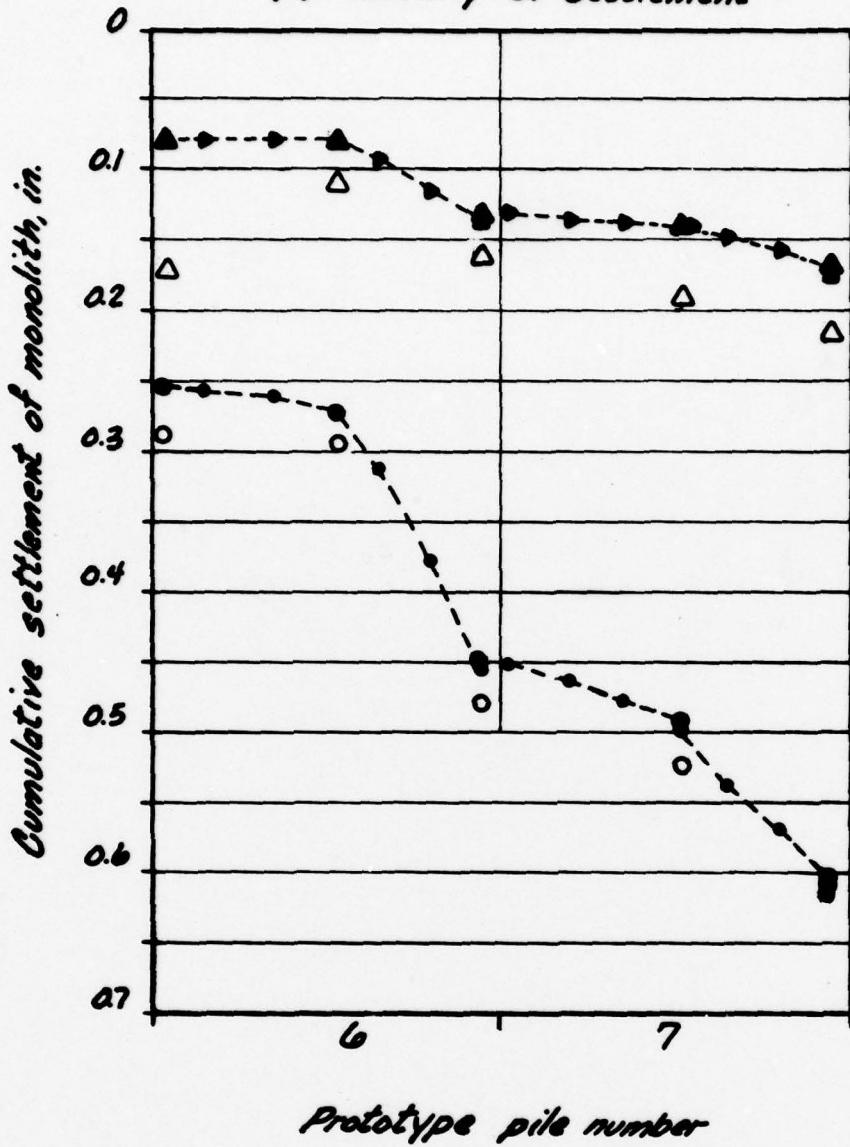
- Reference point data
- Linear potentiometer data corrected for measured reference beam displacement
- Linear potentiometer data corrected for interpolated reference beam displacement

Successive driving of prototype  
piles at a distance of 20 ft  
from monolith, using the primary  
driving system  
(Silcon O10 - HD 14 x 73 pile)



5.

(b) Stability of settlement



At north end  
of monolith

Legend

At south end  
of monolith

○

●

●

Reference point data

Linear potentiometer data  
corrected for measured  
reference beam displacement

Linear potentiometer data  
corrected for interpolated  
reference beam displacement

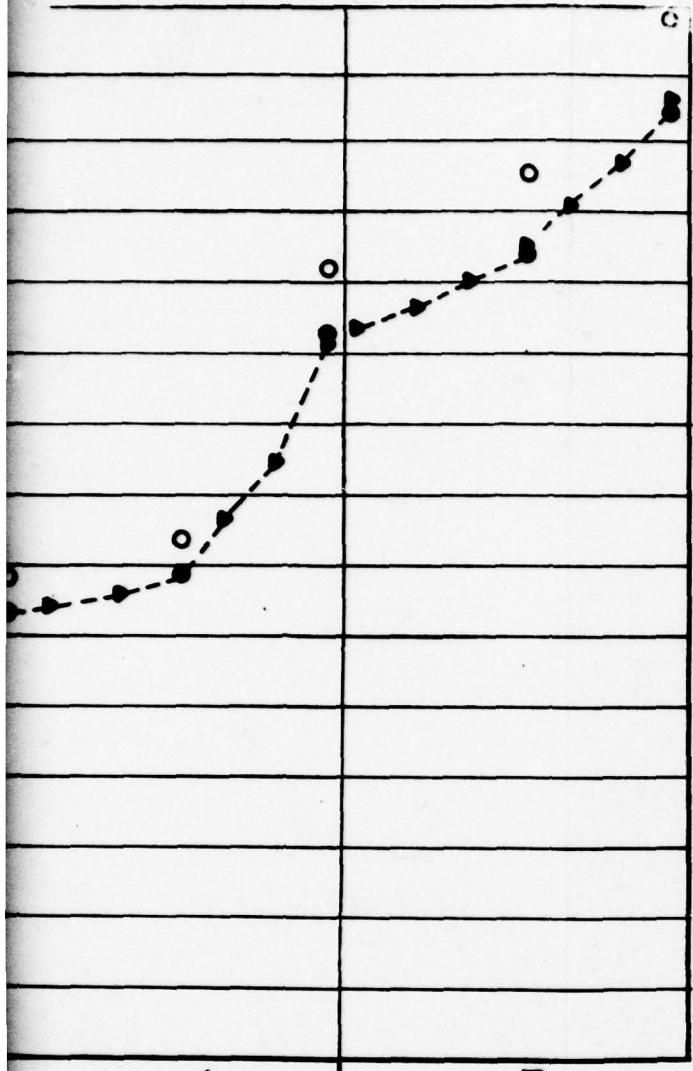
△

▲

▲

○ Re  
● Lin  
○ For  
● Lin  
int

Note  
Su  
pile  
fra  
pile  
(100)



(b) Stability of horizontal displacement

6              7  
Prototype pile number

Legend

Reference point data

Linear potentiometer data corrected  
for measured reference beam displacement

Linear potentiometer data corrected for  
interpolated reference beam displacement

e:  
successive driving of prototype  
piles at a distance of 15 ft  
from monolith, using the primary  
pile driving system  
(ulcon O10 - HP 14 x 73 pile)

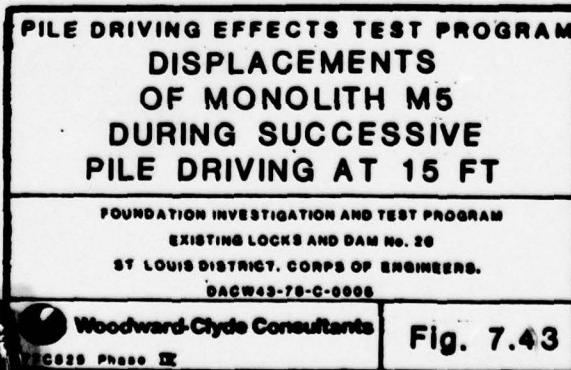
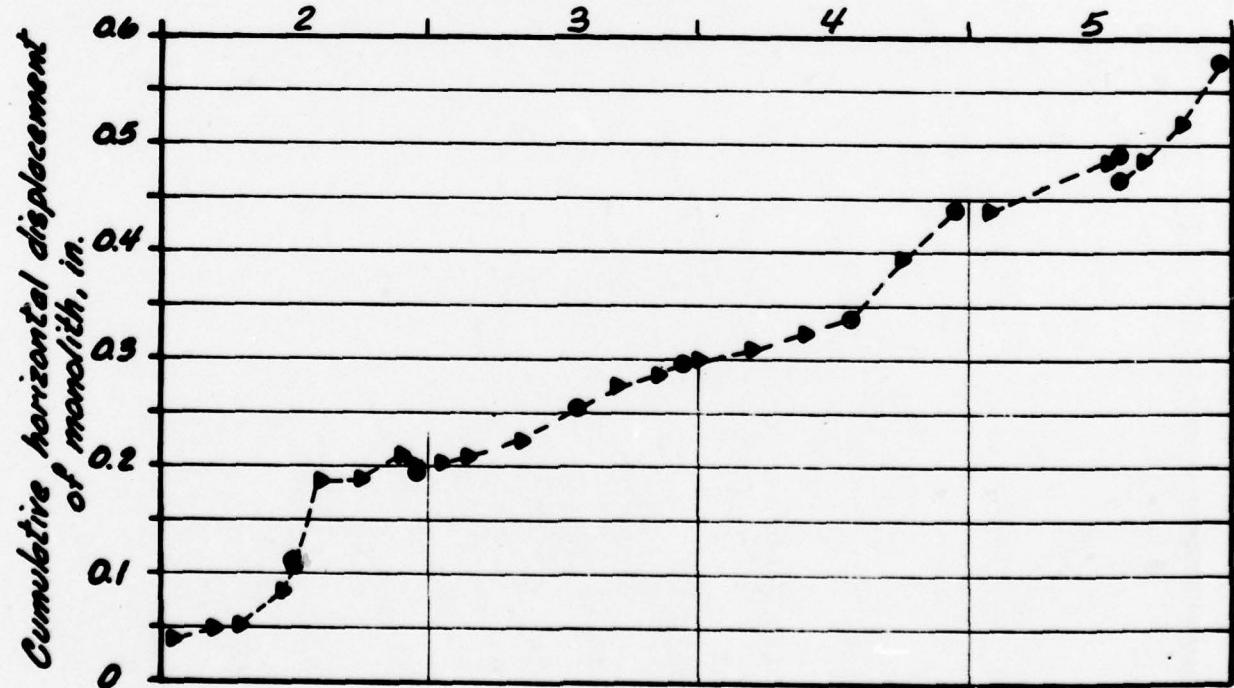
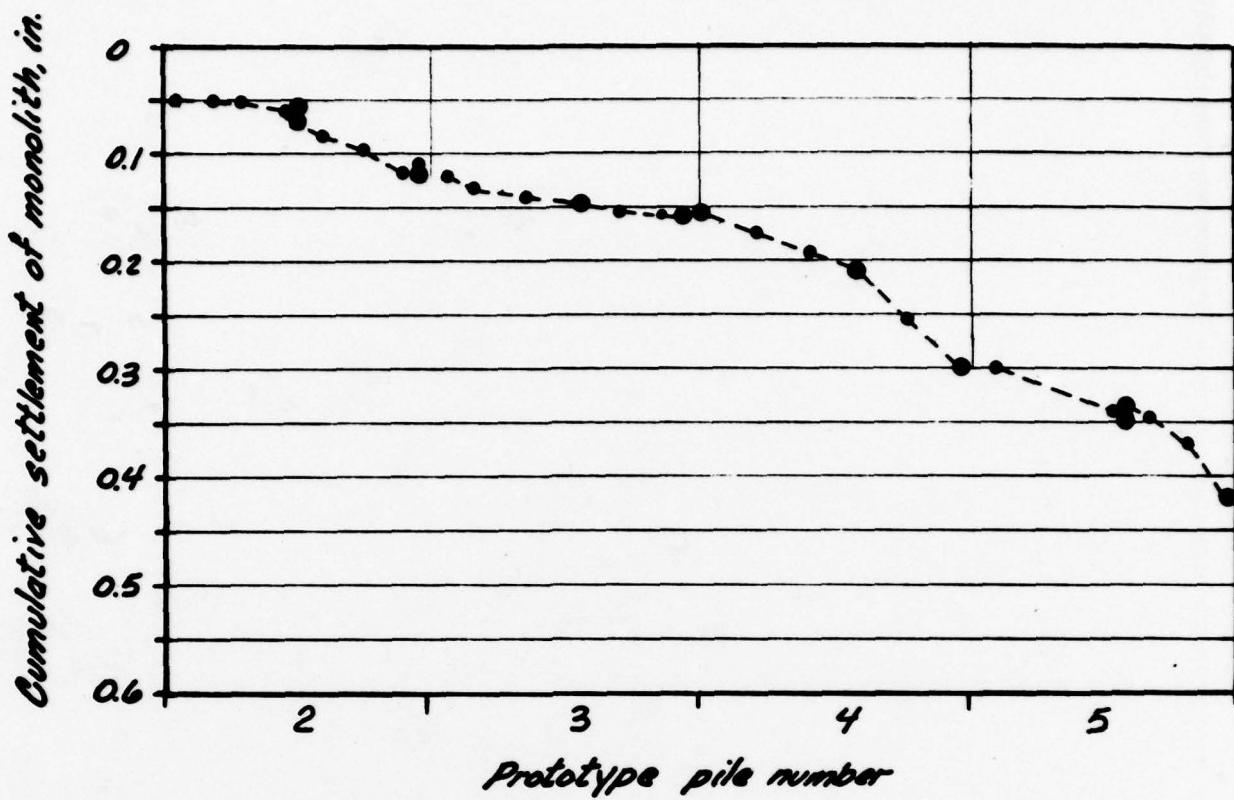


Fig. 7.43

(b) Stability of settlement



(c) Stability of horizontal displacement

*Legend*

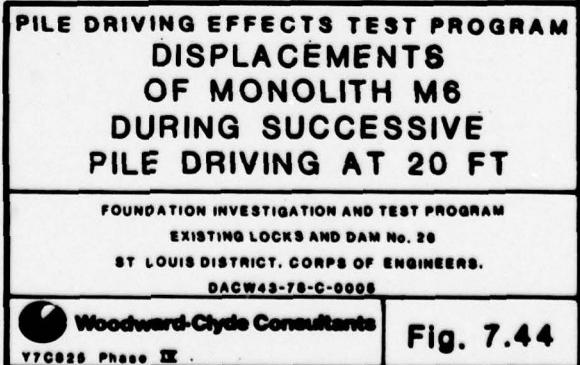
- Linear potentiometer data corrected for measured reference beam displacement
- Linear potentiometer data corrected for interpolated reference beam displacement

*Legend*

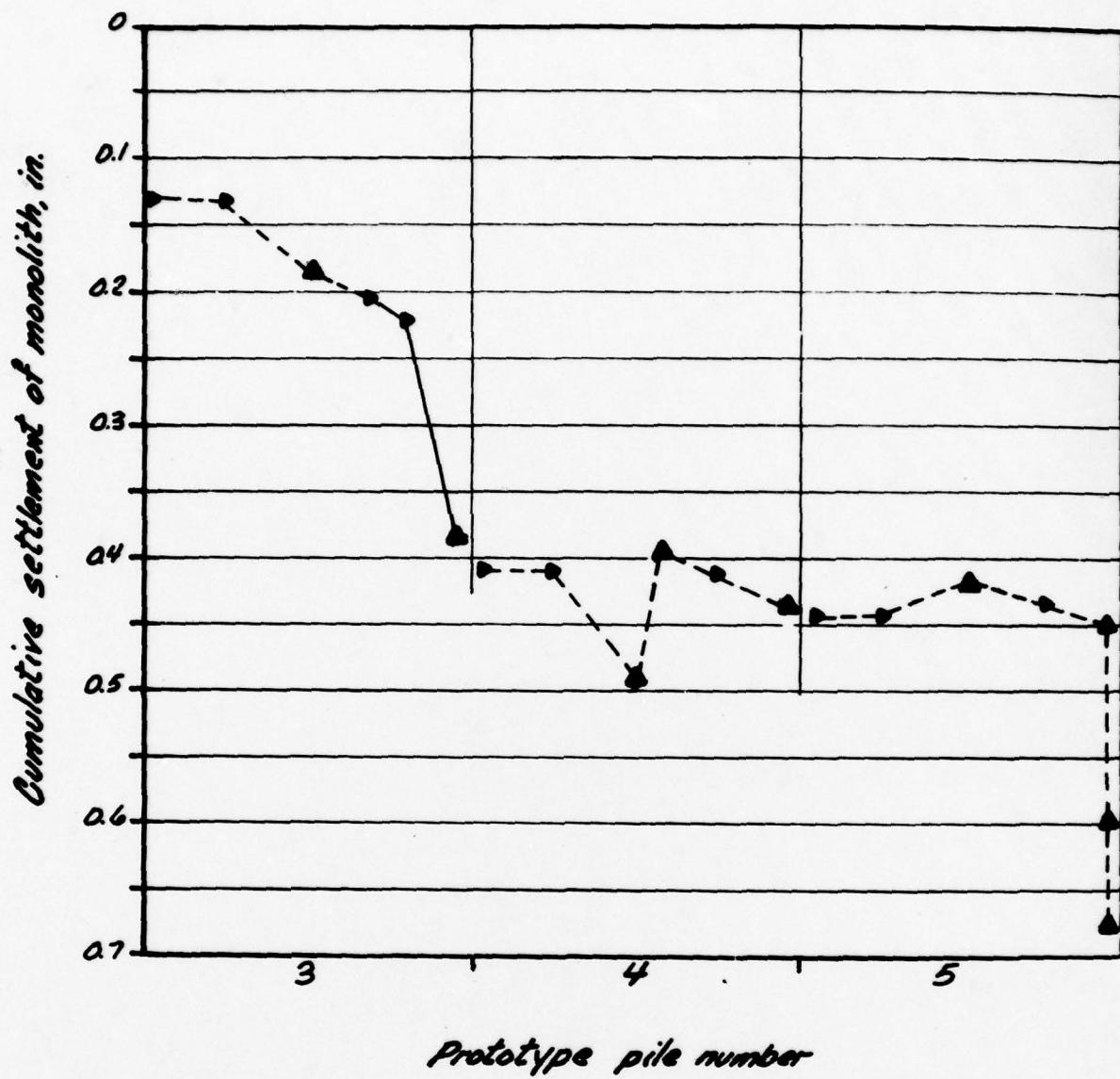
- Linear potentiometer data corrected for measured reference beam displacement
- Linear potentiometer data corrected for interpolated reference beam displacement

*te:*

*Successive driving of prototype  
piles at a distance of 20 ft  
from monolith, using the primary  
pile driving system  
Yukon O10 - HP 14 x 73 pile)*



(b) Stability of settlement



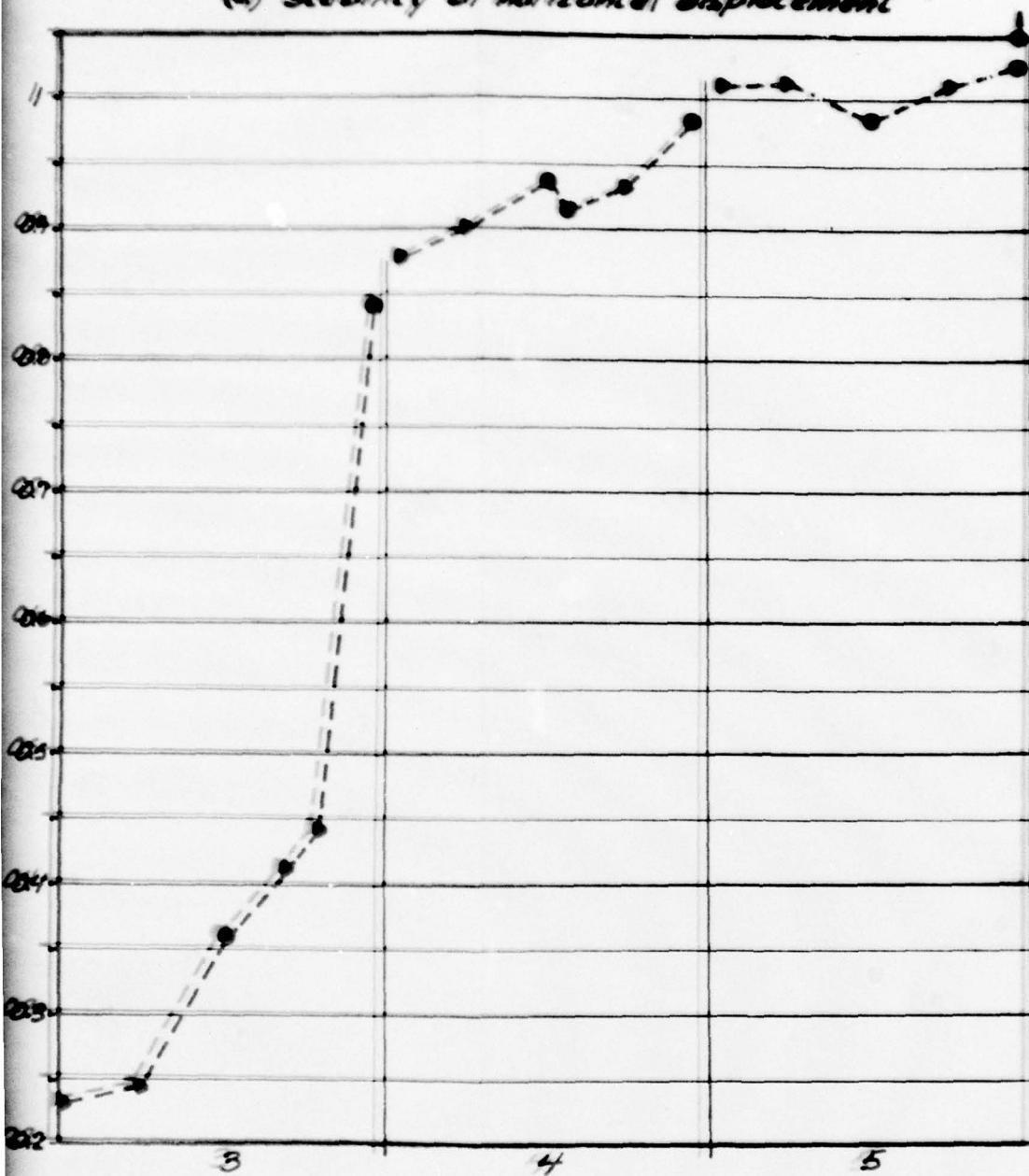
*Legend*

- ▲ Linear potentiometer data corrected for measured reference beam displacement
- Linear potentiometer data corrected for interpolated reference beam displacement

*Note:*

Successive driving of prototype piles at a distance of 20 ft from monolith using the primary pile driving system (Vulcan OIO-HP 14 x 73 pile)

(a) Stability of horizontal displacement



Prototype pile number

Legend

- Linear potentiometer data corrected for measured reference beam displacement
- ▼ Linear potentiometer data corrected for interpolated reference beam displacement

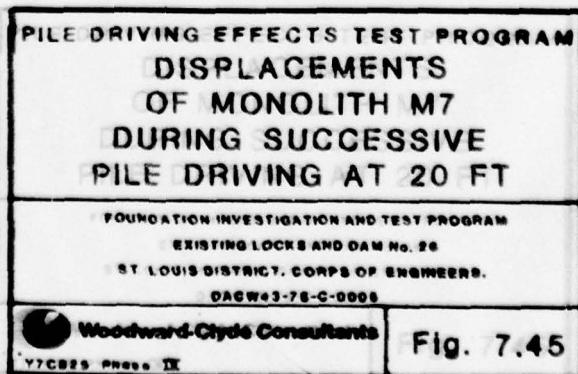
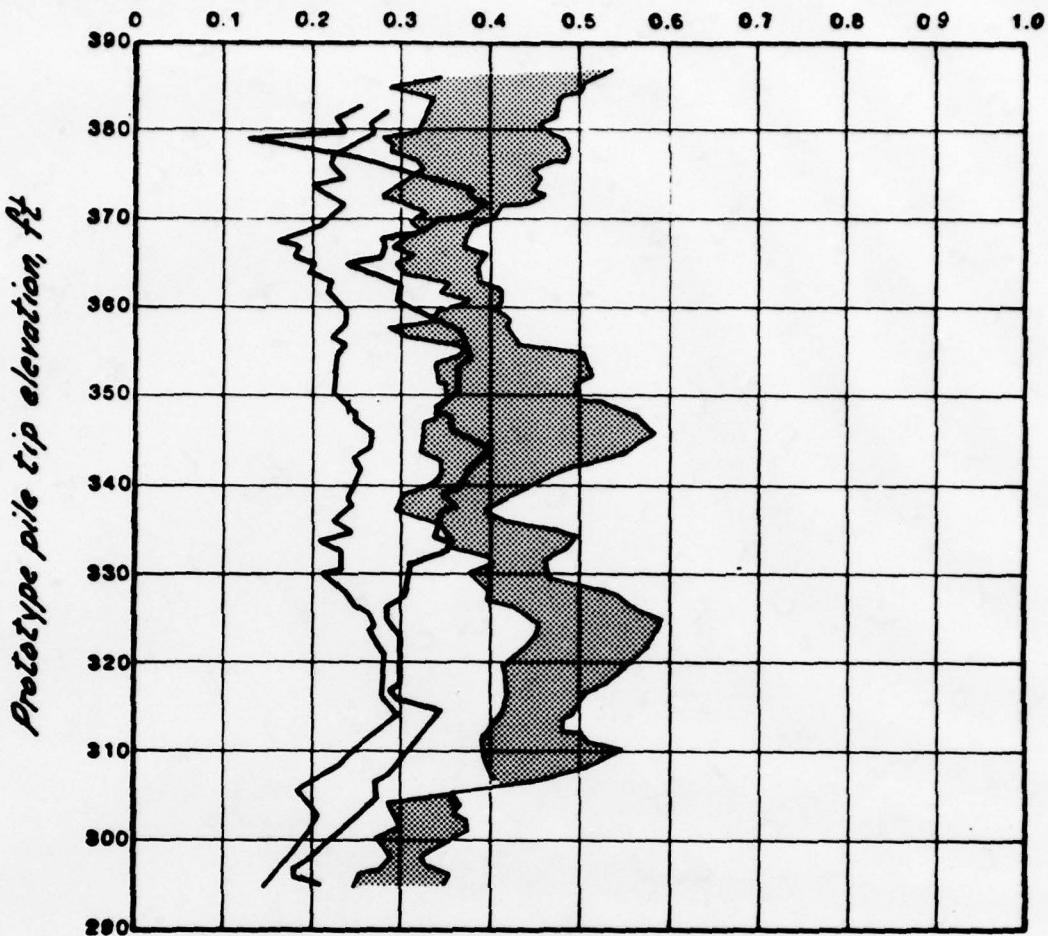


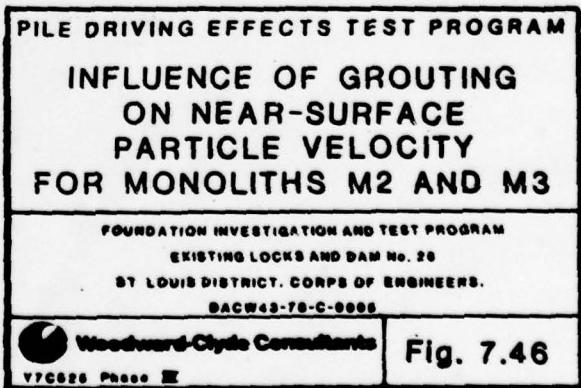
Fig. 7.45

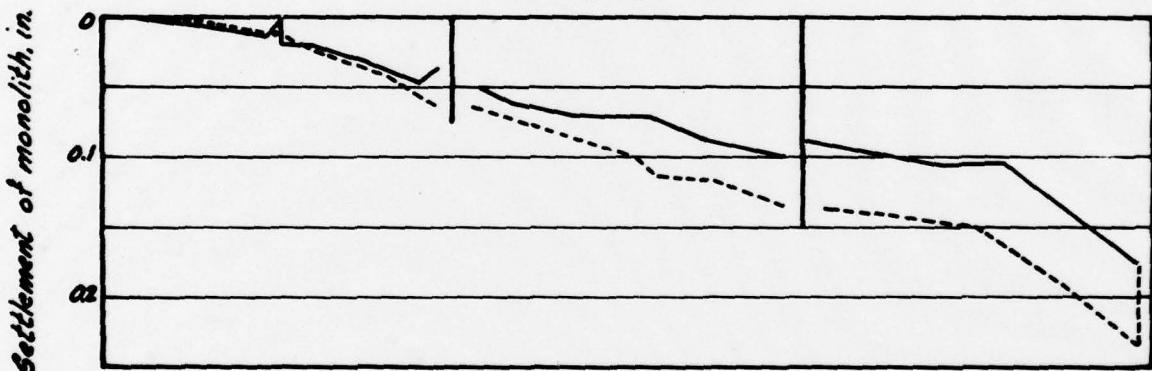
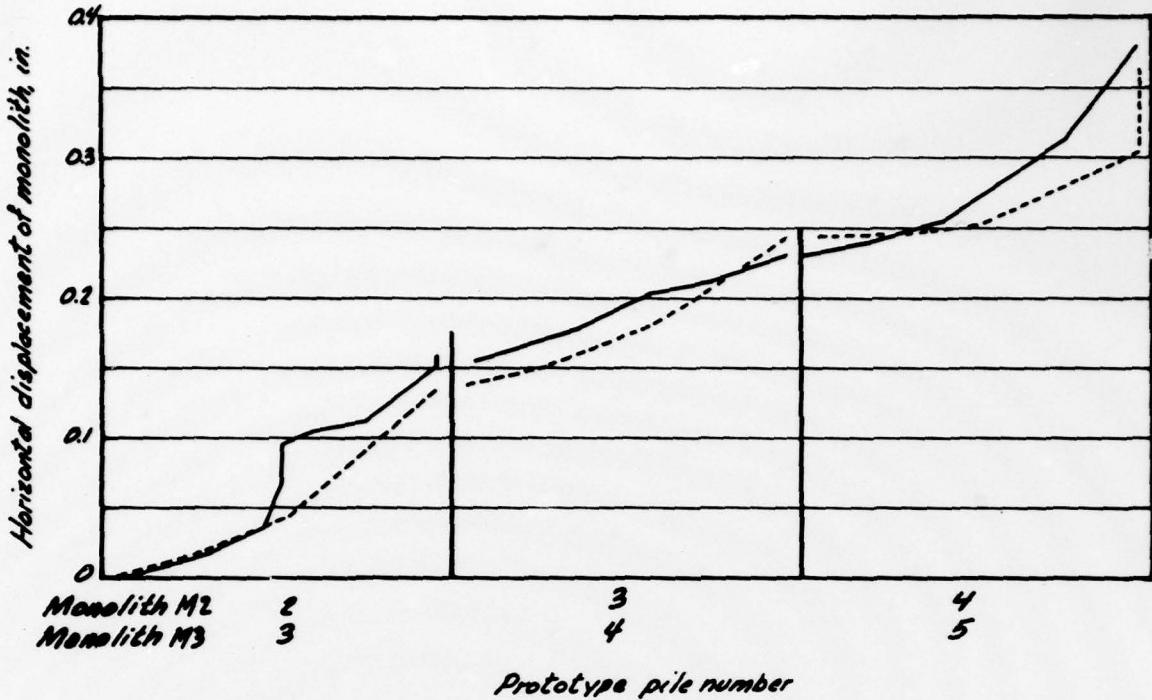
Near-surface peak vectorial particle velocity, in./s



Monolith No.	Distance between prototype pile and monolith, ft	Prototype pile No.
M2	20-21	2,3,4,5
M3	20	3,4,5

Monolith No.	Distance between prototype pile and monolith, ft	Prototype pile No.
M2	20-21	2,3,4,5
M3	20	3,4,5

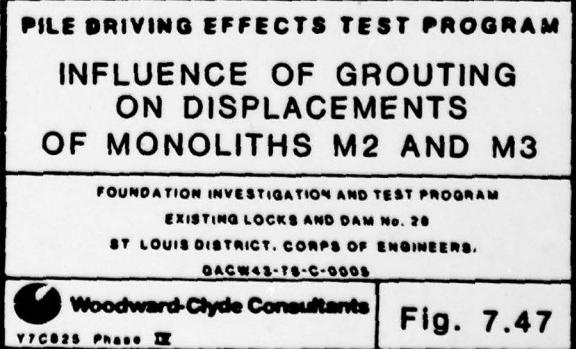




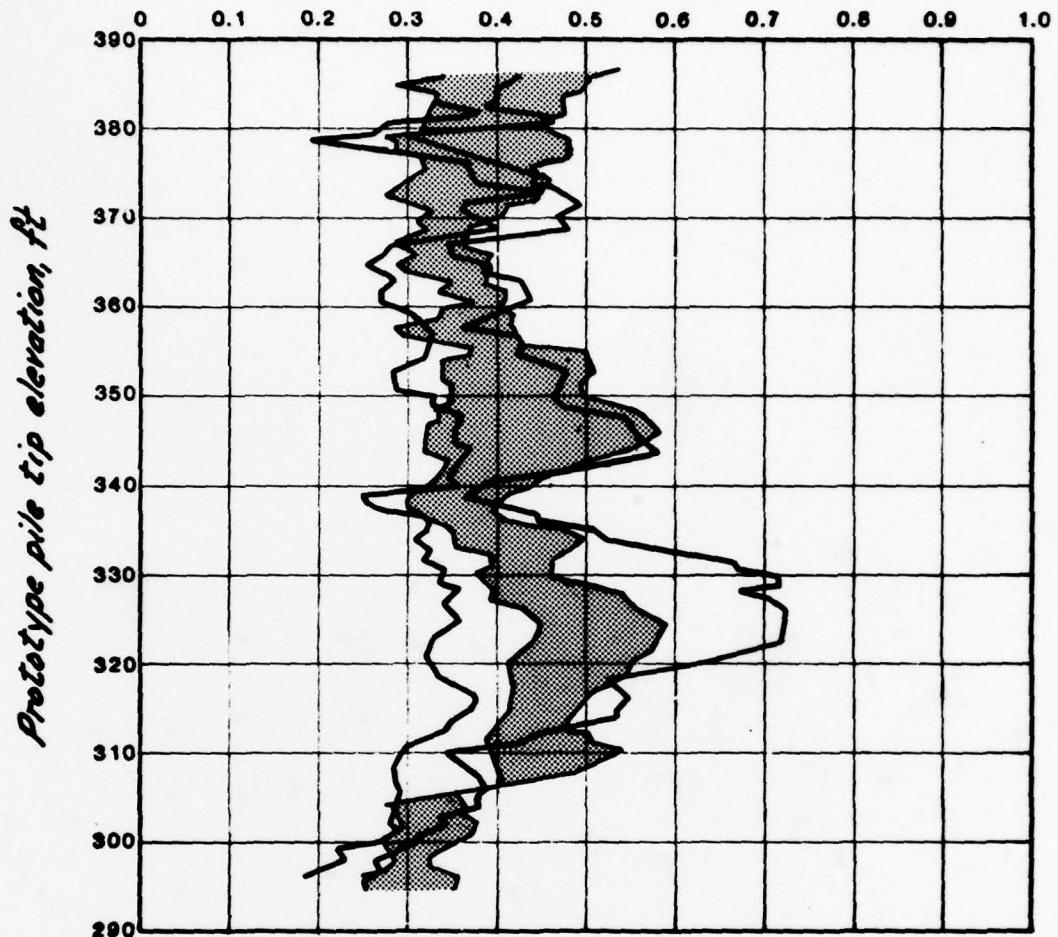
Legend  
 — Displacements of Monolith M2  
 --- Displacements of Monolith M3

Note:

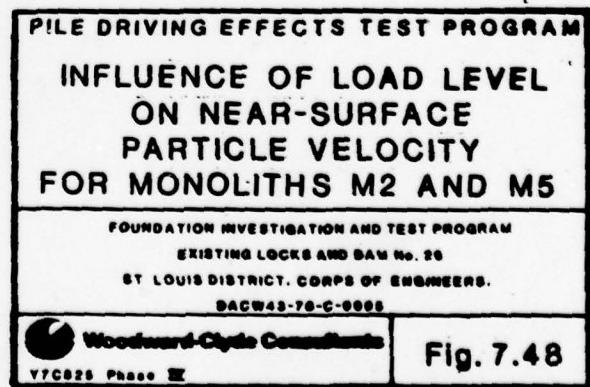
Successive driving of prototype piles at a distance of 20 ft from monoliths, using the primary pile driving system (Vulcan O10 HP 14x73 pile)

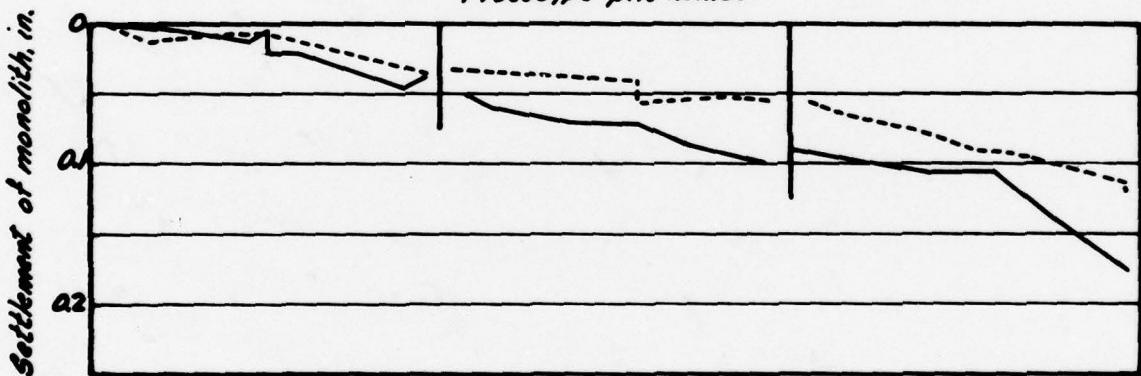
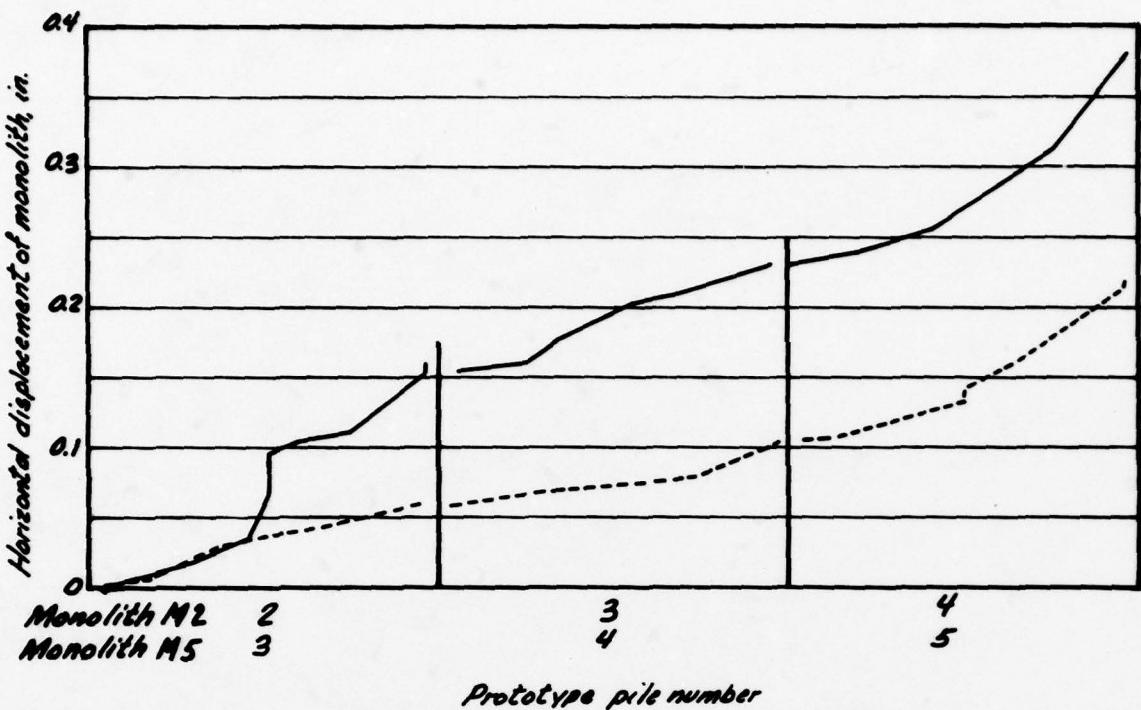


Near-surface peak vectorial particle velocity, in./s



Monolith No.	Distance between prototype pile and monolith, ft	Prototype pile No.
M2	20-21	2,3,4,5
M5	20	3,4,5





*Legend*

— Displacements of Monolith M2  
--- Displacements of Monolith M5

*Note:*

Successive driving of prototype piles at a distance of 20 ft from monoliths, using the primary pile driving system (Vulcan O10 HP 14 x 73 pile)

PILE DRIVING EFFECTS TEST PROGRAM  
INFLUENCE  
OF LOAD LEVEL  
ON DISPLACEMENTS  
OF MONOLITHS M2 AND M5

FOUNDATION INVESTIGATION AND TEST PROGRAM

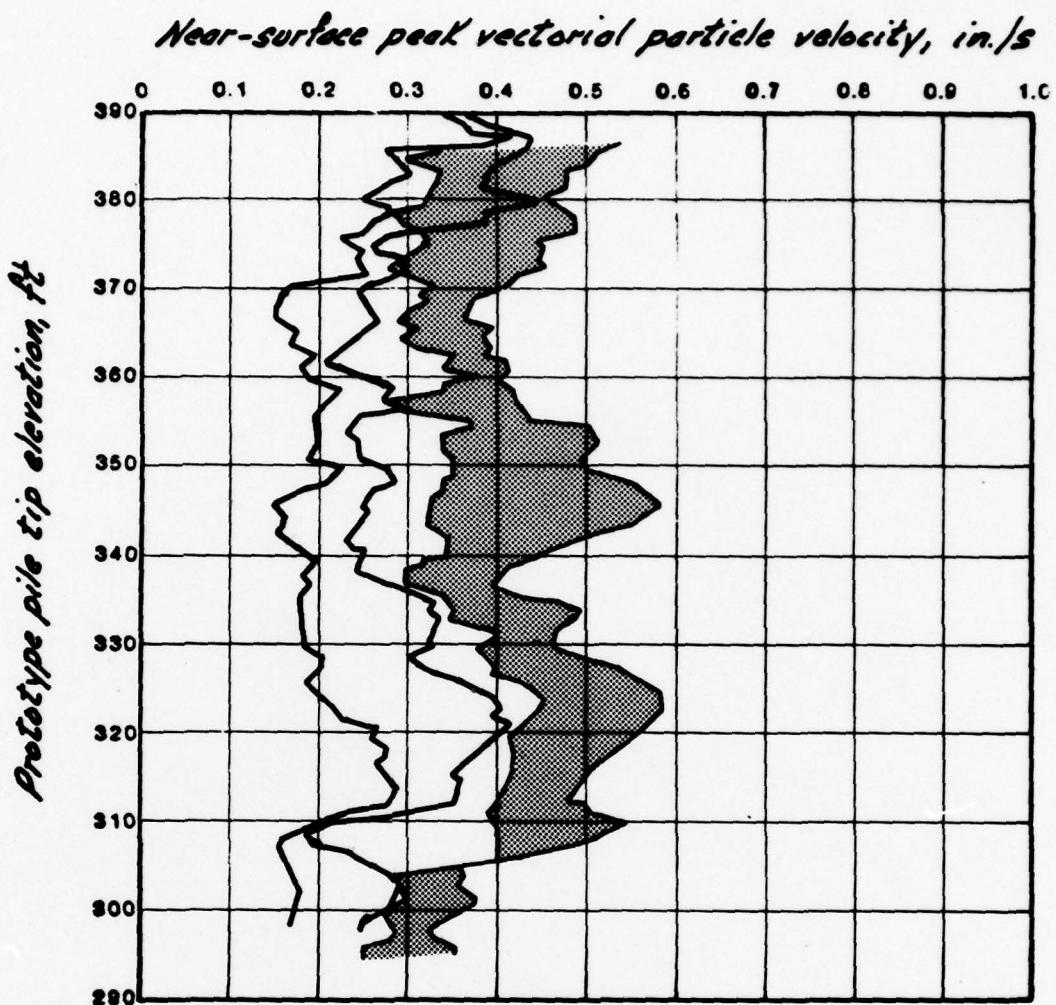
EXISTING LOCKS AND DAM NO. 20

ST LOUIS DISTRICT, CORPS OF ENGINEERS.

DACW43-78-C-0006

Woodward-Clyde Consultants  
YTCB25 Phase II

Fig. 7.49



Monolith No.	Distance between prototype pile and monolith, ft	Prototype pile No.
M2	20-21	2,3,4,5
M1	20	8,9,10

**PILE DRIVING EFFECTS TEST PROGRAM  
INFLUENCE OF  
TIMBER PILE CONFIGURATION  
ON NEAR-SURFACE  
PARTICLE VELOCITY  
FOR MONOLITHS M2 AND M1**

FOUNDATION INVESTIGATION AND TEST PROGRAM

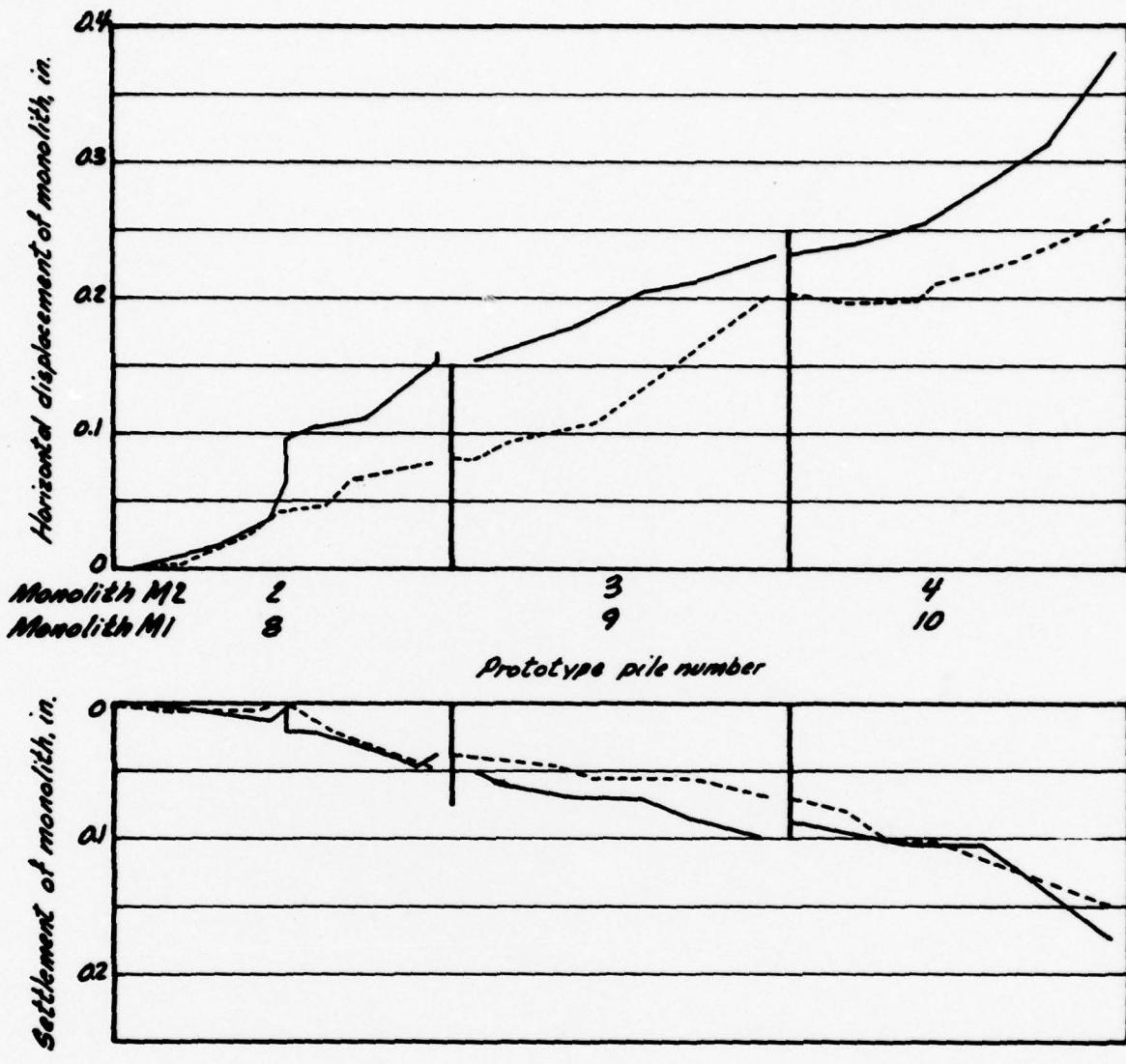
EXISTING LOCKS AND DAM NO. 26

ST. LOUIS DISTRICT, CORPS OF ENGINEERS.

DACW43-78-C-0008

 Woodward-Clyde Consultants  
YTGB25 Phase II

Fig. 7.50



*Legend*  
 — Displacements of Monolith M2  
 --- Displacements of Monolith M1

*Note:*

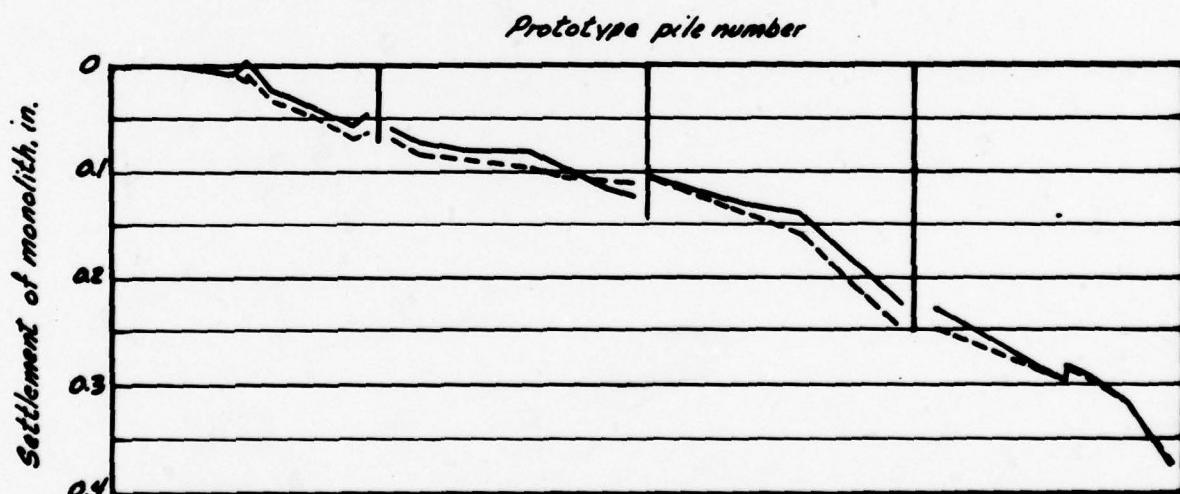
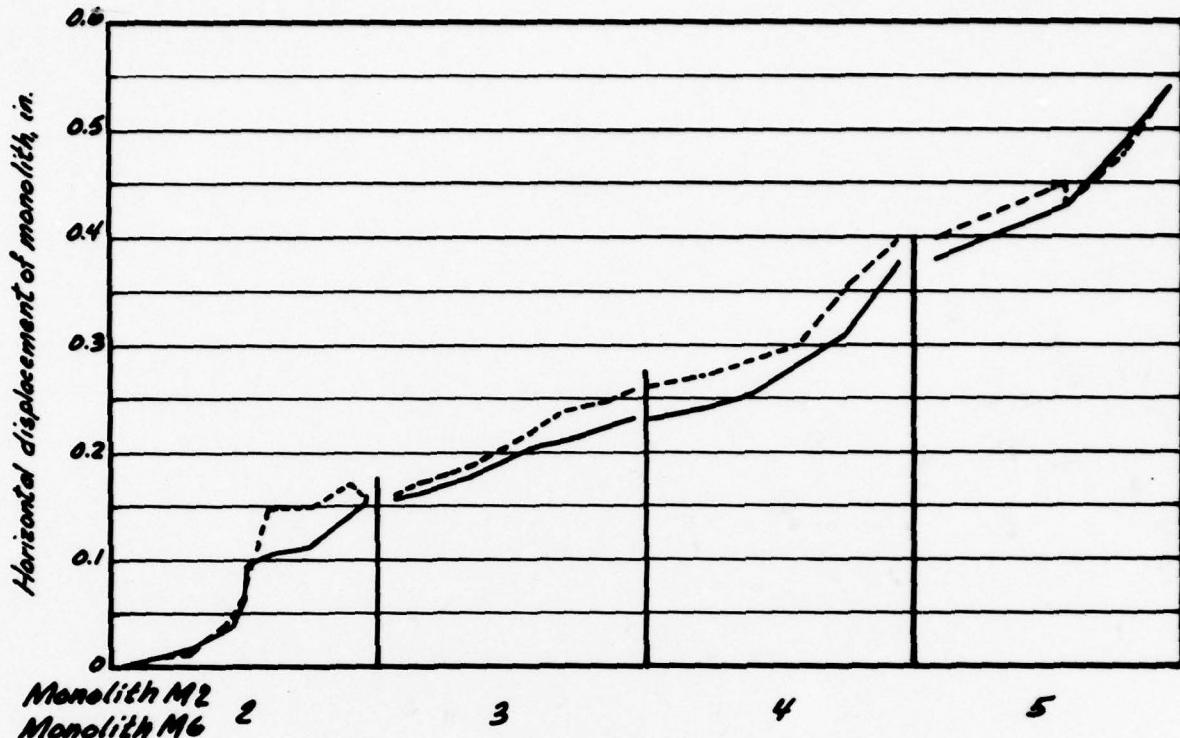
*Successive driving of prototype piles at a distance of 20 ft from monoliths, using the primary pile driving system (Vulcan O10 HP 14 x 73 pile)*

**PILE DRIVING EFFECTS TEST PROGRAM  
INFLUENCE OF  
TIMBER PILE CONFIGURATION  
ON DISPLACEMENTS OF  
MONOLITHS M2 AND M1**

FOUNDATION INVESTIGATION AND TEST PROGRAM  
EXISTING LOCKS AND DAM NO. 26  
ST LOUIS DISTRICT, CORPS OF ENGINEERS.  
DAGW43-76-C-0005

Woodward-Clyde Consultants  
TTCB26 Phase II

Fig. 7.51



Notes:

- (1) Successive driving of prototype piles at a distance of 20 ft from monoliths, using the primary pile driving system (Vulcan O10 HP 14 x 73 pile)
- (2) Horizontal displacement of monolith M6 measured at 33 in. above ground surface
- (3) Settlement of monolith M6 measured at 33 in. above ground surface
- (4) Settlement of monolith M2 is settlement at north end of monolith

Legend  
 — Displacements of Monolith M2  
 --- Displacements of Monolith M6

PILE DRIVING EFFECTS TEST PROGRAM  
 INFLUENCE OF  
 TIMBER PILE CONFIGURATION  
 ON DISPLACEMENTS  
 OF MONOLITHS M2 AND M6

FOUNDATION INVESTIGATION AND TEST PROGRAM  
 EXISTING LOCKS AND DAM NO. 28  
 ST LOUIS DISTRICT, CORPS OF ENGINEERS.  
 DASGW43-78-C-0006

Woodward-Clyde Consultants  
 YTCB25 Phase II

Fig. 7.52

**PHASE IV REPORT**

**VOLUME III**

**RESULTS AND INTERPRETATION OF  
PILE DRIVING EFFECTS TEST PROGRAM**

**SECTION 8**

**MONOLITH LOAD TESTING**

## 8 MONOLITH LOAD TESTING

### 8.1 SCOPE OF TESTS

Upon completion of the pile driving effects stage of testing, each monolith was load tested to failure either axially or laterally. The objective of the monolith load tests, ranked as a secondary objective for the overall pile driving effects test program, was to measure ultimate axial or lateral load capacities of single timber piles and timber pile groups in ungrouted and grouted soil.

Each monolith was tested to failure under a different combination of axial and lateral loads. The following table presents a summary of the various test load combinations.

Monolith No. and Timber <u>Pile Configuration</u>	<u>Soil Conditions</u>	<u>Test Load Combination</u>
M1 (3 x 4)	Ungrouted	Constant axial load of 360 t Increased lateral load to failure
M2 (2 x 4)	Ungrouted	Constant axial load of 240 t Increased lateral load to failure
M3 (2 x 4)	Grouted	Constant axial load of 240 t Increased lateral load to failure
M5 (2 x 4)	Ungrouted	Increased axial load to failure Zero lateral load
M6 (single)	Ungrouted	Increased axial load to failure Zero lateral load; then Constant axial load of 30 t Increased lateral load to failure
M7 (single)	Grouted	Constant axial load of 30 t Increased lateral load to failure

### 8.2 TEST PROCEDURES

#### 8.2.1 Instrumentation and Test Setup

Load tests were made immediately after driving prototype steel piles. The monolith setup generally was unchanged from this earlier stage of testing. The instrumentation monitored was essentially the same as that monitored during pile driving effects tests, except that the geophones, pile driving analyzer system, and dynamic data acquisition system were not used during the load tests.

### 8.2.2 Axial Load Tests

Axial load tests in compression to failure were made on monolith M5 and M6 in ungrouted soil. No lateral load was applied to the monoliths during these tests. The actual procedures for each test did not significantly depart from the general test procedures described below:

- (1) make initial readings and measurements, the monolith being unloaded (load cells, linear potentiometers and dial gages, optical surveys, tiltmeters, tape extensometers, telltales, strain gages, piezometers and thermocouples);
- (2) apply the axial load in increments of 30 t/pile (that is 240-t increments for monolith M5, and 30-t increments for monolith M6); make periodic measurements using automatic data acquisition system (load cells and linear potentiometers) until settlement of monolith stabilized to less than 0.01 in./hr;
- (3) make selected automatic and manual measurements (dial gages, optical surveys, telltales); the actual instruments read were selected by the shift leaders on the basis of monolith settlement and axial load level;
- (4) increase the axial load in 30-t/pile increments, repeating steps (2) and (3) until failure occurred;

The failure criterion was different for the single pile (M6) and the pile group (M5). The single pile was considered to have failed axially when the pile tip settled in excess of 1.5 in. Jacking was halted and the failure load was taken as the load recorded by the load cell 15 min after the jacking stopped. During application of what was the final load increment on monolith M5, the southeast corner of the monolith had settled so much and the monolith was tilting to a point where the stability of the jacks and load frame system was of concern. Rather than risk a collapse of the system, jacking was halted. The load stabilized and the stabilized load was taken as the failure load.

- (5) most instruments were read at failure and the axial load was removed; and
- (6) readings and measurements were repeated after unloading.

### 8.2.3 Lateral Load Tests

Lateral load tests to failure were made on monoliths M1, M2, and M6 in the ungrouted soil, and monoliths M3 and M7 in grouted soil. The general test procedures were as follows:

- (1) make initial readings and measurements, the monolith being unloaded (load cells, linear potentiometers and dial gages, optical surveys, tiltmeters, tape extensometers, ground and pile inclinometers, telltales, strain gages, piezometers, and thermocouples);
- (2) apply an axial load equivalent to 30 t/pile (that is, 360 t for M1, 240 t for M2 and M3, and 30 t for M6 and M7); make periodic measurements using the automatic data acquisition system (load cells and linear potentiometers) until settlement of the monolith stabilized to less than 0.01 in./hr;
- (3) make selected automatic and manual measurements (dial gages, optical surveys, inclinometers, telltales);
- (4) apply a lateral load equivalent to 6 t/pile (that is, 72 t for M1, 48 t for M2 and M3, and 6 t for M6 and M7); make periodic measurements using automatic data acquisition system (load cells and linear potentiometers) until the lateral displacement of the monolith stabilized to less than 0.01 in./hr;
- (5) repeat step (3);
- (6) increase the lateral load in increments equivalent to 3 t/pile (that is 36 t for M1, 24 t for M2 and M3, and 3 t for M6 and M7); make periodic measurements using the automatic data acquisition system at each load level until the lateral displacement of the monolith stabilized to less than 0.01 in./hr; repeat step (3); apply the next load increment;
- (7) repeat step (6) until failure occurred. Failure was defined as structural failure of piles or concrete cap, or continued displacement of the monolith under sustained load (this latter failure mode occurred in all cases);
- (8) maintain failure load long enough to make automatic and selected manual measurements;
- (9) remove lateral load and repeat automatic and manual measurements; and
- (10) remove axial load and repeat automatic and manual measurements.

### 8.3 TEST RESULTS

#### 8.3.1 Monolith M1 (Lateral Load Test)

Monolith M1 rested on a 3 x 4-pile group. The soil around the timber piles was not grouted. At the time of the lateral load test, the toe of the berm leading from the bottom of the monolith trench at el 391 to the bottom of general excavation was approximately 8 ft from the north end of the monolith. The berm had a slope of approximately 1:1 and a height of 9 ft.

The behavior of monolith M1 under constant axial load of 360 t and increasing lateral load is depicted in Fig. 8.1. The lateral load at failure was 172 t, or an average of 14.3 t/pile. Under the failure load, the monolith displacement did not stabilize. The test was terminated at that load because it was feared that the vertical jacks and load frame would slip and collapse. At the time the test was terminated, the monolith displacement was almost 6 in. from beginning of lateral load application. About 4 in. of displacement occurred when the lateral load was increased from 144 t (12 t/pile) to 172 t (14.3 t/pile). Residual horizontal displacement was 2.2 in. after complete unloading (axial and lateral).

There was no evidence of structural failure of the timber piles during the test. The timber piles emitted creaking sounds at the two highest load levels. Gaps about 2 in. wide were observed between the soil and the rear of the piles. Soil deformation at ground surface in front of the piles was obscured by water and snow cover; the ground was not frozen, however, because forced-air heaters were used throughout the test under and around the monoliths, and the groundwater was maintained near ground surface.

### **8.3.2      Monolith M2 (Lateral Load Test)**

Monolith M2 rested on a 2 x 4-pile group. The soil around the timber piles was not grouted. The berm in front of monolith M2 was excavated after cyclic preloading such that its toe was about 25 ft from the north end of the monolith. The berm was approximately 10 ft high and had a nearly vertical slope.

The behavior of monolith M2 under a constant axial load of 240 t and increasing lateral load is depicted in Fig. 8.2. The lateral load at failure was 120 t or an average of 15 t/pile. Under the failure load, the monolith eventually stabilized after more than 5 hours. At this time, the total horizontal displacement was 5.3 in. from beginning of horizontal load application. Residual lateral displacement was 1.4 in. after complete unloading.

There was no evidence of structural failure of the timber piles during the tests, although creaking sounds were heard. Gaps about 1 in. wide were observed between the soil and the rear of the piles. Soil deformation at ground surface in front of the piles was obscured by water and grout spillage from monolith M3.

### **8.3.3      Monolith M6 (Axial Load Test)**

Monolith M6 rested on a single timber pile. The soil around the pile was not grouted. Monolith M6 was on the east side of M2 and was more than 25 ft from the berm.

The behavior of monolith M6 under no lateral load and increasing axial loads is depicted in Fig. 8.3. The maximum axial load applied was 110 t, but the pile continued to settle under that load. At the time the test was discontinued, the total monolith settlement was 2 in. and the pile had significantly deflected laterally in the y-direction (north).

#### **8.3.4      Monolith M6 (Lateral Load Test)**

Monolith M6 was also loaded to failure laterally after the axial load test to failure. Behavior of monolith M6 under a constant axial load of 30 t and increasing lateral load is depicted in Fig. 8.4. The maximum sustained lateral load was 15 t producing a displacement of 2 in. near ground surface. Attempts to increase the lateral load to 18 t were discontinued when it appeared that the axial jack was about to kick out.

#### **8.3.5      Monolith M3 (Lateral Load Test)**

Monolith M3 rested on a 2 x 4-pile group. The soil around the timber piles was grouted to a depth of approximately 20 ft below ground surface, after the monolith had been cyclically preloaded. The toe of the berm was 25 ft from the north end of the monolith.

The behavior of monolith M3 under a constant axial load of 240 t and increasing lateral load is depicted in Fig. 8.5. The lateral load at failure was 118 t or an average of 14.8 t/pile. When attempting to load to 120 t, the monolith kept moving and the test was halted for safety reasons. At the failure load, the monolith displacement was 3.2 in. Residual horizontal displacement was 1.4 in. after complete unloading. There was no evidence of structural failure of the timber piles.

#### **8.3.6      Monolith M7 (Lateral Load Test)**

Monolith M7 rested on a single timber pile to the west of M2. The soil around the pile was grouted. The berm was 25 ft from the north end of the monolith.

Behavior of monolith M7 under a constant axial load of 30 t and increasing lateral load is depicted in Fig. 8.6. The maximum lateral load applied was 20 t. Larger loads could not be sustained nor was a stable monolith displacement obtained. At the failure load of 20 t, the monolith had deflected 2.4 in. near ground surface.

#### **8.3.7      Monolith M5 (Axial Load Test)**

Monolith M5 rested on a 2 x 4-pile group. The soil around the timber piles was not grouted. The berm was 25 ft from the north end of the monolith. The behavior of monolith M5 under no lateral load and increasing axial load is depicted in Fig. 8.7. The maximum sustained axial load was 720 t or an average of 90 t/pile. This load was taken as the failure load. Settlement at the failure load was 2.3 in. at the north end of the monolith and 3.2 in. at the south end. When the load was increased to 750 t, the monolith continued to settle quickly and unevenly, and the settlement did not show signs of stabilization. There was no evidence of structural failure of the timber piles.

The axial load test on monolith M5 will be further discussed in a separate document to be prepared for the Corps of Engineers and Department of Transportation.

#### 8.4 EVALUATION OF TEST RESULTS

##### 8.4.1 Evaluation of Predictions

Results of the lateral load tests are summarized in Table 8.1. The load-deflection predictions made at the design stage do not compare well with actual measurements because of differences between assumed and actual conditions. The monoliths were cyclically preloaded and subjected to the effects of nearby pile driving prior to being load tested. This was not taken into account in the predictions. For this reason, the lateral behavior predictions are compared to the monolith response during initial loading at the beginning of cyclic preconditioning (Section 6).

##### 8.4.2 Effects of Grouting

Grouting in the upper 20 ft of soil surrounding the timber piles in monoliths M3 and M7 (Section 5.5) had different effects on the pile group (M3) and single pile (M7). Comparing monolith M3 (grouted) with monolith M2 (ungrounded), the two monoliths mobilized the same lateral load capacity, but the grouted monolith exhibited slightly stiffer elastic response. The stiffer response in the case of monolith M3, may be the result of a shorter duration of each load increment and incomplete stabilization of horizontal displacement.

Typically, soil grouted with the type of grout used in the tests exhibits a time-dependent deformation response and some strain hardening at large strains. This response was observed in the results of laboratory and in situ tests (Section 9.5.2, Volume II and Section 5.4.2, above) performed on this grout, and lateral load tests on prototype piles (Section 10). No significant creep or strain hardening behavior was noted for monolith M3. This atypical grouted soil behavior may be the result of incomplete grouting near ground surface caused by grout leaks around the timber piles (Section 5.5.5).

The single pile under monolith M7 mobilized a lateral load capacity 33 percent larger than monolith M6 in ungrouted soil. The lateral load-deflection curve in Fig. 8.6 indicates a marked strain hardening response of monolith M7; this is believed to account for the larger load at failure. Lower grouted soil stiffness was also mobilized early in the test, at low lateral load level, as indicated by the elastic portion of the load-displacement curve; this may be due to some creep effects, although the stress duration for this test was short compared to the test in ungrouted soil. On the basis of the results of the lateral load on monolith M7, it can be concluded that grout was effectively injected around the single timber pile.

##### 8.4.3 Effects of Pile Groups

There was some difference in response to lateral load between the two timber pile groups of monolith M1 (3 x 4 pile) and monolith M2 (2 x 4 piles), and the single timber pile of monolith M6. Table 8.1 shows that the lateral load per pile at failure was the same for monoliths M2 and M6. The lateral load per pile at failure for monolith M2 was 5 percent larger than that for monolith M1. The load at

failure for monolith M6 may have been slightly underestimated due to early termination of the test. The single timber pile showed a stiffer response early in the test; the slope of the elastic portion of the load-displacement curve is 30 percent larger for monolith M7 than for monolith M2, and 12 percent larger for monolith M2 than for monolith M1.

Several factors must be considered in comparing the lateral load test results. Monolith M1 was located only 8 ft from the monolith trench berm; monolith M2 was 25 ft away from the berm. The proximity of the berm increased the in situ confining stress which would tend to increase the lateral resistance of the soil and stiffen the response of the monolith. Under similar stress conditions monolith M1 would probably have shown a greater disparity with monolith M2. Also, monolith M1 was surrounded with unloaded timber piles; these piles tended to confine the soil around the loaded timber piles and increase its apparent stiffness.

In comparing the pile groups with single piles, it must be remembered that the heads of the piles in the groups were fixed against rotation. The single pile heads were partially fixed against rotation due to the axial load; this fixity was less than complete, however, because rotation of the pile cap and tilting of the axial jack were observed during the tests. Tilting and translation were so severe at times, that the axial jack had to be unloaded and repositioned on the single pile monoliths. Typically, the deflection of a free-head pile should be twice that of a fixed-head pile under otherwise same conditions. Accordingly, because the observed response of the single timber pile under monolith M6 was somewhat stiffer than that of the pile groups, the lateral resistance of this single pile is larger than that of the eight-pile groups.

Horizontal Monolith Displacement in.  in.	Loads t	Monolith No. and Timber Pile Configuration				
		M1 (3 x 4)	M2 (2 x 4)	M3 <sup>(2)</sup> (2 x 4)	M6 (single)	M7 <sup>(2)</sup> (single)
0.25	Total	24	18	14	4.8	2.4
	Average/pile <sup>(3)</sup>	2	2.3	1.8	4.8	2.4
0.5	Total	44	35	28	8.2	4.8
	Average/pile	3.7	4.4	3.5	8.2	4.8
1.0	Total	84	60	53	11.9	11.2
	Average/pile	7	7.5	6.6	11.9	11.2
Failure <sup>(4)</sup>	Total	172	120	118	15	20
	Average/pile	14.3	15	14.8	15	20

Notes:

- (1) Horizontal displacement measured at 3 ft above ground surface for M1, M2, and M3 9 in. above ground surface for M6 6 in. above ground surface for M7
- (2) Grouted; all other monoliths ungrouted
- (3) Average/pile = Total load/No. of piles
- (4) Failure load = maximum sustained load

**PILE DRIVING EFFECTS TEST PROGRAM**

**SUMMARY OF MONOLITH LATERAL LOAD TEST RESULTS**

FOUNDATION INVESTIGATION AND TEST PROGRAM  
EXISTING LOCKS AND DAM NO. 20  
BY LOUIS DISTRICT, CORPS OF ENGINEERS.  
BACW43-76-C-0000

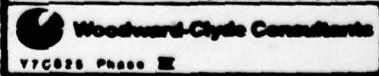
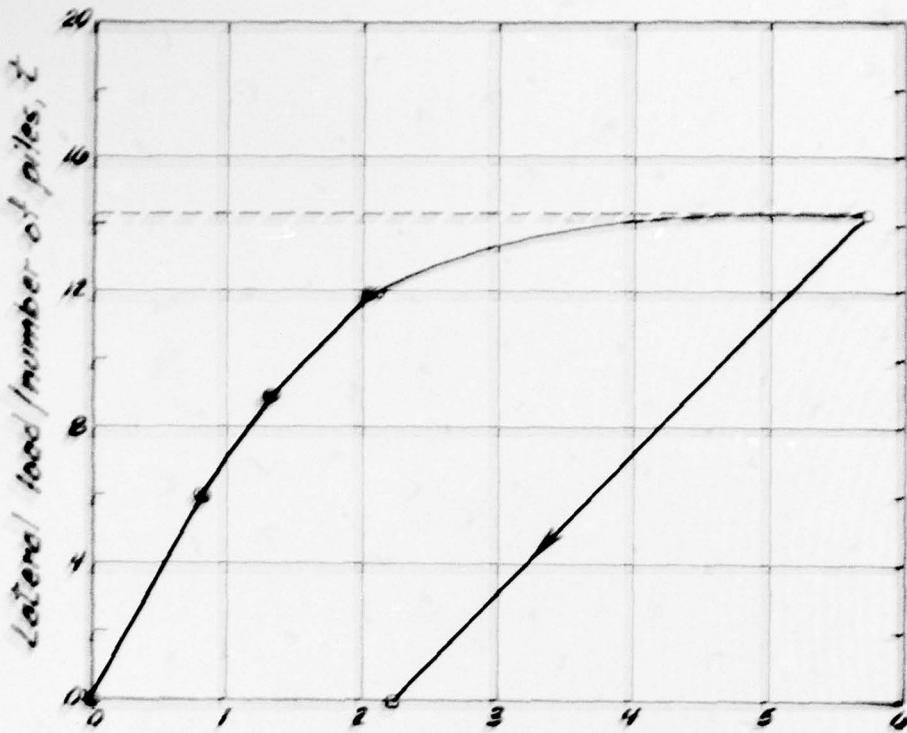


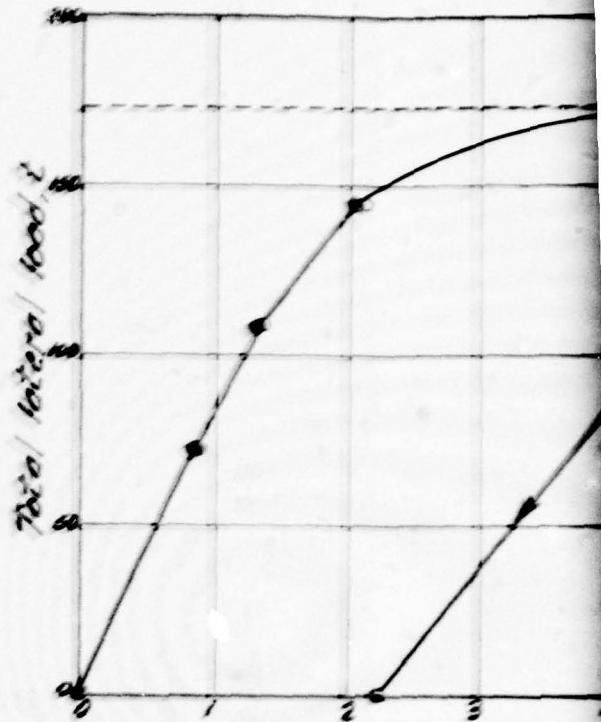
Table 8.1



Horizontal displacement of monolith during lateral load test, in.

Legend

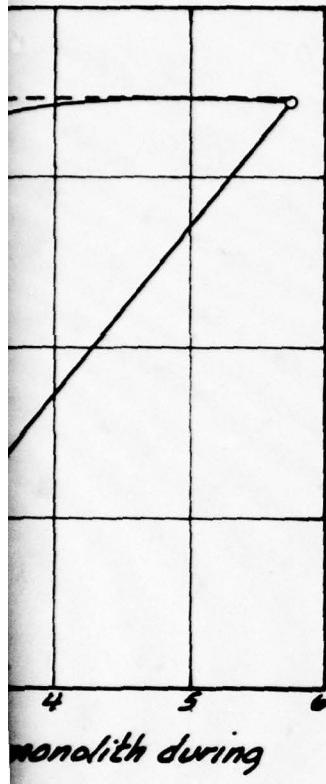
- Reference point data, measured at approximately 3.5 ft above ground surface
- Corrected linear potentiometer data, measured at approximately 3 ft above ground surface
- Residual horizontal displacement after complete unloading (axial and lateral)



Horizontal displacement of monolith during lateral load test, in.

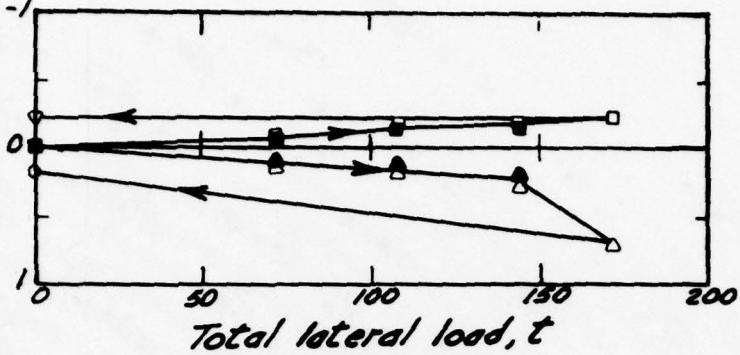
Notes:

- (1) Axial load during test was 300 kips
- (2) Berm toe was 8 ft from north end
- (3) Horizontal displacement of monolith during lateral load testing, was 1.90 in.
- (4) Settlement of monolith prior to lateral load test was 1.11 in. at south end and 2.06 in. at north end
- (5) Residual displacements after completion of lateral load test were reference point data



monolith during

Settlement of monolith during lateral load test, in.



### Legend

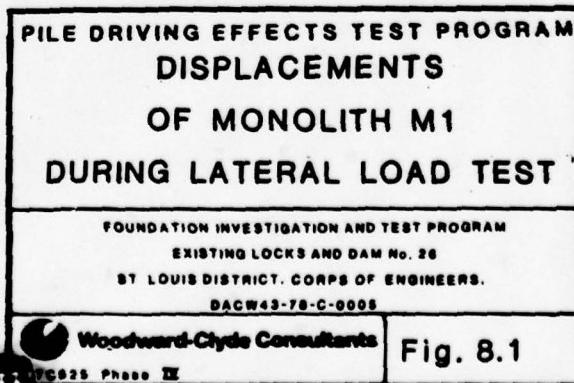
- Reference point data at south end of monolith
- Corrected linear potentiometer data at south end of monolith
- Residual settlement at south end of monolith after complete unloading (axial and lateral)
- △ Reference point data at north end of monolith
- ◆ Corrected linear potentiometer data at north end of monolith
- Residual settlement at north end of monolith after complete unloading (axial and lateral)

360 t

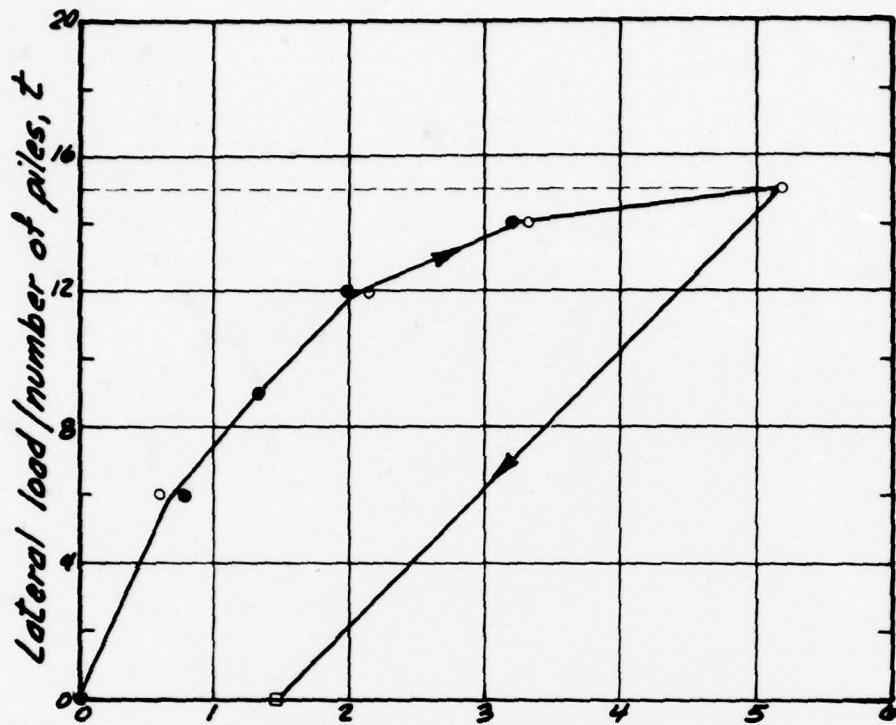
at end of monolith  
dith prior to

to load testing,  
in. at north end

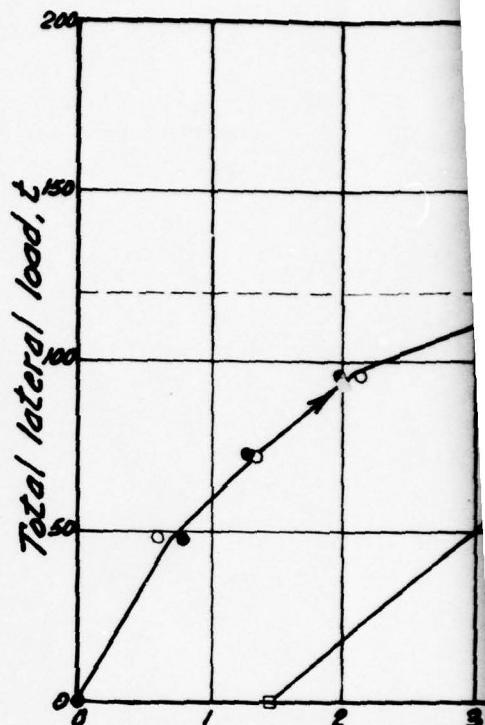
After unloading



7



Horizontal displacement of monolith during lateral load test, in.



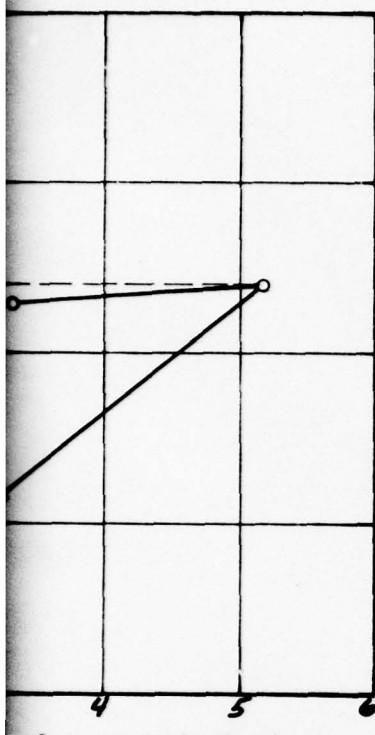
Horizontal displacement lateral load test, in.

#### Legend

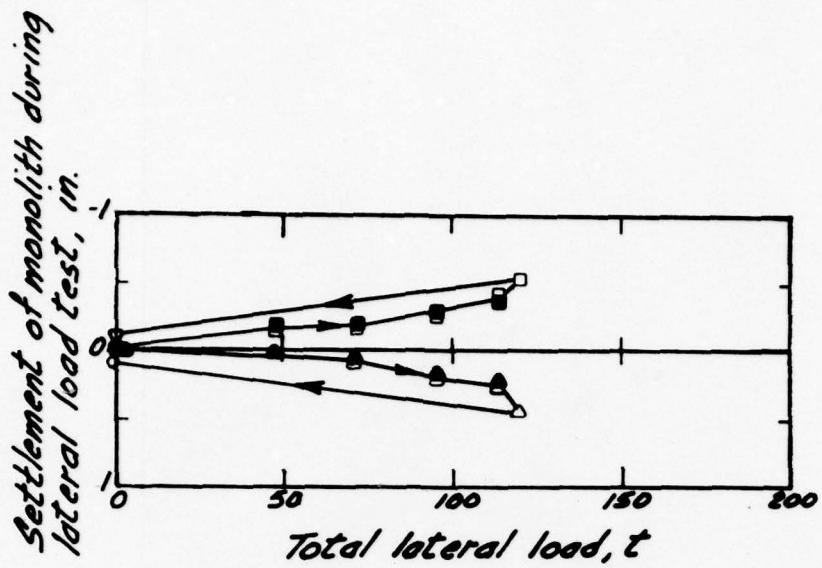
- Reference point data, measured at approximately 4 ft above ground surface
- Corrected linear potentiometer data, measured at approximately 3 ft above ground surface
- Residual horizontal displacement after complete unloading (axial and lateral)

#### Notes:

- (1) Axial load during
- (2) Berm toe was
- (3) Horizontal displace load testing, w
- (4) Settlement of a was 0.95 in. at s of monolith
- (5) Residual displac unloading are



of monolith during



#### Legend

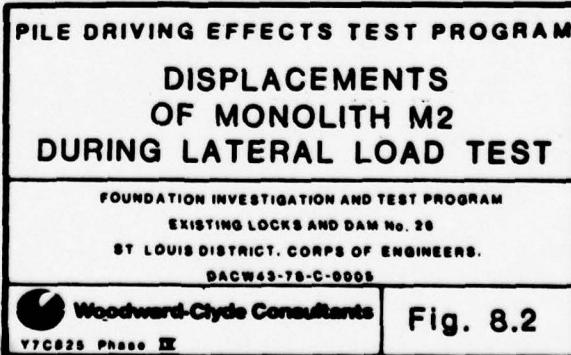
- Reference point data at south end of monolith
- Corrected linear potentiometer data at south end of monolith
- Residual settlement at south end of monolith after complete unloading (axial and lateral)
- △ Reference point data at north end of monolith
- ▲ Corrected linear potentiometer data at north end of monolith
- ◇ Residual settlement at north end of monolith after complete unloading (axial and lateral)

test was 240 t

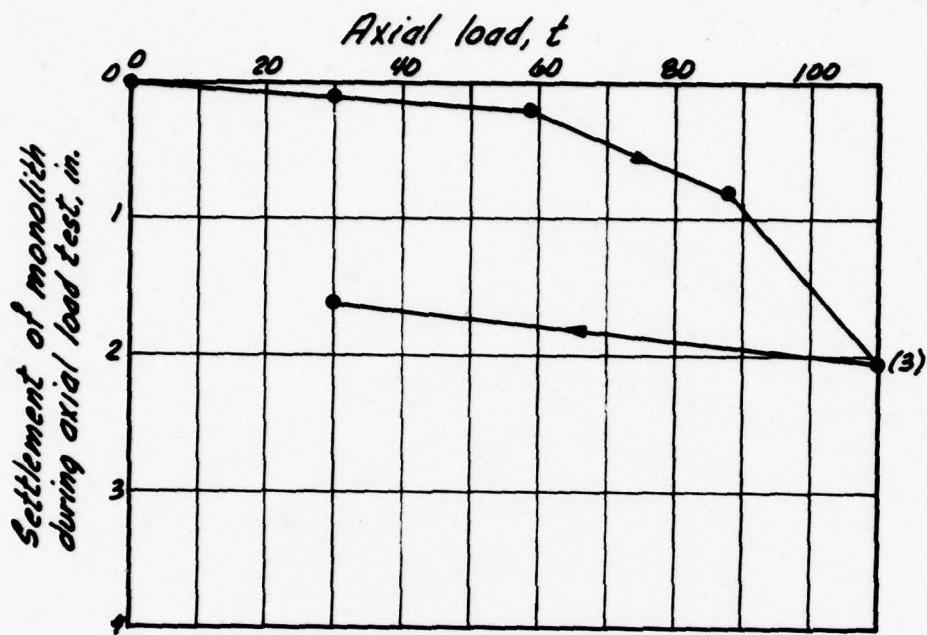
ft from north end of monolith  
ment of monolith, prior to  
2.20 in.

monolith prior to load testing  
th end and 1.54 in. at north end

ments after complete  
reference point data



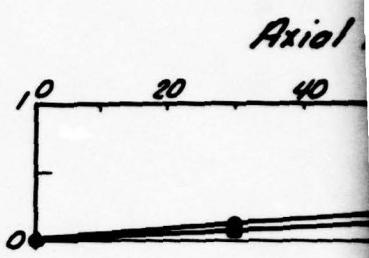
2



Legend

- Corrected linear potentiometer data measured at 33 in. above ground surface

Horizontal displacement of monolith during axial load test, in.



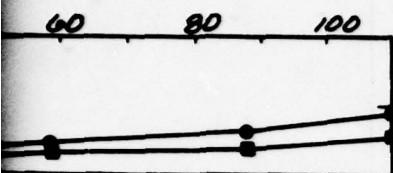
Legend

- Corrected linear data measured at 33 in. above ground surface
- Corrected linear data measured at 9 in. above ground surface

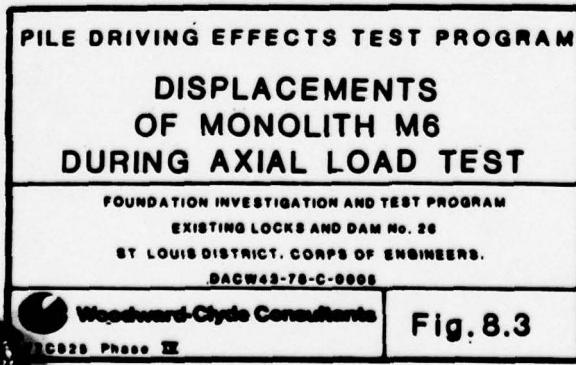
Notes

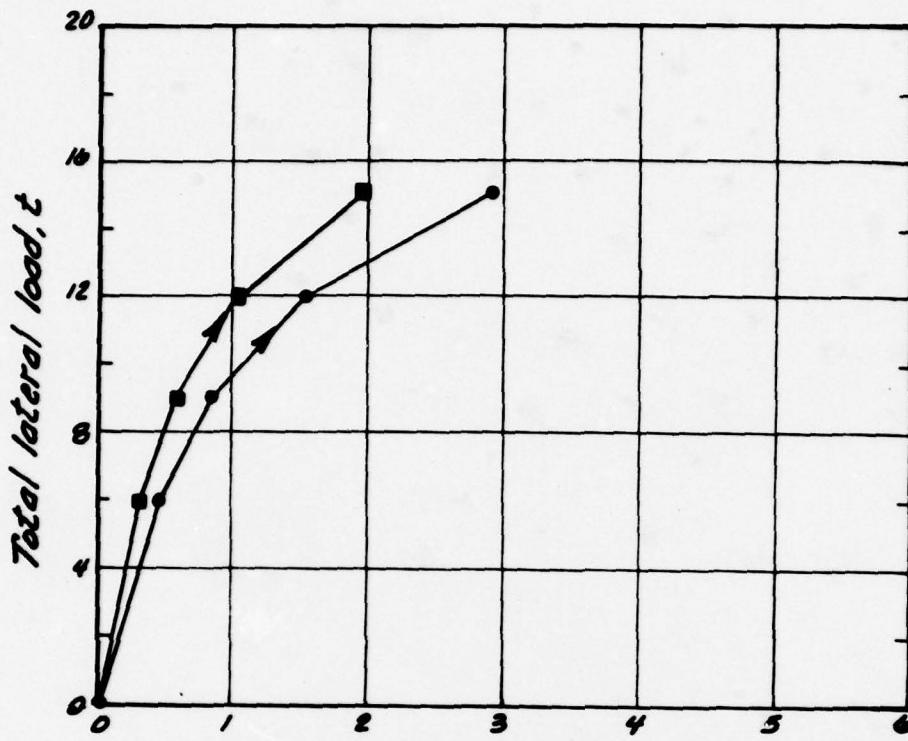
- (1) Berm toe was 25 ft from monolith
- (2) Settlement of monolith, prior to load testing, was 1.76 in., measured at 33 in. above ground surface
- (3) Monolith continued to settle under that load
- (4) No lateral load applied to monolith during axial load test

*load, t*



potentiometer data  
in. above ground surface  
potentiometer data  
in. above ground surface





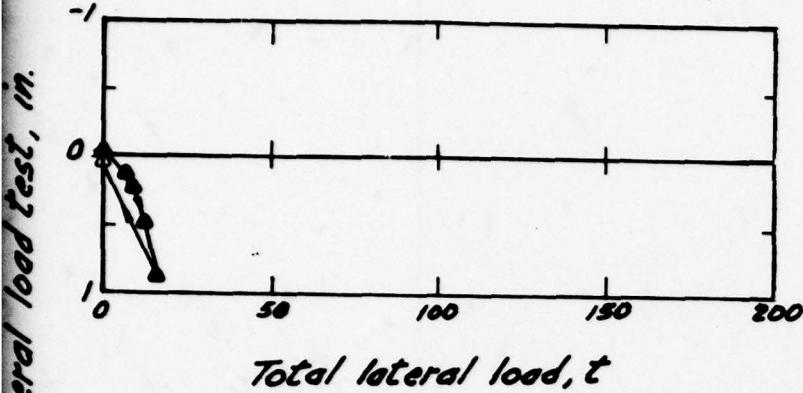
Horizontal displacement of monolith during lateral load test, in.

#### Legend

- Corrected linear potentiometer data measured at 3 in. above ground surface
- Corrected linear potentiometer data measured at 9 in. above ground surface

#### Notes:

- (1) Axial load during test
- (2) Berm toe was 25 ft
- (3) Horizontal displacement during load testing was 2.47 in. above ground surface
- (4) Lateral load was applied 9 in. above ground surface



*Legend*

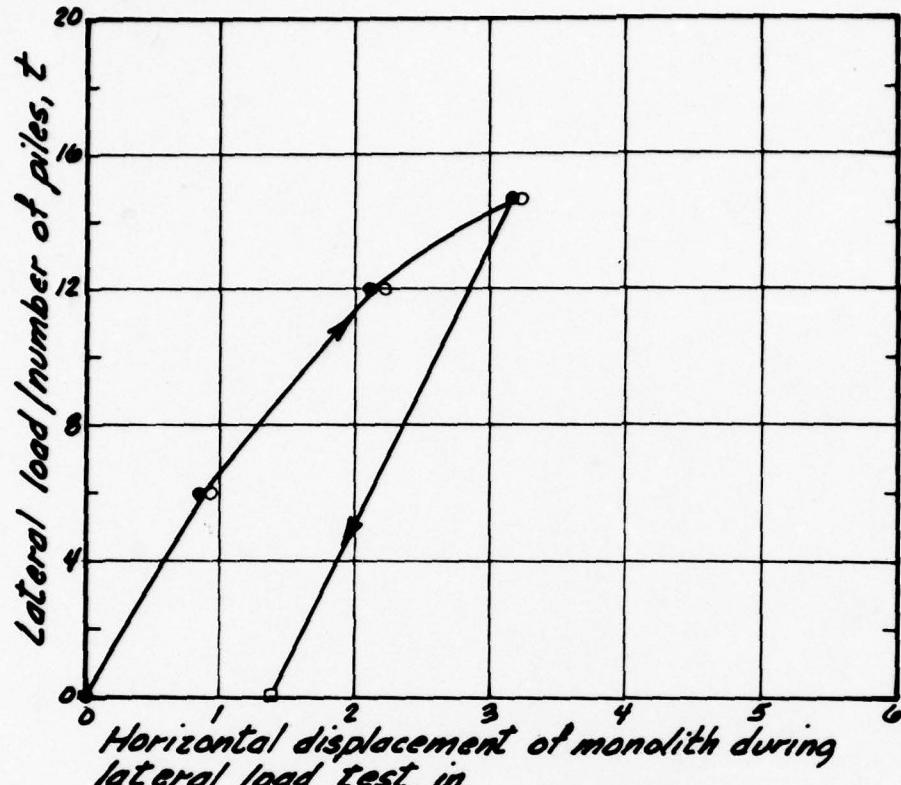
- ▲ Corrected linear potentiometer data measured at 33 in. above ground surface
- △ Residual settlement of monolith after complete unloading (axial and lateral)

test was 30 t  
 from monolith  
 ent of monolith prior to  
 7 in., measured at 33 in.

plied at 20 in.

<b>PILE DRIVING EFFECTS TEST PROGRAM</b>	
<b>DISPLACEMENTS</b>	
<b>OF MONOLITH M6</b>	
<b>DURING LATERAL LOAD TEST</b>	
FOUNDATION INVESTIGATION AND TEST PROGRAM	
EXISTING LOCKS AND DAM NO. 28	
ST LOUIS DISTRICT, CORPS OF ENGINEERS.	
DACW43-76-C-0026	
 Woodward-Clyde Consultants <small>77C025 Phase II</small>	<b>Fig. 8.4</b>

2

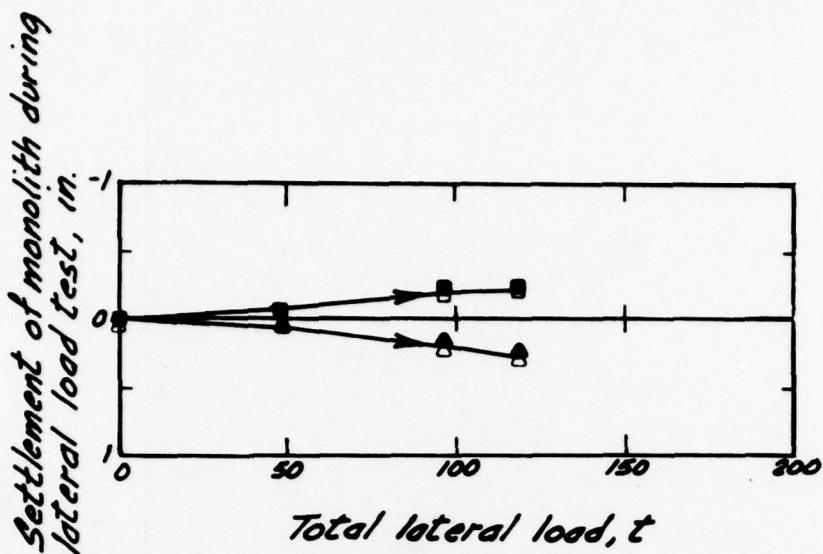


#### Legend

- Reference point data, measured at approximately 4 ft above ground surface
- Corrected linear potentiometer data, measured at approximately 3 ft above ground surface
- Residual horizontal displacement after complete unloading(axial and lateral)

#### Notes:

- (1) Axial load during
- (2) Berm toe was 25 ft
- (3) Horizontal displacement during load testing, was 1.
- (4) Settlement of monolith was 0.38 in. at south end of monolith
- (5) Residual displacements are reference point



*Legend*

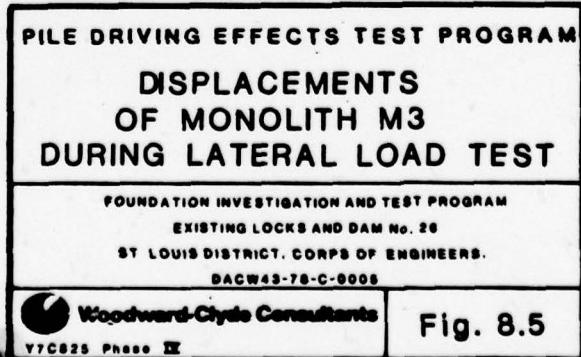
- Reference point data at south end of monolith
- Corrected linear potentiometer data at south end of monolith
- △ Residual settlement at south end of monolith after complete unloading (axial and lateral)
- ◇ Reference point data at north end of monolith
- ◆ Corrected linear potentiometer data at north end of monolith
- Residual settlement at north end of monolith after complete unloading (axial and lateral)

test was 240 t

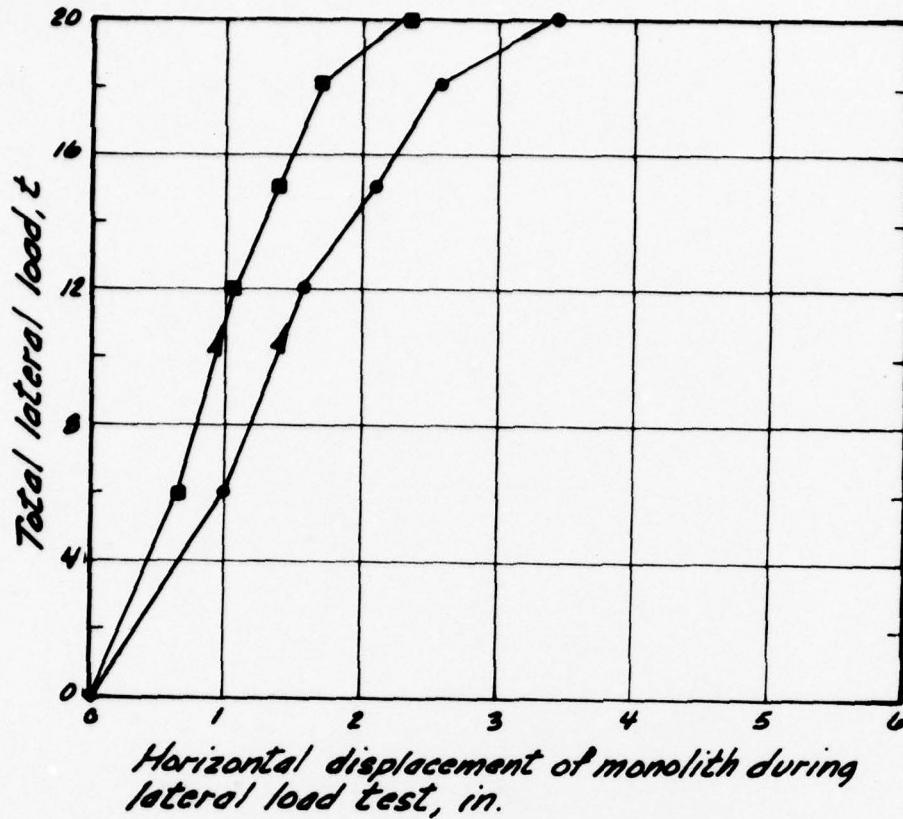
ft from north end of monolith  
ment of monolith, prior to  
1.92 in.

plith, prior to load testing,  
h end and 1.05 in. at north end

's after complete unloading  
data



2



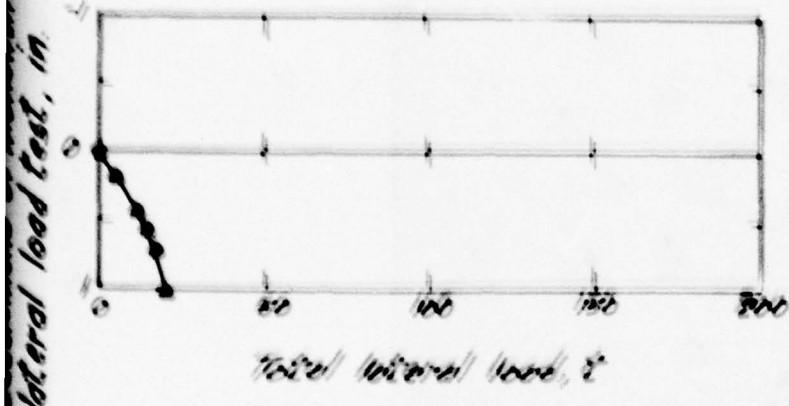
Horizontal displacement of monolith during lateral load test, in.

#### Legend

- Corrected linear potentiometer data measured at 3 in. above ground surface
- Corrected linear potentiometer data measured at 7 in. above ground surface

#### Notes:

- (1) Axial load during
- (2) Berm toe was 2
- (3) Horizontal displa  
load testing ma  
above ground sur
- (4) Lateral load was  
above ground sur



*Legend*

- Correlated linear potentiometer data measured in 1 in above ground surface

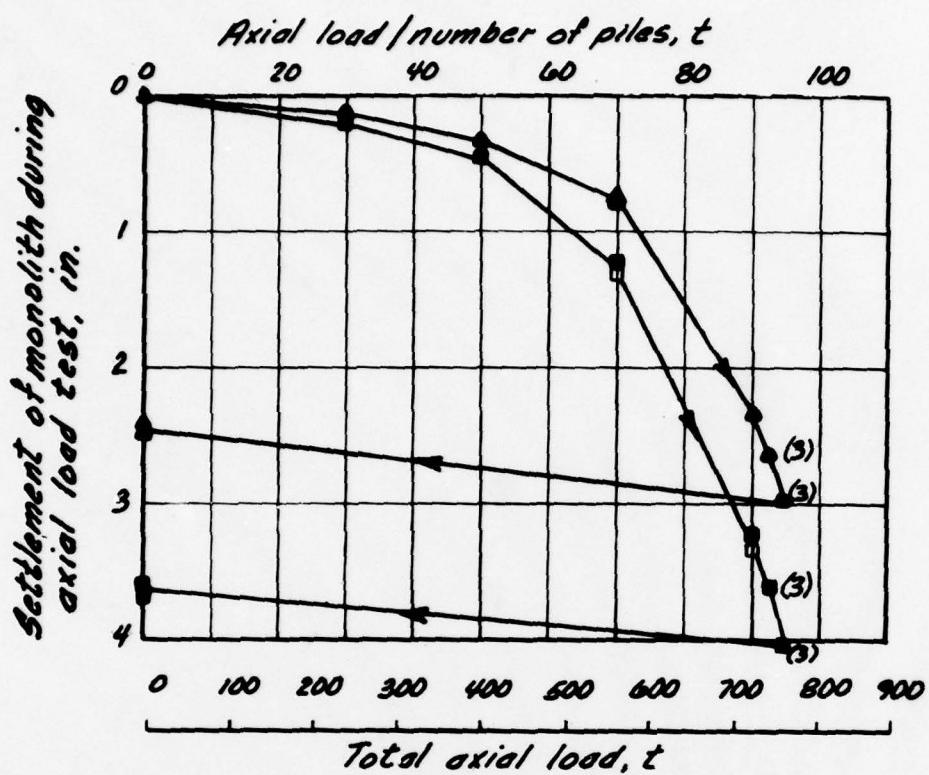
Ring load was 30 k

25 ft from monolith

Distance of monolith, prior to  
no 161 in., measured at 31 in.  
place

• applied at 37.5 in.  
place

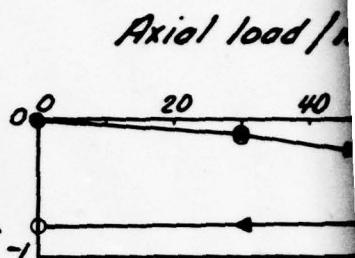




#### Legend

- Reference point data at south end of monolith
- Corrected linear potentiometer data at south end of monolith
- △ Reference point data at north end of monolith
- ▲ Corrected linear potentiometer data at north end of monolith

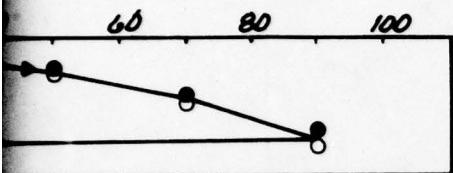
Horizontal displacement of monolith during axial load test, in.



#### Notes:

- (1) Berm toe was at the south end of monolith.
- (2) Settlement measured at south end of monolith.
- (3) Monolith corrected to those loads.
- (4) No lateral movement during axial load test.

number of piles, t



point data

linear potentiometer data

was 25 ft from north  
monolith  
at of monolith, prior to  
ing, was 0.23 in. at  
and 0.77 in. at north  
monolith  
continued to settle under  
load applied to monolith  
load test



J

**PHASE IV REPORT**

**VOLUME III**

**RESULTS AND INTERPRETATION OF  
PILE DRIVING EFFECTS TEST PROGRAM**

**SECTION 9**

**DETAILED EVALUATION OF BEHAVIOR OF MONOLITH M2**

## 9 DETAILED EVALUATION OF BEHAVIOR OF MONOLITH M2

### 9.1 SCOPE OF DETAILED EVALUATION

Monolith M2 is selected as a reference case on which to base comparisons made to evaluate the influence of various test variables. The detailed behavior of monolith M2 is examined to explain the mechanisms governing pile driving effects. Predicted and measured displacements and peak particle velocities at ground surface are compared.

### 9.2 MONOLITH DISPLACEMENTS CAUSED BY PROTOTYPE PILE DRIVING

#### 9.2.1 General

A study was made to investigate potential correlations between observed ground vibration characteristics, such as near-surface peak vectorial particle velocity, and observed monolith displacement. As discussed in Section 7.3.3, the trend of the relationship between cumulative peak velocity (expressed as the summation of the product of peak vectorial particle velocity for each foot of prototype pile penetration times the number of hammer blows required for each foot of penetration) and the prototype pile penetration depth was similar for primary prototype pile driving systems at 40 ft to 15 ft from the monoliths. Plots of cumulative peak velocity vs prototype pile tip elevation are shown in Fig. 7.20 for the various monoliths.

#### 9.2.2 Cumulative Peak Velocity vs Monolith Displacements

Incremental horizontal displacement and settlement of monolith M2 caused by driving prototype piles 1 through 6 are shown in Fig. 9.1 vs prototype pile tip elevation. The data is based on corrected linear potentiometer data; incremental settlement is based on data (Section 7.3.4) obtained at the north end of the monolith, closest to prototype piles. The trend towards larger displacements during the second half of each prototype pile driving is again clear in these figures. More importantly, the general trend of the curves is very similar to that exhibited by the curves in Fig. 7.20 of cumulative peak velocity vs prototype pile tip elevation.

Cumulative peak velocities were calculated for each prototype pile 1 through 6 driven at monolith M2 for corresponding pile tip penetration depth. Examples of these results are shown for prototype piles 3 and 4 in Fig. 9.2. The cumulative peak velocity data was generated for the near-surface geophone G5-1 (1 ft below ground surface) and for the deep geophone G5-50 (located directly below G5-1 and 50 ft below ground surface, Fig. 7.2). The trends of the curves in Fig. 9.2 are similar to those of the curves in Fig. 9.1. The horizontal displacement of monolith M2 correlates better with the near surface geophone data; the settlement of monolith M2 correlates better with the deep geophone data. This is to be intuitively expected.

Incremental displacements shown in Fig. 9.1 are plotted in Fig. 9.3 vs corresponding calculated cumulative peak velocity values. Although there is a certain degree of scatter, there are definite trends in the data of Fig. 9.3. As a first approximation, the data can be fitted by eye by straight lines drawn through the origin. In Fig. 9.3a (horizontal displacement) three lines (A, B, and C), appear to fit the data for distances between prototype pile and monolith of 50 ft, 20 ft and 15 ft, respectively. The slope of these lines is plotted in Fig. 9.3b vs distance between prototype pile and monolith. In Fig. 9.3c (settlement) the data corresponding to all distances appears to be fitted best by a single straight line. The relationship between settlement and cumulative peak velocity is approximately independent of the distance between prototype pile and monolith.

The incremental displacement of a monolith caused by driving any prototype pile at any distance and to any tip penetration depth, can be estimated by multiplying the appropriate value of slope from Fig. 9.3b (horizontal displacement) or Fig. 9.3c (settlement) by the appropriate measured or expected cumulative peak velocity. For example, incremental horizontal displacement caused by prototype pile 3 at 20 ft can be estimated by multiplying the cumulative peak velocity<sub>5</sub> data of Fig. 9.2 by the slope value corresponding to 20 ft (that is,  $34 \times 10^{-5}$  in./in./s per blow/ft in Fig. 9.3b); similarly, the monolith settlement can be calculated using the slope value of  $-57 \times 10^{-4}$  in./in./s per blow/ft in Fig. 9.3c. The curves generated in this manner for prototype piles 1 through 6 at monolith M2 are shown as dashed lines in Fig. 9.1. The agreement between calculated and measured data is reasonably good, considering the approximations involved in the calculation procedure. This good agreement emphasizes the good correlation between cumulative peak velocity and displacements.

The procedure described above has a number of shortcomings; in particular:

- (1) it grossly oversimplifies a complex pile-soil-pile interaction problem by only considering vibration characteristics of a single point in the soil mass (that is, either near-surface geophone G5-1 or deep geophone G5-50);
- (2) it does not take into account prior loading or displacement history of the monolith; and
- (3) it is probably dependent on many of the test variables and specific site conditions.

Nevertheless, the relationship between observed ground vibration characteristics and monolith displacements established above constitutes the first step in the attempt to quantify the mechanisms governing monolith behavior under various conditions. This cumulative peak velocity-displacement relationship is consistent with the approach used for prediction (Section 2.3.2).

### 9.3 DYNAMIC RESPONSE CHARACTERISTICS

#### 9.3.1 General

**Purpose of Study.** The study presented in this section demonstrates the techniques and procedures that may be used to interpret detailed aspects of ground and monolith vibrations, and better understand the dynamic response of the monolith-timber pile foundation system. The scope of this study is by no means complete; it does show an approach for evaluating dynamic mechanisms contributing to the observed behavior of the monoliths.

**Data Base.** The characteristics of ground vibration caused by nearby prototype pile driving, in terms of peak vectorial particle velocity recorded by a near-surface geophone adjacent to the monoliths, are discussed in Section 7.3.3. A potential relationship between cumulative peak velocity and monolith displacement caused by nearby prototype pile driving is presented in Section 9.2.2. Examination of additional dynamic data recorded during the tests (Section 3.2.7), such as peak vectorial and component particle velocity from geophones other than the two mentioned above, and digitized velocity time histories from analog magnetic tape records, indicates a reasonable consistency in the vibration data; vibration data from all these instruments complement each other and can be used in elucidating the mechanisms governing pile driving effects.

**Compatibility of Data.** The time history for the three components ( $x$  = transverse,  $y$  = longitudinal, and  $z$  = vertical) of particle velocity were recorded for all geophones used in a given prototype pile driving test on oscilloscopes (Section 3.2.7). The peak values of each velocity component can be scaled for any prototype pile tip elevation from the oscilloscope traces. The peak values of velocity components for prototype piles 1, 2, and 6 at monolith M2, scaled from the oscilloscope traces, are shown at the left side of Fig. 9.4 through Fig. 9.6, respectively. The corresponding ratios of transverse to vertical ( $x/z$ ) and longitudinal to vertical ( $y/z$ ) components are shown in these figures. The velocities calculated as:

$$x^2 + y^2 + z^2$$

and referred to as the square root of the sum of the squares (SRSS), are compared to peak vectorial velocities directly recorded by the S4 peak vibration monitors (S4) (Section 3.2.7 and Appendix J, Volume IIIA) at the right side of Fig. 9.4 through Fig. 9.6.

Theoretically, the SRSS values should form an upperbound envelope of the peak vectorial velocity values, because the peaks of the three component velocities did not necessarily occur simultaneously. This is generally corroborated by the data in the figures. During a given test, only selected geophones were monitored through the S4 peak vibration monitors or analog magnetic tape recorders; the output of all the geophones was recorded on oscilloscopes. The compatibility of S4 data (either recorded during the tests or played back from the magnetic tapes after the tests) and oscilloscope data confirms that the limited S4 data can be supplemented by the more complete oscilloscope data, if necessary.

### 9.3.2 Component Peak Velocities

From Fig. 9.4 through Fig. 9.6, it appears that generally the values of peak x-component velocity (transverse) were relatively large near ground surface (geophone G5-1), and relatively small at depth (geophone G5-50) for all cases. Considering the radial distribution of the seismic waves generated at a prototype pile tip, the large transverse (x) component observed near ground surface is unexpected.

There is a noticeable difference in the shape of the curves depicting peak vectorial particle velocity vs prototype pile tip elevation for G5-1 at 20 ft and 15 ft in Fig. 9.5 and 9.6, respectively. This difference is mainly due to variations of the peak x-component velocity; the z-component, and to a lesser degree the y-component, are reasonably similar in both cases. The z-component data from geophone G5-15 (15 ft below ground surface) are very similar for both prototype piles driven at 20 ft (Fig. 9.5) and 15 ft (Fig. 9.6) from the monolith.

A summary plot of peak vectorial particle velocity vs prototype pile tip elevation for geophone G5-50 is shown in Fig. 9.7. The peak vectorial velocity for this deep geophone reflects the general trend of the z-component velocity shown in Fig. 9.4 through 9.6. There is also a marked similarity between the trend of the velocity range for prototype piles driven at about 20 ft and the trend of the blowcount range for the same piles (Fig. 7.6).

It was noted in Section 9.2, that the incremental horizontal displacement of monolith M2 caused by nearby prototype pile driving correlated well with the data from near-surface geophone G5-1; the incremental settlement correlated better with the data from deep geophone G5-50. It appears that the horizontal displacement of M2 was more affected by the x- and y-component velocities near ground surface; the settlement appears to have been more affected by the z-component velocity.

### 9.3.3 Velocity and Acceleration Time Histories

Digitized data recorded during the tests on analog magnetic tape (Section 3.2.7 and Appendix I, Volume IIIA) were processed through a computer. Examples of this analysis are presented in Fig. 9.8 in the form of velocity time histories. The data in these figures are from geophones G5-1, G5-15, and G5-50 (Fig. 7.2) for prototype pile 6 at monolith M2, when the pile tip was at a depth of about 50 ft (el 341). Again, it is clear from Fig. 9.8 that near the ground surface, a soil particle motion was in three directions; at greater depth (50 ft), the motion was primarily vertical (z) and longitudinal (y).

The peak values from component velocity time histories for geophone G5-1 data in Fig. 9.8 are summarized below. These values are compared with corresponding values scaled from oscillograph traces, and with SRSS values (Section 9.3.1) calculated from digitized records and oscillograph traces.

Prototype Pile Tip Elevation ft	Peak Velocity, in./s								Vectorial (S4 Peak Vibration Monitors)	
	Digitized Data				Oscillograph Data					
	<u>x</u>	<u>y</u>	<u>z</u>	<u>SRSS</u>	<u>x</u>	<u>y</u>	<u>z</u>	<u>SRSS</u>		
el 341	0.29	0.12	0.23	0.39	0.24	0.17	0.21	0.37	0.36	

The consistency apparent in the three sets of data above existed for almost all the data examined.

The digitized velocity time histories were also converted to acceleration and displacement time histories by numerical differentiation and integration techniques. The acceleration and displacement time histories thus calculated are shown in Fig. 9.9 for near-surface geophone G5-1 (solid curves) and geophone MG1 mounted on the north face of monolith M2 (dashed curve); the velocity data, also shown in Fig. 9.9, were recorded during driving of prototype pile 6, as the prototype pile tip reached at depth of 70 ft below ground surface (el 321). The ground motion was characterized by high acceleration (0.2 g maximum) and low displacement (0.004 in. maximum). The monolith motion in x- and y-directions was considerably smaller than that of the ground; however, vertical motions of the ground and monolith were similar.

From these time histories, it can be seen that the monolith was oscillating both in x- and y-directions at a relatively constant period or frequency during the later part of a hammer blow. The period was 0.14 s in the x-direction and 0.1 s in the y-direction. The period of 0.1 s in the y-direction is consistent with the natural period of monolith M2 that can be calculated on the basis of the lateral load test results.

#### 9.3.4 Response Spectra

Time history plots can be used to derive peak values and duration of vibratory movement; they are not convenient to observe frequency content of the movement. The combined effects of frequency and amplitude can be represented by means of a response spectrum. The velocity or acceleration response spectrum of a given vibration is a plot showing the maximum velocity or acceleration induced by the vibrations in single-degree-of-freedom oscillators of different fundamental periods, but having the same degree of internal damping. The maximum velocity or acceleration is plotted as a function of the fundamental period of the single-degree-of-freedom oscillators.

The velocity and acceleration response spectra at 5 percent damping corresponding to the motions shown in Fig. 9.9 are presented in Fig. 9.10. The ground motion is shown by solid lines; the monolith motion is shown by dashed lines. The relatively small monolith motion, when compared to that of the ground in both the x- and y-directions, is again apparent. For the monolith motion, a small peak

is noted at approximately 0.14 s for the x-direction and 0.1 s for the y-direction. These values represent the free vibration periods of the monolith discussed in Section 9.3.3.

#### 9.3.5 Conclusions

The main purpose for conducting detailed analyses of selected geophone data was to present the type of analyses that can be performed with the large amount of vibration data collected during the tests, and illustrate the nature of the results derived from such analyses. The importance of the motion in x-direction near ground surface was established. The analyses of digitized records showed a clear relationship between ground and monolith vibratory motions.

### 9.4 DEFORMATION OF THE TIMBER PILE-SOIL SYSTEM

#### 9.4.1 General

The deflection of the timber piles of monolith M2 and the deformation of the surrounding soil during prototype pile driving and subsequent lateral load testing are examined in some detail in the following sections. This detailed examination provides a perspective of the timber pile-soil interaction mechanisms. Only selected cases are used to highlight the dominant trends. The data obtained at the end of cyclic preloading are in excellent agreement with the data obtained upon reloading of the monolith before prototype pile driving; the former data are not considered herein. An itemized description of all measurement events is summarized for each monolith in the respective Appendices L through P, Volume IIIA.

#### 9.4.2 Deformation During Prototype Pile Driving

**Horizontal Deformation.** The results of timber pile inclinometer measurements (Section 3.1.5) made during prototype pile driving for monolith M2 are summarized in Fig. 9.11a through 9.11e. In these figures, corresponding horizontal displacements of the monolith, measured three above ground surface, and of the four corner timber piles, measured a few inches above ground surface, are also shown. The monolith and timber pile displacements above ground are based on corrected linear potentiometer data. The cases shown in these figures correspond to:

- (1) initial deflection at W<sub>2</sub> load level (30 t/pile axial load and 6 t/pile lateral load); this load level was maintained throughout prototype pile driving;
- (2) deflection after driving prototype pile 3, except for timber pile 10 (prototype pile 1 was driven at 50 ft, piles 2 and 3 were driven at approximately 20 ft from monolith M2);
- (3) deflection after driving prototype pile 6 (prototype piles 4 and 5 were driven at approximately 20 ft from monolith M2) and pile 6 at approximately 15 ft; and
- (4) deflection after driving prototype pile 12 (prototype piles 7 and 8 were driven with the diesel hammer, H piles 9 and 10 and sheet piles 11 and 12 were driven with the vibratory hammer, all at 15 ft from monolith M2, except pile 7 and 9 that were driven at approximately 20 ft).

In all cases, the inclinometer deflection and monolith displacement values are with reference to initial readings made before cyclic preloading of monolith M2. The inclinometer deflections are projections of vectorial deflections on a vertical, north-south plane (y-direction). In general, the x-components of the inclinometer deflections were at least one order of magnitude smaller than the y-components.

The timber pile-head and monolith displacements derived from the pile inclinometer measurements are less than those measured directly using the linear potentiometers and reference beams. The differences increased with the number of prototype piles driven. The difference was larger for the two northernmost timber piles 10 and 20 (0.6 in. at end of prototype pile driving) than for the two southernmost timber piles 14 and 30 (approximately 0.2 in. at end of prototype pile driving). This tendency was also observed for the other monoliths. The bottom of the pile inclinometers was at 27 ft below ground surface (el 364). The results shown in Fig. 9.11 assume that the bottom of the inclinometers remained stationary. The deviations from the linear potentiometer data above ground surface indicate that this was not the case; progressive lateral deflection of the timber piles occurred below el 364, with larger deflection occurring at the north end of the monolith.

The ground inclinometer data (Section 3.1.6) tend to substantiate the above observation. Ground inclinometer deflections are shown in Fig. 9.12a through 9.12c. Ground inclinometer PD3-D4 was inside the timber pile group and it extended upward through the concrete monolith. Ground inclinometers PD3-D5 and D6 were located immediately north of the timber pile group. The bottom of these inclinometers was approximately 60 ft below ground surface (el 331). The ground inclinometer data in Fig. 9.12 correspond to cases (1), (2), and (4) above.

Results from ground inclinometer PD3-D4 (Fig. 9.12a) within the timber pile group indicate a horizontal deflection on the order of 0.25 in. at the timber pile tip elevation (el 356). This deflection is represented by the sharp kink in the deflected shape of the inclinometer casing at that elevation. The magnitude of this deflection is in agreement with the difference in horizontal displacement above ground between the linear potentiometers and the timber pile inclinometers, particularly for timber piles 14, 30, and 46 (Fig. 9.11) surrounding inclinometer PD3-D4.

The deflected shape of inclinometers PD3-D5 and D6 at the end of prototype pile driving shows a steep slope at the base of the casings, indicating some horizontal deformation of the soil to a depth of at least 60 ft. This is not seen for inclinometer PD3-D4 within the timber pile group. The deflected position of inclinometer PD3-D5 (Fig. 9.12b) assuming the casing bottom was stationary (curve A) has been translated by matching inclinometer deflection and timber pile displacement at ground surface to obtain curve B. Curve B can be considered as representative of an upperbound of the soil deformation at depth. At comparable depths, the soil deformation is larger on the north side of the monolith than within the timber pile group.

Average pile and ground inclinometer results are shown in Fig. 9.13 at beginning and end of prototype pile driving. The deflections shown in this figure confirm that deep-seated horizontal soil deformation and timber pile deflection occurred during prototype pile driving; the soil deformation and pile deflection progressively increased from the north to the south end of the monolith, the larger movement occurring at the point closest to prototype pile driving. Timber piles 10 and 20 (north end) punched laterally into the soil by as much as 0.6 in. Timber piles 14 and 30 translated by only 0.25 in. The bulge in the deflected shape of the ground inclinometers (average of PD3-D5 and D6) implies very deep soil horizontal deformation of the order of 0.5 in. at a depth of 50 ft (el 341). This deep soil deformation was due to the axial and lateral loads applied to the monolith and timber piles, and/or a net volume change in the surrounding soil.

**Settlement.** The settlement measured at ground surface and on monolith M2 during prototype pile driving is shown in Fig. 9.14. The figure indicates that large areal settlement occurred at ground surface. The vertical distance between the solid lines in the figure represents the settlement of monolith M2. The tilting of the monolith, discussed in Section 7.3.4, is also apparent here. The monolith tilt closely followed the trend of ground surface settlement observed several feet from the monolith; this implies that redistribution of the axial load to resist overturning due to application of the lateral load had little influence on the settlement of the monolith.

The distribution of settlement at depth can be best described from the settlement of the reference beam supports. Sondex measurements (Section 3.1.6) were made only sporadically because they were time consuming; the accuracy and reliability of the measurements were also questionable at times. The reference beam supports are described in Section 3.2.1 and are shown in Fig. 3.7. During the course of prototype pile driving, the supports settled. The settlement was about 80 percent of that observed at ground surface, implying that a large portion of the observed surface settlement was caused by settlement at depths exceeding 40 ft.

#### 9.4.3 Deformation During Lateral Load Testing

Timber pile deflection and soil deformation measurements were made at selected lateral load levels during lateral load testing of monolith M2. Timber pile inclinometer deflection is shown in Fig. 9.15 for lateral loads of 0, 48 t, 72 t, and 120 t (equivalent to 0, 6, 9, and 15 t/pile); ground inclinometer deflection is shown in Fig. 9.16 for lateral loads of 0, 48 t, and 96 t (equivalent to 0, 6, and 12 t/pile). Initial values for these data are based on measurements made prior to cyclic preloading of the monolith. Monolith and ground surface did not settle appreciably during lateral load testing, except for the symmetric rotation of the monolith about the x-axis depicted in Fig. 8.2.

The horizontal deflection pattern observed during lateral load testing indicates a different behavior of the timber piles and surrounding soil than during prototype pile driving. The horizontal deflection occurred only at shallow depth, as can be seen in Fig. 9.15; the deflected shapes of the timber pile inclinometers did not change appreciably below a depth of about 10 ft below ground surface (el 381).

The difference between displacement above ground surface measured using linear potentiometers and inclinometers remained constant throughout lateral load testing of the monolith; this observation indicates that ground deformation at depth was very small. The results from ground inclinometers PD3-D5 and D6 (Fig. 9.16) corroborate this conclusion. The somewhat larger deflection at depth of ground inclinometer PD3-D4 within the timber pile group is probably due to interaction between the monolith, timber piles, and soil; above a depth of 10 ft below ground surface, the inclinometer deflection is due to the fact that the top of the inclinometer casing was cast into the concrete monolith and, therefore, followed the monolith displacement. As the lateral load in the monolith increased, there appears to be a reversal in deflection of inclinometer PD3-D4, occurring between 6 ft and 8 ft below ground surface.

## 9.5 MONOLITH-PILE-SOIL LOAD TRANSFERS

### 9.5.1 General

A substantial effort was mobilized for this test program to measure pile strains for interpreting the monolith-timber pile-soil load transfer mechanisms involved during prototype pile driving and lateral load testing. The instrumentation of the piles is described in Sections 3.1.5 and 3.1.7. The location of the upper strain gage levels on the timber piles (36 in. and 18 in. below bottom of the concrete) and the configuration of the test monoliths (3 ft above ground surface) were selected to measure the shear load transfer from the monoliths to the piles in the absence of soil resistance\*.

During testing, strain gage data were directly converted to stresses (Section 3.3) and stored on floppy disks for future processing. The data were later transferred to computer-compatible digital magnetic tapes. The data for monolith M2 were analyzed to derive moment, shear, and axial load distribution in each of the eight timber piles. Telltale data were also used in the analysis. Details of the analysis, including data preparation, geometric relationships, computer programs, and strain gage ranking considerations are given in Appendix T, Volume IIIA. A summary of strain gage measurement events for each monolith is given in Appendices L through P, Volume IIIA.

---

\* In the absence of external forces and stress concentration effects, the shear load transferred from the monolith to timber pile is equal to the slope of the moment distribution curve along the pile shaft

### 9.5.2 Load Transfer During Prototype Pile Driving

Analyses of monolith-timber pile-soil load transfer were made from data obtained during driving of prototype piles 2 through 6, 8 through 10, 12, and 14 at various distances from monolith M2.

**Monolith-Timber Pile Load Transfer.** Changes in bending moment in the timber pile 18 in. below concrete and in shear force transferred to the piles are computed with respect to values at the start of prototype pile driving after full axial ( $V_2$ ) and lateral load ( $H_2$ ) application. These values are shown in Fig. 9.17 for each timber pile under monolith M2. Changes in axial load near the pile butt are computed using the strain gage level 2 ft below ground surface; changes in pile tip strain are based on the two bottom telltales 1 ft and 6 ft above the pile tips. These values are shown in Fig. 9.18.

Equilibrium of axial and lateral forces was found to be satisfied within 15 percent of applied loads in all cases. The large temperature variations experienced above ground surface during testing (Section 7.2.1) were apparently sufficiently uniform at a given strain gage level to make moment calculations meaningful; the axial loads were derived from strain gages below ground surface because uniform changes in temperature above ground resulted in apparent changes in strain of  $-5 \mu\epsilon$  (7 to 10 lb/in<sup>2</sup>) per degree F (Section 3.3.4). Considering that long-term strain effects and temperature changes were neglected, and that the errors tended to overestimate the actual loads, the equilibrium agreement is remarkable. The results of monolith-timber pile load transfer analyses demonstrate some revealing trends which are discussed below.

**Shear Force.** The shear force (Fig. 9.17) transferred to the north-end timber piles 10 and 20 decreased steadily by approximately 2.5 k (a 20 percent decrease from the initial values averaging 13.3 k) as prototype piles were driven. The other timber piles mobilized larger shear forces in compensation; the southernmost piles 14 and 30 received larger shares of the shear force than the intermediate piles 46, 8, 9, and 17.

**Bending Moment.** The bending moments in the timber piles show the same trend as the shear forces. They increased in magnitude more for the southermost piles than for the northernmost; this indicates an increased fixity moment for the south piles.

**Axial Load and Pile Tip Strain.** The redistribution of axial loads at the pile butt and strains at pile tip is more complex. On the basis of observed differential ground settlement, a transfer of axial compression load from the north to the south of the monolith would be expected. The axial load changes show such a tendency, but the axial load decrease is larger for intermediate (piles 8, 17, and 46) piles than for the northernmost piles. The telltale data reflect a complex behavior in regard to changes in axial load near the pile tip. For example, it appears that, although the ground and monolith settled more at the north end, the axial tip load in timber pile 10 increased by 21.6 k (a strain of  $1 \times 10^{-5}$  corresponded to a change in axial load of 1.2 k at the level of the two bottom telltales). Because

the axial load above ground did not change appreciably, a phenomenon akin to negative skin friction is probably the cause of the observed behavior. This phenomenon may not be truly a negative skin friction manifestation, but rather a decrease in shear resistance of the soil along the pile shaft.

**Timber Pile-Soil Load Transfer.** The timber pile-soil load transfer mechanism is examined in the light of the two extreme cases discussed above: before prototype pile driving and after driving of the last prototype pile 14. The computed shear force, bending moment, and axial force distribution along each timber pile are shown in Fig. 9.19, 9.20, and 9.21, respectively. The absence of data points in some of the figures signifies that computed values were obviously in error or, more likely, two or more strain gages at that level malfunctioned and prohibited determination of moment or force altogether.

**Shear Force.** The shear force distribution vs depth is shown in Fig. 9.19 for each timber pile. The data suggest that, in the upper 10 ft below ground surface, the soil shear resistance diminished somewhat around the timber piles in the northern half of monolith M2 and increased slightly around the south piles (furthest from prototype pile driving). This conclusion is based on the fact that, for the north piles, the slope of shear distribution vs depth becomes less steep with respect to depth; this implies that the shear force is transmitted over a longer portion of the shaft length because the shear resistance of the soil has decreased. The reverse is true for the south piles.

**Bending Moments.** The bending moment distribution vs depth is shown in Fig. 9.20 for each timber pile. There is a tendency for the bending moment to redistribute during prototype pile driving in such a manner that the soil resistance must be mobilized at a greater depth to resist the constant applied lateral load for all the timber piles.

**Axial Load.** The axial load distribution vs depth is shown in Fig. 9.21 for each timber pile. The phenomenon of apparent negative skin friction discussed above is again illustrated for timber piles 10 and 20. The tendency of the slope of the axial load distribution curve to flatten out (or decrease), or even reverse sign in the case of pile 20, implies a net decrease in soil resistance. This decrease requires a larger soil resistance to be mobilized at greater depth or a decrease in the axial load transferred from the monolith to the timber pile. The result is a redistribution of axial load along the shaft of the northern timber piles and/or to the other piles in the group. That redistribution is apparent for timber piles 8 and 17, and in the deeper portion of piles 10 and 20.

#### **9.5.3      Load Transfer During Lateral Load Testing**

As it was the case in the analyses of load transfer during prototype pile driving, the force equilibrium was satisfied within 15 percent for force values computed during lateral load testing of monolith M2. The computed shear force, bending moment, and axial force distributions along each timber pile are shown in Fig. 9.22, 9.23, and 9.24, respectively. The data shown in these figures correspond to lateral loads of 48 t, 72 t, 96 t, and 120 t (equivalent to 6, 9, 12, and 15 t/pile).

The trends in shear force and bending moment distributions show a relatively uniform increase as the lateral load increased; this indicates a linear response of the timber pile foundation. Examination of strain gage data collected after unloading of the monolith showed only minor residual gage offsets, if any; this indicates no structural failure of the timber piles occurred during lateral load testing. Failure was exclusively due to excessive soil deformation. Two timber piles were extracted after load testing and visual inspection of the piles corroborated this conclusion.

**Shear Force.** Examination of the slope of the curves in Fig. 9.22 indicates the shear force transferred from the timber piles to the soil was significantly greater for the northernmost piles 10 and 20 than for those towards the south end of monolith M2 (piles 14 and 18). Timber pile 17 was an exception. The softer response of piles tracking the piles in front of them was reasonable.

**Axial Load.** The axial load transfer for timber piles 10 and 14 (Fig. 9.24) is characterized by parallel curves; this implies that full shaft resistance to axial load was mobilized at the strain gage levels (upper 20 ft) and that the load had to be redistributed deeper or shared with the other piles. Piles 17 and 20 show a change in slope which is characteristic of a shaft load increase in response to the axial load increase caused by the behavior of piles 10 and 14. The trend for pile 8 denotes an increase in compression at the pile butt that is amplified at depth by negative skin friction, possibly as a result of the behavior of pile 10 which, having mobilized full shaft resistance, settled more rapidly than pile 8.

The deformation mechanisms of the soil mass surrounding the timber piles in response to the increase in lateral load was reasonable. They differed fundamentally from those exhibited during prototype pile driving.

## 9.6 COMPARISON BETWEEN PREDICTED AND OBSERVED MONOLITH RESPONSE

### 9.6.1 General

A method was established at the design stage to predict displacements of a test monolith caused by nearby prototype pile driving; displacements were predicted using the method for a few selected conditions (Section 2.3.2). Other predictions were made, such as particle velocity induced by pile driving. The prediction process undertaken at the design stage was not so much directed at obtaining numerical values, but more to formulate a procedure based on the best available data at that time.

On the basis of the findings discussed in the preceding sections, it is obvious that the prediction method grossly oversimplified the problem at hand. The parameters used to predict were based on empirical data obtained from a previous pile driving effects test program conducted some 40 years ago, and for which very limited detailed information was available. In addition, among the empirical data, only those yielding the most conservative displacement predictions were used (Section 2.3.2). Nevertheless, the predicted displacements are compared to the actual measurements for monolith M2.

**9.6.2      Predicted Performance**

**Prototype Pile Driving Blowcount.** The horizontal displacement of a monolith was predicted as a function of prototype pile driving blowcount. Piles, similar to those used during this test program, were test driven at the site of the proposed replacement structures for Locks and Dam No. 26 (Fruco 1973). The blowcount reported for the replacement site test piles was as follows:

<b>Pile Tip Depth Range ft</b>	<b>Average Blowcount blow/ft</b>	<b>Total Number of Hammer Blows for Depth Range</b>
0-5	0.5	2.5
5-10	2.5	12.5
10-15	5	25
15-20	7	35
20-25	9.5	<u>47.5</u>
<b>Total Number of Hammer Blows For First 25 ft of Pile Penetration:</b>		<b>122.5</b>

Prototype pile penetration resistance was assumed to be identical to that of the replacement site test piles.

**Monolith Displacement.** The horizontal displacement of a monolith, regardless of its pile configuration, was predicted for each series of 10 hammer blows for the Vulcan 010 hammer, as a function of blowcount and applied lateral load level (Fig. 2.9). For a load level of 6 t/pile, the following values were predicted using the design prediction method, and the average blowcount and total number of hammer blows assumed above. Horizontal distances from prototype piles to monolith M2 of 50 ft, 20 ft, and 15 ft were selected, because they correspond to prototype piles 1, 2 through 5, and 6, respectively. Details of the calculations are shown in Appendix R, Volume IIIA.

Horizontal Distance From Prototype Pile to Monolith ft	Pile Tip Depth Range ft	Average Distance r From Pile Tip to Monolith ft	Hammer Blows	Horizontal Displacement of Monolith in.
50 (Prototype Pile 1)	0-5 5-10 10-15 15-20 20-25 0-25	50.1 50.6 51.5 53 54.8 52	2.5 12.5 25 35 45 122.5	0.0001 0.0012 0.0033 0.0051 0.0074 0.0171
				$\frac{122.5 \text{ blows}}{10 \text{ blows}}$
				0.0014
21 (Prototype piles 2 through 5)	0-5 5-10 10-15 15-20 20-25 0-25	21.1 22.3 24.4 27.3 30.8 25.2	2.5 12.5 25 35 45 122.5	0.0004 0.0042 0.0107 0.0153 0.0204 0.0510
				$\frac{122.5 \text{ blows}}{10 \text{ blows}}$
				0.0042
15 (Prototype Pile 6)	0-5 5-10 10-15 15-20 20-25 0-25	15 16.6 19.4 22.9 26.9 20.2	2.5 12.5 25 35 45 122.5	0.0006 0.0058 0.0139 0.0190 0.0246 0.0639
				$\frac{122.5 \text{ blows}}{10 \text{ blows}}$
				0.0052

The settlement of a monolith was predicted to be about 12 percent of the horizontal displacement. The rotation in degrees was predicted as 0.009 times the horizontal displacement in inches.

**Particle Velocity.** Predictions of particle velocity are depicted in Fig. 2.12. For the range of prototype pile driving distances for monolith M2, the peak particle velocity was expected to vary from 0.2 in./s to 2 in./s.

### 9.6.3 Comparisons

**Prototype Pile Driving Blowcount.** A comparison between assumed and measured blowcount for the first 25 ft of penetration for prototype piles 1 through 6 at monolith M2 is shown below.

Pile Tip Depth Range ft	Assumed Blowcount blow/ft	Measured Blowcount blow/ft
0-5	0.5	N/A
5-10	2.5	2
10-15	5	2
15-20	7	3
20-25	7.5	4
Average	4.9	2.75

**Monolith Displacements.** A comparison between predicted and measured displacements of monolith M2 caused by the first 25 ft of penetration for prototype piles 1 through 6 is shown below.

Prototype Pile No.	Horizontal Displacement per 10 Hammer Blows in.		Settlement per 10 Hammer Blows in.	
	Predicted	Measured	Predicted	Measured
1	0.0014	0.0002	0.0007	0
2,3,4,5 (average)	0.0042	0.00176	0.00050	-0.00136
6	0.0052	0.00196	0.00062	-0.00107

The prediction method overestimated horizontal displacement. Had the prediction method been based on Feagin's monolith 3 (Section 2.3.2), the agreement would have been closer. The settlement was underpredicted. This underprediction would have been larger if the predictions had been based on Feagin's monolith 3.

**Particle Velocity.** Measured particle velocities normalized for a blow-count of 10 blow/ft are compared in Fig. 9.25 with predicted values. Normalization procedures are given in Appendix R, Volume IIIA. The agreement is good, indicating that the attenuation law (eq 2.1) considered is reasonable. The agreement is better with the peak vertical component ( $z$ ) of the particle velocity than with the peak vectorial values.

## 9.7 APPARENT DEFORMATION MECHANISMS

### 9.7.1 General

On the basis of the analyses presented in the preceding sections, it is possible to infer some deformation patterns of the monolith, its timber pile foundation, and the surrounding soil mass. The behavior of these elements is illustrated in the form of schematic representations of horizontal and vertical components of deformation; however, the effects of the combination of these two components on total deformation during prototype pile driving is not entirely understood at present.

### 9.7.2 Pattern of Deformations During Static Lateral Load Testing

The pattern of horizontal and vertical deformations under an increasing lateral load is depicted in Fig. 9.26. The horizontal deflections of the various timber piles (Fig. 9.26a and b) is similar, with only local variations due to structural differences (for example, timber pile properties, fixity conditions, and pile installation conditions). The soil within the pile group deforms and tends to follow the pile deflections; the soil outside the pile group exhibits much less deformation. This tracking effect results in a softer soil response towards the rear (south) end of the monolith where the lateral load is applied. The timber piles at the front (north) end of the monolith punch into the surrounding soil. The effects of prior cyclic loading history tend to reduce the difference between the front and rear pile behavior.

The vertical deformations under static loads are much smaller than the horizontal deformations. These vertical deformations are almost completely recoverable upon unloading. The application of the lateral load results in a small symmetrical tilting of the monolith, imperceptible at the relative scale in Fig. 9.26c.

### 9.7.3 Pattern of Deformations During Prototype Pile Driving

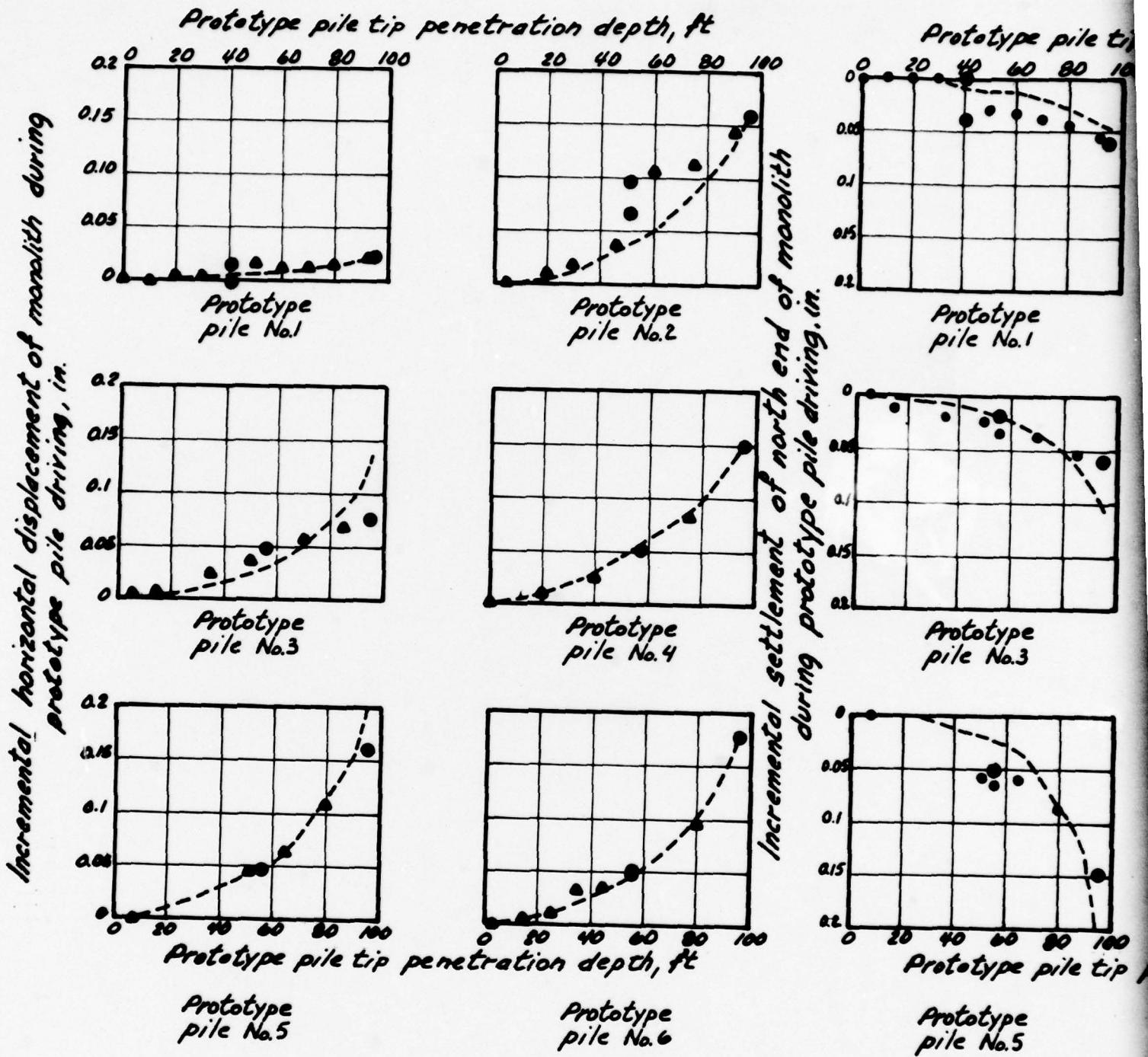
The pattern of deformation associated with prototype pile driving is significantly different than that observed under static loading. The deformations inferred from detailed observation of monolith M2 data are depicted in Fig. 9.27.

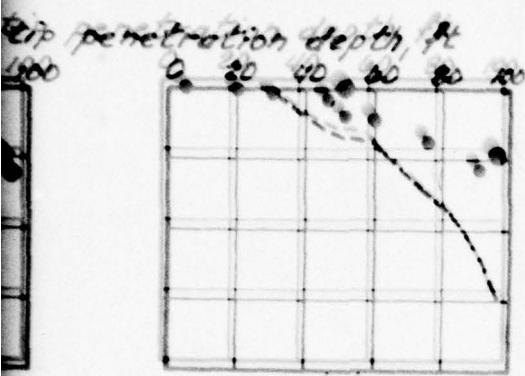
At shallow depth, the soil experiences a transient loss of strength under the effects of nearby pile driving. This transient loss of strength is probably caused by a temporary soil volume change, as no significant pore pressure changes were observed during prototype pile driving. The timber piles, under the static lateral load and because of this temporary soil resistance decrease, deflect towards the prototype pile being driven. The upper part of the timber piles deflect more than the soil deform, and the piles punch into the soil. This deformation is more pronounced for the front timber piles, closer to the driven prototype pile, than for the rear timber piles. As the front timber piles lose support at shallow depth, the axial and shear loads on the piles are transferred deeper along the pile shafts and are redistributed from the front piles to the rear piles.

At greater depth below ground surface, although the soil probably also experiences transient loss of strength, the axial and shear loads on the pile shaft are smaller, and the pile moves laterally with the soil, with no relative pile-soil movement.

The vertical deformation associated with prototype pile driving is characterized by deep settlement of the soil at or beneath the timber piles tip elevation. Although the vertical deformations are probably affected by the axial load, the effects of areal ground settlement dominate.

The gross monolith displacements correlate reasonably well with cumulative peak particle velocity (Section 9.3) which can be considered to be an approximation of transient shear strains in the soil. To extrapolate the results of this correlation to any other structure or to different conditions will require site specific assessment of ground vibration characteristics. The relationship between ground vibrations and structure displacements could then be evaluated on the basis of the data from this test program and the inferred mechanisms of deformation proposed above.

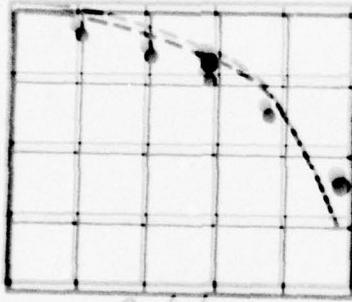




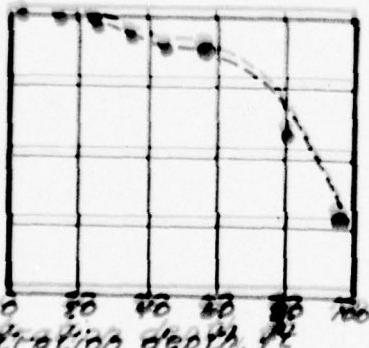
Prototype  
pile No. 2

*Legend*

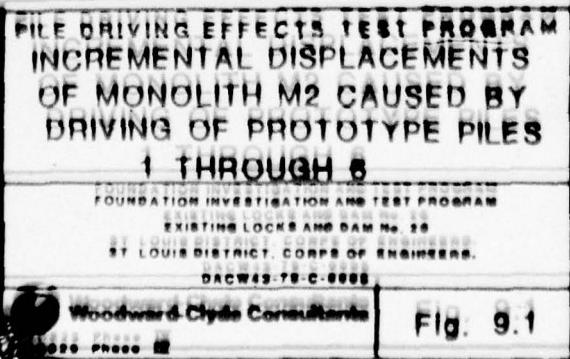
- Linear potentiometer data corrected for measured reference beam displacement
- ▲ Linear potentiometer data corrected for interpolated reference beam displacement
- Displacements calculated on the basis of the method of Fig. 9.3

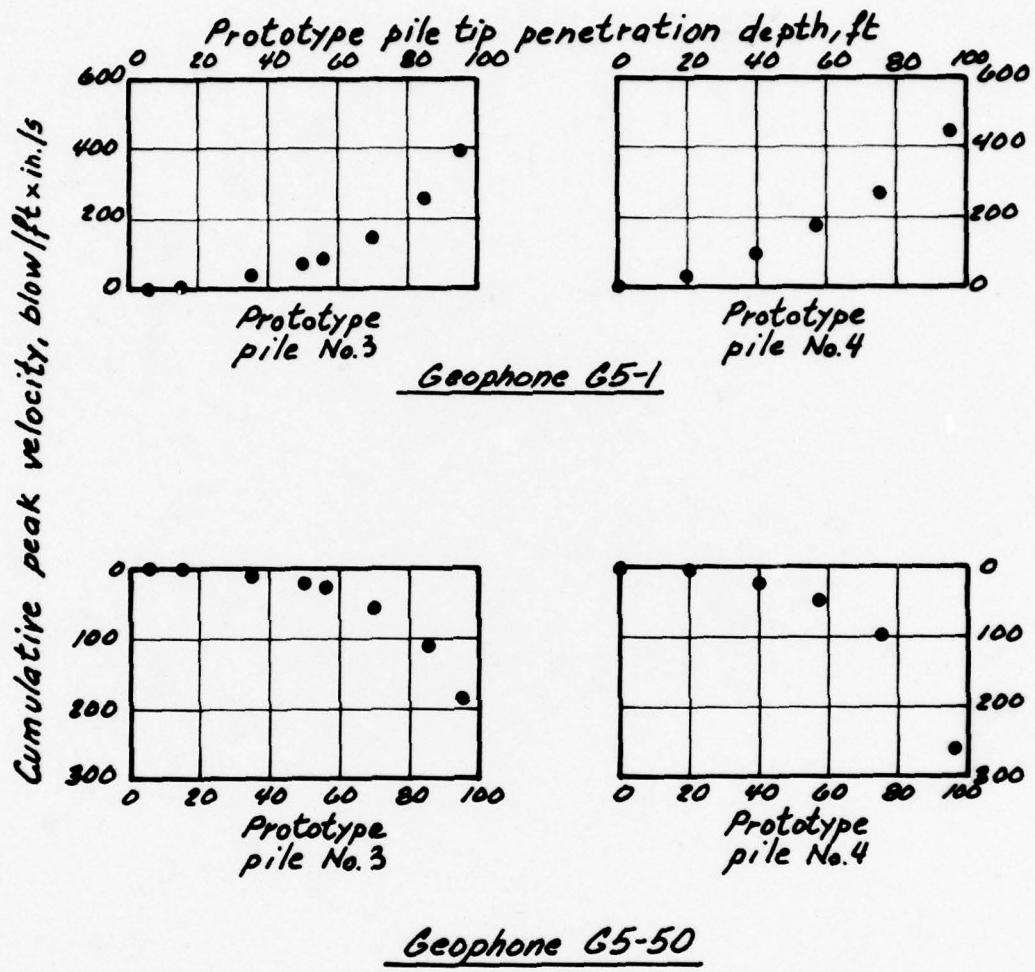


Prototype  
pile No. 4



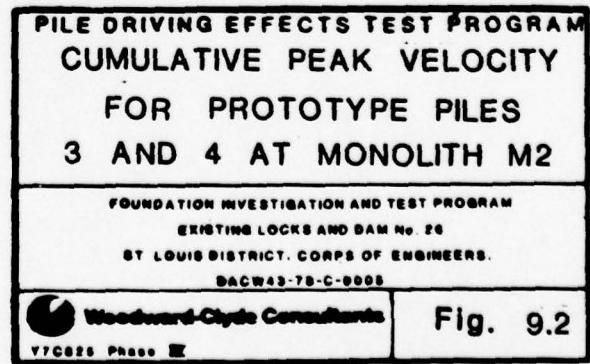
Prototype  
pile No. 6

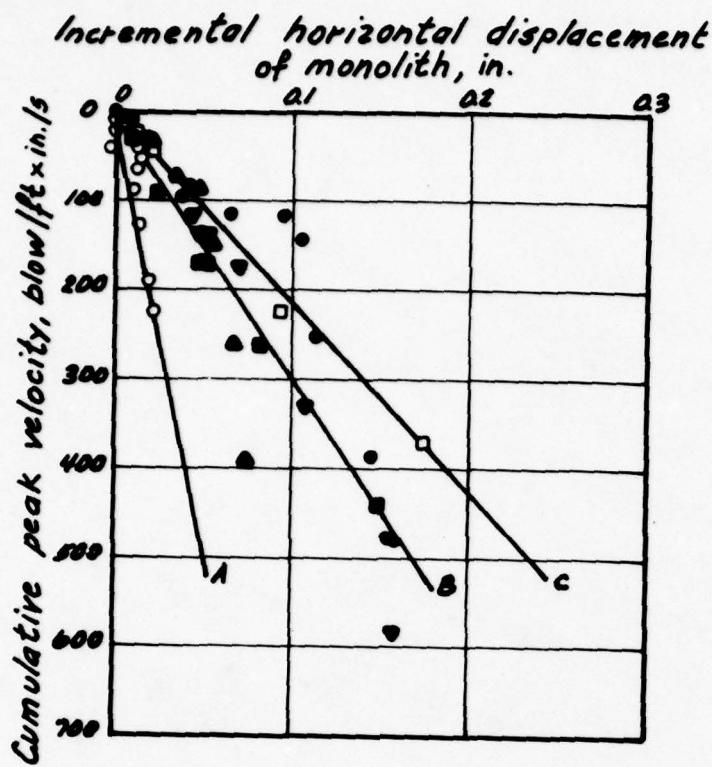




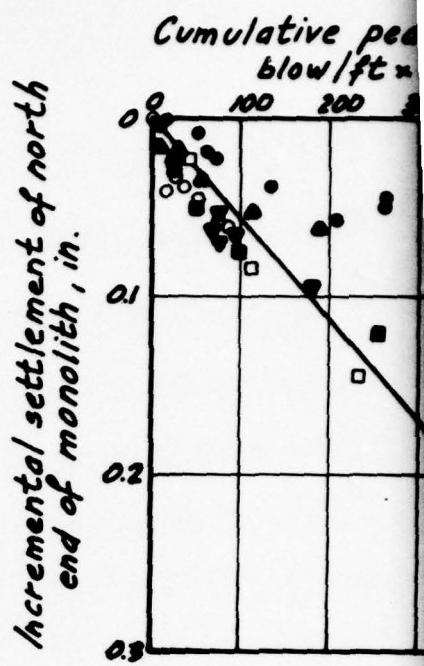
Geophone G5-1

Geophone G5-50

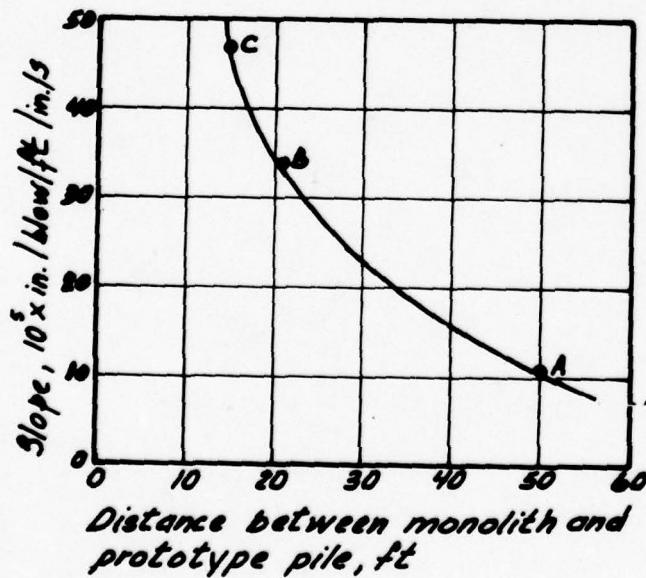




(a) Incremental horizontal displacement



Incremental settlement of north end of monolith, in.



(b) Slopes

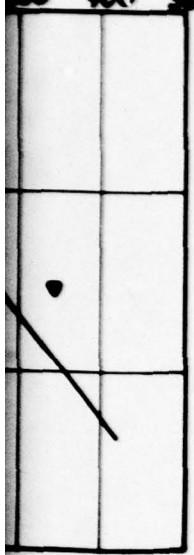
Legend

Prototype pile No.	Distance from proto
○	1
●	2
▲	3
▼	4
□	5
□	6

Note:

Lines A, B, C are the lines fitting the data corresponding to distances between prototype piles and monolith of 50 ft, 20 ft and 15 ft respectively

peak velocity,  
in./s  
200 400 600

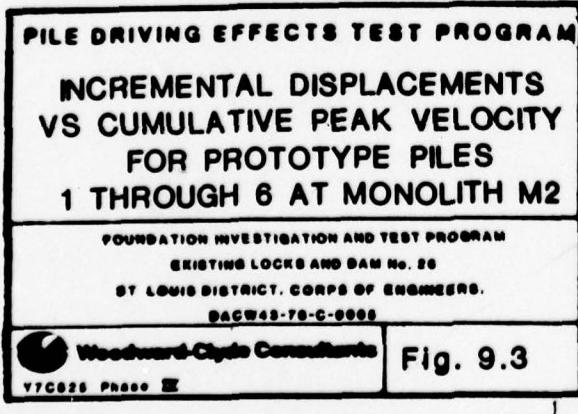


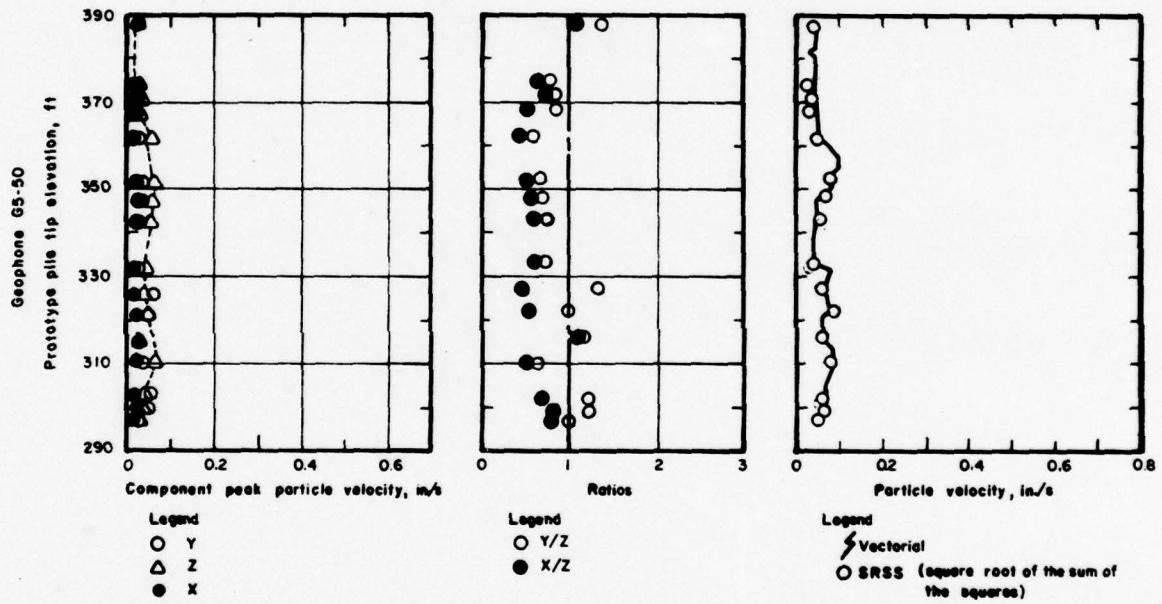
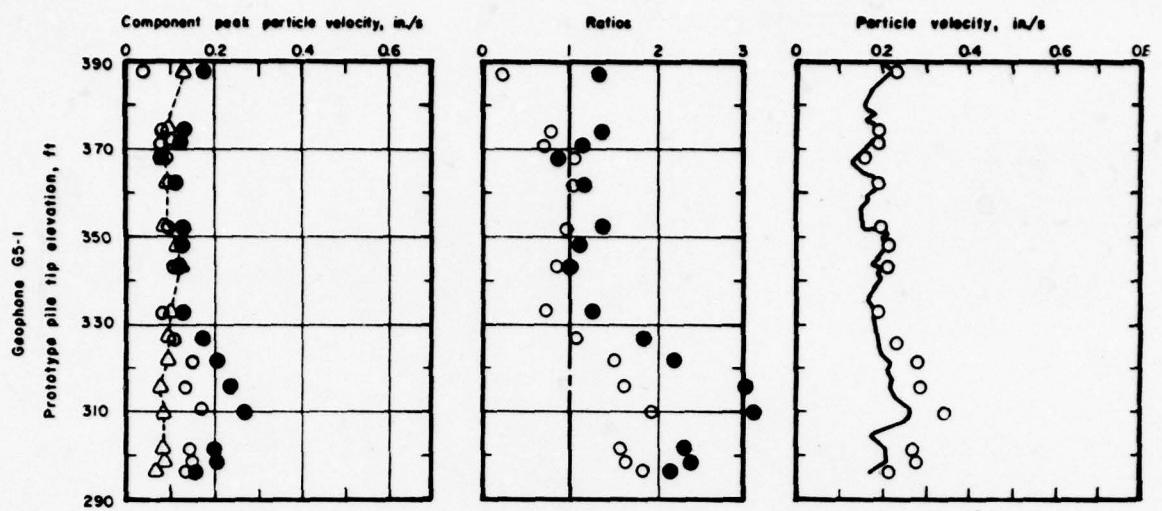
(c) Incremental settlement

Distance between  
monolith and  
prototype pile, ft

50  
21  
20.6  
21.1  
20.8  
14.8

data  
0 ft, 21-





COMPONENT PEAK PARTICLE  
VELOCITIES

LONGITUDINAL/VERTICAL AND  
TRANSVERSE/VERTICAL RATIOS

PEAK VECTORIAL PARTICLE VELOCITY  
AND SRSS FROM COMPONENT PEAKS

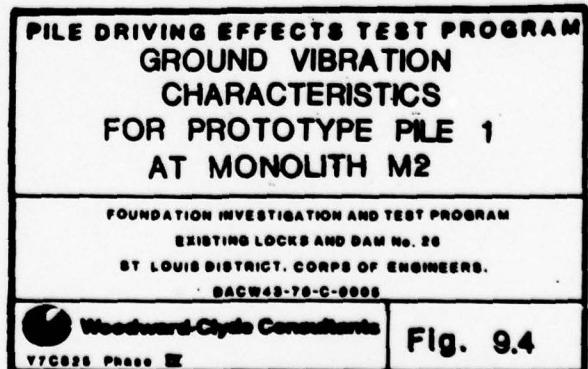
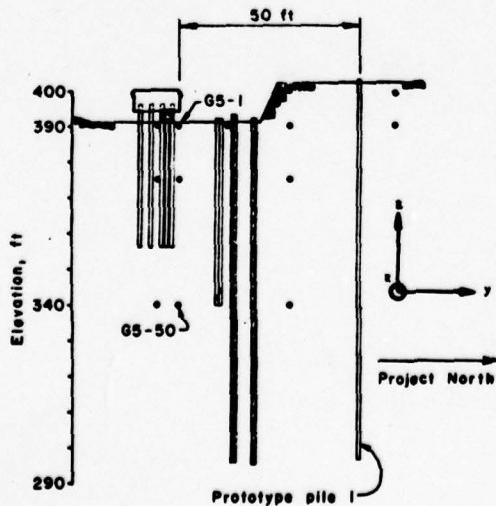
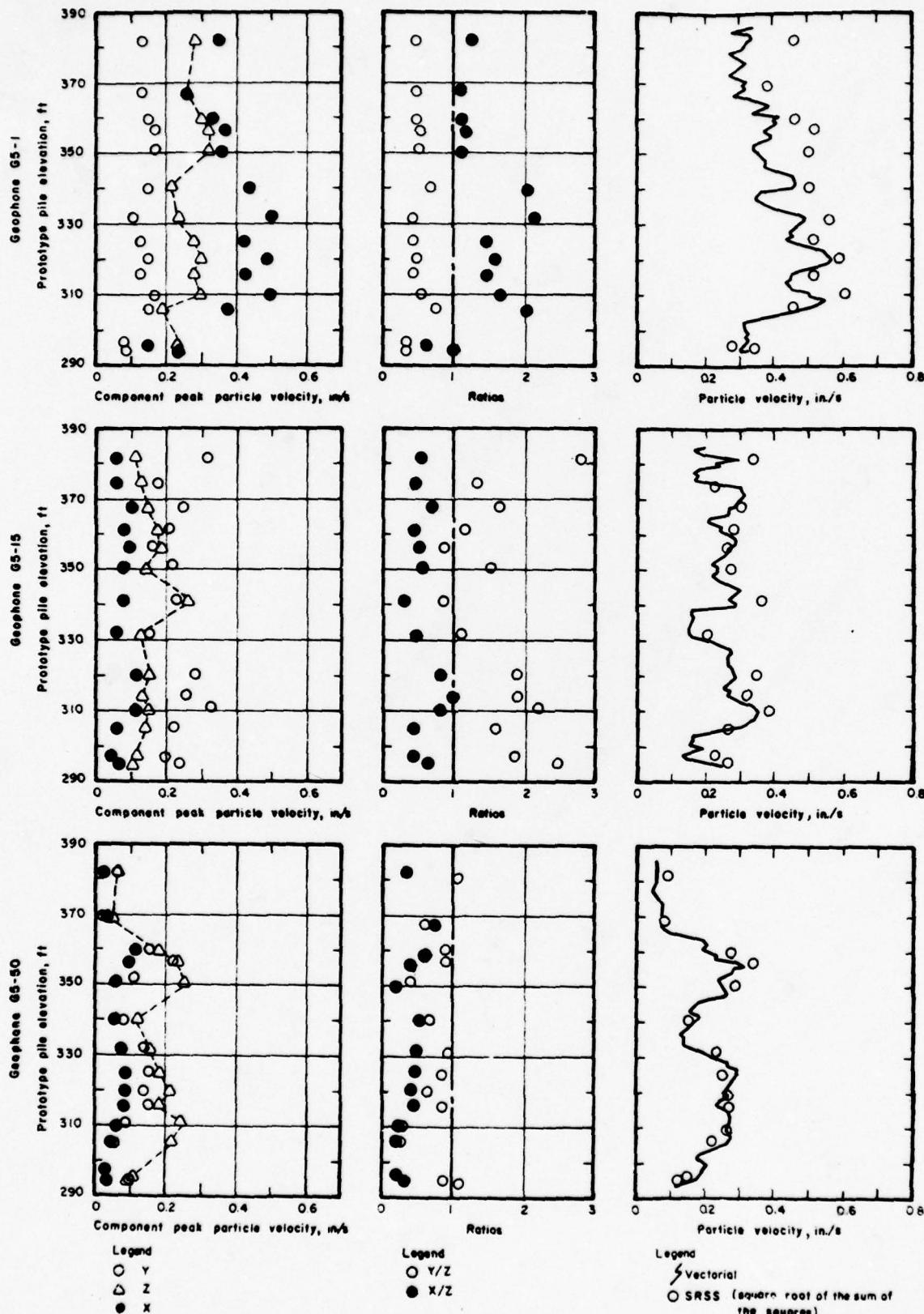


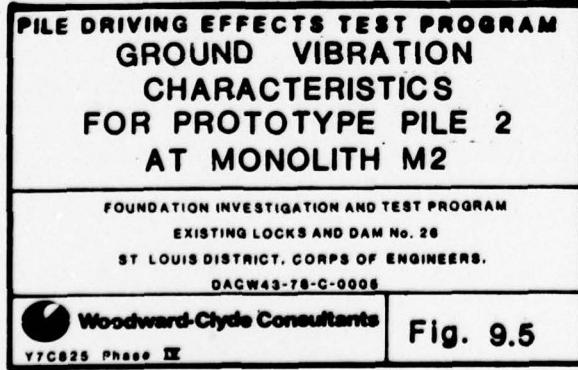
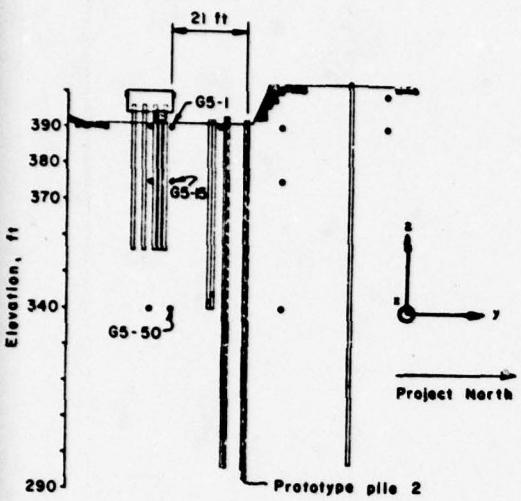
Fig. 9.4



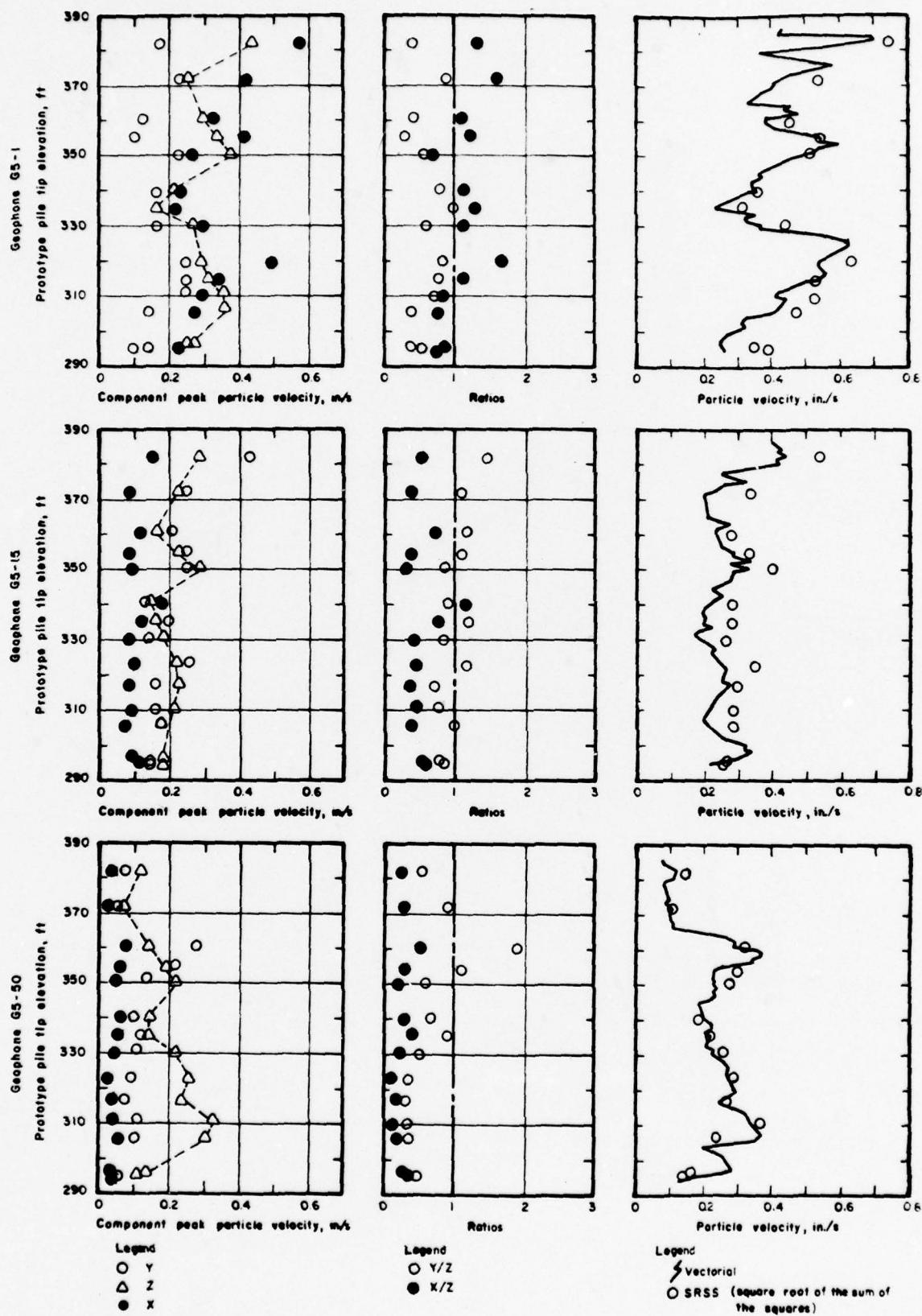
COMPONENT PEAK PARTICLE  
VELOCITIES

LONGITUDINAL/VERTICAL AND  
TRANSVERSE/VERTICAL RATIOS

PEAK VECTORIAL PARTICLE VELOCITY  
AND SRSS FROM COMPONENT PEAKS



8



Legend

- Y
- △ Z
- X

COMPONENT PEAK PARTICLE  
VELOCITIES

Legend

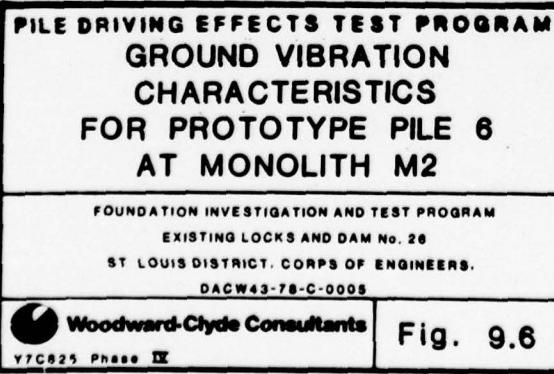
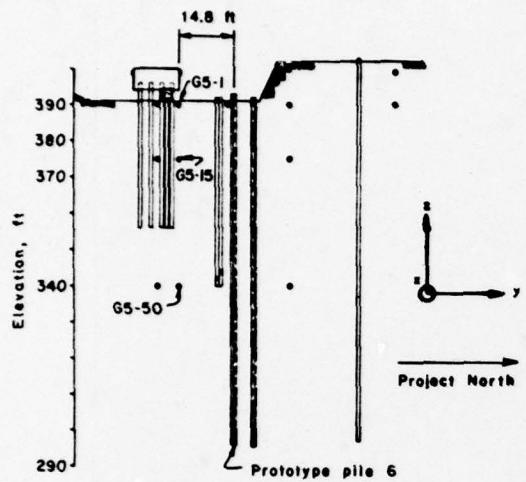
- Y/Z
- X/Z

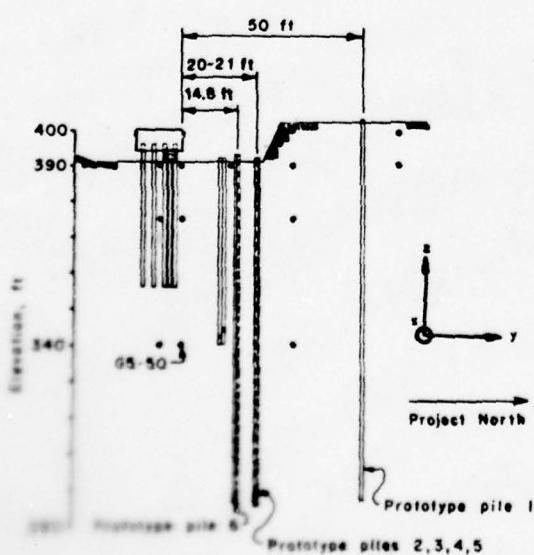
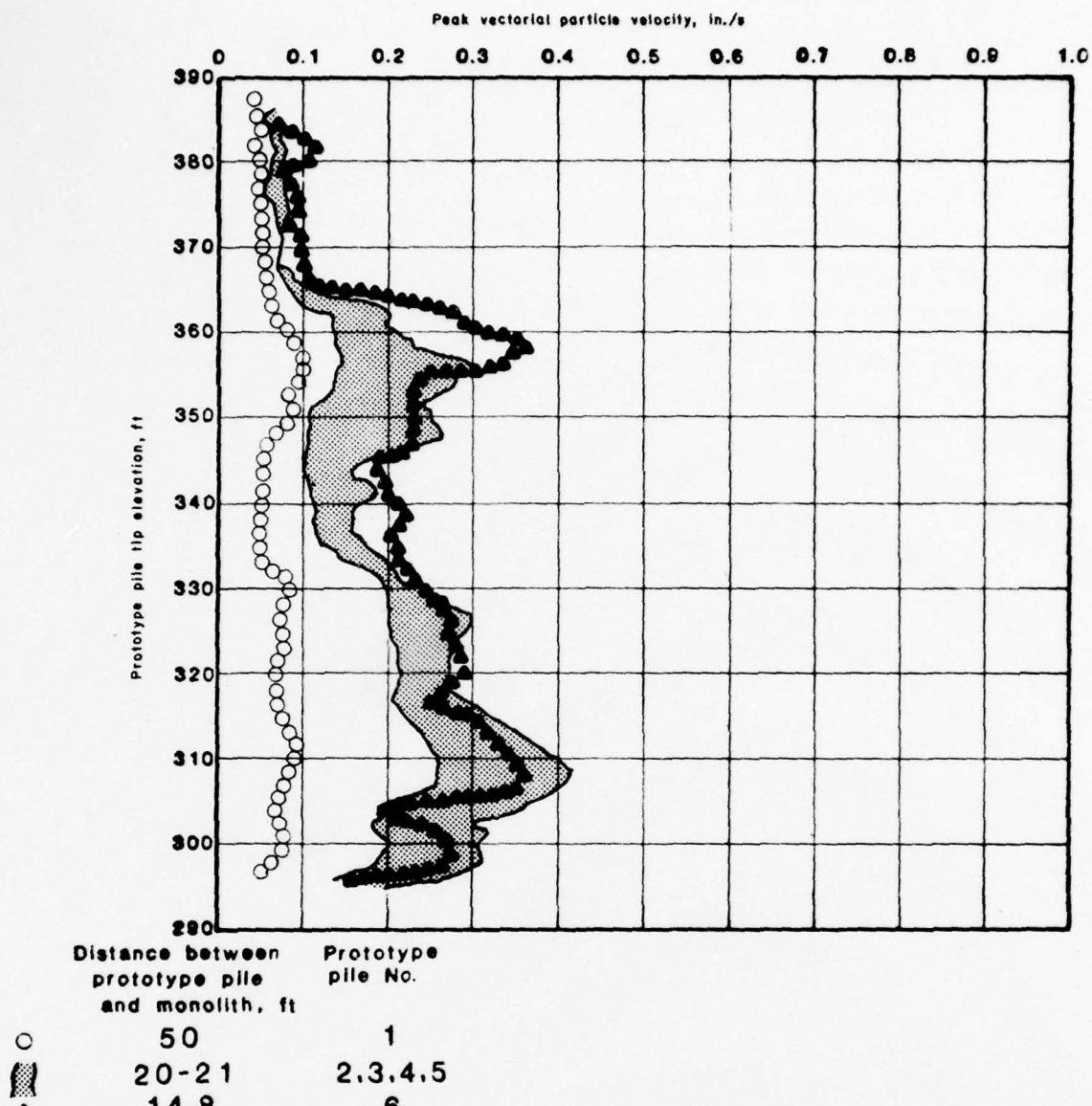
LONGITUDINAL/VERTICAL AND  
TRANSVERSE/VERTICAL RATIOS

Legend

- ⚡ Vectorial
- SRSS (square root of the sum of  
the squares)

PEAK VECTORIAL PARTICLE VELOCITY  
AND SRSS FROM COMPONENT PEAKS



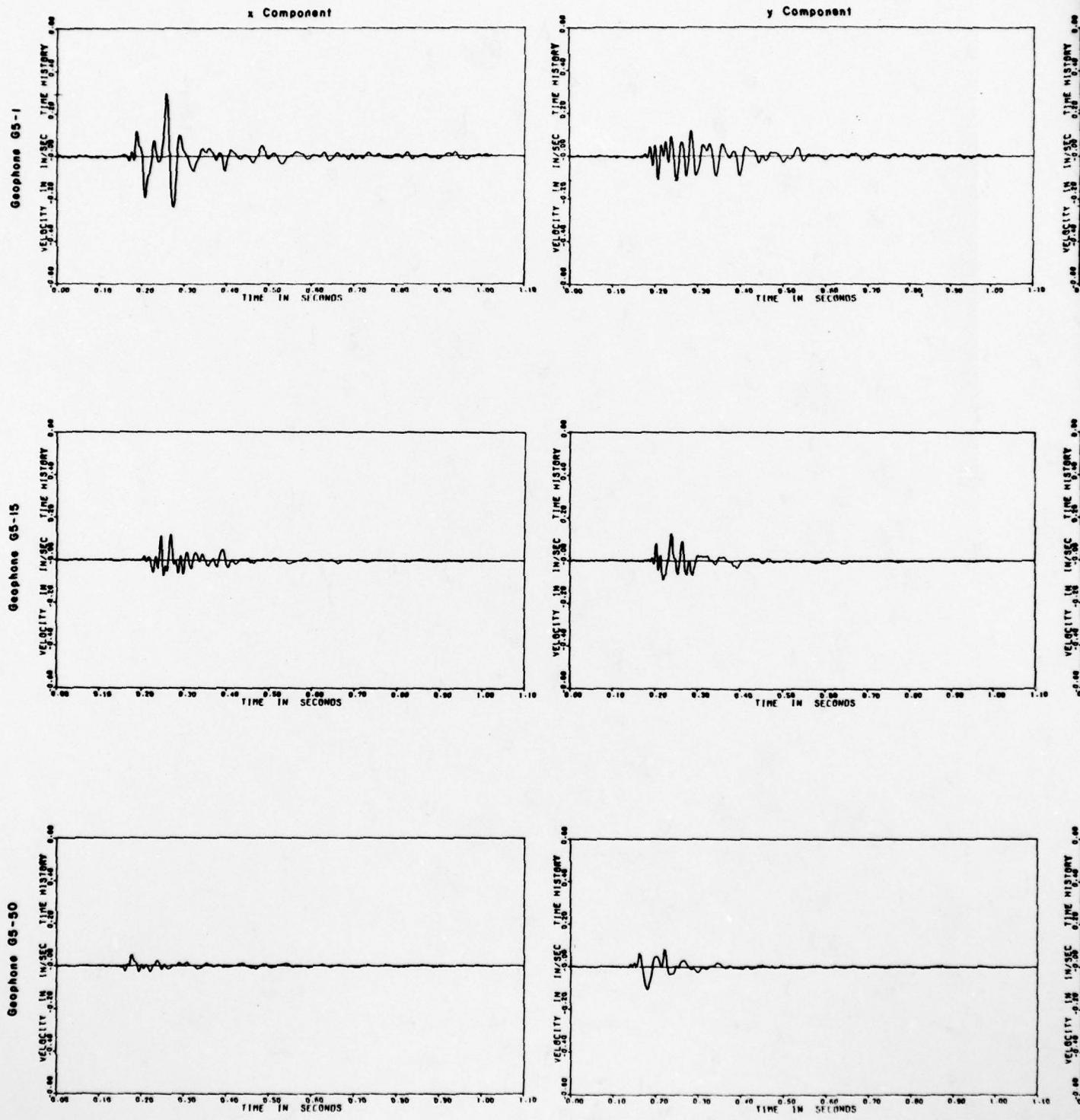


**PILE DRIVING EFFECTS TEST PROGRAM**  
**PARTICLE VELOCITY RECORDED**  
**50 FT BELOW GROUND SURFACE**  
**AT MONOLITH M2**

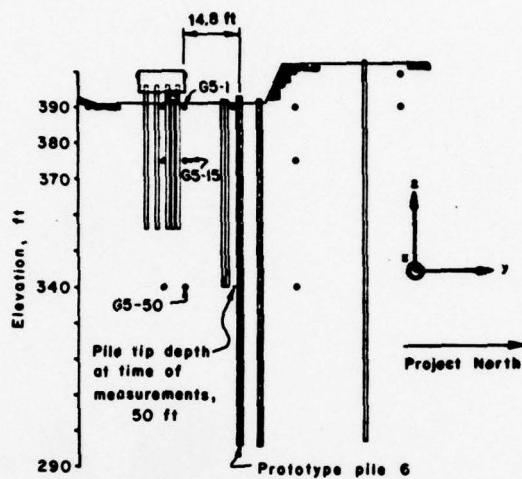
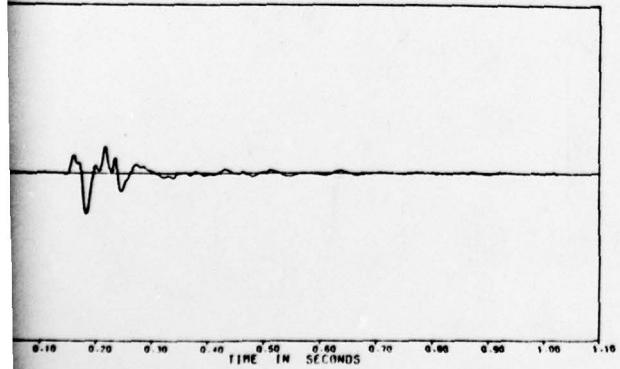
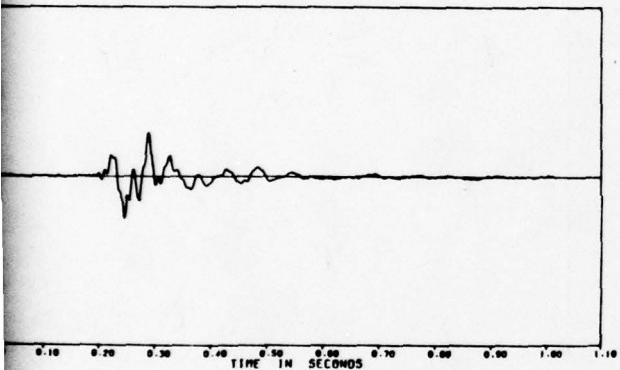
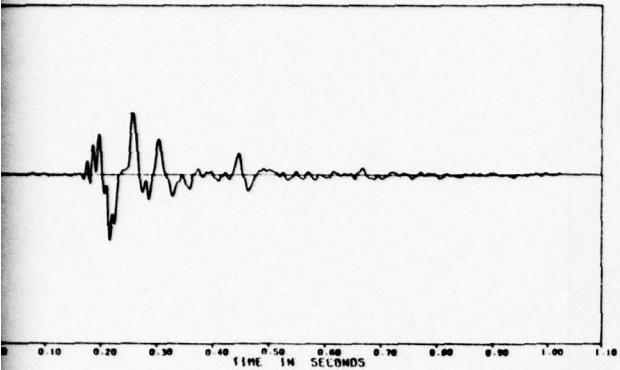
FOUNDATION INVESTIGATION AND TEST PROGRAM  
 EXISTING LOCKS AND DAM NO. 26  
 BY LOUIS DISTRICT, CORPS OF ENGINEERS.  
 BACW43-78-C-0006

 Woodward-Clyde Consultants  
 TTC625 Phase II

**Fig. 9.7**



*z* Component



**PILE DRIVING EFFECTS TEST PROGRAM**

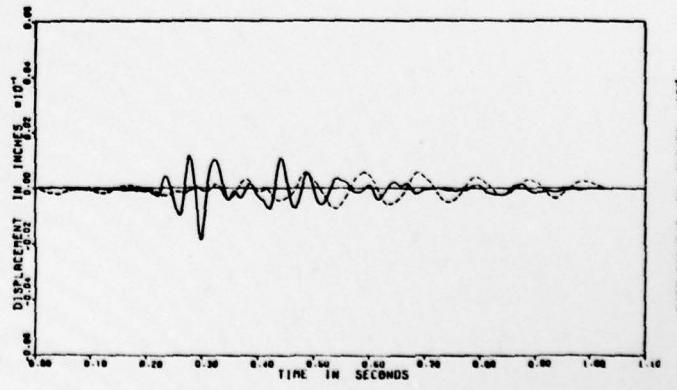
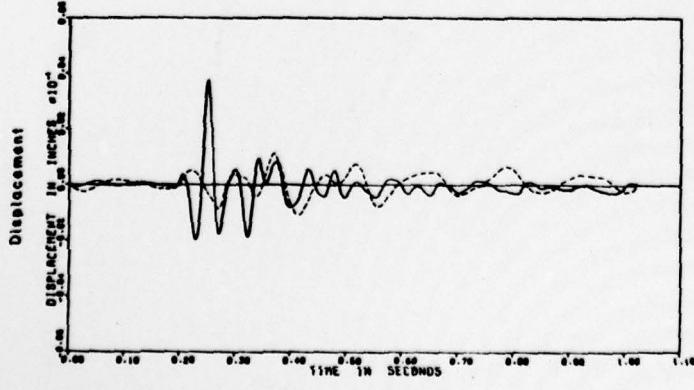
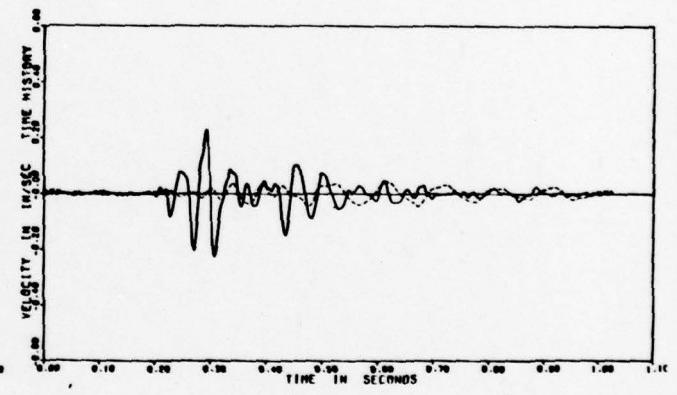
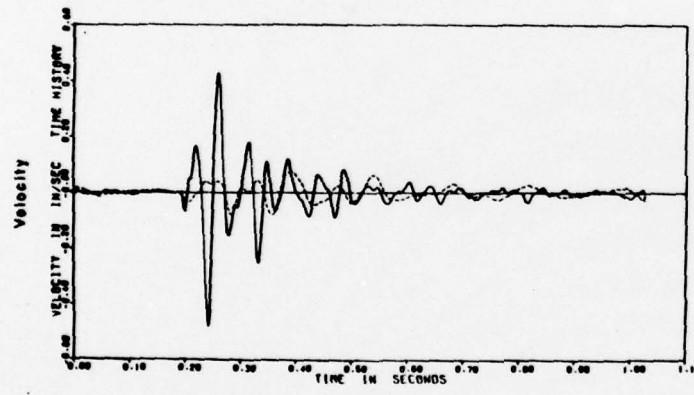
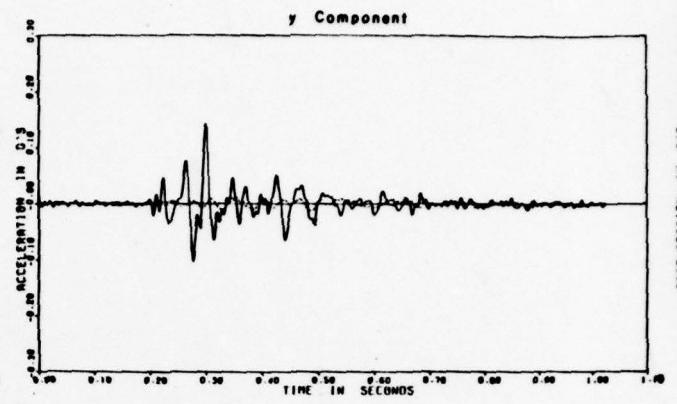
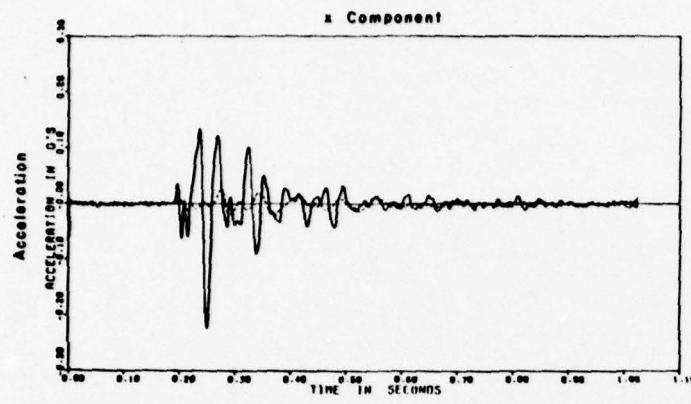
**EXAMPLES OF GROUND  
VELOCITY TIME HISTORIES  
AT MONOLITH M2**

FOUNDATION INVESTIGATION AND TEST PROGRAM

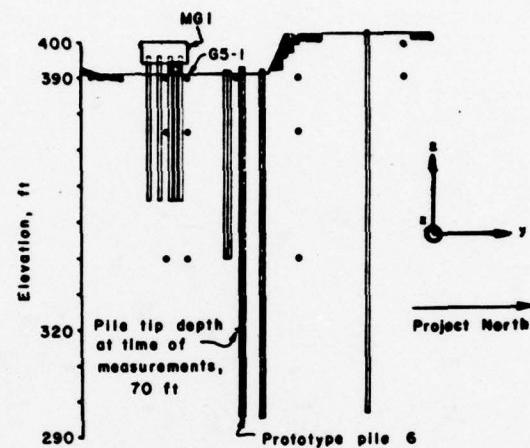
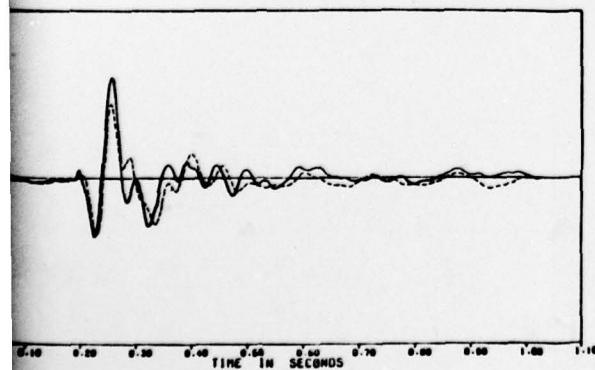
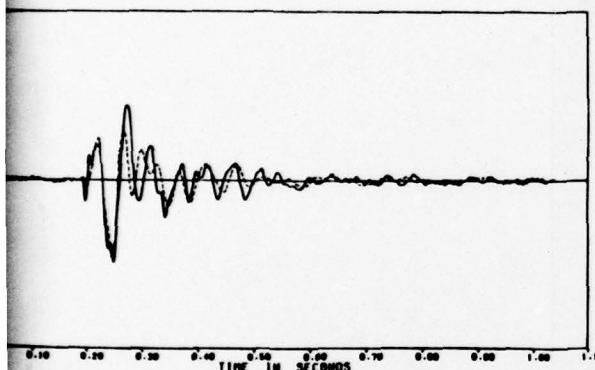
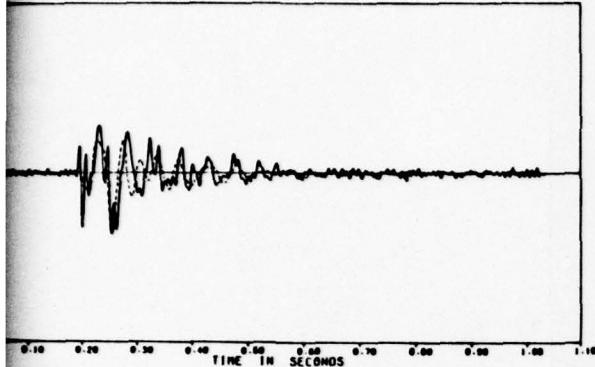
EXISTING LOCKS AND DAM No. 28  
ST LOUIS DISTRICT, CORPS OF ENGINEERS.  
DACPW43-78-C-0008

Woodward-Clyde Consultants  
YTGB25 Phase IV

*Fig. 9.8*



*z* Component



*Legend*

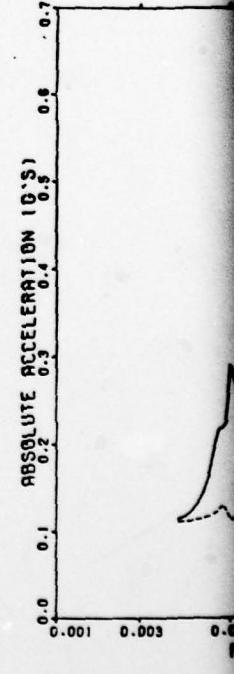
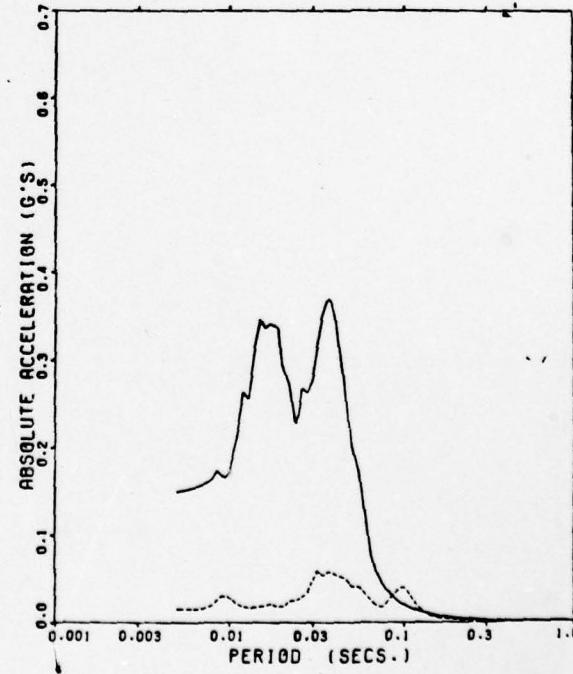
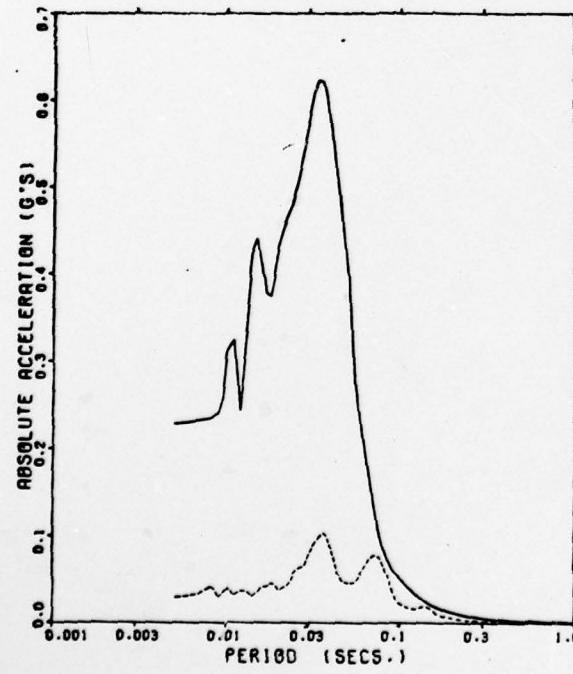
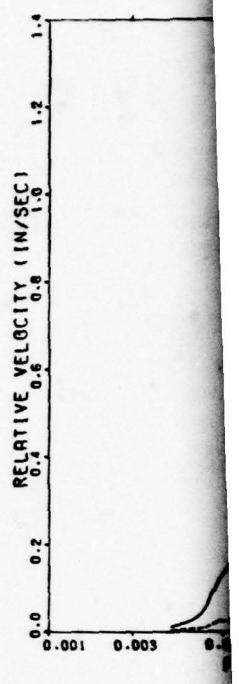
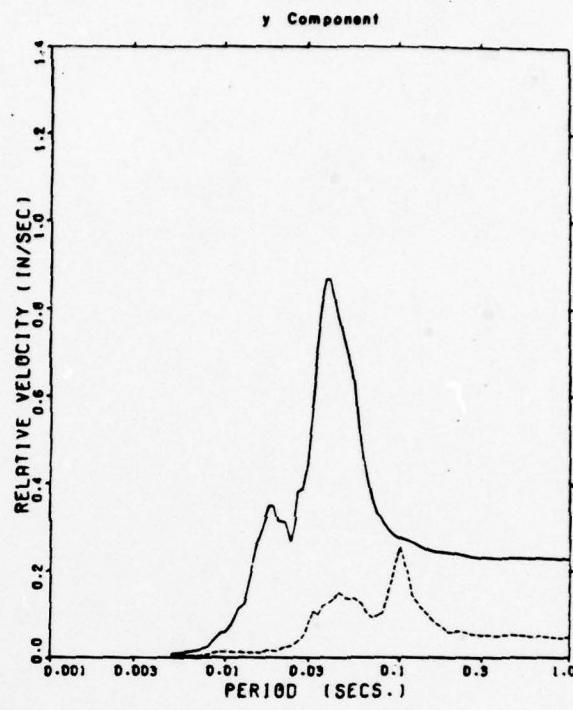
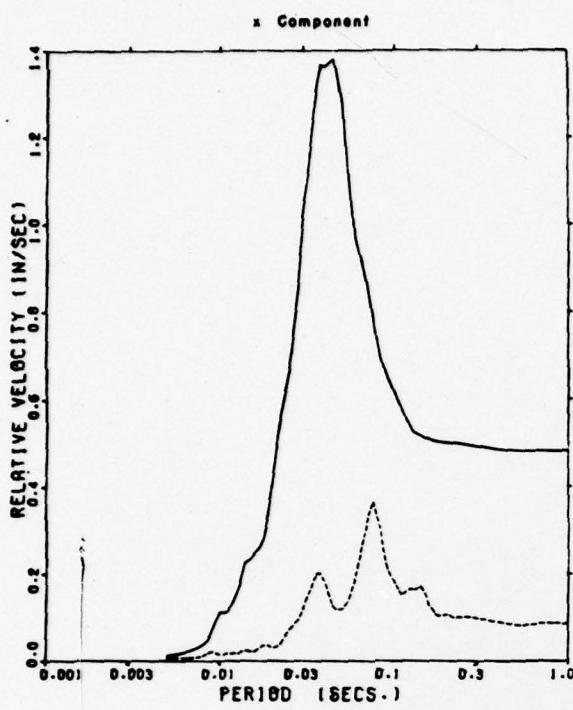
Geophone G5-1  
 Geophone MG-1

**FILE DRIVING EFFECTS TEST PROGRAM**  
**EXAMPLES OF GROUND AND MONOLITH MOTIONS TIME HISTORIES AT MONOLITH M2**

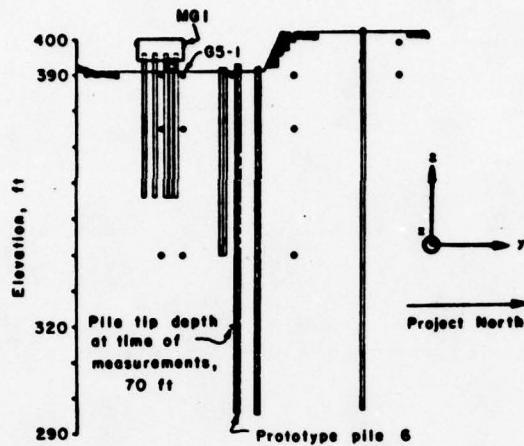
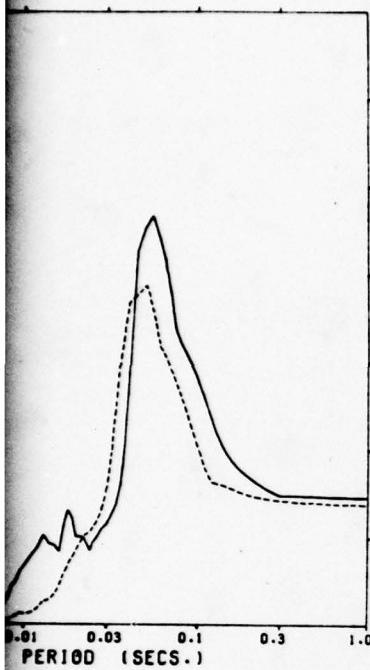
FOUNDATION INVESTIGATION AND TEST PROGRAM  
EXISTING LOCKS AND DAM No. 26  
ST LOUIS DISTRICT, CORPS OF ENGINEERS.  
DACPW43-78-C-0008

Woodward-Clyde Consultants  
V7C825 Phase II

**Fig. 9.9**

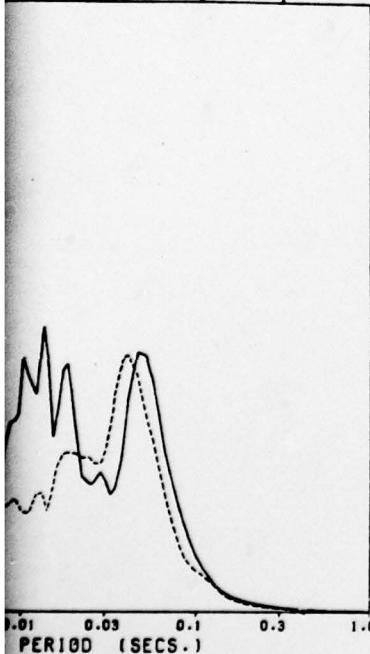


*z* Component

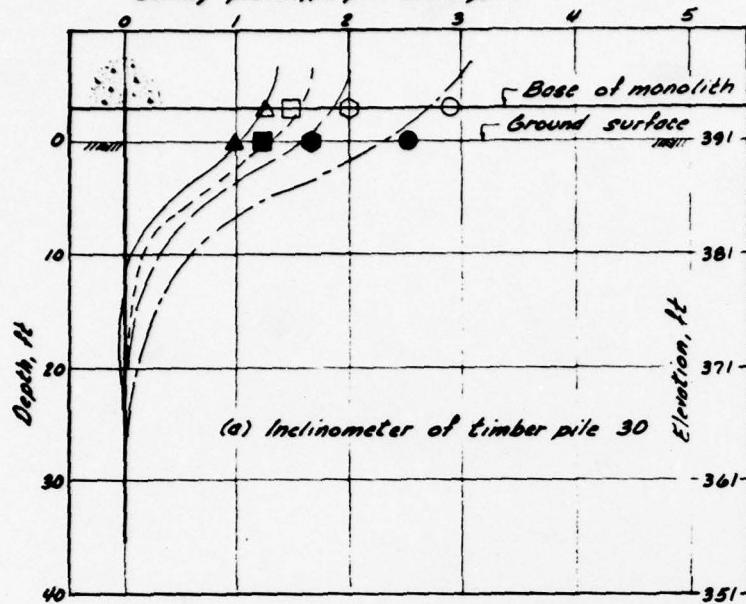


*Legend*

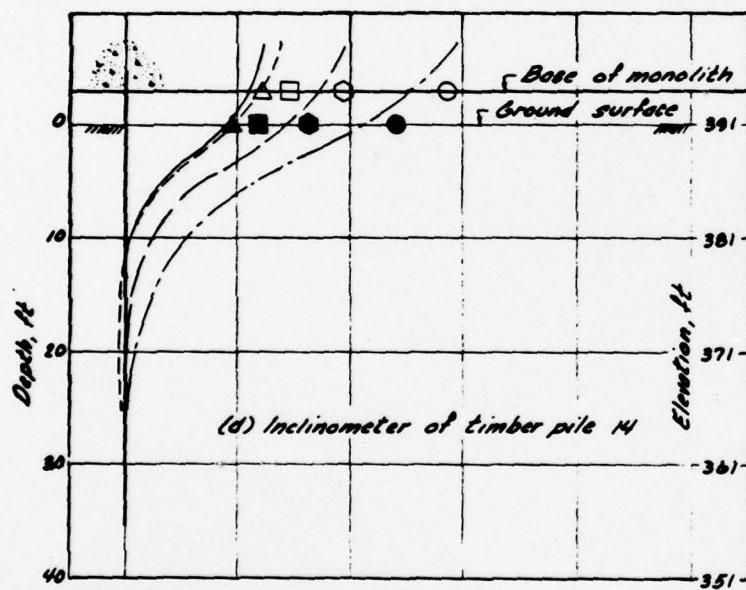
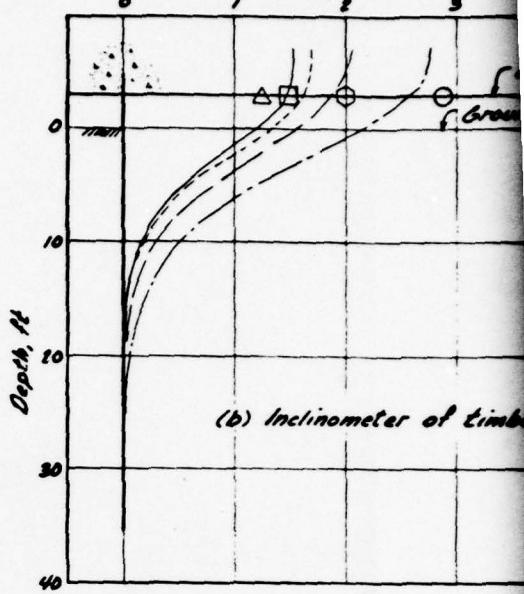
Geophone G5-1  
 Geophone MG1



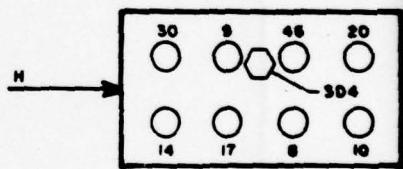
Horizontal deflection of timber pile inclinometer during prototype pile driving, in.



Horizontal deflection of timber pile during prototype pile driving, in.

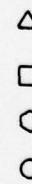


MONOLITH M2 - SCHEMATIC



Legend

Horizontal displacements of  
monolith four corner timber  
piles at ground surface



▲



□

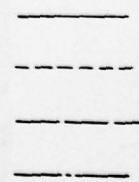


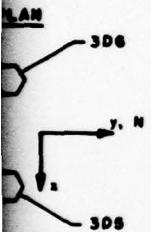
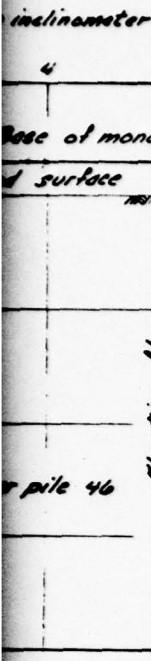
○



●

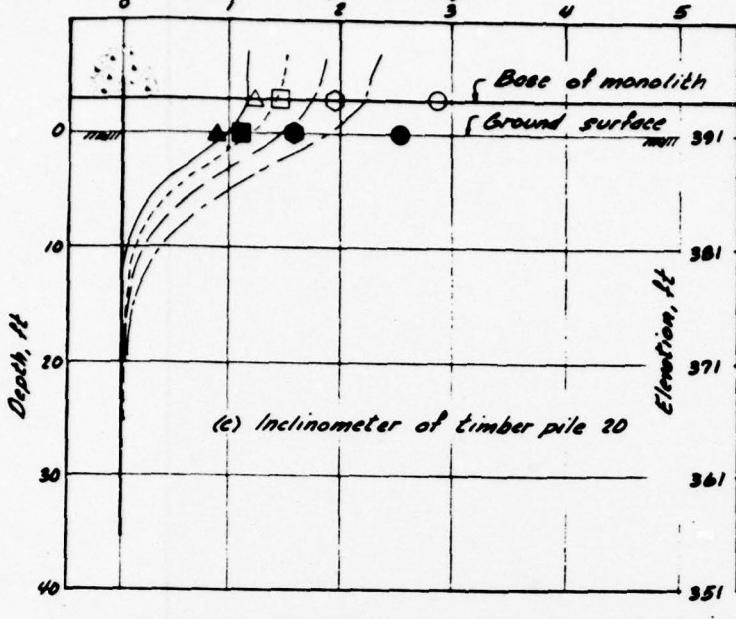
Deflection of timber  
pile inclinometers



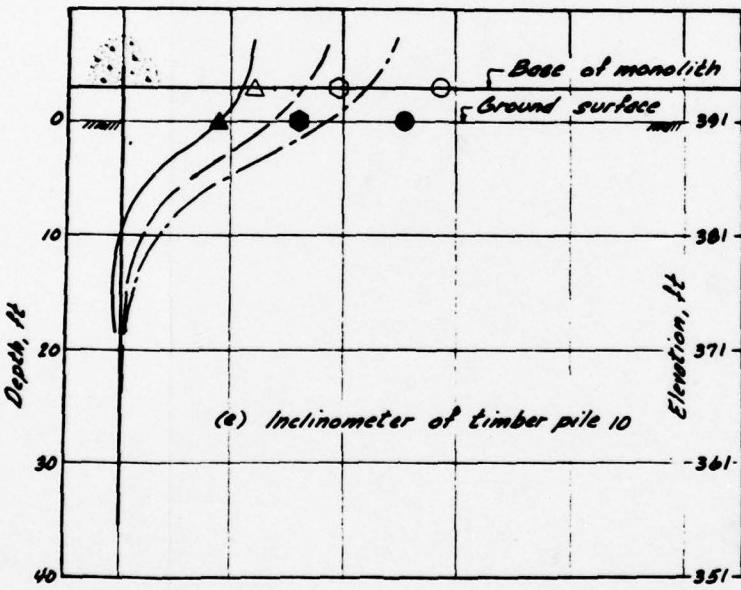


under full test loads,  
prior to prototype  
pile driving  
after driving prototype  
pile 3  
after driving prototype  
pile 6  
after driving prototype  
pile 12

Horizontal deflection of timber pile inclinometer  
during prototype pile driving, in.



(c) Inclinometer of timber pile 20



(c) Inclinometer of timber pile 10

**PILE DRIVING EFFECTS TEST PROGRAM  
DEFLECTION  
OF TIMBER PILE INCLINOMETERS  
DURING  
PROTOTYPE PILE DRIVING  
FOR MONOLITH M2**

FOUNDATION INVESTIGATION AND TEST PROGRAM  
EXISTING LOCKS AND DAM NO. 20  
ST LOUIS DISTRICT, CORPS OF ENGINEERS.

DACW43-78-C-0000

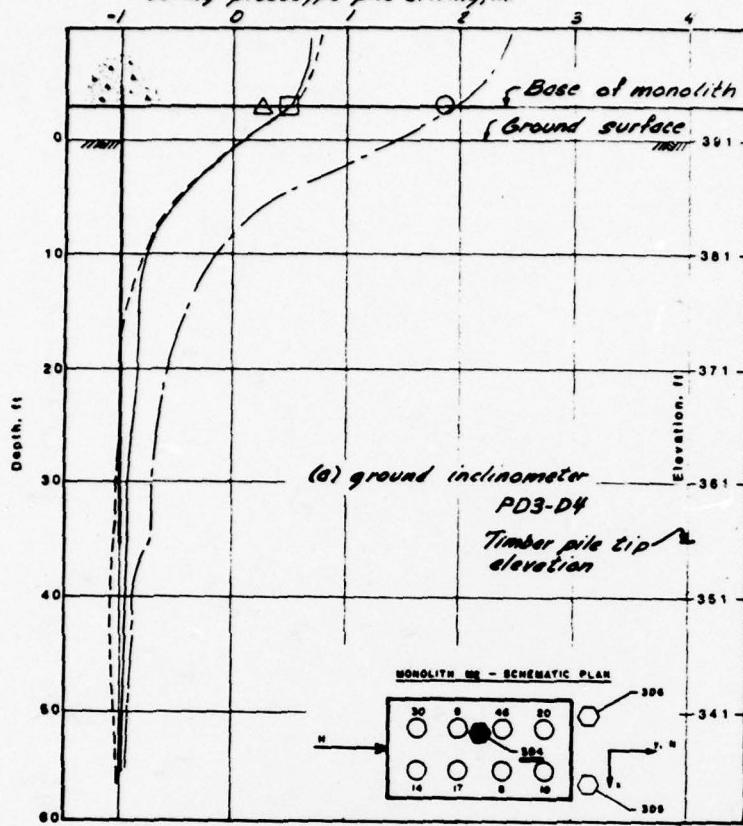
Woodward-Clyde Consultants

1978 Phase II

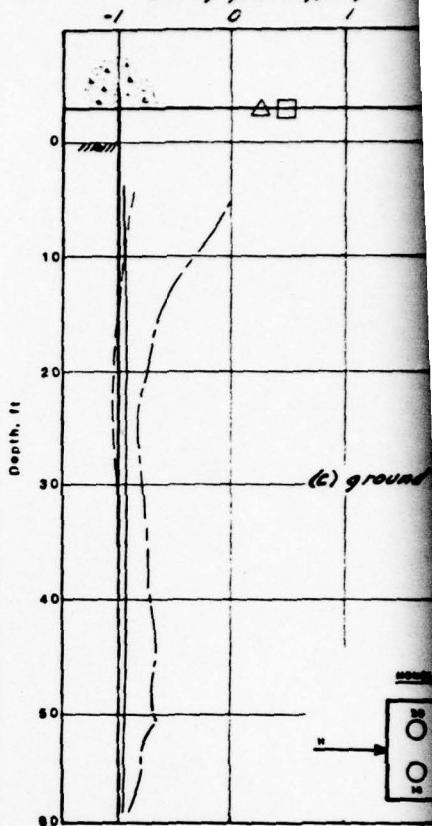
Fig. 9.11

5

Horizontal deflection of ground inclinometer  
during prototype pile driving, in



Horizontal deflection  
during prototype pile



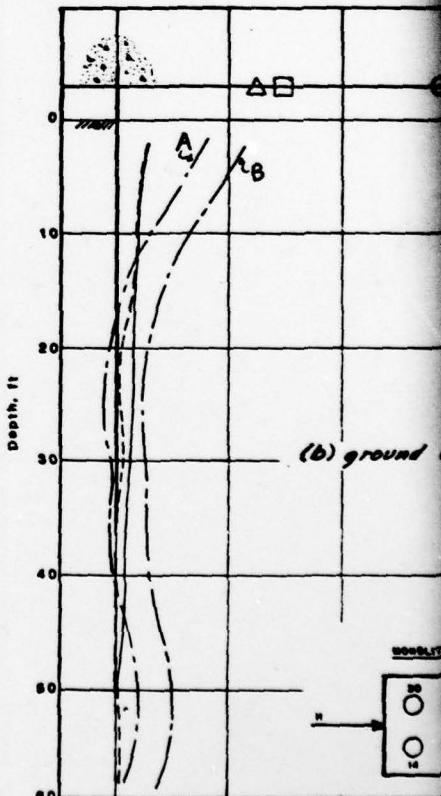
#### Legend

Horizontal displacement of Deflection of ground  
monolith inclinometers

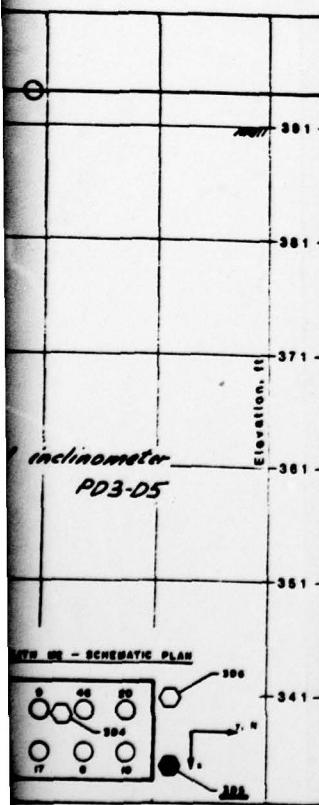
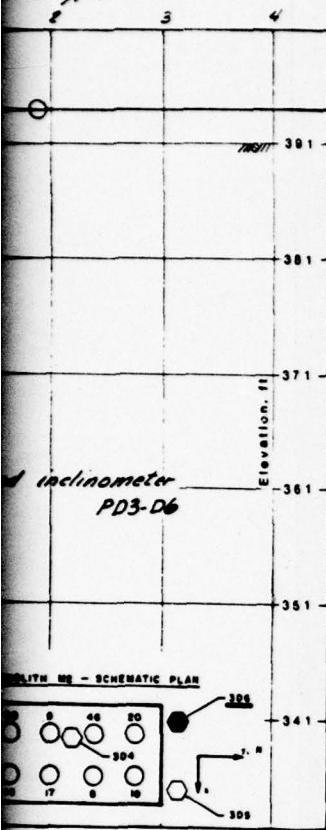
- |   |       |   |
|---|-------|---|
| △ | —     | under full test loads<br>prior to prototype<br>pile driving |
| □ | - - - | after driving prototype<br>pile 3                           |
| ○ | —     | after driving prototype<br>pile 12                          |

#### Note:

Curve A obtained assuming the casing bottom stationary.  
Curve B obtained by translation to match inclinometer  
deflection and timber pile displacement at ground  
surface



at ground inclinometer  
driving, in.



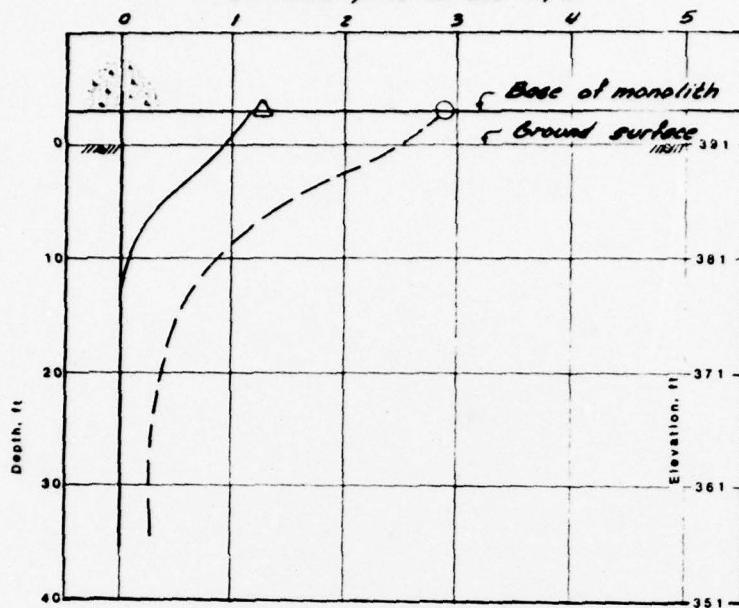
PILE DRIVING EFFECTS TEST PROGRAM  
**DEFLECTION  
OF GROUND INCLINOMETERS  
DURING PROTOTYPE PILE  
DRIVING FOR MONOLITH M2**  
FOUNDATION INVESTIGATION AND TEST PROGRAM  
EXISTING LOCKS AND DAM NO. 20  
ST LOUIS DISTRICT, CORPS OF ENGINEERS.  
DAGW43-78-C-0000

Woodward-Clyde Consultants

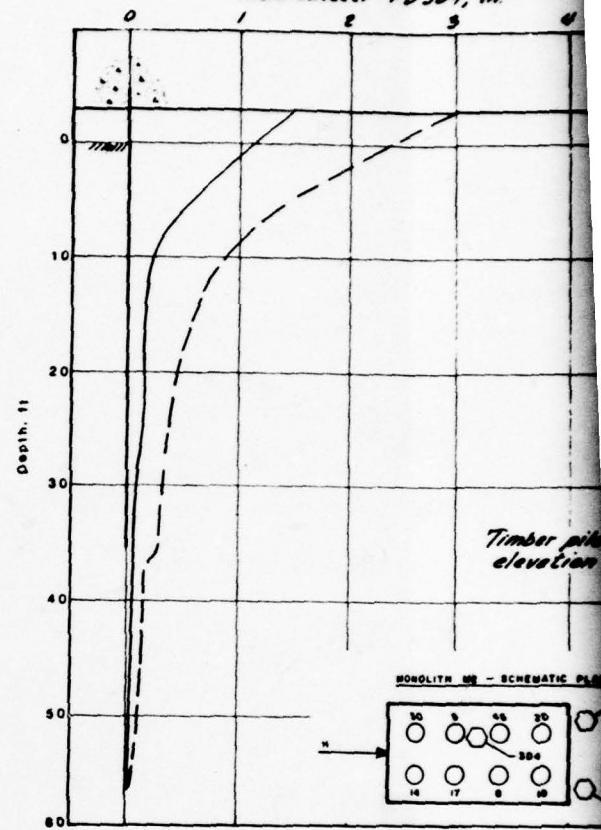
10 PHASE II

Fig. 9.12

Average horizontal deflection of inclinometers  
of timber piles 30 and 14, in.



Horizontal deflection of ground  
inclinometer PD304, in.



#### Legend

Horizontal displacement  
of monolith



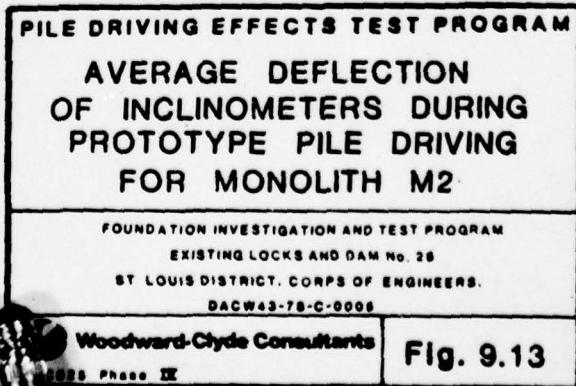
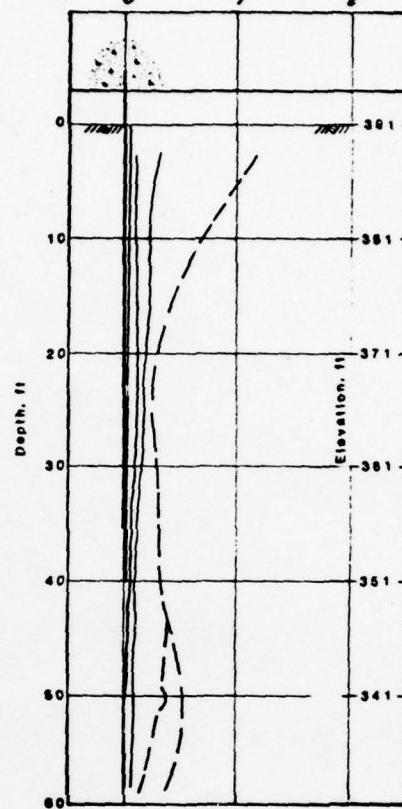
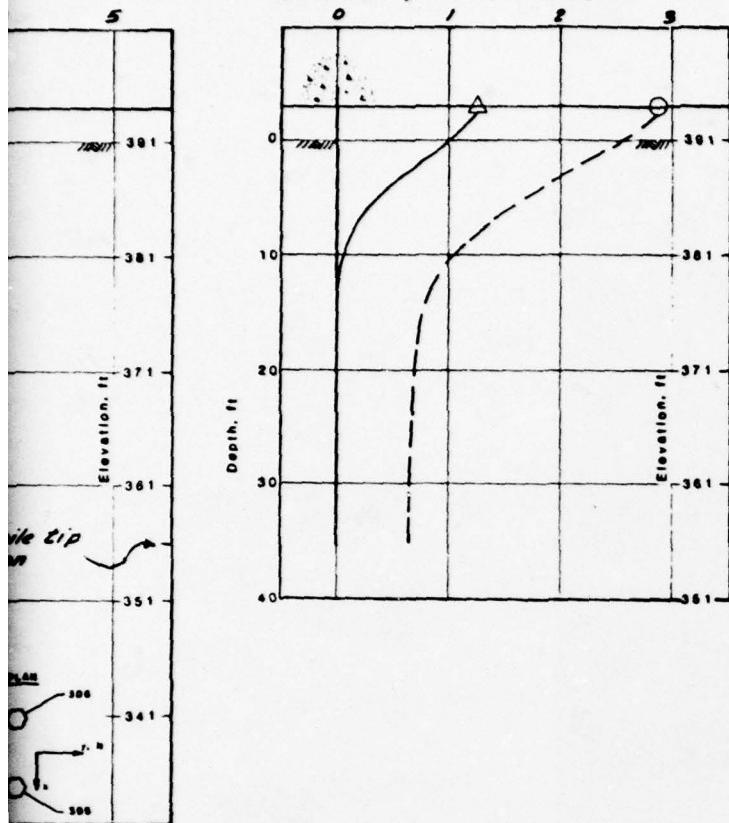
Horizontal deflection  
of inclinometers

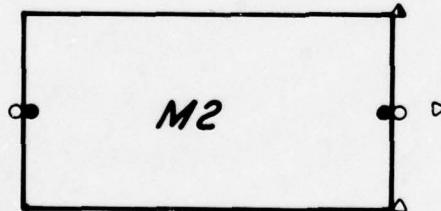
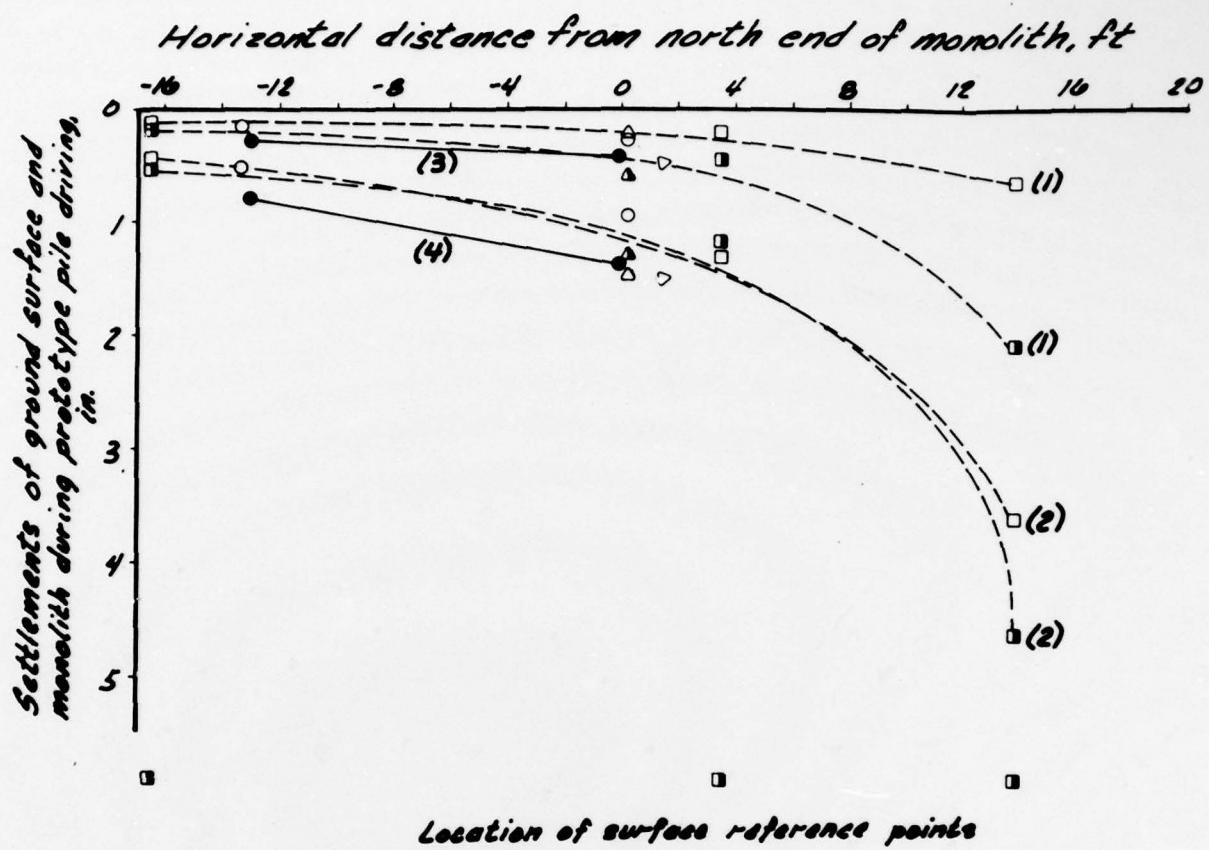


at beginning of  
prototype pile driving  
at end of prototype  
pile driving

Average horizontal deflection of inclinometers  
of timber piles 10 and 20, in.

Average horizontal deflection of ground  
inclinometers PD3-05 and PD3-06, in.





Project N

Note  
(1)  
(2)  
(3)  
(4)

AD-A076 093

WOODWARD-CLYDE CONSULTANTS CHICAGO IL

F/G 13/2

RESULTS AND INTERPRETATION OF PILE DRIVING EFFECTS TEST PROGRAM--ETCIL

JUL 79 J PEREZ , D M HOLLOWAY

DACW43-78-C-0005

NL

UNCLASSIFIED

5 OF 5

AD  
A076093



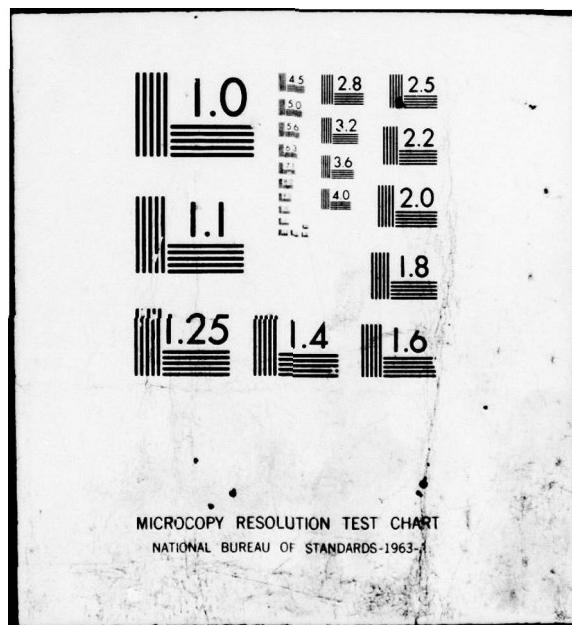
END

DATE

FILMED

11-79

DOC



end

Settlement of monolith at north and south ends of monolith

Settlement of reference beam at north and south ends of monolith

Settlement of east surface reference points

Settlement of west surface reference points

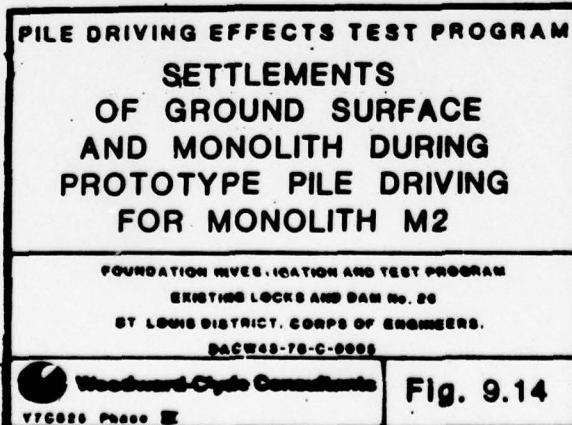
Settlement of middle surface reference point

Settlement of ground surface after driving of prototype pile 5 at 20.8 ft from monolith

Settlement of ground surface after driving of prototype pile 12 at 15 ft from monolith

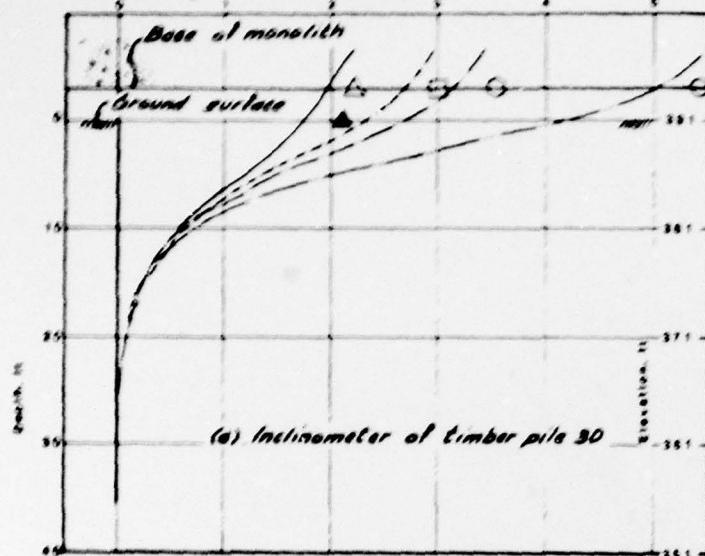
Settlement of monolith after driving of prototype pile 5 at 20.8 ft from monolith

Settlement of monolith after driving of prototype pile 12 at 15 ft from monolith

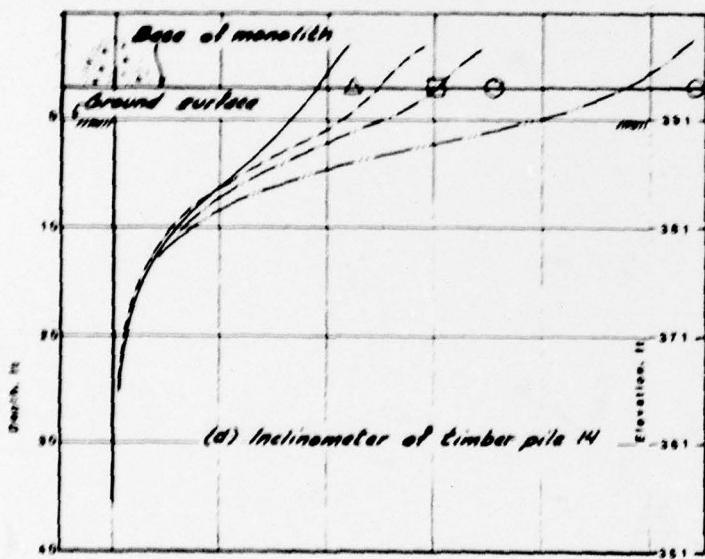
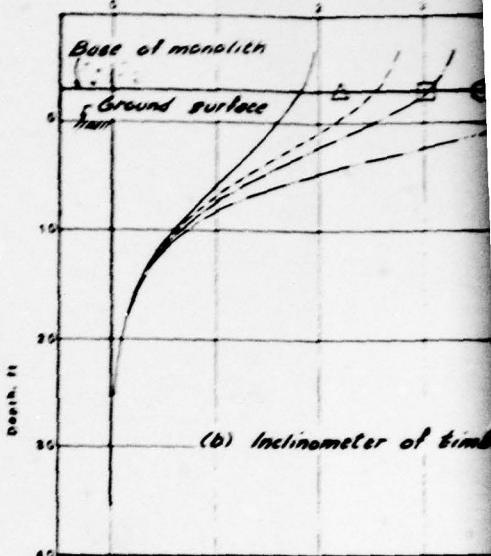


2

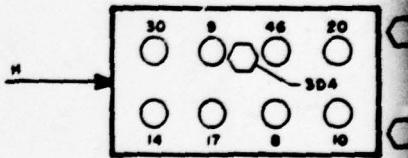
Horizontal deflection of timber pile inclinometer during lateral load testing, in.



Horizontal deflection of timber pile during lateral load testing, in.



MONOLITH MR - SCHEMATIC PIANO

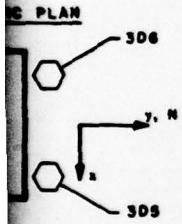
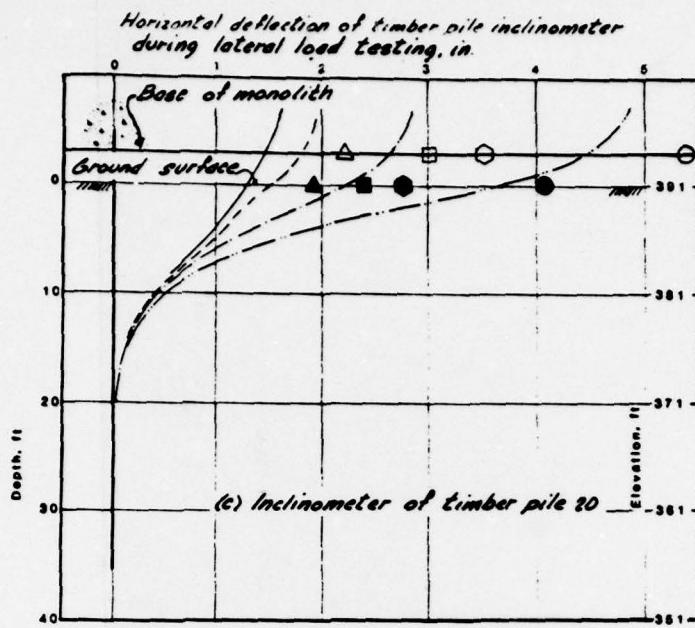
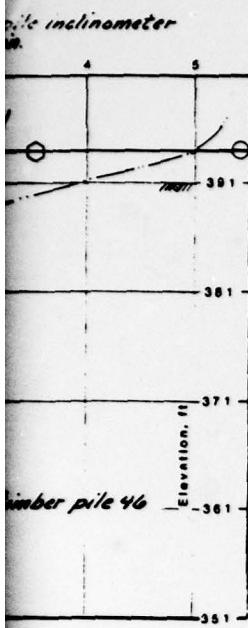


Horizontal displacement of monolith, four corner timber piles at ground surface

Legend

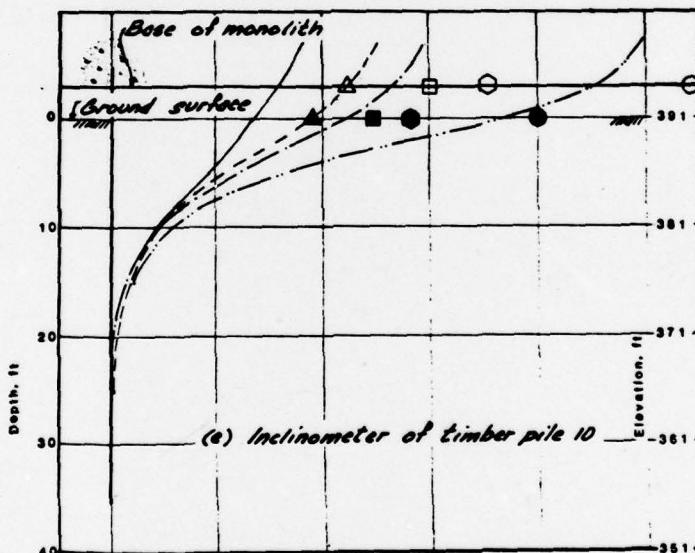
Deflection of pile inclinometers

- |   |   |
|---|---|
| △ | ▲ |
| □ | ■ |
| ○ | ● |
| ○ | — |



of timber For lateral load/pile of  
inclinometers

0t  
6t  
9t  
15t



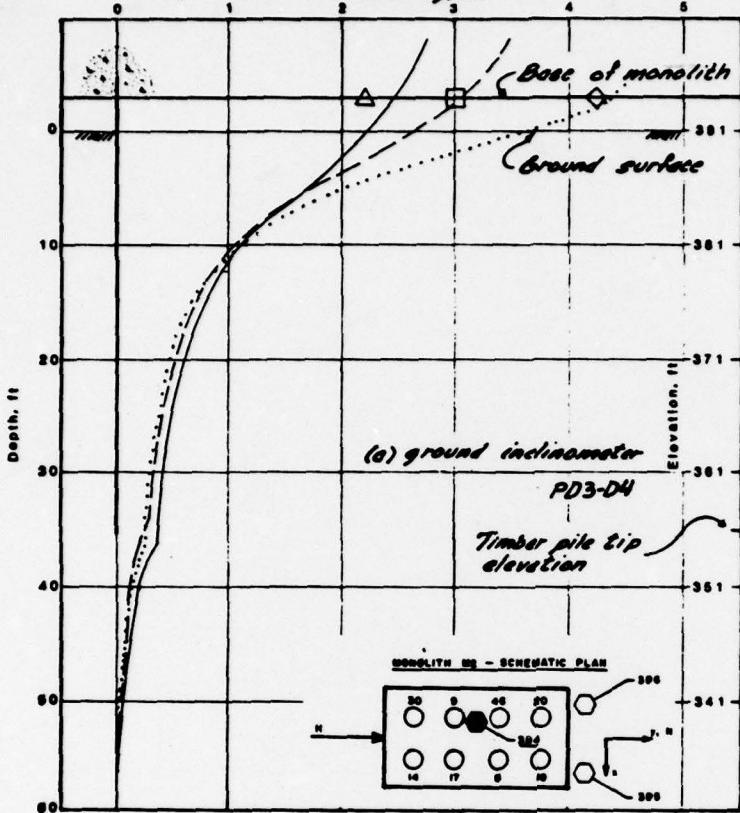
**PILE DRIVING EFFECTS TEST PROGRAM  
DEFLECTION OF TIMBER  
PILE INCLINOMETERS DURING  
LATERAL LOAD TESTING  
OF MONOLITH M2**

FOUNDATION INVESTIGATION AND TEST PROGRAM  
EXISTING LOCKS AND DAM No. 26  
ST LOUIS DISTRICT, CORPS OF ENGINEERS.  
DACPW43-78-C-0008

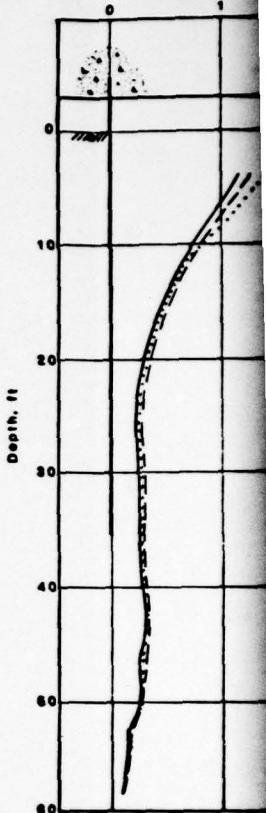
Woodward-Clyde Consultants  
V7C026 Phase IX

Fig. 9.15

Horizontal deflection of ground inclinometer  
during lateral load testing, in.



Horizontal deflection of ground inclinometer  
during lateral load testing, in.



### Legend

Horizontal displacement of monolith



Deflection of ground inclinometers

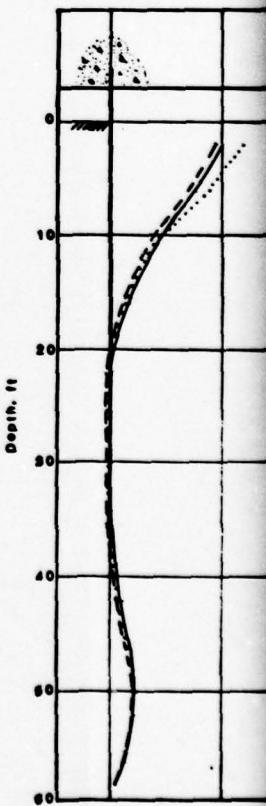


For lateral load/pile of

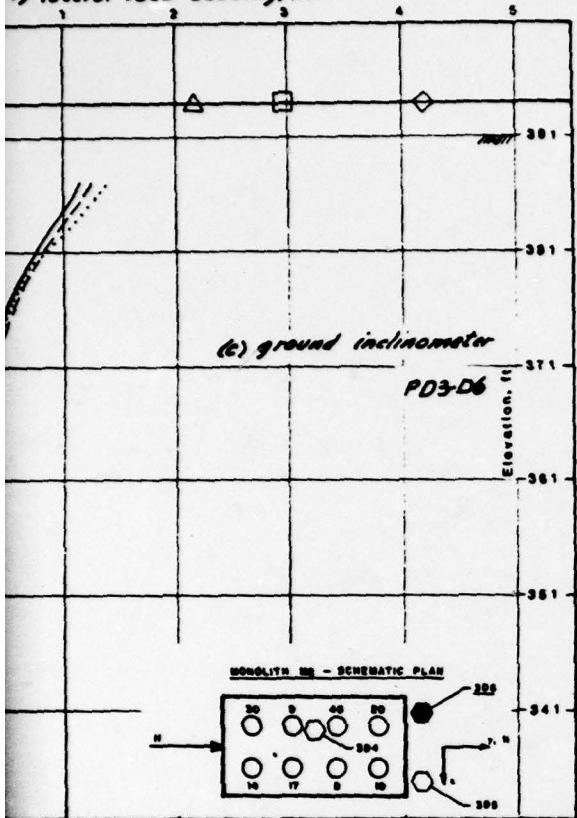
0t

6t

12t



horizontal deflection of ground inclinometer  
during lateral load testing, in.

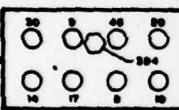


(c) ground inclinometer

PD3-D6

ELEVATION

MONOLITH M2 - SCHEMATIC PLAN



382

384

385

386

341

331

321

311

301

(b) ground inclinometer

PD3-D5

ELEVATION

MONOLITH M2 - SCHEMATIC PLAN



382

384

385

386

341

331

321

311

301

### PILE DRIVING EFFECTS TEST PROGRAM

## DEFLECTION OF GROUND INCLINOMETERS DURING LATERAL LOAD TESTING OF MONOLITH M2

FOUNDATION INVESTIGATION AND TEST PROGRAM

EXISTING LOCKS AND DAM NO. 26

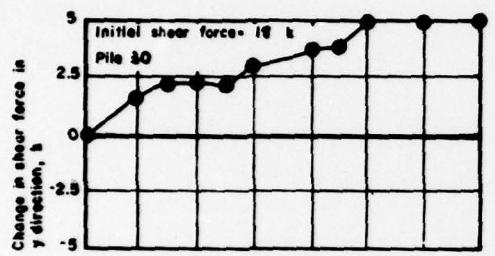
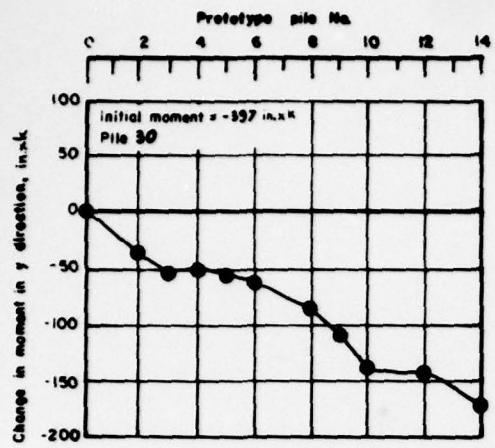
ST LOUIS DISTRICT, CORPS OF ENGINEERS.

DACW43-78-C-0008

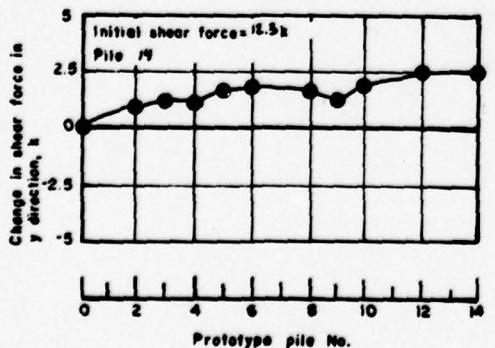
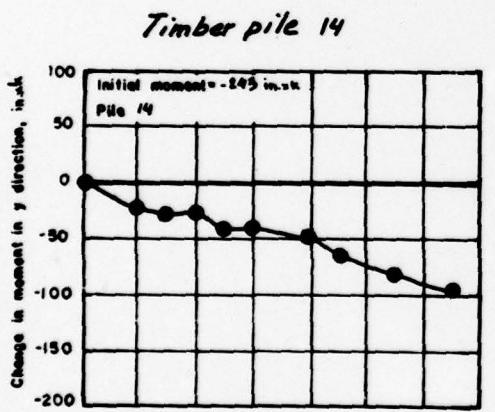
Woodward-Clyde Consultants

VCG25 Phase II

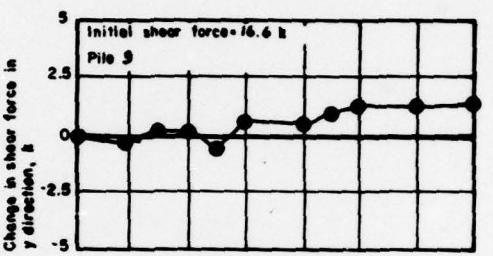
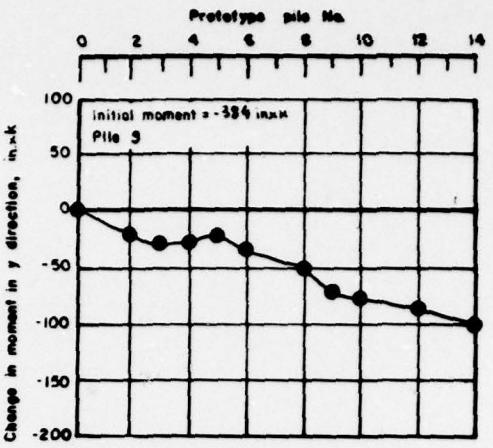
Fig. 9.16



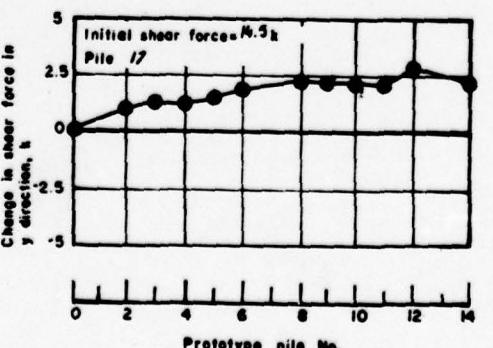
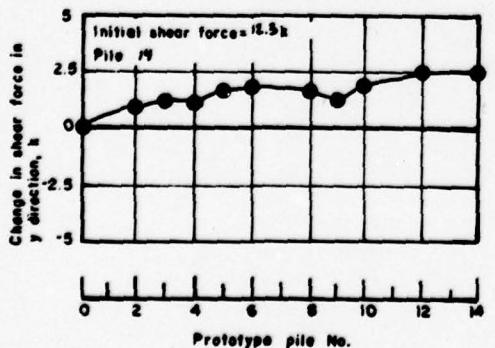
Timber pile 30



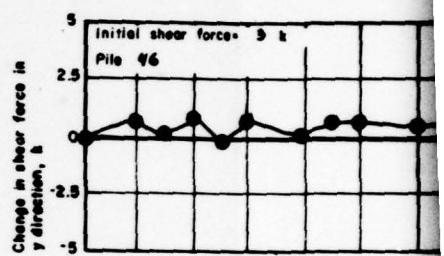
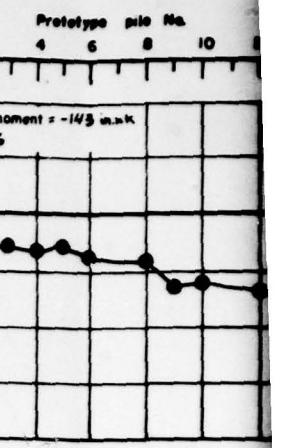
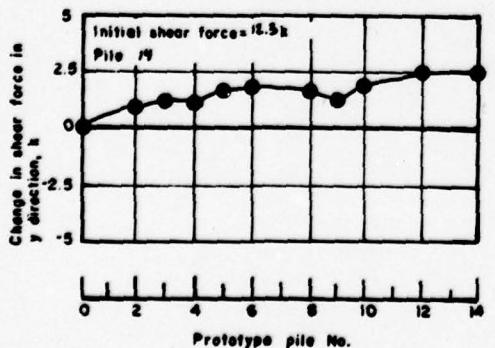
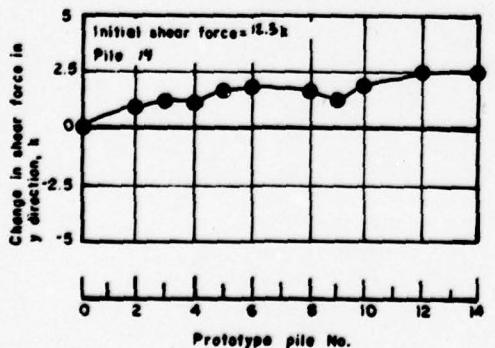
Timber pile 14



Timber pile 9

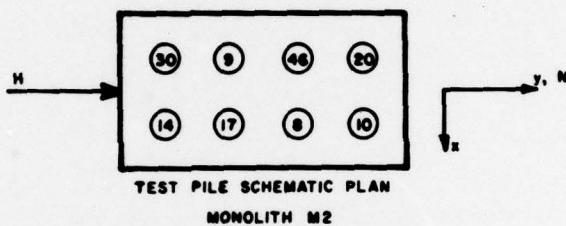
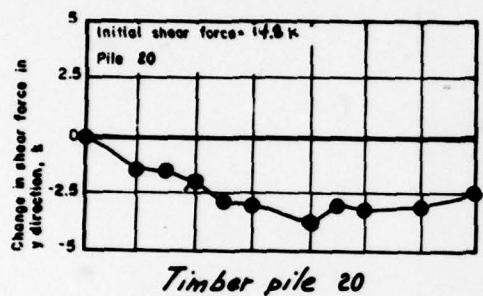
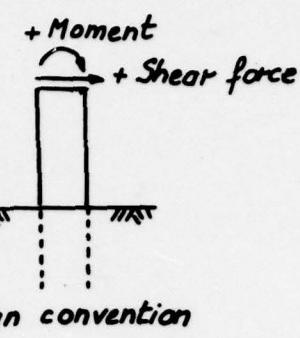
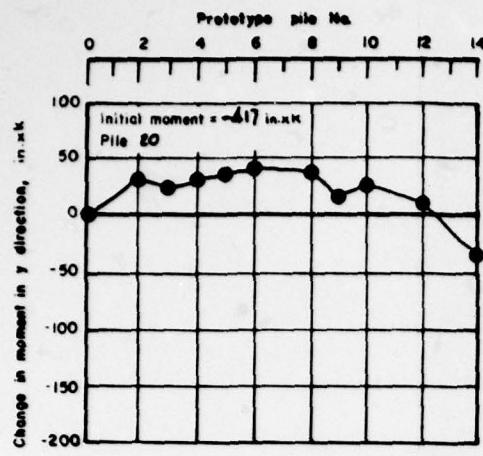


Timber pile 17

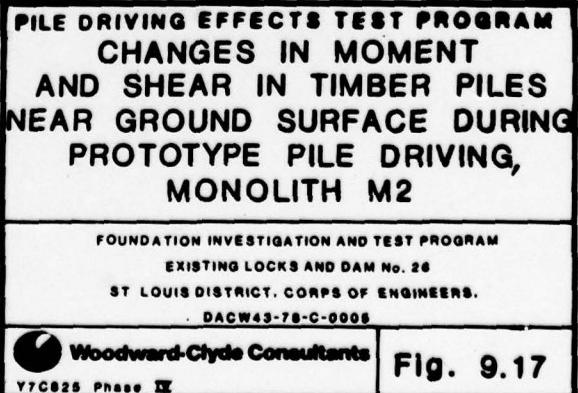
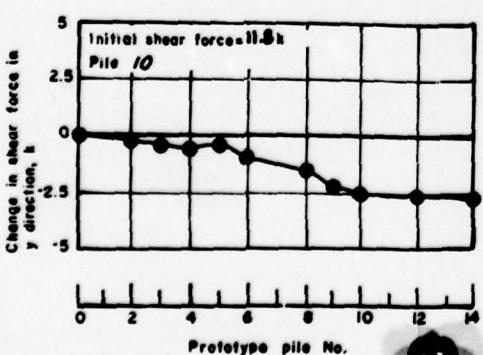
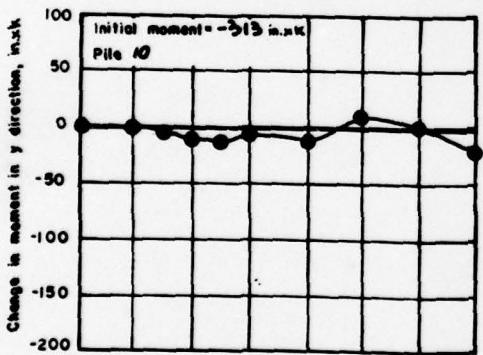


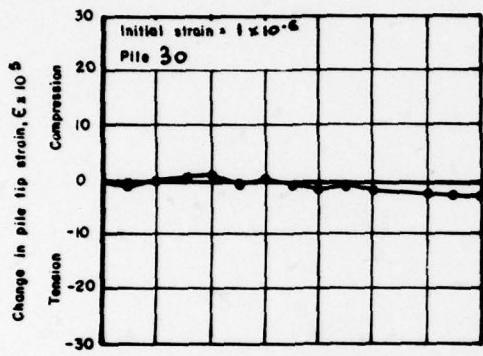
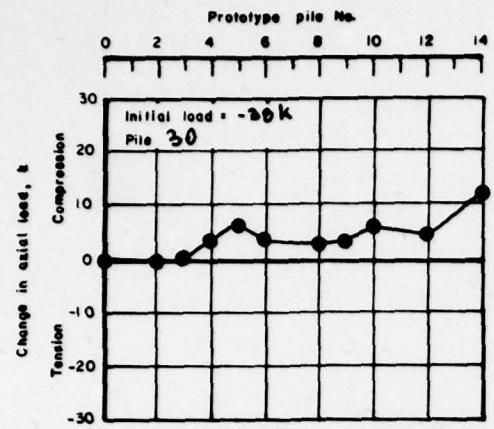
Timber pile 46

Timber pile 8

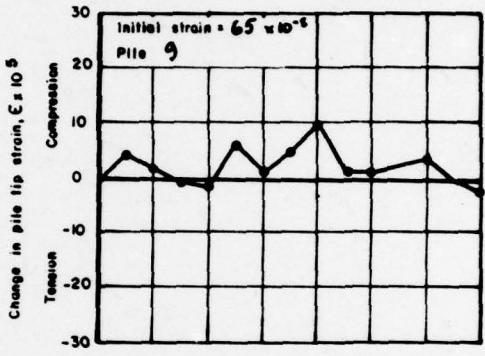
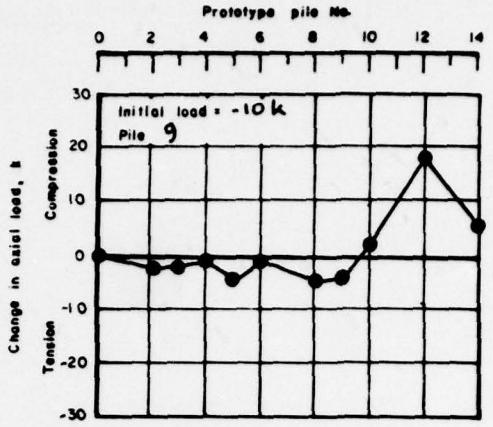


Timber pile 10

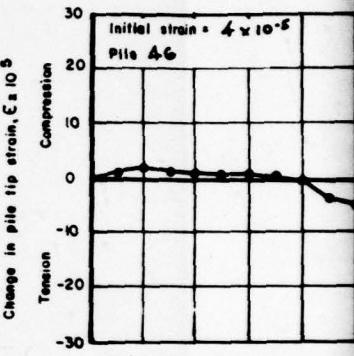
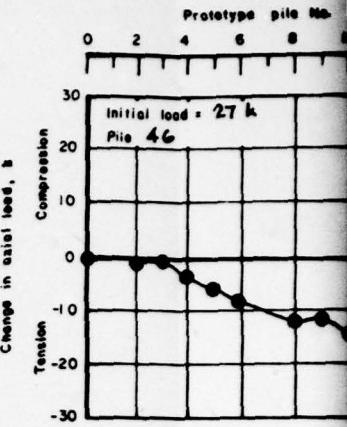




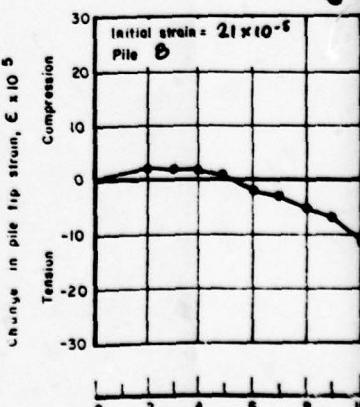
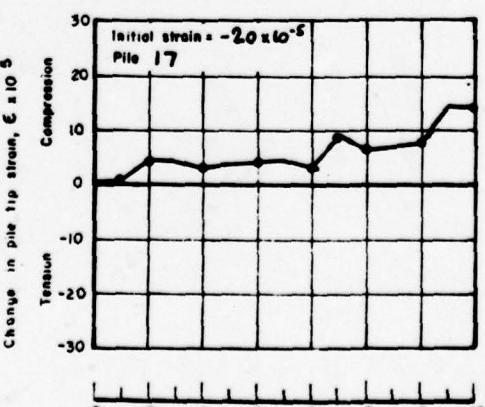
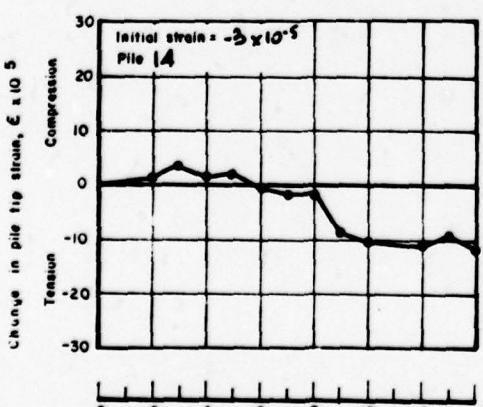
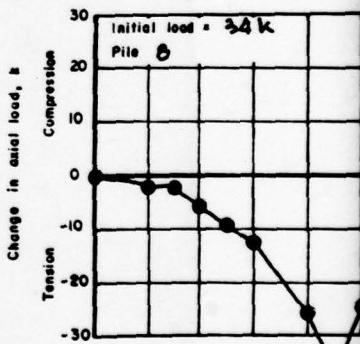
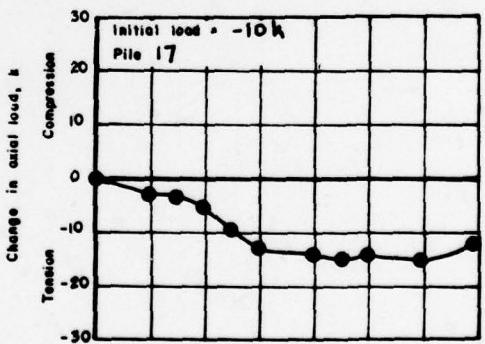
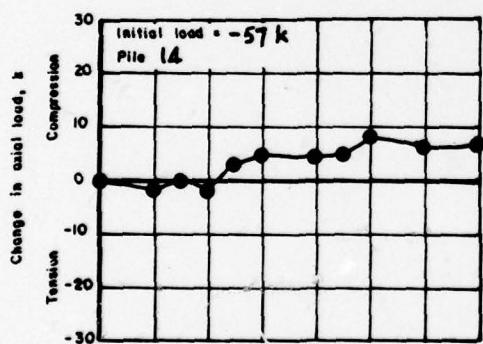
Timber Pile 30  
Timber Pile 14

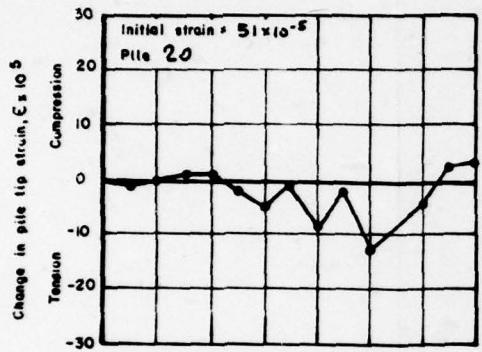
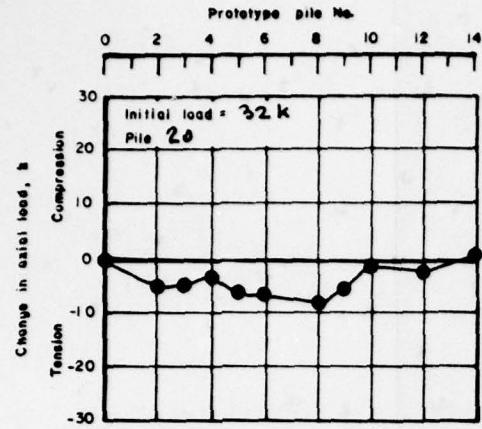
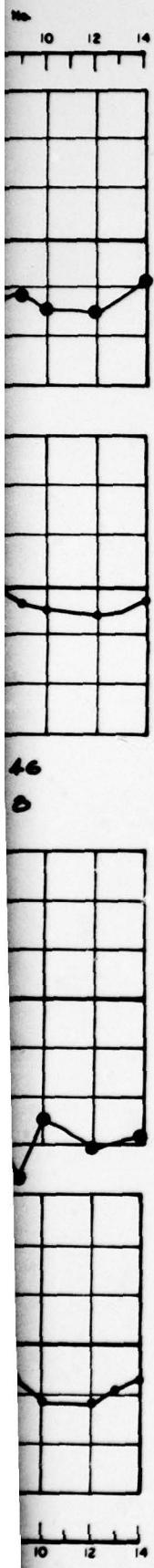


Timber Pile 9  
Timber Pile 17

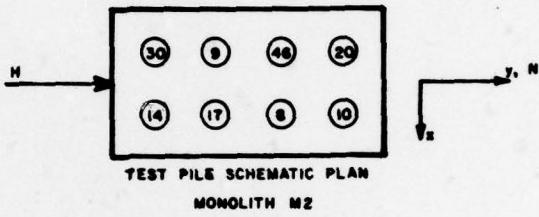
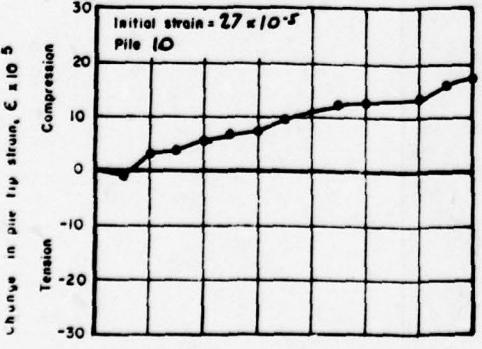
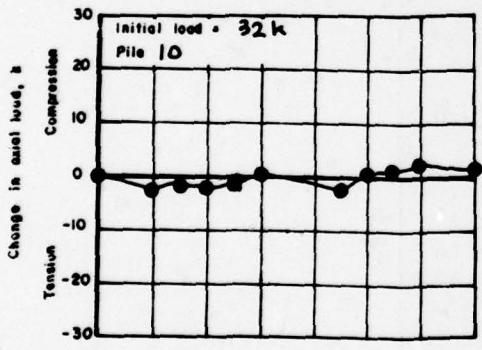


Timber Pile 46  
Timber Pile 8





Timber Pile 20  
Timber Pile 10



#### Legend

Initial axial load refers  
to the value after  
application of full  
lateral load

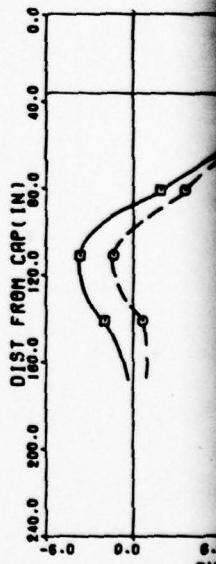
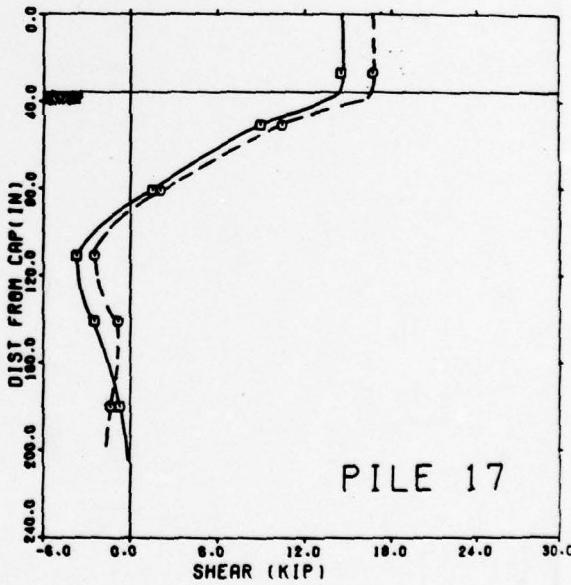
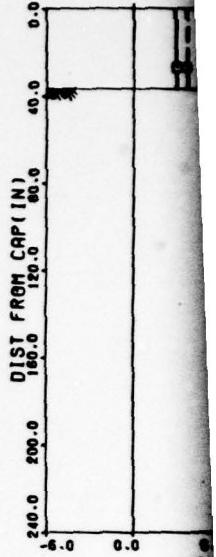
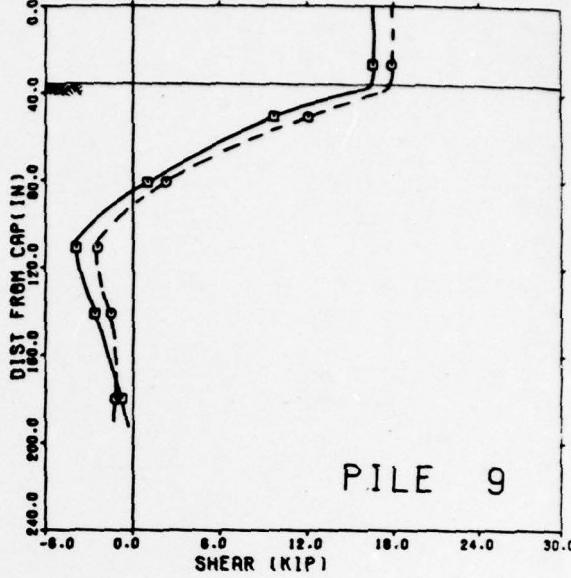
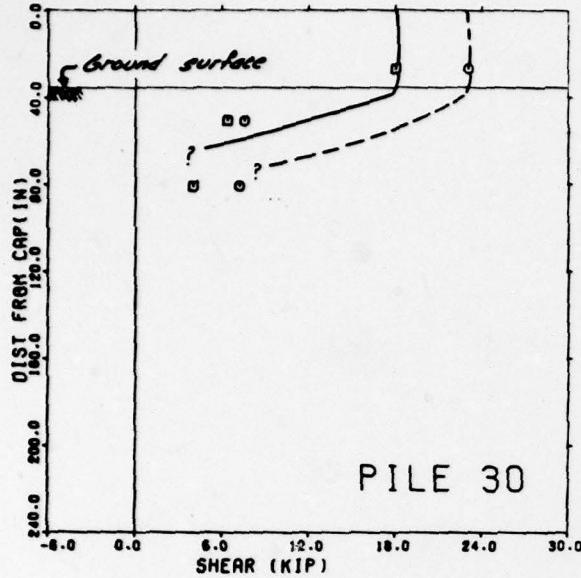
Initial strain computed  
at start of  
prototype pile driving, with  
 $\epsilon = 1 \times 10^{-5}$  corresponding to  
 $6 \times 10^{-4}$  in. change in the  
5 ft gage length.

### PILE DRIVING EFFECTS TEST PROGRAM CHANGES IN AXIAL LOAD AT BUTT AND STRAIN AT TIP OF TIMBER PILES DURING PROTOTYPE PILE DRIVING, MONOLITH M2

FOUNDATION INVESTIGATION AND TEST PROGRAM  
EXISTING LOCKS AND DAM NO. 26  
ST LOUIS DISTRICT, CORPS OF ENGINEERS.  
DACPW43-78-C-0005

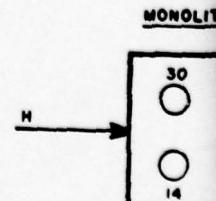
Woodward-Clyde Consultants  
Y7CB25 Phase II

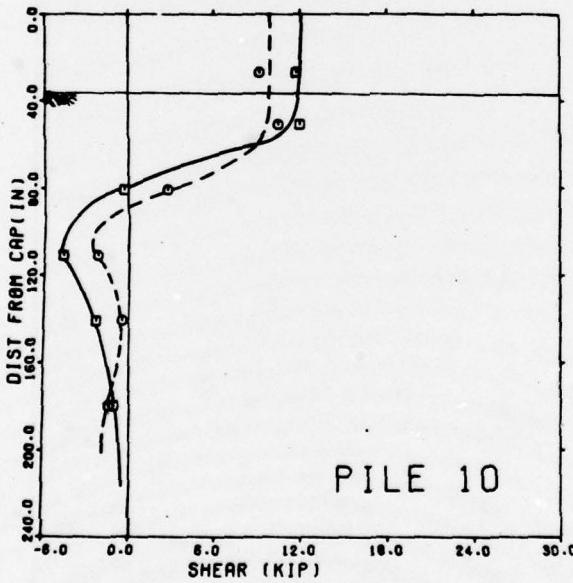
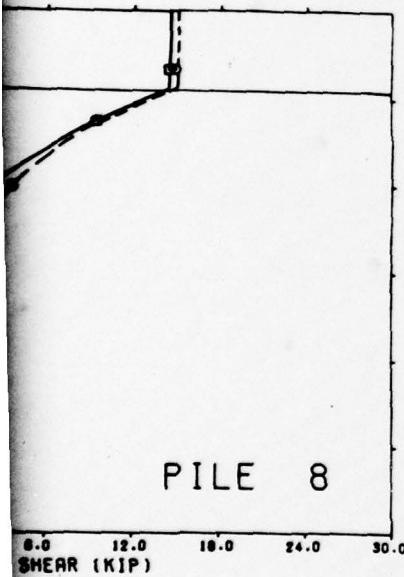
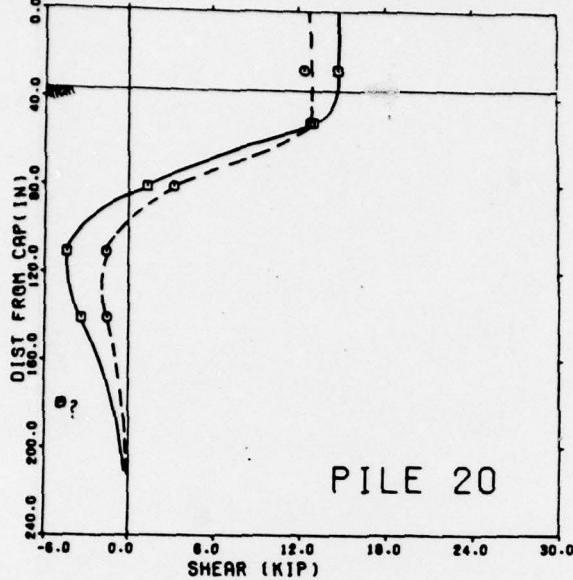
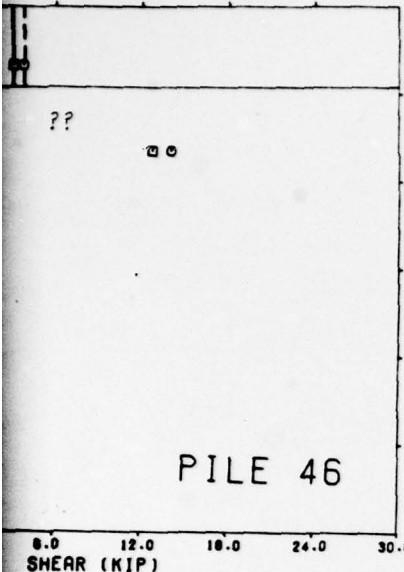
Fig. 9.18



### Legend

- o- Prior to prototype pile driving
- o-- After driving last prototype pile 14





**PILE DRIVING EFFECTS TEST PROGRAM  
SHEAR FORCE DISTRIBUTION  
ON TIMBER PILES DURING  
PROTOTYPE PILE DRIVING,  
MONOLITH M2**

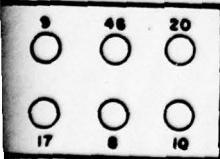
FOUNDATION INVESTIGATION AND TEST PROGRAM  
EXISTING LOCKS AND DAM No. 20  
ST LOUIS DISTRICT, CORPS OF ENGINEERS.  
DRCW43-78-C-9008

Woodward-Clyde Consultants

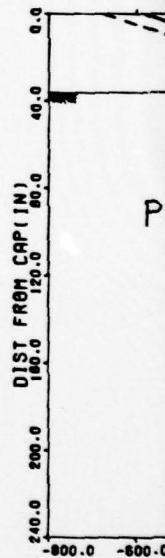
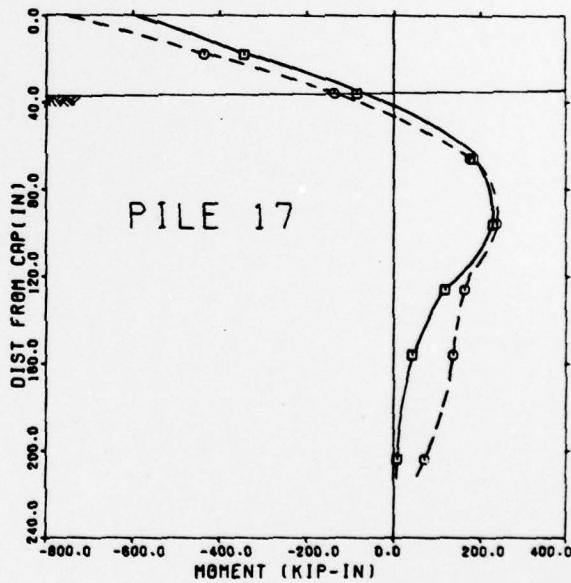
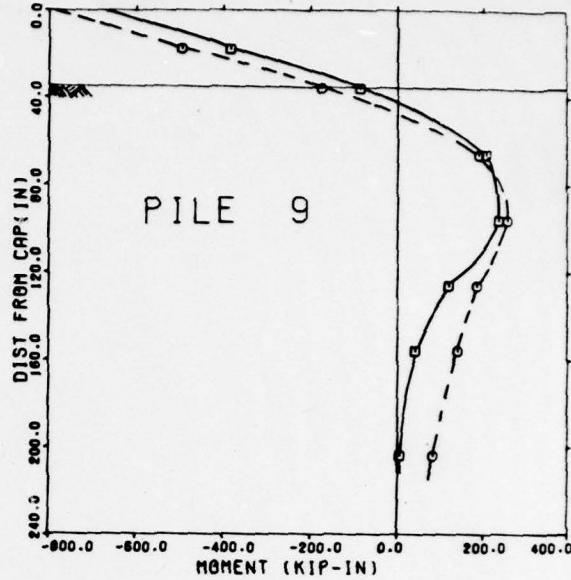
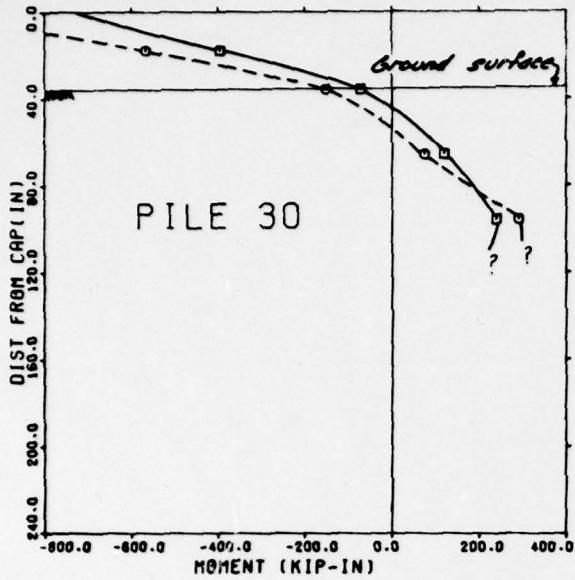
TC028 Photo II

Fig. 9.19

MONOLITH M2 - SCHEMATIC PLAN

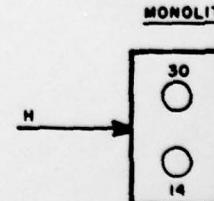


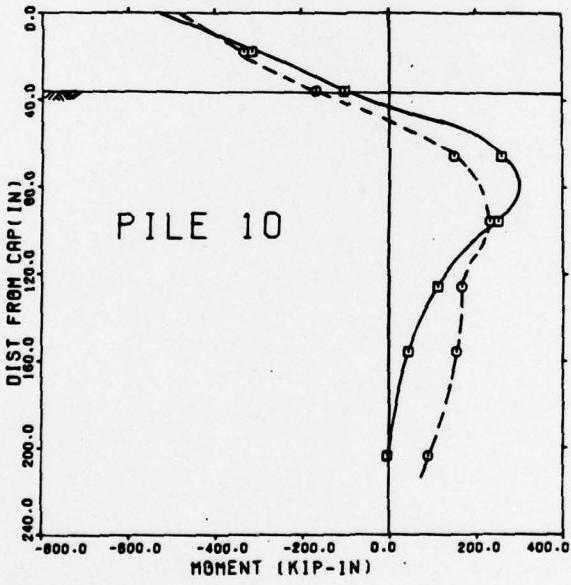
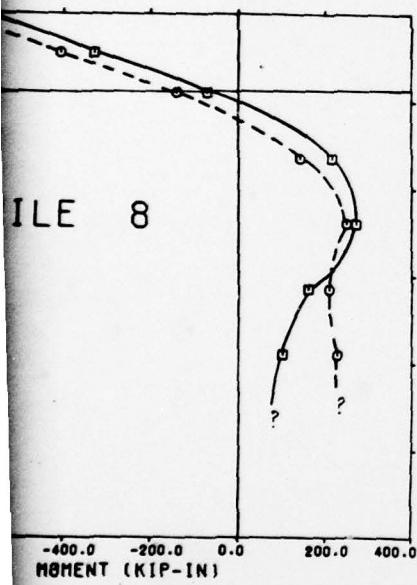
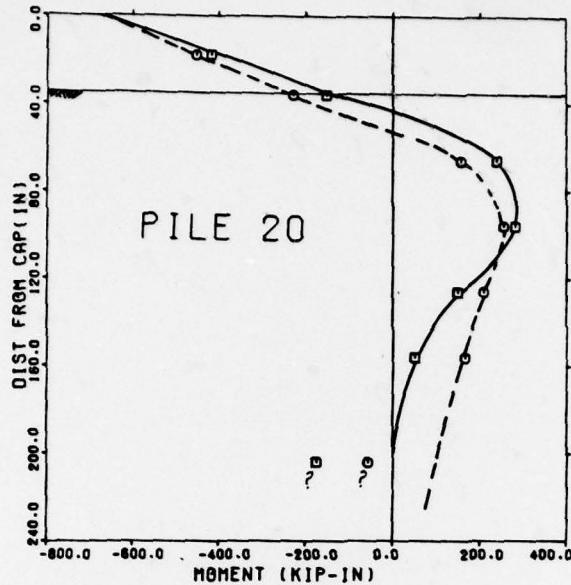
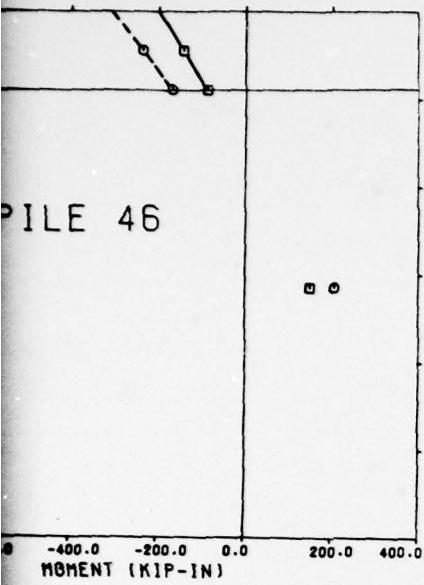
2



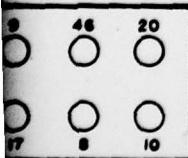
### Legend

- - Prior to prototype pile driving
- After driving last prototype pile 14





M2 - SCHEMATIC PLAN

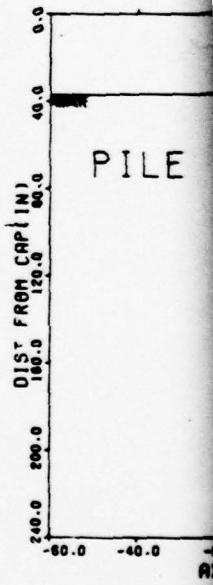
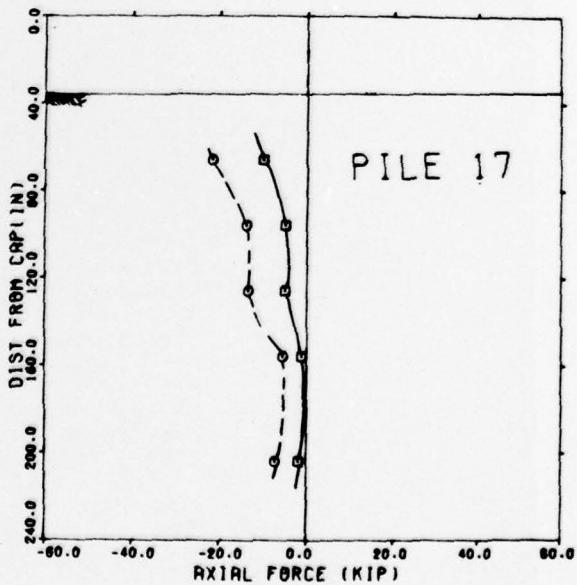
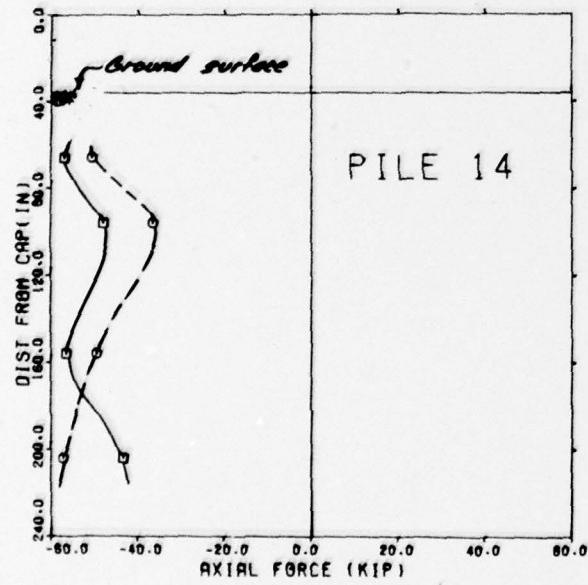
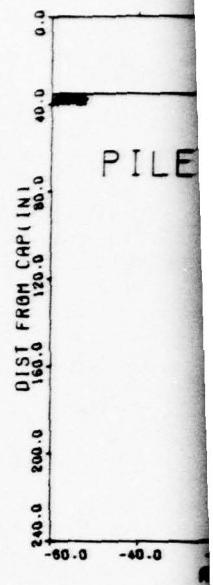
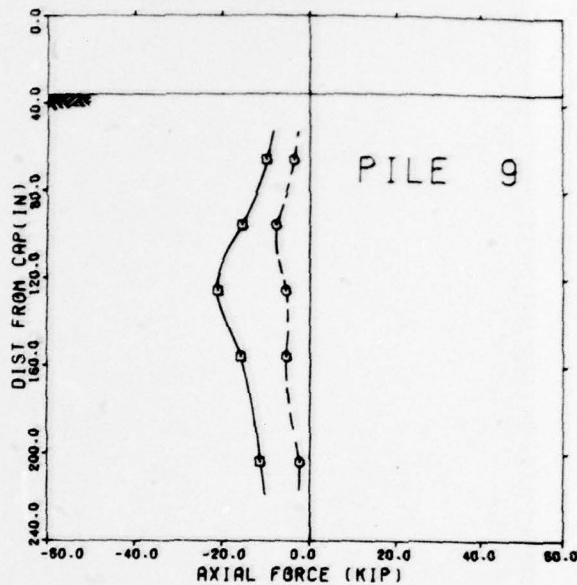
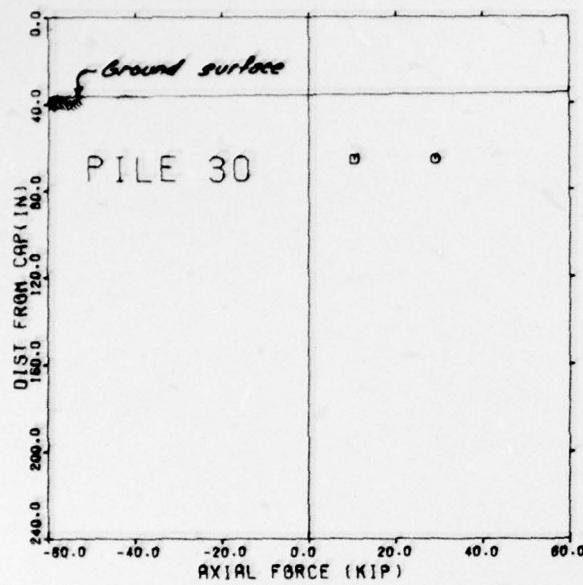


**PILE DRIVING EFFECTS TEST PROGRAM  
BENDING MOMENT DISTRIBUTION  
ON TIMBER PILES DURING  
PROTOTYPE PILE DRIVING,  
MONOLITH M2**

FOUNDATION INVESTIGATION AND TEST PROGRAM  
EXISTING LOCKS AND DAM No. 26  
BY LOUIS DISTRICT, CORPS OF ENGINEERS.  
DACPW43-78-C-0008

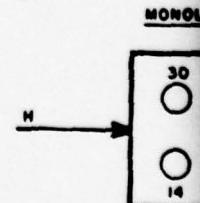
Woodward-Clyde Consultants  
V7C829 Phase II

Fig. 9.20



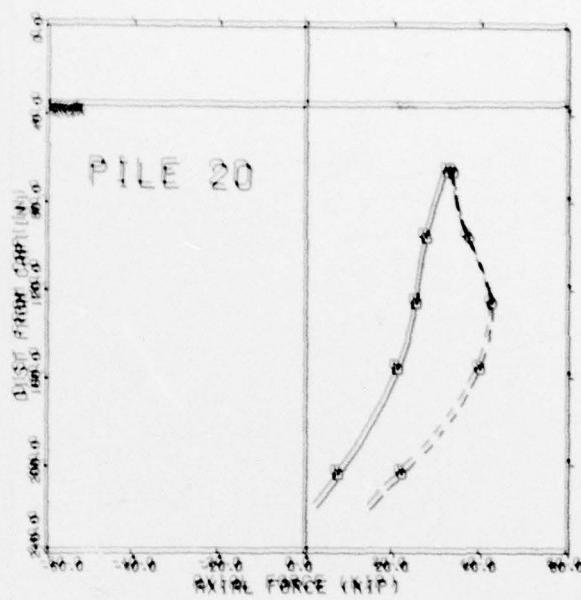
### Legend

- Prior to prototype pile driving
- After driving last prototype pile 14



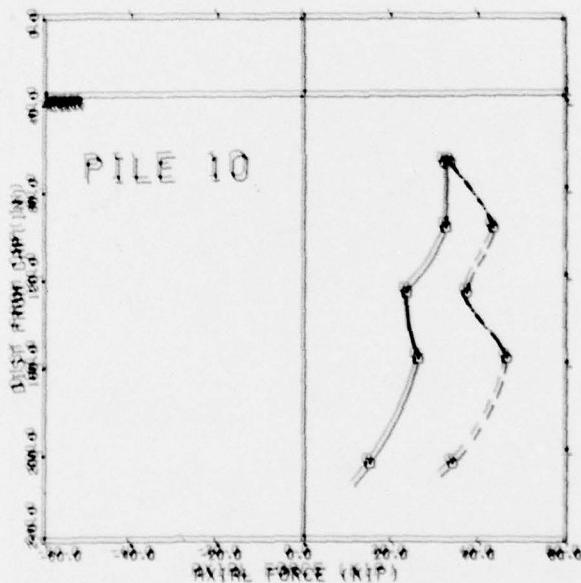
E 46

AXIAL FORCE (KIP)

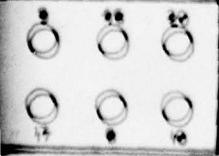


8

AXIAL FORCE (KIP)



ATTACHMENT = SCHEMATIC PLAN

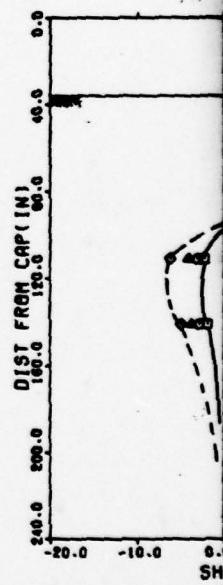
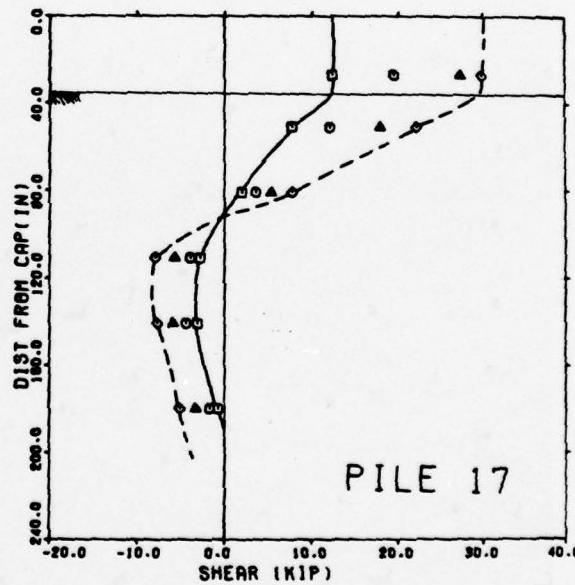
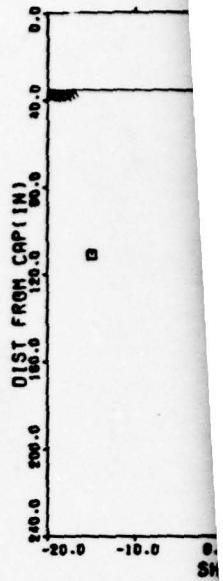
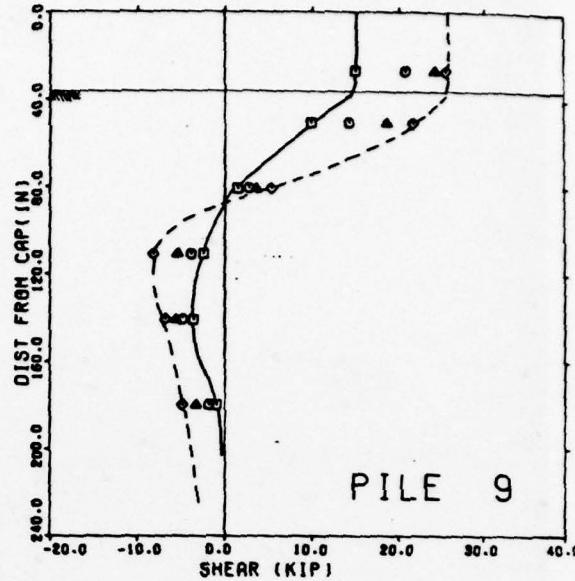
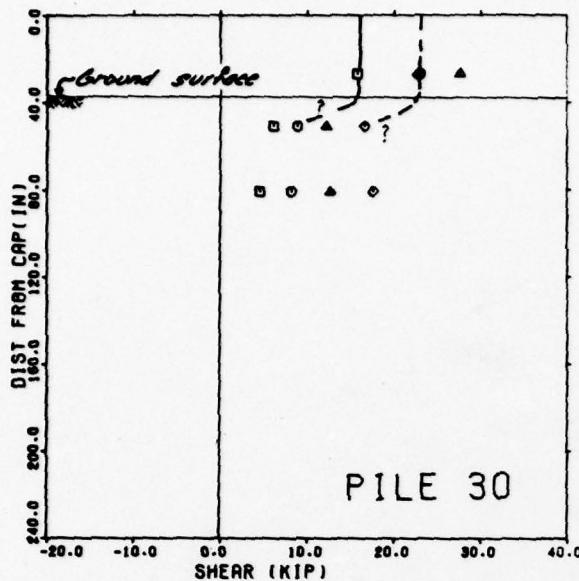


PILE DRIVING EFFECTS TEST PROGRAM  
AXIAL LOAD DISTRIBUTION  
ON TIMBER PILES DURING  
PROTOTYPE PILE DRIVING,  
MONOLITH M2

FOUNDATION INVESTIGATION AND TEST PROGRAM  
EXISTING LOCKS AND DAM NO. 20  
BY ST. LOUIS DISTRICT, CORPS OF ENGINEERS  
BACHELOR OF SCIENCE

Woodward-Clyde Consultants  
ST. LOUIS, MISSOURI

Fig. 9.21

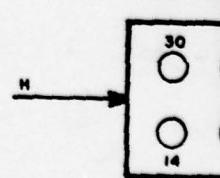


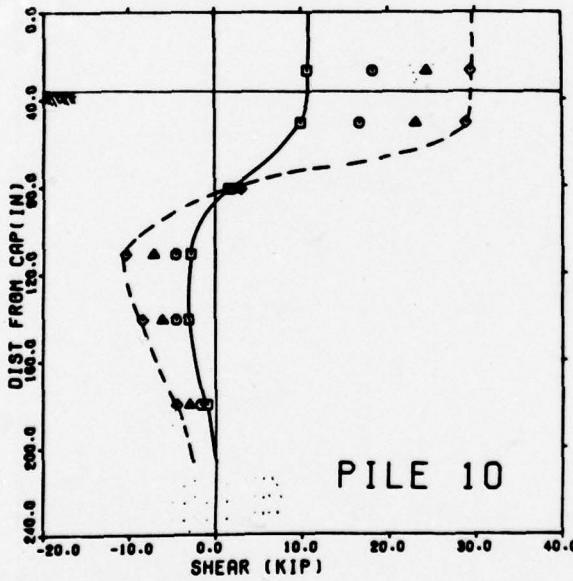
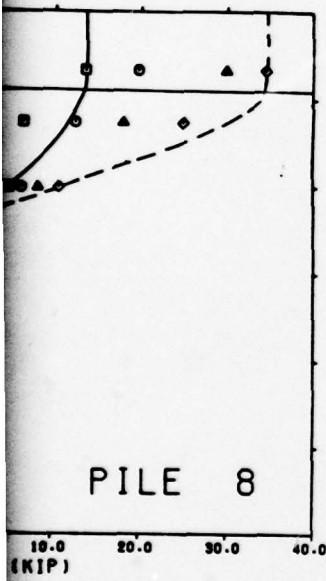
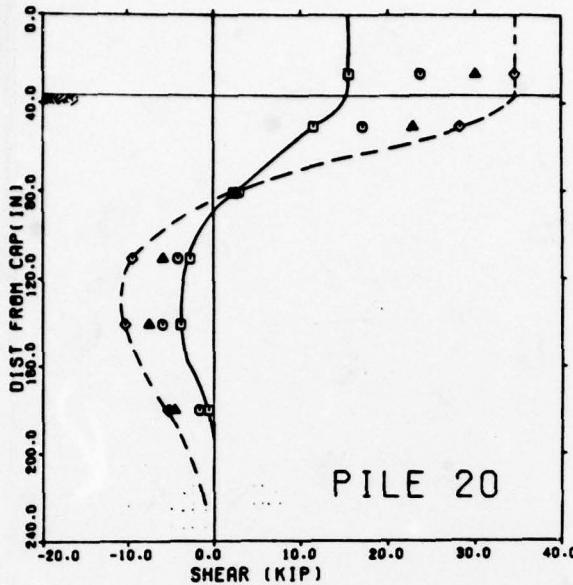
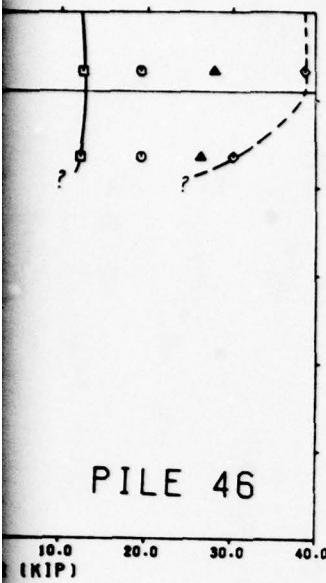
### Legend

Total lateral load,  $t$       Lateral load/pile,  $t$

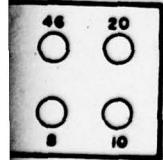
—	48	6
○	72	9
▲	96	12
◆	120	15

MONOLIT





- SCHEMATIC PLAN



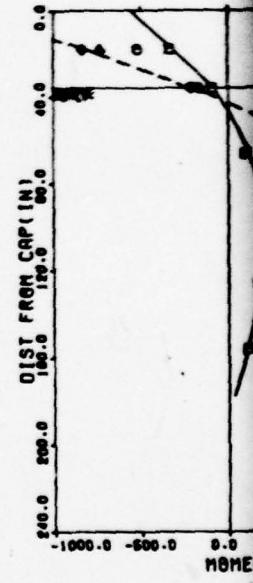
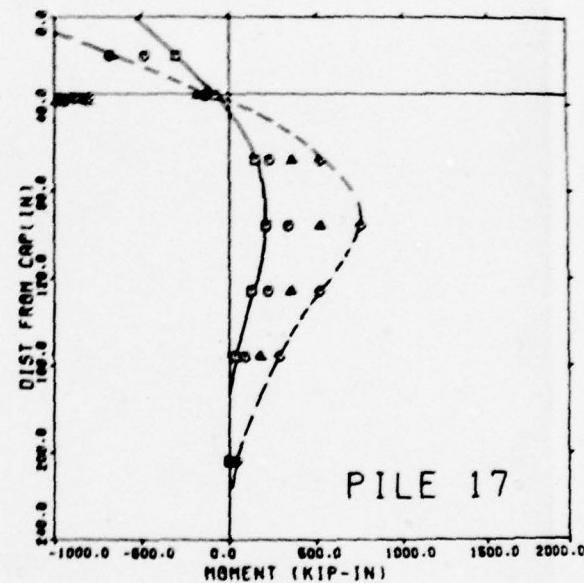
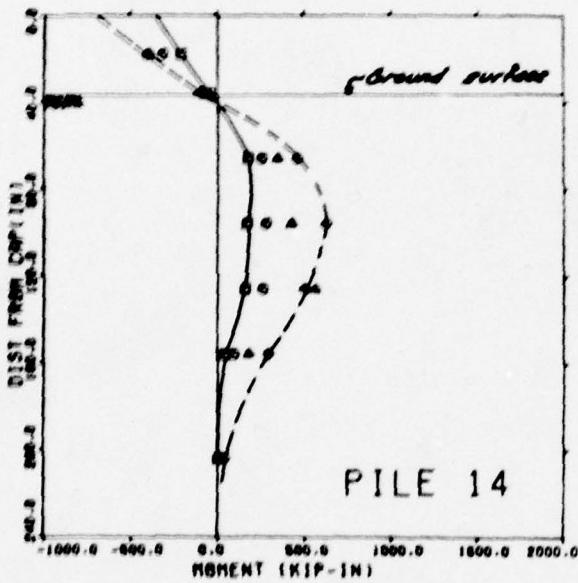
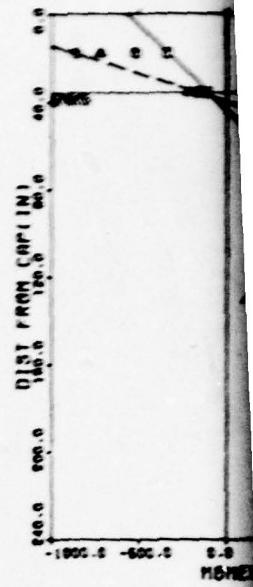
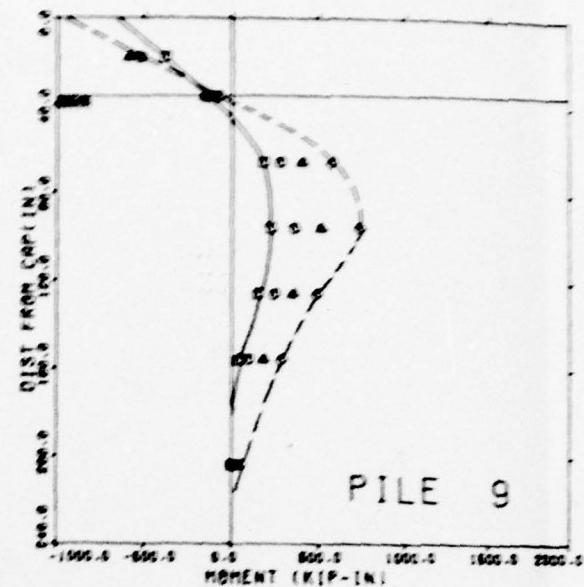
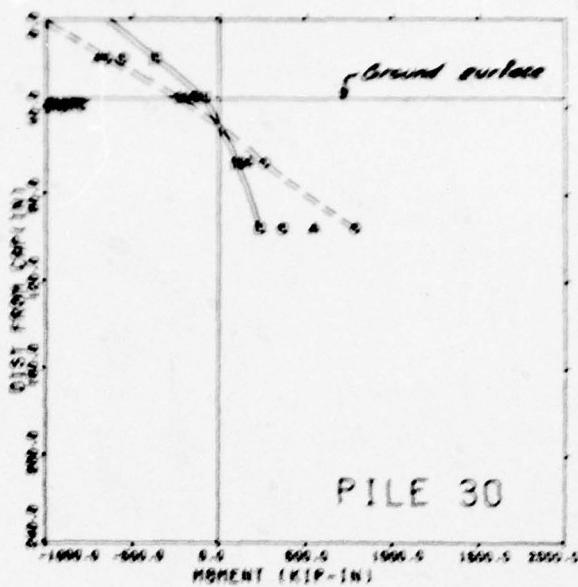
**PILE DRIVING EFFECTS TEST PROGRAM  
SHEAR FORCE DISTRIBUTION  
ON TIMBER PILES  
DURING LOAD TESTING  
OF MONOLITH M2**

FOUNDATION INVESTIGATION AND TEST PROGRAM  
EXISTING LOCKS AND DAM No. 28  
ST. LOUIS DISTRICT, CORPS OF ENGINEERS.  
DACP43-78-C-0008

Woodward-Clyde Consultants  
Y7C828 Phase II

Fig. 9.22

*J*

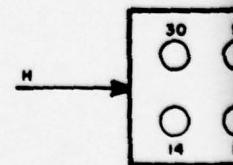


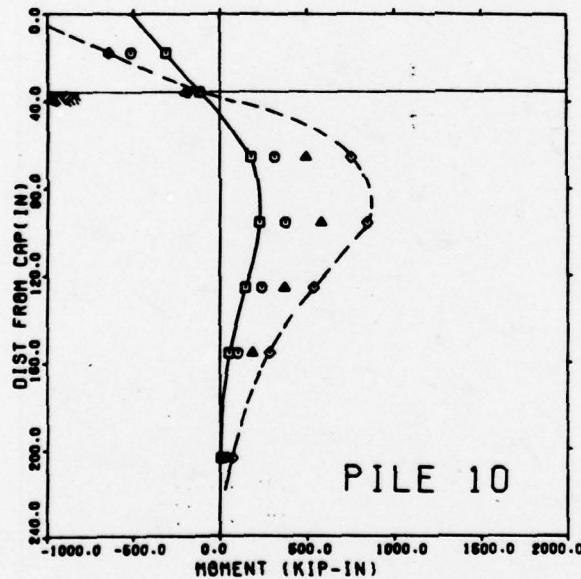
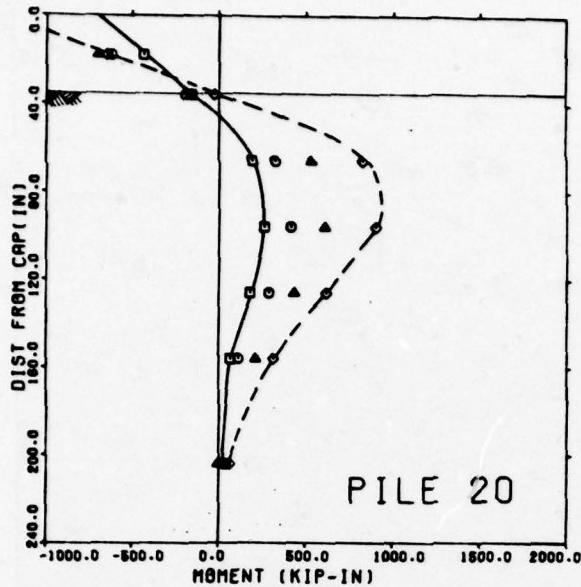
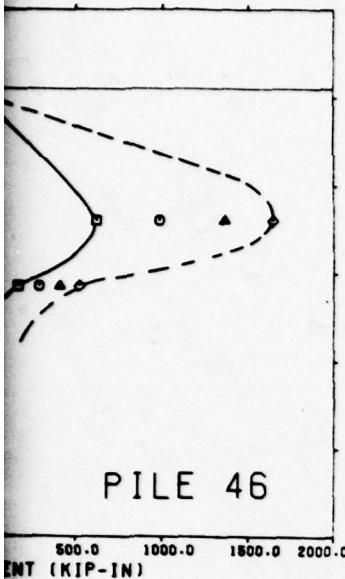
### Legend

Total lateral load,  $t$       Lateral load/pile,  $t$

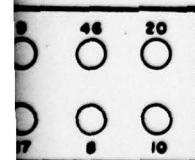
—	48	6
•	72	9
•	96	12
—•—	120	15

MONOLITH





M2 - SCHEMATIC PLAN

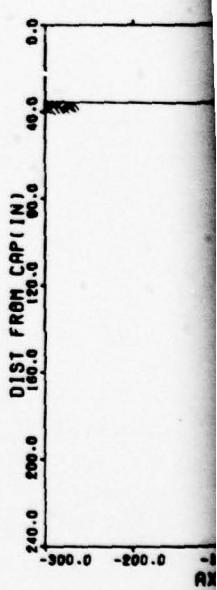
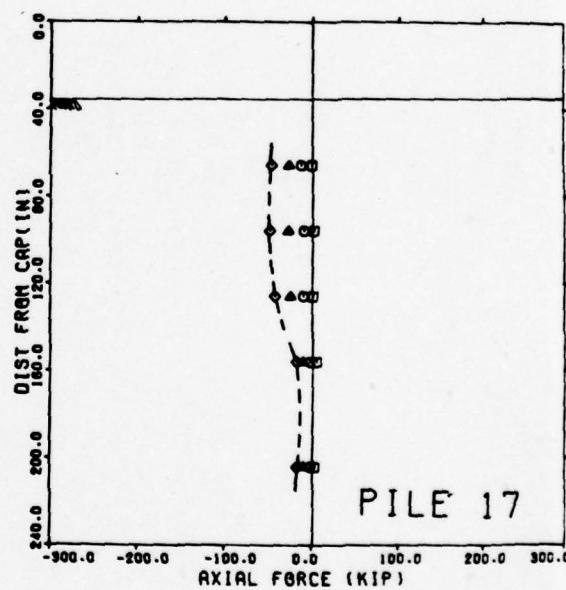
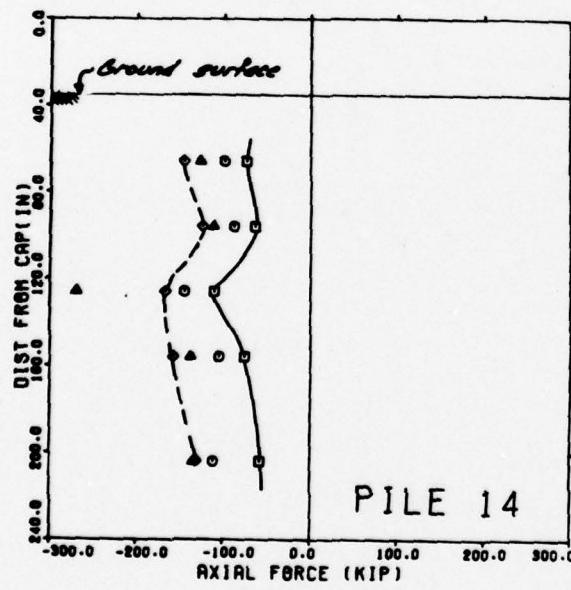
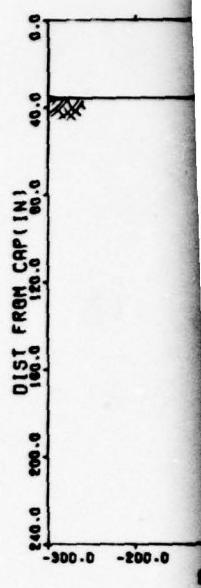
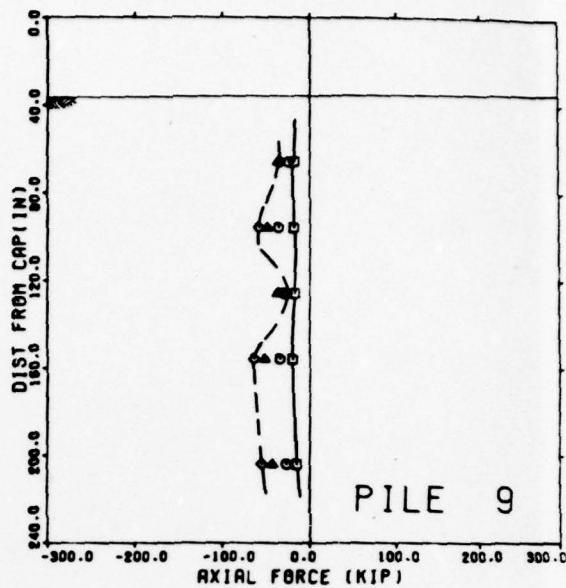
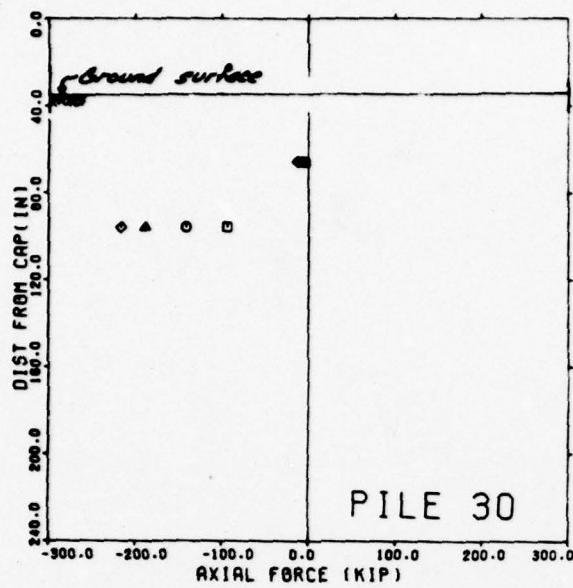


**PILE DRIVING EFFECTS TEST PROGRAM  
BENDING MOMENT DISTRIBUTION  
ON TIMBER PILES  
DURING LOAD TESTING  
OF MONOLITH M2**

FOUNDATION INVESTIGATION AND TEST PROGRAM  
EXISTING LOCKS AND DAM No. 28  
ST. LOUIS DISTRICT, CORPS OF ENGINEERS.  
BACW43-78-C-0008

Woodward-Clyde Consultants  
77C625 Phase II

Fig. 9.23

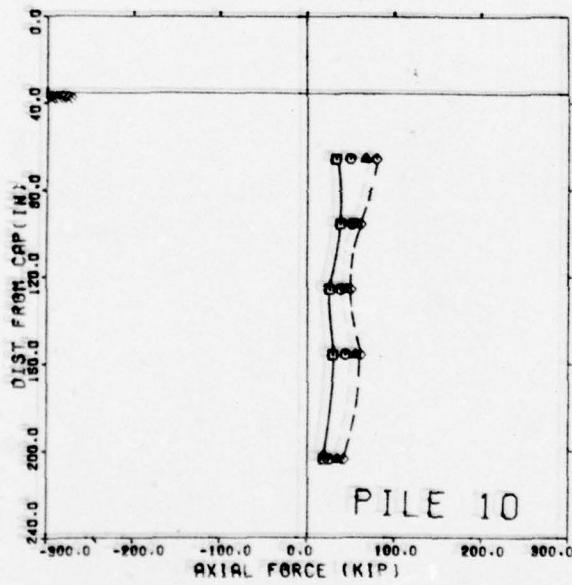
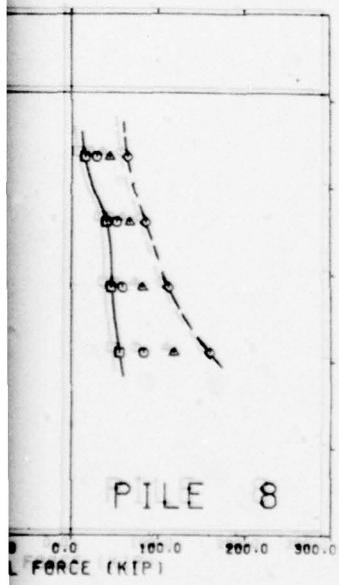
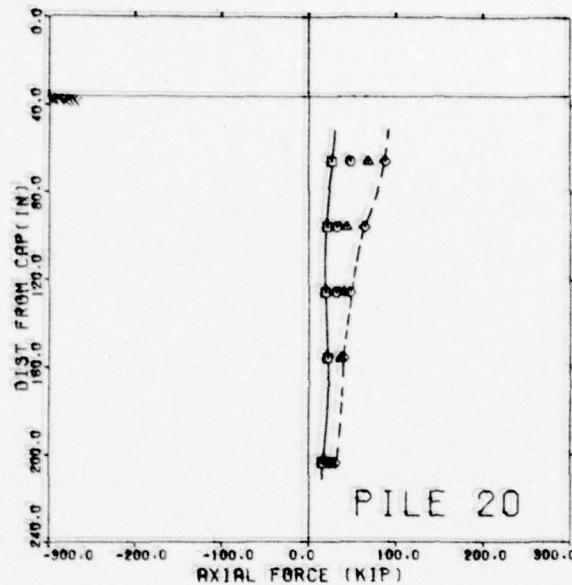
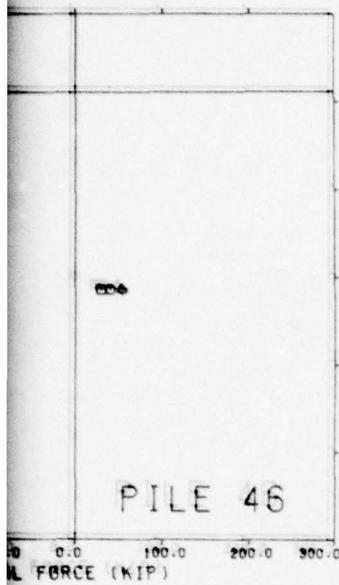


### Legend

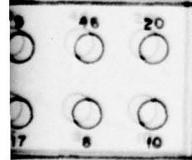
Total lateral load,  $t$       Lateral load/pile,  $t$

—	48	6
•	72	9
▲	96	12
—●	120	15





M2 - SCHEMATIC PLAN

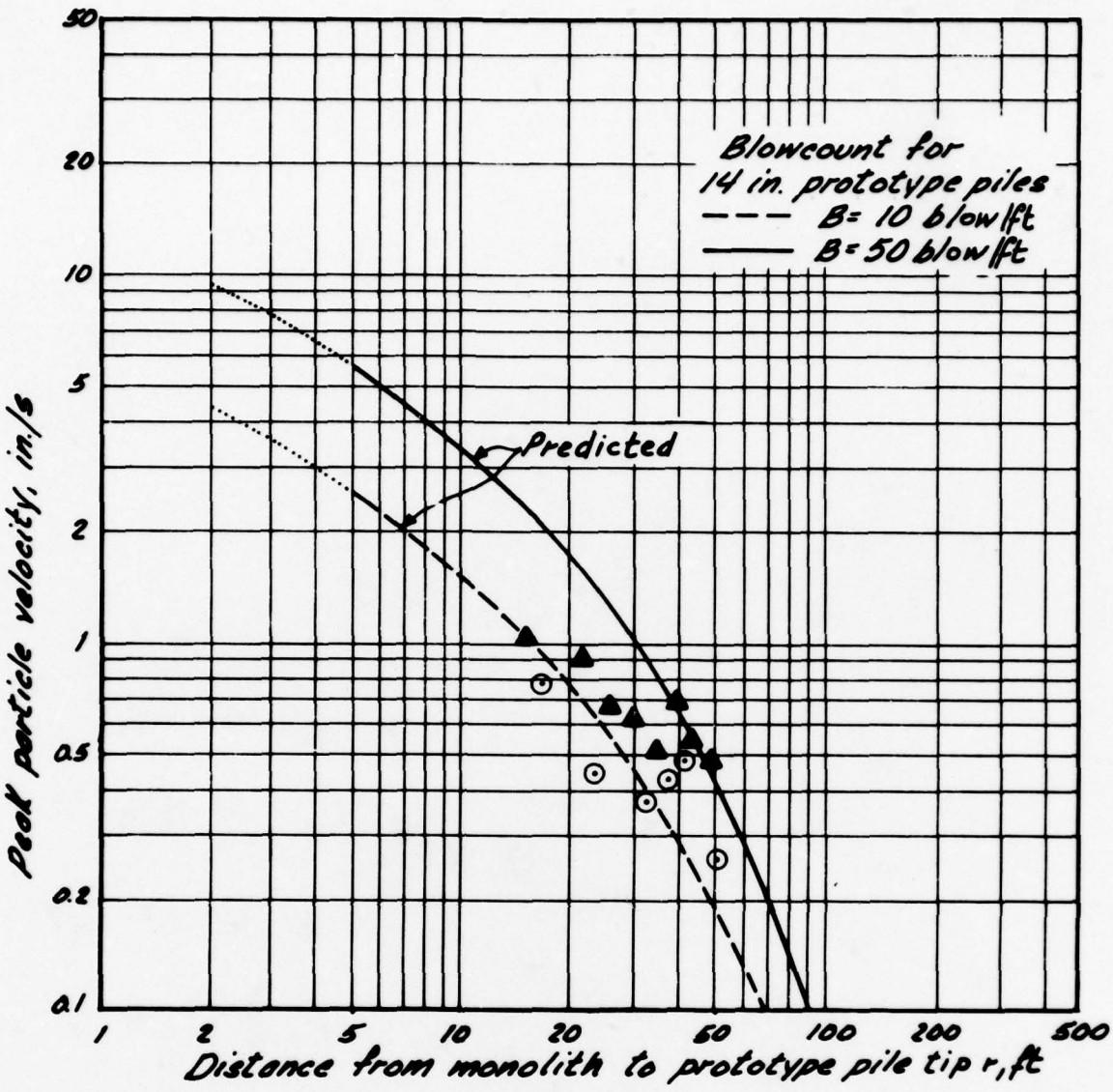


**PILE DRIVING EFFECTS TEST PROGRAM  
AXIAL LOAD DISTRIBUTION  
ON TIMBER PILES  
DURING LOAD TESTING  
OF MONOLITH M2**

FOUNDATION INVESTIGATION AND TEST PROGRAM  
EXISTING LOCKS AND DAM No. 26  
ST. LOUIS DISTRICT, CORPS OF ENGINEERS.  
DARW43-78-C-0008

Woodward-Clyde Consultants  
Y7C829 Phase II

Fig. 9.24



Legend

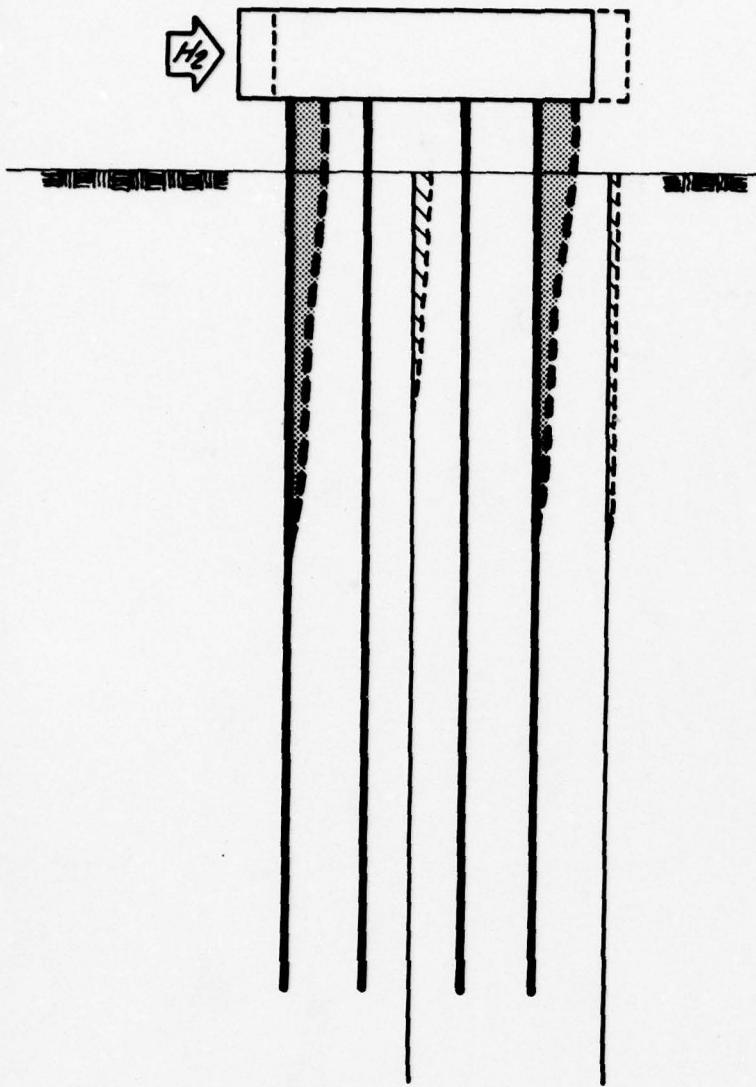
- Measured peak vertical particle velocity
- △ Measured peak vectorial particle velocity

Note

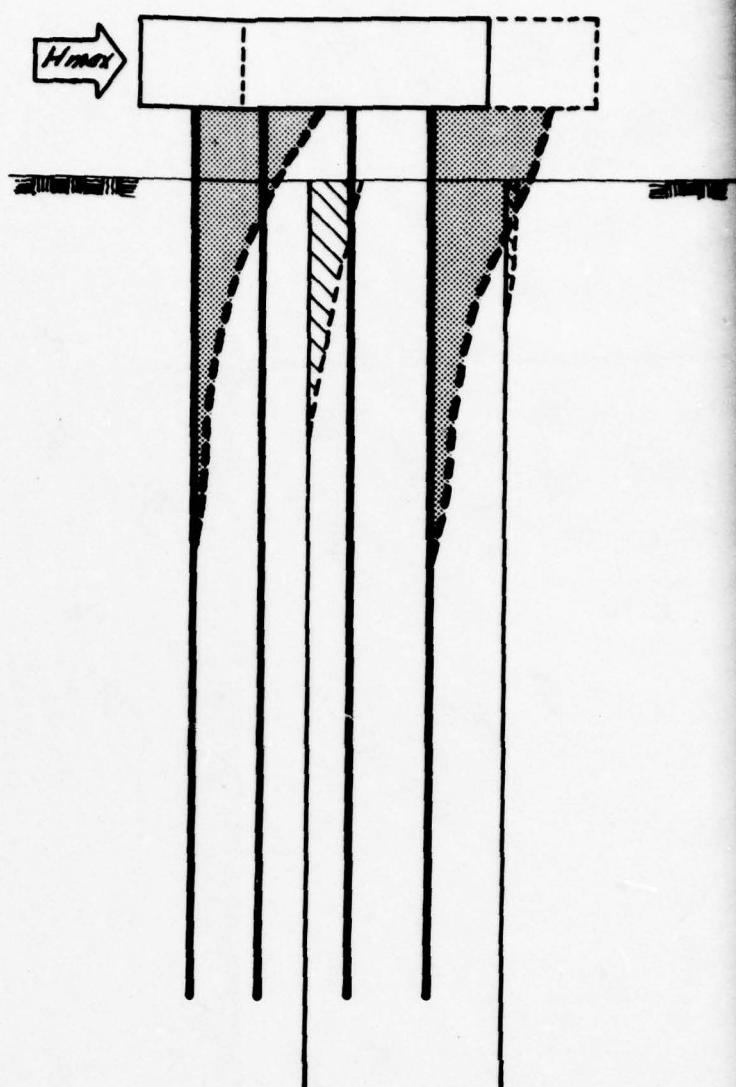
Particle velocity  
normalized for B=10 blow/ft  
(Appendix R, Volume III A)



(a) Design lateral load only



(b) Lateral load at failure

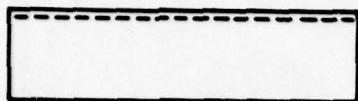


Legend

- [■] Pile deflection
- [▨] Ground deformation

(c) Design axial load only

$\downarrow V_2$

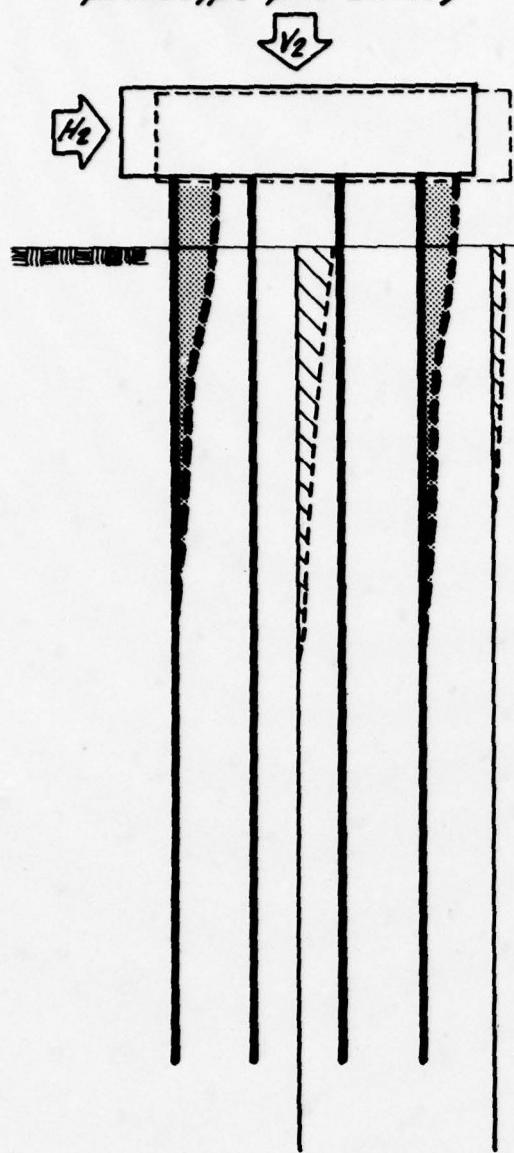


EXISTS EXISTING

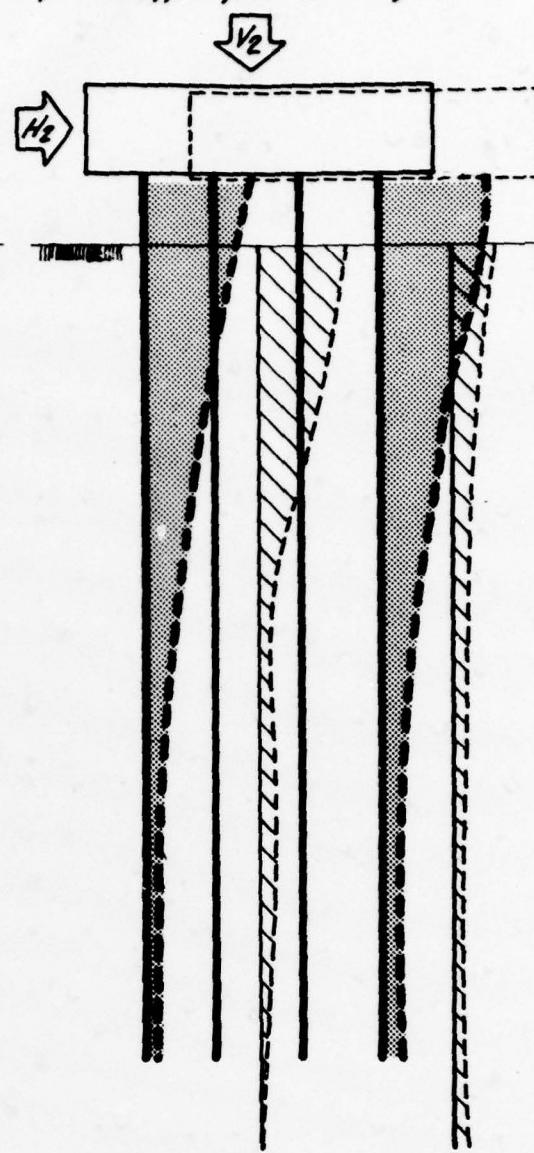
PILE DRIVING EFFECTS TEST PROGRAM	
PATTERN OF DEFORMATIONS DURING STATIC LOAD TESTING	
FOUNDATION INVESTIGATION AND TEST PROGRAM	
EXISTING LOCKS AND DAM No. 26	
ST LOUIS DISTRICT, CORPS OF ENGINEERS.	
DAGW43-78-C-0006	
Woodward-Clyde Consultants Y7C826 Phase II	Fig. 9.26

2

(a) Lateral and axial loads, prior to prototype pile driving

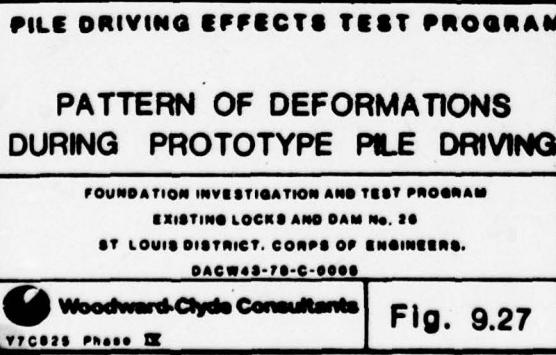


(b) Horizontal deformation due to prototype pile driving



Legend  
■ Pile de  
□ Ground

(c) Settlement due to  
prototype pile driving



2

**PHASE IV REPORT**

**VOLUME III**

**RESULTS AND INTERPRETATION OF  
PILE DRIVING EFFECTS TEST PROGRAM**

**SECTION 10  
LATERAL LOAD TESTING OF PROTOTYPE PILES**

## 10 LATERAL LOAD TESTING OF PROTOTYPE PILES

### 10.1 SCOPE OF TESTS

Lateral load tests were performed on six instrumented prototype piles. The objective of the tests was to examine the lateral load-deflection behavior of prototype H and pipe piles under three conditions:

- (1) piles driven into natural (ungrouted) soil;
- (2) piles driven into natural soil which was subsequently grouted prior to load testing (postgrouted); and
- (3) piles driven into grouted soil (pregrouted).

A secondary aspect of performance of interest was the effects of grouting on pile driving resistance. These effects are discussed in Section 7.3.2, where it was noted that pile driving blowcount increased on the average from 5 blow/ft in ungrouted soil to 10 blow/ft in pegrouted soil.

Three prototype HP 14 x 73 and three PP 14 x 0.375 were driven as test piles; one H and one pipe pile were tested together as a pair in three different setups. The piles were instrumented with strain gages to measure bending strains and with inclinometers to measure pile deflection at depth. Pile-head horizontal displacement at and above ground surface was measured using dial gages. A detailed description of the instrumentation is given in Section 3 and Appendix S, Volume IIIA.

Grouting procedures and grouted soil profiles are discussed in detail in Section 5.5. The grout was a low strength 25% silicate/aluminate. It was injected in the upper 20 ft of Recent alluvium between el 391 and el 371. A static cone penetration sounding (PD4-C1, Fig. 5.14) was made 2 ft from pegrouted H-pile T5 to assess the influence of pile driving on grouted soil properties.

Prototype pile performance during driving and lateral load testing was predicted. The prediction method and predicted performance are discussed in Sections 2.3.2 and 2.3.3.

### 10.2 PILE INSTALLATION AND TEST CONFIGURATION

#### 10.2.1 Pile Driving

Locations of the six test piles T1 through T6 are given in Fig. 10.1. The piles were 55 ft long. They were driven from the bottom of the monolith trench at el 391. The pile driving hammer was either a Vulcan 010 air hammer or an MKT DE 70B diesel hammer. Details of these hammers are discussed in Section 7.3. The H-Piles (T1, T3, and T5) were fitted with APF cast steel shoe No. BP75000. The pipe piles (T2, T4, and T6) were driven open-ended, and were fitted with an APF cast steel inside cutting shoe No. D-14001.

During driving, pile performance was monitored with a pile driving analyzer system (Sections 3.1.3 and 3.2.8). Pile driving resistance in terms of blowcount was recorded for each foot of penetration. An evaluation of pile performance during driving through ungrouted or grouted soil is given in Section 7.4.2. Pile driving records are presented in Appendices M (T3 and T4 ungrouted soil), N (T5 and T6 pregrouted soil), and S (T1 and T2 postgrouted soil), Volume IIIA.

#### 10.2.2 Grout Placement in Pipe Piles

The 55-ft-long pipe piles were driven open-ended. After driving, the soil plug inside the piles was measured. The following results were found:

<u>Pile No.</u>	<u>Soil Conditions At Time of Driving</u>	<u>Depth of Soil Plug Below Ground Surface ft</u>
T2	ungrouted	31
T4	ungrouted	33
T6	grouted	40

Installation of the inclinometer casing and filling of the pipe piles with cement grout were done differently for each pile, because of construction and scheduling difficulties.

**Pipe Pile T2.** Pipe pile T2 was driven on 8 November 1978 into ungrouted soil. The soil plug was flushed out using bentonite drilling fluid and water to a depth of approximately 47 ft below the top of the pile. The pile was left full of water. The inclinometer casing was inserted into the pipe and positioned with centralizers at 10-ft intervals. A sand-cement grout was pumped through a grout pipe lowered to approximately 1 ft from the soil plug surface at the bottom of the pile. As the grout was pumped, the grout pipe was raised slowly. The cement was high early strength Portland, Type III, without any additives. The sand was obtained at the site. The cement content or the water-cement ratio was not carefully controlled. Six standard cylinder grout samples were taken. They were tested by ANCO Testing Laboratory in St Louis. Results are discussed in Appendix S, Volume IIIA. The 28-day strength of the grout samples was 2989 lb/in<sup>2</sup>.

**Pipe Pile T4.** Pipe pile T4 was driven on 17 January 1979 in ungrouted soil. Flushing of the soil plug was attempted on 10 February 1979, but could not be done because of insufficient pump capacity. Grout was placed in the pile as-driven. The inclinometer casing was installed and a sand-cement grout mixture was pumped as was done for T2. Two standard cylinder grout samples were taken and tested (Appendix S, Volume IIIA). The 7-day strength of the grout samples was 3059 lb/in<sup>2</sup>.

**Pipe Pile T6.** Pipe pile T6 was driven on 28 February 1979 into grouted soil. This pile was not filled with grout because of insufficient time for placement and curing. After installation of the inclinometer casing, the pile was filled with sand. Near the top, some compaction of the sand fill was attempted using a 2 x 6 board.

### 10.2.3 Test Setup.

A schematic of the lateral load test setup is shown in Fig. 10.2. A 50-t hydraulic jack was used to apply the load to a pair of piles. The jack was mounted in such a way that the piles could be pushed apart or pulled together. The jack loads were measured with a 100-t, hollow-cylinder load cell (Section 3.2.2).

The pinned joints at the load frame-collar connections ensured that only lateral thrust and no moment was applied to the piles. The collars were placed on the pipe piles so as to be just above the angle steel covers protecting the strain gages. The collar was then mounted on the H piles so that the entire system was level.

Angle sections supported by two remote posts were installed as displacement reference systems for each test pile. Dial gages were mounted on the angles to measure pile-head displacement at three different levels to determine the slope of the pile head. The location of the supporting posts was designed to avoid displacement of the reference system caused by soil deformation in front of the piles.

## 10.3 TEST PROCEDURES

### 10.3.1 Initial Measurements

The first step of a test was to make initial measurements for all instrumentation (dial gages, strain gages, and inclinometers). The as-built geometry of the test setup was also recorded at that time.

### 10.3.2 Short-Term Static Load Tests

The purpose of the short-term static load tests was to assess the ultimate lateral load capacity of the test piles. In all cases, the short-term static load tests were performed jacking the piles apart. The test procedure was as follows:

- (1) apply the lateral load in 5-t increments;
- (2) allow pile deflection to stabilize at each load level. Stabilization was assumed to have occurred when the pile head deflection was less than 0.01 in./hr. During this period, the applied load was maintained constant;
- (3) read dial gages and strain gages; make slope inclinometer measurements; and
- (4) apply next load increment unless failure was observed. Failure was defined as continued deflection of the pile as the load increment was applied.

The load tests were performed while prototype piles were driven, and it was necessary to minimize the effects of pile driving on test results. Therefore,

the load was reduced to zero each time pile driving operations were underway. Afterward, the load was reestablished in increments to the previous level.

#### 10.3.3 Cyclic Load Tests

The purpose of the cyclic tests was to assess the degradation in prototype pile lateral resistance due to repetitive loading. The load was cycled from 0 to one-half the observed load at failure for approximately 25 cycles for the piles in ungrouted soils (T3 and T4) and postgrouted soils (T1 and T2). The piles driven into pregrouted soil were not cyclically tested. In all cases, the cyclic tests were performed by pulling the piles together. The test procedure was as follows:

- (1) load to 17 t and hold for two minutes, then read dial gages; and
- (2) unload to 0 t and hold for two minutes, then read dial gages.

The load was cycled in this manner throughout each test. Strain gages were read and slope indicator measurements were made generally at both load levels every five cycles. During adjacent pile driving operations, the piles were unloaded as it was done during the static tests.

### 10.4 DATA ACQUISITION AND REDUCTION

#### 10.4.1 General

All test measurements were made manually. The data acquired were:

- (1) pile-head displacement, using dial gages;
- (2) bending strains, using strain gages; and
- (3) pile deflection, with depth, using inclinometers.

#### 10.4.2 Pile-Head Displacement

Pile-head displacement was measured at two or three levels above the ground surface. The actual measurement heights are given in various figures in this section. The purpose of the multiple-level displacement measurements was to derive of the pile-head slope.

The displacement at each level was determined by subtracting the dial gage reading from the initial reading. Pile-head displacement at the ground surface was computed based on a linear approximation using these data. The displacement at ground surface computed in this manner were compared with that obtained using the inclinometer and showed general agreement within  $\pm 0.07$  in.

#### 10.4.3 Bending Moment

Strain gages were mounted on the piles so that bending strains could be measured, from which bending moments along the pile were computed. Details of gage installation, circuitry, and calibration are given in Appendix S, Volume IIIA.

For the H piles, measured changes in strain were converted to bending moment using Euler beam theory. Values of elastic modulus for each bridge were obtained from the calibration tests described in Appendix S, Volume IIIA.

Computation of the bending moment from the measured changes in strain was more complicated for the grout-filled pipe piles because concrete has different properties in tension than in compression. Therefore, the composite flexural stiffness of the pile varies with the bending moment.

Moment-curvature relationships were computed for each pile to assess the relationship between strain and bending moment for the concrete-filled pipe piles. Grout strength and stress-strain relationships were evaluated from compression tests on standard cylinders of grout. Test results are given in Appendix S, Volume IIIA. Typical stress-strain curves were used for the steel, as tests were not performed. Bending moment was computed for various values of bending curvature. The bending curvature can be related to measured strain by:

$$\epsilon = \phi d$$

where:  $\epsilon$  = strain;  
 $\phi$  = curvature; and  
 $d$  = distance from centerline of pile to gage along axis of loading.

The resulting strain-bending moment relationships for T2 and T4 are presented in Fig. 10.3.

Pipe pile T6 was filled with sand, not grout. The sand did not contribute to the flexural stiffness of the pile. Therefore, the appropriate linear elastic modulus and geometric relationships were applied based on elastic beam theory.

#### 10.4.4 Pile Deflection With Depth

The deflected shape of each pile was measured using the inclinometer. The inclinometer readings were reduced to pile deflection using standard methods.

### 10.5 TEST RESULTS

#### 10.5.1 General

Measured pile response to lateral loads is compared to the predicted response for each of the three cases investigated: piles in ungrouted soil; piles in pregrouted soil; and piles in postgrouted soil. For the comparison, two aspects of performance were considered: pile displacement at ground surface and maximum bending moment. These two aspects generally provide the limiting criteria in design of laterally loaded piles. A summary of test results and predicted values is presented in Table 10.1.

#### 10.5.2 Piles Driven Into Ungrounded Soil

Figure 10.4 presents the observed and predicted pile displacement at ground surface caused by the applied lateral loads for H pile T3 and pipe pile T4. The predicted values account for the corrected flexural stiffness of the test piles considering the various instrumentation protections welded to the piles (Section 2.2.3). The difference between measured and predicted values is not large, except at lateral loads greater than 20 t.

As seen in Fig. 10.4a, the predicted H pile-head displacement is about 25 percent higher than the observed displacements for loads up to 20 t. At higher loads, the predicted displacement is about twice the observed values.

The predicted displacement at ground surface is in very good agreement with the observed value for pipe pile T4 (Fig. 10.4b) for loads up to 25 t. At higher loads, the pile underwent considerably more deflection than predicted. It is believed that the pile failed structurally at about 25 t and formed a plastic hinge. This is borne out by the moment data presented later.

The comparison between observed and predicted maximum bending moments is presented in Fig. 10.4c for H pile T3. The maximum deviation is about 15 percent, with most of the values within 10 percent. For pipe pile T4, the comparison between predicted and observed maximum bending moments is given in Fig. 10.4d. In general, the observed values are 20 percent higher than the predicted values. Overall, the agreement between observed and predicted behavior is good, considering the approximations made with regard to soil and pile parameters prior to the testing program:

Soil Parameter	Assumed Value For Prediction	Measured Value
Friction Angle, degree	41	40
Effective Unit Weight, lb/ft <sup>3</sup>	70	68
Cohesion, lb/ft <sup>2</sup>	0	0

The distribution of bending moment with depth for piles T3 and T4 is presented in Fig. 10.5 and Fig. 10.6, respectively.

#### 10.5.3 Piles In Postgrouted Soil

The observed and predicted pile displacements at ground surface caused by the applied lateral loads for H-pile T1 and pipe pile T2 are presented in Fig. 10.7a and b. For both piles, the observed displacements are considerably greater than the predicted values.

Figures 10.7c and d present a comparison between predicted and observed maximum bending moments for T1 and T2. As with the displacements, there is poor agreement. The observed bending moments are considerably greater than predicted. This is to be expected because deflections induced greater pile curvature than predicted, and bending moment is proportional to curvature.

Two reasons are believed to account for the large discrepancy between predicted and observed results. The first concerns the assumed strength parameters of the grouted soil:

<u>Soil Parameter</u>	<u>Assumed Value For Prediction</u>	<u>Measured Value (From Vol II)</u>
Friction Angle, degree	40	35
Cohesion, lb/ft <sup>2</sup>	1000	700

However, analyses performed using the actual measured values for friction angle and cohesion, and stress-strain relationships from triaxial compression tests on grouted soil (Volume II), still did not agree with the observed results.

The second, and probably more important, reason concerns the time-dependent properties of grouted soil under sustained load. The grouted soil near the loaded piles underwent considerable deformation with time. Results of triaxial creep tests on grouted sand samples (Section 9.5.2, Volume II) and of pressuremeter tests in borings PD3-PM2 and PD3-PM3 (Section 5.5.5) indicated that sand grouted with 25% silicate/aluminate grout does creep and that creep rate is dependent on stress level.

The distribution of bending moment with depth for piles T1 and T2 is presented in Fig. 10.8 and Fig. 10.9, respectively.

#### **10.5.4 Piles Driven Into Pregouted Soil**

Horizontal displacement at ground surface for piles driven into pregrouted soil (H pile T5 and pipe pile T6) is presented in Fig. 10.10a and b. Observed bending moments are also shown in Fig. 10.10c and d for piles T5 and T6, respectively. As with piles T1 and T2, the agreement between predicted and observed behavior is poor. The reasons are believed to be the same as those cited previously for piles T1 and T2. The distribution of bending moment with depth for piles T5 and T6 is given in Fig. 10.11 and 10.12, respectively.

A profile of static cone penetration resistance measured in boring PD4-C1 near H pile T5, after the pile was driven into pregrouted soil, is compared in Fig. 10.13 to a similar profile obtained in boring PD3-C2 near pile T1, after the pile was driven into ungrouted soil. The difference between the two profiles is insignificant. The short stress duration during a cone penetration test, however, does not model the long-term stress duration associated with the lateral pile load tests; the load test results are affected by the time-dependent properties of the grouted soil.

#### **10.5.5 Cyclic Load Tests**

The reduction in lateral soil resistance due to repetitive load applications is manifested by increased deflection and bending moment with each load application up to a steady-state limit. After that limit is reached, additional applications of load do not cause further increase in these values.

Figure 10.14 presents pile displacement at ground surface at both zero lateral load and maximum applied lateral load (17 t) for various cycles for the four piles cyclically tested. Most of the increase in displacement occurred in the first five load cycles. After that, the displacement increased only slightly with each cycle. For the piles in ungrouted soil (T3 and T4), the cyclic degradation was greater than for the piles in postgrouted soil (T1 and T2).

The maximum bending moment also increased, as shown in Fig. 10.8, 9, 5, and 6 for piles T1 through T4, respectively. Again, most of the increase occurred in the first five cycles for the H piles T1 and T3. The pipe piles T2 and T4 did not show an increase because the piles had failed structurally during the previous static lateral load tests.

## 10.6 EVALUATION OF TEST RESULTS

### 10.6.1 Piles Driven Into Ungrouted Soil

At loads less than 20 t, there was good agreement between the predicted and observed values of maximum bending moment and pile displacement at ground surface. The soil properties assumed were reasonably close to those observed in the subsequent field and laboratory investigations. A comparison is presented in Section 10.5.2. Use of the actual values would not significantly affect the results. The prediction method worked well for piles in ungrouted soil. A summary of measured and predicted results is given in Table 10.1

The loads applied to the test piles were sustained for a relatively short time. For a particular load, the duration ranged from about 1 hr at the 5-t load level to about 12 hr at the 30-t load level. Compared to duration of load application on actual structure, these times are short. However, for a sustained lateral load of 15 t, Fig. 10.15 indicates that further displacement with time should not be anticipated; the rate of displacement is 0.0001 in./log cycle of time.

The cyclic load tests showed that repetitive load applications result in increased pile deflection for the same load (on the order of 50 percent). However, the number of cycles to reach a stable response and the stabilized pile deflection was dependent on the duration of each cycle and the load level. It is also important to note that, upon release of the load, the pile did not return to its original position. The induced permanent pile deflection was relatively large, about 100 percent of the deflection observed during initial static loading.

### 10.6.2 Piles In Postgrouted Soil

The lateral test results showed poor agreement with predicted values for piles in postgrouted soil (T1 and T2); the differences are attributed to the assumptions made regarding the behavior of the grouted soil. The lateral load-displacement curves presented in Fig. 10.7 for piles in postgrouted soil indicate a different response for these piles than for those in ungrouted soil (Fig. 10.4). The H pile T1 exhibited a marked strain hardening behavior for displacements at ground surface larger than 0.5 in.; the pipe pile T2 exhibited a response similar to that of

pipe pile T4 in ungrouted soil. The strain hardening phenomenon tended to stabilize the pile deflection, resulting in a larger load at failure. The strain hardening tendency of the grouted soil was demonstrated by pressuremeter test results (Section 5.4.5).

The time-dependent behavior of the grouted soil adjacent to the laterally loaded piles is illustrated in Fig. 10.15 which is a plot of horizontal displacement vs time of sustained load application. The piles in postgrouted soil exhibited larger creep displacement than any other pile; the average creep rate for the postgrouted piles was 0.117 in./log cycle of time. During the first hour following each lateral load increment, the piles continued to deflect. The rate at which this creep deflection took place was examined; creep displacement rate of each pile measured at ground surface is shown vs lateral load level in Fig. 10.16a. For the piles in postgrouted soil, the creep displacement rate increased faster with load level than for the piles in ungrouted soil; and was similar to that for the piles in pregrouted soil. The time required for the lateral displacement due to each lateral load increment to stabilize is shown in Fig. 10.16b vs lateral load level for each pile. The stabilization time (displacement rate less than 0.01 in./hr) for the piles in postgrouted soil is much larger than that for the piles in ungrouted soil, and is similar to that for the piles in pregrouted soil.

The creep tendency of the grouted soil surrounding the piles resulted in a softer response to lateral load than for the piles in ungrouted soil; however, the lateral load, at failure, was not very different in all cases. The large displacement observed for pipe pile T2 could be explained by the formation of a plastic hinge, similar to that noted for pipe pile T4.

#### 10.6.3 Piles Driven Into Pregrouted Soil

Driving the prototype piles into pregrouted soil (T5 and T6) did not significantly affect the response of the piles to lateral load. As shown in Table 10.1, pipe pile T6 underwent less deflection than the pipe piles in postgrouted or ungrouted soil at the same lateral load levels. The contrary is true for H pile T5. Strain hardening phenomenon was more pronounced for T6 than for T5 (Fig. 10.10). The creep rate for the piles driven into pregrouted soil averaged 0.057 in./log cycle of time (Fig. 10.15) much larger than that for piles driven into ungrouted soil; however, it was less than that for piles in postgrouted soil. The creep displacement and the load stabilization time (Fig. 10.16) were slightly less for the piles in pregrouted soil than for the piles in postgrouted soil; they were much larger than those observed for piles in ungrouted soil. The small differences for the pregrouted and postgrouted cases were probably due to effects of driving. Pile driving through the pregrouted soil appears to have reduced the creep behavior of the grouted soil and magnified its strain hardening behavior more so for the point-displacement pipe pile than for the H pile.

	Ungrouted Sand		Piles Driven Followed by Grouting		Piles Driven Through Grouted Soil	
	H-Pile T3	Pipe Pile T4	H-Pile T1	Pipe Pile T2	H-Pile T5	Pipe Pile T6
Predicted Load for 0.25 in. Deflection	6.5 ton	5.0 ton	26.5 ton	12.5 ton	4.0 ton	3.5 ton
Observed Load for 0.25 in. Deflection	8.5 ton	5.5 ton	12.0 ton	4.5 ton	7.0 ton	8.0 ton
Predicted Load for 0.5 in. Deflection	11.5 ton	8.5 ton	>40 ton	24.5 ton	8.5 ton	7.8 ton
Observed Load for 0.5 in. Deflection	15 ton	10.5 ton	16.5 ton	8.5 ton	10.5 ton	12 ton
Predicted Load for 1.0 in. Deflection	18.0 ton	15.5 ton	>40 ton	>40 ton	>35 ton	32.5 ton
Observed Load for 1.0 in. Deflection	21.5 ton	17.0 ton	25.0 ton	15.5 ton	16 ton	18.5 ton
Predicted Deflection at 30-ton Load	3.15 in.	2.65 in.	0.30 in.	0.65 in.	0.92 in.	0.95 in.
Observed Deflection at 30-ton Load	1.65 in.	3.85 in.	1.30 in.	3.50 in.	2.30 in.	1.78 in.

Notes

- (1) All deflection values are pile-head displacements at ground surface.
- (2) Load application was 9 in. to 18 in. above ground surface.

**PILE DRIVING EFFECTS TEST PROGRAM**

**SUMMARY OF  
LATERAL LOAD TEST RESULTS  
ON PROTOTYPE PILES**

FOUNDATION INVESTIGATION AND TEST PROGRAM  
EXISTING LOCKS AND DAM NO. 20  
ST LOUIS DISTRICT, CORPS OF ENGINEERS.  
DARW42-78-C-0005

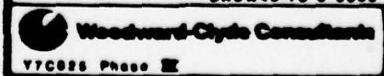
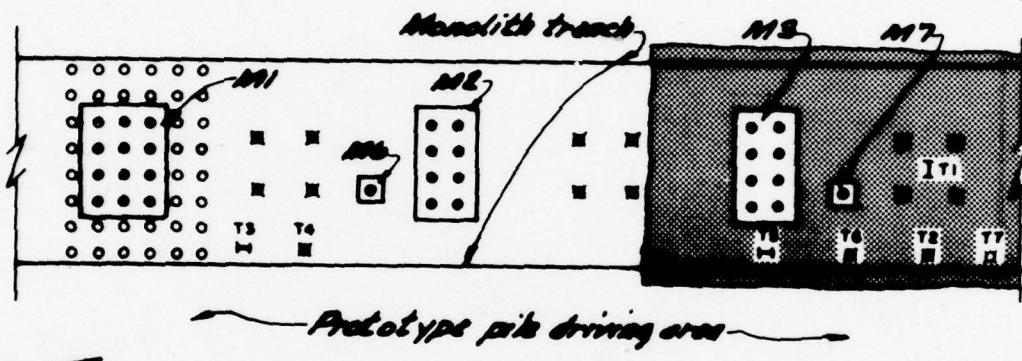


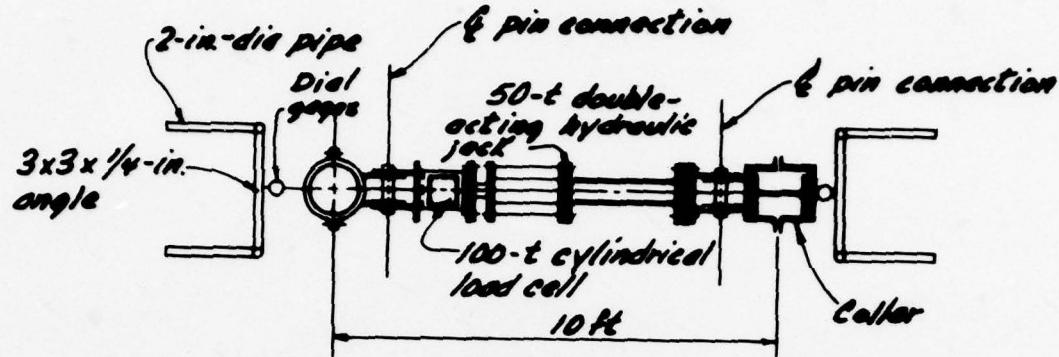
Table 10.1



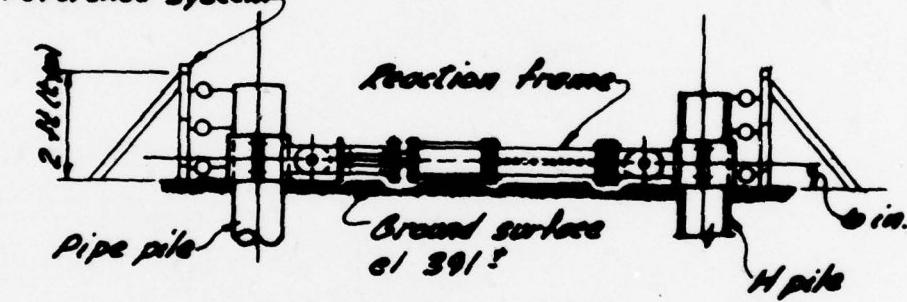
Legend

- Instrumented HP 14x73 prototype pile
- Instrumented PP 14x0.375 prototype pile
- Horizontal limit of grouted zones
- Vertical reaction rock anchor
- Instrumented timber pile
- Uninstrumented timber pile

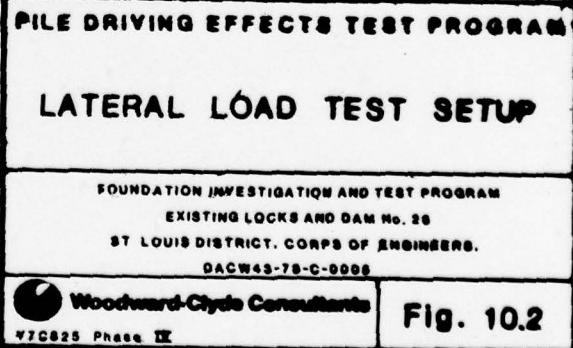
<b>PILE DRIVING EFFECTS TEST PROGRAM LOCATION PLAN FOR PROTOTYPE PILES T1 THROUGH T6</b>	
<small>FOUNDATION INVESTIGATION AND TEST PROGRAM EXISTING LOCKS AND DAM NO. 28 ST LOUIS DISTRICT, CORPS OF ENGINEERS. DACPW43-78-C-0008</small>	
 Woodward-Clyde Consultants YTGB25 Phase III	<b>Fig. 10.1</b>

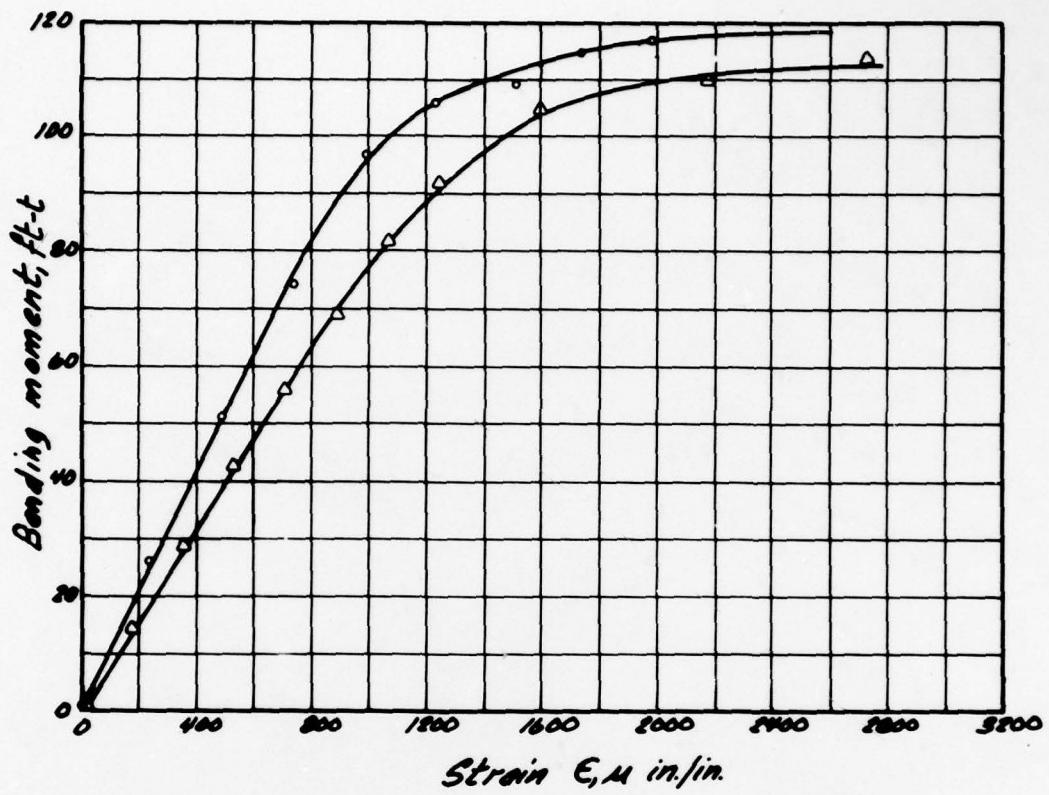


Plan



Elevation



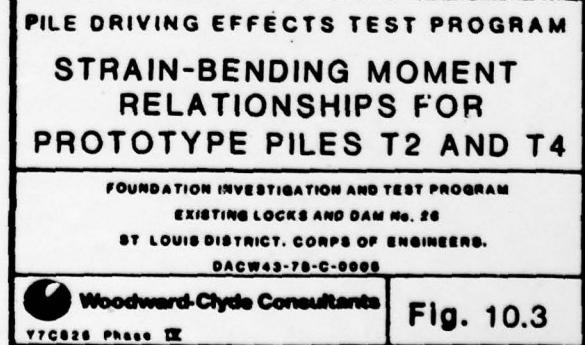


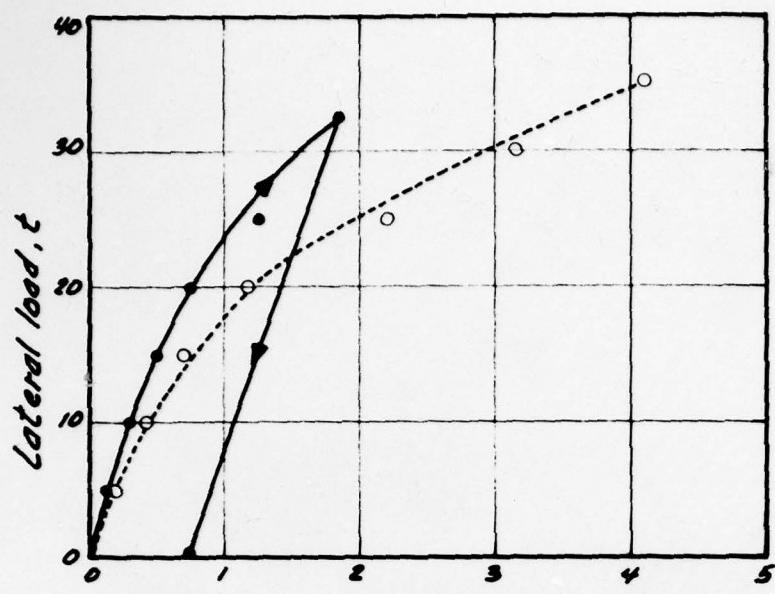
Legend

- Pipe pile T2
- △— Pipe pile T4

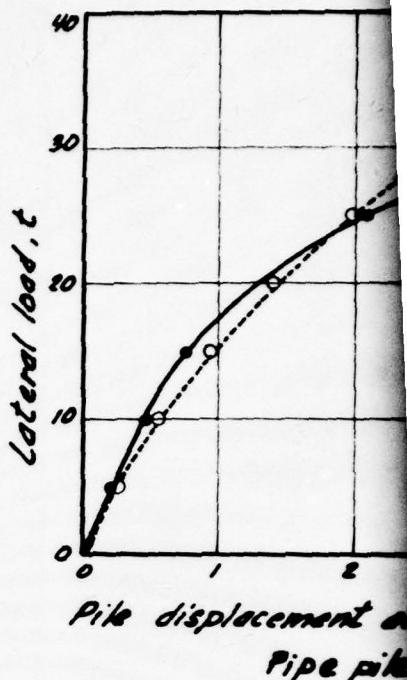
Note:

Both pipe piles  
T2 and T4 were  
concrete-filled

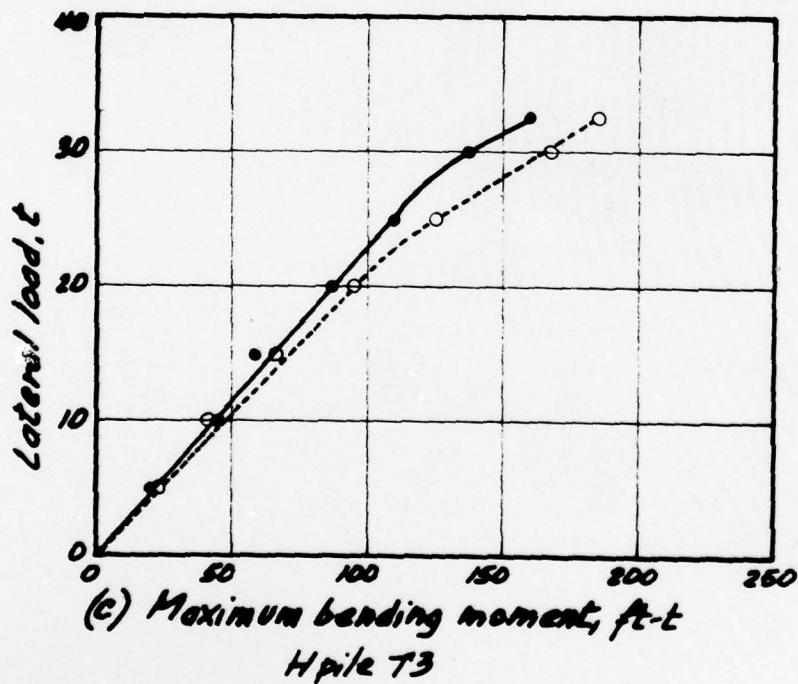




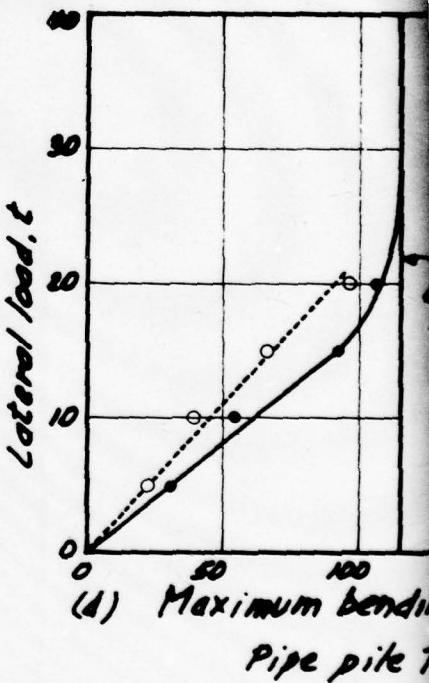
(a) Pile displacement at ground surface, in.  
H pile T3



Pile displacement at ground surface, in.  
Pipe pile 1

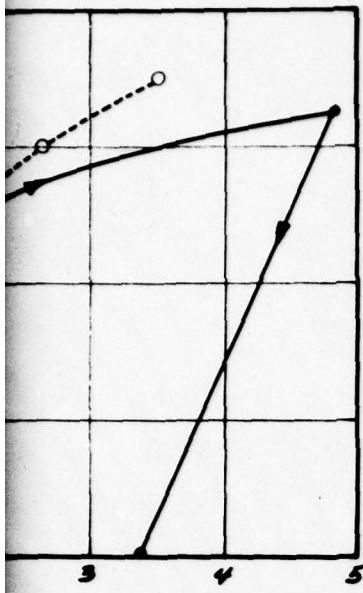


(c) Maximum bending moment, ft-lb  
H pile T3



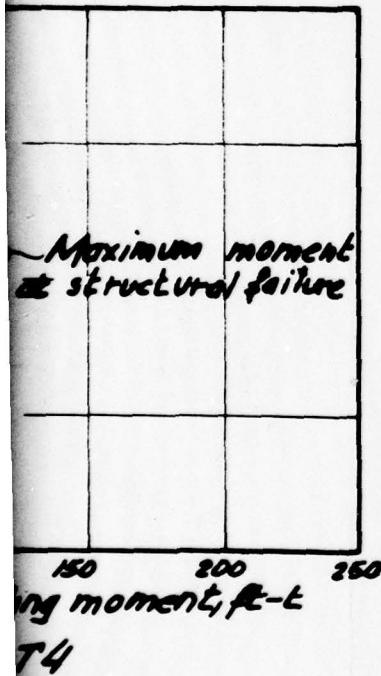
(d) Maximum bending moment, ft-lb  
Pipe pile 1

Note:  
Results  
static /



t ground surface, in.  
T4

Legend  
 -•- Observed values  
 -○- Predicted values

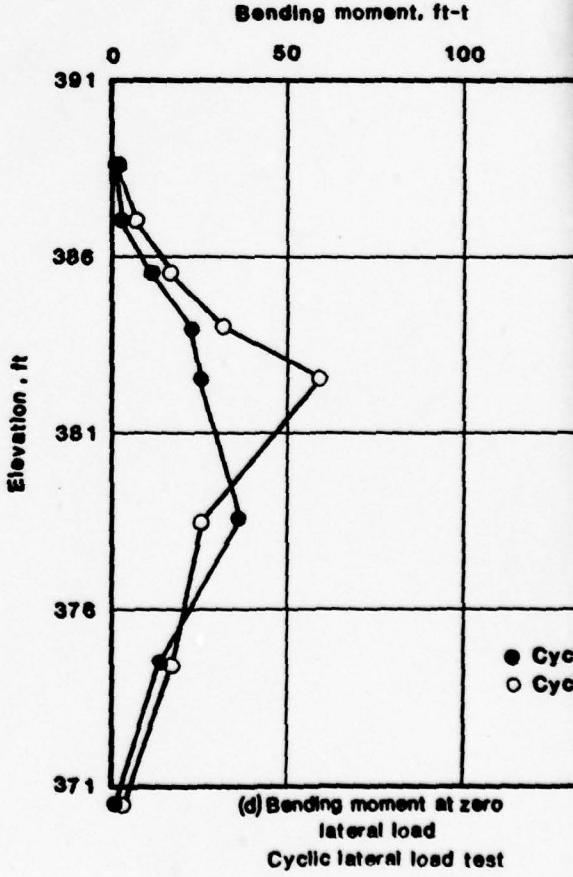
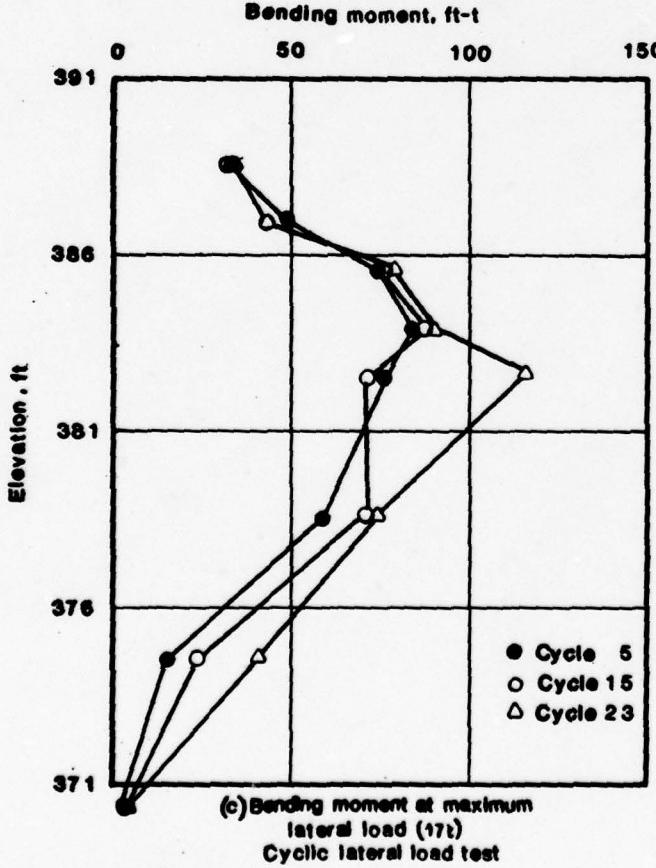
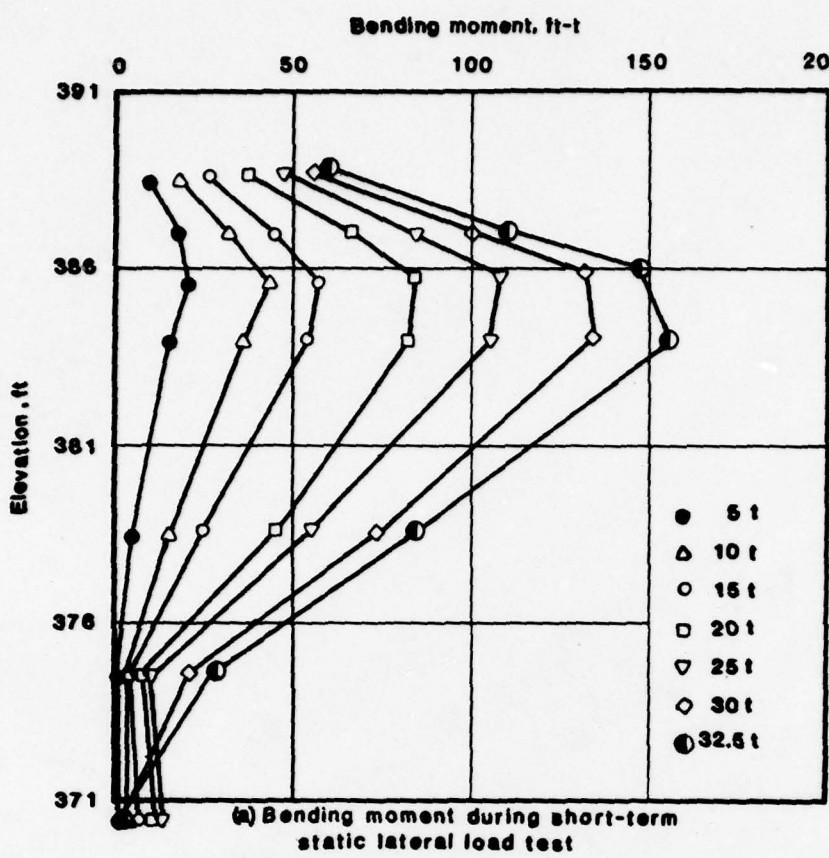


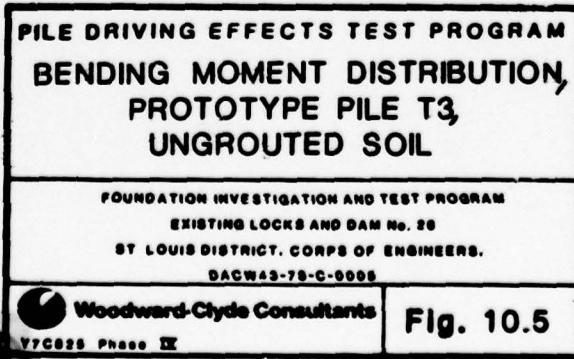
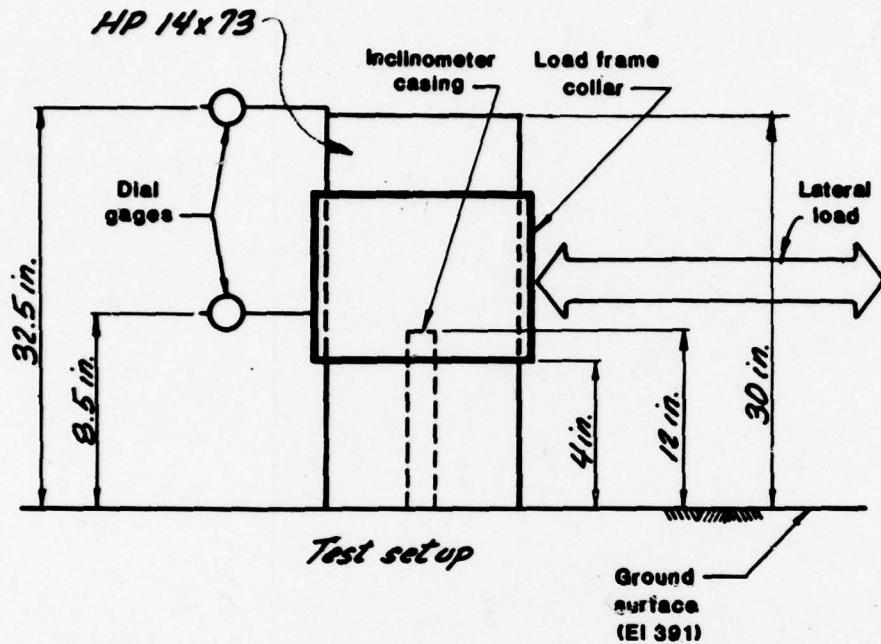
Maximum moment  
at structural failure  
T4

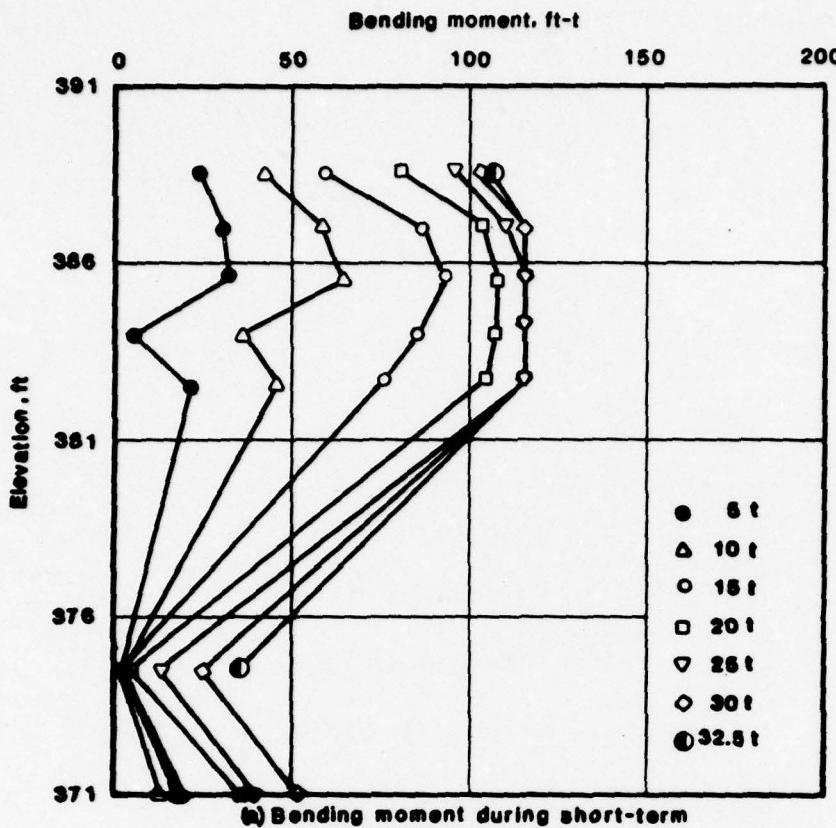
from short term  
lateral load test



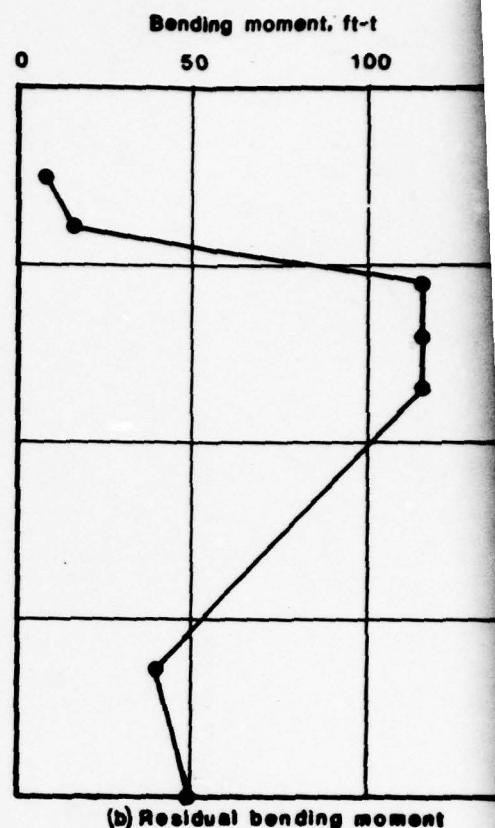
2



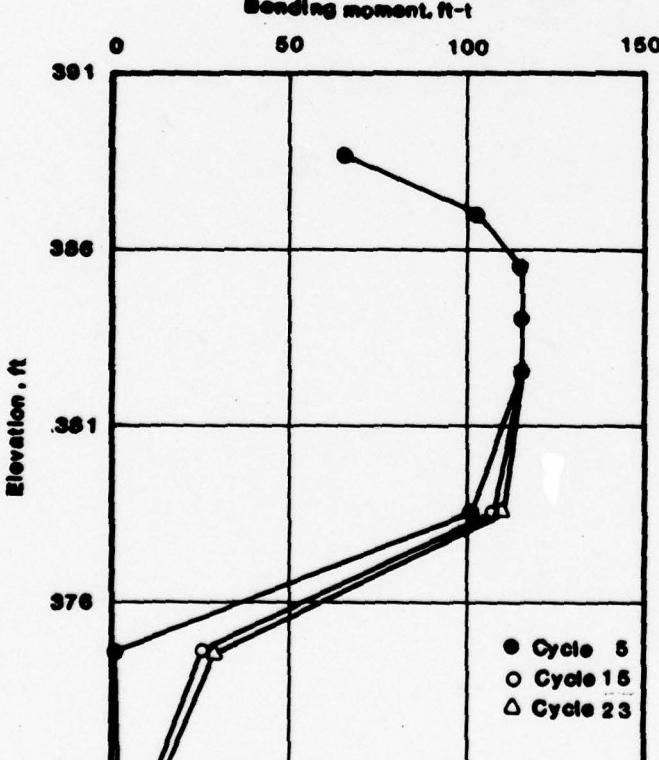




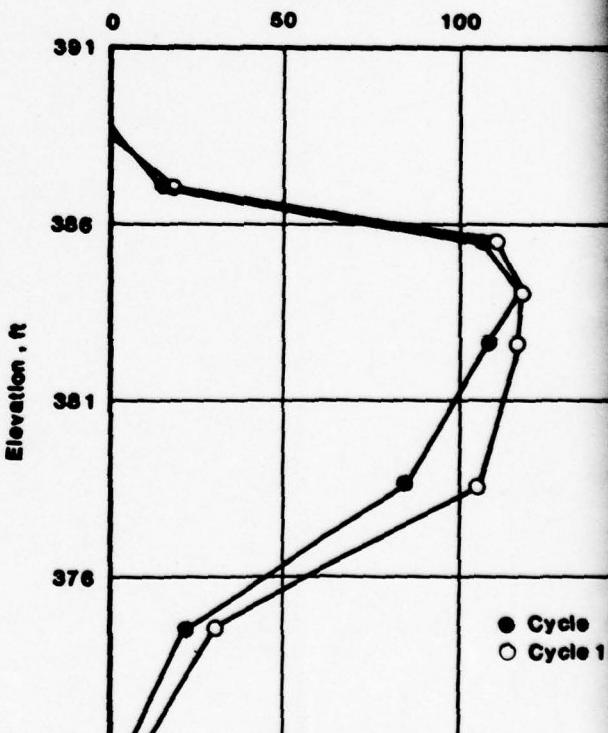
(a) Bending moment during short-term static lateral load test



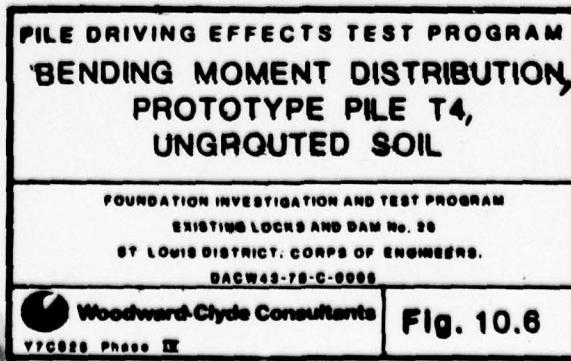
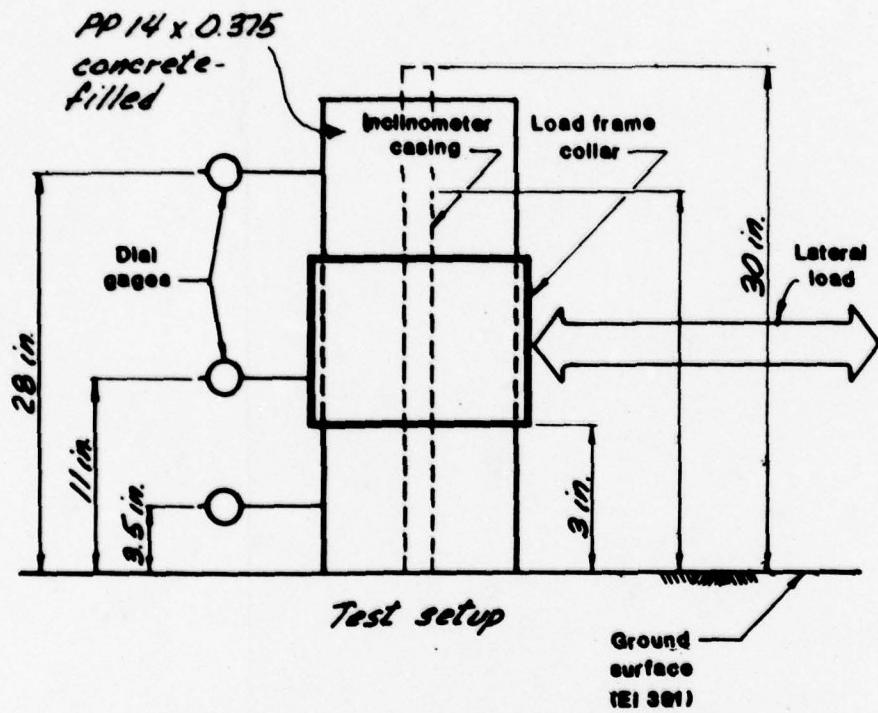
(b) Residual bending moment after unloading

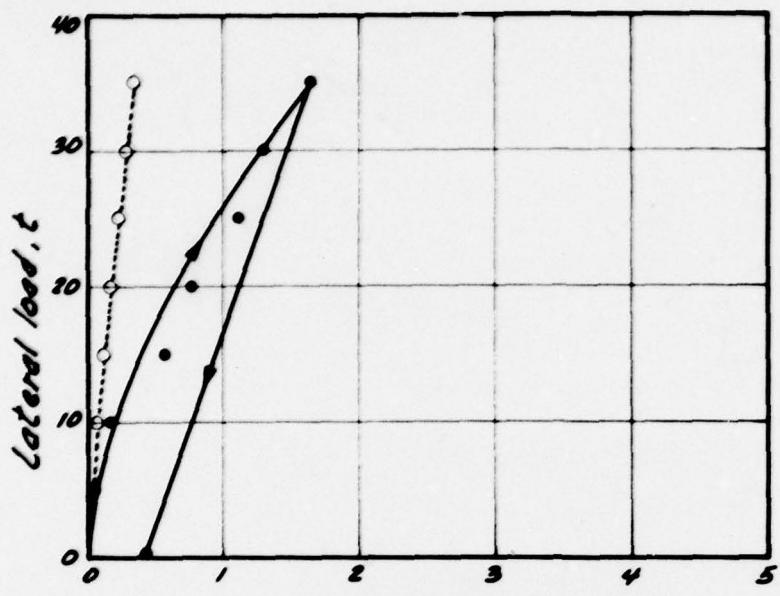


(c) Bending moment at maximum lateral load (17t)  
Cyclic lateral load test

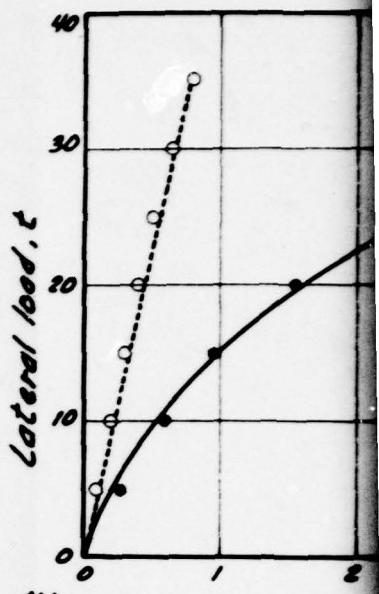


(d) Bending moment at zero lateral load  
Cyclic lateral load test

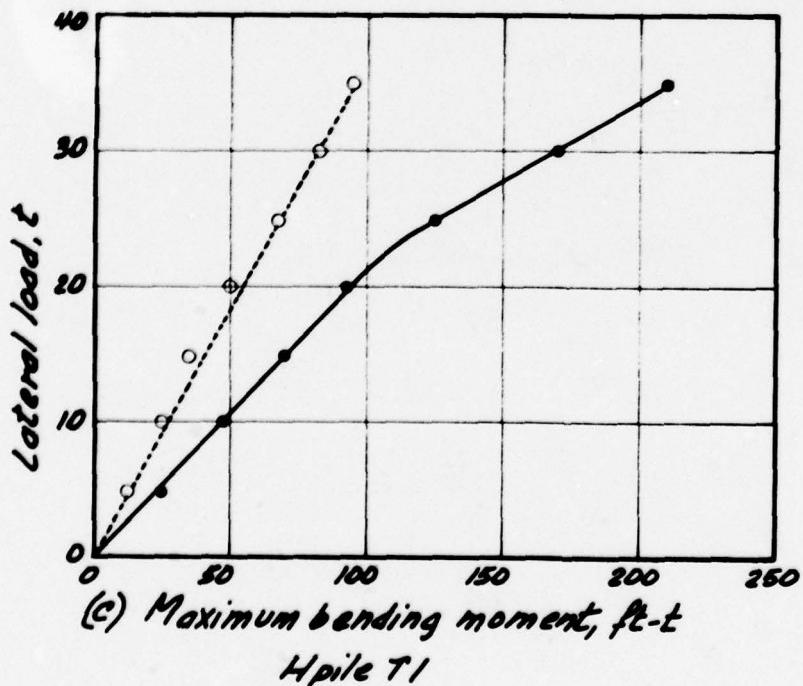




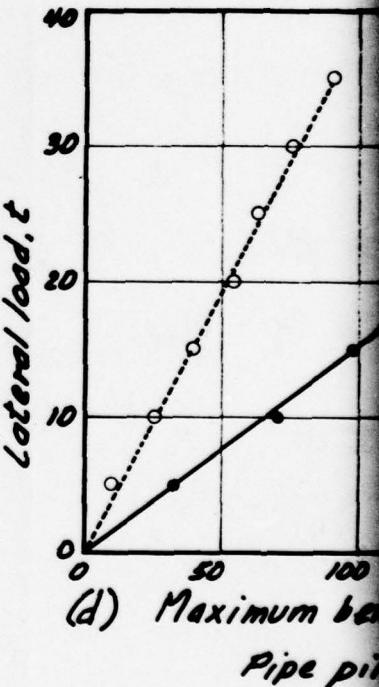
(a) Pile displacement at ground surface, in.  
H pile T1



(b) Pile displacement  
Pipe p1

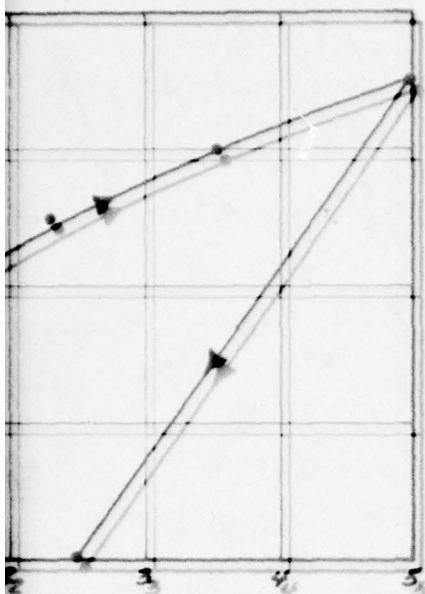


(c) Maximum bending moment, ft-t  
H pile T1



(d) Maximum bending moment, ft-t  
Pipe p1

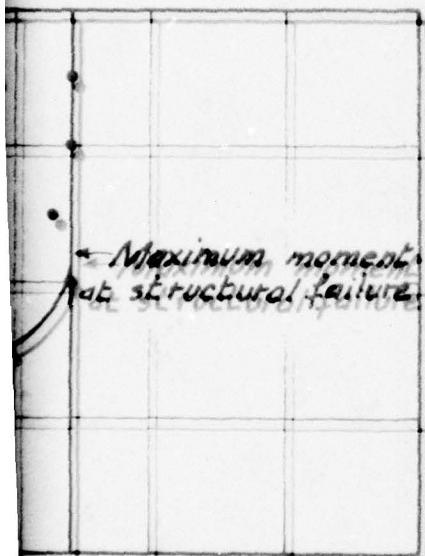
Note  
Res  
stan



pile T2

### Legend

- Observed values
- o- Predicted values



pile T2

Results from short term  
static lateral load test

**PILE DRIVING EFFECTS TEST PROGRAM**

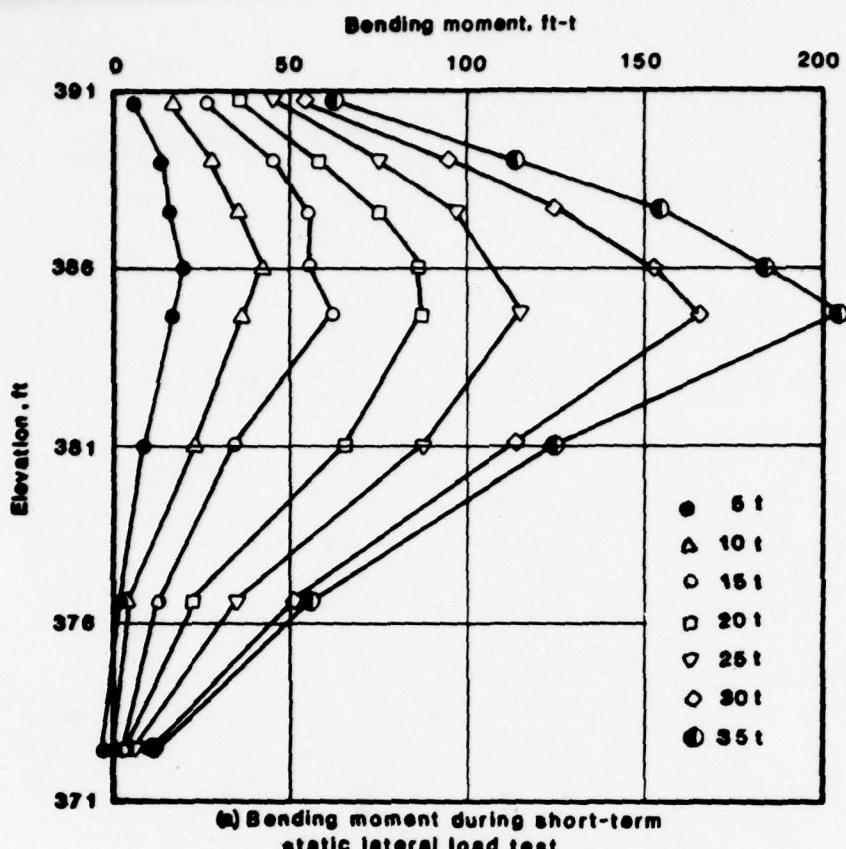
**SHORT-TERM LOAD BEHAVIOR**

**PROTOTYPE PILES T1 AND T2,**

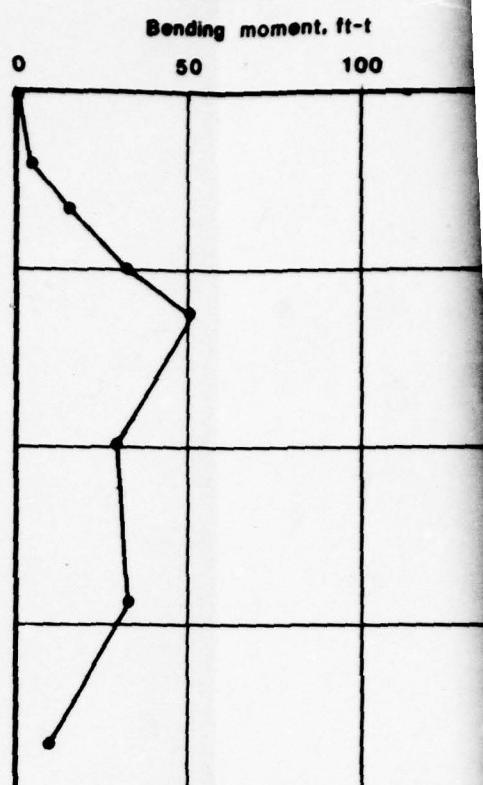
**POSTGROUTED SOIL**

FOUNDATION INVESTIGATION AND TEST PROGRAM	
EXISTING LOCKS AND DAM NO. 36	
ST. LOUIS DISTRICT, CORPS OF ENGINEERS.	
DAGW43-78-C-9888	
Woodburn & Gandy Consultants	Fig. 10.3
100-28 Phase II	

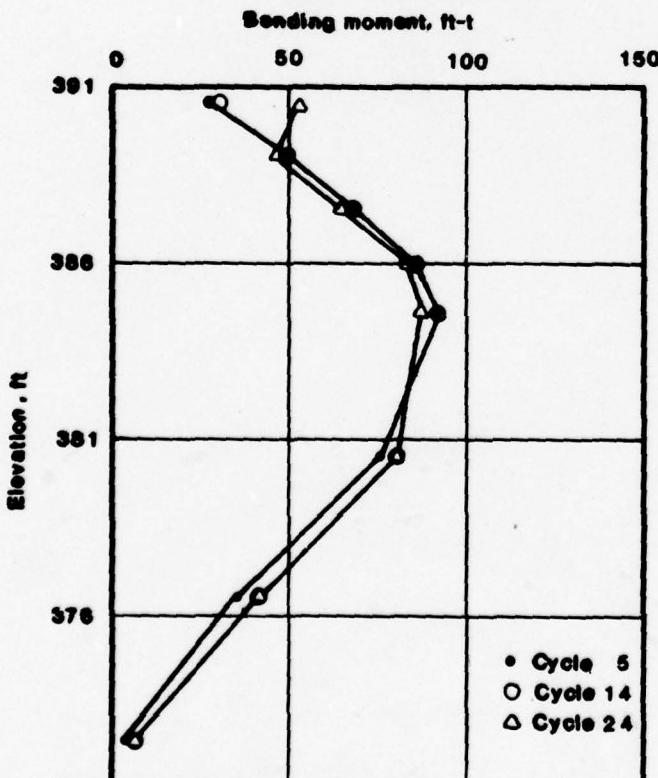
2  
J



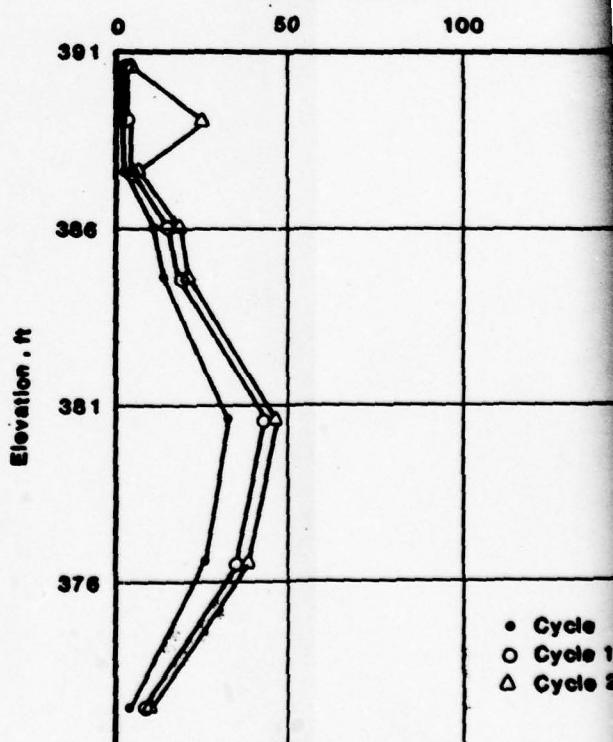
(a) Bending moment during short-term static lateral load test



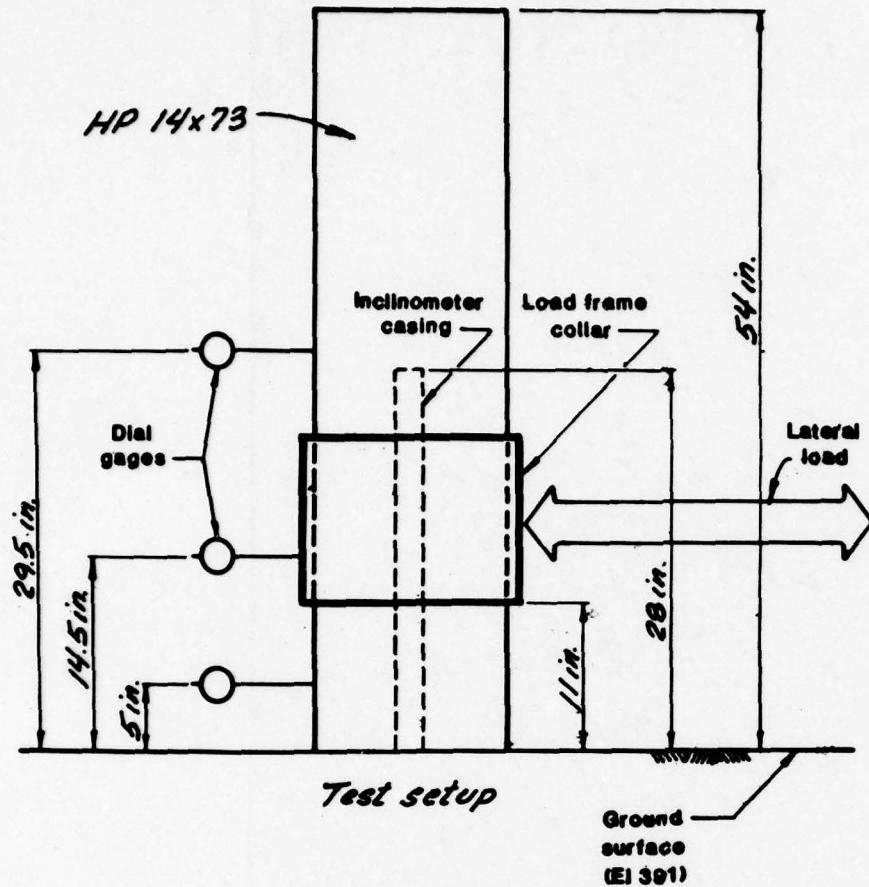
(b) Residual bending moment after unloading

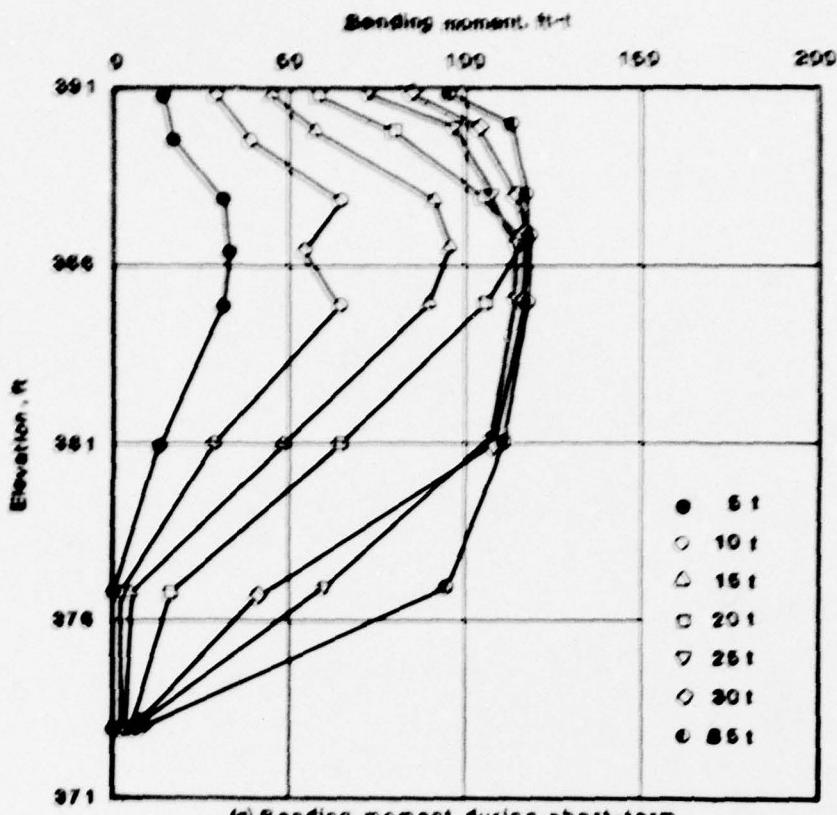


(c) Bending moment at maximum lateral load (17t)  
Cyclic lateral load test

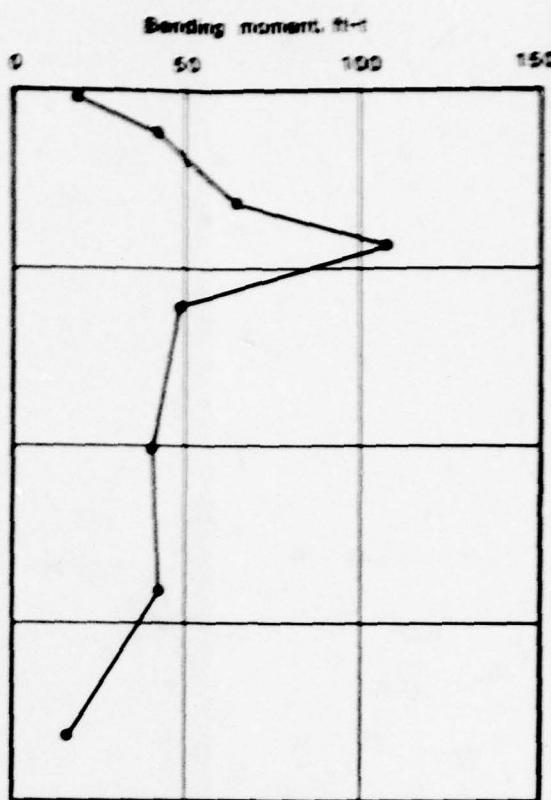


(d) Bending moment at zero lateral load  
Cyclic lateral load test

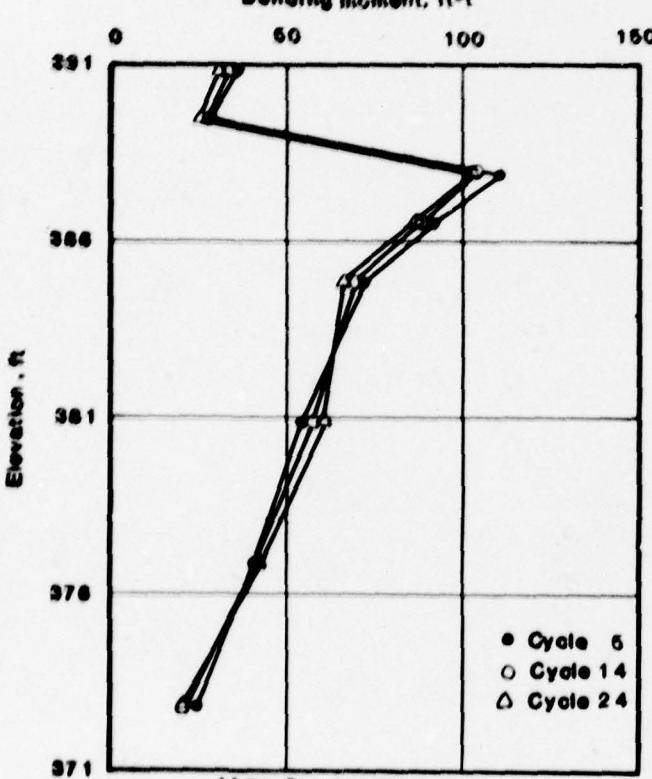




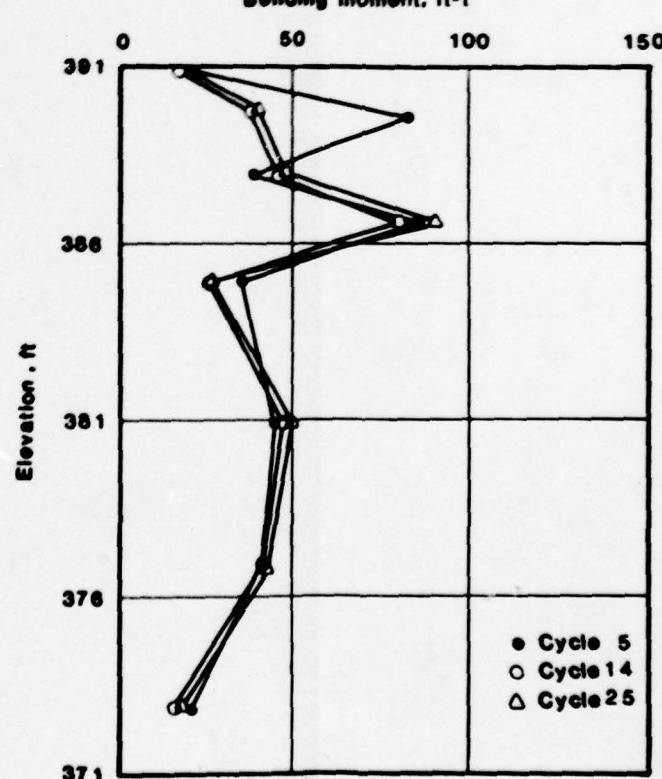
(a) Bending moment during short-term static lateral load test



(b) Residual bending moment after unloading



(c) Bending moment at maximum lateral load (17t)  
Cyclic lateral load test



(d) Bending moment at zero lateral load  
Cyclic lateral load test

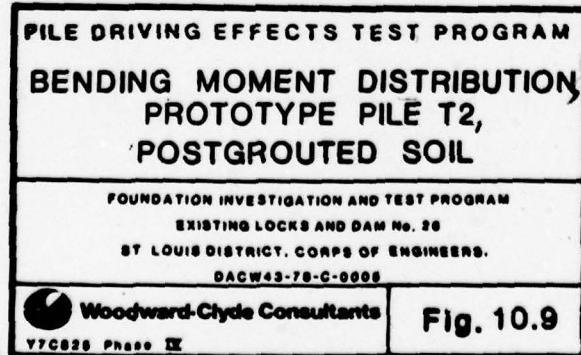
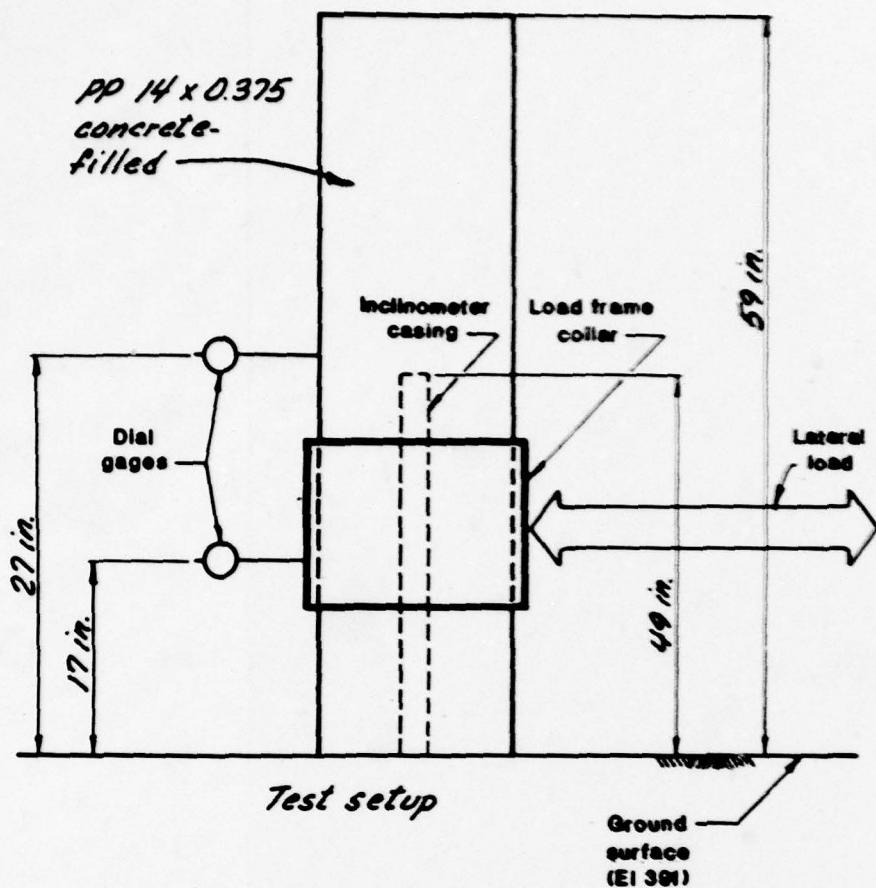
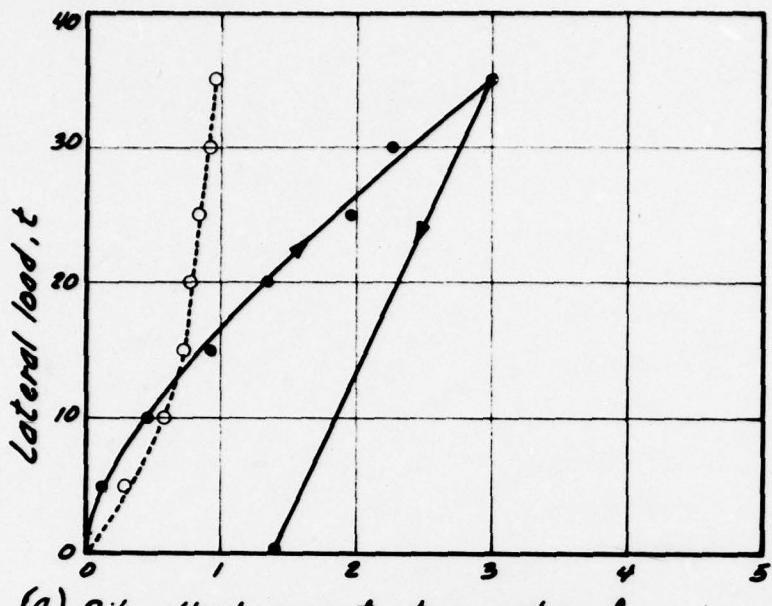
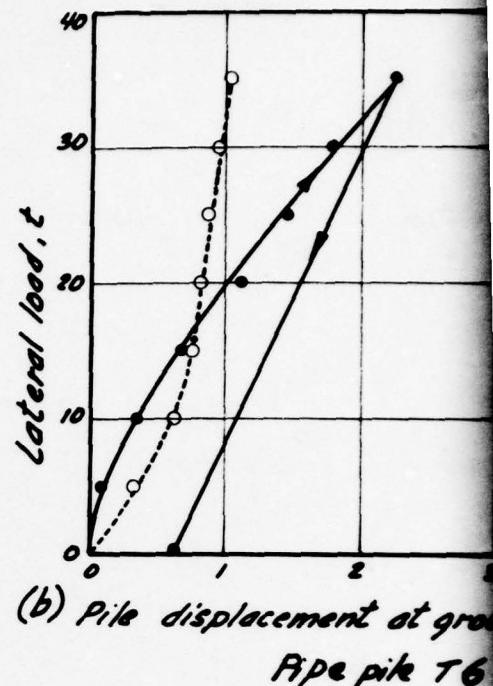


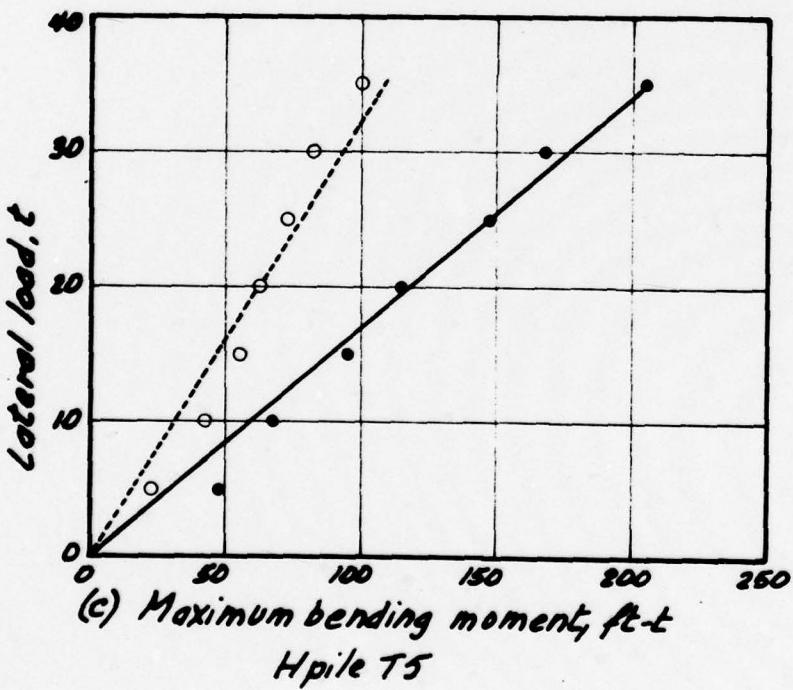
Fig. 10.9



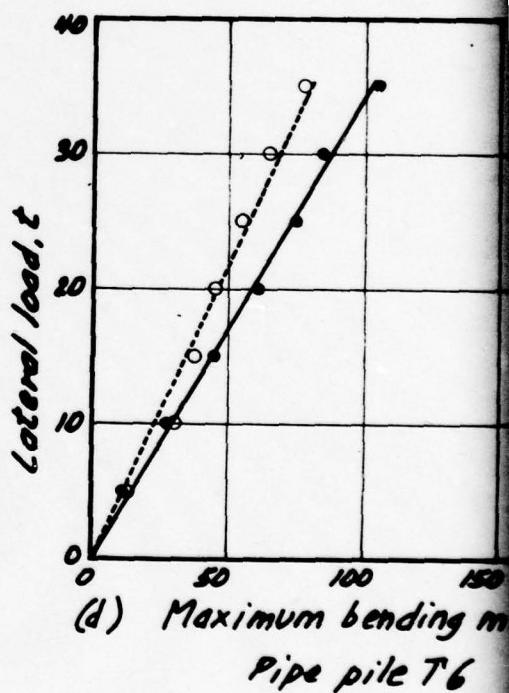
(a) Pile displacement at ground surface, in.  
H pile T5



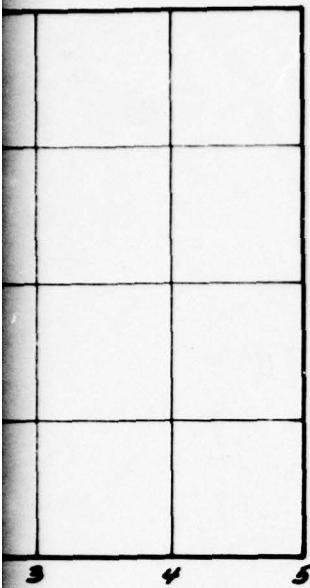
(b) Pile displacement at ground surface, in.  
Pipe pile T6



(c) Maximum bending moment, ft-lb  
H pile T5

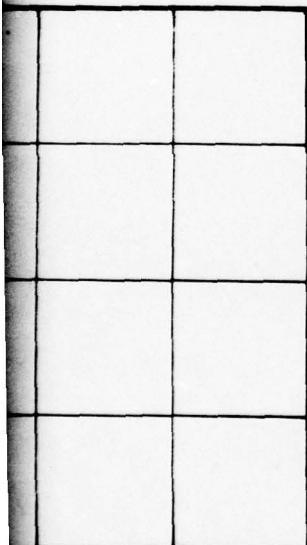


Note:  
Results for static lateral load tests



ground surface, in.

6



20 200 250  
moment, ft-lb

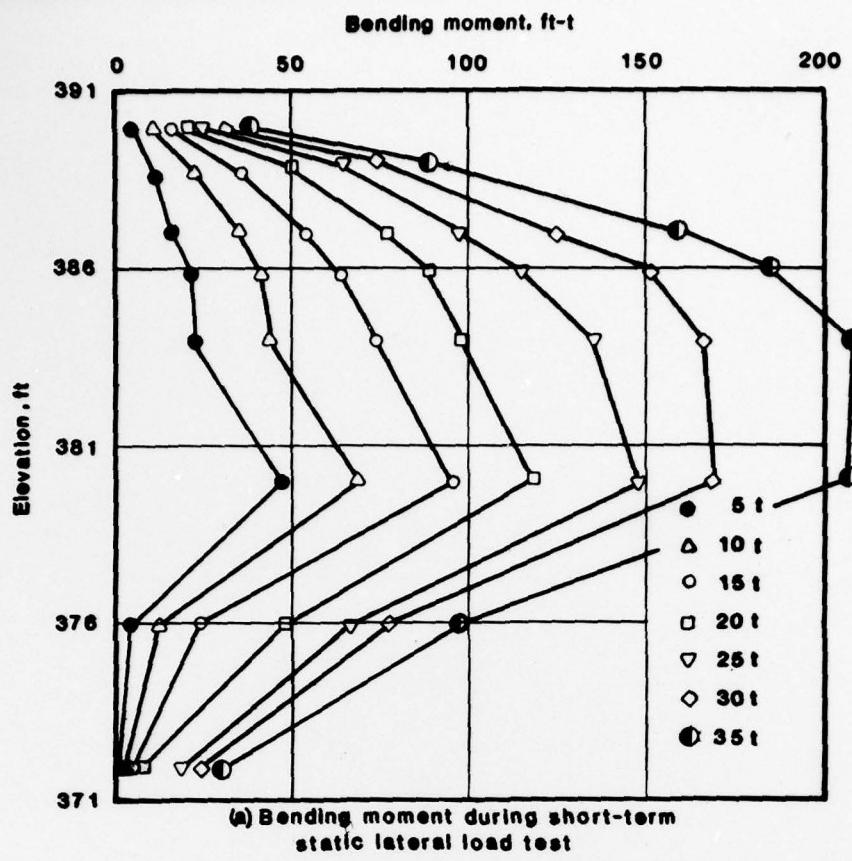
from short term  
lateral load test

### Legend

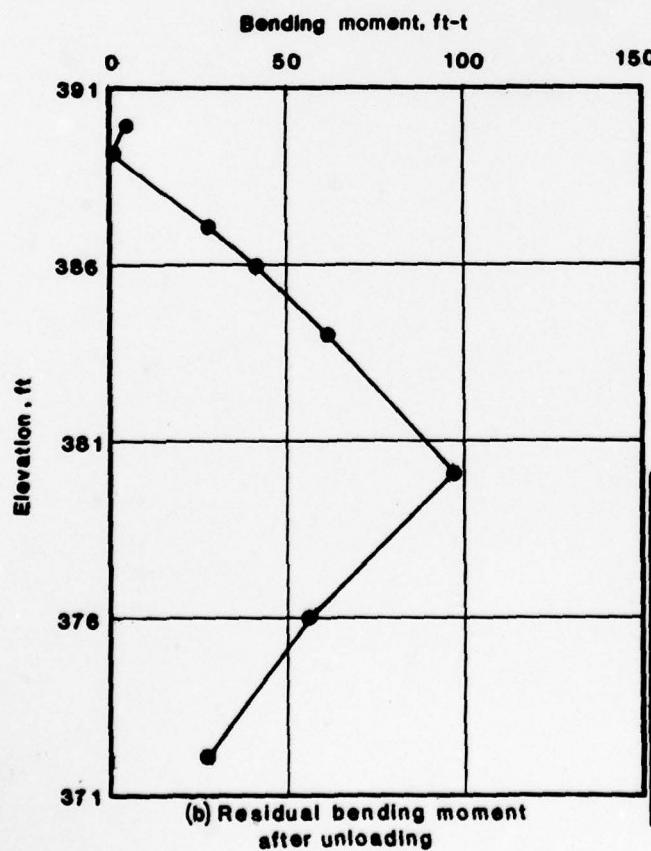
- Observed values
- Predicted values



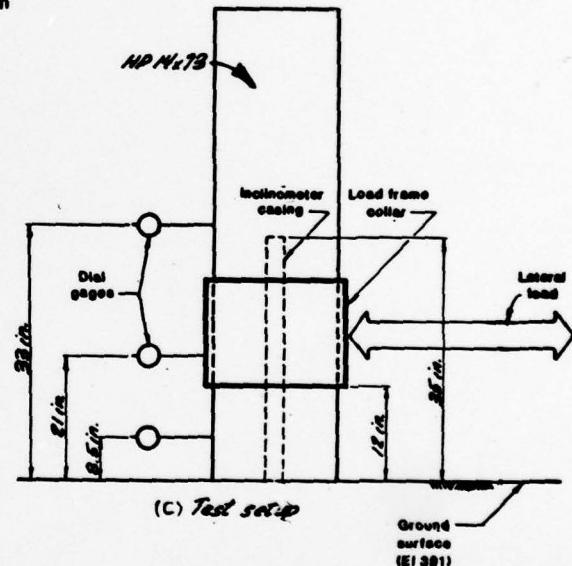
2



(a) Bending moment during short-term static lateral load test



(b) Residual bending moment after unloading

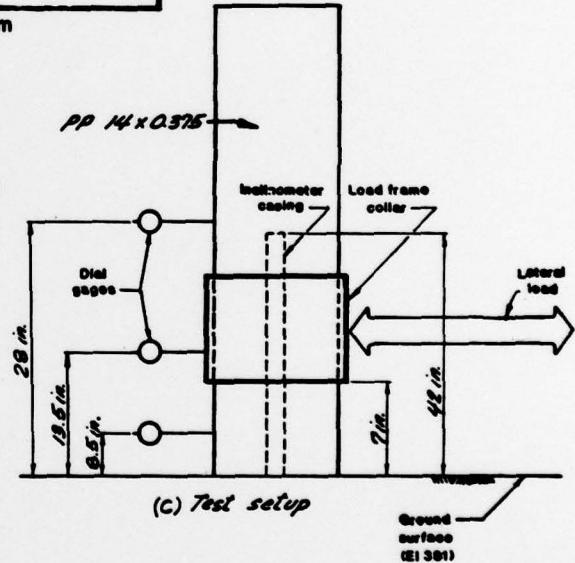
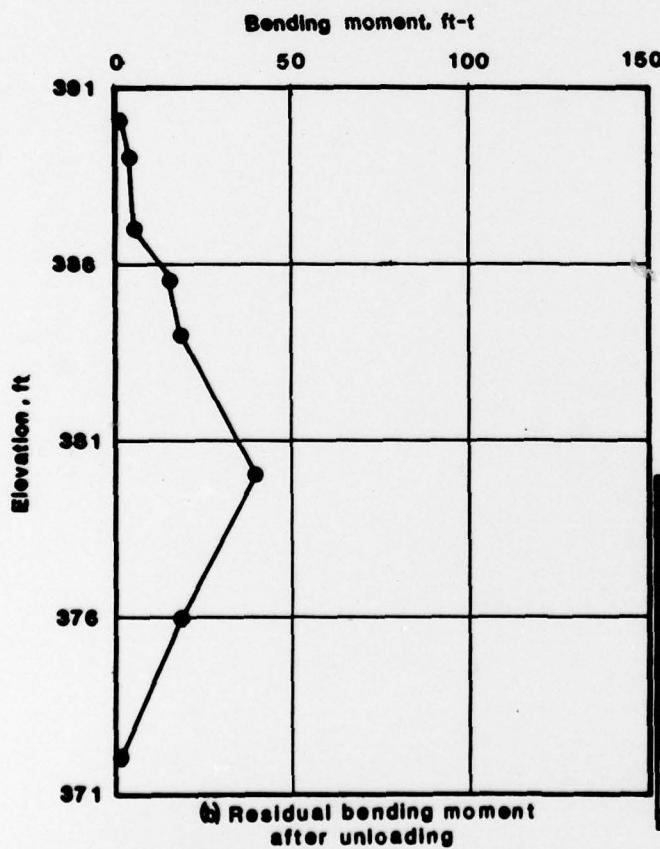
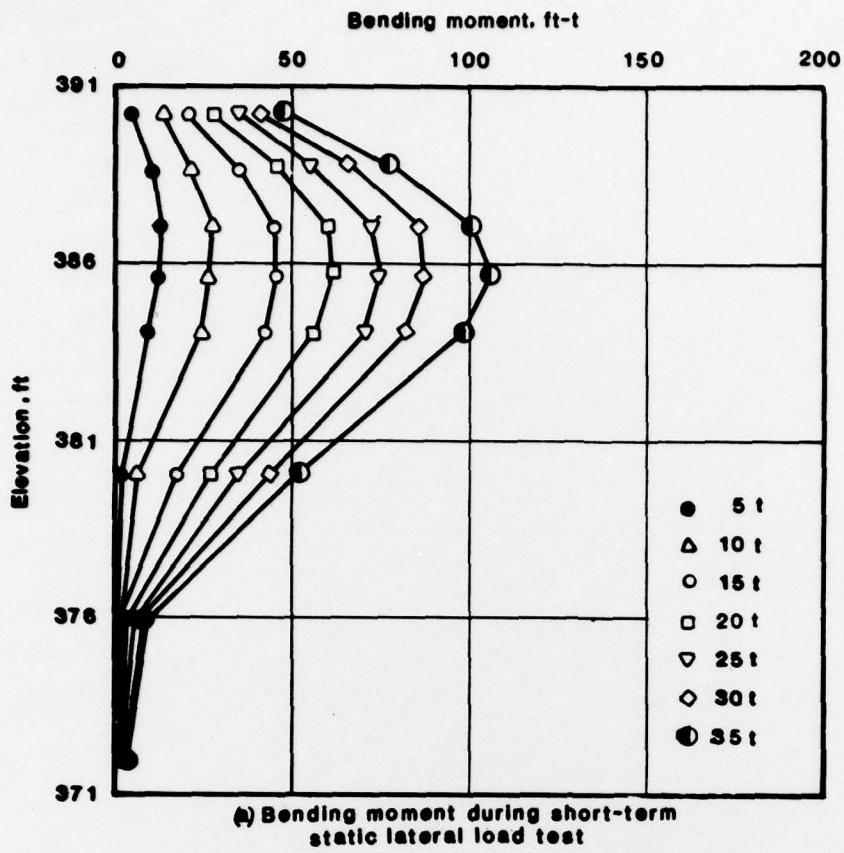


**PILE DRIVING EFFECTS TEST PROGRAM**  
**BENDING MOMENT DISTRIBUTION,**  
**PROTOTYPE PILE T5,**  
**PREGROUTED SOIL**

FOUNDATION INVESTIGATION AND TEST PROGRAM  
 EXISTING LOCKS AND DAM No. 20  
 ST LOUIS DISTRICT, CORPS OF ENGINEERS.  
 DABW43-10-C-0000

Woodward-Clyde Consultants  
 V7C028 Phase III

Fig. 10.11

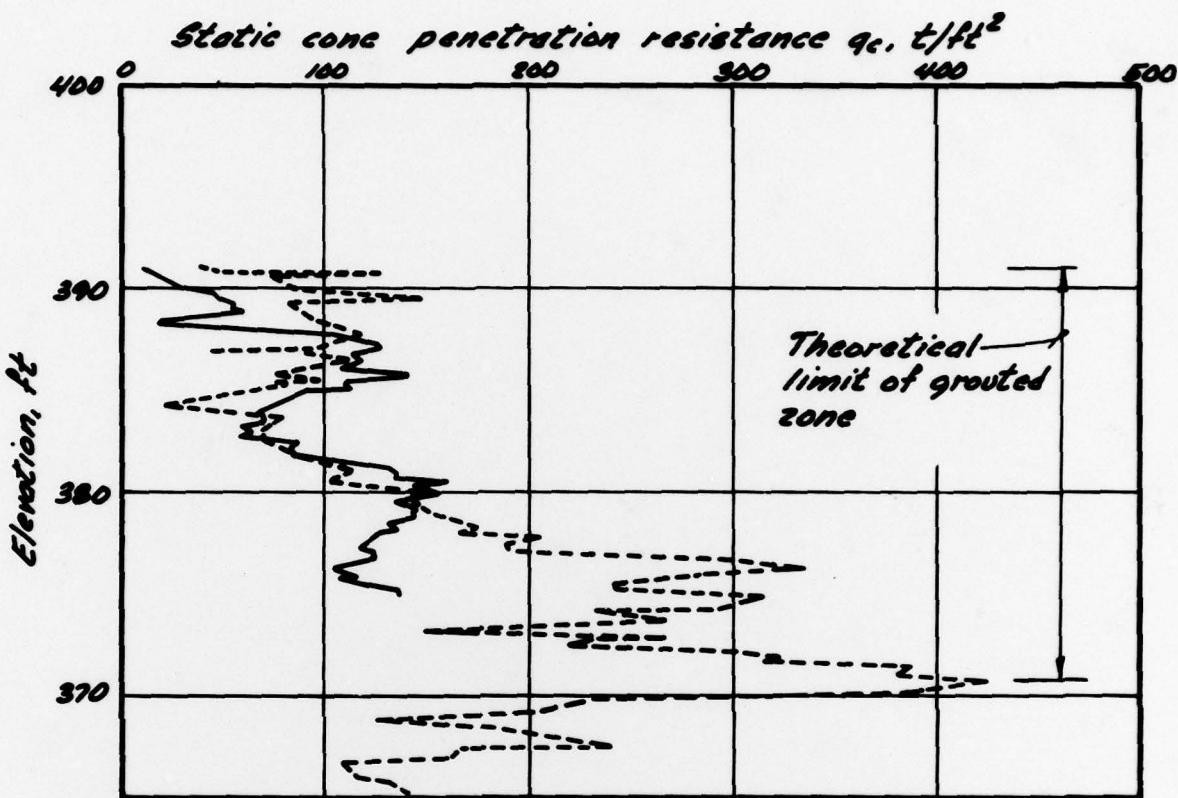


**PILE DRIVING EFFECTS TEST PROGRAM  
BENDING MOMENT DISTRIBUTION,  
PROTOTYPE PILE T6,  
PREGROUTED SOIL**

FOUNDATION INVESTIGATION AND TEST PROGRAM  
EXISTING LOCKS AND DAM NO. 26  
ST. LOUIS DISTRICT, CORPS OF ENGINEERS.  
DACW43-78-C-0008

Woodward-Clyde Consultants  
Y7C626 Phase II

**Fig. 10.12**

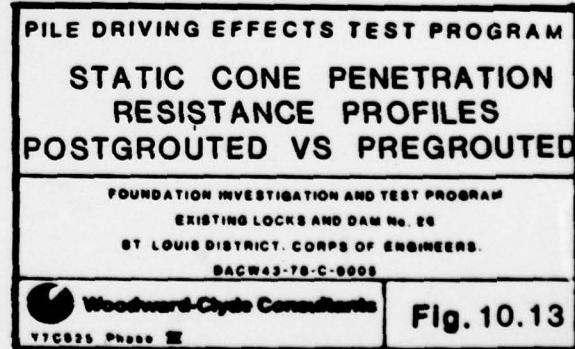


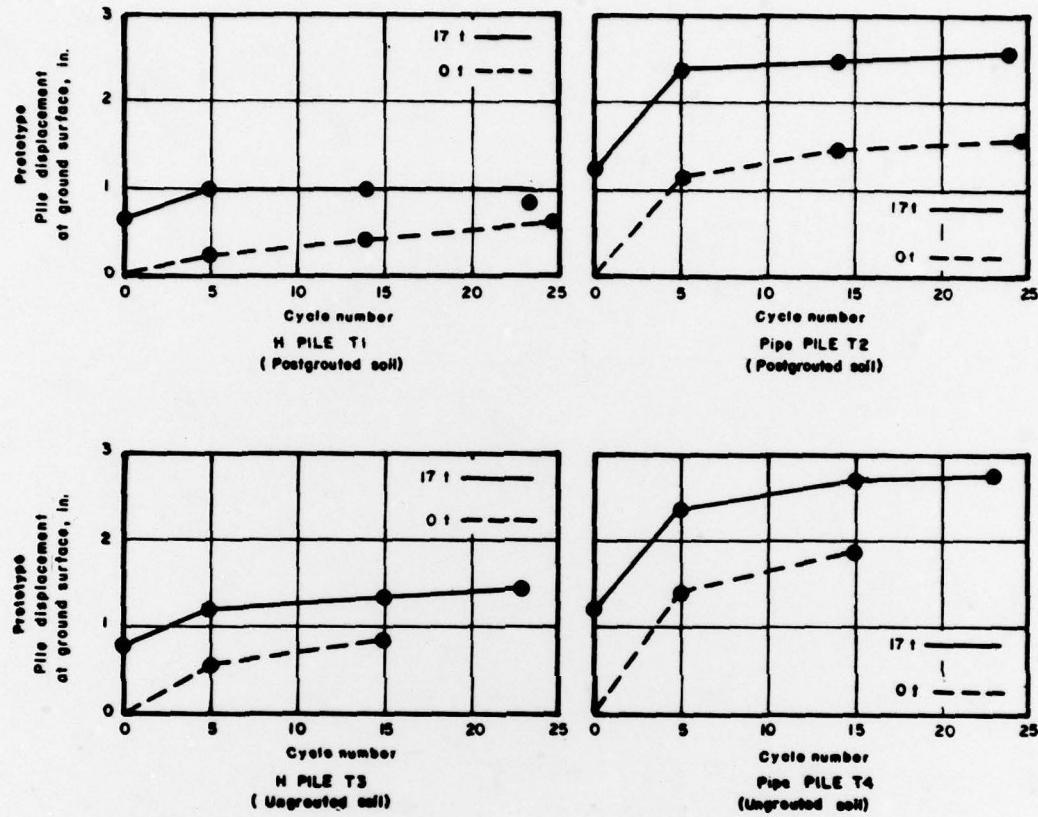
*Legend*

- Prototype pile driven into ungrouted soil,  
soil then grouted (Postgrouted)
- Boring PD3-C2
- Prototype pile driven into pregrouted soil (Pregrouted)
- Boring PD4-C1

*Note:*

*Location of borings  
shown in Fig. 5.14*



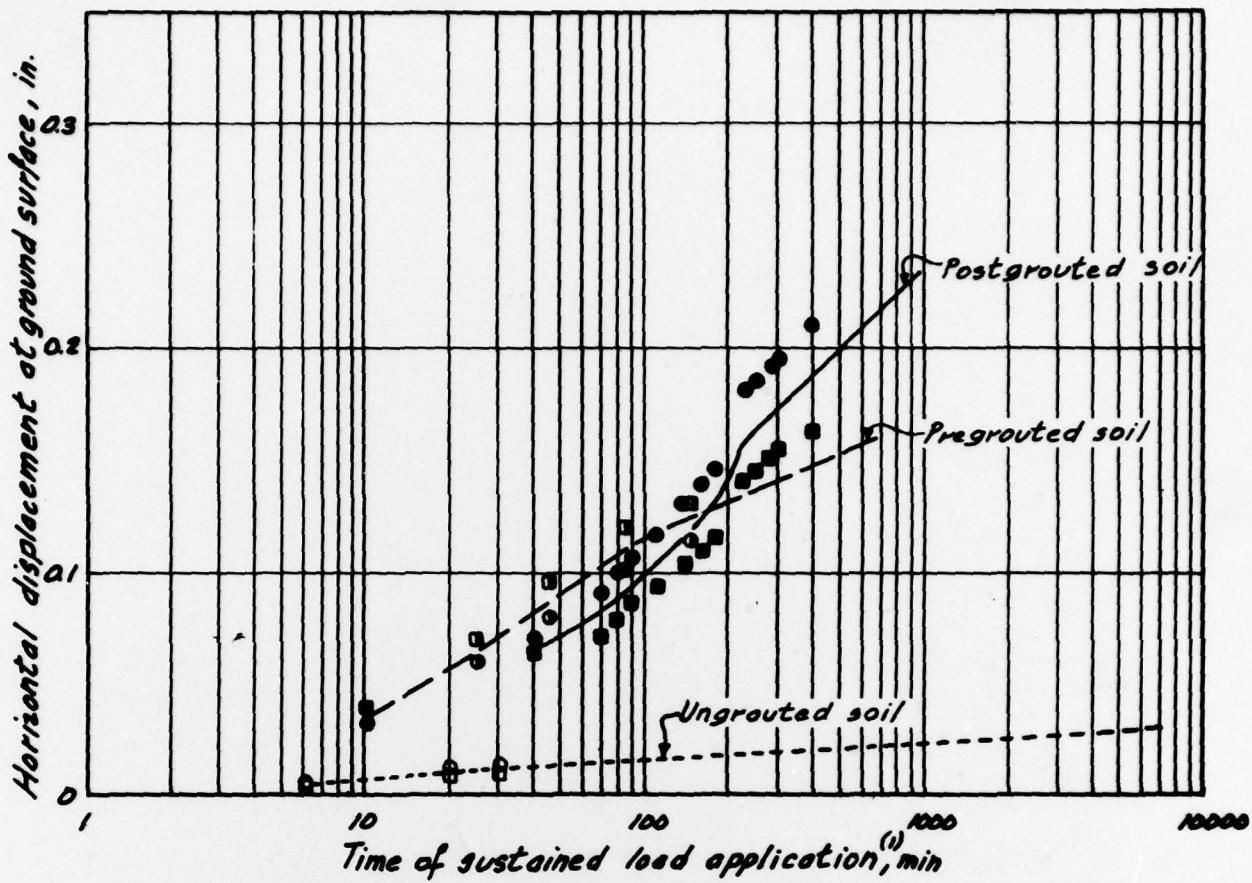


**PILE DRIVING EFFECTS TEST PROGRAM  
PROTOTYPE PILE DISPLACEMENTS  
AT GROUND SURFACE DURING  
CYCLIC LATERAL LOAD TESTS,  
PROTOTYPE PILES  
T1 THROUGH T4**

FOUNDATION INVESTIGATION AND TEST PROGRAM  
EXISTING LOCKS AND DAM NO. 26  
ST. LOUIS DISTRICT, CORPS OF ENGINEERS.  
DAGW43-78-C-0008

Woodward-Clyde Consultants  
V7C826 Phase II

**Fig. 10.14**

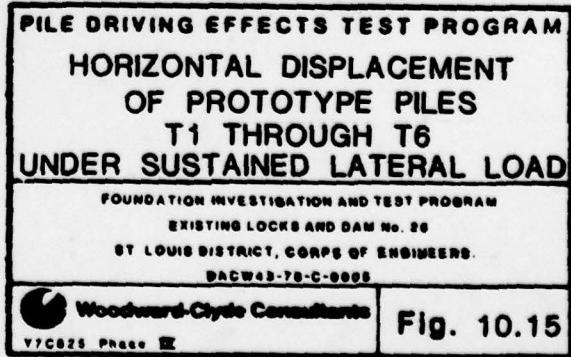


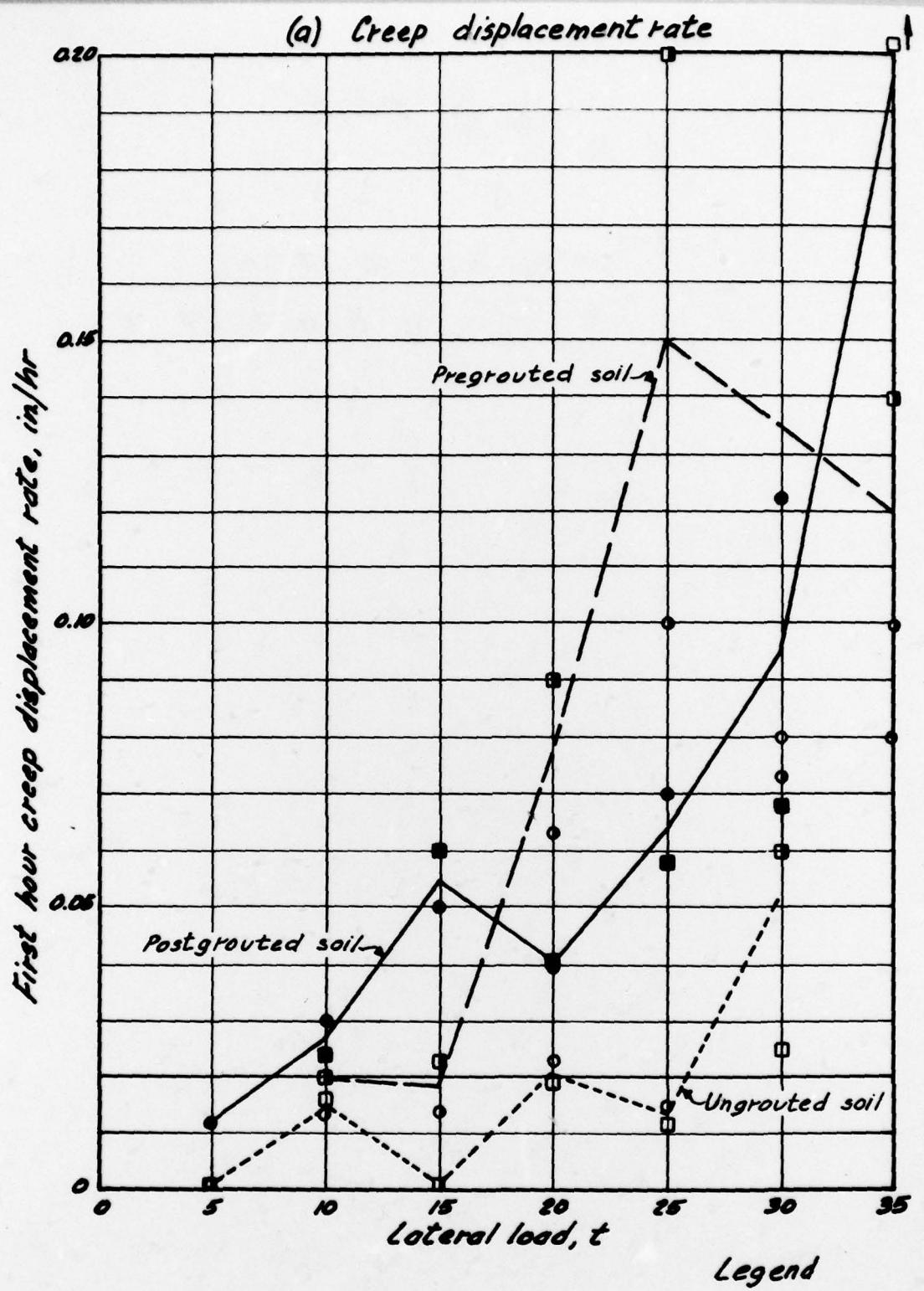
*Legend*

<u>Prototype pile type</u>	<u>Prototype pile No.</u>	<u>Soil type</u>	<u>Prototype pile No.</u>	<u>Prototype pile type</u>
T3	○	Ungrouuted	□	T4 PP 14 x 0.375
HP 14 x 73	T5	• Pregrouuted	□	T6 concrete-filled
T1	●	Postgrouted	■	T2

*Notes:*

- (1) Horizontal displacements at ground surface measured under a sustained load of 15 t
- (2) Prototype pile T6 was backfilled with sand





Legend

Prototype pile type   Prototype pile No.

HP 14 x 73

T3   T5   T1

Soil type

Ungrouted   Pregrueted   Postgrouted

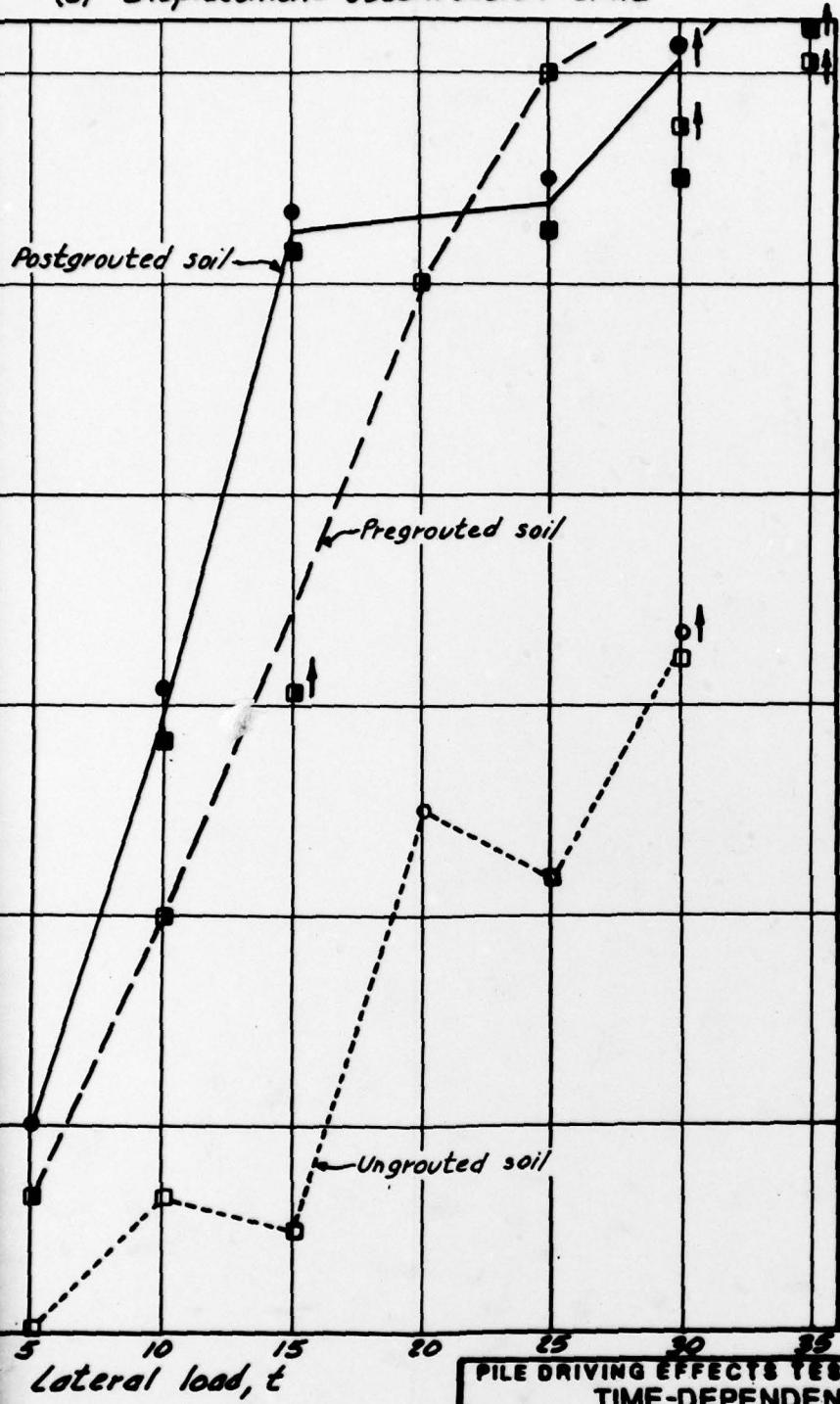
Prototype pile No.   Prototype pile

T4   T6   T2   PP 14 x concrete

Note:

Prototype pile T6 was backfilled with sand

(b) Displacement stabilization time



**PHASE IV REPORT**

**VOLUME III**

**RESULTS AND INTERPRETATION OF  
PILE DRIVING EFFECTS TEST PROGRAM**

**SECTION 11  
PILE INSPECTION AFTER EXTRACTION**

## 11 PILE INSPECTION AFTER EXTRACTION

### 11.1 TIMBER PILES

At the end of the test program, two timber piles under monolith M2 (piles 17 and 13, Fig. 5.2) were extracted. The concrete monolith was partially demolished using a large jack-hammer mounted on a backhoe boom. The timber piles were extracted using a Foster 40E vibratory extractor. No difficulty was experienced during this operation. Photographs of the two piles after extraction are shown in Fig. 11.1. Information concerning the installation of the two piles is given below:

Pile No.	Jetted Depth ft	Final Blowcount During Installation blow/ft	Blowcount Upon Restriking blow/ft
17	27	25	148
30	27	100	334

Complete driving records for these two timber piles are given in Appendix M, Volume IIIA.

Timber pile 30 was not seriously damaged, except for longitudinal cracks at the butt (probably caused by the jackhammer and extractor). Timber pile 17 was much more damaged. The butt of that pile was damaged by the jackhammer and extractor; more importantly, the pile tip was split and a large piece of wood was missing. Undoubtedly, the hard driving required to install pile 17 to the desired tip elevation was the cause of the observed, substantial damage. Otherwise, none of the two piles showed signs of structural failure which could be attributed to lateral load testing.

### 11.2 PROTOTYPE PILES

One H, one open-ended pipe, and the two steel piles were extracted at the end of the test program, using Foster 40E vibratory extractor. No difficulty was experienced in these operations; the pipe pile required somewhat more effort to extract.

The H pile which was extracted was prototype pile 3 driven at 125 ft from monolith M1 using the Vulcan 010 hammer. Driving records for this pile are given in Fig. 7.6 and Fig. 7.10, and in Appendix L, Volume IIIA. A photograph of the H pile tip after extraction is shown in Fig. 11.2a. No damage was observed.

The pipe pile which was extracted was prototype pile 12 driven open-ended at 7 ft from monolith M1 using the Vulcan 010 hammer. Driving records for this pile are given in Fig. 7.5 and Fig. 7.13, and in Appendix L, Volume IIIA. No damage was observed.

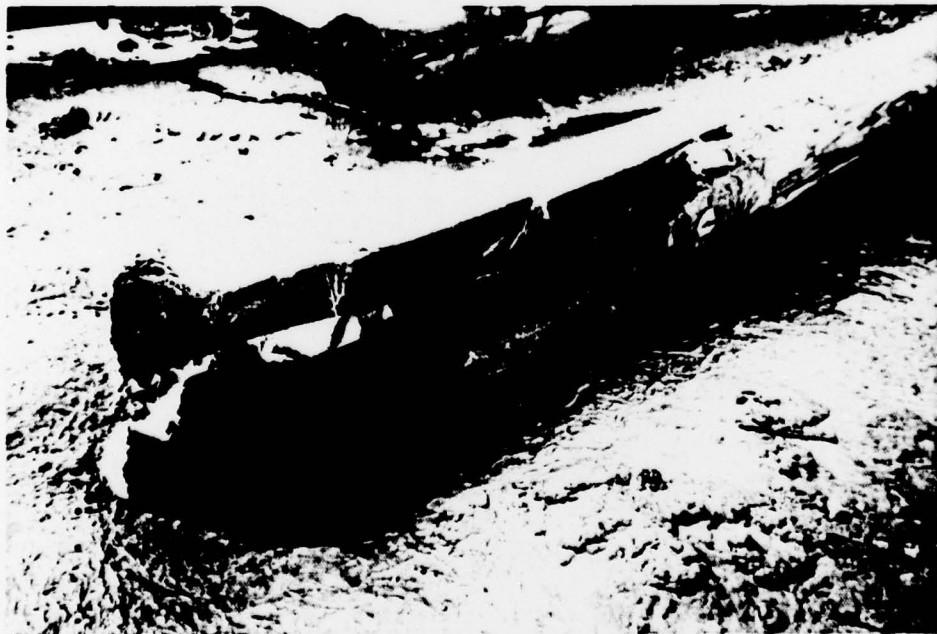
The two sheet piles which were extracted were prototype piles 11 and 12 driven as a pair at 15 ft from monolith M2 using the Foster 4000 vibratory hammer. Driving records of these piles are shown in Fig. 7.15. They were also extracted as a pair. A photograph of the tip portion of the sheet piles after extraction is shown in Fig. 11.2 b. No damage was observed.



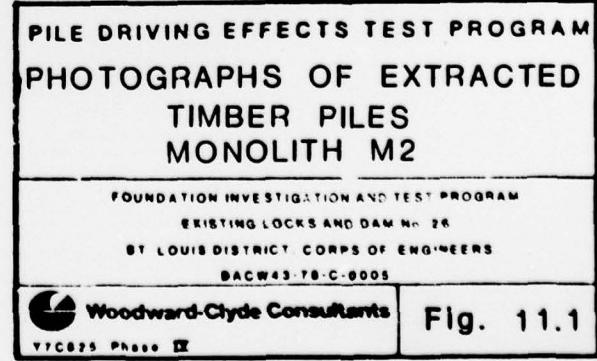
Timber pile 17

Timber pile 30

(a) Pile butts

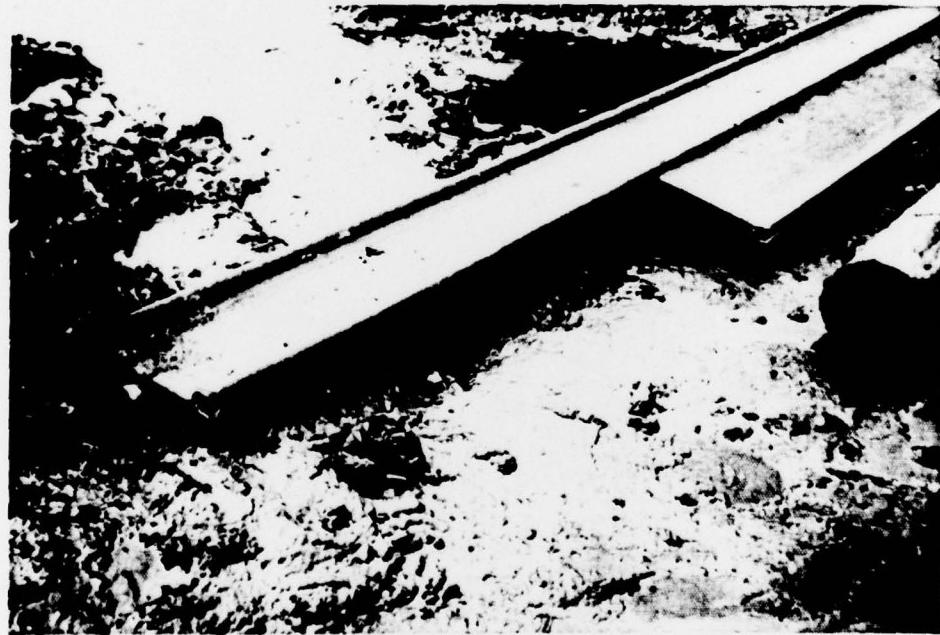


(b) Tip of  
timber pile 17





(a) H-pile  
prototype  
pile 3  
monolith M1



(b) Sheet piles  
prototype  
piles 11 and 12  
monolith M2

PILE DRIVING EFFECTS TEST PROGRAM  
PHOTOGRAPHS OF EXTRACTED  
H AND SHEET PILES  
MONOLITHS M1 AND M2

FOUNDATION INVESTIGATION AND TEST PROGRAM  
EXISTING LOCKS AND DAM NO. 28  
BY LOUISIANA DISTRICT CORPS OF ENGINEERS  
BACW43-78-C-8005

Woodward-Clyde Consultants  
VTC875 PHASE II

Fig. 11.2

R-i

**PHASE IV REPORT**

**VOLUME III**

**RESULTS AND INTERPRETATION OF  
PILE DRIVING EFFECTS TEST PROGRAM**

**REFERENCES**

#### REFERENCES

- Barkan, D.D. (1962) "Dynamics of Bases and Foundations" (translated from Russian by L. Draskevska; translation edited by G.P. Tschebotarioff), McGraw-Hill Book Co, New York
- Bogard, D. and Matlock, H. (1977) "A Computer Program for the Analysis of Beam-Columns Under Static and Lateral Loads" Proc IX Offshore Technology Conference, Houston
- Clough, G.W., Tan, D.Y., Kuck, W.M., and Koenzen, P.J. (1977) "Development of Design Procedures for Stabilized Soil Support Systems for Soft Ground Tunneling" I and II, Report to Dept of Transportation, DOT-TST-77-74
- Feagin, L.B. (1936) Dam No. 11 Round Timber Pile Lateral Stability Test, War Dept Corps of Engineers, US Army, US Engineer Office, Rock Island, IL
- Feagin, L.B. (1936a) "Pile Loading Tests - Dam No. 26 Within Cofferdams No. 1 and 2" Report to District Engineer, St Louis, MO
- Feagin, L.B. (1937) "Pile Loading Tests - Dam No. 26 Within Cofferdam No. 3" Report to Acting District Engineer, St Louis, MO
- Feagin, L.B. (1937a) "Lateral Pile Loading Tests" Trans ASCE, 63, 8, Part 2
- Feagin, L.B. (1948) "Performance of Pile Foundations of Navigation Locks and Dams on the Upper Mississippi River" Proc 2nd ICSMFE, Rotterdam, IV, Article VII a 10
- Feagin, L.B. (1953) "Lateral Load Tests on Groups of Battered and Vertical Piles" Proc Symp on Lateral Load Tests on Piles, ASTM, STP154, Atlantic City, NJ
- Fruco and Associates (1973) "Overwater Steel H-Pile Driving and Testing Program, Locks and Dam No. 26 (replacement)", report prepared for St Louis District, Corps of Engineers
- Gibbs, H.J. and Holtz, W.G. (1953) "Research on Determining the Density of Sands by Spoon Penetration Testing" Proc 4th ICSMFE, 1, p. 35-39
- Goble, G.G. and Rausche, R. (1970) "Pile Load Test by Impact Driving" Highway Research Board, Record No. 333, Washington, DC
- Hughes, J.M.O., Wroth, C.P., and Windle, D. (1977) "Pressuremeter Tests in Sands" Geotechnique, 27, No. 4, Dec

- Koenzen, P.J. (1977) "Time Dependent Stress-Strain Behavior of Silicate-Grouted Sand" JGED, ASCE, 103, GT8, Aug
- Kolbuszewski, K.J. (1948) "An Experimental Study of the Maximum and Minimum Properties of Sand" 2nd ICSMFE, Rotterdam, 1
- Lo, M-B. (1977) "Attenuation of Ground Vibration Induced by Pile Driving" Proc 9th ICSMFE, 2, Tokyo
- Lucks, A.S. (1970) "Influence of Particle Shape on Strength of Granular Materials" PhD Thesis, MIT, June
- Matlock, H. and Reese, L. (1956) "Non-Dimensional Solution for Laterally Loaded Piles With Soil Modulus Assumed Proportional to Depth" Proc V Texas Conf on Soil Mech and Fdn Engr
- McClelland, B. and Focht, J.A. (1958) "Soil Modulus for Laterally Loaded Piles" Trans ASCE, 123
- Meyerhof, G.G. (1974) "Penetration Testing Outside Europe" General Report Proc European Symp on Penetration Testing, Stockholm, Sweden, 2.1
- Mirafuente, N., Zurflueh, E., and Statton, C.T. (1975) "Improved Shear Wave Measurement Techniques for Better Earthquake Resistant Design" WCC Geotechnical/Environmental Bulletin, VII, No. 2
- O'Neill, M.W., Ghazzaly, O.L., and Ha, H.B. (1977) "Analysis of Three-Dimensional Pile Groups with Non-Linear Soil Response and Pile-Soil-Pile Interaction" Paper 2838, Proc Offshore Technology Conference
- Richart, F.E., Hall, J.R., and Woods, R.D. (1970) Vibrations of Soils and Foundations, Prentice Hall
- Schmertmann, J. (1976) "An Updated Correlation Between Relative Density, Dr and Fugro-type Electric Cone Bearing,  $q_c$ " Contract Report DACW39-76-M-6646, Waterways Experiment Station, Vicksburg, MS
- Terzaghi, K. (1955) "Evaluation of Coefficients of Subgrade Reaction" Geotechnique, 8
- Vesic, A.S. (1970) "Test on Instrumented Piles, Ogeechee River Site" JSMFD, ASCE, 96, SM2, Mar
- Warner, J. (1972) "Strength Properties of Chemically Solidified Soils" JSMFD, ASCE, 98, No. SM11, Nov
- Woodward-Clyde Consultants (1971) "Foundation Preparation, Chemical Grouting, Crystal River Unit No. 3" 10 May